ISTANBUL TECHNICAL UNIVERSITY ★ GRADUATE SCHOOL OF SCIENCE ENGINEERING AND TECHNOLOGY

MODELLING WELLBORE HYDRAULICS THROUGH THERMAL RHEOLOGICAL SEPIOLITE MUD PROPERTIES

Ph.D. DISSERTATION

ALI ETTEHADI

Department of Petroleum and Natural Gas Engineering

Petroleum and Natural Gas Engineering Programme

JANUARY 2016

ISTANBUL TECHNICAL UNIVERSITY ★ GRADUATE SCHOOL OF SCIENCE ENGINEERING AND TECHNOLOGY

MODELLING WELLBORE HYDRAULICS THROUGH THERMAL RHEOLOGICAL SEPIOLITE MUD PROPERTIES

Ph.D. DISSERTATION

ALI ETTEHADI
(505102500)

Department of Petroleum and Natural Gas Engineering

Petroleum and Natural Gas Engineering Programme

Thesis Advisor: Assoc. Prof. Dr. Gürşat ALTUN

JANUARY 2016

İSTANBUL TEKNİK ÜNİVERSİTESİ ★ FEN BİLİMLERİ ENSTİTÜSÜ

SONDAJ KUYUSU HİDROLİĞİNİN SEPİYOLİT ÇAMURU ISIL REOLOJİK ÖZELLİKLERİYLE MODELLENMESİ

DOKTORA TEZİ

Ali ETTEHADİ
(505102500)

Petrol ve Doğal Gaz Mühendisliği Bölümü

Petrol ve Doğal Gaz Mühendisliği Programı

Tez Danışmanı: Doç. Dr. Gürşat ALTUN

OCAK 2016

ALI ETTEHADI, **a Ph.D.** student of ITU **Graduate School of Science Engineering and Technology** student ID 505102500, successfully defended the **dissertation** entitled "**MODELLING WELLBORE HYDRAULICS THROUGH THERMAL RHEOLOGICAL SEPIOLITE MUD PROPERTIES**", which he prepared after fulfilling the requirements specified in the associated legislations, before the jury whose signatures are below.

Thesis Advisor : **Assoc. Prof. Dr. Gürşat ALTUN** ....
İstanbul Technical University

Jury Members : **Prof. Dr. İ. Bedii ÖZDEMİR** ....
İstanbul Technical University

Prof. Dr. Niyazi AKSOY ....
Dokuz Eylül University

Assoc. Prof. Dr. Metin MURADOĞLU ....
Koç University

Asst. Prof. Dr. Şenol YAMANLAR ....
İstanbul Technical University

Date of Submission : 11 December 2015
Date of Defense : 13 January 2016

This dissertation is dedicated to my gorgeous wife Farnaz and lovely baby Ela whose unyielding love, support, and encouragement have enriched my soul and inspired me to pursue and complete this study

FORWARD

I would like to present my endless thanks to my advisor, Associate Professor Dr. Gürşat Altun, for his encouragement, guidance, support and patience during my Ph.D. study. He had given useful criticism and assistance during all stages of this study. It was a great honor working with him.

In addition, I would like to address special thanks to the Department of Petroleum and Natural Gas Engineering at the Istanbul Technical University for motivating me during the study. The greatest thanks go to TUBITAK (The Scientific and Technological Research Council of Turkey) and Turkish Petroleum Corporation (TPC), to provide financial support and infrastructural facilities for this study.

Finally but yet importantly, I would like to say my grateful thanks to my family for their support and patience for motivating me during this study.

January 2016

Ali ETTEHADI
(MSc in Petroleum and Natural Gas Engineering)

TABLE OF CONTENTS

Page

ABBREVIATIONS

API : American Petroleum Institute
AAPE : Average absolute percentage error
BC : Boundary condition
BP : Bingham Plastic
CFD : Computational fluid dynamics
CFL : Chrome free lignosulfonate
CMC : Carboxymethyl cellulose
DGD : Dual Gradient Drilling
DPM : Discrete phase model
ECD : Equivalent circulation density
FPL : Frictional pressure loss
FF : Formation fracture pressure
FP : Formation pressure
GS : Gel strength
HB : Herschel Bulkley
HTHP : High temperature high pressure
LPC : Lignit/Polymer reaction complex
MSE : Mean square error
MPD : Managed pressure drilling
MTA : Mineral Research and Exploration
PV : Plastic viscosity
PAC-LV : Polyanionic cellulose-low viscosity
PL : Power Law
RMSE : Root mean square error
SPP : Stand pipe presure
SST : Total sum of squares
SSR : Sum of squares of the regression
SSE : Residual sum of squares
TP : Turkish Petroleum
TSPD : Thermally stable polymetric deflocculant
XCD : Xantham gum
YP : Yield point
YPL : Yield power law

NOMENCLATURE

$\boldsymbol{A}$: Area of slot geometry, m^2

$\boldsymbol{AV}$: Annular velocity, m/sec or ft/sec

$\boldsymbol{C_a}$: Herschel Bulkley model parameter, dimensionless

$\boldsymbol{C_c}$: Herschel Bulkley model parameter, dimensionless

$\boldsymbol{C_D}$: Drag coefficient, dimensionless

$\boldsymbol{d}$: Diameter of pipe, inch

$\boldsymbol{d_1}$**:** Inner diameter of pipe/annulus, inch

$\boldsymbol{d_2}$**:** Outer diameter of pipe/annulus, inch

$\mathbf{d_s}$ **:** Diameter of spherical particle, inch

$\boldsymbol{d_h}$: Hole diameter, inch

$\boldsymbol{d_p}$: Pipe diameter, inch

$\boldsymbol{\frac{dP_f}{dL}}$**:** Frictional pressure loss per unit length, kPa/m or psi/ft

$\boldsymbol{\frac{dv}{dy}}$: Shear rate, s^{-1}

$\boldsymbol{f}$: Fanning friction factor, dimensionless

$\boldsymbol{f_b}$: Bingham fluid modified friction factor, dimensionless

$\boldsymbol{f_s}$: Power Law fluid modified friction factor, dimensionless

$\boldsymbol{f_l}$: Laminar flow regime friction factor, dimensionless

$\boldsymbol{f_t}$: Turbulent flow regime friction factor, dimensionless

$\boldsymbol{F_T}$**:** Cutting transport ratio, dimensionless

GS: Gel strength, Pa or lbf/100 ft^2

$\boldsymbol{h}$: Thickness of slot (annular clearance), m

$\boldsymbol{I_{cc}}$: Carrying capacity index, dimensionless

$\boldsymbol{K}$: Consistency index, Pa-s^n or eq cp

$\boldsymbol{\overline{K}}$: Mud clinging constant, dimensionless

$\boldsymbol{K_{sc}}$: Sticking coefficient, dimensionless

$\boldsymbol{L}$: Measured length, m

$\boldsymbol{n}$**:** Flow-behavior index, dimensionless

$\boldsymbol{N_{Re}}$ **:** Reynolds number

PV: Plastic viscosity, Pa-s or eq cp

$\boldsymbol{q}$: Flow rate of drilling fluid

$\boldsymbol{q_{plug}}$: Flow rate in plug region

$\boldsymbol{R}$: Inside drillpipe radius, m

$\boldsymbol{Re}$: Reynolds number, dimensionless

$\boldsymbol{R_1}$: Inner radius of annulus, m

$\boldsymbol{R_2}$: Outer radius of annulus, m

$\boldsymbol{r_1}$: Inner radius of slot, m

$\boldsymbol{r_2}$: Outer radius of slot, m

$\boldsymbol{R_{em}}$: Reynold number during tripping, dimensionless

$\boldsymbol{Re_{eq}}$: Equivalent Reynolds number, dimensionless

$\boldsymbol{Re_{eqcr}}$: Critical equivalent Reynolds number, dimensionless

$\boldsymbol{S}$: Plasticity, dimensionless

$\boldsymbol{V}$: Velocity of drilling fluid, ft/s

$\boldsymbol{V_{sl}}$**:** slip velocity, m/sec or ft/sec

$\boldsymbol{V_a}$**:** Mean annular velocity, m/sec or ft/sec

$\boldsymbol{V_T}$**:** Transport velocity, m/sec or ft/sec

$\boldsymbol{V_{sl}}$**:** Slip velocity, m/sec or ft/sec

$\boldsymbol{V_p}$: Pipe velocity, m/sec or ft/sec

$\boldsymbol{\overline{v}_{ae}}$: Effective mean velocity, ft/min or m/sec

$\boldsymbol{\overline{v}}$: Velocity due to mud displacement, m/sec or ft/sec

$\boldsymbol{W}$: Slot width, m

YP: Yield point, Pa or lbf/100 ft^2

$\boldsymbol{y}$: Herschel Bulkley model parameter, dimensionless

$\boldsymbol{z}$: Herschel Bulkley model parameter, dimensionless

Greek Letters

$\boldsymbol{\rho}$: Density of drilling fluid, pound per gallon, kg/m^3 or lbm/gal

$\boldsymbol{\tau_y}$**:** Yield point, Pa or lbf/100 ft^2

$\boldsymbol{\mu}$ **:** Viscosity, Pa-s or eq-cp

$\boldsymbol{\rho_f}$ **:** Density of fluid, kg/m^3 or lbm/gal

$\boldsymbol{\rho_s}$ **:** Density of particle, kg/m^3 or lbm/gal

$\boldsymbol{\mu_a}$ **:** Apparent viscosity, Pa-s or eq cp

$\boldsymbol{\theta_{600}}$: Dial reading of viscometer at 600 rpm, Pa

$\boldsymbol{\theta_{300}}$: Dial reading of viscometer at 300 rpm, Pa

γ_{300}: Shear rate at the rotor speed of 300 rpm, s^{-1}

τ: Shear stress, Pa or lbf/100 ft^2

α: Ratio of pipe diameter to hole diameter, dimensionless

$\bar{\gamma}$: Conductance number, dimensionless

λ: Coefficient of pick point distance in slot geometry, dimensionless

λ_1: Coefficient of lower limit of plug region, dimensionless

λ_2: Coefficient of upper limit of plug region, dimensionless

μ_{eff}: Effective viscosity, Pa-s or eq cp

LIST OF TABLES

Page

LIST OF FIGURES

Page

MODELLING WELLBORE HYDRAULICS THROUGH THERMAL RHEOLOGICAL SEPIOLITE MUD PROPERTIES

SUMMARY

Design of wellbore hydraulics has the fundamental contribution during drilling operations. An optimized hydraulic strategy can lead to minimize drilling time and cost. Accurate prediction of pressure distributions through the wellbore is one of the important focus points of drilling operators. Selecting an appropriate drilling fluid also plays a vigorous role in terms of reducing pressure losses. The thermal rheological behavior of selected drilling fluid should be taken into account to provide efficient hydraulic optimization.

Through this study, sepiolite drilling fluid as a thermal stable fluid system, was selected and evaluated in terms of modelling wellbore hydraulics using a new semi-analytical method and validated with experimental data, analytical methods, and Computational Fluid Dynamics (CFD). Thermal rheological properties of unweighted and barite-weighted fresh water sepiolite base muds as well as salt saturated sepiolite muds were extensively investigated using both conventional viscometer and HTHP rheometer. Rheological parameter analysis was performed to determine the best rheological fit model at elevated temperatures. Other thermal properties such as filtration, lubricity, differential pressure sticking tendency of mud samples were also studied at extreme conditions to achieve complete evaluation of thermal behavior of sepiolite drilling fluids. Parameters derived from rheological properties were used to analyze comprehensive hydraulic optimization involving estimation of surge and/or swab pressures caused by pipe movement as well as frictional pressure losses caused by mud circulation for the sepiolite muds using the new derived semi-analytical model and CFD approach based on three well-known rheological models. In addition, hole cleaning ability of sepiolite muds as another part of wellbore hydraulic design were evaluated using an existing empirical method and CFD.

The comparative study on thermal rheological properties of sepiolite muds resulted in substantial differences between the results obtained from conventional viscometer and thermal HTHP rheometer. These differences in rheological measurement using rheometer and conventional viscometer were stretched out with increasing temperature. Therefore, any hydraulic optimization based on conventional viscometer rheological measurements conducted after thermal aging and cooling of mud samples might lead to noticeable errors. This situation causes misleading through drilling program, particularly in calculating surge pressures caused by drillstring movement.

Findings of this study proved the successful laboratory application of sepiolite base muds as highly tolerable to hostile drilling conditions particularly at high temperature. Investigated and introduced of different sepiolite mud types put forward the efficient properties of this mud that could be a good alternative for drilling in harsh conditions. On the other hand, extensive experimental and theoretical work details almost all

required sepiolite mud characteristics helping industry to be more familiar with properties of this mud.

SONDAJ KUYUSU HİDROLİĞİNİN SEPİYOLİT ÇAMURU ISIL REOLOJİK ÖZELLİKLERİYLE MODELLENMESİ

ÖZET

Gün geçtikçe, sondaj teknolojisi ve yöntemlerindeki ilerlemeye rağmen, zorlu ortam koşullardan dolayı ortaya çıkan problemlerin anlaşılması ve çözümleri daha da karmaşık ve güç hale gelmektedir. Bu karmaşıklığı tetikleyerek daha da zor hale sürükleyen bazı faktörler dönüşü olmayan sonuçlara neden olabilmektedir. Bu durumlardan önemli olan bazıları derin sondaj operasyonlarında ortaya çıkan yüksek sıcaklık, yüksek basınç ve derin denizaltı bölgelerinde arama ve hidrokarbon üretiminin maliyetini artıran kuyu stabilitesi problemleridir. Bundan dolayı, derinlikle formasyon basıncı ve formasyon çatlatma basınç değişimi hakkında doğru bilgilere sahip olmak, özellikle yukarıdaki söz konusu zorlu ortamlarda kuyu planlama açısından çok önemli ve kritik hale gelmektedir. Örneğin, formasyon basıncının ve formasyon çatlatma basıncının arasındaki farkın özellikle açık deniz sondajlarında artan su derinliğine bağlı olarak azalması beklenen bir durumdur ve kuyu stabilitesi sorunlarının artmasına ve kontrol edememesine neden olmaktadır. Bu durum, dizi manevrası sırasında veya matkap değişimi sırasında kuyu ve sondaj güvenliğini riske atmaktadır. Petrol ve doğal gaz endüstrisinde formasyon basıncı ve formasyon çatlatma basıncı arasındaki farkın yapay bir şekilde arttırılması için uzun zamandan beri araştırmalar yapılmaktadır. Günümüzde, bu problemin araştırılması bilim insanları için önemli konulardan biri olmakla birlikte, konuyla ilgili petrol ve doğal gaz endüstrisi tarafından kısmi olarak kabul edilen birkaç yöntem vardır. Bu yöntemlerden en yaygın olan ikili gradyen sondaj (Dual Gradient Drilling) tekniğidir. Bu yöntem anülüsteki basınç değişimini belirlemek ve izlemek için anülüsün seçilen bölümlerinde birden fazla basınç gradyeni oluşturulması olarak tanımlanmaktadırlar. Ancak, bu tekniklerin uygulaması örneğin dizi değişimi sırasında ağırlaştırılmış sondaj çamuru ve düşük yoğunluklu malzemeler arasında faz ayrışmasına (separation) ve tabakalaşmaya (stratification) yol açabilmektedir. Kabul edilmiş ve yaygın olarak kullanılan bir yöntem yoktur ve konu üzerinde bilimsel çalışmalar devam etmektedir.

Sondaj mühendisliğinde iyi bilinen bir gerçek olarak ve API standardına göre, su bazlı çamurlar için, akma noktasının plastik viskoziteye oranının minimize edilmesi yukarıda bahsedilen problem için kısmi bir çözüm yolu olabilmektedir. Bu nedenle, sondaj çamuru özelliklerinin iyi bilinmesi sondaj operasyonu sırasında oluşan basınç değişikliklerini incelemek ve kontrol etmek açısından önemli bir parametredir.

Günümüzde, ileri teknoloji ve iyi mühendislik yöntemleri esas olan zorlu sondaj ortamlarında, özellikle güvenli sondaj bölgesinin dar olduğu (formasyon basıncının formasyon çatlatma basıncına yakın olduğu bölgeler) derin deniz kuyularında, sondaj operasyonları devam etmektedir. Böylesi dar ve hassas aralıkta sondaj yapmak eşdeğer sirkülasyon yoğunluğunun doğru hesaplanmasını zorunlu kılmaktadır. Buna ek olarak, sondaj operasyonlarında tüketilen güç maliyeti yüksektir ve bunun en aza indirilmesi de gerekmektedir. Sondaj kuyusunun içinde oluşan basınç değişiklikleri

hakkında olgusal ve daha sağlam bilgilere sahip olmak herhangi bir işleme başlamadan önce operatörlerin bir adım önde olmasını sağlayabilir. Kuyu içi akışkan hareketinden dolayı oluşan basınç dalgalanmaları ikiye ayrılmaktadır. Kuyu içindeki akışkanın sirkülasyonu nedeniyle hidrolik devrede ortaya çıkan sürtünme basınç değişimleri “Stand Pipe” basıncı olarak tanımlanmaktadır. Diğer yandan, dizi veya koruma borusu (casing) hareketinden dolayı oluşan basınç değişimlerine “surge” veya “swab (negatif surge)” basınçları denilmektedir. Manevra sırasında dizinin kuyu içine indirilmesinden doyalı oluşan basınç dalgalanması nedeniyle oluşan artışı surge basıncı adı verilmektedir. Buna karşılık, dizinin kuyudan yukarı doğru çekilmesinden dolayı oluşan basınç dalgalanması nedeniyle olan azalım swab basıncı olarak tanımlanmaktadır.

Günümüzde enerji kaynaklarına olan talep artışı nedeniyle petrol, gaz ve jeotermal kaynak arayışları önemini daha da arttırarak korumaktadır. Bu talep artışını karşılamak amacıyla daha önce araştırma yapılmamış yeraltı derinliklerinde ve su derinliğinin 3000 m’yi geçtiğini açık denizlerde yeni kaynak araştırmaları devam etmektedir. Sondaj operasyonları sırasında özellikle sirkülasyon sisteminden kaynaklanan maliyetler önemli bir yer tutmaktadır. Sondaj çamurunun toplam kuyu maliyeti üzerindeki payı yaklaşık %5 olmasına rağmen, özellikleri kontrol edilmezse kuyunun terkine varan milyonlarca dolarlık kayıplara neden olabilmektedir. Bu nedenle, oluşan maliyetlerin sondaj sırasında en aza indirilmesi için sondaj akışkanı özellikleri ile ilgili ve akışkanın hareketinden dolayı oluşan sürtünme basınç kayıpları hakkında iyi bilgilenme gereksinimi kaçınılmaz bir gerçektir. Böylesi bir amaca ulaşmak için şirketlerin çabalarının büyük bir kısmı hidrolik çözümlerini optimize etmek için yoğunlaşması zorunlu hale gelmektedir. Dolayısıyla, sondaj sektöründe kuyu içi hidrolik tasarımı önemli bir yer tutmaktadır. Diğer bir ifade ile sondaj operasyonunun hemen hemen her aşaması bir akışkanın hareketini içermesi nedeniyle, sıvının basınç kayıpları ile ilişkili hidrolik optimizasyonunu iyi tasarlamak için akışkanın kuyu içinde davranışın ve özelliklerindeki değişimin araştırılması gerekmektedir.

Manevra sırasında dizi hareketinden, sirkülasyon sırasında yüksek sirkülasyon debilerinde ve koruma borusunun kuyu içine indirilmesi sırasında oluşan sorunlar özellikle güvenli sondaj çamur yoğunluğu aralığının dar olduğu bölgelerde daha da önemli olmaktadır. Dizi veya koruma borusunun kuyuya yüksek hızla indirilmesi sırasında kuyu içinde yüksek “surge” basıncı oluşmaktadır. Bu basınç artışı, en kötü koşul olarak, formasyon çatlatma basınç limitini aşarak delinen formasyonda çatlak meydana getirilmesine ve kayıp sirkülasyon olarak adlandırılan yoğun çamur kaçaklarına yol açabilmektedir. Tersi durumda, “swab” basıncından dolayı kuyu içi basıncı formasyon basıncının oldukça altına düşerek formasyondaki bulunan akışkanın kuyu içine akmasına ve diğer bir ifade ile kuyunun canlanmasına (kick) sebep olmaktadır. Dolayısıyla, surge ve swab basınçlarının doğru bir şekilde tahmin edilmesi maksimum dizi hızını kuyu içi basıncının gözenek ve formasyon basınç limitleri arasında sağlanarak belirlenmesi açısından son derece önemli ve kritiktir. Ayrıca bu basınçların doğru bilinmesi dar anülüs açıklıkları içinde koruma borularının indirilmesi sırasında da aktif bir rol oynamaktadır. Diğer yandan, kuyu içi basınç dalgalanmasının değişimi doğrudan çamurun akma noktası ve jel kuvvetinden etkilenmesinden dolayı seçilen çamurun reolojik özellikleri iyi bir şekilde incelenip kontrol altına alınmalıdır. Yüksek sıcaklık ve yüksek tuzluluk gibi zorlu sondaj koşulları, çamurun reolojik özelliklerini etkilediği için çamur stabilitesini bu koşullarda korumak sondaj mühendisinin önemli sorumlulukları arasındadır. Yüksek sıcaklık çamur sisteminin flokülasyonuna yol açarak kabul edilmeyecek değerlerde akma noktası ve jel kuvvetlerine sebep olmaktadır. Bu nedenle, böyle bir çamurun kuyuda dolaşımı sirkülasyon ve manevra sırasında yüksek sürtünme basınç kayıplarına neden olarak kuyu stabilitesi sorunlarını, sondaj süresini ve maliyetini arttırmaktadır.

Bentonit kilini içeren sondaj çamurları genellikle sahalarda ucuz olmaları nedeniyle tercih edilmektedir. Ancak, yaygın olarak kullanılan bentonit kili ile hazırlanan katkılı sondaj çamurları sıcaklığın 150^{o}C ve tuzluluğun 35000 ppm'i geçtiği zorlu sondaj ortamlarında görev yapamaması nedeniyle varil maliyeti 100 ABD Dolarını geçen sentetik çamurların kullanılmasını zorunlu kılmaktadır. Bu çamurlara alternatif olarak sepiyolit bazlı çamurların kullanılabilirliği daha önce gerçekleştirilen bir çalışmada ortaya konulmuştur, (A. E. Osgouei, 2010). Bu çalışma kapsamında formüle edilen sepiyolit bazlı sondaj çamurlarının su kaybı özelliğinin yüksek sıcaklık ve tuzluluk koşullarında kontrol altına alınabildiği deneysel olarak gösterilmiştir. Fakat sepiyolit çamurlarının sondaj akışkanı olarak görevlerini yerine getirebilmesi ve sektörde etkin kullanıma sunulması amacıyla sepiyolit çamurunun kuyu koşullarında (yüksek sıcaklık ve yüksek basınç) reolojik özelliklerinin incelenmesi gerekmektedir. Bilgisayar kontrollü "Rheometer Model 50 SL High Temperature" adlı yüksek sıcaklık reometresinin kullanılması ile sondaj akışkanının reolojik özelliklerinin kuyu şartlarında (in-situ) belirlenmesi bu doktora çalışmasının amaçlarından birisidir. Genel olarak yaygın ve klasik bir yöntem olan yaşlandırma hücresi kullanılarak çamurların reolojik özellikleri belirlenmektedir. Klasik yöntemde istenen sıcaklık altında yaşlandırma hücresinde (aging cell) şartlandırılmış örneklerin soğutulmalarından sonra viskometre kullanılarak reolojik özellikler belirlenmektedir. Literatürde her iki yöntem arasında çamur türüne bağlı olarak önemli farkların olabildiği ve reometre ile belirlenen reolojik özelliklerin sondaj kuyusu koşullarını daha doğru canlandırdığı bildirilmektedir. Bu çalışmanın diğer bir önemi ise her iki yöntem ile reolojik özellikler belirlenerek iki yöntem arasındaki farklılık sepiyolit çamurları üzerinde incelenmiştir. Ayrıca bu çalışma kapsamında sepiyolit çamurları için elde edilen deneysel sonuçlar kullanılarak örnek bir kuyuda oluşan sürtünme basınç kayıpları ve bu çamurların kesinti taşıma yeteneği ampirik yöntemin yanı sıra sayısal yöntem (CFD analizi) ile de hesaplanarak modellenmiştir. Dolayısıyla bu çalışma deneysel ve teorik olarak iki fazdan oluşmaktadır.

Çalışmanın birinci fazında sepiyolit çamurlarının ısıl etki altında özellikleri kapsamlı bir şekilde incelenmiştir. Sepiyolit çamurlarının ısıl reolojik özellikleri yukarıda bahsedilen her iki yöntemle araştırılmıştır. Yaşlandırma (aging) deneyinden elde edilen sonuçlar (statik koşul) ile kuyu koşullarını simüle edebilen reometreden elde edilen sonuçlar (dinamik koşul) karşılaştırılmıştır. Ayrıca sepiyolit temelli sondaj akışkanının yüksek sıcaklık ve yüksek tuzluluk içeren ortamlarda etkin bir reoloji sağlayabildiği gösterilmiştir. Sondaj akışkanlarının sadece reolojik ve su kaybı özelliklerinin uygun olması sahada kullanılabilecekleri anlamına gelmez. Bu özelliklerin yanı sıra yağlama ve dizi sıkışmasına neden olmaması da istenen özellikler arasındadır. Bu çalışmada, sepiyolit çamurlarının yağlama özelliği ve dizi sıkışmasına neden olup olmayacakları da deneysel olarak incelenmiştir.

Çalışmanın ikinci fazında kuyu içinde dizi hareketinden dolayı oluşan basınç dalgalanmalarına doğru bir şekilde tahmin edebilme amacıyla bir yarı-analitik yöntem geliştirilmiş ve bu yöntemin doğruluğu literatürde bulunan deneysel veriler ve deneye dayalı iki ampirik yöntemle (Burkhardt ve Schuh model) teyit edilmiştir. Gerçek kuyu koşullarını canlandırabilen reometre ile elde edilen sonuçlar çalışmanın ikinci fazında kullanılarak ve örnek bir kuyu geometrisi için hidrolik hesaplamalar yapılarak, kuyu içi hidrostatik basıncın ve sürtünme basınç kayıplarının nasıl değişebileceği hem analitik (Bingham Plastic, Power law ve Yield Power Law modeller), hem de geliştirilen yarı-analitik yöntem ile ve ayrıca CFD analizi kullanılarak gösterilmiştir. Diğer taraftan, sepiyolit çamurlarının kesinti taşıma yeteneği iki farklı yöntem ile karşılaştırmalı olarak yapılmıştır. Bu yöntemlerden birisi ampirik yöntem (Moore korelasyonu) olup çamurların "kesinti taşıma indeksi" olarak adlandırılan terim ile ifade edilmektedir. Kesinti taşıma yeteneğini belirlemek için ikinci bir yöntem olarak hesaplamalı akışkanlar dinamiği (CFD) yaklaşımı kullanılmış ve hesaplamalar İTÜ bünyesinde akademik ve araştırma kullanımına açık olan Ansys Fluent yazılımı ile gerçekleştirilmiştir.

Bu araştırma çalışması sepiyolit çamurunun zorlu sondaj ortamlarında etkin çamur olduğunu göstermek için gerekli tüm özelliklerini inceleme amacıyla yapılan kapsamlı bir deneysel çalışmadır. Bu çalışmanın sonuçlarına göre sepiyolit bazlı çamurun özellikle zorlu sondaj koşullarında başarılı bir laboratuvar performansı gösterdiği kanıtlanmıştır. Bulgular klasik viskometre kullanılarak elde edilen örneklerin reoloji ölçümlerinin gerçek sıcaklıktaki değerlerden farklı olduğunu göstermiştir. Reometre ve klasik viskometre kullanılarak belirlenen viskozitelerdeki farklılık genel olarak artan sıcaklık ile daha da artmaktadır. Bu nedenle, ısıl işlem yapıldıktan sonra oda sıcaklığına soğutularak klasik viskometre ile elde edilen viskozite değerlerine göre yapılan hidrolik optimizasyonda dikkate değer hatalara yol açabilecek, böylece kuyu sondaj programlarından sapmalara, kuyu stabilitesi ve kuyu kontrolü sorunlarına, sondaj zamanının ve maliyetinin artmasına sebep olabilecektir.

1 INTRODUCTION

Day to day, in conjunction with technological advancement in drilling operations, problems encountered due to hostile conditions become more challenging and complicated. Some factors and conditions trigger this complexity to be more severe cause to reach to the point of no return. High temperature and pressure resulting from drilling in deeper formations, exploration in deep subsea regions, and wellbore stability problems making the oil and gas production costly are some of these important conditions. Therefore, accurate knowledge about the variation of formation pressure (FP) and formation fracture pressure (FF) with depth are so critical, especially in planning wells in aforementioned hostile environments. Formation Pressure (Pore Pressure) is defined as a pressure exerted by fluids within the pore spaces of the formation. The drill pipe gauge pressure plus the hydrostatic pressure of the drilling fluid equals the formation pressure. On the other hand, the pressure gradient at which the formation accepts whole fluid from the well bore is called formation fracture gradient. The leak-off pressure plus the hydrostatic pressure of the drilling fluid is the formation fracture pressure (API RP 59, 2006).

The most critical events may take place as the gap between FP and FF gets narrow with increasing depth of drilling and/or sea water coupled with hostile environment conditions. This situation puts drilling safety in jeopardy during trip process for the sake of switching drillstring or drill bit. It is long time that oil and gas industry has been searching a way to extend the gap between FP and FF artificially. To date, investigation about this problem is one of the major subjects of scientists, and there exists a few methods that are partially accepted by the oil and gas industry. The most common one is called Dual Gradient Drilling (DGD) techniques that are defined as intentionally creation of multiple pressure gradients within selected sections of the annulus to manage the annular pressure profile. Techniques to achieve a dual gradient include injecting a lower-density fluid through a parasite casing string in a land well or through the marine riser when operating subsea, or actively pumping return fluids from the seafloor through lines external to a seawater-filled riser. These techniques suffer from the unavoidable and very inconvenient separation and stratification of the heavy drilling mud and lighter injected components once pumping is interrupted, e.g., when making a drill-string connection.

As a well-known fact in drilling engineering and according to the American Petroleum Institute (API) standard, minimizing the ratio of yield point (YP) to plastic viscosity (PV) could be a partial solution of the above-mentioned problem for water base muds. Therefore, a good knowledge of drilling mud properties is an essential factor to provide efficient wellbore hydraulic optimization.

1.1 Problem Statement

Drilling engineers open holes in harsh environments where advanced technology and good engineering methods are a must, particularly in deep water offshore wells where safe mud weight windows are reported to be approximately zero. Such a low mud weight margin dictates calculating accurate equivalent circulation density (ECD) even for managed pressure drilling (MPD) operations. In addition, cost of power consumed in drilling operations is quite high and aimed to be minimized. Having factual and more solid information about surge pressure changes through wellbore could have a strong contribution on knowledge of operators making them one step ahead before employing any operation. Wellbore pressure changes caused by fluid flow can be classified in two ways. The first is frictional pressure changes caused by fluid circulation in a hydraulic circuit that is known as stand pipe pressure. The second one is the pressure variations produced by drillstring movement or running casing string that is called surge or swab (negative surge) pressures.

Today oil and gas companies are planning to drill wells in offshore arctic regions with depths reaching to 15240 meters (50,000 ft). Circulation of drilling fluid from surface to bottom hole creates pressure drops through different parts of drilling equipment and borehole. Minimizing cost of drilling operation leads to study of mud properties and related frictional pressure losses. To reach such goal, the companies are imposed to intensify most of their efforts to optimize hydraulics. Basically in the drilling industry, the circulation hydraulic takes important place. Almost every phase of drilling engineering involves the movement of the fluid such as muds, cuttings and gases through the pipes and fittings. Therefore, good hydraulic optimization associated with pressure losses of the fluid mandates an accurate knowledge of the fluid behavior in a circulation system. In the course of tripping in/out pipe, circulating the mud with high rates, and running close-end casing string into the wellbore, the encountered operational difficulties get accelerated and become more complex and problematic, particularly in deep and narrow hole (slim hole) drilling. If a casing string or drillstring is lowered in the well, the pressure at a given point in the well increases. This pressure increment is known to be surge pressure. In contrary, upward movement of pipe or casing string causing a decrement in the pressure at wellbore is named as swab pressure or negative surge. Running the pipe or casing into the wellbore with high velocities generate high surge pressures. As a worse condition, drilled formations are fractured and results in lost circulation if the fracture gradient limit is exceeded. Conversely, if the pressure in the well sourcing from the swab pressure falls below the formation pore pressure, flowing of formation fluid into the well would be unavoidable, and the well gets kick. Therefore, accurate predictions of surge and swab pressures are extremely critical in terms of estimating the maximum safe tripping speeds to keep the wellbore hydraulics within the limits of pore and fracture pressures. It also plays an active role in running casings where narrow annular clearances are encountered.

On the other hand, rheological properties of any fluid system must be in the focus point of view because the rate of induced surge pressure in a wellbore are directly influenced by the yield point and gel strength of drilling mud being circulated. Hostile conditions such as high temperature and high salinity affect the rheological properties of fluid system; and hence, special attention must be paid to maintain mud stability. High temperature might lead to mud flocculation and generate excessive yield point and gel strength. Therefore, using such fluid in drilling causes high pressure drops that indicates higher equivalent circulation density. As a result, an efficient mud providing acceptable thermal stability and a model predicting better drilling hydraulics are required particularly in hostile drilling environments.

1.2 Hypothesis

Annular pressure drops cannot be underestimated and become a significant factor with increasing circulation flow rates. A more accurate pressure loss calculation and prediction is mandatory, especially at depths where margin between pore pressure and fracture pressure is low. Consequently, calculations of precise frictional pressure losses (FPL) to realize better stand pipe pressures (SPP) and effective optimization of drilling hydraulics become an extremely crucial issue. Therefore, more accurate FPL predictive methods are required in advance to develop efficient strategy for experimentally expensive and unpredictable oil and gas wells drilling.

Presented in this study is to estimate, model, and verify pressure surges caused by drillstring movement or tripping in a well with the consideration of thermal rheological properties of drilling fluid. The estimation approach is based on deriving new semi-analytical expressions for Herschel Bulkley (or known as Yield Power Law) non-Newtonian fluid. The modelling approach is based on calculating surge pressures using both a new proposed semi-analytical method and Computational Fluid Dynamics (CFD) method. The verification approach is based on obtaining numerical results from the new semi-analytical model and comparing them with the results from experimental data (Crespo, et al, 2011), existing other methods (Burkhardt and Schuh models), and CFD method. A special emphasis will be given to in-situ rheological properties of sepiolite muds to analyze the temperature effect on surge pressures. Therefore, the hypothesis of this study consists of two phases.

In the first phase, sepiolite mud is proposed as an alternate fluid to prevent or minimize mud stability related problems by considering the thermal rheological properties of this proposed mud. Comprehensive experimental investigation of sepiolite mud properties will be performed in details. Determination of in-situ rheological behavior, thermal filtration properties, thermal differential pressure sticking tendency, and lubricating quality of the proposed sepiolite mud would be the other major objectives through this study. The properties of other commonly used drilling muds (lignosulfonate and bentonite/polymer base muds) are also investigated to have better evaluation on pros and cons of the sepiolite fluid systems.

In the concept of second phase of this study, an exhaustive hydraulic optimization will be applied and modeled using CFD method as well as existing analytical-empirical methods in order to investigate hole cleaning ability and wellbore pressure distribution profile, prediction of surge/swab pressures resulting from drillstring or casing movement. A new semi-analytical solution will be developed and introduced to estimate wellbore pressure losses during circulation (stand pipe pressures) and tripping operations (surge and swab) for Power Law, Bingham Plastic, and Herschel Bulkley rheological models.

1.3 Sepiolite Base Muds: Proposed Mud to Minimize Drilling Problems

Nowadays, the significance of the exploration for oil, gas and geothermal resources keeps up due to increasing demand for energy resources. Search for new resources is continued to meet this demand in depths that have never been exploited before and offshore fields with a water depth of more than 3000 m. Drilling operations constitute the major part of the exploration costs. A fluid so-called drilling mud is used in drilling operations to (1) clean the rock fragments from the borehole and carry them to the surface, (2) exert hydrostatic pressure to prevent fluid influx from subsurface formations, (3) prevent the collapse of subsurface formations until casing string is set, (4) cool and lubricate the rotating drillstring and the bit, and (5) reduce the borehole frictional pressure losses. It is required to solve or control many technical problems caused by the search for new resources in the harsh drilling conditions known as high temperature, high pressure, and high salinity. Temperatures more than 150°C, salinity more than 35000 ppm and formation pressures more than 68948 kPa (10000 psi) are the basic foundation of hostile conditions. One of the key factors for drilling safe and economical wells in these environments depends on the drilling fluid or mud meeting the desired needs for hostile conditions. While constituting about 5% of the total drilling cost, the consequences might be catastrophic economical loss along with abandoning the well if the properties of drilling fluid are not controlled.

Drilling muds having bentonite clay are usually preferred due to their low cost. However, synthetic muds with a cost of more than 100 $/bbl have to be used since the drilling muds having bentonite and additives do not function well in hostile drilling environments. Alternative to these muds, the effective usage of muds having sepiolite clay in hostile environments has been experimentally proven by a joint venture project carried out by Turkish Petroleum Corporation (TPC) and Department of Petroleum and Natural Gas Engineering of Istanbul Technical University (ITU) with a title of "Controlling Rheological and Water Loss Properties of Sepiolite Base Drilling Muds at High Temperature and High Pressure" (Revolving fund project DS861, 2012). It has been demonstrated experimentally in the content of this project that the water loss properties of specially mixed sepiolite base drilling muds can be controlled under high temperature and salinity conditions. On the other hand, the rheological properties of sepiolite muds at the in-situ wellbore conditions (high temperature and high pressure) must be investigated in order to officiate as a drilling fluid and to bring it into use effectively by the sector.

Bought in 2009 and available in the laboratory of ITU Petroleum and Natural Gas Engineering, the usage of computer controlled high temperature rheometer named as “Rheometer Model 50 SL High Temperature” for determining the rheological properties of drilling fluids (under in-situ conditions) constitutes one of the main objectives of this study. The common and classical method for determining the thermal rheological properties using aging cell has also been achieved. In this classic method, the rheological properties of samples conditioned in a roller oven at the desired temperature and cooled afterwards to ambient conditions are determined by using a Couette type viscometer. It is stated in literature that some differences between the two methods are possible depending on the mud types. Also, the rheological properties obtained from a rheometer simulate the in-situ wellbore conditions better.

Another importance of this study is that the rheological properties of sepiolite mud will be determined first time ever from the both methods, and whether or not a difference will be examined by comparing the results. A possible difference yields more accurate wellbore hydraulic calculations; and hence, helps both safer and more economic drilling by providing better effective wellbore stability. Moreover, investigation of hydraulics and flow characteristics of sepiolite muds in terms of cutting transport and frictional pressure drops in a sample well will be determined using numerical application through well-known software, Ansys Fluent. In addition, lubrication quality properties of sepiolite muds on drillstring and bit using an apparatus named “Lubricity Tester” and differential pressure sticking properties of sepiolite mud in a borehole using an apparatus named “Differential Sticking Tester” will be investigated too.

It has been established within the scope of various projects carried out by Institute of Mineral Research and Exploration (MTA) that the world largest sepiolite deposits after Spain are in Turkey. On behalf of our nation having the world largest sepiolite deposits (Balcı 1999, Öztürk ve Kavak 2004), substantial economic opportunities might be created by the usage of sepiolite clay in the drilling industry. Unlike bentonite and attapulgite, API standards related to sepiolite are not well defined. Another objective of this work is to make contribution for providing standards and to introduce new definitions by determining the general properties of sepiolite muds under high temperature and salinity conditions.

1.4 Modelling Drilling Hydraulics: Stand Pipe (SPP) and Surge/Swab Pressures

Pressure drop, as known, occurs owing to friction between the fluid and the contacting surface during fluid circulation in a well. The total pressure drop that takes places in consequence of this event is called stand pipe pressure (SPP). Accurate prediction of the SPP for non-Newtonian drilling fluid throughout a hydraulic circuit of a well, from surface to bottom inside stand pipe, rotary hose, kelly, drill pipe, drill collar and drill bit and then bottom to surface in annular section is a significant factor to determine optimum jet bit nozzle sizes and control pump rates to achieve better hole cleaning with a minimum cost. Improper estimation of pressure drop may lead to major drilling problems, such as stuck pipe, kicks, loss circulation, and inadequate rig power selection during drilling. In this study, CFD technique will be applied to determine SPP through the usage of sepiolite drilling fluid properties. The effect of temperature on SPP will be investigated to get the better insight about this event that is not available through traditional calculation methods. In addition, non-Newtonian fluids behavior such as Bingham Plastic, Power Law, and Herschel Bulkley are considered to provide a comprehensive comparison during modelling.

The investigation of pressure surges in a wellbore, (second phase) is planned to carry out by two different approaches. The first one defined in the literature is given as a semi analytical solution to calculate surge pressure for yield power law (YPL) drilling fluids (Crespo et.al, 2012). This method presents a steady-state theoretical model which is based on a dimensionless correlation to predict surge and swab pressures for YPL fluids. An analytical solution for steady-state laminar flow in narrow slot geometry was developed to approximate and model the flow in a concentric annulus with inner pipe's axial movement. The semi-analytical solution involves in solving a system of non-linear equations by the assumption of constant frictional pressure loss gradient perpendicular to flow direction. Accurate predictions were presented as a family of curves, though not in convenient forms. Thus, a numerical scheme has been developed to solve the system of non-linear equations. However, it is difficult to follow the derivations and understand the notation used in their study.

This dissertation involves above-mentioned method in a different dimensional notation to make it better understandable. This semi-analytical solution will be assigned for Bingham plastic, Power Law and Herschel Bulkley rheological models. In order to have a comprehensive understanding about accuracy of predicted results using semi-analytical method, it is aimed to make a comparison between obtained results and other approaches such as Burkhardt and Schuh models validated for Bingham Plastic and Power Law rheological models, respectively. The validity of semi-analytical results for Herschel Bulkley model will be investigated by comparing the obtaining results with experimental outcomes available in literature. In addition, the semi-analytical model derived in this dissertation has another advantage of applying it to determine not only surge and swab pressures caused by tripping but also stand pipe pressures caused by circulation of drilling fluid.

1.5 Significance and Common Impact of the Study

Through this study, an attempt is made to bridge the gap between theoretical knowledge and field application of an effective mud employed on severe conditions especially in high temperatures. The results of this study can emphasize that sepiolite based muds could be good candidate for drilling in hostile environments such as deep water oil and gas wells, geothermal wells, and drilling through unstable shale formations causing borehole stability issues. In short, this study could contribute on introducing and developing sepiolite drilling fluid concept since a few studies have been previously reported in literature. On top of that, because field and laboratory applications are mostly based on bentonite or polymer base mud systems, results presented in this study can help industry to fill up their gap in terms of application of sepiolite as a major component of water base drilling fluid. Findings of this study are the result of two years ceaselessly effort and study through lots of repeated experiments providing a valuable contribution and comprehensive guideline for understanding the rheology and fluid loss behavior of sepiolite base drilling fluids.

Second phase of this study focuses on borehole hydraulics. Excessive surge and swab pressure caused by tripping operation and/or running casing string can lead to serious well problems. Decrease in hydrostatic head in the wellbore due to swabbing is a major source of blowouts. Swabbing can lead to invasion of formation fluid toward well annulus or in a technical terminology, getting a kick. Reversely, high surge pressure can lead to loss of mud either suddenly by fracturing the formation or slowly by continuous efflux to permeable formation. The drilling fluid enters the fractures and this produces a drop in fluid level, causing a decrease in the wellbore hydrostatic pressure. This can allow formation fluids to enter the wellbore and may lead to an underground blowout. Therefore, the need for calculating accurate surge pressures has been recognized as a big challenge.

The main hypothesis of this study is to investigate pressure surges in the wellbore through developing a semi-analytical model based on considering the usage of thermal rheological properties of a specially formulated (special mixing order) sepiolite mud systems. In addition, the thermal effect on frictional pressure losses resulting from fluid circulation were evaluated in details using the proposed semi-analytical approach based on rheological parameters estimated for sepiolite mud at elevated temperatures. The possibility of kick and lost circulation in tripping or running a casing string could be prevented by predicting the optimum safe trip velocities that might also results in saving in time and operational cost. Safe trip speeds depend on the margins between the formation pressure and formation fracturing pressure. Therefore, the correct determination of trip speeds allows drillers to use this margin to the maximum extent so that the drillstring can be moved faster without causing serious problem. In other words, faster pipe movements will reduce the drilling time and cost without sacrificing the safety. Brief glance in literature is enough to figure out the importance of pressure surges prediction. It has been emphasized that in most of rig time-analysis results, more than 19% of the time required to drill and complete a well was spent in tripping to change bits (Bourgoyne et. al., 1991). Note also that the amount of high cost for offshore drilling is more than one million dollars per day.

Application of CFD to confirm the analytical solution of pressure surges will be the exclusive aspect of this study to evaluate the effect of temperature. CFD analysis can provide valuable insight that helps engineers to understand what is physically happening when such above-mentioned events are faced prior to any stage of oil and gas well operations. The priority of CFD analysis on analytic and experimental examinations in prediction of oil and gas well events is the other concern of this study that might help petroleum engineers to become familiar with the wide range of CFD application in the oil and gas industry.

1.5.1 Computational fluid dynamics

Computational Fluid Dynamics (CFD) is a powerful way of modelling fluid flow, heat transfer, and related processes for a wide range of important scientific and engineering problems. Unlike experiments that are only permitting data to be extracted at a limited number of locations in the system (e.g. pressure and temperature probes, heat flux gauges, etc.), CFD allows the analyst to examine a large number of locations in the region of interest, and yields a comprehensive set of flow parameters for examination. Simply, CFD offers a strong way to simulate theoretically any physical condition.

Computational fluid dynamics constitutes a new approach in the scientific study and development of a whole discipline of fluid dynamics. It provides a cost effective means of simulating real flows by the numerical solution of the governing equations. The governing equations for Newtonian fluid dynamics, namely Navier-Stokes equations, have known for many years. However, the development of reduced forms of these equations is still an active area of research, in particular, the complex problems like turbulent flows. On top of that, there are less progress in developing non-Newtonian fluid dynamics, chemically reacting flows, and multi-phase flows.

Governing equations of the flow are extremely complicated such that analytic solutions have not been obtained for most practical applications. General approximate solutions to the Navier-Stokes equations must be obtained using numerical methods, this is where computational fluid dynamics (CFD) comes into play. Computational techniques replace the governing partial differential equations with systems of algebraic equations that are much easier to solve using computers. The steady improvement of computing power has led to the emergence of CFD. This branch of fluid dynamics complements experimental and theoretical fluid dynamics by providing alternative potentially cheaper means of testing fluid flow systems. It can also allow for the testing of conditions that are not possible or extremely difficult to measure experimentally and are not amenable to analytic solutions.

1.5.2 CFD in petroleum engineering

Utilization of the CFD has been extended broadly across all industries, and it has been used increasingly in the oil and gas industry. Increasing demand for energy resulted in the exploration more sources and subsequently expansion of drilling activities all over the world. Any improvement in terms of well planning, drilling and production operations can result in significant saving for the operators. Therefore, it is crucial to have an idea and to develop efficient strategy in the case of experimentally expensive and unpredictable oil and gas wells operations in advance. CFD has an important role in petroleum engineering applications such as studying optimization of bit performance, convective heat transfer between casings and annular fluids, flow in porous media like mud filtrate invasion, simulation of multi-phase flow for designing separators, cement displacement, erosion prediction, risk analysis during blowout event, optimization of drilling hydraulics and hole cleaning, wellbore stability analysis, cutting transport in wellbore and modelling flow through oil and gas wells.

It is an undeniable fact that the most of operations related to oil and gas extraction including exploration, drilling and production are very costly so that even a little miscalculation and inaccurate estimation might lead to lose a substantial investment of an operator company. On the other hand, time is a really significant parameter affecting feasibility of any process, especially in the cases that petroleum engineer is supposed to make a quick decision during operation. Some unforeseen problems might happen during drilling or production process while quick remediation is necessary to recover and apply related treatments. For instance, a petroleum engineer must adjust pump pressure and density of mud to avoid loss circulation or kick intrusion through drilling unknown formation having variable pore pressures. Introducing of successful strategy in the face of naturally fractured formation is another case that requires great knowledge about the mechanism of flow in such formations that can help engineer to put forward a logical approach against probable problems.

In addition, creating real and ideal condition of a physical process is experimentally hard to get essential engineering data for designing purpose. Modelling and investigation of the nature, and predicting the natural convection heat transfer coefficient in the annulus through the mud, which is hard to predict due to the large length-to-spacing ratio, might need to generate real condition that seems to be unreasonable in terms of time and cost. Frequently experienced such events, especially in petroleum industry, infer that the need for effective tools in order to estimate and model all these events before operation is an inevitable essential. Application of CFD to overcome oil and gas well's touchy problems is in parallel with this necessity because of being cost-effective, fast and ability to simulate real and ideal conditions.

This study uses CFD approach as a numerical solution for some aspect of wellbore hydraulic design. It was applied to simulate sepiolite mud as a non-Newtonian fluid flowing through a vertical pipe and annulus at different temperatures. The pressure and velocity distribution profiles were modeled through a commonly used part of drillstring interior and its corresponding annulus. The results were compared with existing analytical methods for three well-known non-Newtonian rheological models. In addition, the cutting transport event through wellbore was numerically simulated using CFD as another part of wellbore hydraulic optimization. Assuming being spherical, drilled cuttings are injected through a sample wellbore geometry and two-phase flow were modeled based on Discrete Phase Model (DPM). The result were also verified with an empirical model.

2. METHODS AND MATERIALS

2.1 Concept of Study

As described in the previous section, this study consist of two phases that each one includes different subtasks. To be clear, this study is a combination of theoretical, experimental, and simulation works to investigate thermal sepiolite mud properties exhaustively and to evaluate surge pressure related hydraulic optimization through this mud system by employing a new semi-analytical model. The schematic view given in Figure 2.1 pictures scope and steps of this dissertation that contains all part of experimental, theoretical, and simulation sections for achieving the hypothesis.

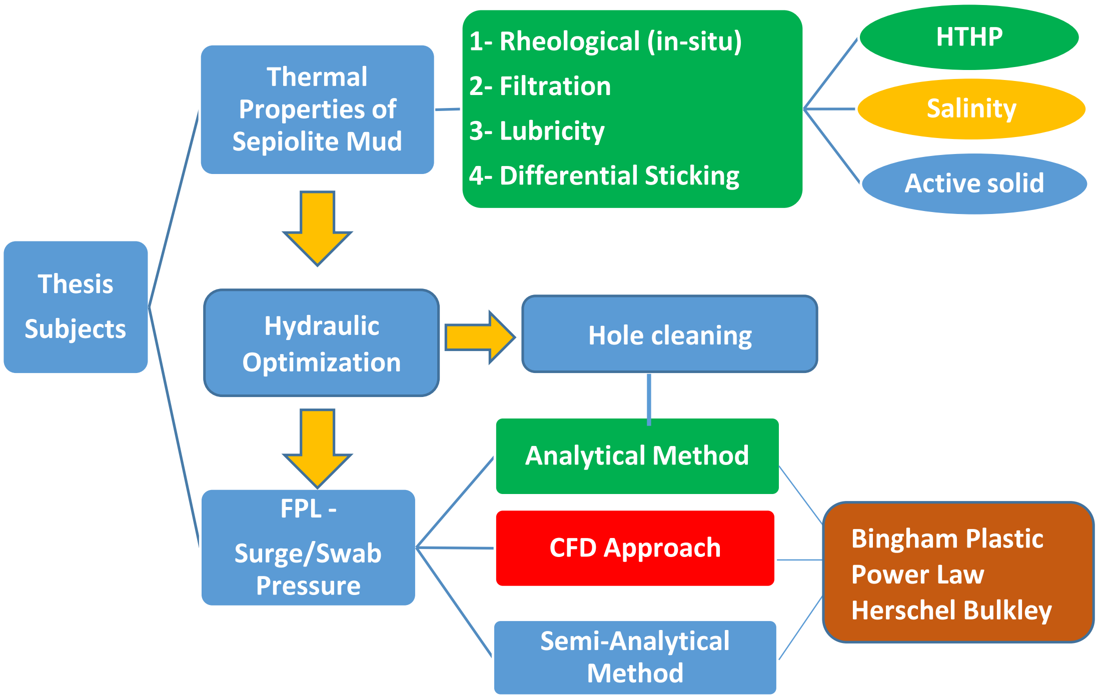

Figure 2.1: Schematically introduction for scope of study.

As seen in Figure 2.1, the first phase of study involves experimental investigation of thermal properties of sepiolite mud. In the concept of this phase, thermal effects on rheological and filtration properties, lubricity, and differential sticking tendency of sepiolite mud were studied under harsh drilling conditions such as HTHP, high salinity and active solid contamination. The experimentally obtained results were used to perform a complete wellbore hydraulic modelling including estimation of circulation pressure losses, surge and swab pressures, and hole cleaning ability of sepiolite mud at elevated temperatures. New developed semi-analytical method, CFD approach, and already existing analytical models were used through well-known three non-Newtonian rheological models to evaluate the hypothesis.

This dissertation consists of ten chapters. The first two chapters involve in general introduction and methods and materials used throughout the study. The following five chapters focus on comprehensive laboratory works to investigate thermal properties of sepiolite mud in details to get some properties using different methods, simulations, and experimental procedures. Chapter 3 explains the properties of active-clay contaminated sepiolite drilling muds at harsh drilling conditions. Thermal effects on differential pressure sticking tendency and lubricity of sepiolite fluid system are experimentally investigated through Chapters 4 and 6, respectively. Chapter 5 comprises the modelling and evaluating thermal in-situ rheological properties of seven types of sepiolite fluid systems.

The effect of high temperature and high pressure, salinity and active solid contamination on above mentioned sepiolite mud properties are the major concerns through experimental part of this study. A new semi-analytical solution proposed for steady state laminar flow is developed to predict accurate pressure surges for a non-Newtonian fluid through Chapter 7. The other two chapters use experimental data to perform a well-rounded optimization on wellbore hydraulics using semi-analytical, CFD and existing analytical/empirical methods. The study is terminated with the final chapter including culminated conclusions and recommendations for further research. The order in chapter presentations is based on subject's precedency so that the presentation of experimental phase of study was terminated with investigating thermal rheological properties of sepiolite muds to obtain rheological parameters used in the theoretical phase. The lubricity results of sepiolite muds was presented after Chapter 5 involving in-situ rheological measurement results to avoid repetition in listing mud compositions.

Since this study considers wide range of subjects such as extensive experimental work, developing new semi-analytical model, and simulation and verification, it is difficult to report literature review and methodology in a single chapter. Consequently, reporting the literature review and methodology were presented in the beginning of each chapter separately to accomplish for easy following and understanding. In this chapter, experimental equipment used throughout the study are introduced in details.

2.2 Preparation of Sepiolite Clay Samples

A raw sepiolite clay sample, a commercial product known as Turk Taciri Bej (TTB) produced near Sivrihisar-Eskisehir district of Turkey by AEM Company (AEM, 2014), was used in this experimental phase. Sepiolite clay rock samples was subjected to several physical grinding processes in the laboratory of Mineral Processing Engineering Department at ITU. First of all, sepiolite clay rocks have been crushed into smaller pieces (around 1 cm of diameter) using rock crusher equipment as shown in Figure 2.2.

Figure 2.2: Rock crusher equipment.

Then as shown in Figure 2.3, obtained 0.5 – 1 cm grain size clays were placed in a jar roller mill to make finer grain sizes. Jar Rolling Mill, electrically driven roller mechanisms for spinning or rotating milling jars, which were used for dry size reduction, or dispersing. The milling jar was half filled with grinding media or balls and as the mill rotates the solids were trapped between the ball and were milled down to as little as 1 micron by the cascading and tumbling action of the ball charge.

In the next step, grinded sepiolite clay samples were passed through the 300 mesh sieve. Clay samples remained above the sieve were retune to the grinding process again. Clay samples at the bottom of the sieve were entered into the segregation process using vacuum separator equipment to obtain desired grain size of clay.

Figure 2.3: Jar roller mill.

Vacuum separator equipment shown in Figure 2.4 was run at different working conditions that were consisted of the different fan speeds, separator speeds and feeding rate. Clay samples were taken back from three different outputs of this equipment. Coarse grain particles were taken from the Separator Output A. Fine grain particles were taken from the Output C, and very fine grain particles were taken from Output B. After each tests, grain size analysis of sepiolite clay samples was performed in Particulate and Ceramic Materials Characterization Laboratory of Metallurgical and Materials Engineering Department at ITU.

Results of desired sepiolite particle size analysis at the end of sixth tests conducted by vacuum separator equipment was determined and depicted in Figure 2.5 by volume percentage. Particle size analysis report was given in Appendix A. This report cited three values as the D10, D50, and D90. The D10, D50 and D90 are commonly used to represent the midpoint and range of the particle sizes of a given sample. Particle size distributions have been traditionally calculated based on sieve analysis results, creating an S-curve of cumulative mass retained against sieve mesh size, and calculating the intercepts for 10%, 50% and 90% mass. The D50, the median, is defined as the diameter where half of the population lies below this value. Similarly, 90 percent of the distribution lies below the D90, and 10 percent of the population lies below the D10. According to the results 10% of sepiolite particles were smaller than 7 micron (D10 = 7µm), 50% and 90% of them were smaller than 29 micron and 53 micron, respectively (D50 = 29µm and D90 = 53µm).

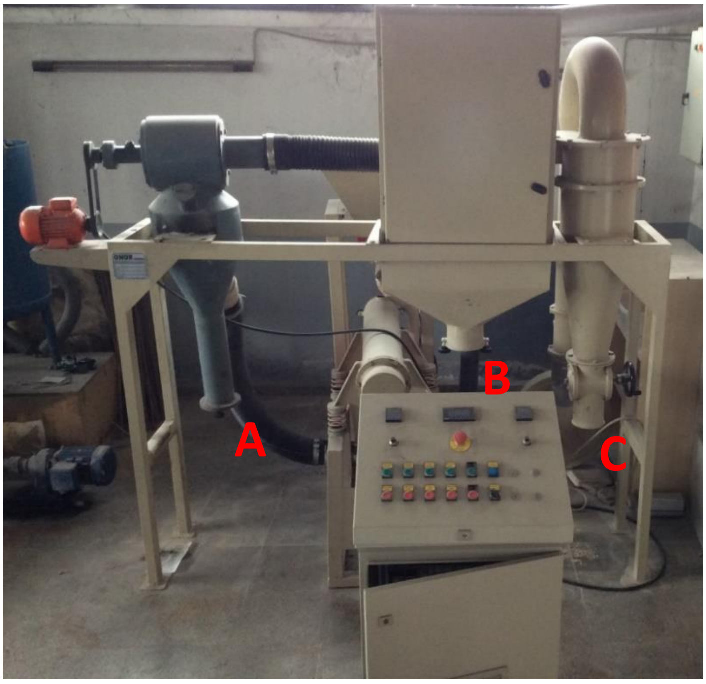

Figure 2.4: Vacuum separator equipment.

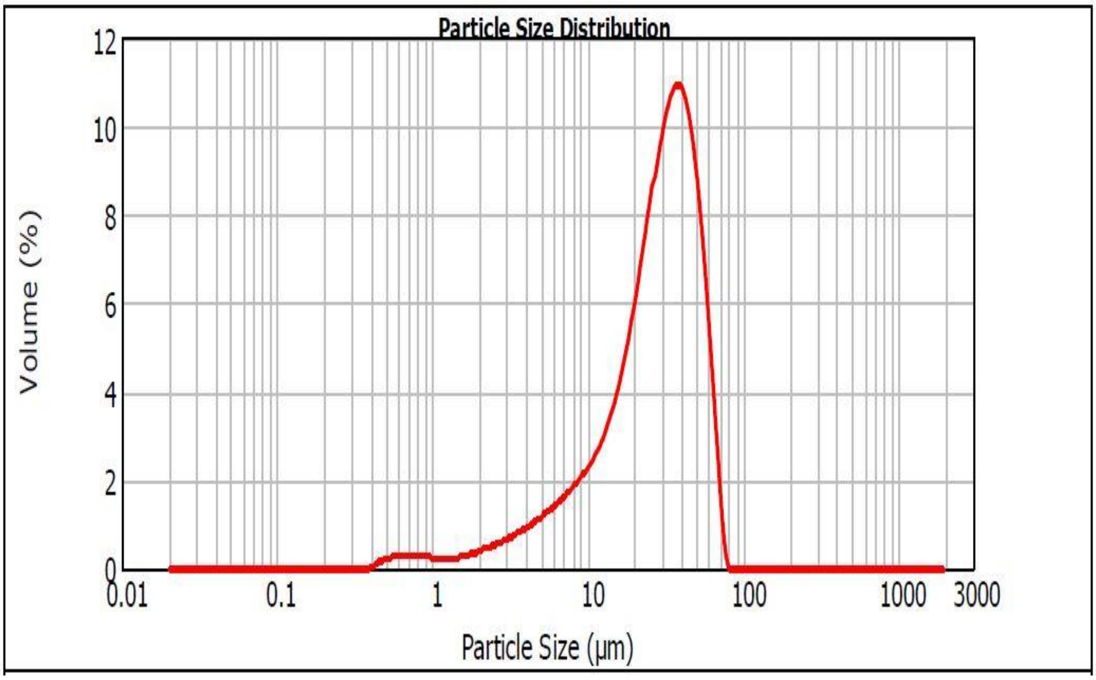

Figure 2.5: Fine grained sepiolite particle size distributions after sixth sieving test.

2.3 Chemical and Mineralogical Properties of Sepiolite Clay

The <62 µm (230 mesh) fraction was examined by X-ray Fluorescence Spectrometry (XRF) using a Spectro Xepos 3 model apparatus and analyzed with fusion method on Cu anode tube, running conditions of 0.9 mA, 40 kV at the research center of Turkish

Petroleum Corporation (Figure 2.6-pie shape distribution). X-ray powder diffraction pattern of the sepiolite sample was obtained on a Bruker D8 Advance model XRD with CuKα radiation (1.54178°A) running conditions of 40 mA, 40 kV, scan-speed of 0.005°, time/scan of 0.1 sec and 0.2 mm soller slit using LynxEye detector (Ni-filter) at Istanbul Technical University (Figure 2.6). The XRD analyses conducted at Geological Engineering Department of ITU indicate that the TTB sepiolite includes about 10% dolomite by weight and negligible gangue minerals. More information related to the calculation of dolomite content of sepiolite clay is given in Appendix A. Note also that the TTB sepiolite was not purified by any physical or chemical method.

The surface morphology of used sepiolite clay was investigated by the Scanning Electron Microscope (SEM) analysis using a Quanta FEG 250 Microscope. This analysis was performed at National Research Center on Membrane Technologies located at ITU. Figure 2.7 clearly shows the fibrous structure of selected TTB sepiolite clay along with dolomitic impurities. It is known that sepiolite is a kind of fibrous silicate clay mineral rich of magnesium with a structure of layer and chain. The sepiolite has a unique crystal structure. In a suspension of sepiolite, the fibers intersect each other to form a network frame which is an important factor to keep the suspension stable. Therefore, the rheological behavior of sepiolite suspension depends on the fibrous structure rather than the electrostatic attraction between particles, (Ke and Stroeve, 2005).

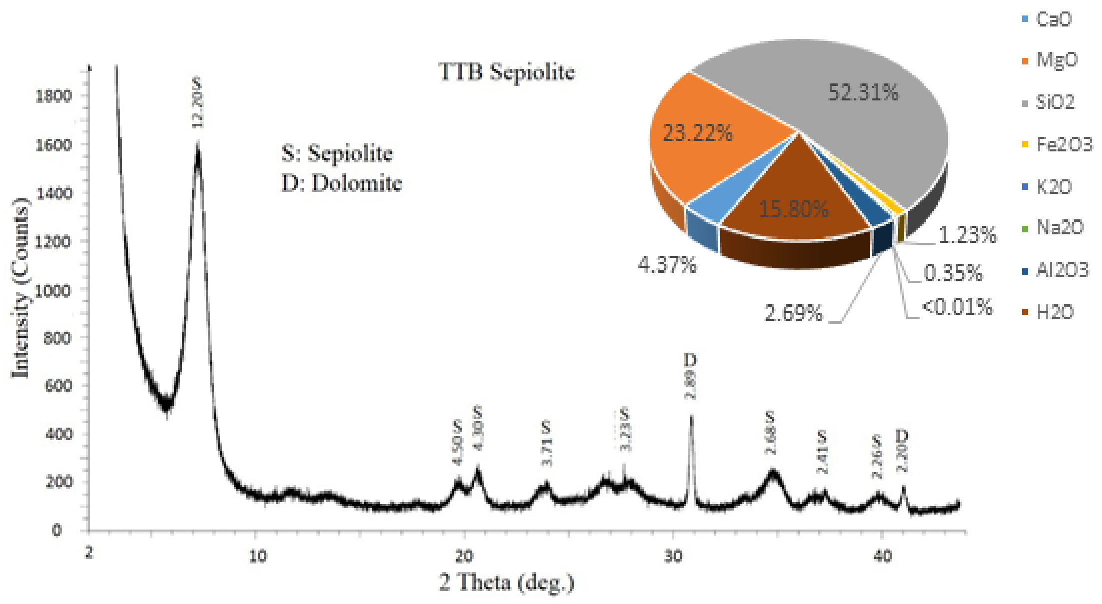

Figure 2.6: XRD and XRF analysis of sepiolite clay.

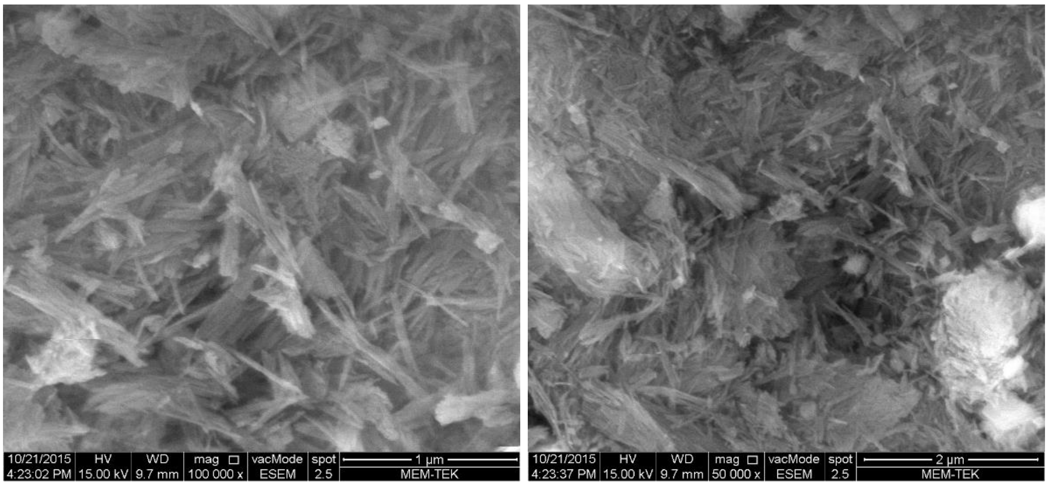

Figure 2.7: Fibrous structure of TTB sepiolite.

2.4 Experimental Equipment

Following experimental equipment were used through this study:

2.4.1 HPHT (High Temperature, High Pressure) filter press

Measurement of the filtration behavior and cake building characteristics of drilling mud are fundamental parameters to make better treatment and consequently increase its efficiency. Filtration characteristics of a drilling fluid are affected by the quantity, type, size of solid particles, and properties of the liquid phase. Interactions of these various components may be influenced by temperature and pressure. Therefore, filtration tests are often performed from ambient to high-temperature conditions to provide data for comparison purposes. 500 ml volume of HPHT Filter Press unit was designed for this purpose (Figure 2.8). It can be pressurized to 12.41 MPa (1800 psig) on the cell and 750 psig on the backpressure receiver. Maximum operating temperature is 260°C (500°F).

2.4.2 Conventional viscometer

The FANN Model 35SA/SR-12 viscometer are direct reading instruments which are available in 6 speed and 12 speed designs for use on either 50 Hz or 60 Hz electrical power. The standard power source is 115 volts but all of the models may be fitted with a transformer which makes operation with 220/230 volts possible. These are true Couette coaxial cylinder rotational viscometer since the test fluid is contained in the annular space (shear gap) between an outer cylinder and the bob. Viscosity measurements are made when the outer cylinder, rotating at a known velocity, causes a viscous drag to be exerted by the fluid. This drag creates a torque on the bob, which is transmitted to a precision spring where its deflection is measured and then compared with the test conditions and the instrument's constants. A Couette type FANN Model 35SA/SR-12 viscometer was used in this study to measure rheological properties of aged fluid samples at ambient conditions (Figure 2.9). This method of measurement was named throughout this study as conventional or classical rheological measurements method.

Figure 2.8: 500 ml HTHP filter press.

Figure 2.9: FANN Model 35SA/SR-12 viscometer.

2.4.3 Aging cell

Drilling fluid aging is the process in which the rheological and filtration properties of prepared drilling fluid sample is allowed to more fully develop. The time period needed to more fully develop properties varies from as little as several hours (usually 16 hours) to as much as several days. The aging can be done at either ambient or elevated temperatures. It is also done under conditions which vary from static to dynamic and from ambient to highly elevated temperatures using specially manufactured cells (Figure 2.10).

Figure 10: Aging cells.

2.4.4 Roller oven

Fann Roller Oven provides an excellent environment to age fluid samples at different temperatures for a desired time. Aging cells containing sample fluids are placed in the roller oven where they are subjected to homogeneous heat and rolling on power driven rollers. Samples may also be heated without rolling (static aging). These roller ovens are constructed of polished stainless steel and other corrosion resistant materials. They are well insulated and the temperature is regulated by a digital electronic controller. Fann Model 704ET Roller Oven was used to provide hot rolling condition for fluid samples in this study (Figure 2.11).

Figure 2.11: Fann roller oven.

2.4.5 Mixing mud samples

Most drilling fluid formulations contain a base liquid and additives which must be dissolved or mechanically dispersed into the liquid to form a homogenous fluid. The resulting fluid may contain one or more of the following: water-dispersible (soluble) polymers or resins, clays or other insoluble but dispersible fine solids, and soluble salts. The fluids are mixed or sheared for times appropriate to achieve a homogenous mixture. The Five-Spindle Multi-Mixer® Model 9B mixer (Figure 2.12) is recommended for use in general purpose mixing of drilling fluids in preparation for laboratory tests of mud materials.

Figure 2.12: Five-spindle multi-mixer.

Five Spindle Multi-Mixer mixers are supplied with impeller blades. It conforms to American Petroleum Institute (API) Specification 13A for mixing water base and oil base drilling fluids.

2.4.6 High temperature rheometer

The Model 50SL High-Temperature Rheometer (Figure 2.13) is a rotational viscometer designed for testing fluids at temperatures up to 500°F (260°C) and pressures to 1000 psig (7000 kPa) in a coaxial cylinder chamber. Heating, pressurization and rotor speed are controlled by input from specialized software. The thermal in-situ rheological properties of prepared sepiolite samples were measured using this rheometer to have better insight with more details about temperature effect on rheological properties. The rheometer is a computer controlled one that can provide accurate measurements at wide range of rotor speed through tight temperature intervals.

Figure 2.13: High temperature rheometer (Model 50 SL).

2.4.7 Lubricity tester

The combination EP (Extreme Pressure) and Lubricity Tester measures the lubricating quality of drilling fluids. It provides data to evaluate the type and quantity of lubricating additives that may be required, and predict wear rates of mechanical parts in known fluid systems. The EP tests are performed by applying a measured torque with a torque arm to a torque-sensitive, rotating bearing cup. This provides a means of testing lubrication under extreme pressure conditions and produces an indication of the film strength of the fluid being tested.

The problem of reduction of friction between the drillstring and the borehole requires a different simulation. The more common lubricity tester (Figure 2.14) measures fluid resistance (lubricating character) between two hardened steel moving surfaces at 100 pounds force. During the lubricity test, a steel block is pressed against a rotating steel ring. Load in inch-pounds (in-lb) is read directly from the dial on the torque arm. Measure of friction is a requirement for the determination of the film strength of a lubricant, for bit bearing wear, as is obtained in EP test and for the determination of torque or drag of the drill pipe as determined in the lubricity test.

Figure 2.14: Fann Model 212 EP/Lubricity Tester.

2.4.8 Differential sticking tester

The Differential Sticking Tester apparatus was designed to determine how likely a given drilling fluid will be to produce a "stuck pipe" situation, and how effective a given drilling fluid remediation or application of spotting fluid in any given drilling fluid would be in reducing this tendency. This measurement is called the "Stuck Tendency Coefficient". It takes into account both the stickiness and the cake building capability of the drilling fluid. The "Stuck Tendency Coefficient" is determined by the Timed Filtrate Test.

The unit can be pressurized by the CO_2 regulator assembly or from any nitrogen source. If nitrogen is to be used, the Differential Sticking Tester (Figure 2.15) must be fitted with a suitable nitrogen regulator, gauges, relief valve, hose and fittings. The tests use 477.5 psi (3292 kPa) differential pressure applied to a stainless steel vessel of approximately 200 ml capacity. The measurement can be made using either the flat-faced torque plate or the 31.75 cm (12.5 inch) spherical radius plate which approximates pipe in casing or collars in borehole contact geometry. In the event of a "sticky" sample that tends to adhere more to the torque plate than to the filter paper, stainless steel micro-corrugation disks are provided, along with extra-strength paper to ensure success of the test.

Figure 2.15: Fann Model 21150 Differential Sticking Tester.

3. INVESTIGATION AND REMEDIATION OF ACTIVE-CLAY CONTAMINATED SEPIOLITE DRILLING MUDS

3.1 Introduction

Unconventional gas and oil development has gained remarkable attention in recent years. However, the high content of active clays in shales makes drilling difficult. Since most formations drilled for oil and gas exploration are shales, active solid dispersion into the drilling mud is a common problem. This might results in severe problems, such as stuck pipes, circulation loss, excessive torque and drag, inadequate cuttings transport, poor log quality, poor primary cement job, and borehole instability.

In this study, active clay contamination effects on sepiolite muds were experimentally investigated for hostile drilling conditions. Rheological properties of both unweighted and barite-weighted sepiolite drilling muds with and without sodium chloride additions were tested at ambient to 204°C (400°F) temperatures. Filtration loss properties were determined at a 0.689 MPa (100 psig) pressure differential. The drill-hole cleaning efficiency of sepiolite drilling muds was investigated too. Methylene blue tests were also performed to determine the tolerance of sepiolite muds to solids accumulation. Special emphasis of this chapter is to investigate and show the suitability of sepiolite base muds at high temperatures and salinity when subjected to active-clays intrusion. Through this laboratory work, it is aimed to bridge the gap between theoretical knowledge and field development of providing adequate muds applicable to severe drilling conditions. The main objective is to justify the introduction of the sepiolite clay as a major component of water base mud tolerating excessive active clay contamination sourcing from clay rich formations such as shales. This chapter was published in Journal of Applied Clay Science (Altun and Osgouei, 2014).

3.2 Literature Review

An important drilling engineer duty is to select and maintain drilling fluid properties. As deeper formations are drilled, different sediments are mechanically fragmented, chemically hydrated, and dispersed into the drilling mud system. These sediments can contain active and/or inactive (inert) materials. In general, active solids contain clay minerals with different hydration abilities. Montmorillonite clays are known to have a high hydration ability, which can cause formations to swell. This can produce some difficulties with rheological and filtration properties of the drilling fluid if no treatments are used (Bourgoyne et al., 1991).

Active shales sourcing from clay rich formations are problematic during drilling operations because of their tendency to degrade when exposed to aqueous media. Very fine shale particles in drilling fluid lead to further absorption of water and accelerate drilling fluid related borehole instability. Swelling of shale induces stresses, loss of mechanical strength, and shale failure. For these reasons, rheological and water loss properties of a drilling mud should be continuously monitored and controlled in the case of active clays intrusion.

Different approaches to design water base mud (WBM) have been suggested (Bol et al., 1992; Cook et al., 1993; Mody and Hale, 1993). More recent studies on shale-fluid contacts have suggested a new approach to WBM design (Lomba et al., 2000; Schlemmer et al., 2002; Van Oort, 2003). This approach has basically focused on the process called inhibition which means reducing swelling ability of active clays to maintain borehole integrity. Beside of these ongoing research efforts, there is no widely accepted solution by the drilling industry. Yet the drilling fluid stability problems continue to be one of the main fluid formulation challenges.

3.2.1 Drilling fluid contamination

Any of the liquid, chemical, or solid components of drilling muds and formation solids can become a contaminant under certain circumstances. It is very difficult to foresee the worst problems resulted by potential contaminants in an exploration well. The prevalent problems results from (1) high active solids or clay concentration sourcing from shale zones, (2) high electrolyte concentration, and (3) high temperature (Bourgoyne et al., 1991). These three items are known to be the main causes of mud flocculation that refers to thickening (intolerable high viscosities) of the mud and unacceptable high filtration losses. One of the worst situations in drilling is the presence of these three hostile conditions simultaneously. Hence, it is crucial to visualize changes in the properties of the mud frequently, and make the necessary adjustments when needed. If a high amount of salt intrusion into the mud is expected, salt-water mud must be prepared to provide both the mud and the borehole stability. Salinity greatly affects the hydration ability of clays and results in inherent problems for treatment and maintenance of a mud system. More importantly, severe mud problems are expected from the combined effects of high temperature and salt intrusion.

Viscosity of drilling fluids is the most commonly monitored and controlled parameter. Mud treatment is arranged to accomplish desired yield point (YP), plastic viscosity (PV), gel strength (GS), and filtration rate at the minimum possible cost. Typical ranges of YP and PV at 49^{o}C (120°F) for clay (bentonite)/water mud systems are given by Bourgoyne et al. (1991). However, there is no specifically accepted standard by the drilling industry for YP and PV ranges at high temperatures.

Contaminants also have unfavorable effects on the mud filtration rate that can be directly related to borehole instability by activating clay or clay rich formations. It is a fact that the fluid loss rate increases with increasing temperature, pressure differential, and salt content, and slightly decreases with increasing mud density. Even though the American Petroleum Institute (API) does not provide a specific water loss value for sepiolite muds, the entire effort in this study is to achieve a maximum of 15 ml/30 min at ambient conditions that is the defined standard value for bentonite base mud systems. In addition, the filtration characteristics of sepiolite muds under harsh conditions will intentionally be presented in this study in order to emphasize the efficiency of sepiolite base muds.

3.2.2 Hole cleaning efficiency of drilling fluids

Carrying capacity index (I_{CC}) of a drilling mud is a very significant criterion to evaluate the efficiency of a drilling fluid. In general, 0.254 m/s of annular velocity in vertical wells is sufficient for adequate hole cleaning for a typical mud under normal conditions (Bourgoyne et al., 1991). Minimum required annular mud velocity to carry cuttings out of annulus considerably increases for harsher conditions. The I_{CC} is an empirical relationship from real data and the equation is below:

$$I_{cc} = \frac{AV.MW.K}{244} \quad (3.1)$$

where I_{CC} is the Carrying Capacity Index (dimensionless), AV is the annular velocity (m/s), MW is the mud weight (kg/m^3), K is the consistency index in the Power Law model (Pa-s^n), and 244 is the empirical constant [(m/s)(kg/m^3)(Pa-s^n)]. In field units constant 244 becomes 400000 if AV in ft/sec, MW in lbm/gal and K in eq cp.

Only three drilling-fluid parameters are controllable to enhance transportation of drilled solids from the wellbore: annular velocity (AV), density or mud weight (MW), and viscosity (K). By testing cuttings discarded from shale shakers in vertical and near-vertical wells during a 10-year period, it was learned that sharp edges on the cuttings resulted when the product of those three parameters was about 244 or higher. When the product of these three parameters was around 122, the cuttings were well rounded indicating that the cuttings were grinded during the transportation. When the product of these parameters was 61 or less, the cuttings were small, almost grain sized, (API RP 13D, 2006).

To ensure a good hole cleaning, I_{CC} should be 1 (one) or greater. Equation 3.1 applies to wellbores up to an inclination angle of 35^o. The AV chosen for the calculation should be the lowest value encountered in a circulation system where the area open for the drilling mud is at maximum (e.g., drillpipe annulus or probably the riser for offshore operations). Quantification indicates that if the I_{CC} is too low for adequate cleaning, Equation 3.1 can be rearranged to predict the change of K in Equation 3.2 in order to accomplish efficient cutting transport by assuming I_{CC} is equal to 1 (ASME, 2005).

$$K = \frac{244}{(MW).(AV)} \tag{3.2}$$

Consistency index (K) in the Power Law model can be calculated using the flow behavior index (n) and related shear stresses as defined in Equations 3.3 and 3.4 (API 13D, 2006).

$$n = 3.32 log \frac{\theta_{600}}{\theta_{300}} \tag{3.3}$$

$$K = 510 \frac{(\theta_{300})}{(\gamma_{300})^n} \tag{3.4}$$

where **n** is the flow behavior index in the Power Law model (dimensionless), θ_{600} is the dial reading from Couette type of viscometer at 600 rpm (Pa), θ_{300} is the dial reading from Couette type of viscometer at 300 rpm (Pa), and **K** is the consistency index in the Power Law model (Pa-s^n). γ_{300} (s^{-1}) is the amount of shear rate on the viscometer bob at the rotor speed of 300 rpm. γ_{300} is equal to 511 (=1.703 × 300) for a Couette type of viscometer with the bob radius of 1.7245 cm. Multiply dial reading value by constant 0.4788026 to obtain result in Pascal.

3.2.3 Sepiolite base drilling fluids

Sepiolite, a magnesium silicate clay mineral with fibrous texture, is proposed to be used in both high temperature and/or high saline environments. Some investigators have reported that sepiolite is a temperature resistant clay up to 260^{o}C (Carney et al., 1976, 1980; Güven et al., 1988; Serpen, 1999; Serpen et al., 1992). Also, the basic structure of sepiolite is known to be firm in a saturated saline-water phase. Although the sepiolite muds yield appropriate rheological properties in harsh drilling conditions, unacceptable high filtration loss is the major deficiency (Altun et al., 2005; Carney and Meyer, 1976; Serpen et al., 1992). On the other hand, recent studies revealed that the filtration properties of sepiolite mud could economically be controlled based on the addition of commercial additives (Altun et al., 2010; Osgouei, 2010; Osgouei et al., 2014).

3.3 Methods and Materials

A raw sepiolite clay sample, a commercial product known as Turk Taciri Bej (TTB) and produced near Sivrihisar-Eskisehir district of Turkey by AEM Company (AEM, 2014), was used in this experimental study. The <62 µm (230 mesh) fraction was examined by X-ray Fluorescence Spectrometry (XRF) using a Spectro Xepos 3 model apparatus and analyzed with fusion method on Cu anode tube, running conditions of 0.9 mA, 40 kV at the research center of Turkish Petroleum Corporation (Figure 2.6). X-ray powder diffraction pattern of the sepiolite sample was obtained on a Bruker D8 Advance model XRD with CuKα radiation (1.54178°A) running conditions of 40 mA, 40 kV, scan-speed of 0.005^{o}, time/scan of 0.1 sec and 0.2 mm soller slit using LynxEye detector (Ni-filter) at Istanbul Technical University (Figure 2.6). The XRD and XRF analyses indicate that the TTB sepiolite includes about 10% dolomite by weight and negligible gangue minerals. TTB sepiolite was not purified by any physical or chemical methods.

After grinding, the TTB sample was dry sieved to <74 µm (<200 mesh). Other additives, all in technical grades, used in formulation of muds were i) Sodium carbonate (soda ash, Na_2CO_3, product of Karakaya) for controlling pH, ii) A commercial deflocculant (polymer-1, anionic acrylic copolymer used as thinner, product of Halliburton) for controlling rheological properties in water base systems for up to 232°C and providing high temperature stability, iii) Filtration control agent (polymer-2, vinyl amide/vinyl sulfonate copolymer, product of Halliburton), iv) GEM GP (polyalkyline glycol, product of Halliburton) for providing stability, lubricity, and reducing dilution rates and ineffective drill bit performance, v) Oil Company Materials Association (OCMA) clay (API test calibration bentonite, product of Baker Hughes Inteq) for simulating active clay contamination, vi) Sodium chloride (NaCl, product of Karakaya) for controlling salinity, and vii) Weighting agent (API Barite, product of Karakaya).

API RP-13B Standard was employed throughout the experiments. All mud samples were based on the formulation of 350 ml of water phase (distilled water) having different amount of sepiolite and commercially available additives (polymers) in both unweighted and barite-weighted systems. Rheological properties such as apparent viscosity, PV, YP, and GS were measured on a Couette type viscometer (Fann Model 35SA/SR-12) before and after aging mud samples at elevated temperatures. The static filtration properties of the samples at elevated temperatures were measured using high temperature high pressure (HTHP) filter press (Fann 500 ml HTHP filter press).

A total of seven sepiolite base muds coded as BM1 to BM7 were prepared, representing two unweighted and five barite-weighted systems (Table 3.1). A total of 39 mud samples were investigated under these 7-base-mud systems. Each base mud system followed by letter S indicates a different sample for various conditions, such as temperature, salt and contaminant contents (Tables B.1–B.3). For example, the mud coded with BM3-S8 indicates barite-weighted Base Mud 3, Sample-8.

3.3.1 Preparation of fresh-water mud

Typical compositions of unweighted and barite-weighted sepiolite (TTB clay) base muds for fresh water systems are also listed in Table 3.1. After preparing mud samples through a mixing order given in Table 3.1, rheological properties of the samples were measured at ambient conditions. Then the samples were poured into pressurized cells that were placed in a roller oven for 16 hours of aging at elevated temperatures. Finally, the properties of sepiolite mud samples with and without active clay were measured.

Table 3.1: Compositions of sepiolite-base mud systems.

Substance	Quantity (kg/m³)				
	Unweighted		Barite-Weighted		
	Base mud	Contaminated (fresh water)	Base mud	Contaminated (fresh water)	Contaminated (salt water)
Mud system	BM1	BM2	BM3	BM4	BM5, BM6, BM7
Sepiolite	57	57	57	28.5-57	28.5-42.75-57
Soda Ash	0.286	0.286	0.286	0.286	0.286
Polymer - 1	11.43	11.43	11.43	11.43	11.43
Polymer - 2	14.28	14.28	14.28	14.28	20.00
API Barite	None	None	429	429	429
Glycol, % by vol.	None	3	None	3	3
NaCl	None	None	None	None	343
Contaminant (OCMA[1])	None	228	None	228	228

[1] Oil Company Materials Association (OCMA): Pertaining to a drilling-grade bentonite with API/ISO specifications

In the first stage, rheological properties of aged samples without active clay at the specified temperature were measured at both 27°C and 49°C using heating jackets. The filtration loss measurements of all of the samples were performed at 149^{o}C. In the second stage, an amount of 228 kg/m^3 OCMA clay as the active clay contaminant was added into the muds (Table 3.1).

3.3.2 Preparation of salt-water mud

Typical compositions of barite-weighted salt-water muds are given in Table 3.1 for three sepiolite concentrations. A concentration of 343 kg/m^3 NaCl known as the most extreme salinity condition (Bourgoyne et al., 1991) was used to have a fully saturated system. Effects of adding salt into the mud were to increase the mud weight and to simulate the salt contamination. The process of measuring rheological and filtration properties were as defined in the previous section.

3.3.3 Methylene blue properties (MBT)

MBT measured in accordance to API RP13B-1 (2004) is one of the most meaningful tests available to indicate the amount of active clays present in the mud. The test is performed by adding methylene blue solution to a sample of drilling fluid (which has been treated with hydrogen peroxide and acidified to remove organic substances) until saturation is noted by formation of a dye halo around a drop of solids suspension placed on filter paper. In general, a non-dispersed polymer drilling fluid should have a MBT value no greater than 57 kg/m^3.

For high density drilling fluids, 42.75 kg/m^3 should be considered as the upper limit, (ASME, 2005). The MBT value of a salt water base mud was suggested to be 50 kg/m^3 and could be allowed 14.25 kg/m^3 more if all of the other parameters were acceptable and stable (KDS, 2001). High temperatures rapidly promote the yield of active solids and increase in values obtained from MBT.

3.4 Results and Discussions

3.4.1 Properties of fresh water mud system without contamination

3.4.1.1 Rheological properties

Rheological and filtration properties of fresh water sepiolite muds were listed in Table B.1. Moreover, The YP values measured at 49^{o}C for unweighted and barite-weighted fresh muds were given in Figure 3.1 illustrating the variation of YP versus mud density. The YP of the unweighted mud system (BM1) decreased up to 177^{o}C and increased beyond this temperature (Figure 3.1). Similar behavior was observed for the barite-weighted mud system (BM3) up to 149^{o}C, and then the YP again increased with increasing temperature. This behavior is a clear indication of thermal degradation of the muds. For example in BM3, the YP in ambient condition decreased from 10.54 to 5.27 Pa at 149^{o}C, and then increased to 11.50 Pa at 204^{o}C. Similar trends were also obtained for the PV and GS values. An increase in the YP and GS above 149^{o}C was more noticeable than that of the PV. This behavior is one of the characteristic properties of sepiolite clays and indicates that sepiolite begins to be converted to a smectite at 149°C, and this reaction is fully completed at 260°C (Güven et al., 1988). The new smectite in the mud has a thin flakey morphology and increases the viscosity and filtration losses (Güven et al., 1988). Therefore, it would be logical to use a lower amount of sepiolite in the case of salt and/or active clay contamination. As a result of this fact, mud samples having different concentrations of sepiolite were investigated particularly for the barite-weighted systems. Water base drilling fluids can be easily flocculated while drilling salt zones or shale formations (the main source of active clays) when coupled with high temperatures. However, the rheological properties obtained under these conditions for the sepiolite muds formulated in this study are comparable to those of results given by Bourgoyne et al. (1991), even though the referenced results are valid for a bentonite system at 49°C (Figure 3.1). After comparison, it can be concluded that YP values obtained from the sepiolite muds at 177 or 204°C were superior both in unweighted (BM1) and barite-weighted (BM3) fresh water mud systems.

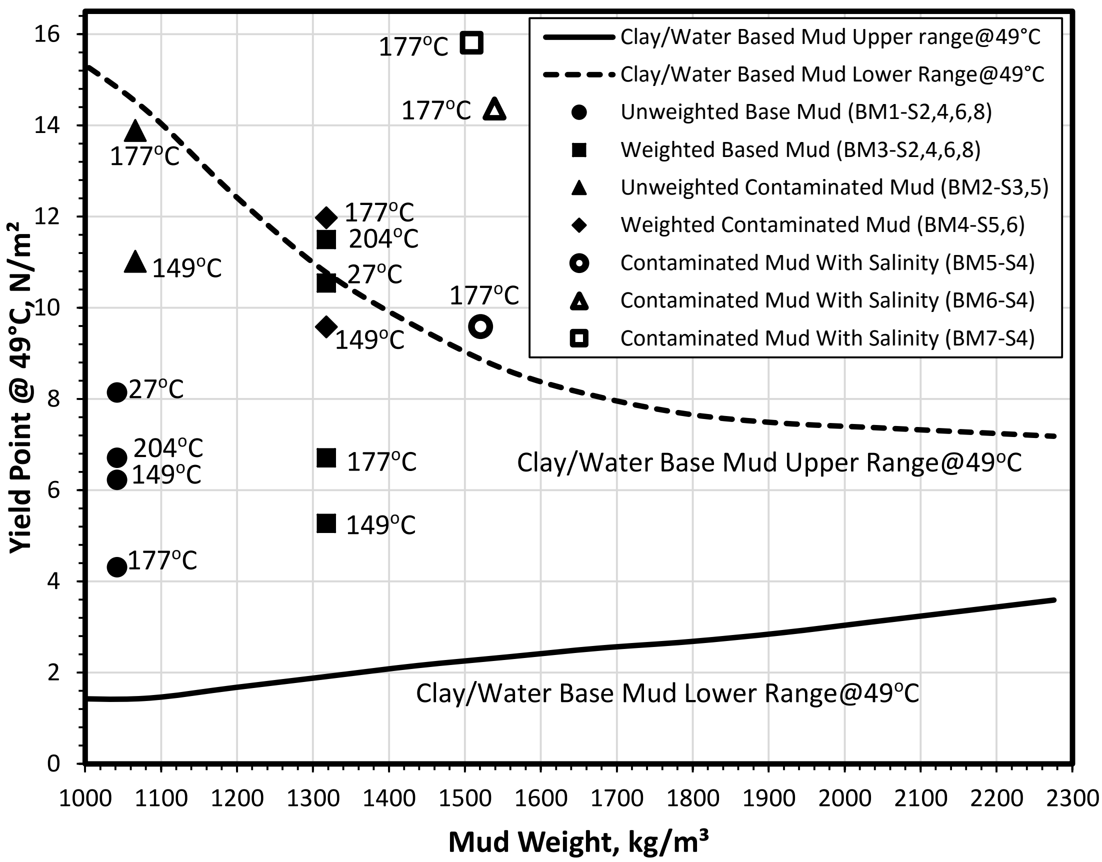

Figure 3.1: The upper and lower range of YP measured at 49°C for clay/water base muds regenerated from Bourgoyne et al., (1991) including the values measured for sepiolite mud samples.

3.4.1.2 Filtration properties

The filtration losses of all the mud samples had appropriate values even at high temperatures (Table B.1). Water loss at high temperatures especially for the weighted mud samples (BM3) aged at 177°C were in the proper interval between 6.5 and 9 ml/30 min. The water loss values slightly increased with increasing aging temperature as expected. Filtration amount of the sample (BM3-S8) aged at 204°C (15.5 ml/30 min) was slightly higher in comparison to those obtained at lower temperatures due to decrease in polymer efficiency and increase in rate of clay alteration at aging temperatures above 177°C. However, the amount of water loss was still in an acceptable range at such high temperatures. In the case of unweighted mud samples

(BM1), the filtration rates were high to some extent due to their lower solids content.

3.4.2 Properties of fresh water mud system with contamination

3.4.2.1 Rheological properties

By adding an amount of 228 kg/m^3 OCMA clay as the contaminant into the unweighted mud system, viscosity tended to increase slightly with increasing temperature after 16 hr aging at 149^{o}C and 177^{o}C (Table B.2). Similar behavior was observed for the barite-weighted mud system as well. However, the amount of sepiolite in barite-weighted mud systems should be decreased to 28.5 kg/m^3 concentration in order to preserve the rheological values at desirable levels. In short, the increase in the YP was insignificant indicating that the mud successfully preserved its rheological properties even under high contamination conditions and at high temperature conditions, particularly in the barite-weighted samples.

3.4.2.2 Efficiency of hole cleaning and carrying capacity

Assuming a value of 1 for I_{CC}, calculated minimum required AV values of the unweighted mud system (BM2) at high temperatures are given in Table B.2. For example, suppose a vertical well is being drilled with this typical sepiolite mud (BM2-S3) contaminated with 228 kg/m^3 of active clay and being circulated in an annulus with a mud weight of 1066 kg/m^3, PV of 0.019 Pa-s, and YP of 11.02 Pa at a temperature of 149^{o}C. The values of n and K for BM2-S3 sample were calculated as 0.5381 and 0.747 Pa-s^n, respectively, using 600 and 300 rpm dial readings of the viscometer. Solving Equation 2 for AV gave 0.305 m/s assuming 1 for I_{CC} to carry cuttings efficiently. Likewise AV was calculated as 0.244 m/s for the sample (BM2-S5) aged at a temperature of 177^{o}C. Similar calculations were performed for the other samples, and the results are given in Table B.2. In case of barite-weighted mud samples (BM4) also given in Table B.2, AV was obtained as 0.417 m/s for the mud (BM4-S5) aged at 149^{o}C and 0.269 m/s for the mud (BM4-S6) aged at 177^{o}C.

The required value of AV decreased with increasing temperature for both unweighted and barite-weighted mud samples due to the increased viscosity. These calculated AV values clearly indicate that sepiolite muds under harsh conditions have excellent ability to remove cuttings through the annulus. The carrying capacity of the mud could result in better hole cleaning since the mud is flocculated due to temperature effect. If this assumption is true, then the filtration loss value of flocculated mud must also be substantially higher. However, for the unweighted and barite-weighted systems the changes in filtration losses at the both aging temperatures (149^{o}C and 177^{o}C) were negligible indicating that the mud was not flocculated (Table B.2).

3.4.2.3 Filtration properties

There existed insignificant filtration differences between aging at ambient temperature and 177^{o}C for BM2 samples without contaminant (Table B.2). This was an expected behavior since the sepiolite clay was suggested for high temperature environments. While the amount of water loss at ambient temperature was 13 ml/30 min for BM2-S1, this value at an aging temperature of 177^{o}C was 14 ml/30 min for BM2-S2. Filtration rates of 5 ml/30 min for BM2-S3 and 6.5 ml/30 min for BM2-S5 were obtained when contaminant was introduced to the samples at aging temperatures of 149 and 177^{o}C, respectively. Filtration rates for contaminated samples were substantially lower because of the high solid content of the muds.

Similar to the unweighted muds, noticeable low filtration rates were obtained for the barite-weighted samples. The amount of filtration in contaminated and barite-weighted mud samples are also given in Table B.2. Filtration rates were measured as 6 ml/30 min for BM4-S5 and 7.5 ml/30 min for BM4-S6 at aging temperatures of 149 and 177^{o}C, respectively. In addition, the barite-weighted sample without contaminant (BM4-S4) at aging temperature of 177^{o}C gave a filtration loss of 6.5 ml/30 min. This result indicates a negligible difference between BM4-S4 and BM4-S6 under the same conditions. This is a clear indication of insensitiveness of sepiolite muds when exposed to active clay contamination. In addition, it is also important to note that the minor filtration loss variations imply that the muds are not flocculated even at high temperatures.

3.4.2.4 MBT properties

MBT measurement on base sepiolite mud (BM2-S1 or S2) indicated that sepiolite had a low value of 14.28 kg/m^3 MBT, which was in the range of 12.21-20.35 kg/m^3 (Table B.2**)**. More importantly, after the introduction of 228 kg/m^3 clay into both unweighted and barite-weighted systems, the amount of active clays in the mud system was still at acceptable levels as evidenced by the MBT analyses, which fell within the range of recommended values for MBT. The value of the MBT was 34.28 kg/m^3 for MB2-S4 or S5 in the unweighted samples and 37.14 kg/m^3 for BM4-S6 in barite-weighted sample. In short, sepiolite muds are extremely tolerable for active clays. As mentioned before, even though high temperatures rapidly promoted the yield of active solids and increased the MBT values, sepiolite muds were not affected by temperatures up to 177^{o}C.

3.4.3 Properties of barite-weighted salt water mud systems with contamination

3.4.3.1 Rheological properties

Lower amounts of sepiolite should be used for preparing barite-weighted mud in order to have better rheological and filtration properties when active clay (contaminant) intrusion is introduced into the system. In this section, the experiments were conducted with three different concentrations of sepiolite to analyze the effects of both weighting agent and solid contaminant.

Rheological and filtration properties were determined at high temperature and high saline conditions (Table B.3). The mud with a concentration of 28.5 kg/m^3 sepiolite (BM5-S4) yielded the best rheological performance compared to the other muds having 42.75 kg/m^3 (BM6-S4) and 57 kg/m^3 (BM7-S4) sepiolite, respectively. In other words, the amount of sepiolite in a weighted mud system should be maintained at low concentrations when it is used in environments having high amount of active clay (unstable formations) coupled with high salt content. When a large amount of active clay invades the mud system, the values of YP and GS increase. This condition along with high temperature and high salinity might result in mud flocculation; consequently, initial concentration of sepiolite should be lowered to preserve appropriate mud stability. As stated before, sepiolite begins to convert a smectite above 149^{o}C and exhibits higher YP and GS values (Güven et al., 1988). This reaction in conjunction with salinity and the introduction of substantial amounts of active clay leads to an increase in rheological properties expeditiously. Therefore, using low amounts of sepiolite are a reasonable decision while drilling shale zones. For example, the YP values for the mud with 28.5 kg/m^3 of sepiolite (BM5-S1) decreased from 12.93 to 4.79 Pa after the introduction of 343 kg/m^3 of salt for BM5-S2 (Table B.3). However, the values of YP were still in acceptable ranges with respect to the values given by Bourgoyne et al. (1991), for the fresh water bentonite mud systems. Keeping the YP and GS at acceptable minimum values is a critical factor, especially in clay base muds, in order to preserve mud stability and reduce costs. The increase in the rheological values is not progressive with the introduction of active clay, higher temperatures, and salinity conditions.

A basic strategy in designing a water base mud is to prevent an excessive increase in rheological properties. Sepiolite concentration, particularly in the barite-weighted muds, had a substantial effect on the rheological properties, especially on the YP and GS values. When for example the sepiolite concentration was increased from 28.5 kg/m^3 (BM5-S4) to 57 kg/m^3 (BM7-S4), the YP value increased from 9.58 to 15.81 Pa at 49^{o}C. In addition, increasing the amount of sepiolite resulted in undesired progressive GS behavior (Table B.3). According to the literature (KDS, 2001), the 3-rpm viscometer dial reading defining the lifting capacity at very low flow rates and the 10-sec GS defining the suspension capability of the system are also known as important rheological parameters. In order to provide for the best possible hole cleaning and reduce accumulation of cuttings in a mud, keeping these parameters within certain margins is of critical importance. These specifications may depend on different factors such as temperature, pressure, and salinity. However, the common specification is to control the 3-rpm dial reading and 10-sec GS without producing high 10-min gel values. This condition was best approached by the mud system (BM5) with 28.5 kg/m^3 of sepiolite rather than the higher concentrations (Table B.3).

3.4.3.2 Hole cleaning and carrying capacity

AV for BM5-S4 was calculated as 0.315 m/s for a mud weight of 1522 kg/m^3, PV of 0.021 Pa-s, and YP of 9.58 Pa using Equations 2 and 3 with a K value of 0.507 Pa-s^n, and I_{CC} value of 1 (one) at high temperature condition of 177^{o}C (Table B.3). The mud sample BM5-S4 could be a good choice for harsh drilling conditions that would have high salinity, high formation pressure, and high contaminants at high temperatures. Interestingly the lower value of AV was not the reason of the mud flocculation because the filtration losses of the muds having sepiolite content of 28.5 kg/m^3 for BM5-S4 and 42.75 kg/m^3 for BM6-S4 resulted in almost the same filtration losses (Table B.3). Further increase of sepiolite concentration in the mud formulation to e.g. a sepiolite content of 57 kg/m^3 in BM7-S4 decreased the AV value even more as if hole cleaning were getting better. However, this decrease in the AV value could be as a result of mud flocculation based on the high filtration loss value of 16.5 ml/30 min (almost double of the value obtained for the mud with 28.5 kg/m^3 sepiolite content). Relatively low AV values, in general, indicate that even in hostile drilling conditions, the sepiolite muds provide effective borehole cleaning and cutting transport ability at low circulation rates, which in turn requires less pumping energy.

3.4.3.3 Filtration properties

The amounts of HTHP filtration rates were relatively low and acceptable for the given harsh drilling conditions when the sepiolite amount in the mud formulation was kept at 42.75 kg/m^3 or less (Table B.3). The amount of filtration was 8.5 ml for BM5-S4 and 9.5 ml for BM6-S4 having 28.5 kg/m^3 and 42.75 kg/m^3 sepiolite, respectively. However, at 149°C a high filtration rate of 16.5 ml was observed when the sepiolite content was further increased to 57 kg/m^3 for BM7-S4. The optimum sepiolite concentration in the barite-weighted muds for the specified conditions should be kept around 28.5 kg/m^3 or no more than 42.75 kg/m^3 to provide acceptable filtration losses as well as desired rheological properties, hole cleaning ability, and MBT values.

3.4.3.4 MBT properties

Extremely good results (less than the field specified value of 50 kg/m^3) for MBT values were obtained in spite of the high amount of active clay invading the mud system. The MBT values of sepiolite muds were in the range of 31.43 to 34.28 kg/m^3 indicating that the sepiolite muds were exceptionally endurable while subjected to active clay contamination, particularly in drilling clay rich active formations like shales (Table B.3). Higher amount of contaminants, more than 228 kg/m^3, should be further investigated to ensure the active solid contamination tolerance of sepiolite base systems.

3.5 Chapter Conclusions

In general, sepiolite clay is resistant to high temperature and saline environment. Therefore, substantial experimental work has been performed to demonstrate whether water base mud with bentonite clay can be used together or totally replaced by sepiolite to extend the limits of drilling fluids at hostile conditions (Carney et al., 1980, 1982; Güven et al. 1988) and particularly for geothermal wells (Serpen, 1999, 2000). In these studies, sepiolite base muds with good rheological properties have been proposed for hostile drilling environments since the late 1970. Even though the extensive researches, filtration rate of sepiolite muds could not be controlled until recently (Altun et al., 2010; Osgouei 2010).

The results of this study form a valuable contribution and comprehensive guideline for understanding the rheology and fluid loss behavior of sepiolite base drilling fluids with both rheological and filtration properties in acceptable limits at temperatures up to 204°C and a saline condition of 342 kg/m^3 (fully saturated). In addition, the tolerance to active solid contamination (MBT), hole cleaning efficiency, and carrying capacity of both barite-weighted and unweighted sepiolite muds at hostile drilling conditions have been studied for the first time in this study as far as the authors are aware.

It is important that the results of this experimental work should be validated in the field to confirm the effectiveness of this mud both technically and economically. Additionally, further research need to be conducted on borehole instability while drilling shale sections and plugging ability of sepiolite muds in induced fractures.

- Experimental results verified that sepiolite base drilling muds yield extremely good rheological properties at temperatures >177°C. In addition, the rheological properties were not greatly affected by water salinity. However, sepiolite mud rheological properties started to degrade at 177°C coupled with increased mud density and high amounts of active clay contaminants. Sepiolite concentration in barite-weighted mud should be decreased to overcome problems related to degradation. Flocculation started to occur at sepiolite contents > 42.75 kg/m^3 for the barite-weighted muds coupled with harsh conditions. Even though sepiolite muds are known to have high filtration losses, this study proved that sepiolite muds formulated with commercially available additives yield exceptionally low filtrate volumes at harsh conditions, such as high temperatures, high salt concentrations, and active solid concentrations.

- The capacities of sepiolite muds to transport cuttings were sufficient as indicated by low annular velocities (AV). The cleaning effects increased with increased temperature due to increased viscosities. However, low filtration rates proved that the viscosity increase was not caused by mud flocculation. Relatively low AV values under hostile drilling conditions indicated that the sepiolite muds have provided effective hole cleaning and cuttings transport at low circulation rates with less pumping energy. Sepiolite muds were insensitive both to active clay and salt contaminations.

- In summary, sepiolite muds could provide effective borehole stability when drilling unconventional oil and gas wells, particularly for directional or extended-reach wells experiencing high temperatures and/or high salt intrusion. As a result, laboratory proven sepiolite mud is ready to be used or tested in the field.

4. THERMAL EFFECTS ON DIFFERENTIAL PRESSURE PIPE STICKING TENDENCY

4.1 Introduction

Differential pressure pipe sticking as one of the common borehole instability mechanisms occurs when there is an overbalance pressure pushing drillstring into filter cake that is formed over permeable formations. This part of study is an experimental attempt to determine the possibility of "stuck pipe" tendency taking place during the usage of two commonly used drilling fluids (Bentonite/Polymer and Lignosulfonate base drilling fluids) and one new developed drilling fluid system (Sepiolite base drilling fluid) at elevated temperatures. Samples of drilling fluids were thermally aged for 16 hours up to 204°C (400^{o}F).

Rheological and filtration properties of samples were also measured for initial confirmation. Afterwards, the samples were subjected to the differential sticking test under differential pressure of 3.447 MPa (500 psi). Amount of sticking coefficients and corresponding sticking times were measured at various set times. Since few studies were reported in the literature, hence this part of study could contribute on providing database about the differential pressure pipe sticking tendency of various drilling fluids coupled with thermal effect.

4.2 Literature Review

Borehole instability continues to be an updated difficulty for oil and gas industry despite of numerous advances in drilling techniques (Bradley, 1979; Bailey et al., 1991; Aadnoy, 2003; Bell, 2003; Wang and Dusseault, 2003; Zoback et al., 2003; Aadnoy and Belayneh, 2004; Al-Ajmi and Zimmerman, 2006; Al-Bazali et al., 2008). This problem has been a special focus point since drilling horizontal and extended reach wells have been growing up to find more resources. From economic point of view, a loss of one billion dollar per year due to the wellbore instabilities (Zeynali, 2012), on top of missing time corresponding to 40% of all drilling related non-productive time increases the importance of wellbore stability issue for the drilling industry (Schmidt et al., 2004).

Generally a combination of different controllable and uncontrollable reasons and mechanisms may lead to wellbore instability (Bowes and Procter, 1997; Chen et al., 1998; Mohiuddin et al., 2001). Some instability mechanisms are recognized by the analysis of initial drilling fluid weight, drilling fluid weight increment, and hole enlargement of vertical wells. Instability due to collapse of the wellbore wall, drilling fluid invasion, and drillstring sticking (stuck pipe) are the most troublesome types of these mechanisms (Mohiuddin et al., 2006). Drillstring sticking could be a result of both mechanical problems and differential pressure. Inadequate hole cleaning (pack off), borehole collapse and caving, and key seating are recognized as dominant causes of mechanical pipe sticking. On the other hand, while the pressure in the annulus passes over the formation pressure, created differential pressure pushes drillstring through the wall and make it sink into the filter cake which was formed through permeable formations. When drillstring contacts to the filter cake, internal cake pressure decreases, and this situation causes the pipe to be held against the borehole wall. This mechanism refers to differential pressure pipe sticking firstly reported by Outmans in 1958 (Outmans, 1958). Some researchers expressed the importance of differential pipe sticking as one of the stuck pipe mechanisms that influences the drilling operation and cost of the well (Adams, 1977; Weakley, 1990; Wisnie and Zheiwei, 1994). Several studies also stressed the emphasis of differential pipe sticking severely affecting well cost and operation time as a non-productive time (Adams, 1977; Biegler and Kuhn, 1994; Wisnie and Zheiwei, 1994; Aadnoy et al., 1999). In spite of these adversities, stuck pipe incidences can be reduced by proper manage of the filter cake and drilling fluid properties (Haden and Welch, 1961; Annis and Monaghan, 1962).

Importance of pipe sticking can also be realized by considering some industrial reports and statistics. Reported in 1991 for British Petroleum, the cost of stuck pipe has exceeded $30 million per year; however, this rate for the industry was so crucial and reported to be more than $250 million annually (Bradley et al., 1991). Stuck pipe related to differential pressure sticking has been presented by BP as a major reason for 61% of total cost in the Gulf Coast region. However, packing off (mechanical sticking) accounted for one third of the total Gulf Coast stuck pipe cost (Bradley et al., 1991).Within Sedco Forex, the stuck pipe has been recognized as a main source for 36% of all reported drilling problems over a 15-month period in the world (Jardine et al., 1992).

Although the cost of stuck pipe in deep oil and gas wells is estimated to be a quarter of total budget (William C et. al 2011), in some cases 40% of the total well cost stems from events related to differentially stuck pipe (Siruvuri et. al 2006). Furthermore, a performed analysis on drilling data, extracted from sixty wells in a field, presented the differential pipe sticking and hole pack off as two significant factors responsible for 13% and 8% of stability problems, respectively. Although the share of these factors were lower than stability problems related to tight-holes (65%), stuck pipe was mentioned as the major reason of productivity loss for evaluated wells (Mohiuddin et al., 2006). Even though the reported statistics considerably vary, the common point in all of them indicate and emphasize the importance of the instability problems resulting from the differential pressure pipe sticking.

Drilling fluid properties and its behavior under different drilling condition directly influence the possibility of pipe sticking. Proper drilling fluid weight and quality of mud cake deposited at the wellbore wall are the essential factors playing undeniable role on stuck pipe event. It is obvious that the temperature, an essential factor, has a detrimental effect on the rheological and filtration properties of drilling fluids. High temperature causes clay particles to be flocculated resulting in unacceptable high viscosities and water losses with excessive thick mud cake. Stickiness of mud cake and drilling fluid lubricity must be evaluated to help engineers to select an effective drilling fluid. In the absence of an efficient filter cake, sourcing from the effect of temperature on properties of drilling fluid, a rise in a bottom hole pressure may lead to differential pipe sticking stability problems. A quick glance to literature is enough to understand the importance of differential pipe sticking. Several researchers tried to deal with this subject in order to help industry to avoid stuck piping. The effect of using lubricant on the water base drilling fluid was studied in some of recent studies. One of them concluded that sticking tendency of the drilling fluid is reduced significantly by using vegetable oil and it may be quite suitable for the prevention of differential pipe sticking problems (Mahto, 2013). However, interestingly there is not published data about the stuck pipe caused by differential pressure coupled with thermal effect.

4.3 Sepiolite base drilling fluid

Sepiolite, a magnesium silicate clay mineral with fibrous texture, is proposed to be used in both high temperature and high saline environments known as hostile drilling conditions. Some investigators have reported that the sepiolite drilling fluid is a temperature resistant clay up to 260°C (Carney and Meyer, 1976; Carney and Güven, 1980; Güven, 1988; Serpen, 1992; Serpen, 1999). Although the sepiolite drilling fluid yields appropriate rheological properties in harsh drilling conditions, unacceptable high filtration loss is the major deficiency of this drilling fluid (Carney and Meyer, 1976; Serpen, 1992; Altun and Serpen, 2005). On the other hand, recent studies indicated that the filtration properties of a new developed sepiolite drilling fluid could economically be controlled using commercial additives by mixing in a special order (Altun et al., 2010; Osgouei, 2010; Altun et al., 2014). Moreover, the properties of active-clay contaminated sepiolite base drilling fluid were also investigated and remediated through comprehensive experimental study (Altun and Osgouei, 2014).

4.4 Methods and Materials

Bentonite/polymer and lignosulfonate drilling fluids were selected as the two prevalent drilling fluids. Sepiolite base drilling fluid prepared in the concept of recent study was introduced as a new developed drilling fluid to clarify the differential sticking tendency of this fluid and compared with others when the temperature was the main parameter (Altun and Osgouei, 2014).

First stage of this study involved in determining the rheological and filtration properties of all fluid samples at elevated aging temperatures to define the efficient and proper functioning area of selected drilling fluid systems. In the second stage, the fluid samples were subjected to differential sticking experiments using differential sticking apparatus to identify comparative parameters such as sticking coefficient and sticking time for different set times (contact times) at various aging temperatures. Sepiolite clay commercially named as Turk Taciri Bej (TTB) obtained from near Sivrihisar-Eskisehir district of Turkey was used in this study. Performed XRF and XRD analysis indicates that selected clay sample was dominantly sepiolite with approximately %10 dolomite (Altun et al., 2014). Raw sepiolite clay sample was not purified by any physical or chemical methods before and after grinding. After grinding, the sepiolite was sieved to < 74 µm (<200 mesh). Commercial bentonite clay provided by Karakaya Company was used as a major additive for bentonite/polymer and lignosulfonate drilling fluids. The other additives, all in technical grades, used in formulation of drilling fluids were i) Sodium carbonate (soda ash, Na_2CO_3, product of Karakaya) and Sodium hydroxide (caustic, NaOH, product of Karakaya) to remove water hardness and PH control, ii) A commercial deflocculant (polymer-1, anionic acrylic copolymer used as thinner, product of Halliburton) for controlling rheological properties in water-base systems for up to 232°C and providing high temperature stability, iii) Filtration control agent (polymer-2, vinyl amide/vinyl sulfonate copolymer, product of Halliburton), iv) Chrome free lignosulfonate (CFL) as deflocculants, temperature stabilizer, filtration control additive and gel strength reducer, v) Xanthum Gum (XCD), a biopolymer, used as a viscosifier to enhance drilling fluid rheology, ensuring efficient hole cleaning, vi) Carboxymethyl cellulose (CMC) acts as a viscosity modifier and water retention agent, vii) Polyanionic cellulose (PAC-LV) acts as a filtration control chemicals with negligible effect on viscosity, viii) Weighting agent (API Barite).

API RP-13B Standard was employed throughout the experiments. All drilling fluid samples were base on the formulation of 350 ml of water phase (distilled water) containing sepiolite, bentonite, and different amount of commercially available additives (polymers) in both unweighted and barite-weighted mud systems. Rheological properties such as apparent viscosity (AV), plastic viscosity (PV), yield point (YP), and gel strength (GS) were measured with a Fann Model 35SA viscometer after aging mud samples at elevated temperatures. The static filtration properties of the samples were measured using a high temperature high pressure (HTHP) filter press. Table 4.1 summarizes the compositions of three drilling fluids. Amount of 429 kg/m^3 (150 lb/bbl) of barite were added to drilling fluid systems to prepare barite-weighted drilling fluid samples. Rheological properties of the samples were measured at ambient conditions after 16 hours of aging at elevated temperatures. Filtration measurements were performed at the corresponding aging temperatures only for unweighted drilling fluid samples. In order to specify the possibility of stuck pipe tendency of a given drilling fluid circulating in the wellbore, Differential Sticking Tester can be a useful device to impose a comparative idea. It can also help to investigate the success of any treatment performed to reduce the tendency of pipe sticking.

Table 4.1: Compositions of drilling fluid samples.

Substance	Quantity (kg/m^3)		
	Lignosulfonate	Bentonite/Polymer	Sepiolite
Sepiolite	None	None	57
NaOH	0.17	0.17	None
Soda Ash	0.286	0.286	0.286
Bentonite	57	57	None
Polymer - 1	None	5.7	11.43
Polymer - 2	None	None	14.28
CFL	8.58	None	None
CMC	8.58	None	None
PAC-LV	None	5.7	None
XCD	None	5.7	None
*Barite	429	429	429

* USED ONLY IN WEIGHTED DRILLING FLUID SAMPLES.

Fann Model 21150 Differential Sticking Tester was used to measure Sticking Coefficient (K_{sc}) of drilling fluid samples. To measure the sticking coefficient, drilling fluid filled apparatus is set up and subjected to 3.447 MPa (500 psi) gas (nitrogen) pressure. It lets loaded drilling fluid sample to filtrate for a predetermined time. Then torque plate is pressed down usually for two minutes using lever against the screen until pressures are equalized sufficiently to allow the plate to stick formed mud cake. If the sticking take places, the filtrate time is recorded as the sticking time. Otherwise, the test is repeated using a new mud sample for a longer time period until determining the appropriate sticking time. Several set times are considered to evaluate the effect of contact time. The time required to the steel plate contacts with the filter cake is defined as the set time. Then the plate is rotated by means of the torque wrench, and then the force required for rotation, filtrate volume and time corresponding to that volume are recorded. The sticking coefficient is calculated using these data.

It must be mentioned that locking mesh disc was used through all sticking tests in order to get the comparative results. As shown in Equation 4.1 and 4.2 (url_01, 2014), the average torque reading is used to determine the sticking coefficient of drilling fluid. If cake stuck radius is less than 1 inch (2.54 cm), Equation 4.1 is used. If the cake stuck radius is equal or higher than 1 inch, cake edge effect must be taken into account. In this case, Equation 4.2 including cake height parameter in the edge of the plate is used.

$$K_{sc} = \frac{(average\ torque\ reading) \times 0.001}{(stuck\ cake\ radius)^3} \tag{4.1}$$

$$K_{sc} = \frac{(average\ torque\ reading) \times 0.001}{1 + 1.33 \times (cake\ height\ on\ edges)} \tag{4.2}$$

4.5 Results and Discussions

4.5.1 Rheological and filtration properties of drilling fluid samples

Rheological properties of unweighted and weighted bentonite/polymer, lignosulfonate, and sepiolite drilling fluids aged at different temperatures were measured. The results were used to obtain yield point (YP) values of each drilling fluid system. Moreover, in order to visually illustrate the efficient thermally stable region of these fluid systems, measured YP's of both unweighted and weighted drilling fluid samples were depicted through Figures 4.1, 4.2, and 4.3. The figures also illustrate the water losses of unweighted samples. Note that the data points on figures were linearly connected to each other to increase visualization.

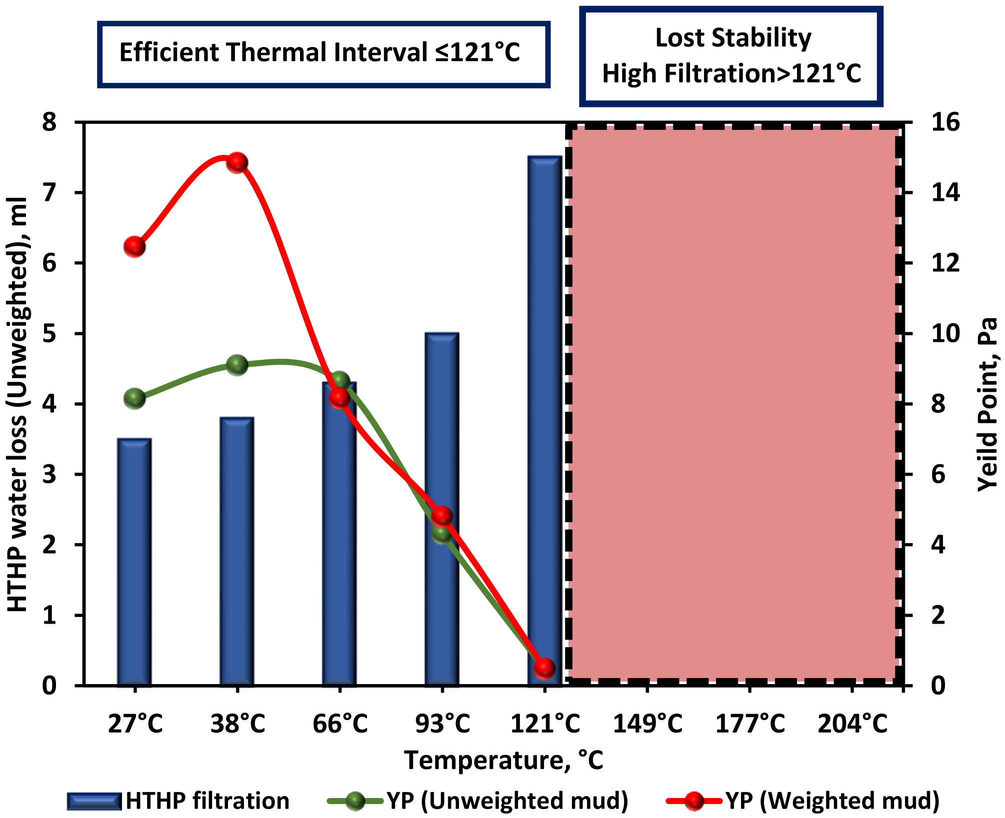

Figure 4.1: Yield point and water loss behaviors of bentonite/polymer drilling fluids.

As seen in figures, the thermal efficiency of a drilling fluid is directly proportional to the variation of thermal properties, especially filtration and rheological behaviors. These properties must be considered and evaluated all together to determine whether or not the selected fluid system is adequately designed and functioned. From the rheological properties point of view, the yield point (YP) and gel strength (GS) are the most important factors playing critical role to evaluate drilling fluid effectiveness.

The YP indicates the ability of the drilling fluid to carry cuttings out of a borehole. In addition, frictional pressure loss is directly related to the YP. High YP implies existence of high frictional pressure loss while the drilling fluid is being circulated. In the case of unweighted and barite-weighted bentonite/polymer drilling fluid system, the measured yield points (8.143 and 12.454 Pa) right after preparation of samples, were a little bit lower than the yield points obtained for the samples aged 16 hours at 38°C (9.58 and 14.849 Pa). This behavior can be related to the effect of aging on increasing the hydration ability of the clay particles. After that the value of YP decreased down to 0.479 Pa (1 lb/100 ft^2) with increasing temperature up to 121°C in both unweighted and weighted bentonite/polymer drilling fluid systems (Figure 4.1). Such a lower YP is the clear indication of undesired function of this fluid system regarding to the ability of lifting cuttings to the surface.

In the case of filtration properties, lower amount of water losses without any spurt loss and an impermeable thin filter cake are so notable parameters that obviously clarify if the drilling fluid is convenient for a given condition or not. Water loss of clay base drilling fluids is extremely sensitive to temperature increment. Thermal degradation of clay particles causes drilling fluid to be flocculated easily by deteriorating filter cake quality along with high water loss. Consequently, thermally instable drilling fluid reduces drilling efficiency by slowing the rate of penetration and creating severe borehole stability problems. Low amounts of water losses from high temperature and high pressure (HTHP) measurements for unweighted bentonite/polymer drilling fluid systems up to 121°C were observed as shown in Figure 4.1. However, the filtration measurement was not possible due to excessive amount of spurt losses above 121°C even though the samples was rheologically stable up to 149°C. This observation was a clear indication that the bentonite/polymer drilling fluid was not thermally stable at temperatures above 121°C. Similar to bentonite/polymer drilling fluid system, rheological measurements for unweighted and weighted lignosulfonate drilling fluids resulted in slightly lower YP values in ambient condition without aging than those of aged samples at 38°C. A rise in aging temperature caused decreases in YP values; however, the rate of decrease in YP for lignosulfonate fluid system was substantially lower than that of the bentonite/polymer system. Amounts of 2.874 and 3.832 Pa (6 and 8 lb/100ft^2) YP values measured for unweighted and weighted lignosulfonate drilling fluid at 121°C, respectively (Figure 4.2). These values depending on drilling conditions were relatively acceptable to provide efficient hole cleaning at high annular fluid velocity. Therefore, in point of rheological properties, the lignosulfonate fluid system was significantly functional compare to the bentonite/polymer system by providing a value of 3.832 Pa (8 lb/100ft^2) YP at 121°C. Relatively comparable results of HTHP water losses were obtained for both unweighted lignosulfonate and bentonite/polymer drilling fluids up to 121°C. Nevertheless, similar to the bentonite/polymer fluid system, a high amount of spurt loss signified thermal instability of lignosulfonate fluid beyond 121°C (Figure 4.2). Amount of YP for unweighted sepiolite fluid system decreased up to 149°C and then increased beyond this temperature.

Similar behavior was observed for barite-weighted sepiolite fluid system up to 177°C (Figure 4.3), and then, the YP tended to increase with the further increase in temperature. This behavior is a clear indication of the thermal alteration of sepiolite clays and specifies that the sepiolite clay begins to be converted to smectite at 149°C, and this reaction is fully completed at 260°C (Güven et al., 1988). The thermal alteration of smectite increases the viscosity and filtration losses. It was noticeable that the sepiolite drilling fluids provided more appropriate YPs even at high temperatures than those of both the lignosulfonate and the bentonite/polymer fluid systems that were not thermally stable at temperatures above 121°C. For example, while unweighted sepiolite drilling fluid exhibited 6.706 Pa (14 lb/100ft^2) at 121°C, unweighted bentonite/polymer and lignosulfonate drilling fluids demonstrated extremely low YP amounts of 0.479 and 2.874 Pa (1 and 6 lb/100ft^2), respectively. This means that the sepiolite drilling fluid can provide more efficient hole cleaning at lower pump rates that are the direct indication of less energy consumption and cost. In addition and more importantly, the lower circulation rates result in less erosion on the mud cake indicating less filtration loss to the formation and minimum instable zone around the borehole.

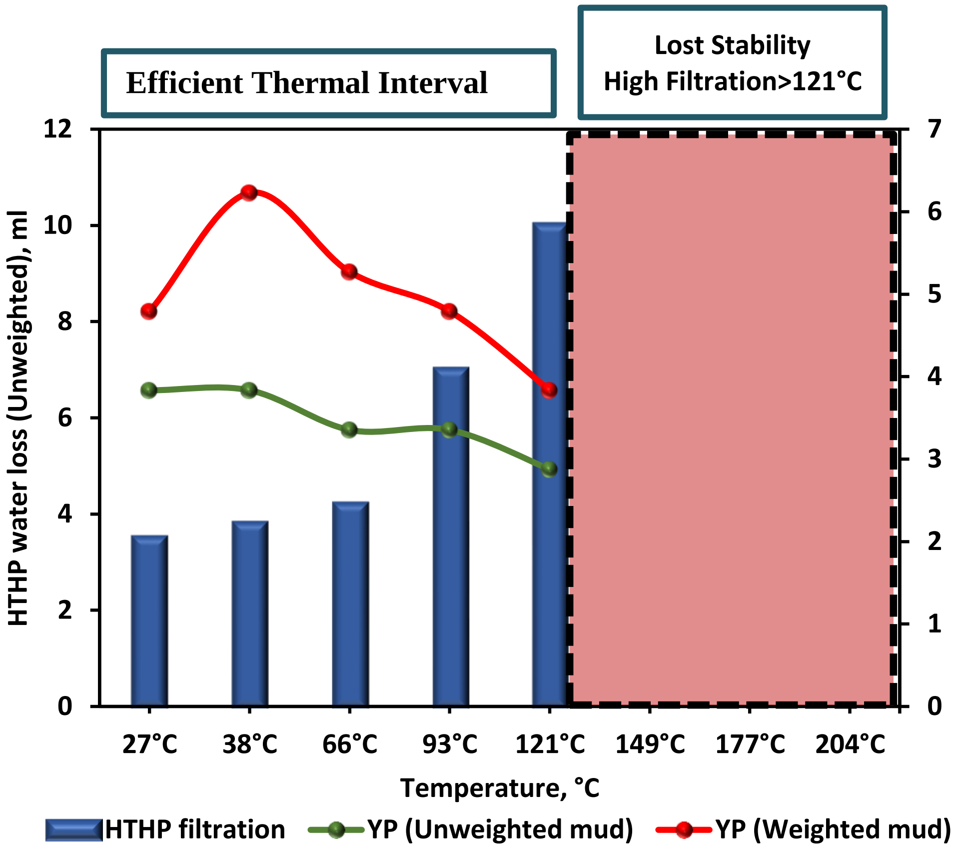

Figure 4.2: Yield point and water loss behaviors of lignosulfonate drilling fluids.

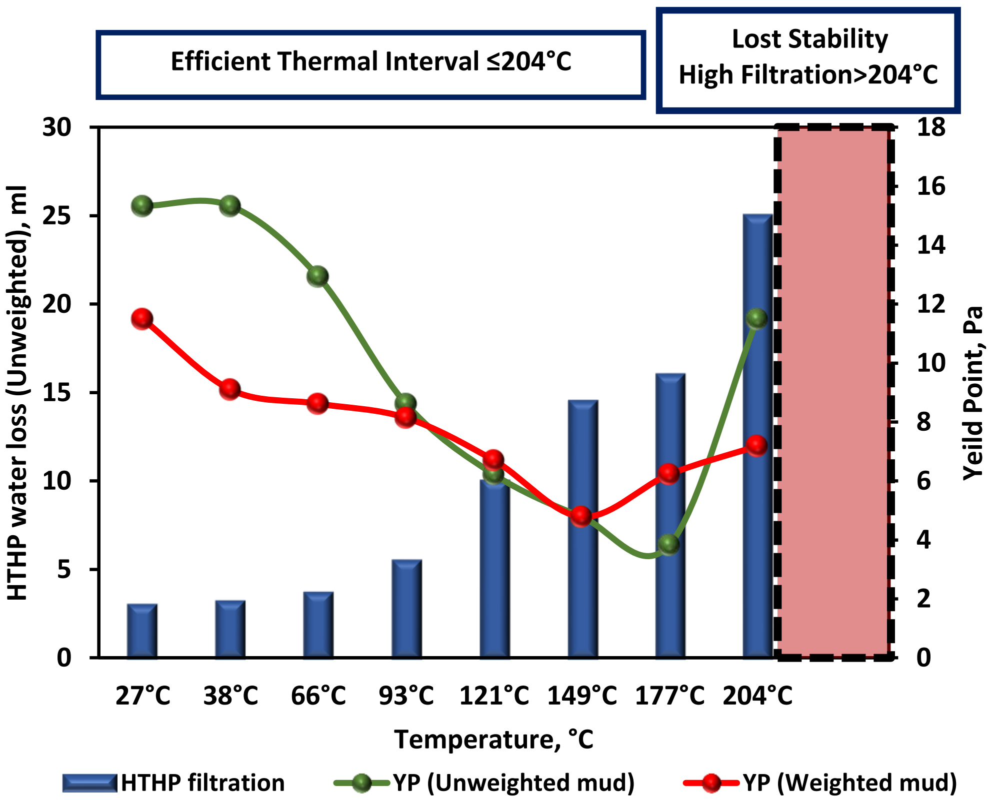

Figure 4.3: Yield point and water loss behavior of sepiolite drilling fluids.

The filtration losses of the unweighted sepiolite drilling fluid samples illustrated in Figure 4.3 were very convenient and attractive in terms of field usage even at high temperatures where the other two drilling fluid systems did not function. Ranging between 3 ml/30min at 38^{o}C to 15.5 ml/30min at 177^{o}C, the water loss values for the unweighted sepiolite fluid samples aged at corresponding temperatures were still acceptable. The water loss values insignificantly increased with increasing aging temperatures up to 177^{o}C as expected. The filtration amount of the sample aged at 204°C (25 ml/30 min) was slightly high in comparison to those of obtained at lower temperatures due to the loss in polymer efficiency and increase in the rate of clay alteration at aging temperatures above 177°C. Even though the amount of 25 ml/30 min filtrate is not far from agreed for such a high temperature, the lower amount of water loss for the weighted sepiolite fluid sample would be expected due to the high amount of solid content (Altun and Osgouei, 2014). A photographic view of both stable and degraded bentonite/polymer drilling fluid system is given in Figures 4.4a and 4.4b at aging temperatures of 66°C and 149°C, respectively. Figure 4.5 shows degradation of lignosulfonate drilling fluid visually at 149°C.

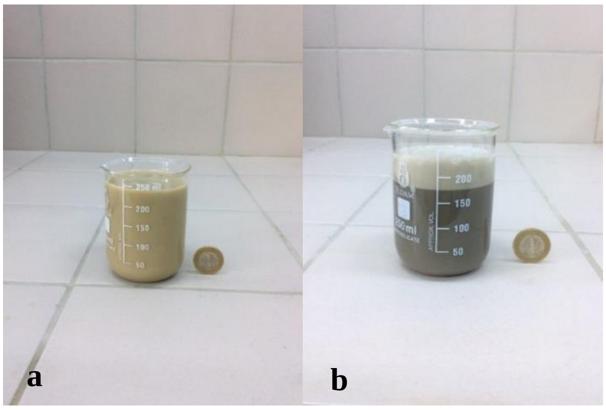

Figure 4.4: Bentonite/Polymer unweighted drilling fluid aged at a) 66°C b) 149°C.

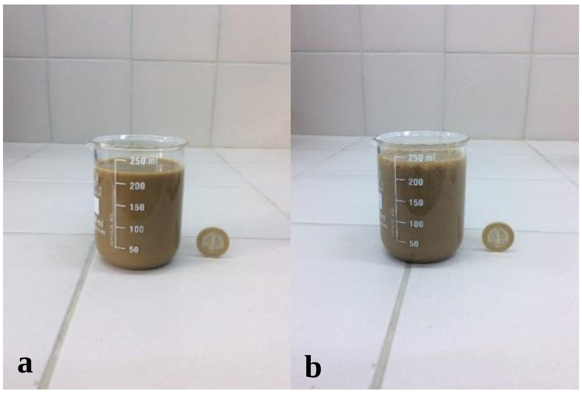

Figure 4.5: Lignosulfonate unweighted drilling fluid aged at a) 66°C b) 149°C.

4.5.2 Differential sticking tendency of drilling fluid samples

The effect of some parameters such as created differential pressure, filter cake quality (being sticky or not), pipe contact area, contact time, and on top of them wellbore temperature must be considered by drilling team. Helping to achieve this goal, the possibility of pipe sticking incidence of these fluid systems were evaluated in this study by the consideration of differential pressure, pipe contact time, and especially high temperature effects. Differential sticking test was conducted for both unweighted and weighted bentonite/polymer and lignosulfonate fluid samples aged at elevated temperatures of 27 to 121°C (80 to 250°F). Attained results were graphically represented in Appendix C through Figures C.1 to C.6 and numerically listed in Tables 4.2 and 4.3. The unweighted and weighted sepiolite samples were also subjected to the same test, and results were given in Figures C.7 to C.10 and summarized in Tables 4.4 and 4.5. Being thermally stable, the sepiolite samples were allowed to thermal aging up to 204°C (400°F). The differential pressure sticking tests on unweighted bentonite/polymer drilling fluid samples aged at 27 to 121°C (80 to 250°F) presented quite low amount of sticking coefficients (0.002) for a set time of 10-minutes and pretty high sticking time of 540 minutes, (Figure C.1). Amount of sticking coefficient slightly increased from 0.0020 to 0.0033 up to 93°C, however it became approximately double (0.0062) for the sample aged at 121°C. This could be a sign of drilling fluid degradation and improper filter cake quality. The sticking time decreased from 540 minutes for the sample aged at 27 and 38°C to 280 minutes for the drilling fluid sample aged at 121°C. It means that at least 540 minutes was required to actualize sticking between the cake and plate for the unweighted bentonite/polymer fluid aged at 27 and 38°C (Figure C.1). In addition, 420 minutes and 320 minutes were enough for unweighted bentonite/polymer drilling fluid aged at 66 and 93°C, respectively to accomplish sticking between the cake and plate. It was obvious that the time required for pipe sticking tends to significantly decrease with increasing temperature. The barite-weighted bentonite/polymer drilling fluid samples reasonably provided higher sticking coefficients and lower sticking times than those of the unweighted drilling fluid samples due to the higher solid content.

Figure C.3 exhibits amount of the sticking coefficient obtained for the weighted bentonite/polymer fluid at different set times. The sticking coefficient slightly and continuously increased with increasing set time. The increase in sticking coefficients were not progressive up to 93°C, however an excessive increase (especially for 60 minutes set time) was observed in the sticking coefficients acquired for the weighted bentonite/polymer sample aged at 121°C indicating possible triggered degradation fluid sample (Figure C.3). Edge effect was witnessed for the bentonite/polymer sample aged at 121°C for the sticking tests only at 90 and 120 minutes (Figure C.3). It means that high the temperature adversely affected the drilling fluid properties and caused the formation of thick mud cake. Therefore, the plate (representing drill pipe) embedded into the formed mud cake so that it caused to form edge surrounding the plate (Figure 4.6).

The calculated sticking coefficients at 10-minutes set time for the unweighted lignosulfonate fluid system were slightly higher than the sticking coefficient values for the unweighted bentonite/polymer fluids. The sticking coefficients were measured to be 0.0030 to 0.0035 for the unweighted lignosulfonate sample aged at 27 to 93°C (Figure C.4). Similar to the bentonite/polymer drilling fluid, severe increase in the sticking coefficients was also observed for the unweighted lignosulfonate fluid aged 121°C. Relatively high sticking times were also recorded for the unweighted lignosulfonate fluid aged at 27 to 121°C. The steel plate was stuck to formation filter cake just after 600 minutes for the sample aged at 27°C. The time required for plate to be stuck decreased rapidly with the increasing aging temperature such that it recorded as 300 minutes in the case of unweighted lignosulfonate fluid aged at 121°C (Figure C.4).

Required sticking times for the unweighted lignosulfonate fluid were somewhat more than the recorded sticking times for the unweighted bentonite/polymer fluid. Effect of barite added to the fluid system to make weighted lignosulfonate fluid was very striking on the measured sticking coefficient as well as the sticking time. The obtained sticking coefficients at 10-minutes set time for the weighted lignosulfonate fluid increased around 10 (0.003 to 0.03) and 15 (0.0065 to 0.1) times compare to the unweighted samples aged at 27 and 121°C, respectively. Besides, the sticking times for the weighted lignosulfonate fluid decreased 80% and 83% with respect to the unweighted samples aged at 27 and 121°C (Figure C.5). The sticking test was repeated at higher set times in order to investigate the effect of contact time on the measured torque and consequently the sticking coefficient. The results of these tests were detailed in Figure C.6.

Table 4.2: Sticking coefficient of Bentonite/Polymer fluid system.

Temperature °C	Sticking Time, minutes		Set Times, minutes						
	unweighted	weighted	unweighted	weighted					
			10	10	30	60	90	120	
27	540	100	0.002	0.023	0.029	0.033	0.043	0.068	Sticking Coefficient
38	540	90	0.0022	0.031	0.038	0.051	0.062	0.113	
66	420	90	0.003	0.055	0.065	0.072	0.084	0.227	
93	320	80	0.0033	0.091	0.103	0.110	0.122	0.143	
121	280	40	0.0062	0.130	0.135	0.140	0.150	0.170	

Table 4.3: Sticking coefficient of Lignosulfonate fluid system.

Temperature °C	Sticking Time, minutes		Set Times, minutes						
	unweighted	weighted	unweighted	weighted					
			10	10	30	60	90	120	
27	600	120	0.0030	0.031	0.057	0.096	0.124	0.140	Sticking Coefficient
38	600	120	0.0030	0.035	0.065	0.106	0.132	0.145	
66	480	90	0.0032	0.054	0.075	0.114	0.139	0.158	
93	360	70	0.0036	0.058	0.078	0.116	0.140	0.160	
121	300	50	0.0067	0.099	0.115	0.162	0.150	0.170	

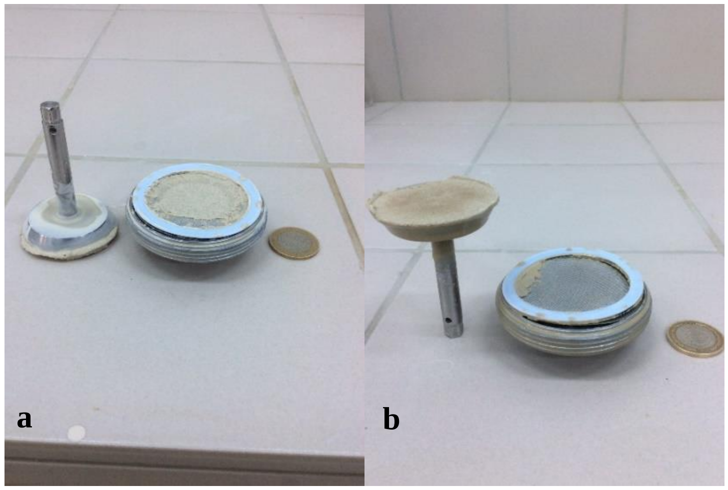

Figure 4.6: Formation mud cake edges at 121°C for 120 minutes set time. a) Bentonite/Polymer, b) Lignosulfonate barite-weighted drilling fluids.

Similar to the bentonite/polymer drilling fluid, continuous increase in the sticking coefficient was recognized with the increasing set time. In contrary of samples aged up to 93°C, an extreme sticking coefficients increase was measured for the weighted lignosulfonate sample aged at 121°C (Figure C.4). Similar to the bentonite/polymer drilling fluid, the edge effect was also detected for the weighted lignosulfonate sample aged at 121°C after 60 minutes set time (Figure C.6).

Performed sticking test for the sepiolite unweighted fluid indicated that at least 30 minutes was required to actualize contact between the cake and plate for the samples aged at 177 and 204°C. The minimum required sticking time was 45, 60, 75, 90, 110, 120 minutes for the unweighted sepiolite samples aged at 149, 121, 93, 66, 38, 27°C, respectively (Table 4.4). The amount of sticking coefficient slightly increased up to 177°C, and a moderate increase in the sticking coefficient was attained for the unweighted sepiolite fluid sample aged at 204°C (Figure C.7). In the case of the barite-weighted sepiolite drilling fluid sample, 10-minutes was sufficient to accomplish sticking plate into the mud cake for the samples aged at 121 to 204°C whereas the minimum sticking time was 30 minutes for the weighted sample aged at 27°C (Figure C.8). The sticking time decreased when the aging temperature of fluid samples rose up in both the unweighted and the barite-weighted sepiolite drilling fluids. This meant that the deposition of mud cake was formed rapidly at high temperatures. The amount of sticking coefficients at lower set times (up to 60 minutes) for the barite-weighted sepiolite samples are higher than those of the unweighted samples

(Table 4.5). However, the difference in sticking coefficient values measured at high contact times between the unweighted and weighted sepiolite fluids were getting less. Although the measured sticking coefficient at 10-minutes for the unweighted sepiolite fluid became more than twice the weighted sample aged at 204°C (0.062 to 0.150), this rate was severely decreased about by half (1.11) in the case of measured sticking coefficient at 120 minutes (0.18 to 0.2) as shown in Figures C.9 and C.10. Figure 4.7 shows the imprint of the torque plate impression on the mud cakes that was used to calculate the sticking coefficient as the stuck cake radius in Equation 4.1.

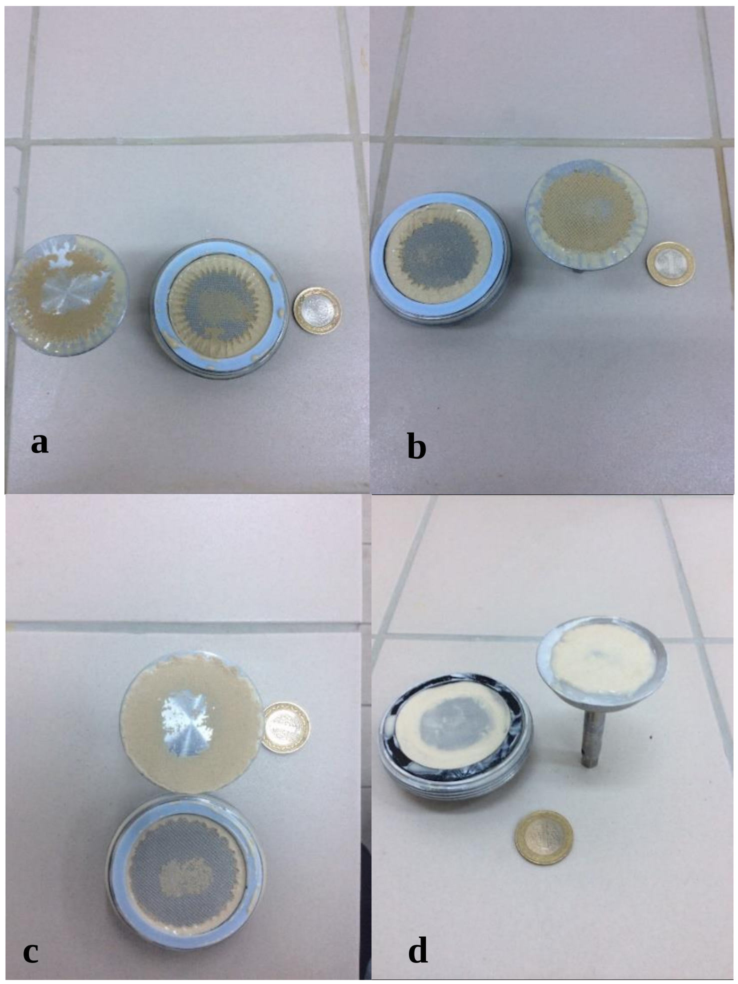

Figure 4.7: Mud cake imprint formation at 66°C for 90 minutes set time.
a) Bentonite/Polymer. b) Lignosulfonate. c) Sepiolite weighted d) Sepiolite unweighted drilling fluids.

Table 4.4: Sticking coefficient of unweighted Sepiolite fluid system.

Temperature °C	Sticking Time minutes	Set Times, minutes						
		10	20	30	60	90	120	
27	120	0.037	0.063	0.065	0.067	0.067	0.067	Sticking Coefficient
38	110	0.037	0.067	0.068	0.069	0.069	0.069	
66	90	0.038	0.070	0.086	0.088	0.089	0.092	
93	75	0.038	0.074	0.100	0.102	0.107	0.107	
121	60	0.044	0.073	0.091	0.112	0.129	0.129	
149	45	0.046	0.048	0.051	0.069	0.072	0.074	
177	30	0.047	0.086	0.123	0.145	0.156	0.157	
204	30	0.062	0.100	0.127	0.167	0.178	0.180	

Table 4.5: Sticking coefficient of weighted Sepiolite fluid system.

Temperature °C	Sticking Time minutes	Set Times, minutes					
		10	30	60	90	120	
27	30	0.077	0.085	0.095	0.102	0.105	Sticking Coefficient
38	25	0.077	0.087	0.104	0.119	0.120	
66	20	0.078	0.093	0.106	0.114	0.115	
93	15	0.084	0.122	0.159	0.169	0.170	
121	10	0.100	0.116	0.118	0.121	0.121	
149	10	0.050	0.080	0.085	0.090	0.091	
177	10	0.144	0.146	0.163	0.182	0.183	
204	10	0.154	0.162	0.187	0.196	0.200	

Attained sticking coefficients for the unweighted sepiolite system were considerably higher than those of the unweighted bentonite/polymer and the lignosulfonate systems. On the other hand, in the case of unweighted sepiolite fluid system, the sticking plate occurred at a quite shorter time than the unweighted bentonite/polymer and the lignosulfonate systems aged at the same temperatures. Unlike the bentonite/polymer and lignosulfonate drilling fluids, the sticking coefficients were not continuously increased with increasing plate contact time for the sepiolite fluid sample. In both unweighted and weighted sepiolite fluid samples, the measured sticking coefficients remained almost constant after 60 minutes of set time (Figures C.9 and C.10). Interestingly, the sepiolite drilling fluid aged at 149°C provided the lowest sticking coefficient values that could be the result of a proper cake quality and drilling fluid properties. This observation was a common result in both the unweighted and weighted sepiolite fluid samples unlike the other two fluid systems. Further studies should be carried out to prove this observation such as XRD and XRF analyses on the mud cake samples.

4.6 Chapter Conclusions

Investigation of differential pipe sticking as one of the borehole instability mechanisms is the staple topic of this study. A brief search in literature reveals that the major loss of time and productivity during drilling operation are due to the stuck pipes. Furthermore, lack of information and knowledge fold the occurrence of this event. Despite the significant attempts exerted by the industry on developing stuck pipe prevention measures, the incidence of stuck pipe has not been avoided. In addition, adverse effect of high temperature on drilling fluid properties can trigger the stuck pipe incident. Thermal effects on differential pipe sticking tendency of three different unweighted and barite-weighted fluid systems were experimentally investigated in this chapter. These fluids are bentonite/polymer, lignosulfonate, and sepiolite drilling muds, respectively. The results presented the impression of temperature, contact time, drilling fluid type and its rheological and filtration properties on sticking pipe possibility by determining sticking time and sticking coefficient for the aforementioned drilling fluids.

High temperatures were the dominant factor on the rheological and filtration properties of all drilling fluids. The variation on the rheology and fluid loss properties of the drilling fluids with temperature indicated that both bentonite/polymer and lignosulfonate fluids were thermally stable up to 121°C, whereas the stability of sepiolite drilling fluids extended to a temperature of 204°C. Among the mud samples, the bentonite/polymer drilling fluids exhibited the worst yield point (YP) performance with increasing temperature. The filtration characteristics of both bentonite/polymer and lignosulfonate fluids could not be obtained above 121°C since the both fluids were flocculated as a result of degradation of bentonite clay above this temperature.

The sticking coefficient (indicator or tendency of differential pipe sticking) of all drilling fluid samples was strongly affected by the temperature variation and noticeably increased with increasing temperature. It was also observed that the sticking time decreased with increasing temperature. The sticking time of the barite-weighted fluid samples were excessively lower than those of the unweighted samples at all temperatures. The decrease in sticking time due to increase in drilling fluid weight is the most for the bentonite/polymer fluid, then followed by the lignosulfonate and sepiolite fluids, respectively.

Both bentonite/polymer and lignosulfonate drilling fluids resulted excessive sticking coefficient values at 121°C which was also another clear indication of flocculation. In addition, unlike the sepiolite drilling fluid, the sticking coefficient values of both bentonite/polymer and lignosulfonate fluids were not stabilized (undesired behavior) and increased with increasing setting time. However, it was observed that the sticking coefficient values of sepiolite fluid samples for various setting time were stable even at 204°C.

The following major findings were obtained in this experimental work:

- Considering both rheological and fluid loss characteristics, the bentonite/polymer and lignosulfonate drilling fluids were thermally stable up to 121°C, whereas the stability of sepiolite drilling fluids extended to a temperature of 204°C.
- Among the fluid samples, the bentonite/polymer drilling fluid performed the most appropriate sticking time for a set time of 10-minutes, then lignosulfonate and sepiolite drilling fluids, respectively up to 121°C.

- The higher the temperature, the higher the sticking coefficient and the higher the tendency of differential pipe sticking were.
- Increased mud weight promotes the occurrence of differential pipe sticking. In general, the higher the mud density, the higher the tendency of differential pipe sticking was observed.
- The sticking coefficients of all drilling fluids for various set times steadily increased with increasing temperature.
- Both bentonite/polymer and lignosulfonate fluids exhibited edge effect (not desirable in terms of pipe sticking) for the setting times of 90 and 120 minutes at 121^{o}C. No edge effect was observed for the sepiolite fluid even at 204^{o}C indicating the superiority of these drilling fluids.
- Even though the sepiolite drilling fluid provided better stability at high temperatures, lubricity agents should be used in sepiolite mud design to extend the sticking time.
- Both bentonite/polymer and lignosulfonate drilling fluids are suitable and preferred for drilling environments exhibiting low to medium temperatures. The sepiolite drilling fluids, however, should be preferred particularly in high temperature environments.

5. THERMAL IN-SITU RHEOLOGICAL PROPERTIES OF SEPIOLITE MUD USING HTHP RHEOMETER

5.1 Introduction

Rheology is the study of the deformation and flow of matter. Viscosity is a measure of the resistance offered by that matter to a deforming force. Shear rate dominates most of the viscosity-related aspects of drilling operations. Because of that viscosity of drilling fluids is the property that is most commonly monitored and controlled.

Formation temperatures and/or drilling fluid properties are two important versatile parameters during circulation, tripping and shut-in processes. It is a well-known fact that the thermo-physical and rheological properties of drilling fluid are affected by the temperature variation in a borehole. Generally, formation temperature increases with increasing depth. Heat transfers to the drilling fluid which is circulating in wellbore due to its direct contact with drilled formations. Therefore, the temperature of wellbore return fluid is relatively higher than fluid pumped from surface. Due to this temperature variation, the viscosity of drilling fluid would be intensively affected. Decrease in viscosity of drilling fluid with temperature increasing was reported in quite many studies. This effect is getting more meaning particularly in geothermal well drilling where temperature is a crucial parameter. Therefore, drilling in formations with high temperatures causes to degradation of drilling fluid. Temperature is reported as one of the main flocculation sources for drilling fluids while it is subjected to hot formations (Bourgoyne et al. 1991).

Viscosity plays an active roles through the solution of most problems in drilling engineering such as well control, cementing, bit optimization, hole cleaning and wellbore hydraulic optimization. Viscosity is the critical factor along with rheological model especially in drilling hydraulics calculation. It is known that viscosity is a function of density that shows significant changes with temperature variations. Density and especially viscosity of drilling fluid could exhibit impressive variation if the temperatures in a well are quite high, indicating high temperature difference between the surface and bottomhole conditions. Therefore, accurate determination of fluid viscosity has the decisive importance so that poor knowledge of the actual behavior of the drilling mud properties with varying temperature might cause some sort of difficulties in programing and controlling drilling operations. The possible difference between measured and calculated viscosity values might directly affect drilling hydraulic design. Hence, it cause to encounter stability problems and leads to poor hole cleaning and accumulation of cutting in wellbore, eventually will cause the abandonment of the well.

Classic Couette type rotational viscometer is traditionally used to measure the viscosity of drilling fluids in ambient condition. Through this traditional method according to American Petroleum Institute (API) standards (API RP13B-1, 2004), following procedure is applied to investigate the effect of temperature on drilling fluid viscosity. The fluid samples are poured into pressurized cells that are placed in a roller oven for 16 hours of aging at elevated temperatures (thermal aging). The samples were subjected to ambient condition to be cooled, and then the rheological properties of the samples were measured using Couette type rotational viscometer (like FANN 35SA/SR-12) at different rotor speeds. This traditional method has generally been applied by drilling operators. However, it is not sufficient method to measure viscosity variations in a real well condition. The temperature of drilling fluid is gradually increased through its way to the bottomhole, and then tends to decrease during going back to the surface. Therefore, the variation of viscosity in a wellbore during drilling operation is an unavoidable fact.

Conventional viscometer along with thermal aging method commonly used to determine rheological properties of drilling muds can be fallacious to project the effect of temperature on drilling mud behavior. The effect of cooling after the thermal aging could be the major reason of possible misleading in the viscosity measurements. On the other hand, values measured with conventional viscometer might be away from reality due to temperature variations. For this reason, it is necessary to use more effective method in order to obtain accurate rheological behavior of drilling fluids. HTHP rheometer measurements, the main objective of experimental part (first phase) in this study, can be used for this purpose.

This part of study consisted of experimentally measurement of rheological properties of the sepiolite base mud under dynamic and high temperature/pressure conditions (in-situ) using thermal rheometer. In addition, bentonite base and KCl polymer muds were also subjected to same tests to provide elaborative comparison among the fluid systems. The viscosities of mud samples were measured in a programmable temperature range of 40 to 260^{o}C at 5 MPa constant pressure at six different rotor speeds (shear rates). Rheological properties of sample fluids were also measured using conventional viscometer after 16 hours of thermal aging up to 232°C and cooling down to room temperature. The results have been compared to build a better understanding of thermal rheological properties of mud samples and difference between the two measurement methods. At the end, the compatibility of rheological behaviors with the well-known rheological models was investigated by the application of curve fitting method.

5.1.1 Literature review

There are many studies in the literature related to clay sepiolite, but a large part of the studies include in the application of sepiolite in other area rather than the usage in drilling muds. These subjects contain a large area such as mineralogical properties of sepiolite clay, physical properties and sepiolite applications in different purposes. Carney and Meyer (1976) were among the pioneer researchers using sepiolite clay to formulate drilling mud. Numerous investigators have studied to formulate a water base mud system that can be used in the high temperature and high saline environments, Carney et al., (1976, 1980, and 1982), Hillscher and Clements (1982), Moussa (1985), Guven et al., (1988), Zilch et al., (1991), Serpen et al., (1992), Serpen (1999), and Serpen (2000). Such mud can also be used in very deep oil and gas wells exhibiting similar temperature conditions to the geothermal environment. One common point among the investigators is that almost all mud samples prepared with sepiolite clay also contain abundant different additives to obtain suitable viscosity and filtration properties that are necessary to execute safe drilling operations at minimum cost. Also, in all of these studies, the traditional standard models were followed in order to evaluate the properties of these kinds of drilling muds such that all muds were subjected to static thermal aging process to simulate related temperature of the wellbore, and the rheological properties were measured after cooling the muds.

Poor filtration property of sepiolite base mud has been a well-known fact and has already been addressed by some investigators such as Carney and Meyer (1976), Serpen et al., (1992), and Altun et al., (2005). High water loss problem was resolved to some degree by using polymers such as Na-polyacrylates (cypan) and synthetic resin (resinex).

In 1976, Carney and Meyer demonstrated a new approach to high temperature drilling fields. They showed the work done on sepiolite mineral in an effort to obtain a drilling fluid capable of withstanding temperatures in the ultra-high range. This included a study on the rheology of sepiolite slurries that have been subjected to temperatures up to 800°F (427°C). There appears to be some changes in the sepiolite after being subjected to temperatures up to 800°F (427°C); however, the basic structure of sepiolite seems to be stable.

In the studies of slurries containing sepiolite, it was observed that the rheological properties of the slurries showed a slight increase in viscosity when measured at elevated temperatures and pressures. Due to this apparent temperature stability, formulations containing sepiolite were prepared and tested at these extreme conditions. Parameters that were important for good drilling fluid performance were measured and recorded. In their study, sepiolite slurries were subjected to temperatures of 750°F (399°C) using a specially designed ultra-high temperature, high pressure thickening time tester. The viscometer data showed an increase in viscosity after thermal aging, but not desirable for good mud rheology. The yield point has experienced little change. Moreover, in an effort to control fluid loss, the slurries were formulated containing sepiolite in conjunction with thinners and various polymers. This approach looked more promising than the previous work, but the fluid loss was still considered to be excessive or unacceptable. After thorough investigation, reasonable fluid losses were obtained with small additions of Wyoming bentonite in conjunction with various polymers. Considering to data obtained from this composition, the reasonable rheological properties such as yield point and gel strength were not obtained.

Drilling fluids prepared with clay of sepiolite without additives protect their structure at temperatures up to 300°F (149°C) and perform better than bentonite and attapulgite when exposed to the same conditions (Carney and Güven, 1980). Sepiolite clay used in conjunction with saponite clay at higher temperatures provided better rheological properties. Sepiolite begins to convert to a smectite at 300°F (149°C) and this reaction is fully completed at 500°F (260°C). However, the fluid loss of drilling muds could not be control in these studies, and the field usage of formulated sepiolite mud was reported to be inadequate.

Structural changes of sepiolite have been investigated by Güven et al., (1988). In this study, rheological properties of the suspension containing sepiolite clay and 1% sodium and potassium salts were examined at high pressure and high temperatures. In their study, it was observed that 60% and 80% of the sepiolite clay was altered into a smectite at temperatures of 700°F and 800°F, respectively. It was also mentioned that the large part of sepiolite clay was transformed to smectite, tremolite and talk (water-containing magnesium silicate) as a result of structural change.

In an experimental work, Serpen et al., (1992) compared sepiolite mud with bentonite and attapulgite muds at room condition and showed that sepiolite mud yielded relatively better rheological and filtration properties for various salinities. The grain size effect on the rheological properties at room temperature of sepiolite slurries were investigated by Carney et al., (1976) and revealed the considerable differences.

It is well known fact that the effects of mixing speed, the mixing time, and the grain size on rheological and filtration properties for the bentonite base muds have trivial effect at room condition and can easily be neglected. In contrast, in an experimental study, Altun et al., (2005) observed that the sepiolite base muds behave in an entirely unusual manner under specified conditions mentioned above. Better viscosities and filtration properties were obtained from the sepiolite muds when the mixing speed and mixing time were increased and grain size was decreased. Also in 1982, Hischer and Clements developed a new high temperature drilling fluid. The system which uses a thermally stable deflocculant and fluid loss additive has been tested in the laboratory at temperatures up to 450°F (232°C). It provided stable rheological properties and good filtration control even in the present of severe cement contamination. Lime may be used with the system to inhibit shale swelling and dispersion. This study investigated the prospects of preparing good high temperature, low lime drilling of green cement. It was found that the low lime mud could be stabilized at high temperatures by the use of a thermally stable polymeric deflocculant (TSPD). Filtration control was enhanced by the addition of the lignite/polymer reaction complex (LPC). The utility and general behavior of this system at 204°C (400°F) and 232°C (450°F) has been characterized. However, using significant amount of LPC polymer (about 42.9 kg/m^3 or 15 lb/bbl) was weak point of this study.

Massive sepiolite deposits are found around Eskisehir, Turkey. In fact, Turkey has the biggest sepiolite reserves in the world, Balci (1999) and Ozturk and Kavak (2004). These clays, having different dolomite content and organic materials, are deposited within the lacustrine series in white, brown, and black colors. In addition, the usage of sepiolite in drilling industry might create important economic opportunities for Turkey.

Recent studies indicated that the filtration properties of sepiolite mud could inexpensively be controlled using commercial additives (Osgouei, A. E, 2010 and Altun et al, 2010). Sepiolite clays used in these studies were taken from the region of Yenidogan-Sivrihisar, and their geological formation and structure were investigated. Unlike bentonite clay, API standards about sepiolite are not well defined; and hence, recent studies could contribute to enhance standard and to develop new definitions by identifying common features of sepiolite clay (Osgouei, A. E, 2010 and Altun et al, 2010).

Santayo et al., (2001) evaluated the rheological properties of eleven drilling fluids that were sampled from field area using a thermal rheometer. They developed an empirical correlation which was expressed the variation of rheological parameters with temperature. Their experiments were carried out at temperatures between 25-180°C under 100 rpm shear rate. The other common rheometer shear rates (3, 6, 200, 300, 600 rpm) were not considered that was a weak point of this study. Moreover, they did not use sepiolite muds in their study.

As a result of the literature review, it is obvious that the works on sepiolite base drilling fluids are not sufficient. In other words, all the attempts have been failed in terms of controlling rheological and filtration characteristics of sepiolite muds. Sepiolite was used in most of the work as additive to improve properties of main clays such as bentonite, saponite, and attapulgite. Thus it is obvious that considering sepiolite clay as a main component of drilling muds can be important area of research on helping drilling fluid industry to have more stable mud at high temperatures.

5.1.2 Preparation of sepiolite base muds

API RP-13B Standard procedures were employed throughout the laboratory work to prepare unweighted and weighted mud samples. All the sample muds were based on the formulation of 350 ml of fresh and salt water that contains 57 kg/m^3 (20 gr/350 ml) of sepiolite clay and some commercial additives. 429 kg/m^3 (150 gr/350ml) barite was added to fresh water mud sample to prepare weighted sepiolite drilling fluid. In addition, the effect of salinity on sample properties was investigated in two different ways.

In the first case, sodium chloride (NaCl) was mixed with water phase to prepare two different brine (NaCl) concentrations, 200 g/l (semi saturated) and 400 g/l (fully saturated), respectively. In the second case, sodium chloride (NaCl) was added to the fresh water sepiolite base mud as a contaminant. In this case, two different NaCl concentrations (171 and 342 kg/m^3) were added to the fresh water mud composition. Moreover, commonly used two drilling fluids (Bentonite/Polymer, and Lignosulfonate base drilling fluids) were selected and examined in the same tests for making comprehensive comparison to sepiolite base mud.

Commercial bentonite clay provided by Karakaya Company was used as a major additive for bentonite/polymer and lignosulfonate drilling fluids. The other additives, all in technical grades, used in formulation of drilling fluids were i) Sodium carbonate (soda ash, Na_2CO_3, product of Karakaya) and Sodium hydroxide (caustic, NaOH, product of Karakaya) to remove water hardness and PH control, ii) A commercial deflocculant (polymer-1, anionic acrylic copolymer used as thinner, product of Halliburton) for controlling rheological properties in water-base systems for up to 232°C and providing high temperature stability, iii) Filtration control agent (polymer-2, vinyl amide/vinyl sulfonate copolymer, product of Halliburton), iv) Chrome free lignosulfonate (CFL) as deflocculants, temperature stabilizer, filtration control additive and gel strength reducer, v) Xanthum Gum (XCD), a biopolymer, used as a viscosifier to enhance drilling fluid rheology, ensuring efficient hole cleaning, vi) Carboxymethyl cellulose (CMC) acts as a viscosity modifier and water retention agent, vii) Polyanionic cellulose (PAC-LV) acts as a filtration control chemicals with negligible effect on viscosity, viii) Weighting agent (API Barite).

Seven types of sepiolite base mud listed in Table 5.1 along with bentonite/polymer and lignosulfonate mud samples were prepared to be evaluated in terms of thermal rheological stability. Composition of the above mentioned sepiolite and other two muds were given in Table 5.2.

Table 5.1. Sepiolite mud types

No	Mud	Specification	Description
1	Water + sepiolite clay	No additives	Fresh water
2	Fresh water	With additives	Fresh water
3	Semi-saturated	additives + NaCl	Brine
4	Fully-saturated	additives + NaCl	Brine
5	Fresh water + 171 kg/m^3 NaCl	additives + NaCl intrusion	Fresh water
6	Fresh water + 342 kg/m^3 NaCl	additives + NaCl intrusion	Fresh water
7	Weighted fresh water	additives + Barite	Fresh water

Table 5.2. Compositions of drilling fluid samples.

Substance	Quantity (kg/m^3)				
	Lignosulfonate	Bentonite Polymer	Sepiolite Fresh water/brine	Sepiolite + NaCl	
Sepiolite	-	-	57	57	57
NaOH	0.17	0.17	-	-	-
Soda Ash	0.286	0.286	0.286	0.286	0.286
Bentonite	57	57	-	-	-
Polymer -	-	5.7	11.43	11.43	11.43
Polymer -	-	-	14.28	14.28	14.28
CFL	8.58	-	-	-	-
CMC	8.58	-	-	-	-
PAC-LV	-	5.7	-	-	-
XCD	-	5.7	-	-	-
*Barite	-	-	429	-	-
NaCl	-	-	-	171	342

* USED ONLY IN WEIGHTED DRILLING FLUID SAMPLES.

5.1.3 Determination of rheological properties

The rheological properties such as apparent viscosity (AV), plastic viscosity (PV), yield point (YP), and gel strength (GS) were measured and determined using two different equipment. The first one was Couette type viscometer (Fann Model 35A/SR-12) that was used to measure rheological properties of mud samples before and after thermal aging process. Prepared muds were subjected to hydrothermal treatments in an aging cell that was rolled in an oven at temperatures up to 232°C (450°F) for 16 hours. During this period, it was accepted that all chemical reactions as well as clay mineralogical alteration by the effect of temperature were completed. Aging cells containing mud samples were pressurized using nitrogen gas to prevent vaporization.

To accomplish this, amount of appropriate nitrogen pressure corresponding to 10-20% higher than vapor pressure of water was used. For example, for the highest temperature condition (260°C) about 5 MPa (700 psi) gas pressure was applied. The maximum applicable aging temperature for the aging cell was reported as 260°C (500°F) by the manufacturer. However, the all mud samples aged at this temperature were failed due to vaporization. This might be due to mechanical faults formed because of the excessive usage. Therefore, all mud samples were aged up to 232°C in the concept of first way (traditional method) to determine rheological properties.

The rheological properties of thermally aged mud samples were measured at six different viscometer speeds (600, 300, 200, 100, 6 and 3 rpm). An extra devise (heating jacket) was used along with the conventional viscometer to maintain measurements at constant temperature. Using this additional equipment, the rheological measurements were carried out at two different temperatures of 27°C (80°F) and 49°C (120°F).

The rheological properties measured by conventional viscometer might cause some sort of deceptive results that were far from reality. The reason might stem from the preparation process when the mud samples were required to be cooled down in order to be ready for viscometer measurements. It is well-known fact that the viscosity of liquid phase of mud samples changes with temperature variations. The viscosity of most water base fluids will be decreased with increasing temperature. However, because it was not possible to measure the in-situ thermal rheological properties of mud samples, the HTHP rheometer introduced previously was used to achieve this goal. The rheological properties of mud samples might demonstrate significant differences depending on mud composition and additive materials. Therefore, determination of rheological behavior in the borehole temperature conditions has vital importance in terms of proposing effective drilling well program and hydraulic optimization.

This study is mainly based on determining the in-situ thermal rheological properties of sepiolite mud using HTHP rheometer (Fann Model 50). The rheological properties of mud samples listed in Table 5.1 along with bentonite/polymer and lignosulfonate muds were measured using HTHP rheometer at temperature variations of 37 and 260°C (100-500°F) with 5.5°C (10°F) increments under differential pressure of 50 bar (≃700 psi). This compare controlled device can save all the measured data such as temperature, pressure, shear rates, shear stress, time, and viscosity at the specified temperature. Another advantage of this device is to measure the rheological properties of sample in cycles; i.e., both heating and cooling. Cycling rheological measurements can provide better insight to understand rheological variations due to thermal alteration in the clay structure. The rheological variation can be reported as a function of temperature as well as time.

5.2 Rheological Properties of Sepiolite Mud Using Conventional Viscometer

The rheological properties of sepiolite muds listed in Table 5.1 were measured using classic viscometer according to the first method explained in the previous section. API RP 13 B-1 (2004) was followed during all measurements on prepared mud samples. The results of rheological measurements using conventional viscometer were tabulated and given in Appendix-D through Tables D1 to D7. The values of plastic viscosity and yield point given in tables were calculated using dial reading values at 600 and 300 rpm. These values are known as the parameters of Bingham Plastic rheological model. However, the rheological parameters for each rheological model, also given in this chapter, were determined based on the six dial readings from the viscometer. Similarly, the values of gel strength measured at 10 second, 1 minute, and 10 minutes were presented for the each sepiolite mud sample and tabulated. Evaluation of rheological properties of sepiolite muds were discussed in the following section. The results were also given graphically, and visualization was increased on figures by connecting data points to each other using continuous line.

5.2.1 Fresh water sepiolite base muds

The formulation of fresh water sepiolite mud was given in Table 5.2. The rheological measurements were conducted on thermally aged mud samples ranging from 38°C to 232°C. The results of measurements for each sample were tabulated in Appendix-D and specified by aging temperature. As an example, the results for the mud sample aged at 65°C were given in Table 5.3. To compare results, the values of shear stress measured at 27 and 49°C and conducted at 600 rpm were also given graphically for the thermally aged mud samples. The shear stress variation of unweighted fresh water sepiolite mud sample for the specified conditions was shown in Figure 5.1. The shear stress values measured at 49°C were lower than those measured at 27°C through all aging temperatures, as expected. Decrease in viscosity with increasing temperature was observed until the gelation temperature.

Table 5.3. Rheological properties of unweighted fresh water sepiolite mud aged at 65°C.

Aging Temperature, °C		65	
Measured temperature, ˚C		27	49
*Dial readings	600 rpm	70	46
	300 rpm	44	30
	200 rpm	35	23
	100 rpm	23	14
	6 rpm	5	3
	3 rpm	4	3
Plastic viscosity, Pa-s		0.026	0.016
Yield point, Pa		8.622	6.706
*Gel strength (1sec/1min/10min), dial reading		5 / 9 / 20	3 / 7 / 15

*Multiplying dial reading to 0.479 to obtain in Pascal

It was observed that the amount of viscosity steadily decreased up to 149°C, and then tended to increase up to the final aging temperature of 232°C. The amount of shear stress decreased from 37.78 Pa at 27°C to 19.42 Pa at 149°C and then increased to 26.55 Pa at 232°C of aging temperatures in the case of unweighted fresh water mud sample when measured at 27°C. On the other hand, amount of shear stress started with 26 Pa at 27°C and decreased to 14.29 Pa at 149°C and finalized with 20.42 Pa at 232°C of aging temperatures when measured at 49°C.

The reason of increment in viscosity after 149°C might refer to the degradation of polymers used in the mud composition. However, despite of this condition, the rheological values measured at 149°C and above this temperature were still in acceptable range and have met the requirements. Therefore, it can be inferred that the sepiolite mud provided desirable rheological properties and efficiency at such high temperatures. The change in rheological behavior of sepiolite muds will be discussed in Section 5.3.

The values of shear stress at 600 rpm measured at 27 and 49°C for barite-weighted fresh water sepiolite mud sample were depicted in Figure 5.2. Similar to unweighted mud sample, the shear stress values measured at 49°C were lower than those measured at 27°C through all aging temperatures. Due to existing weighting agent (barite), the viscosity of weighted mud sample was measured higher than that of unweighted sample. The same rheological behavior as in the unweighted sample was observed in the case of weighted sample. Viscosity decreased until 177°C and then increased beyond this temperature.

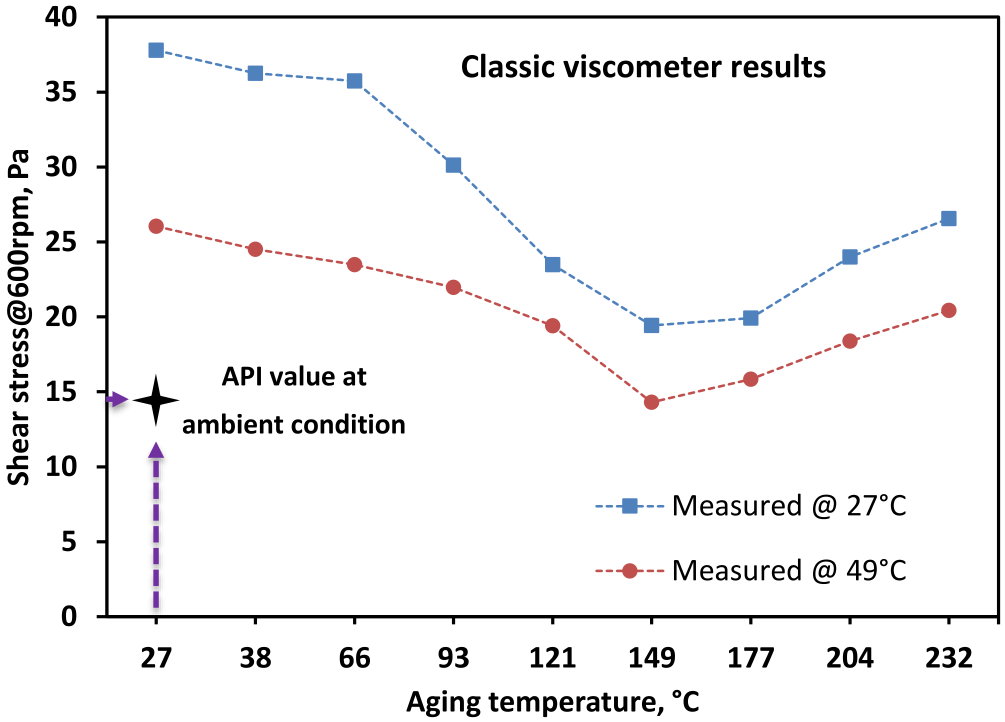

Figure 5.1: Shear stress at 600 rpm for unweighted fresh water sepiolite mud.

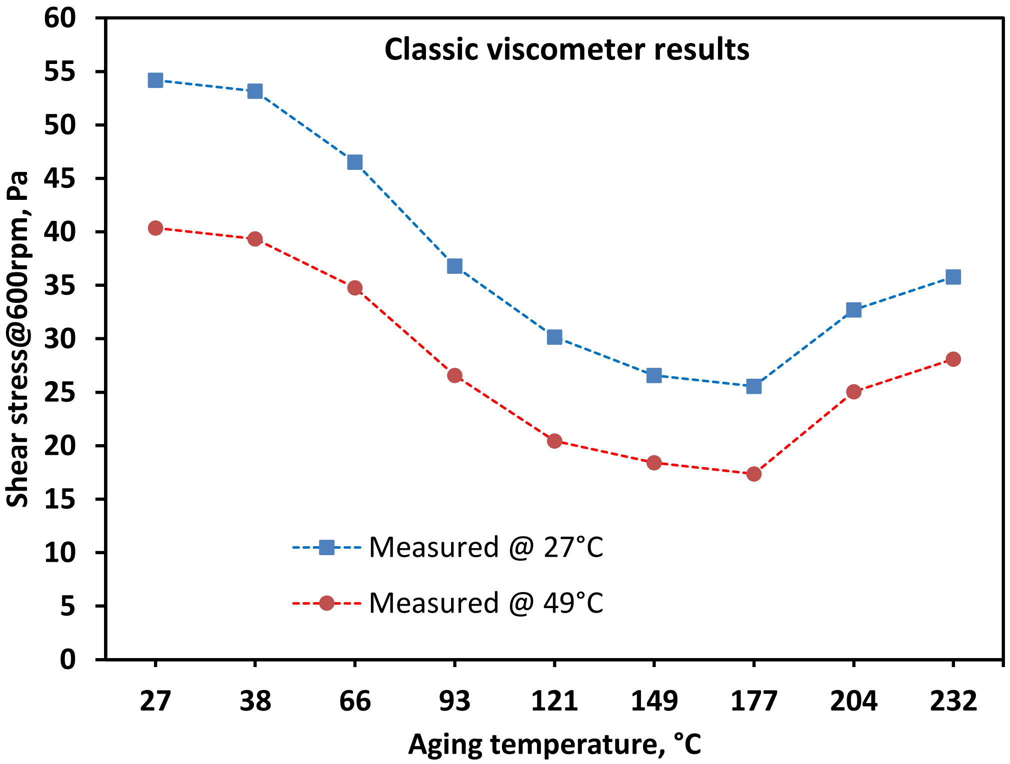

Figure 5.2: Shear stress at 600 rpm for barite-weighted fresh water sepiolite mud.

The amount of shear stress decreased from 54.17 Pa at 27°C to 25.55 Pa at 177°C and then increased to 35.77 Pa at 232°C of aging temperatures in the case of weighted fresh water mud sample when measured at 27°C. On the other hand, amount of shear stress initiated with 40.37 Pa at 27°C and decreased to 17.37 Pa at 177°C and finalized with 28.11 Pa at 232°C of aging temperatures when measured at 49°C. In addition, similar to unweighted mud, barite-weighted sepiolite mud yielded effective rheological properties at extremely high temperatures too. The aging temperature required to reach minimum shear stress (also the indication of apparent viscosity) in the case of barite-weighted sample was higher than that of the unweighted sample. This observation should be further investigated in another research study.

5.2.2 Salt saturated sepiolite muds

The variation of shear stress at 600 rpm measured at 27 and 49°C for semi-saturated and fully-saturated sepiolite muds were shown in Figure 5.3 and 5.4, respectively. Similar to the weighted and unweighted muds, the shear stress values measured at 49°C were lower than those measured at 27°C through all aging temperatures. The value of shear stress measured at 27°C decreased from 37.78 Pa in the case of unweighted sample to 12.24 Pa and 11.24 Pa in the case of semi and fully saturated muds respectively for samples with the aging temperature of 27°C.

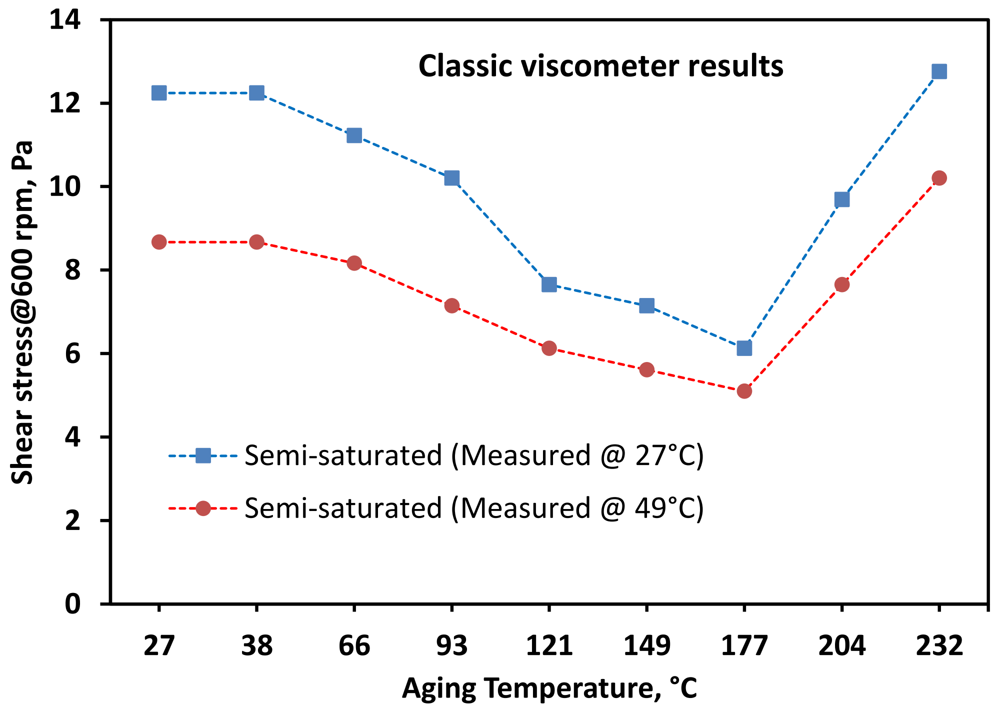

Figure 5.3: Shear stress at 600 rpm for semi-saturated sepiolite mud.

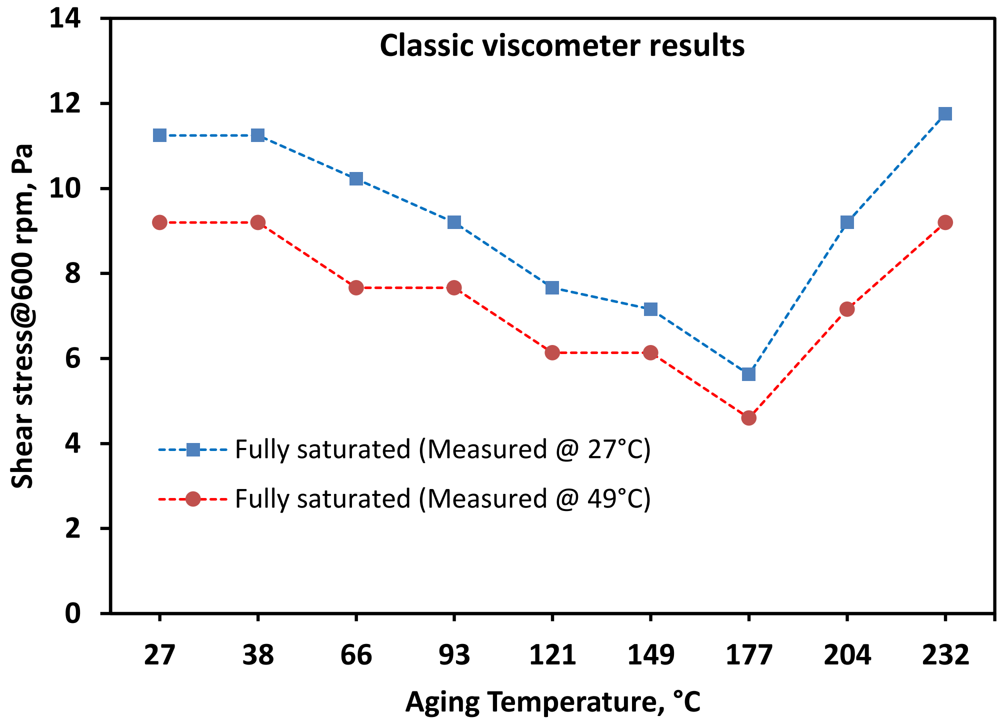

Figure 5.4: Shear stress at 600 rpm for fully-saturated sepiolite mud.

Addition of salt resulted in higher aging temperature to reach minimum shear stress. It was observed that the sepiolite mud prepared with NaCl was able to provide appropriate rheological values especially at high temperatures even though some decrease in shear stress values with respect to unweighted sepiolite muds were observed. Interestingly, the rheological values were not significantly changed with increasing salinity (doubling the amount of NaCl). Such that the values of shear stresses for the fully-saturated mud were almost the same with those of the semi-saturated sample at all aging temperatures. The amount of shear stress measured at 27°C decreased from 12.24 Pa at 27°C to 6.12 Pa at 177°C and then increased to 12.73 Pa at 232°C of aging temperatures in the case of semi-saturated mud sample. The same trend followed by the fully-saturated sample with the values of 11.24, 5.62, and 11.75 Pa at the corresponding aging temperatures. This was the clear indication of efficiency of the sepiolite muds in high saline environments.

5.2.3 Properties of sepiolite muds with salt intrusion

The variation of shear stress at 600 rpm measured at 27 and 49°C for sepiolite muds containing 171 and 342 kg/m^3 NaCl were shown in Figure 5.5 and 5.6, respectively. Similar to the weighted and unweighted muds, the shear stress values measured at 49°C were lower than those measured at 27°C through all aging temperatures.

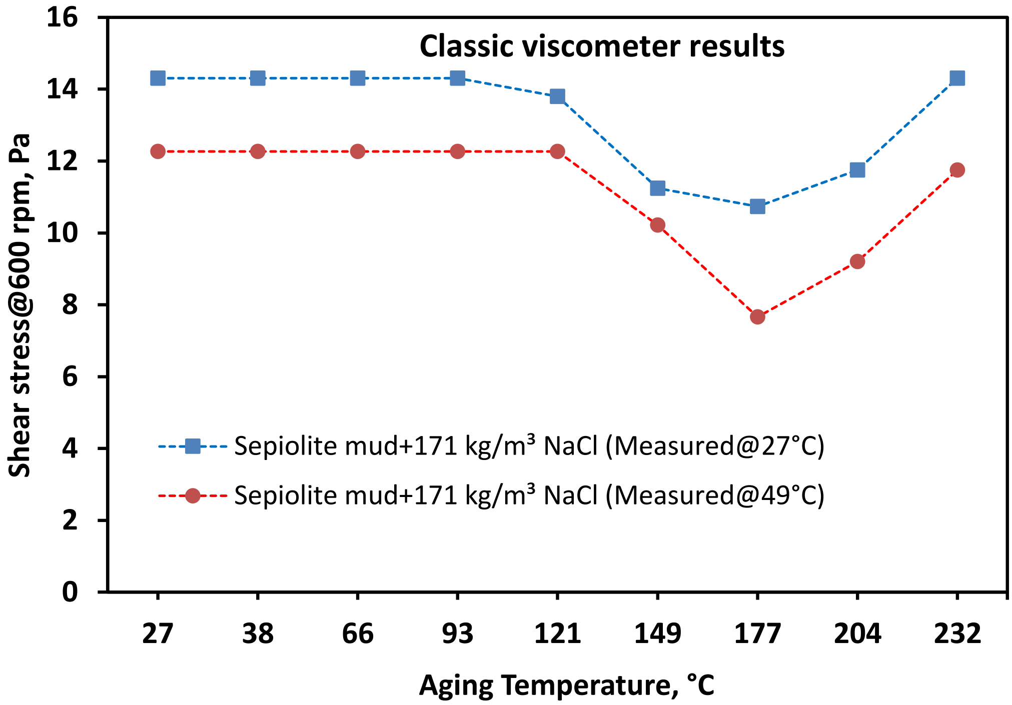

Figure 5.5: Shear stress at 600 rpm for sepiolite mud with 171 kg/m^3 NaCl.

The value of shear stress measured at 27°C decreased from 37.78 Pa in the unweighted sample to 14.31 Pa and 16.35 Pa for sepiolite mud with 171 and 342 kg/m^3 NaCl intrusion at the aging temperature of 27°C, respectively. Similar observation with salt saturated mud samples was recorded in the case of testing sepiolite muds when subjected to huge amount of salt intrusion. There was not significant change in the shear stress of this sepiolite mud up to 121°C which was recorded as around 14 Pa. After that it tended to decrease until 177°C to 10.73 Pa and then increased to 14.31 Pa at 232°C of aging temperatures when amount of 171 kg/m^3 NaCl were externally added to the mud system. These results were obtained at 27°C of rheological measurement using conventional viscometer.

The amount of viscosity increased with increasing amount of salt intrusion as seen in Figure 5.6. Similarly, there was not significant change in the shear stress of sepiolite mud when subjected to amount of 342 kg/m^3 NaCl up to 149°C (recorded around 16 Pa). Then, shear stress measured at 600 rpm decreased to 14.8 Pa at 177°C and rose to 28 Pa at 232°C of aging temperatures. Increment in viscosity could be the sing of initiation gelation in the mud. This observation should be further investigated along with filtration properties of such sample. It can be inferred that the sepiolite muds are more tolerable to salt intrusions than the sepiolite muds prepared with salt water. Shear stress at aging temperature of 232°C was two-fold higher than the values obtained at

27°C of aging temperatures. The shear stress difference between the measurement temperatures of 27°C and 49°C remained almost constant up to the aging temperature of 149°C (so-called gelation temperature) and diminished fast beyond this temperature.

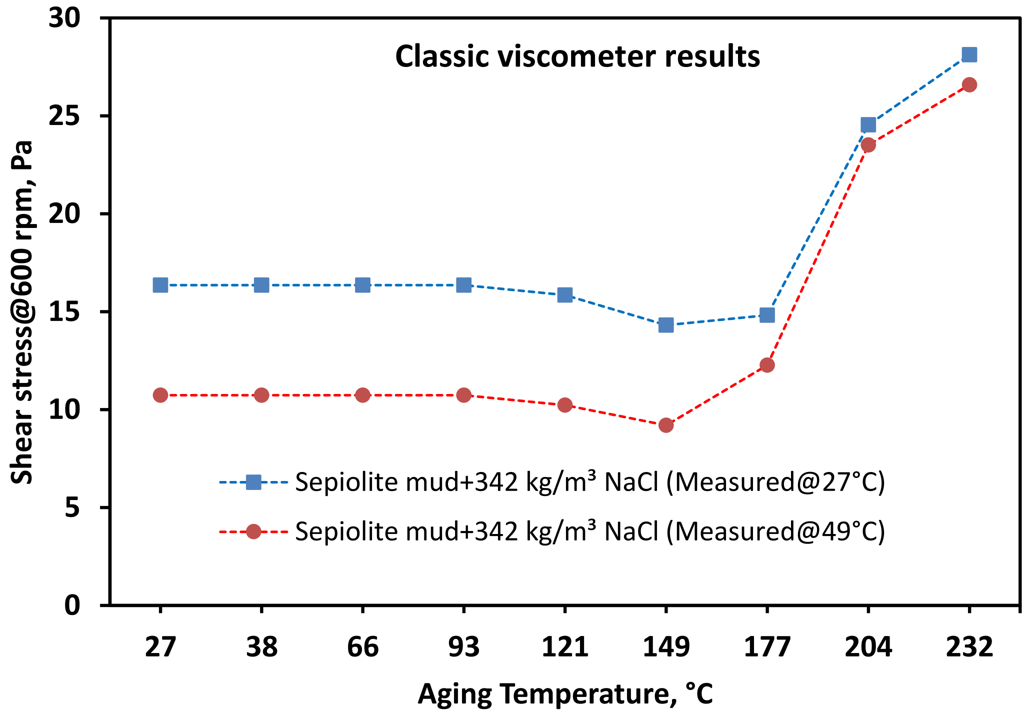

Figure 5.6: Shear stress at 600 rpm for sepiolite mud with 342 kg/m^3 NaCl.

Salt intrusion did not affect the shear stress up to aging temperature of 121°C. In addition, the overall change in the shear stress considering the all aging temperatures in the case of external salt intrusion was smaller than those of the other sepiolite mud types. The maximum shear stress variation was observed in the fresh water unweighted mud sample. Less shear stress values were obtained for the semi and the fully saturated sepiolite muds than those of the sepiolite muds under the influence of external salt intrusion.

The rheological behavior of all sepiolite muds were illustrated in Figure 5.7. The effectiveness of sepiolite mud was the impressive point and clearly exhibited in this figure. The change in shear stress and its corresponding viscosity for the salt water sepiolite muds is much less than viscosity variation through fresh water sepiolite mud. As seen in Figure 5.7, the amount of maximum change in shear stress was 18.36 Pa recorded between aging temperatures of 27°C and 149°C for the unweighted fresh water sepiolite mud sample. However, the value of shear stress in fully-saturated and semi-saturated mud samples was measured with the maximum change of 5.62 and 6.12 Pa between the aging temperatures of 27°C and 177°C, respectively. Therefore, the usage of sepiolite mud as an effective mud system through drilling salt domes or formations containing water with high concentration of salt would be highly sensible idea.

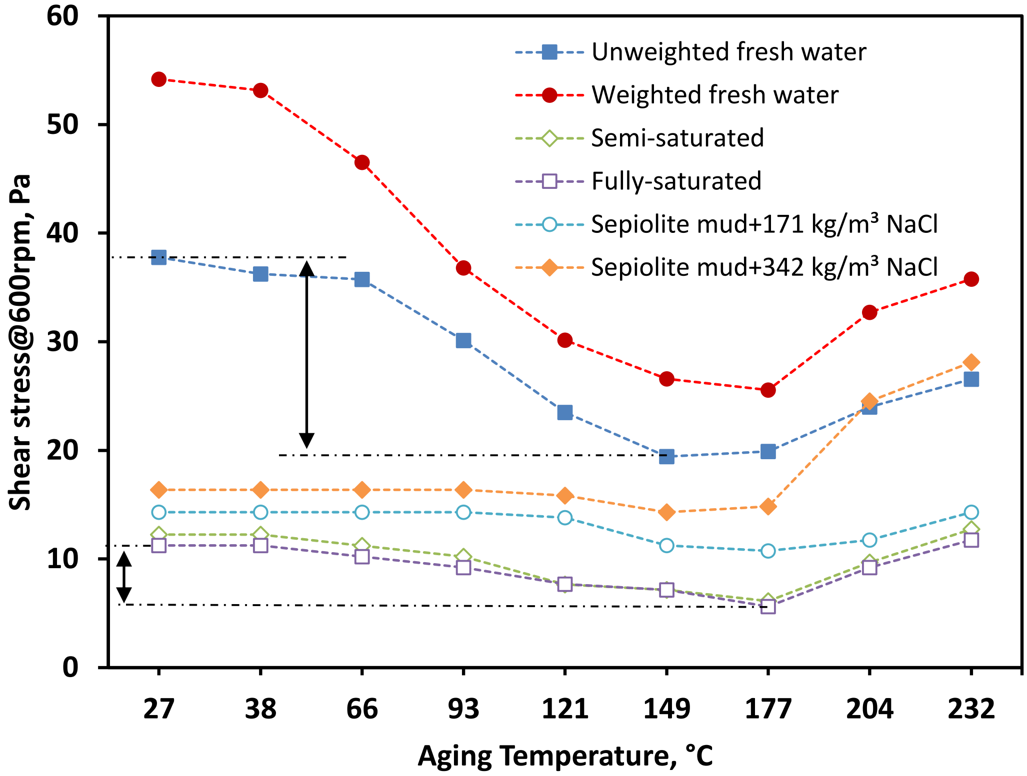

Figure 5.7: Shear stress at 600 rpm for sepiolite muds, (Measured @ 27°C).

5.3 Thermal In-Situ Rheological Properties of Sepiolite Mud Using HTHP rheometer

Knowledge of in-situ rheological properties of a drilling fluid concerning temperature variations has indisputable importance for minimizing borehole instability and enhancing well design. It is also fact that safe drilling practices in environments with narrow mud weight windows dictate rigorous assessment and analysis of temperature and pressure effects on the rheological properties of drilling muds. As mentioned before, rheological evaluation based on thermal aging method with conventional viscometer might bring out illusory results in drilling optimizations. Therefore, it is essential to determine accurate rheological properties at elevated temperatures when assessing drilling optimization properly.

Thermal rheological properties of sepiolite muds were measured using Fann Model 50 SL high temperature rheometer (Figure 2.13) and the related results were presented in this section. In addition, obtained results at elevated temperatures have been compared with those from the conventional viscometer relying on thermal aging method. Moreover, commonly used two drilling muds (bentonite/polymer and lignosulfonate mud) were also subjected to the test with HTHP rheometer to determine the thermal rheological properties and to provide a comparison with the sepiolite muds. Therefore, the mud samples were subjected to in-situ thermal rheological measurements using Rheometer 50 SL at temperature ranges of 38^{o}C to 260^{o}C with a temperature increments of 5.55^{o}C (10°F). 12 dial readings have been recorded for each temperature and each rotation speed by the rheometer to get the higher accuracy.

Reported results were based on the average values of these readings. Rheological measurements were applied to seven categories of sepiolite muds listed in Table 5.1. Obtained results for each mud system were tabulated and presented in Appendix-E through Tables E1 to E7 at in-situ temperatures ranging from 38^{o}C to 260^{o}C at six different rotor speeds of the rheometer. These tables have contained the shear stress obtained at 600 rpm, elapsed time, temperature, and Newtonian viscosity. These data were extracted from raw data sheet provided by computer software connected to the rheometer. Each mud system was evaluated in the following sections.

5.3.1 Thermal rheological behavior of fresh water sepiolite suspension (without additives)

The sample of sepiolite suspension was prepared by adding only 20 gr sepiolite clay to 350 ml water. Amount of shear stress at 600 rpm rotation speed is an important index as mentioned in API standard. Therefore, the results were given here based on this value at different temperatures. Thermal rheological properties of fresh water sepiolite mud (without additive) were depicted in Figure 5.8. HTHP rheometer is capable to record the rheological properties while heating the sample as well as cooling it down.

Therefore, investigating the variation on the rheological properties of mud sample due to possible mineral alteration in the structure of sepiolite clay, the mud sample without additives were tested during the cooling period down to 38°C after heating up to 260°C. As stated in literature review section, an alteration in sepiolite clay structure was started at 149°C and completed at 260°C. As also mentioned, sepiolite structure mainly turns into saponite with increasing temperature and time that means the amount of sepiolite decreases in the mud system. Therefore, sepiolite slurry without additive subjected to HTHP rheometer test is very important in terms of having deep insight about the effect of such alteration on the rheological properties.

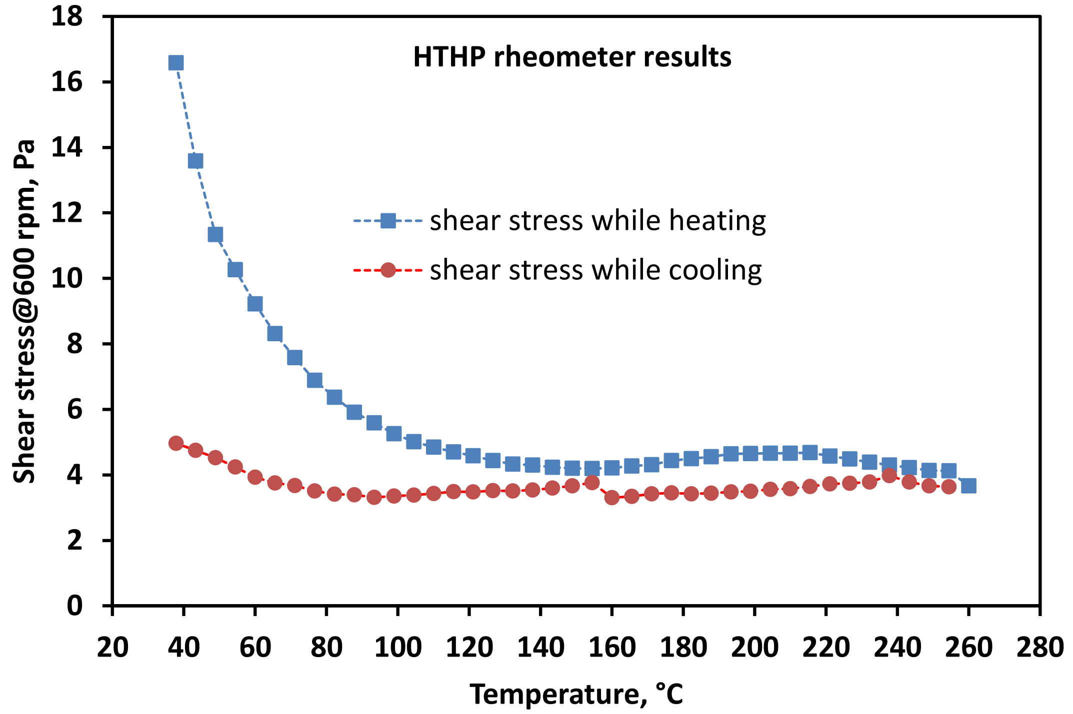

Figure 5.8: Thermal rheological behavior of fresh water sepiolite suspension (600 rpm).

Square shaped points representing the shear stress values at 600 rpm shown in Figure 5.8 was obtained during the heating period from 38ºC to 260ºC. The amount of 16.58 Pa (37 lb/100ft^2) for shear stress was recorded at 38ºC. The value of shear stress decreased rapidly with increasing temperature until 120°C, and then the shear stress decline rate decreased and made a plateau with the further temperature increment. After 120ºC, no changes were observed in shear stress such that amount of about 4.8 Pa (10 lb/100ft^2) was stabled up to 260ºC. It was obvious that decrement in shear stress meant viscosity reduction at the same time. This behavior clearly indicated that sepiolite clay could provide and maintain viscosity at high temperature even if alteration was occurred in the sepiolite clay structure.

Figure 5.8 also indicated the rheological behavior of fresh water and sepiolite clay suspension during cooling period from 260 to 38ºC right after the heating process. The amount of shear stress was remained almost constant at 3.83 Pa (8 lb/100ft^2) through cooling period down to 65ºC. It started to increase slightly up to 4.8 Pa during cooling period between 65 and 38^{o}C. The recorded shear stress value for sepiolite water suspension after cooling down to 38 ^{o}C was lower than the shear stress value (16.58 Pa) measured for the sample in the beginning of the test at the specified temperature. This behavior was another evidence verifying thermal alteration of sepiolite clay structure to form other clay as stated in the literature. It was also observed that the alteration was not reversible during the period of cooling.

The results also demonstrated that the shear stress values during cooling period were lower than those recorded while heating the sample up (Figure 5.8). The little increase in shear stress (viscosity) trend in the cooling period could be mainly attributed to the increase in viscosity of liquid phase rather than the effect of solid phase (sepiolite). The clay effect in this trend was postulated to be negligible. The amount of differences was not significant at 121 ^{o}C and beyond this temperature. However, this gap increased with decreasing temperature.

Thermal rheological properties of sepiolite clay and semi and fully saturated water suspensions were also investigated using HTHP rheometer to dissect the effect of temperate in details as well as salinity. In addition, the thermal rheological properties of commercial bentonite clay and fresh water suspension were also examined to provide a better comparison between two clays. The results of measurements for the suspensions were illustrated in Figure 5.9. The clear observation inferring from the results indicated the shear stress (viscosity) increment with increasing salinity in the case of sepiolite suspensions. The amount of shear stress measured at 177^{o}C was recorded as 5.05, 7.94, and 9.04 Pa for the sepiolite clay and fresh water, semi saturated, and fully saturated suspensions, respectively. This was a clear indication of sepiolite clay efficiency in saline environments as mentioned in the literature.

The second notable observation withdrawn the figure was the clear view of flocculation behavior in the bentonite suspension with increasing temperature up to 77°C (Figure 5.9). The shear stress of bentonite suspension was excessively increased from 10 Pa at 38^{o}C to 17.4 Pa at 77 ^{o}C, and then tended to sharp decrease up to 260^{o}C. The reason of this behavior must be further investigated using XRD and XRF analysis through all sepiolite and also bentonite samples to determine thermal alteration in the structure of clays.

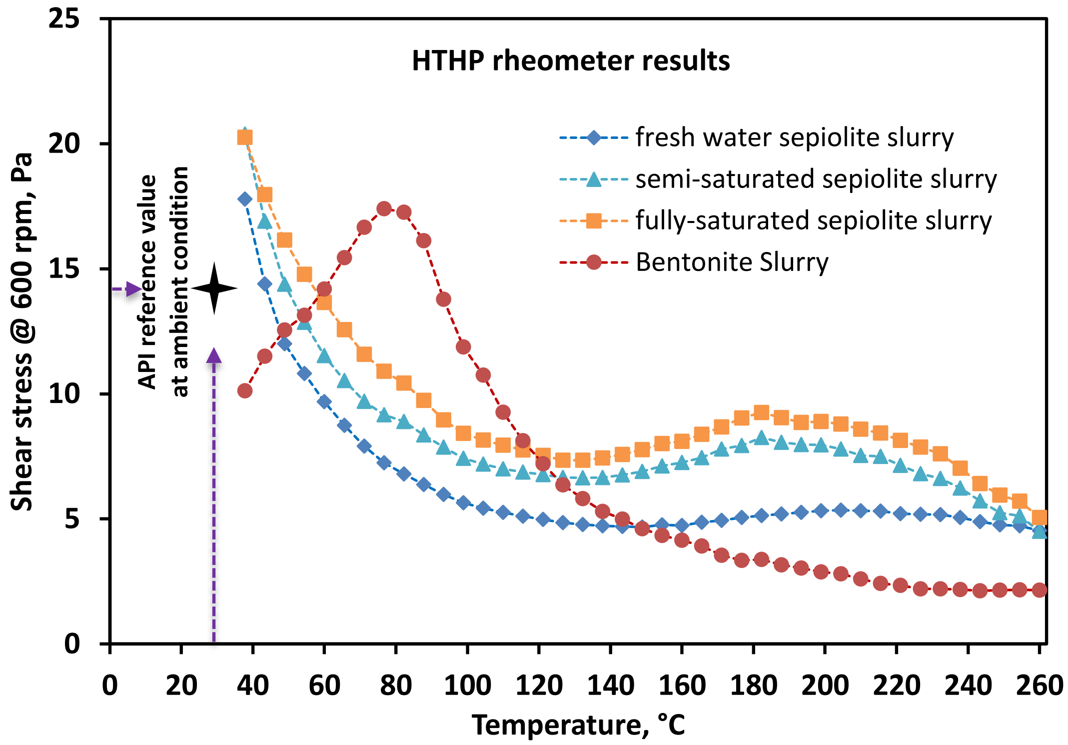

Figure 5.9: Thermal rheological behavior of bentonite and sepiolite suspensions (600 rpm).

5.3.2 Thermal rheological behavior of fresh water sepiolite mud (with additives)

The composition of unweighted and weighted fresh water sepiolite muds containing additives was given in Table 5.2. Thermal rheological properties of unweighted and weighted fresh water sepiolite muds were depicted in Figures 5.10 and 5.11, respectively. The rheological properties of samples from the conventional viscometer were also demonstrated in the figures to show differences. HTHP filtration loss of sepiolite muds was determined using HTHP filter press up to 204°C. The filtration results were included to the graphical view along with in-situ rheological behavior of mud samples in order to demonstrate the efficiency of sepiolite muds in terms of both rheological and filtration properties.

Extremely high and unacceptable fluid losses were obtained beyond 204°C, and it was shown with purple colored area in the figures. It was observed that at low temperature, sepiolite mud with additives had shear stresses about two-fold higher than those with no additives (Figure 5.8 and 5.10). However, this ratio decreased with increasing temperature. The rheological difference between samples with and without additives was eliminated and became insignificant at temperature of 149°C and above. Additives used to prepare sepiolite mud had primary and perhaps the secondary functions. For example, polymer 2 was added to the mud system to prevent water loss; however, it had exhibited secondary function as the viscosity increment at well.

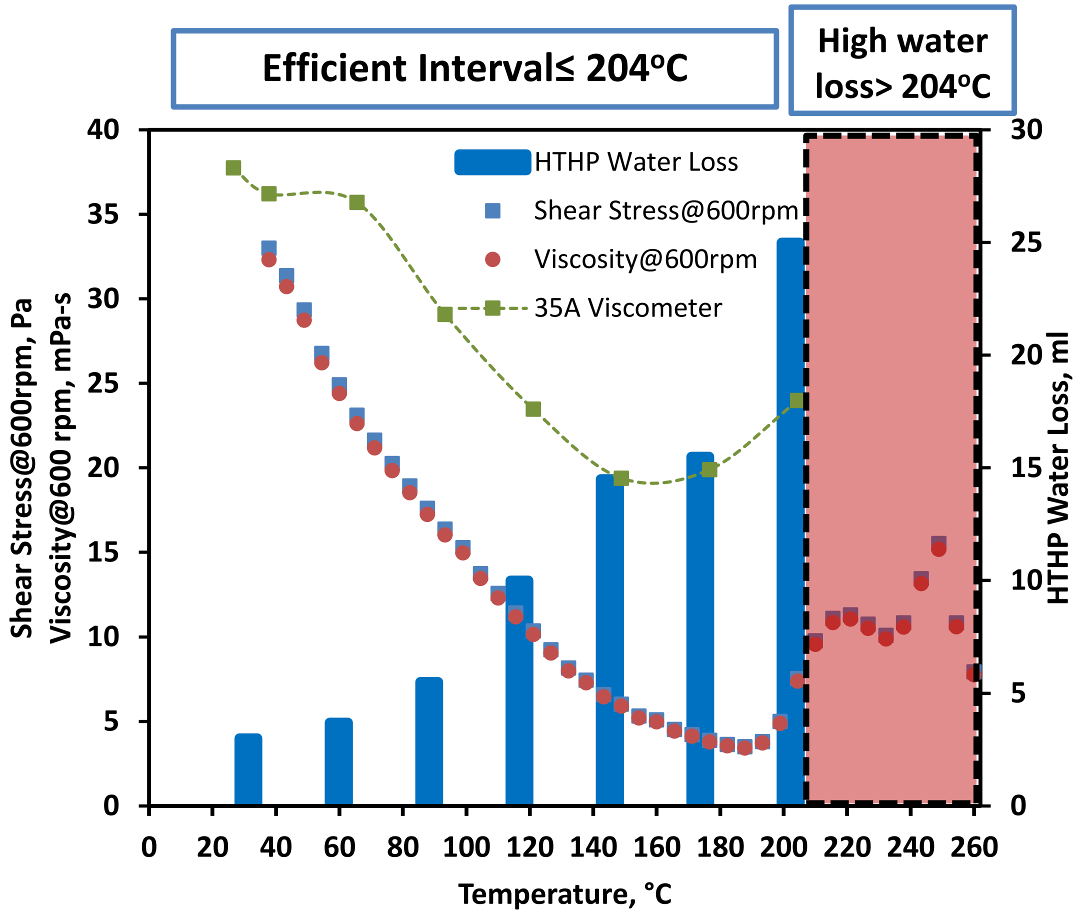

Figure 5.10: Thermal rheological and filtration behavior of unweighted fresh water sepiolite mud.

The contribution of this polymer increased the viscosity of the mud sample at low temperatures and lost its effect at temperature above 149°C, as expected. However, the other viscosity controller additive (polymer-1) successfully fulfilled its function as a thinner at 121°C and above. The amount of shear stress for the unweighted sepiolite mud with additives was observed about 33.53Pa (70 lb/100ft^2). It was also clear that the shear stress values decreased rapidly with increasing temperatures. This declining trend continued until 190°C (375°F), then tended to rise until the maximum tested temperature of 260°C (500°F). As seen in Figure 5.11 and as expected, the weighted fresh water sepiolite mud sample had exhibited higher shear stress than those of the unweighted sample. The reason could related to addition of significant amounts of barite causing higher solids content in the mud system. It is a known fact that the amount of solids in the drilling mud causes an increase in the rheology, particularly in plastic viscosity. Amount of shear stress for the weighted mud samples at 38°C was recorded approximately as 47.9 Pa (100 lb/100ft^2).

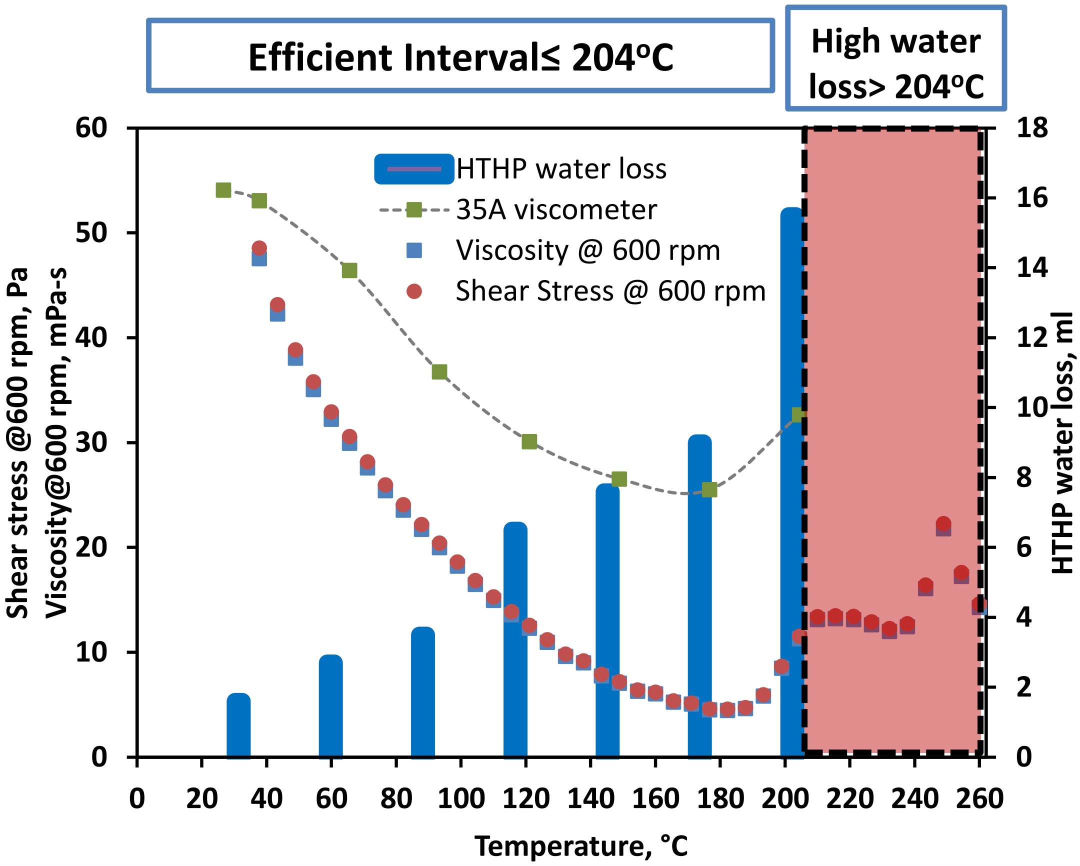

Figure 5.11: Thermal rheological and filtration behavior of barite-weighted fresh water sepiolite mud.

In addition, the weighted mud samples followed the same decline trend with the behavior of unweighted system. However, the difference between two was significant despite the decrease in the shear stresses with increasing temperatures. The results also indicated a significant difference between the conventional viscometer measurements with those obtained from the rheometer. Therefore, it is inferred that the hydraulic optimization analysis based on conventional viscometer and using aging method might be far from the reality and yields results with significant errors. The results of measured HTHP water losses were strong indicator of thermal stability and efficiency of sepiolite muds up to 204°C (400°F).

5.3.3 Thermal rheological behavior of sepiolite mud subjected to salt intrusion (with additives)

Amount of 171 kg/m^3 and 342 kg/m^3 NaCl were added to the sepiolite base mud composition given in Table 5.2 to simulate high amounts of externally salt intrusion into the sepiolite mud system. Thermal rheological properties of sepiolite mud sample containing 171 and 342 kg/m^3 NaCl were depicted in Figures 5.12 and 5.13, respectively.

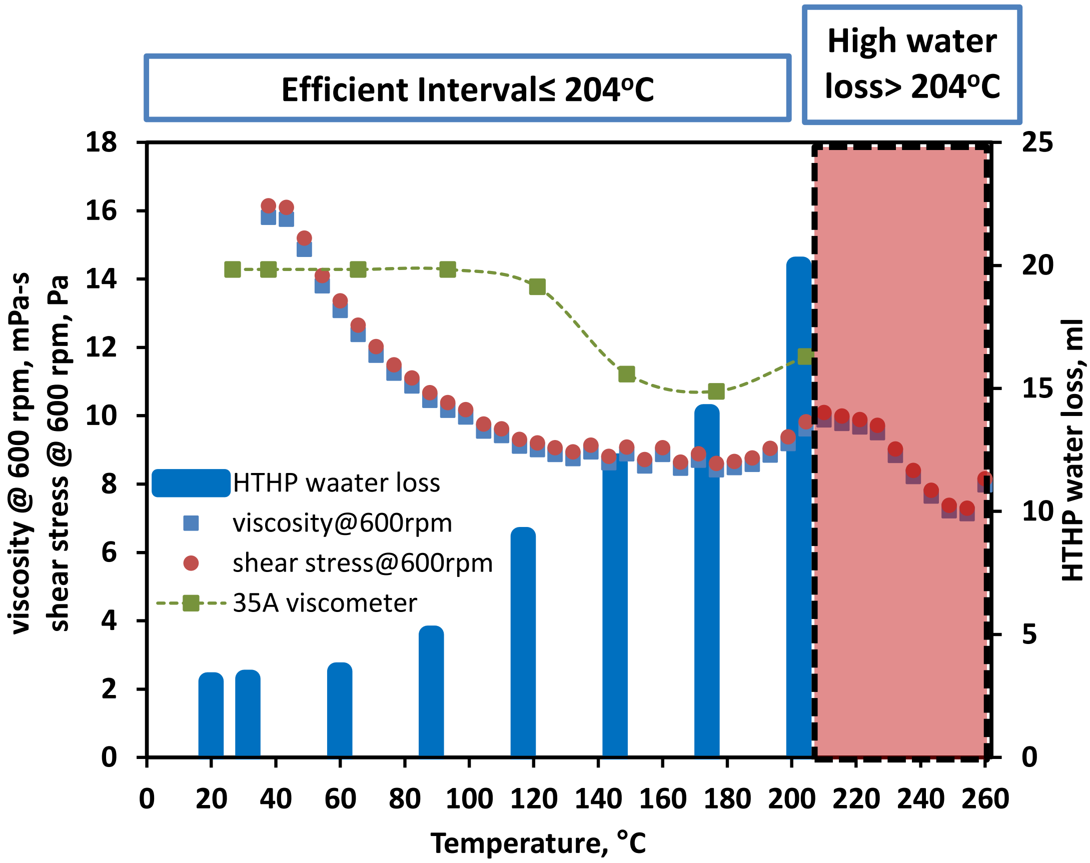

Figure 5.12: Thermal rheological and filtration behavior of sepiolite mud containing 171 kg/m^3 NaCl.

As seen from Figure 5.12, the salt intrusion caused decrease in viscosity at significant rate. The viscosity measured at 38°C decreased almost two-fold from 32.31 mPa-s in the fresh water sepiolite mud sample to 16.15 mPa-s in the mud sample containing 171 kg/m^3 NaCl. However, a little bit increment in the viscosity was observed when doubling the amount of salt intrusion to 342 kg/m^3 (Figure 5.13). The amounts of shear stress and viscosity in the mud sample containing 342 kg/m^3 NaCl were relatively higher than those measured for the mud sample containing 171 kg/m^3 NaCl. This observation confirmed the results obtained using the conventional viscometer (aging method) and proved the saline effectiveness of the sepiolite mud.

As another finding from Figure 5.13 that the rheological variation range in the sepiolite mud with salt intrusion of 342 kg/m^3 (8 - 18 Pa) was noticeably lower than the range for the fresh water mud system (3.43 - 33 Pa) as shown in Figure 5.10. The sepiolite muds used in this study exhibited more stability in saline environments and was a proof of the statement mentioned in the literature too.

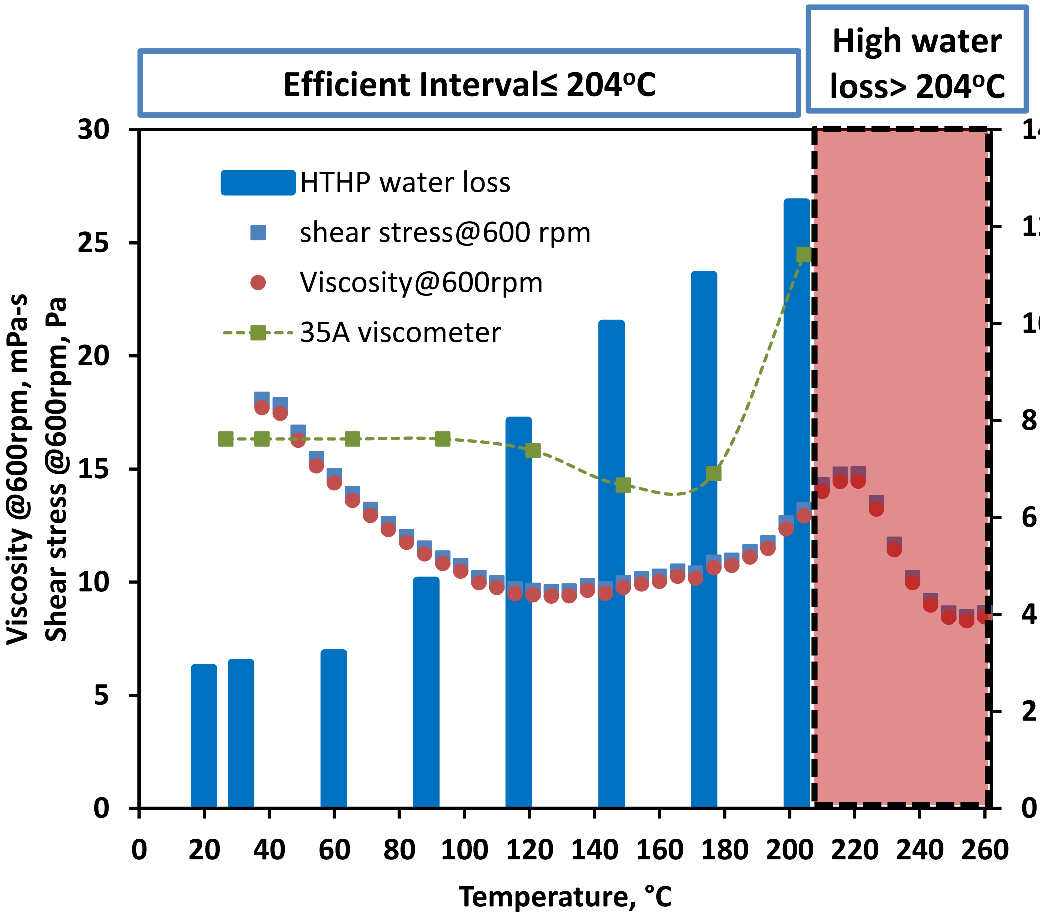

Figure 5.13: Thermal rheological and filtration behavior of sepiolite mud containing 342 kg/m^3 NaCl.

Shear stress tended to decrease with increasing temperature. Shear stresses in Figure 5.12 and 5.13 showed upward trends after 137 and 121°C, respectively. It could be inferred that the mud samples started to be flocculated at these temperatures; however, the lower amount of HTHP water losses could prove the efficiency of these mud sample up to 204°C. Therefore, the rheological and filtration properties of samples must be evaluated simultaneously to have better insight in efficiency of these sepiolite muds at high temperate and high salinity.

The amount of HTHP water losses at 204°C decreased from 25 ml in the unweighted fresh water system to 20 ml and 12.5 ml in the sepiolite mud systems containing 171 kg/m^3 and 342 kg/m^3 of NaCl, respectively. This is another confirmation of sepiolite mud efficiency at high salinity.

5.3.4 Thermal rheological behavior of salt saturated sepiolite mud (with additives)

57 kg/m^3 of TTB sepiolite clay was added to pre-prepared salt water in concentrations of 200 gr NaCl/l and 400 gr NaCl/l to simulate semi and fully saturated sepiolite mud system, respectively (Table 5.2). The results in the form of shear stress and viscosity values were depicted in Figures 5.14 and 5.15 for semi-saturated and fully saturated fluids, respectively. As seen in Figure 5.14, similar to the salt intrusion case, fully saturated system also exhibited viscosity decrement at a substantial rate. However, it could be observed that the decreasing rate in the case fully-saturated sepiolite mud system was relatively higher than the effect of salt intrusion to the mud system. The shear stress values measured at 38°C decreased almost from 33 Pa in fresh water sepiolite mud sample to 18 Pa in mud sample containing 342 kg/m^3 NaCl. However, the decreasing rate in the case of fully saturated mud system was more than two-fold such that 33 Pa in the fresh water sepiolite mud sample and 13.12 Pa in the fully-saturated system. Therefore, the external salt intrusion effected the mud system less than that of mud sample initially prepared with semi or fully saturated water.

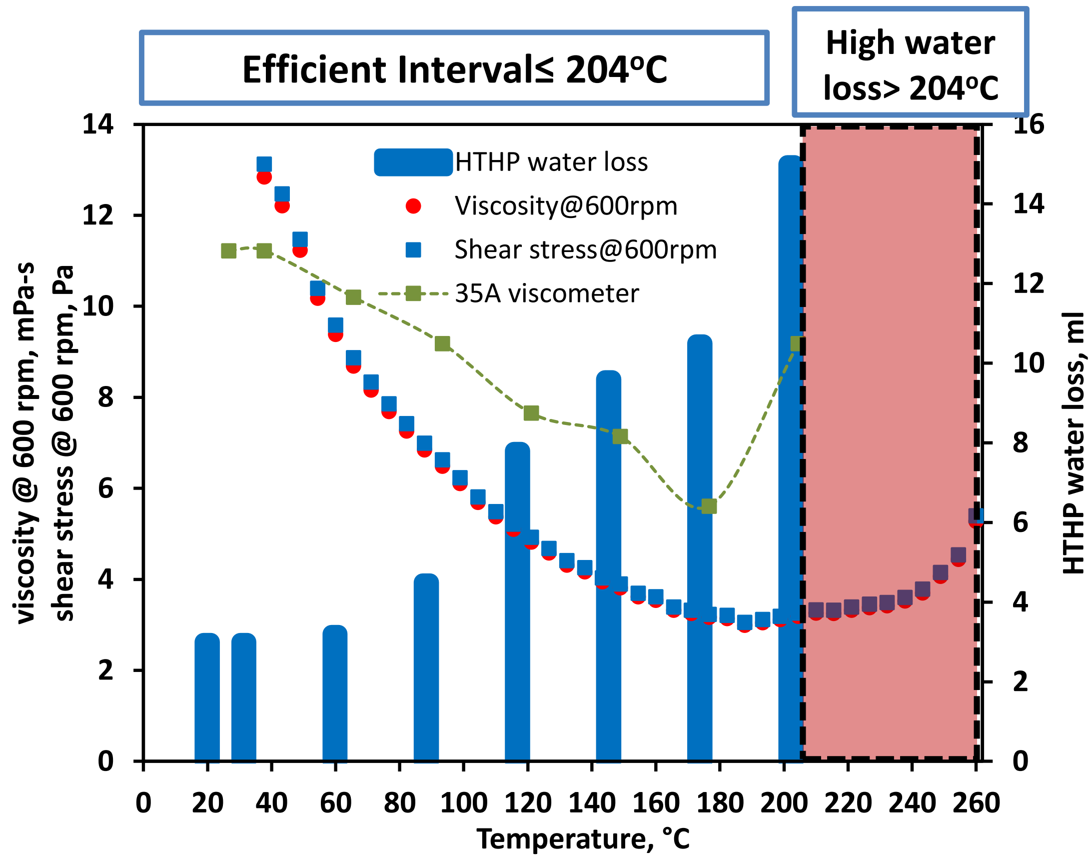

Figure 5.14: Thermal rheological and filtration behavior of fully-saturated sepiolite mud with additives.

The viscosity measured at 38°C decreased almost two-fold from 32.31 mPa-s in the fresh water sepiolite mud sample (Figure 5.10) to 12.96 mPa-s in the semi-saturated mud sample (Figure 5.15). However, the viscosity was remained almost the same (12.85 Pa) with increasing salinity in the case of fully saturated system. Similar to the system with external salt intrusion, this observation confirmed that the sepiolite mud was not substantially affected with increasing salinity and was able to preserve its rheological properties even in the fully-saturated system.

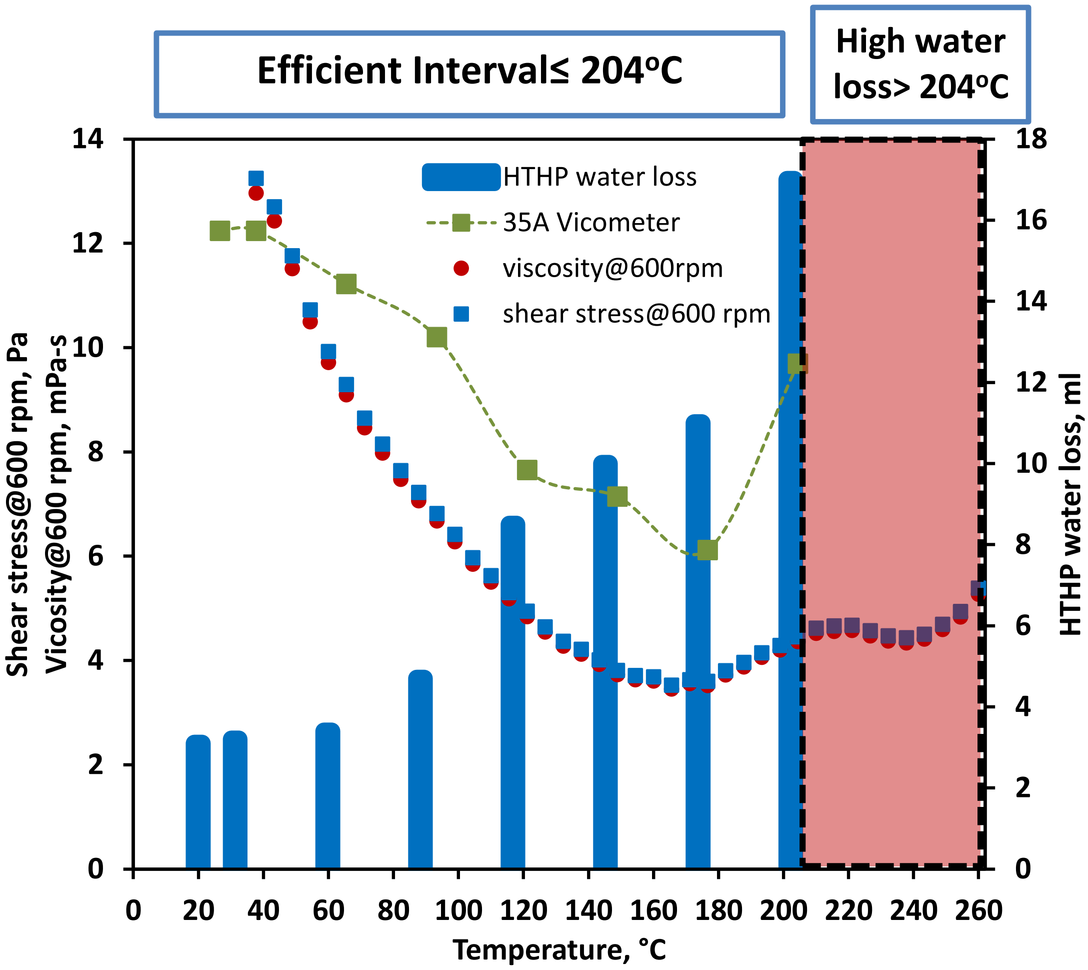

Figure 5.15: Thermal rheological and filtration behavior of semi-saturated sepiolite mud with additives.

According to the previous studies, sepiolite clay efficiency increases with increasing salt content and higher viscosity of fully saturated mud samples in this study support this evidence. Similar behavior was also observed through samples prepared and analyzed using thermal aging method. However, it can be concluded that the thermal aging at low temperatures have not significant effect on the sepiolite mud rheological properties. The lower amount of HTHP filtration was so impressive in the case of salt saturated sepiolite systems. As stated in the previous section, the rheological and filtration properties of samples must be considered together to better interpretation of mud behavior. The amount of HTHP water losses at 204°C decreased from 25 ml in the unweighted fresh water system to 17 ml and 15 ml in the semi saturated and fully saturated mud systems.

As noted in the literature, sepiolite clay base mud prepared with salt especially recommended for high-temperature environments. Behaviors shown in Figures 5.14 and 5.15 clearly supported this statement for the TTB sepiolite clay used in this study. The fresh water sepiolite mud provided more viscosity at low temperatures than those of the salty mud sample. This behavior was protected up to 121°C, and then it was diminished especially at higher temperatures. The rheological advantages of saltwater sepiolite mud was particularly manifest at 177^{o}C and higher temperatures.

5.4 Thermal Rheological Properties of Lignosulfonate Mud

Thermal rheological behavior of lignosulfonate mud were investigated using two afore mentioned methods. Similar to the sepiolite mud, conventional viscometer, the concept of first method, was also used to measure rheological properties of thermally aged samples. In addition, the thermal rheological properties of lignosulfonate mud was evaluated using HTHP rheometer to provide an inclusive comparison on results. Such comparison can help to understand better the possible differences between two methods in hydraulic design of wellbore.

The results of rheological measurements through these two methods were illustrated in Figure 5.16 for the lignosulfonate mud. Similar to the previous sections, the results were given based on shear stress at 600 rpm rotation speed at different temperatures. The amount of apparent viscosity was also depicted in Figure 5.16 based on the results from HTHP rheometer. As expected, the viscosity decreased with increasing temperature. The rheological stability of lignosulfonate mud sample was preserved up to 149°C. However beyond this temperature, the viscosity and shear stress decreased continuously so that the mud system could not provide sufficient yield point and gel strength to meet its mission adequately. Interpretation of rheological properties measured by the classic viscometer indicated that the value of shear stress was higher than those measured by the HTHP rheometer up to 93°C, as expected. However, this behavior was changed above 93°C and adverse behavior was observed. The amount of shear stresses measured by the HTHP rheometer were higher than the shear stresses obtained by the conventional viscometer beyond 93°C. The viscosity of thermally aged mud samples measured by the classic viscometer decreased with increasing temperature up to the final measurable temperature (149°C) due to mud flocculation.

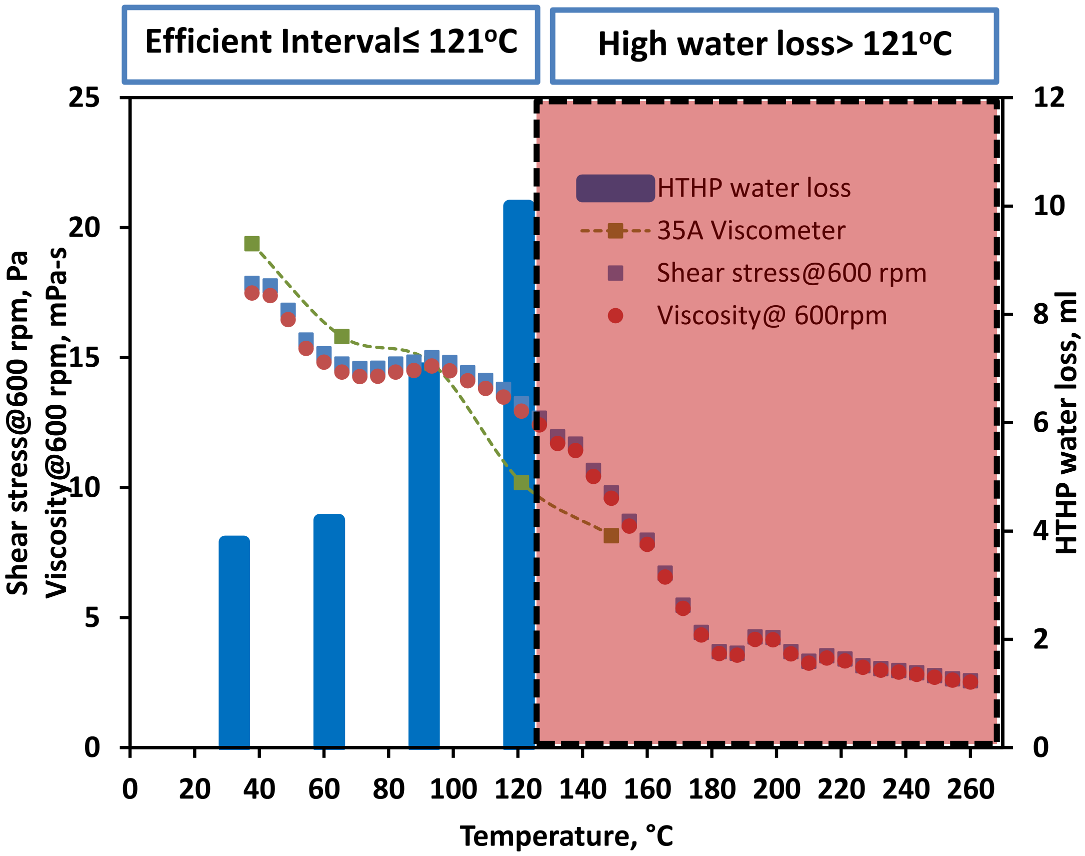

Figure 5.16: Thermal rheological and filtration behavior of lignosulfonate mud.

The flocculation of mud and degradation in clay particles were observed clearly after thermal aging when emptying sample out of the aging cell. The results of HTHP fluid losses were the clear confirmation of this situation. The HTHP filtration test above 121°C was failed due to high amount of spurt losses. The amount of desired HTHP water losses up to 121°C could be the sign of this fact that the lignosulfonate mud was effective below 149°C. The hydraulic optimization results might cause significant differences for this kind of mud type since the rheological behavior measured through two methods did not follow the same trend.

5.5 Thermal Rheological Properties of Bentonite/Polymer Base Mud

Thermal rheological properties of bentonite/polymer mud was also evaluated using HTHP rheometer. Moreover, similar to the sepiolite mud, the conventional viscometer was used to measure the rheological properties of pre-heated samples to be able to compare obtained results using two rheological measurement methods. The results of rheological measurements through these two methods were illustrated in Figure 5.17 for the bentonite/polymer mud.

The amount of apparent viscosity was also depicted on Figure 5.17 based on the obtained results from the HTHP rheometer. The bentonite/polymer mud provided the similar rheological behavior with the lignosulfonate mud; however, the bentonite/polymer mud lost its stability at lower temperature (121°C) than that of the lignosulfonate mud. In addition, bentonite/polymer mud demonstrated lower rheological values than those of the lignosulfonate mud at the same aging temperatures. The viscosity decreased with increasing temperature continuously similar to the lignosulfonate mud. But, the fluid did not provide a measurable viscosity value at 200°C. The rheological values measured by the classic viscometer were higher than the values obtained using the HTHP rheometer. Similar to the lignosulfonate mud, the flocculation and degradation in clay particles were observed after thermal aging at 121°C.

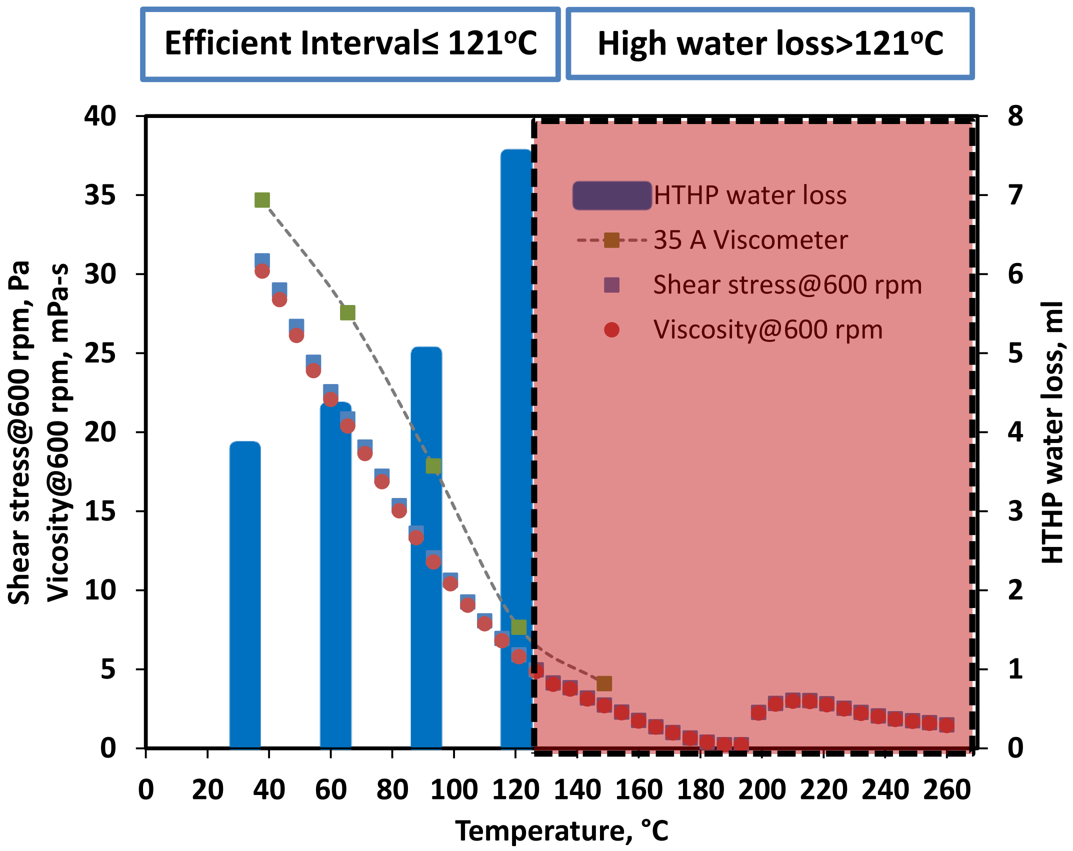

Figure 5.17: Thermal rheological and filtration behavior of bentonite/polymer mud.

The results of HTHP fluid losses confirmed this result. The HTHP filtration test above 121°C was not measured because of existing high amount of spurt losses. The bentonite/polymer mud provided convenient HTHP water losses up to 121°C similar to the lignosulfonate mud. It could be concluded that the efficient and applicable interval of this mud was up to 121°C. Comparing to the sepiolite mud, the bentonite/polymer and lignosulfonate muds was not recommended to be used at temperature higher than 149°C. The sepiolite mud was able to provide proper rheological properties as well as filtration characteristics especially at temperatures higher than 149°C. Therefore, the usage of sepiolite clay instead of the bentonite as the main component of drilling fluid could be reasonable decision at hot wells.

5.6 Determination of the Best Rheological Model and Rheological Parameters

The rheological models are used to estimate the behavior of non-Newtonian fluids. Since the most of drilling fluids exhibit non-Newtonian behavior, the application of these models to describe the rheological properties of drilling fluids is very helpful especially during drilling, well completion, workover, and acidizing operations. The rheological parameters assigned for each mathematically described rheological model are used to describe the viscous forces in fluids. Accurate estimation of these parameters can play essential role to design wellbore hydraulics. Frictional pressure loss equations including these parameters are used to calculate pressure drops in a circulation system including surface facilities, drill strings, drill bit, and annulus. Accurate prediction of pressure losses during circulation as well as tripping period is quite important in terms of bit hydraulic optimization, estimation of equivalent circulating density (ECD), hole cleaning, and drilling fluid compressibility as well as well control. The benefits of a more accurate estimation of ECD is to have efficient hole cleaning to enhance the rate of drilling. All of these lead to reduce total drilling cost. In addition, some critical problems such as circulation loss, maintenance of under-balanced drilling conditions, and kick can be prevented by precise ECD prediction.

Bingham Plastic and Power Law models are commonly used in optimizing drilling hydraulics. Wellbore hydraulic design in API standard are based on these two models. Recently, the Herschel Bulkley model has been used frequently because it includes the yield point (Bingham plastic) as well as the nonlinearity relationship between the shear stress and shear rate (Power Law). Therefore, it is a kind of the combination of two models so that it is also named as Yield Power Law model. Hemphill et al., (1993) proposed Herschel Bulkley model, as a three parameter model, to approximate the non-Newtonian behavior of polymeric fluids accurately. Moreover, rheological behavior of drilling mud was reported to be estimated in the best fit using this model. This model, as a result, was adopted as a standard by API (API RP 13D, 2006).

In this study, data from the HTHP rheometer and conventional viscometer were used to determine the rheological model fitting the data in the best way. The major goal of this part of study is to investigate the effect of temperature variations on the rheological parameters and along with the rheological models. Statistical regression technique, least-square regression approximating functions, was used to specify the appropriate models. Matlab curve fitting toolbox was used to solve each non-linear model function using a quasi-Newton's numerical iterative approach. Results of the regression analysis were plotted, and the residual sum of squares were analyzed. Due to the small sample size, residual mean squares (SSE) were employed as a statistical tool to account for the error variance. The model with the minimum residual mean squares was selected.

5.6.1 Regression analysis and model comparison

Regression analysis has been suggested as a theoretically simple method to investigate functional relationship among variables (Samprit and Ali, 2006). Regression analysis categorized into two major linear and non-linear concepts. Least-square method, the maximum likelihood method, the ridge method, Lagrangian interpolation, piecewise linear polynomials or splines, and the principal components method are some of the methods in regression analysis to estimate model parameters. Least-square is the frequently used method for function approximation. Linear and non-linear regression are based on two assumptions that make it easy to apply. It assumes the scatter follows a Gaussian (Normal) distribution, and standard deviation of scatter is the same for all values. Least-square regression minimizes the sum of squares of the vertical distance between data points and curve based on these two assumptions (Motulsky and Christopoulos, 2003). Wier and Bailey (1996), Bailey and Peden, (2000), Guo and Hong (2010), and Ali et. al (2001) used mean sum-of-squares criterion to select perfect rheological models for various types of drilling fluid used in the oilfield. They selected a model with the minimum mean sum-of-squares as the best fit to estimate model parameters. Absolute percentage error (AAPE) was suggested by Aswad and Saleh (1990) as the most suitable statistical technique to select the fit rheological model for a given non-Newtonian fluid. The model with the lowest average absolute percentage error (AAPE) was proposed as the best rheological model. Jawad and Akgun (2002) used AAPE as a criterion to select the best rheological model for non-Newtonian drilling fluids among six rheological models. The use of R-square (coefficient of determination) as an indicator to quantify goodness of fit was discussed by numerous researchers (Crocker, 1972; Barrett, 1974; Draper and Smith, 1981; Ranney and Thigpen, 1981; Healy, 1984; Kvalseth, 1985; Helland, 1987; Willett and Singer, 1988; Nagelkerke, 1991; Scott and Wild, 1991). Some of them reported some cautionary notes about using R-square. Kvalseth (1985) represented that except for linear models with an intercept term, the various R-square statistics generally yield different values for instance in linear no-intercept models or nonlinear models. Draper (1984) suggested that R-square causes misleading in data sets which replicate data points, and suggested that the Box-Wetz (1973) criterion was more appropriate. Healy (1984) reported that R-square was not suitable measure of ordinary least-squares regression relationship. He highlighted that this misleading was more likely in any non-linear model. Motulsky and Christopoulos (2003) in their paper cautioned that the use of R-square as the main criterion for whether a fit was reasonable or not. A high R-square indicated that the curve came very close to the points, but it didn't mean the fit is "good" in other ways. The best-fit values of the parameters may have values that make no sense or the confidence intervals might be very wide. Therefore, it was recommended to look at all the results to evaluate a fit, not just the R-square.

In this part of study, data sets from the classic viscometer with thermally aged samples and the HTHP rheometer were used to approximate the best fit rheological model using least-square regression. It was aimed to look for a function relating shear stress (dependent variable) to shear rate (independent variable) such that the sum of squares of error was minimized. For minimizing the square of the error, the partial derivative of the function with respect to each model parameters had to be approximately equal to zero. The Matlab curve fitting toolbox was used to apply least-square regression and obtain SSE, R-square, adjusted R-square and Root mean squared error (RMSE) as explained below.

5.6.1.1 Evaluating Goodness of Fit

After fitting measured data to rheological models, the goodness of fit should be evaluated to obtain perfect fit rheological model. The good fit might be a model:

- that data could reasonably come from, and have given the assumptions of least-squares fitting,
- in which the model coefficients can be estimated with little uncertainty,
- that explains a high proportion of the variability in data, and is able to predict new observations with high certainty.

A visual examination of the fitted curve displayed in Curve Fitting toolbox in Matlab can be used to achieve these purposes. The toolbox provides following methods to assess goodness of fit for both linear and nonlinear parametric fits:

- Goodness-of-Fit Statistics,
- Residual Analysis,
- Confidence and Prediction Bounds.

A particular application might still dictate the other aspects of model fitting that are important to achieving a good fit such as a simple model that is easy to interpret. Graphical and numerical methods can help to determine goodness of fit in all these sense. Plotting residuals and prediction bounds are graphical methods that aid visual interpretation while computing goodness-of-fit statistics and coefficient confidence bounds yield numerical measures that aid statistical reasoning.

Graphical measures are more beneficial than numerical measures because they allow user to view the entire data set at once, and they can easily display a wide range of relationships between the model and the data. The numerical measures are more narrowly focused on a particular aspect of the data and often try to compress that information into a single number. In practice, depending on measured data and analysis requirements, it might need to use both types for determining the best fit.

5.6.1.2 Goodness of Fit Statistics

After using graphical methods to evaluate the goodness of fit, the goodness-of-fit statistics should be examined. Matlab Curve Fitting Toolbox software supports these goodness of fit statistics for parametric models as follows.

1. Sum of squares due to error

This statistics measures the total deviation of the response values from the fit to the response values. It is also called the summed square of residuals and is usually labeled as SSE.

$$SSE = \sum_{i=1}^{n} w_i(x_i - \hat{x}_i)^2 \tag{5.1}$$

A value of SSE closer to zero indicates that the model has a smaller random error component, and the fit will be more useful for prediction.

2. R-square

This statistic measures how successful the fit is in explaining the variation of the data. Put another way, R-square is the square of the correlation between the response values and the predicted response values. It is also called the square of the multiple correlation coefficient and the coefficient of multiple determination. R-square is defined as the ratio of the sum of squares of the regression (SSR) and the total sum of squares (SST). SSR is defined as

$$SSR = \sum_{i=1}^{n} w_i(\hat{x}_i - \bar{x})^2 \tag{5.2}$$

SST is also called the sum of squares about the mean and is defined as

$$SST = \sum_{i=1}^{n} w_i(x_i - \bar{x})^2 \tag{5.3}$$

where SST = SSR + SSE.

Given these definitions, R-square is expressed as

$$R - square = \frac{SSR}{SST} = 1 - \frac{SSE}{SST} \tag{5.4}$$

R-square can take on any value between 0 and 1, with a value closer to 1 indicating that a greater proportion of variance is accounted for by the model. For example, an R-square value of 0.95 means that the fit explains 95% of the total variation in the data about the average. Note that it is possible to get a negative R-square for equations that do not contain a constant term. Because R-square is defined as the proportion of variance explained by the fit, then R-square is negative if the fit is actually worse than just fitting a horizontal line. In this case, R-square cannot be interpreted as the square of a correlation. Such situations indicate that a constant term should be added to the model.

3. Degrees of freedom adjusted R-square

This statistics uses the R-square statistics defined above, and adjusts it based on the residual degrees of freedom. The residual degrees of freedom is defined as the number of response values (n) minus the number of fitted coefficients (m) estimated from the response values.

$$v = n - m \tag{5.5}$$

v indicates the number of independent pieces of information involving the n data points that are required to calculate the sum of squares. Note that if parameters are bounded, and one or more of the estimates are at their bounds, then those estimates are regarded as fixed. The degrees of freedom are increased by the number of such parameters.

The adjusted R-square statistics is generally the best indicator of the fit quality when comparing two models that are nested in a series of models of which each adds additional coefficients to the previous model.

$$adjusted\ R - square = 1 - \frac{SSE(n-1)}{SST(v)} \tag{5.6}$$

The adjusted R-square statistics can take on any value less than or equal to 1 with a value closer to 1 indicating a better fit. Negative values can occur when the model contains terms that do not help to predict the response.

4. Root mean squared error

This statistics is also known as the fit standard error and the standard error of the regression. It is an estimate of the standard deviation of the random component in the data, and is defined as

$$RMSE = \sqrt{MSE} \tag{5.7}$$

where MSE is the mean square error or the residual mean square

$$MSE = \frac{SSE}{v} \tag{5.8}$$

Just as with SSE, an MSE value closer to 0 indicates a fit that is more useful for prediction.

5.6.2 Non-Newtonian Fluid

As a known fact, Newtonian fluids are characterized as any fluid that exhibits a constant viscosity regardless of any external stress applied on it. The viscosity of non-Newtonian fluids is a function of shear rate. This is one of the distinct property associated to non-Newtonian fluids, which can become thicker or thinner when stress is applied. Another way to describe non-Newtonian fluids is that they have a non-linear relationship between share rates and shear stresses. Unlike Newtonian fluids, regarding to the shear stress applied to these fluids, the coefficient of viscosity will change. In non-Newtonian fluid, there is a nonlinear relationship between the magnitude of applied shear stress and the rate of angular deformation. The viscosity is not independent of the velocity gradient. Namely, the viscosity will vary with the rate of shear (the difference between velocities of parallel faces of a fluid element divided by the distances between the faces) of the fluid. They have a variable viscosity at a constant temperature. There are many types of non-Newtonian fluids that each of them has distinct properties. Non-Newtonian fluids are classified into two categories, which are time independent non-Newtonian fluids (Pseudo plastic, Shear thickening, and Bingham fluids) and time dependent non-Newtonian fluids (Thixotropic and Rheopectic). An apparent viscosity, μ_a is often used to describe the flow behavior of Newtonian fluids, can be defined as follows:

$$\mu_a = -\frac{\tau}{\gamma} = -\frac{Shear\ stress}{rate\ of\ shear} \tag{5.9}$$

The most drilling fluids and cement slurries are pseudo plastic and thixotropic. In general, the pseudo plastic behavior of drilling fluids and cement slurries can be approximated by Bingham Plastic and Power Law, and Herschel Bulkley rheological models.

5.6.2.1 Bingham Plastic model

A different kind of time-independent behavior is characterized by materials known as Bingham Plastics, which exhibit a yield stress, τ_y. If subjected to shear stress smaller than the yield stress, they retain a rigid structure and do not flow. It is only at stresses in excess of the yield value that flow occurs. In the case of Bingham Plastic model, the shear rate is proportional to shear stress in excess of the yield stress:

$$\tau = \tau_y + \mu_p\gamma \qquad (5.10)$$

where,

τ: Shear stress, Pa or lbf/sq ft
τ_y: Yield point, Pa or lbf/sq ft
μ_p : Plastic viscosity, Pa-s or cp
γ: Shear rate, s^{-1}

In the Bingham model equation, τ_y and μ_p are both constants referring to the yield stress and coefficient of plastic viscosity, respectively. The Bingham equation describes the shear stress/shear rate behavior of many shear-thinning materials at low shear rates.

5.6.2.2 Power Law Model

It should be noted that for shear thinning and shear thickening behavior, the shear stress-shear rate curve passes through the origin. This type of behavior is often approximated by the 'Power Law' and such materials are called 'Power Law fluids'. The power law, also called Ostwald-de Wale equation is usually written as:

$$\tau = k|\gamma|^{n-1}\gamma \qquad (5.11)$$

where,

τ: Shear stress, Pa or lbf/sq ft
k : Consistency index, eq. Pa*s or eq. cp
γ: Shear rate, s^{-1}
n: Flow behavior index, dimensionless.

The power n is known as the Power Law index or flow behavior index, and K as the consistency index. The constants K and n are determined by fitting the equation to data. Clearly, shear thinning behavior corresponds to $n<1$ and shear thickening behavior to $n>1$. The special case, $n=1$, is that of Newtonian behavior, and in this case the consistency coefficient K is identical to the Newtonian viscosity, μ.

5.6.2.3 Herschel Bulkley Model

Herschel Bulkley model looks like combination of Bingham Plastic model and Power Law model. Consequently, it is also called Yield-Power Law (YPL) model. This model takes into account yield stress, stress which should be applied to initiate the motion and change in viscosity with shear rate. Herschel Bulkley model is described with the equation below.

$$\tau = \tau_y + k\gamma^n \tag{5.12}$$

where,

τ : Shear stress, Pa or lbf/sq ft
τ_y: Yield point, Pa or lbf/sq ft
k : Consistency index, eq. Pa*s or eq. cp
γ : Shear rate, s^{-1}
n: Flow behavior index, dimensionless.

Herschel Bulkley model can be reduced to either Newtonian Model, Bingham Plastic Model or Power Law Model by modifying Equation 5.12. If yield stress, τ_y is set to zero (τ_y=0), then Equation 5.12 reduces to Power law model. If flow behavior index (n) in Equation 5.12 is set to one (n=1), then Equation 5.12 reduces to Bingham Plastic model and consistency index, K becomes plastic viscosity ($K=\mu_p$). If flow behavior index (n) set to one and yield point τ_y set to zero, then Equation 5.12 is reduced to Newtonian flow equation and consistency index K, becomes apparent viscosity ($K=\mu_a$). The Newtonian and three common non-Newtonian rheological model behaviors were shown in Figure 5.18.

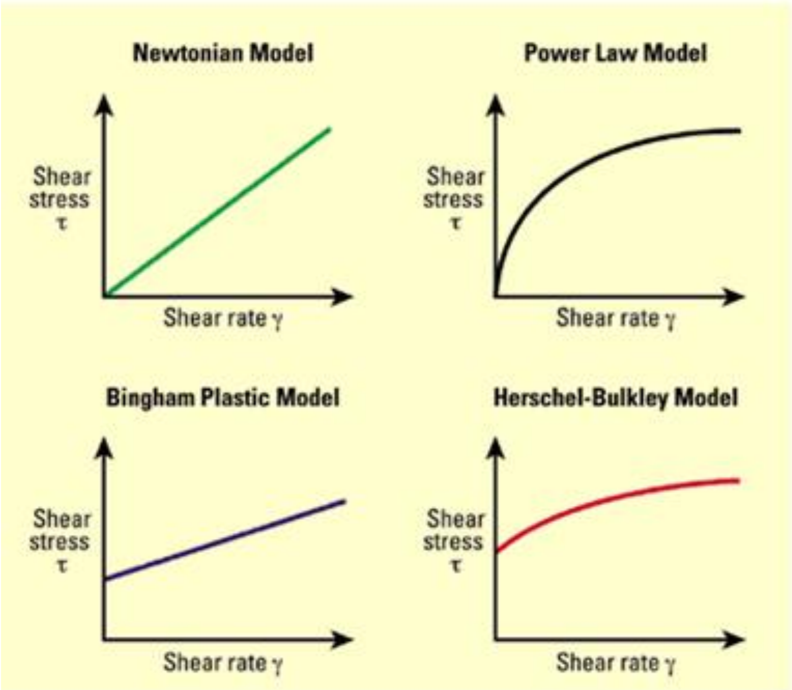

Figure 5.18: Rheological behaviors (Url-1).

5.7 Evaluating Rheological Models and Rheological Parameters.

The rheological model constants of all seven types of sepiolite mud systems defined in Table 5.2 were determined using Matlab curve fitting toolbox as explained in previous section. The fresh water sepiolite suspension formulated according to API SPEC 13A (2010) was used as a reference mud to help in making comparison. Other types of sepiolite muds containing additives were already specified in Table 5.1 and formulated according to Table 5.2. The evaluation of rheological model constants is presented in this section under two main subheadings. In the first subheading, the rheological model constants were determined based on rheological data from the conventional viscometer. The rheological parameters given in the second subheading were obtained from HTHP rheometer. At the end of this section, the comprehensive comparison was performed on the results obtained from these two methods of rheological measurements. The negative values of viscosity and shear stress were recorded at low rotor speeds (6 and 3 rpm) in some temperatures when using HTHP rheometer. The reason might be due to the effect of a physical slip existing between rotor and bob, especially at low shear rates. This slip occurred during rheological measurements using HTHP rheometer when the viscosity of sample decreased in high rate with increasing temperature. Because the negative shear stress values were against the nature of the event, they were not included to the process of rheological parameter determination. Such phenomenon was not observed in the classic viscometer measurements, since the viscosity of samples was high due to cooling process.

5.7.1 Model constants obtained from conventional viscometer

The rheological model constants obtained from conventional viscometer were tabulated through Tables F.1-F.7 in Appendix-F. The experiments were performed at 9 different aging temperature ranging from 27°C to 232°C. The Herschel-Bulkley rheological model was the perfect one describing the best fit model at each condition and all aging temperatures. This was the first notable results extracting from Tables F.1-F.7. The values of residual sum of squares (SSE) and fit standard error (RMSE) for unweighted fresh water sepiolite mud system was shown in Figure 5.19. The results of statistical analysis related to other types of sepiolite muds were given in Appendix-G through Figures G.1-G.7. These figures illustrated the values of residual sum of squares (SSE) and fit standard error (RMSE) for all types of mud systems in different aging temperatures. As mentioned before, these values are deterministic factors in selecting the best rheological model fitting the data. The value of R-square was not considered as a comparative parameter among the rheological models in this study because no significant differences from the models were obtained in some data sets. As shown in Figure 5.19, the Herschel Bulkley model provided the minimum values of SSE and RMSE in all aging temperatures. Power Law rheological model followed the Herschel Bulkley model with slightly higher SSE and RMSE values. Results depicted in Figure 5.19 indicated that the Bingham Plastic model presented the highest SSE and RMSE values; and consequently, it was the worst rheological model in describing the data. Such results emphasized the compatibility of Herschel Bulkley model to simulate rheological behavior of fresh water sepiolite mud with high accuracy with the advantage of having three rheological constant parameters. The statistical results through analysis of data from conventional viscometer for other types of sepiolite muds implied that Herschel Bulkley model provided the minimum SSE and RMSE values for all the mud systems at each temperature. Therefore, it was concluded that the Herschel Bulkley model was the best fit modelling rheological behavior of all seven types of sepiolite muds while using aging method. Error decreased with increasing temperature, and tended to increase with the further temperature increment after gelation was observed.

As known, the three constant parameters characterizing Herschel Bulkley rheological model are; flow behavior index (n), consistency index (K), and yield point (YP). The consistency is a simple constant of proportionality while the flow behavior index measures the degree to which the fluid is shear-thinning or shear-thickening. Finally, the yield stress quantifies the amount of stress that the fluid may experience before it yields and begins to flow. Power Law model are characterized by two constant parameters as flow behavior index (n), consistency index (K). In addition of these two non-linear models, Bingham plastic is a linear model with two parameter as plastic viscosity (PV) and yield point (YP). The variation of these parameters with temperature were illustrated in Appendix-G through Figures G.8-G.21 for all sepiolite mud types examined in aging method. In addition, the change in estimated rheological constant parameters with respect to temperature variation was illustrated in Figures 5.20 and 5.21 in the case of unweighted fresh water sepiolite mud.

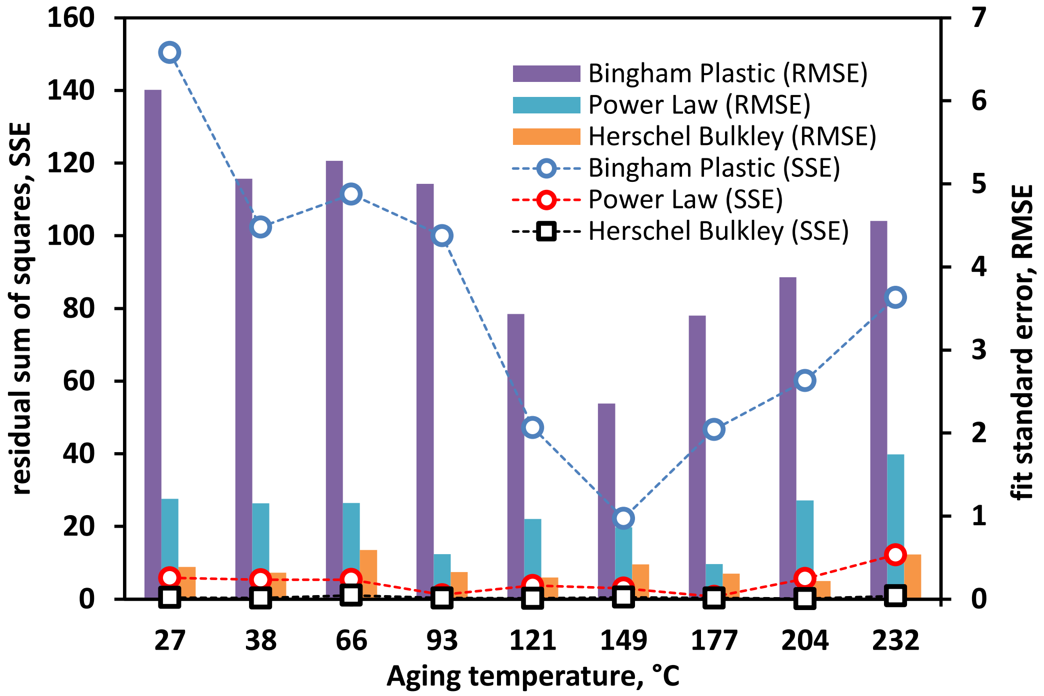

Figure 5.19: SSE and RMSE for unweighted fresh water sepiolite mud-viscometer

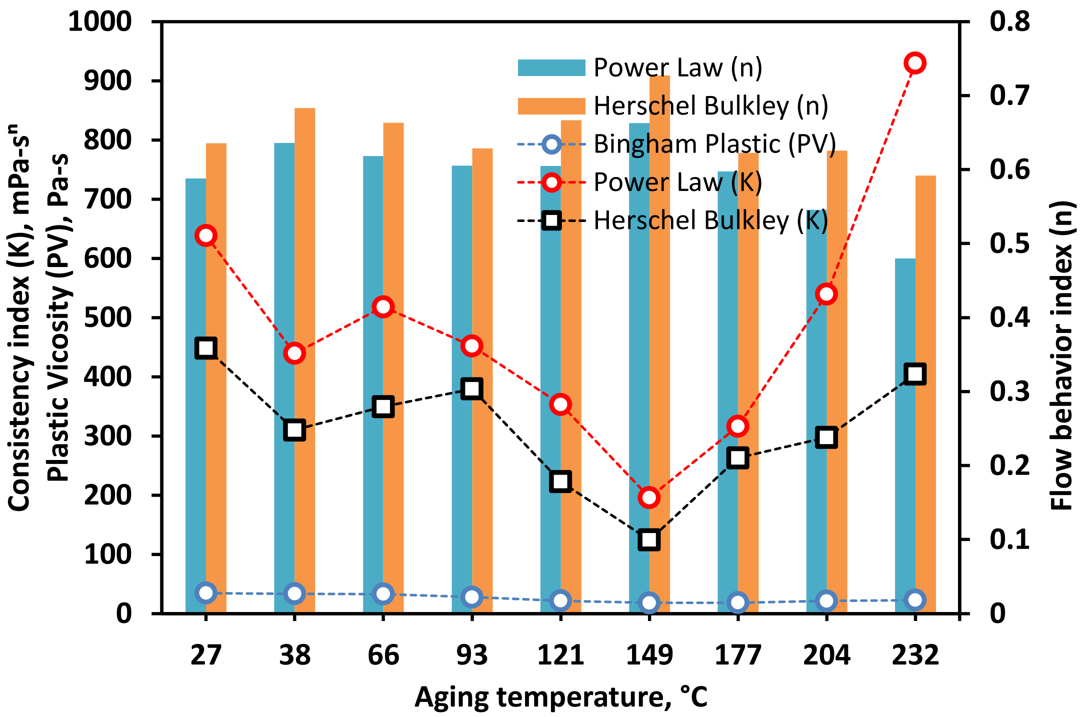

Figure 5.20: Rheological parameters of unweighted fresh water sepiolite mud-Viscometer.

The results sketched in Figure 5.20 exhibited that plastic viscosity was not affected with increasing temperature as much as consistency index was. Plastic viscosity (PV) of fresh water sepiolite mud decreased from 34 mPa-s at 27°C to 18 mPa-s at 149°C and then increased slightly to 23 mPa-s at 232°C of aging temperature. However, the consistency index of Power Law model decreased more than three-fold from 638 mPa-s^n at to 27°C to 195 mPa-s^n at 149°C, and then excessively increased to 930 Pa-s^n at 232°C of aging temperature. The consistency index of Herschel Bulkley model also followed the same behavior with the consistency of Power Law model. The amount of flow behavior index (n) of Power Law and Herschel Bulkley models was minimally influenced from the temperature increase. The minimum value of flow behavior index (n = 0.663) in Herschel Bulkley model was recorded at 232°C where the consistency index was recorded the highest. In addition, the higher value of flow behavior index (n = 0.592) in the same model was at 149°C where the consistency was minimum. The similar behavior was observed in the case of Power Law model. Approximately the same behaviors in both Bingham Plastic and Herschel Bulkley model were identified for the variation of yield point with temperature increases. For instance, it decreased from 4.90 and 1.17 Pa at 27°C to 2.44 and 0.33 Pa at 177°C, and then extremely increased to 4.97 and 2.02 Pa at 232°C for Bingham Plastic and Herschel Bulkley model, respectively. Moreover, it was observed that the amount of consistency index in Power Law model was higher than those recorded for Herschel Bulkley model at all aging temperatures. Conversely, the values of flow behavior index of Herschel Bulkley at all temperatures were observed higher than those in Power Law model. The variation of rheological parameters with temperature for weighted fresh water sepiolite mud was almost similar to the unweighted mud sample explained in details above (Figures G.18 and G.19).

The effect of temperature increment on PV and consistency indexes was not noticeable up to 177°C in the case of semi-saturated sepiolite mud (Figure G.10). However, an extreme increase was noted in Power Law consistency index from 177 to 232°C while the PV of Bingham Plastic model and consistency index of Herschel Bulkley model increased marginally. Similar to the fresh water sepiolite mud, the consistency index in Power Law model was higher than Herschel Bulkley consistency index at all aging temperatures. The same observation with fresh water sepiolite mud was made in terms of flow behavior index too. YP values for HB and BP models decreased somewhat up to 149°C, and then the trend was changed and increased very sharp up to 232°C. The fully-saturated sepiolite mud followed the parallel variations on the rheological parameters with the semi-saturated mud system discussed above (Figures G.12 and

G.13). In general, the amount of YP increased with increasing salinity in the majority of temperatures (Figures G.11and G.13).

The same commentaries can be made on the sepiolite mud systems containing 171 kg/m^3 and 342 kg/m^3 of external NaCl intrusion (Figures G.14 thru G.17).

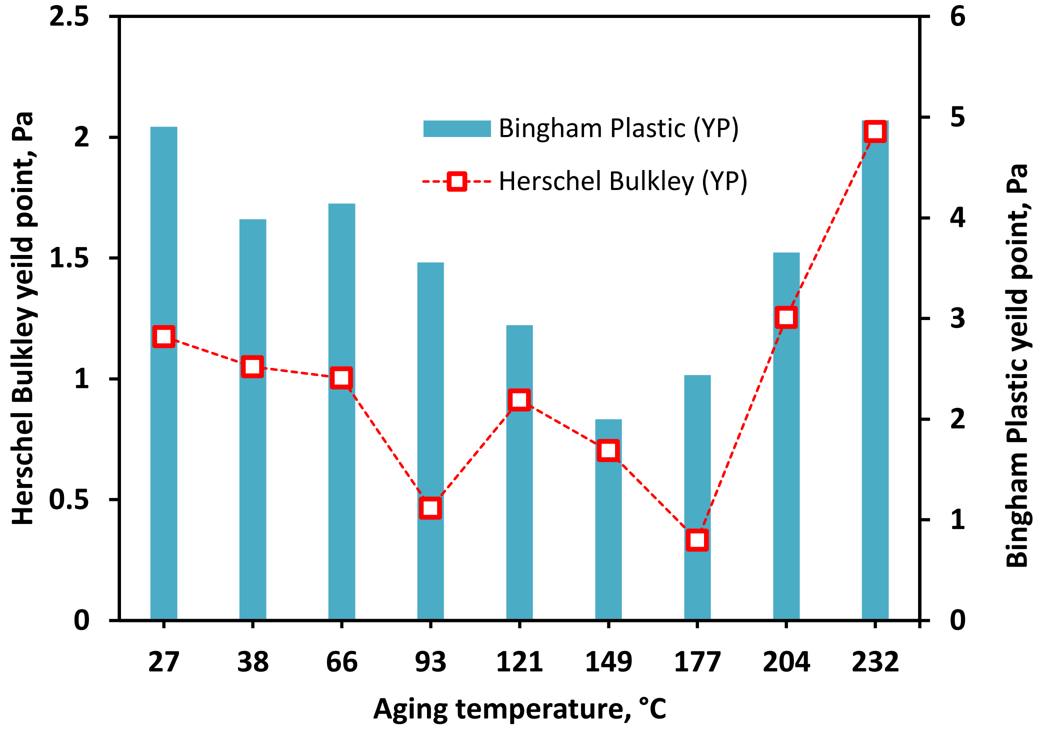

Figure 5.21: Yield point for unweighted fresh water sepiolite mud-viscometer

5.7.2 Model constants obtained from HTHP rheometer

The rheological model constants obtained from the data measured by HTHP rheometer were listed in Tables F.8 thru F.14 in Appendix-F. The Herschel Bulkley rheological model was the best one describing the dominant fit model at majority of temperatures, except in moderate temperatures. It was observed that any of three rheological models could be used as the best fit in moderate temperatures (138°C-193°C) due to resulting close values of SSE and RMSE. This conclusion was practiced in all sepiolite mud types except for the sepiolite mud system subjected to external salt intrusion of 171 kg/m^3 and 342 kg/m^3. The results of statistical analysis related to other types of sepiolite muds were given in Appendix-G in Figures G.22 thru G.28. These figures illustrated the values of residual sum of squares (SSE) and fit standard error (RMSE) for all types of mud systems with respect to varying temperatures. In addition, these figures covered the results of 17 selected temperatures ranging between 27°C and

232°C to have better visuality. The values of residual sum of squares (SSE) and fit standard error (RMSE) was illustrated in Figure 5.22 for the unweighted fresh water sepiolite mud system tested using HTHP rheometer. As shown in Figure 5.22, Herschel Bulkley model provided the lowest amount of SSE and RMSE up to 138°C. Power Law rheological model followed the Herschel Bulkley model with a slightly higher SSE and RMSE values in the same temperature interval. Similar to the results in the aging method, Bingham Plastic model presented the maximum amount of SSE and RMSE indicating that it was the worst rheological model among all to fit the data.

Approximately the same values of SSE and RMSE from the three rheological models were calculated from 138°C to 193°C. Power Law model was yielded the best fit in this temperature interval because it provided the lowest values of SSE and RMSE. However, no big differences were observed in the calculated SSE and RMSE for all three rheological models. After 193°C, Herschel Bulkley with lower values of SSE and RMSE was the best fit model up to 232°C. Interestingly, Power Law was the best fit model at 232°C because ~~of~~ negative yield point was calculated for Herschel Bulkley model.

These results stressed the importance of evaluating rheological behavior based on HTHP rheometer measurements. Any decision based on the commonly used aging method via conventional viscometer leads to obtain the rheological constants far away from reality for the fresh water sepiolite mud particularly in the temperature ranges of 138°C-193°C. The statistical results through analysis of data measured by HTHP rheometer for other types of sepiolite muds signified that the same trends with the fresh water sepiolite mud were witnessed, except for the sepiolite mud systems with 171 kg/m^3 and 342 kg/m^3 of NaCl intrusion. However, the temperature intervals where all three rheological models provided almost the same SSE and RMSE values were seen to be different. For example, this interval was recorded from 66°C to 232°C in the case of fully saturated sepiolite mud system (Figure G.24). Herschel Bulkley model provided the lowest amount of SSE and RMSE for sepiolite mud systems with 171 kg/m^3 and 342 kg/m^3 of NaCl at all testing temperatures. Similar to the aging method, as a results of HTHP rheometer test on the sepiolite mud system with171 kg/m^3 and 342 kg/m^3 of NaCl, the Herschel Bulkley was the best fit model exhibiting appropriate rheological behavior for this kind of mud system (Figures G.25 and G.26).

The variation of rheological parameters of three selected rheological models with temperature were given in Appendix-G with Figures G.29 thru G.42 for all sepiolite mud types examined via HTHP rheometer. In addition, the change of rheological parameter constants with respect to temperature in the case of unweighted fresh water sepiolite mud subjected to HTHP rheometer test was visualized in Figures 5.23 and 5.24. The results pictured in Figure 5.23 also revealed that similar to the aging method, both plastic viscosity and consistency index were minimally affected by the variations in temperature.

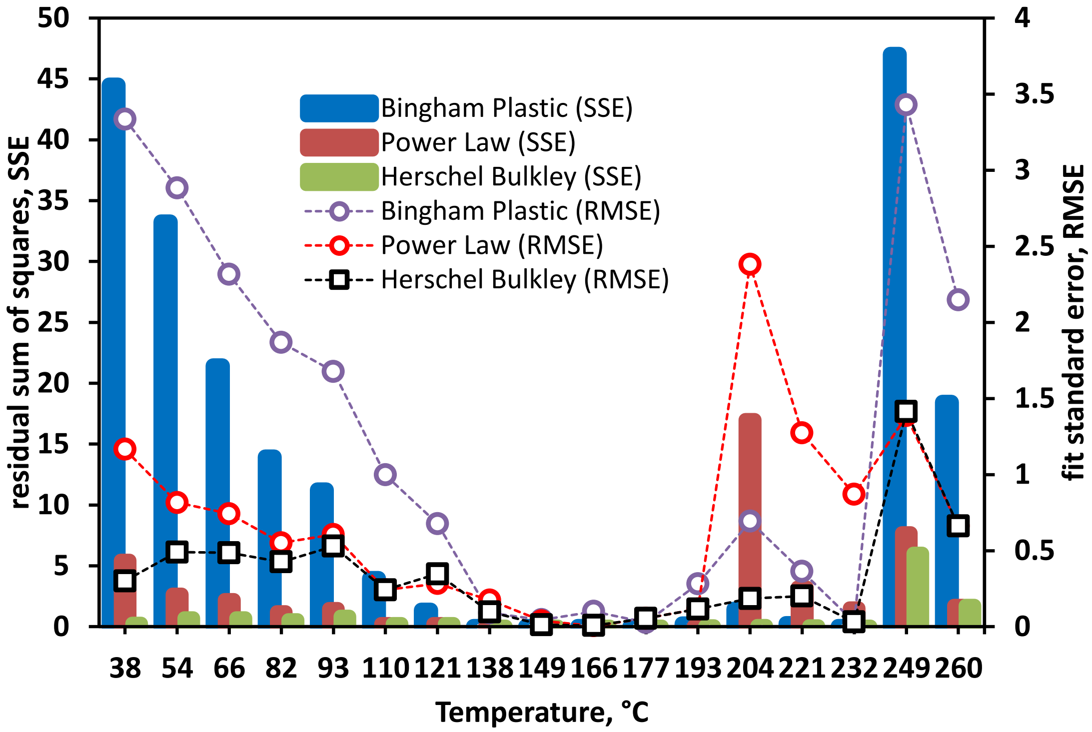

Figure 5.22: SSE and RMSE for unweighted fresh water sepiolite mud-HTHP rheometer.

Plastic viscosity (PV) of fresh water sepiolite mud decreased from 31 mPa-s at 27°C to 3.62 mPa-s at 193°C, and then increased to 12.63 mPa-s at 249°C. However, the consistency index of Power Law model decreased more than hundred times from 235 mPa-s^n at to 27°C to 2 mPa-s^n at 177°C, and then extremely increased to 1672 Pa-s^n at 204°C. Afterward, it decreased one more time to 485 mPa-s^n at 260°C. The consistency index of Herschel Bulkley model also demonstrated approximately the same behavior as in Power Law model, but the sharp increase in consistency value was recorded at lower temperature (232°C). It was recognized that the PV variation range in the fresh water sepiolite mud subjected to aging method using conventional viscometer (34 - 18 mPa-s) is remarkably lower than the range for the same mud system tested by HTHP rheometer (31 – 3.62 mPa-s). The same detection was also observed considering consistency indexes of Power Law and Herschel Bulkley models. Unlike to aging method results, the amount of flow behavior index (n) in both Power Law and Herschel Bulkley models followed the same trend up to 193°C, and then the flow behavior index (n) of Power Law model extremely increased to 1.5 (shear thickening) at 204°C whereas it enormously decreased from 0.846 at 193°C to 0.192 at 204°C in the case of Herschel Bulkley model.

Almost the same behavior was recorded on the variation of yield point with temperature for both Bingham Plastic and Herschel Bulkley model, similar to what detected in aging method. It decreased from 2.75 Pa at 27°C to 0 Pa at 149°C up to 193°C, and then extremely increased to 5.56 Pa at 221°C and again decreased to 1.85 Pa at 260°C for Bingham Plastic model (Figure 5.24). As an interesting observation, it seemed that the fresh water sepiolite sample followed Newtonian behavior rather than non-Newtonian in moderate temperatures (between 110 and 193°C) due to extremely low amount of yield point. In addition, the value of flow behavior index (n) obtained as the constant parameter for Power Law model confirmed this observation. The amount of flow behavior index (n) for Power Law model based on HTHP rheometer measurements generally increased with increasing temperature up to 188°C, and then tended to decrease up to the final rheometer test temperature. It was observed that the value of flow behavior index (n) was equal to 1 at 149°C and increased to 1.094 at 177°C. It continued to be above 1 up to 188°C, and then decreased to less than 1. It meant that when considering Power Law model, the shear thinning (pseudo plastic) behavior tended to change into shear thickening (dilatant) behavior by increasing the value of n above 1 under the effect of temperature up to 188°C. Fluid again switched to shear thinning (pseudo plastic) behavior beyond this temperature. Moreover, it was also observed that the amount of K in Power Law model was higher than that recorded for Herschel Bulkley model up to 110°C, and then it was recorded the same for both model up to 193°C. The variation of rheological parameters with temperature for the weighted fresh water sepiolite mud was almost similar to the unweighted mud sample explained above (Figure G.39).

There was no significant change in the PV and K up to 177°C in the case of using semi-saturated sepiolite mud (Figure G.31). Nevertheless, the PV of Bingham Plastic model and K of Herschel Bulkley model slightly increased whereas the K of Power Law model experienced an extreme increase from 177 to 260°C (Figure G.31).

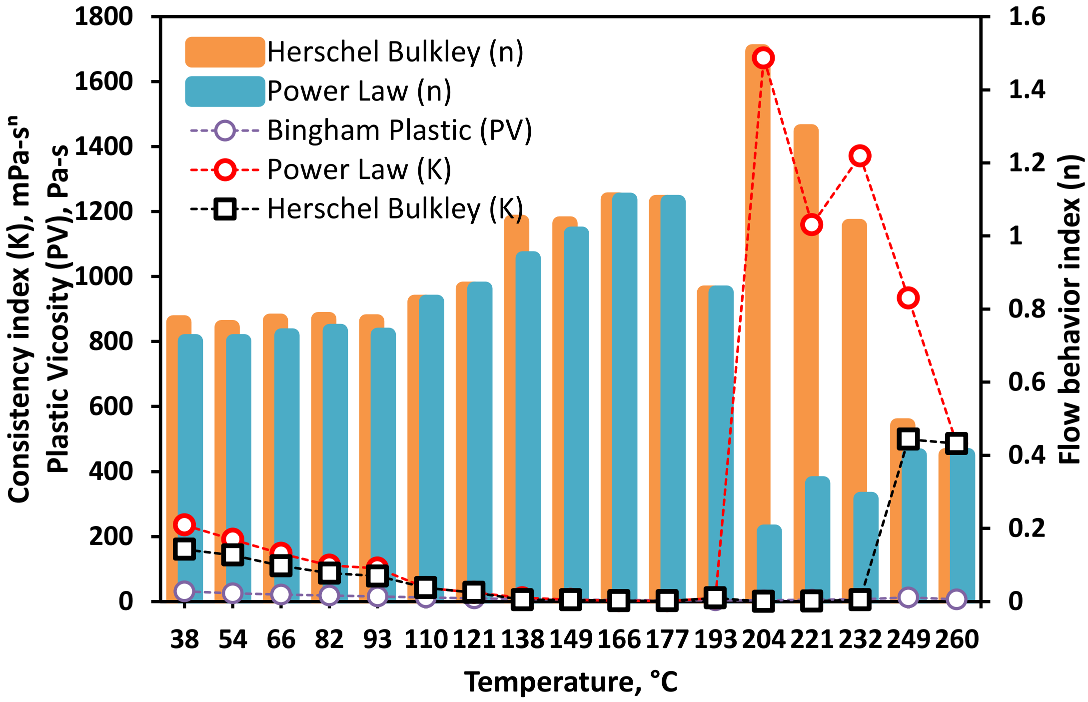

Figure 5.23: Rheological parameters of unweighted fresh water sepiolite mud-HTHP rheometer.

This was what exactly happened for the semi-saturated sepiolite mud system examined with aging method as well. The consistency index representing viscosity in Power Law and Herschel Bulkley models was recorded almost the same value and also very close to the plastic viscosity of Bingham Plastic model up to 177°C for the semi-saturated sepiolite mud. Flow behavior index (n) of Power Law model was slightly increased to 1.022 at 149°C, and then decreased to 0.494 at 260°C. The same trend was seen in flow behavior index (n) of Herschel Bulkley model.

The variation in the yield points of Herschel Bulkley and Bingham Plastic model with temperature for the semi-saturated sepiolite mud did not follow a specific trend, (Figure G.32). Generally, it decreased up to 166°C, and then increased up to 260°C. Although the rheological properties of a non-Newtonian fluid system must consider the change in viscosity and yield point all together, the values of yield point have more importance than those of consistency and flow behavior indexes. YP is used to evaluate the ability of a mud to lift cuttings out of the annulus. A high YP implies a non-Newtonian fluid that carries cuttings better than a fluid of similar density with lower YP. Results also indicated that the YP decreased with increasing salinity in the sepiolite mud systems. However, the rate of decrease in YP with increasing salinity (from semi to fully-saturated) was quite low than that was observed in increasing salinity from fresh water to semi-saturated.

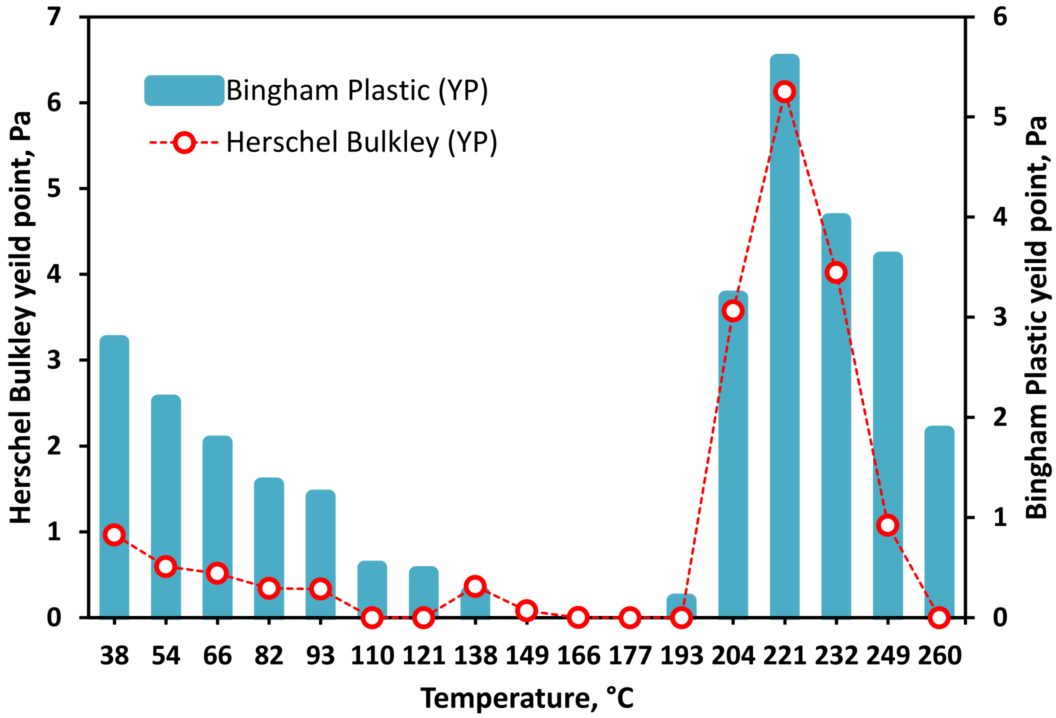

Figure 5.24: Yield point for unweighted fresh water sepiolite mud-HTHP rheometer

The fully-saturated sepiolite mud subjected to HTHP rheometer test followed the similar variations through rheological parameters observed in the semi-saturated mud system discussed above (Figures G.33 and G.34). In addition, the same interpretations could be made about the sepiolite mud system containing 171 kg/m^3 and 342 kg/m^3 of NaCl (Figures G.35-G.38) in the case of using HTHP rheometer to measure rheological properties.

5.8 Chapter Conclusions

Thermal in-situ rheological properties of seven types of sepiolite muds were measured with direct measurement method using HTHP rheometer and compared to the results obtained from the aging method conducted by conventional viscometer. The rheological parameters from these two methods were determined based on three well-known non-Newtonian rheological models. Matlab curve fitting toolbox was used to identify rheological constants for Bingham Plastic, Power Law, and Herschel Bulkley methods and to select the best fit model for the sepiolite muds at elevated temperatures. The results indicated that:

- In-situ rheological measurement confirmed the thermal stability of sepiolite clay in spite of structural changes during heating. The thermal rheological test results for the fresh water sepiolite suspension verified the alteration in sepiolite clay structure during heating period up to 260°C; however, this alteration was not reversible as it proved based on the rheological measurements during cooling to room condition.
- The performance of sepiolite clay to provide an acceptable rheological properties in saline environment was quite impressive such that the viscosity of fresh water sepiolite suspension increased with increasing salinity.
- Thermal in-situ rheological properties of unweighted fresh water sepiolite mud indicated that the viscosity of sample decreased with increasing temperature up to the gelation temperature (193°C), and then tended to increase with the further temperature increase. This behavior was similar to what observed during rheological measurements using conventional aging method. However, the gelation event began at earlier temperatures based on viscometer data than those of obtained from HTHP rheometer.
- Compare to the commonly used drilling fluids (Bentonite/polymer and Lignosulfonate muds), sepiolite muds provided more efficient rheological and filtration properties particularly at temperatures above 149°C.
- The variation in thermal viscosity of salty water sepiolite muds was much less than what was observed in the fresh water sepiolite muds. On the other hand and more interestingly, HTHP filtration test on salty water sepiolite muds indicated that the water losses decreased with increasing salinity. Therefore, the efficiency of sepiolite mud at high salinity could be an exclusive advantage of this mud making its usage reasonable through drilling salt domes or formation waters having high salt content.
- The sepiolite mud had tolerated excessive NaCl invasions as it was observed during thermal rheological measurements as well as HTHP filtration measurements at elevated temperatures. Impressively, the amount of water loss decreased noticeably with increasing salt intrusion for the sepiolite base mud.

- The difference between the rheological results conducted based on HTHP rheometer and conventional viscometer increased with increasing temperature. Therefore, wellbore hydraulic design based on viscometer data cannot represent the in-situ conditions, thereby leading to waste ~~in~~ of time and cost by the result of making conservative and unrealistic decisions.
- The statistical analysis performed based on data measured by conventional viscometer resulted in lower SSE and RMSE values for all mud systems in the case of the Herschel Bulkley model at each temperature. It turned out that the Herschel Bulkley model was the best fit rheological model to capture the rheological behavior of all sepiolite mud types based on thermal aging method via conventional viscometer.
- Unlike to thermal aging method, implementation of the statistical analysis through rheometer results revealed that Power Law model was more accurate than Herschel Bulkley model in terms of being best fit model representing the rheological behavior of mud samples with lower amount of SSE and RMSE at moderate temperatures (138°C-193°C).
- The rheological parameters of all sepiolite muds were determined using Matlab curve fitting toolbox, and the effect of temperature variation on parameters using viscometer and rheometer measurements were studied to have better understanding of thermal rheological properties of sepiolite muds.

6. LUBRICITY

6.1 Introduction

During drilling operation of a wellbore, any contact might happen between drillstring and wellbore wall due to the possible well deviation, and a compaction pressure applied to the drillstring. This contact causes to some difficulties through drillstring (especially in drill collar) in terms of wellbore stabilities. Specifically, it causes wear on drillstring and enlargement on wellbore wall. It is known that drilling fluid flows between drillstring and wellbore wall; therefore, it causes friction between them due to having different mechanical properties. The value of this friction is proportional to the problem that might occur. In other words, the value of this friction decreases with increasing lubricity of drilling fluid, thereby minimizing the stability of wellbore and drillstring. For this purpose, the lubricity of drilling fluid plays an active role in evaluation of drilling fluid performance as well as proper drilling fluid selection. Therefore, the lubricity properties of sepiolite drilling fluid was investigated during this study to achieve this goal. It must also be mentioned that there is neither specification on lubricity test method nor standard test equipment defined by American Petroleum Institute (API). In addition, no accepted universal method is available in the drilling industry.

Lubricity (coefficient of friction) is the important parameter through drilling because of the fact that low lubricity (high coefficient of friction) increases drilling costs and causes a great waste of time. High torque and drag become critical issues in drilling. This is particularly true for water base muds since the water base muds have high coefficient of friction between drillstring and wellbore compared to that of oil base muds. Although oil base muds have lower coefficient of friction values and better wellbore stabilizing characteristics, the current trend in the oil and gas drilling industry is to increase the usage of water base muds. Some of the factors influencing this trend include chancing environmental regulation intended to restrict toxic and non-biodegradable materials, logistical problems in remote locations, gas solubility in oil base fluids, advances in lubricant additives and borehole stabilizers, and the lower cost of water base muds.

Although general tribology literature is rather extensive, information regarding wear and friction of drillstring and casing is limited. It generally describes the composition of complex lubricating agents, the effect of lubricant addition to a mud on overall torque, or the results of small-scale lubricity tests.

6.2 Literature Review

Bradley and Fontenot's (1975) conclusion on casing wear are rather general and identify drillstring rotation as the major cause of wear. Also dogleg severity, and thus contact force, is shown to have a major impact on wear. Rough tool joints are identified as the cause of severe casing wear, whereas bentonite, barite, and nonabrasive drilled solids are shown to decrease wear. True and Weiner (1975) reached similar results with respect to the detrimental effect of rough tool joints, in particular rough hard facings. They did not investigate the effect of mud composition. Williamson (1981) emphasized the importance of the contact pressure as opposed to the contact load as the key factor determining casing wear. All his experiments were performed in a simple, unweighted bentonite mud and thus do not lead to any conclusions on the effect of mud composition.

Best (1986) showed the importance of using smooth tool joints to prevent excessive wear. He also showed that a thin layer of solids in the contact area can have a highly protective effect. White and Dawson (1985) studied wear and friction simultaneously in full-scale equipment, using smooth steel tool joints, actual contact loads, and both weighted and unweighted muds. A model is presented that assumes a linear relationship between the wear volume and the friction force.

Schoenmakers (1986) found good agreement between the results of the casing-wear test facility and field measurements. He also reconfirms the importance of smooth tool joints and presents criteria and an inspection method to evaluate tool-joint roughness in the field.

According to Bol (1986), the appropriate range of lubricity coefficient varies from 0.09 to 0.14 for water base muds with lubricants. Redburn at al., (2013) emphasized range from 0.15 to 0.45 for water base drilling fluids. Founded lubricity coefficient range from lubricity test of formulated sepiolite mud is in the range of 0.10 to 0.20. In addition, it was observed that there are no significant changes in lubricity coefficient values with increasing temperature.

6.3 Experimental Study on Lubricity Properties of Sepiolite Muds

Fann Model 212 EP/Lubricity Tester basically consists of a rotating steel ring against which a metal block can be compressed at variable loads with a torque wrench. Ring and block are immersed in the mud during the test, and the friction force between the two is measured. The coefficient of friction is calculated from the applied torque and the friction force. Before a test is started, the test block has to be conditioned in distilled water. As shown in the Equation 6.1, torque meter reading values and correction factor are used to calculate lubricity coefficient of mud.

$$\text{Lubricity Coefficient} = \frac{\text{Torque Meter Reading} \times \text{ Correction Factor}}{100} \qquad (6.1)$$

To determine the value of Torque Meter Reading and Correction Factor, test procedure is as follows:

- Sample cup is filled with sample.
- Lubricity test ring is attached to the instrument. Device is run for 15 minutes at 60 rpm and 0 torque then device is switched off.
- Torque arm and lubricity test block are attached to the instrument. Torque arm is attached to torque wrench clam. As a results, block and ring surfaces touch to each other.
- Filled sample cup is placed to the instrument so that block and ring are dipped in sample. Device is run for 5 minutes at 60 rpm and 0 in-lb torque. After 5 minutes, values of rpm and torque are checked.
- Torque adjust handle is rotated clockwise to apply 150 in-lb (16.95 N·m) of torque. After 5 minutes, torque value is read on the dial.
- Device is switched off and torque adjust handle is rotated counterclockwise to get zero load.

The average of the read values are used in the Equation 6.2 to calculate Correction Factor. If the average of the read values were not in the range of 28 to 48, the apparatus must be calibrated.

$$\text{Correction Factor } (CF) = \frac{34}{\text{average reading}} \tag{6.2}$$

The experimentally obtained data related to the lubricity of sepiolite muds and calculated lubricity coefficient using Equations 6.1 and 6.2 were given in Table 6.1.

Table 6.1: Lubricity coefficient of sepiolite muds.

	Temperature, °C								
Mud system	**27**	**38**	**65**	**93**	**121**	**149**	**177**	**204**	**232**
Fresh water base mud	0.15	0.15	0.15	0.16	0.15	0.16	0.16	0.18	0.19
Base mud+171 kg/m^3	0.22	0.21	0.21	0.20	0.20	0.18	0.19	0.20	0.21
Base mud+342 kg/m^3	0.20	0.20	0.19	0.18	0.17	0.15	0.17	0.15	0.17
Semi-saturated mud	0.20	0.20	0.19	0.19	0.19	0.19	0.18	0.18	0.19
Fully-saturated mud	0.17	0.17	0.17	0.17	0.17	0.17	0.15	0.15	0.17
Fresh water weighted mud	0.31	0.30	0.29	0.28	0.30	0.30	0.29	0.31	0.31

The lubricity coefficient of sepiolite muds were determined using the lubricity tester after 16 hour of thermal aging in the aging cells and cooling in ambient condition. The variation of lubricity coefficient of all sepiolite mud types with increasing temperature were depicted in Figure 6.1.

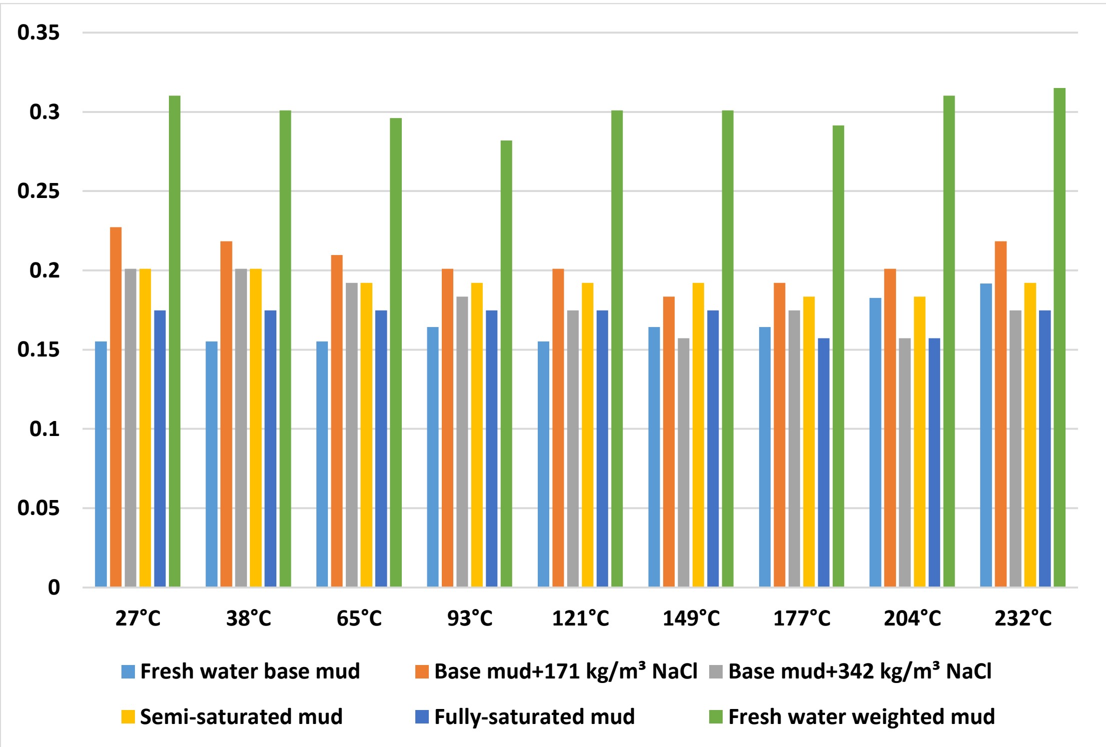

Figure 6.1: the variation of lubricity coefficient of sepiolite muds with temperature.

6.4 Results and Discussions

The effect of temperature increment on lubricity of sepiolite mud types listed in Table 5.2 were evaluated, and it was concluded that the lubricity coefficient and consequently the amount of friction between drillstring and wellbore wall increased with increasing temperature. It is obvious that this event causes increment in the drillstring wearing.

It was clear from the results depicted in Figure 6.1, a slight increase was observed in lubricity coefficient with salinity. However, the rate of increase was not different with what explained through study conducted by Ke and Foxenberg (1998). Lubricity coefficient increased in semi-saturated sepiolite mud with increasing salinity; however, the lubricity coefficient decreased again in fully-saturated sepiolite mud sample with the further increase in salinity. The amount of lubricity coefficients were slightly lower in salt water saturated sepiolite than those recorded for sepiolite muds subjected to external NaCl intrusion. The barite-weighted sepiolite mud system was recognized with the highest values of lubricity coefficient.

The amount of lubricity coefficient in the weighted mud system was approximately twice more than that of the unweighted fresh water mud system. It was due to the abrasiveness of weighted agent (Barite) used in formulation of the weighted mud system. When both salinity and temperature effects were taken into account, it was revealed that the lubricity coefficient of sepiolite mud types were in the appropriate interval specified in the study performed by Redburn et. al., (2013). It must be considered that the results given by Redburn et. al., (2013) was valid for unweighted mud systems at low temperatures. The lubricity coefficient of sepiolite mud systems slightly increased with increasing temperature; however, this increase was not significant as seen from Figure 6.1. Therefore, this could be another advantage of the sepiolite muds in terms of using them in hot wells. In other word, the insignificant effect of temperature on lubricity value of sepiolite mud is the important evidence to confirm the usage of this kind of mud at high temperatures. As a result, it is not expected high increments in the lubricity coefficient and consequently in the friction factor if sepiolite mud is used. Therefore, the effect of wearing between drillstring and wellbore wall would be minimized. There is no doubt that this situation could be a great advantage of sepiolite base mud.

6.5 Chapter Conclusion

Thermal effects on the lubricity of sepiolite muds were presented in this chapter. Seven types of sepiolite muds listed in Table 5.2 were tested using lubricity tester after thermal aging at different temperatures. The results indicated that:

- The lubricity coefficient of sepiolite suspension (only sepiolite and fresh water mixing) was very high as recording its value was out of apparatus measurement ranges. Therefore, using polymers and lubricants (in extreme conditions) as additives to prepare mud samples is mandatory and proposed.
- Lubricity coefficient of sepiolite muds containing additives were in the range of recommended values provided in the literature even at high temperatures.
- Increasing temperature and salt content have not significant effects on the measured lubricity coefficient of sepiolite muds.
- Weighted mud proved higher amount of lubricity coefficients due to effect of weighting agent and high amount of solid content in the mud.
- Lubricity investigations of sepiolite base muds should be continued with the addition of various lubricants into the mud.

7. A NOVEL SEMI-ANALYTICAL MODEL FOR PRESSURE SURGES THROUGH NON-NEWTONIAN FLUIDS

7.1 Introduction

Down-hole pressure as an important part of well control must continuously be monitored during drilling operation. Circulating pressures resulted from pump operation are usually calculated using monographs, slide rules, or simple computer programs. Clark (1955, 1956), Burkhardt (1960), and Schuh (1964) tried to describe bottom-hole pressure variations due to drillstring movement (swab/surge pressures). Approximate methods developed by Burkhardt (1960) for Bingham Plastic model or Schuh (1964) for Power-Law model are generally used to determine these pressure changes. However, these rheological models cannot adequately describe the flow behavior of most of drilling fluids used in the field. The yield-power-law (YPL) model (or known as Herschel Bulkley) describes the rheology of most common drilling and completions fluids in the best way. Despite its high accuracy in predicting the flow properties of drilling fluid, there is a clear gap in literature in predicting surge and swab pressures for a YPL fluid.

7.2 Literature Review

As known, frictional pressure loss of a non-Newtonian fluid using annular geometry cannot be calculated analytically. In this study, slot geometry solution method is employed to analytically model frictional pressure loss (FLP) for non-Newtonian fluids. As drilling fluid exhibits non-Newtonian rheological properties, calculation of surge and swab pressure due to drillpipe movement becomes important from the point of drilling engineer view. Some researchers (Horn 1950; Cannon 1934; Goins et al.1951) accomplished several studies on surge and swab pressures. As a common point in all of these studies, it was expressed that high pressure changes in wellbore due to extreme tripping speeds caused some wellbore problems such as formation fracture, kicks, lost circulation, and blowouts. Some researchers (Ormsby 1954;

Cardwell 1953) considered only pressure drops due to viscous drag of flowing Newtonian fluid in a stationary pipe wall. They introduced prediction techniques to determine these pressures in both laminar and turbulent flow regimes. Clark (1955) added the effect of inner pipe motion in his study by presenting idealized graphs and equations to estimate surge and swab pressures in a concentric annulus for a Bingham Plastic fluid. A well-known study (Burckhardt 1960) in literature proved that running closed-end casing or drillpipe in the hole produced high surge pressures. A semi-empirical method was developed in this study that ended up to get the quantitative techniques representing pressure surges by the Bingham Plastic fluid. Schuh (1964) considered Power Law fluid using numerical method for this problem. Like Burckhardt (1960), Schuh evaluated concentric annulus at steady state flow. An exhaustive study, carried out by Fontenot and Clark (1974), provided a computer program that involved in some models presented by previous researchers to determine surge pressures for the both BP and PL fluids. This program included the effect of some factors such as mud properties, geometries, closed and open-ended pipe. They obtained the convergent results with field measurements in their study. Some other investigator (Bing et al. 1995; Wang and Chukwu 1996; Lal 1983) developed unsteady state models to conclude bottom hole pressure variations during tripping. Real life situations like pipe acceleration effect have been taken into account in these studies. Hussain and Sharif (2009) indicated the decrease of surge pressure with increase in eccentricity.

7.2.1 Commonly used surge pressure models

Numerous models have been suggested to predict the surge and swab pressures in a concentric annulus. However, the most commonly used models to calculate surge and swab pressures have been developed by Burkhardt (1960) for a Bingham Plastic fluid and Schuh (1964) for a Power Law fluid. A brief introduction of these models were presented in the following part of this chapter.

7.2.1.1 Burkhardt model

Burkhardt (1960) suggested a simplified technique to compute surge pressure component stemming from the viscous drag forces due to pipe movement. The effect of pipe movement on the fluid velocity is very difficult to be mathematically expressed because the movement of pipe makes the fluid velocity in the annulus more complex.

Therefore, it is required to calculate the axial mean velocity from the displaced mud volume to be used for hydraulic calculations. Burkhardt method is based on the use of an effective mean velocity ($\bar{v}_{ae},$ ft/min) in the annular flow equations as follows;

$$\bar{v}_{ae} = \bar{v} + \bar{K} v_p \tag{7.1}$$

where the constant $\bar{K}$, the mud clinging constant, can be obtained using special chart developed by Burkhardt or following equation if the flow regime is laminar.

$$\bar{K} = \frac{\alpha^2 - 2\alpha^2 ln\alpha - 1}{2(1-\alpha^2) ln\alpha} \tag{7.2}$$

where α is the ratio of pipe diameter to hole diameter. The volumetric component of the velocity due to mud volume displacement ($\bar{v}$) is given by the following expression:

$$\bar{v} = \left(\frac{d_p^2}{d_h^2 - d_p^2}\right) v_p \tag{7.3}$$

where the d_p is pipe diameter, d_h is the hole diameter, and pipe velocity is presented by v_p.

Dimensionless quantity S, plasticity or Bingham number, and conductance ($\bar{\gamma}$) defined by Melrose (1958) are used to link viscous drag forces of the Bingham Plastic model to Newtonian fluid. These parameters are used to determine the flow regime and consequently friction factor. The plasticity is defined by following equation;

$$S = 2394 \frac{(d_h - d_p)\tau_o}{\mu_p v_{ae}} \tag{7.4}$$

where τ_o is the yield stress (lbf/100 ft^2), μ_p is the plastic viscosity (cp), and v_{ae} is the effective mean velocity (ft/min).

Following relationship is defined to calculate the conductance. An iterative technique should be applied to obtain conductance.

$$\bar{\gamma} = 1 - \frac{\bar{\gamma}\, S}{8} + \frac{1}{2}\left(\frac{\bar{\gamma}\, S}{12}\right)^4 \tag{7.5}$$

A modified friction factor-Reynolds number chart for use in Bingham Plastics was developed by Burkhardt (1960). In addition, the Reynolds number for annular flow of Bingham Plastics was defined by:

$$R_e = 15.44 \frac{(d_h - d_p) v_{ae} \rho}{\mu_p} \tag{7.6}$$

The modified friction factor for Bingham Plastic fluids can also be determined using the following equations. In order to compute the friction factor for turbulent flow regime, an iterative technique is required.

For laminar flows, $S\bar{\gamma} \leq 2000$,

$$f_b = \frac{24}{\gamma R_e} \tag{7.7}$$

For turbulent flows, $S\gamma > 2000$,

$$f_b = \left[4log\left(R_e \times \sqrt{f_b}\right) - 0.4\right]^{-2} \tag{7.8}$$

Finally, the pressure surge generated by the average effective mud velocity in the annulus resulting from the movement of closed pipe in the borehole is given by the conventional Fanning equation;

$$\frac{\Delta P}{\Delta L} = \frac{f_b v_{ae}^2 \rho}{9.282 \times 10^4 (d_h - d_p)} \quad \left(\frac{psi}{ft}\right) \tag{7.9}$$

7.2.1.2 Schuh model

Further study was performed by Schuh (1964) to estimate surge and swab pressures for a Power Law fluid. He tried to investigate the effect of rheological properties of mud through open and close ended pipe with different diameter ratios on pressure drop while circulating mud as well as tripping operation. He developed a computer program to make calculations easy and fast. He used the concept of Burkhardt (the mud clinging constant) to calculate effective mean velocity in the annular flow. The rheology parameters for a Power Law fluid, K and n were determined and the Reynolds number during tripping operation was approximated by Equation (7.10).

$$R_{em} = \frac{v_{ae}^{2-n} (d_h - d_p)^n \rho}{K \left(\frac{2n+1}{2n}\right)^n 8^{n-1}} \tag{7.10}$$

where v_{ae} is the effective mean velocity (m/sec), ρ is density (kg/m^3), K is consistency index Pa-s^n, d_p is pipe diameter, d_h is the hole diameter (meter), and n is flow behavior index for Power Law fluid. The friction factor is determined using Reynolds number as follows.

For laminar flows (Re < 3470 – 1370n),

$$f_s = \frac{24}{R_e} \tag{7.11}$$

For turbulent flows (Re > 4270 – 1370n),

$$f_s = \left[\frac{4}{n^{0.75}} log\left(R_e \times f_s^{\frac{1-n}{2}}\right) - \frac{4}{n^{1.2}}\right] \tag{7.12}$$

For transition flows (3470 – 1370n < Re < 4270 – 1370n)

$$f_s = \frac{16}{R_e} + \left[\frac{R_e - (3470 - 1370n)}{800}\right](f_t - f_l) \tag{7.13}$$

Consequently using effective velocity, surge pressure was determined by Schuh (1964) as:

$$\frac{\Delta P}{\Delta L} = \frac{2 f_s v_{ae}^2 \rho}{\left(d_h - d_p\right)} \quad \left(\frac{Pa}{m}\right) \tag{7.14}$$

In this part of study, a comprehensive dimensional theoretical technique (semi-analytical) using fundamental equations was developed and programmed for computer solution for Yield Power Law (Herschel Bulkley) model. The validation of semi-analytical method was verified by data sets taken from literature. The surge and swab pressure generated while using sepiolite mud was calculated using new derived method.

7.3 Semi-Analytical Model Derivation for Surge and Swab Pressure for a Herschel Bulkley Fluid

The analytical solution method of frictional pressure loss (FPL) in non-Newtonian fluid to get the general solution has been used to calculate surge and swab pressure due to the movement of plate in slot geometry as shown in Figure 7.1. According to literature (Bourgoyne et.al 1991), annular flow can be approximated using equation developed for flow through slot geometry, as long as the ratio of inner diameter to outer diameter is more than 0.3. Application of slot flow equation to represent flow in annular geometry is allowed to make solution simple. Annular geometry and its corresponding acceptable slot geometry to find FPL are given in Figure 7.2. The area (A) and thickness (h) of slot geometry can be written as:

$$A = Wh = \pi(r_2^2 - r_1^2) \tag{7.15}$$

$$h = r_2 - r_1 \tag{7.16}$$

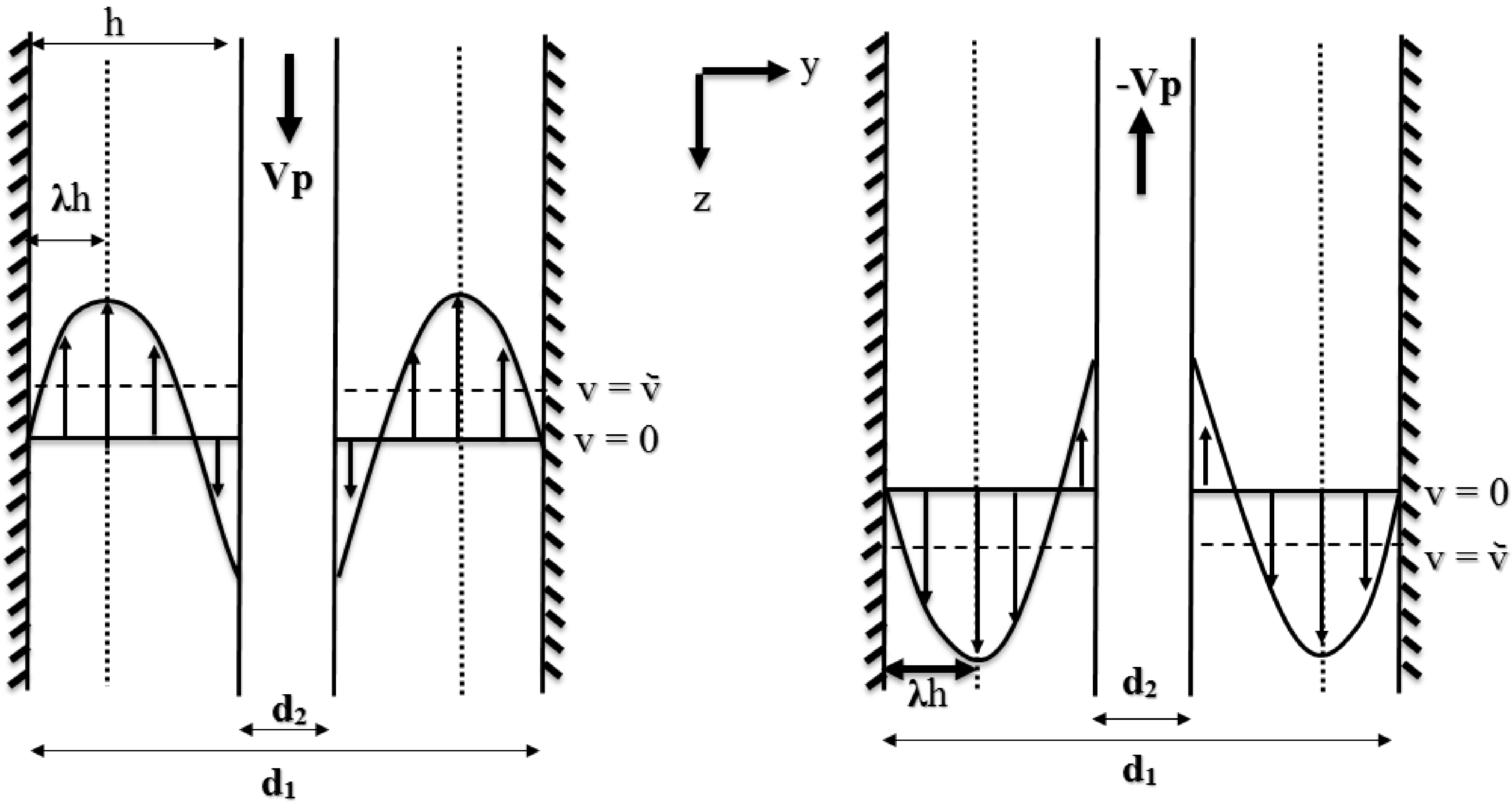

Figure 7.1: Velocity profile generated at annulus due to drill pipe movement (surge and swab).

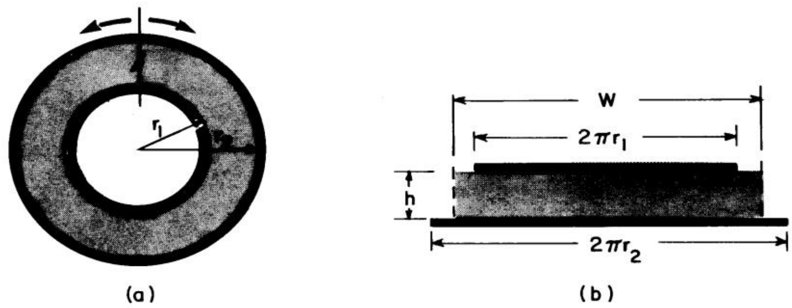

Figure 7.2: Representing annulus as a slot: (a) annular and (b) equivalent slot (Bourgoyne et. al. 1991).

Differential equation provided in literature (Bourgoyne et.al 1991) to calculate frictional pressure loss for annular flow by the help of slot flow approximation is as follows:

$$\frac{dP_f}{dL} - \frac{d\tau}{dy} = 0 \tag{7.17}$$

Equation 7.17 gives the relationship between shear stress and frictional pressure gradient for a flow in the slot that can be obtained regarding to the pressure and viscous forces acting on an element of fluid in the slot. This study also concerns this equation as a beginning point of analytical solution. Figure 7.3 depicts pressure and viscous forces acting on an element in the slot for a Herschel Bulkley fluid.

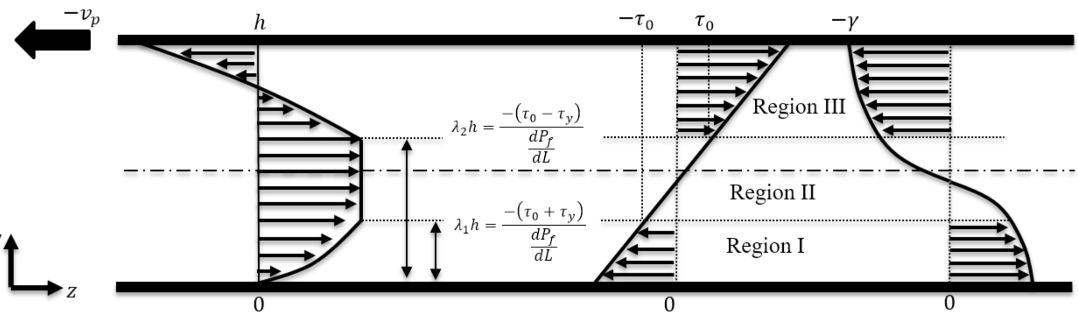

Figure 7.3: Slot geometry for a Herschel Bulkley fluid with axial movement of inner pipe.

Equation 7.17 can be integrated over boundary conditions expressed by independent variable to find required constant values. Since frictional pressure gradient represented by the Equation 7.17 is constant along y direction (perpendicular to flow direction), it can be integrated with respect to y in an interval of y=0 to y=h. h is the height of the slot. The result of integration would be;

$$\tau = y\frac{dP_f}{dL} + C_1 \tag{7.18}$$

C_1 is the constant of the integration that can be calculated by employing boundary condition. For a Herschel Bulkley fluid, portion of the fluid having a shear stress less than the yield point must move as a rigid plug down the conduit. At the inner layer of the plug,

$$\tau_1 = -\tau_y = \tau_0 + \lambda_1 h \frac{dP_f}{dL} \qquad \rightarrow \qquad \tau_y + \tau_0 = -\lambda_1 h \frac{dP_f}{dL} \tag{7.19}$$

Likewise at the outer layer of the plug the shear stress must be given by:

$$\tau_2 = \tau_y = \tau_0 + \lambda_2 h \frac{dP_f}{dL} \qquad \rightarrow \qquad \tau_y - \tau_0 = -\lambda_2 h \frac{dP_f}{dL} \tag{7.20}$$

So it can be inferred:

$$\lambda_2 h - \lambda_1 h = \frac{-(\tau_0 - \tau_y)}{\frac{dP_f}{dL}} + \frac{(\tau_0 + \tau_y)}{\frac{dP_f}{dL}} \tag{7.21}$$

$$h(\lambda_2 - \lambda_1) = \frac{2\tau_y}{\frac{dP_f}{dL}} \tag{7.22}$$

$$\frac{dP_f}{dL} = \frac{2\tau_y}{h(\lambda_2 - \lambda_1)} \tag{7.23}$$

7.3.1 Velocity profile for the first region (inner layer)

As seen from Figure 7.3 for the first region, shear stress τ, is negative whereas shear rate γ, corresponding to dv/dy has positive value. Therefore, Equation (5.12) defined for Herschel Bulkley fluids can be rewritten as below regarding to the above mentioned conditions:

$$\tau = -K(\gamma)^n - \tau_y \tag{7.24}$$

The equality given in Equation (7.24) can be written as follows according to definition of shear stress at first region.

$$\tau = -K\left(\frac{dv}{dy}\right)^n - \tau_y = \tau_0 + y\frac{dP_f}{dL} \tag{7.25}$$

This relation is valid for the first region where $0 \leq y \leq \lambda_1 h$. For this region shear rate conventional sign is:

$$\frac{dv}{dy} > 0 \quad \rightarrow \quad \gamma = -\frac{dv}{dy} < 0 \tag{7.26}$$

So:

$$-K\left(\frac{dv}{dy}\right)^{n} - \tau_y = \tau_0 + y\frac{dP_f}{dL} \tag{7.27}$$

Velocity profile equation that is valid for the first region at $0 \le y \le \lambda_1 h$ can be rewritten by as follows:

$$\left(\frac{dv}{dy}\right)^{n} = \frac{-(\tau_0 + \tau_y)}{k} - \frac{y}{K}\frac{dP_f}{dL} \tag{7.28}$$

$$\frac{dv}{dy} = \left[\frac{-1}{K}\left[\left(\tau_0 + \tau_y\right) + y\frac{dP_f}{dL}\right]\right]^{\frac{1}{n}} \tag{7.29}$$

$$\frac{dv}{dy} = \left[\frac{-1}{K}\left[y\frac{dP_f}{dL} - \lambda_1 h\frac{dP_f}{dL}\right]\right]^{\frac{1}{n}} = \left[\frac{1}{K}\frac{dP_f}{dL}\left[\lambda_1 h - y\right]\right]^{\frac{1}{n}} \tag{7.30}$$

$$\frac{dv}{dy} = \left(\frac{1}{K}\right)^{\frac{1}{n}}\left(\frac{dP_f}{dL}\right)^{\frac{1}{n}}(\lambda_1 h - y)^{\frac{1}{n}} \tag{7.31}$$

$$dv = \left(\frac{1}{K}\right)^{\frac{1}{n}}\left(\frac{dP_f}{dL}\right)^{\frac{1}{n}}(\lambda_1 h - y)^{\frac{1}{n}}dy \tag{7.32}$$

$$v_{inner} = \left(\frac{1}{K}\right)^{\frac{1}{n}}\left(\frac{dP_f}{dL}\right)^{\frac{1}{n}}\frac{(\lambda_1 h - y)^{1+\frac{1}{n}}}{1+\frac{1}{n}} + v_0 \tag{7.33}$$

Applying BC $y = 0 \rightarrow v_0 = 0$ velocity profile for inner layer would be

$$v_0 = \left(\frac{1}{K}\frac{dP_f}{dL}\right)^{\frac{1}{n}}\frac{(\lambda_1 h)^{1+\frac{1}{n}}}{1+\frac{1}{n}} \tag{7.34}$$

$$v_{inner} = \frac{1}{1+\frac{1}{n}}\left(\frac{1}{K}\frac{dP_f}{dL}\right)^{\frac{1}{n}}\left[(\lambda_1 h)^{1+\frac{1}{n}} - (\lambda_1 h - y)^{1+\frac{1}{n}}\right] \tag{7.35}$$

Flow rate equation can be obtained by integrating velocity equation over the flow area considering the relation between flow rate and velocity defined as:

$$q = VdA = VWdy \tag{7.36}$$

Eventually, the flow rate relationship for the first region can be developed as:

$$q_1 = \frac{w}{1+\frac{1}{n}}\left(\frac{1}{K}\frac{dP_f}{dL}\right)^{\frac{1}{n}}\left[(\lambda_1 h)^{1+\frac{1}{n}}y - \frac{(\lambda_1 h - y)^{2+\frac{1}{n}}}{2+\frac{1}{n}}\right]_0^{\lambda_1 h} \quad (7.37)$$

$$q_1 = \frac{-w}{1+\frac{1}{n}}\left(\frac{1}{K}\frac{dP_f}{dL}\right)^{\frac{1}{n}}\left[\frac{(\lambda_1 h)^{2+\frac{1}{n}}}{2+\frac{1}{n}} - (\lambda_1 h)^{2+\frac{1}{n}}\right] \quad (7.38)$$

$$q_1 = \frac{w}{2+\frac{1}{n}}\left(\frac{1}{K}\frac{dP_f}{dL}\right)^{\frac{1}{n}}(\lambda_1 h)^{2+\frac{1}{n}} \quad (7.39)$$

$$q_1 = \frac{w(h)^{2+\frac{1}{n}}}{2+\frac{1}{n}}\left(\frac{1}{K}\frac{dP_f}{dL}\right)^{\frac{1}{n}}(\lambda_1)^{2+\frac{1}{n}} \quad (7.40)$$

7.3.2 Velocity profile for the third region (outer layer)

Similar to the concept performed in the first region, Velocity Profile and Flow Rate relationship can be obtained for the third region (outer layer). As seen from Figure 7.3, for the outer region, shear stress τ, is:

$$\tau = K\gamma^n + \tau_y = K\left(-\frac{dv}{dy}\right)^n + \tau_y = \tau_0 + y\frac{dP_f}{dL} \quad (7.41)$$

This relation is valid for the first region where $\lambda_2 h \leq y \leq h$. For this region shear rate conventional sign is:

$$\frac{dv}{dy} < 0 \quad \rightarrow \quad \gamma = -\frac{dv}{dy} > 0 \quad (7.42)$$

So:

$$(\frac{-dv}{dy})^n = \frac{1}{K}\left[(\tau_0 - \tau_y) + y\frac{dP_f}{dL}\right] = \frac{1}{K}\left[-\lambda_2 h\frac{dP_f}{dL} + y\frac{dP_f}{dL}\right] \quad (7.43)$$

$$\frac{dv}{dy} = -\left(\frac{1}{K}\frac{dP_f}{dL}\right)^{\frac{1}{n}}(y-\lambda_2 h)^{\frac{1}{n}} \quad (7.44)$$

$$dv = -\left(\frac{1}{K}\frac{dP_f}{dL}\right)^{\frac{1}{n}}(y-\lambda_2 h)^{\frac{1}{n}}dy \quad (7.45)$$

$$v = -\left(\frac{1}{K}\frac{dP_f}{dL}\right)^{\frac{1}{n}} \frac{(y - \lambda_2 h)^{1+\frac{1}{n}}}{1+\frac{1}{n}} + v_c \tag{7.46}$$

Applying boundary conditions:

$$\tau_0 - \tau_y = -\lambda_1 h \frac{dP_f}{dL} \tag{7.47}$$

$$y = h \rightarrow v = -v_p$$

$$-v_p = -\left(\frac{1}{K}\frac{dP_f}{dL}\right)^{\frac{1}{n}} \frac{(h - \lambda_2 h)^{1+\frac{1}{n}}}{1+\frac{1}{n}} + v_c \tag{7.48}$$

$$v_c = \left(\frac{1}{K}\frac{dP_f}{dL}\right)^{\frac{1}{n}} \frac{(h - \lambda_2 h)^{1+\frac{1}{n}}}{1+\frac{1}{n}} - v_p \tag{7.49}$$

Replacing the Equation 7.48 in Equation 7.49, velocity at outer layer would be:

$$v_{outer} = \left(\frac{1}{K}\frac{dP_f}{dL}\right)^{\frac{1}{n}} \frac{1}{1+\frac{1}{n}} \left[(h - \lambda_2 h)^{1+\frac{1}{n}} - (y - \lambda_2 h)^{1+\frac{1}{n}}\right] - v_p \tag{7.50}$$

So using the definition of relationship between flow rate and velocity profile in Equation (7.36), flow rate equation for the second region can be obtained as:

$$q_{outer} = \left(\frac{1}{K}\frac{dP_f}{dL}\right)^{\frac{1}{n}} \frac{w}{1+\frac{1}{n}} \left[\int (h - \lambda_2 h)^{1+\frac{1}{n}} dy - \int (y - \lambda_2 h)^{1+\frac{1}{n}} dy\right] - \int v_p \, w dy \tag{7.51}$$

$$q_{outer} = \left(\frac{1}{K}\frac{dP_f}{dL}\right)^{\frac{1}{n}} \frac{w}{1+\frac{1}{n}} \left[(h - \lambda_2 h)^{1+\frac{1}{n}} [y]_{\lambda_2 h}^{h} - \left[\frac{(y - \lambda_2 h)^{2+\frac{1}{n}}}{2+\frac{1}{n}}\right]_{\lambda_2 h}^{h}\right] - [v_p w y]_{\lambda_2 h}^{h} \tag{7.52}$$

$$q_{outer} = \left(\frac{1}{K}\frac{dP_f}{dL}\right)^{\frac{1}{n}} \frac{w}{1+\frac{1}{n}} \left[(h - \lambda_2 h)^{2+\frac{1}{n}} - \frac{(h - \lambda_2 h)^{2+\frac{1}{n}}}{2+\frac{1}{n}}\right] - v_p w (h - \lambda_2 h) \tag{7.53}$$

$$q_{outer} = \frac{w}{2+\frac{1}{n}}\left(\frac{1}{K}\frac{dP_f}{dL}\right)^{\frac{1}{n}}(h-\lambda_2 h)^{2+\frac{1}{n}} - v_p w(h-\lambda_2 h) \tag{7.54}$$

$$q_{outer} = q_2 = \frac{w(h)^{2+\frac{1}{n}}}{2+\frac{1}{n}}\left(\frac{1}{K}\frac{dP_f}{dL}\right)^{\frac{1}{n}}(1-\lambda_2)^{2+\frac{1}{n}} - v_p w(1-\lambda_2) \tag{7.55}$$

7.3.3 Velocity profile for the plug region

Plug velocity can be obtained based on inner and outer layer as follows;

Plug velocity based on inner layer velocity $(y = \lambda_1 h)$

$$v_{plug_1} = \frac{1}{1+\frac{1}{n}}\left(\frac{1}{K}\frac{dP_f}{dL}\right)^{\frac{1}{n}}(\lambda_1 h)^{1+\frac{1}{n}} \tag{7.56}$$

Plug velocity based on outer layer: $(y = \lambda_2 h)$

$$v_{plug_2} = \left(\frac{1}{K}\frac{dP_f}{dL}\right)^{\frac{1}{n}}\frac{1}{1+\frac{1}{n}}(h-\lambda_2 h)^{1+\frac{1}{n}} - v_p \tag{7.57}$$

We know that:

$$v_{plug_1} = v_{plug_2}$$

$$\left(\frac{1}{K}\frac{dP_f}{dL}\right)^{\frac{1}{n}}\frac{1}{1+\frac{1}{n}}(h-\lambda_2 h)^{1+\frac{1}{n}} - v_p = \frac{1}{1+\frac{1}{n}}\left(\frac{1}{K}\frac{dP_f}{dL}\right)^{\frac{1}{n}}(\lambda_1 h)^{1+\frac{1}{n}} \tag{7.58}$$

$$\frac{1}{1+\frac{1}{n}}\left(\frac{1}{K}\frac{dP_f}{dL}\right)^{\frac{1}{n}}\left[(h-\lambda_2 h)^{1+\frac{1}{n}} - (\lambda_1 h)^{1+\frac{1}{n}}\right] - v_p = 0 \tag{7.59}$$

The objective is to find the pressure change per unit length (pressure gradient). Therefore, Equation (7.59) can be rewritten as following:

$$\left(\frac{1}{K}\frac{dP_f}{dL}\right)^{\frac{1}{n}} = \left(1+\frac{1}{n}\right)\frac{v_p}{\left[(h-\lambda_2 h)^{1+\frac{1}{n}} - (\lambda_1 h)^{1+\frac{1}{n}}\right]}$$

$$= \frac{1+\frac{1}{n}}{(h)^{1+\frac{1}{n}}}\frac{v_p}{\left[(1-\lambda_2)^{1+\frac{1}{n}} - (\lambda_1)^{1+\frac{1}{n}}\right]} \tag{7.60}$$

Therefore, frictional pressure gradient for HB fluid in annular geometry due to drill pipe movement can be obtained using following equation:

$$\frac{dP_f}{dL} = \frac{K}{h^{n+1}} \frac{\left[v_p(1+\frac{1}{n})\right]^n}{\left[(1-\lambda_2)^{1+\frac{1}{n}} - (\lambda_1)^{1+\frac{1}{n}}\right]^n} \tag{7.61}$$

For plug region flow rate equation can be written as:

$$q_{plug} = v_{plug_1} wh(\lambda_2 - \lambda_1) \tag{7.62}$$

$$q_{plug} = \frac{w(h)^{2+\frac{1}{n}}}{1+\frac{1}{n}} \left(\frac{1}{K}\frac{dP_f}{dL}\right)^{\frac{1}{n}} (\lambda_1)^{1+\frac{1}{n}}(\lambda_2 - \lambda_1) \tag{7.63}$$

7.3.4 Flow rate – surge pressure relation for entire slot geometry

Total flow rate for the fluid flowing in defined slot geometry shown in Figure 7.3 can be obtained by summing up developed flow rates for three defined regions.

$$q_{total} = q_1 + q_2 + q_{plug} \tag{7.64}$$

With substituting equations obtained for the first and the third and plug regions flow rates (Equations 7.40, 7.55 and 7.63) in Equation (7.64), the total flow rate expression can be written as:

$$q_t = \frac{w(h)^{2+\frac{1}{n}}}{2+\frac{1}{n}} \left(\frac{1}{K}\frac{dP_f}{dL}\right)^{\frac{1}{n}} \left[(\lambda_1)^{2+\frac{1}{n}} + (1-\lambda_2)^{2+\frac{1}{n}} + \frac{2+\frac{1}{n}}{1+\frac{1}{n}}(\lambda_1)^{1+\frac{1}{n}}(\lambda_2 - \lambda_1)\right] - wv_p h(1-\lambda_2) \tag{7.65}$$

Also we know

$$q_{total} = \frac{\pi}{4} v_p (d_c)^2 \tag{7.66}$$

Determination of mean velocity:

$$\bar{v} = \frac{h^{1+\frac{1}{n}}}{2+\frac{1}{n}} \left(\frac{1}{K}\frac{dP_f}{dL}\right)^{\frac{1}{n}} \left[(\lambda_1)^{2+\frac{1}{n}} + (1-\lambda_2)^{2+\frac{1}{n}} + \frac{2+\frac{1}{n}}{1+\frac{1}{n}}(\lambda_1)^{1+\frac{1}{n}}(\lambda_2 - \lambda_1)\right] - v_p(1-\lambda_2) \tag{7.67}$$

$$\left(\frac{1}{K}\frac{dP_f}{dL}\right)^{\frac{1}{n}} = \left(\frac{2+\frac{1}{n}}{h^{1+\frac{1}{n}}}\right)\frac{\bar{v} + v_p(1-\lambda_2)}{\left[(\lambda_1)^{2+\frac{1}{n}} + (1-\lambda_2)^{2+\frac{1}{n}} + \frac{2+\frac{1}{n}}{1+n}(\lambda_1)^{1+\frac{1}{n}}(\lambda_2-\lambda_1)\right]} \quad (7.68)$$

$$\frac{dP_f}{dL} = \frac{K}{h^{n+1}}\frac{\left[\bar{v} + v_p(1-\lambda_2)\right]^n\left(2+\frac{1}{n}\right)^n}{\left[(\lambda_1)^{2+\frac{1}{n}} + (1-\lambda_2)^{2+\frac{1}{n}} + \frac{2n+1}{1+n}(\lambda_1)^{1+\frac{1}{n}}(\lambda_2-\lambda_1)\right]^n} \quad (7.69)$$

Therefore there are three equations with three unknowns as $\frac{dP_f}{dL}, \lambda_1, \lambda_2$. Regarding surge and swab movements, these equations can be written as:

$$\frac{dP_f}{dL} = \frac{K}{h^{n+1}}\frac{\left[\bar{v} \pm v_p(1-\lambda_2)\right]^n\left(2+\frac{1}{n}\right)^n}{\left[(\lambda_1)^{2+\frac{1}{n}} + (1-\lambda_2)^{2+\frac{1}{n}} + \frac{2n+1}{1+n}(\lambda_1)^{1+\frac{1}{n}}(\lambda_2-\lambda_1)\right]^n} \quad (7.70)$$

$$\frac{dP_f}{dL} = \frac{\pm K}{h^{n+1}}\frac{\left[v_p(1+\frac{1}{n})\right]^n}{\left[(1-\lambda_2)^{1+\frac{1}{n}} - (\lambda_1)^{1+\frac{1}{n}}\right]^n} \quad (7.71)$$

$$\frac{dP_f}{dL} = \frac{2\tau_y}{(\lambda_2-\lambda_1)h} \quad (7.72)$$

The sign positive in Equation 7.70 and 7.71 is related to surge pressure and negative sign is for swab pressure. Simultaneous solution of these three equations using a Matlab iteration code based on grid search method results in unknown parameters. The Matlab code was given in Appendix-H.

7.4 Semi-Analytical Solution for Surge and/or Swab Pressure for Bingham Plastic Fluids

Because Herschel Bulkley model looks like combination of Bingham Plastic model and Power Law model. With replacing n equal to 1 and k = μ_p in Equations (7.70) and (7.71) and (7.72) the pressure losses equations for Bingham Plastic fluid can be obtained as:

$$\frac{dP_f}{dL} = \frac{\mu_p}{h^2}\frac{3\left[\bar{v} \pm v_p(1-\lambda_2)\right]}{\left[(\lambda_1)^3 + (1-\lambda_2)^3 + \frac{3}{2}(\lambda_1)^2(\lambda_2-\lambda_1)\right]} \quad (7.73)$$

$$\frac{dP_f}{dL} = \frac{\pm\mu_p}{h^2} \frac{2v_p}{[(1-\lambda_2)^2-(\lambda_1)^2]} \tag{7.74}$$

$$\frac{dP_f}{dL} = \frac{2\tau_y}{(\lambda_2-\lambda_1)h} \tag{7.75}$$

7.5 Semi-Analytical Solution for Surge and/or Swab Pressure for Power Law Fluids

Similar to previous section substituting τ_p=0 and λ_1=λ_2 in Equations (7.70) and (7.71) and (7.72) the pressure losses equations for Power Low fluid can be obtained as following equations with two unknowns of $\frac{dP_f}{dL}, \lambda$:

$$\frac{dP_f}{dL} = \frac{K}{h^{(n+1)}} \left[\frac{(\overline{V} \pm V_p(1-\lambda))\left(2+\frac{1}{n}\right)}{(1-\lambda)^{\left(2+\frac{1}{n}\right)} + \lambda^{\left(2+\frac{1}{n}\right)}} \right]^n \tag{7.76}$$

$$\frac{dP_f}{dL} = \frac{\pm K}{h^{(n+1)}} \left[\frac{V_p\left(1+\frac{1}{n}\right)}{(1-\lambda)^{\left(1+\frac{1}{n}\right)} - \lambda^{\left(1+\frac{1}{n}\right)}} \right]^n \tag{7.77}$$

Through Equations (7.73), (7.74), (7.76) and (7.77) the sign positive is assigned to surge pressure and negative sign is dedicated to swab pressure. An iterated grid search Matlab code given in Appendix-H has been written that ended up to find unknown parameters.

7.6 Validation of Semi-Analytical Method

Published experimental data and existing models were used to evaluate the outcomes of the developed semi-analytical model. To do so, the rheological properties of unweighted fresh water sepiolite mud were selected to determine surge and swab pressure gradients at different temperatures. In addition, a geometry commonly used in medium depth drilling was selected. Table 7.1 defines the selected geometry data to investigate the variation on surge and swab pressures. The objective was to select the section of drill collar where the fluid was circulated with relatively high velocity. The value of surge and swab pressures will be relatively high in such geometry due to existing narrow annular clearances. Therefore, the influence of temperature on variation of surge pressures can be clearly demonstrated.

Table 7.1. Selected geometry information.

	Field unit	SI unit
Pipe inner diameter (ID)	2.75 in	0.06985 m
Pipe outer diameter (OD)	6.25 in	0.15875 m
Wellbore diameter (D_w)	7.875 in	0.2 m
Fluid density	8.7 lb/gal	1043 kg/m^3

First of all, the calculated results of semi-analytical model for Bingham Plastic and Power Law models were compared with the results of existing Burkhardt (1960) and Schuh (1964) models, respectively in the above defined geometry. The results were listed in Appendix-I in Tables I.1 and I.2. In addition, the results were graphically pictured in Figures 7.4 and 7.5 to show the differences between semi-analytical model outputs and existing models predictions by employing error bars.

Figure 7.4 depicted the comparative results of Burkhardt (1960) model and developed semi-analytical model in this study for Bingham Plastic rheological parameters of fresh water sepiolite mud system. Moreover, the comparative results of Schuh (1964) model and developed semi-analytical model was illustrated in Figure 7.5 for Power Law rheological parameters of fresh water sepiolite mud system. The results of developed model exhibited an excellent agreement with the semi-empirical model developed by Burkhardt (1960) and Schuh (1964). As clarified in Figures 7.4 and 7.5, the outputs of semi-analytical model were predominantly between $\pm 5\%$ with a great consistency with Schuh and Burkhardt's models for Power Law and Bingham Plastic fluids, respectively.

Further evaluation on success of the semi-analytical model was made by comparing the results of semi-analytical model with the experimental data published by Crespo et. al., 2011. The geometry definition and tested fluids properties were given in Table 7.2.

Table 7.2: Geometry definition and tested fluids properties, (Crespo et. al., 2011).

Pipe diameter	33.5 mm		
Hole diameter	50.8 mm		
Power Law Fluid	n = 0.5	K = 0.774 Pa-s^n	
Herschel Bulkley Fluid I	n = 0.52	K = 0.359 Pa-s^n	τ_o = 3.44 Pa
Herschel Bulkley Fluid II	n = 0.5	K = 0.554 Pa-s^n	τ_o = 7.8 Pa

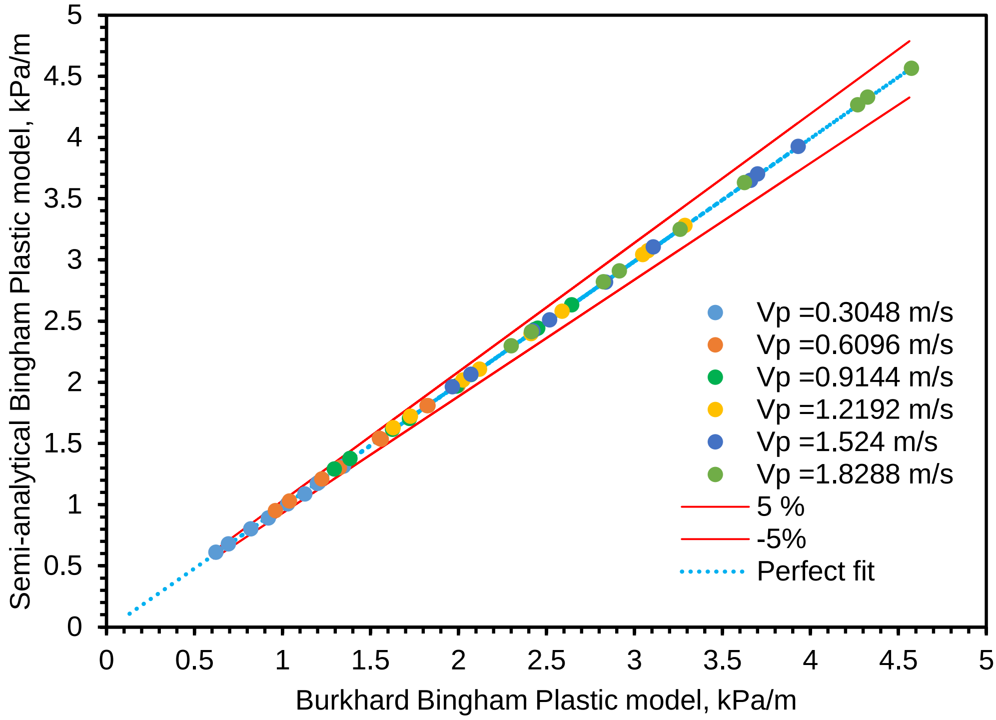

Figure 7.4: Comparative results of Burkhardt (1960) model and semi-analytical model for Bingham Plastic sepiolite mud.

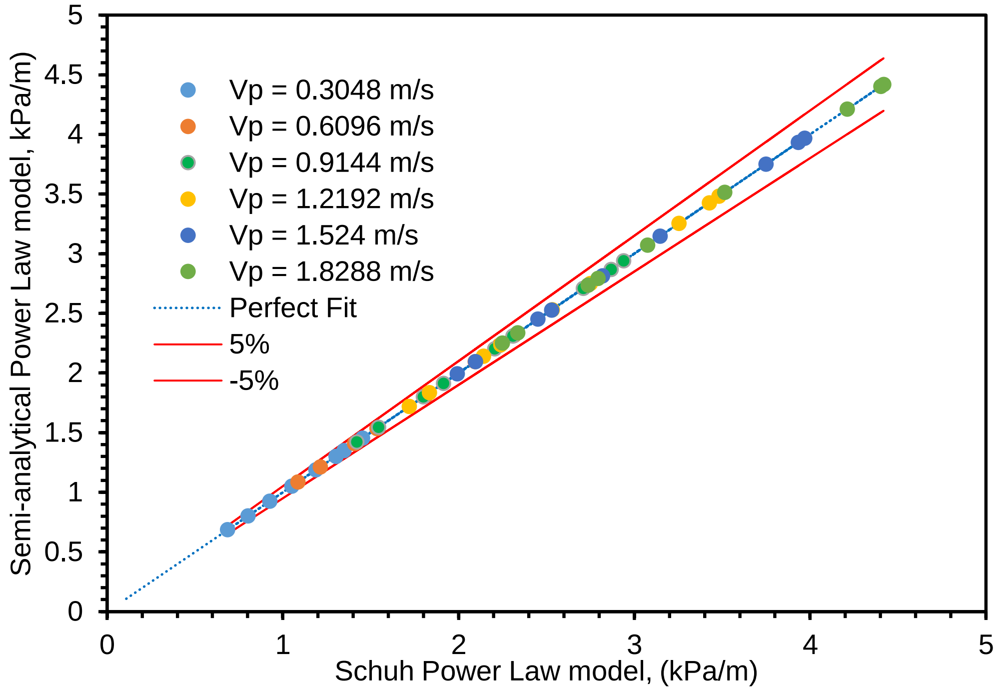

Figure 7.5: Comparative results of Schuh (1964) model and semi-analytical model for Power Law sepiolite mud.

The performance evaluation was made for Power Law and Herschel Bulkley fluids with parameters defined and experimentally tested by Crespo et. al., 2011 to obtain surge pressure gradients. The comparison between the surge pressure gradient using the semi-analytical method and existing Schuh model was given in Figure 7.6 by employing experimental data for the Power Law fluid defined in Table 7.2.

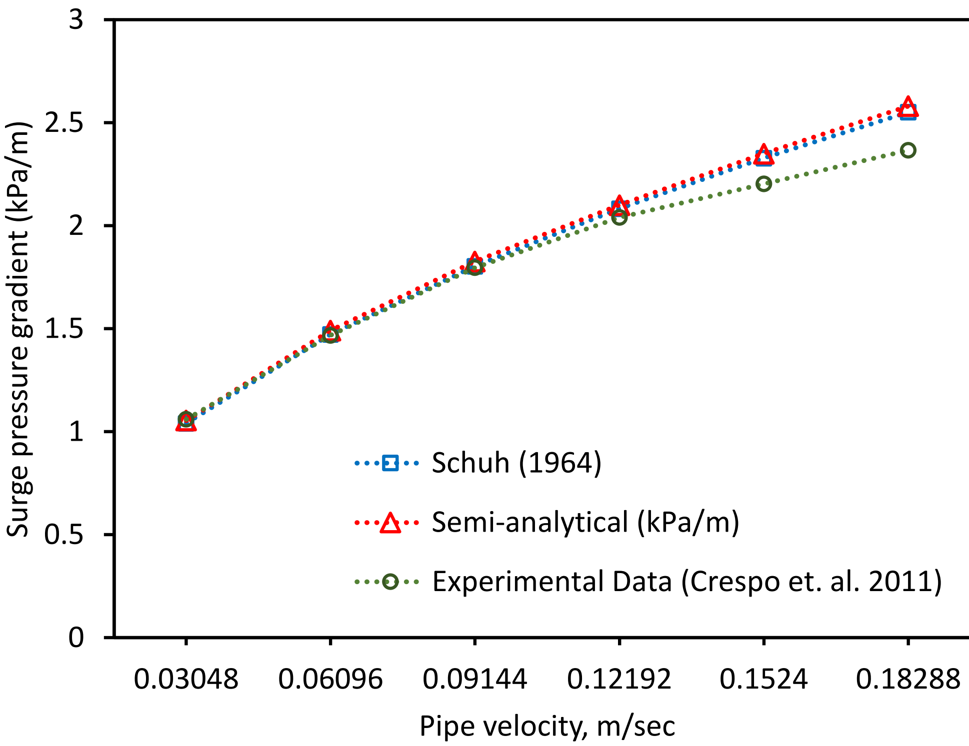

Figure 7.6: Comparison between the surge pressure gradient obtained using semi-analytical method and Schuh model.

High degree of agreement between the results especially at low pipe velocities was the clear indication of accuracy resulted from the semi-analytical model. The results were also numerically listed in Table 7.3.

Table 7.3: Comparing semi-analytical method with Schuh 1964 and Crespo et. al. 2011 (Power Law).

Pipe velocity m/s	Surge pressure gradient kPa/m		
	Schuh 1964	Semi-analytical	Experimental data (Crespo et. al. 2011)
0.03048	1.041	1.054	1.061
0.06096	1.473	1.491	1.468
0.09144	1.803	1.827	1.796
0.12192	2.082	2.1	2.04
0.1524	2.328	2.35	2.203
0.1829	2.55	2.58	2.366

Figure 7.7 and 7.8 signifies the comparison between the surge pressure gradient obtained using the semi-analytical method and the experimental data for two different Herschel Bulkley fluids defined in Table 7.2 and given by Crespo et. al., 2011.

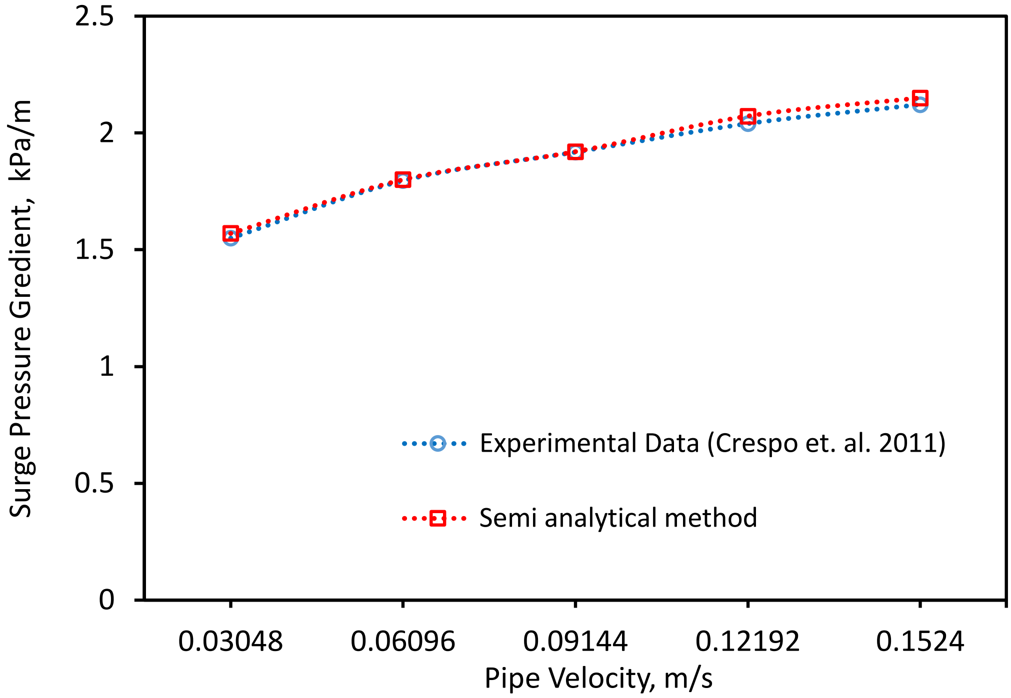

Figure 7.7: Surge pressure gradient obtained using semi-analytical method vs. experimental data (HB-I).

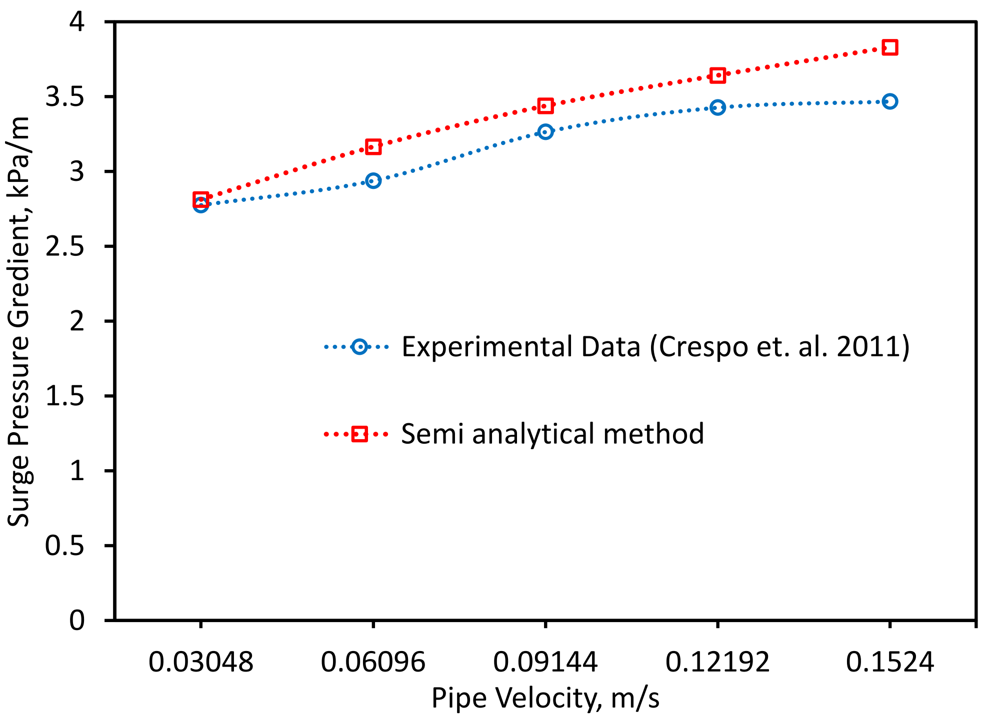

Figure 7.8: Surge pressure gradient obtained using semi-analytical method vs. experimental data (HB-II).

As seen from Figures 7.7 and 7.8, the experimentally measured surge pressure gradients were predicted with high accuracy using the new semi-analytical model for Herschel Bulkley fluid. In the case of Herschel Bulkley fluid II, a little bit overestimations were observed that could be due to inaccuracy of using regression analysis through calculation of rheological parameters or wrong experimental data. The results were also numerically listed in Table 7.4 for Herschel Bulkley model.

Table 7.4: Comparing semi-analytical method with Crespo et. al. 2011 (Herschel Bulkley).

Pipe velocity m/s	Herschel Bulkley fluid I		Herschel Bulkley fluid II	
	Measured	Semi-analytical	Measured	Semi-analytical
0.03048	1.5495	1.57	2.77547	2.8122
0.06096	1.796	1.8	2.9383	3.1649
0.09144	1.9182	1.92	3.2641	3.4378
0.12192	2.04032	2.072	3.4269	3.642
0.1524	2.12175	2.15	3.4676	3.83

7.7 Surge pressure gradient of fresh water sepiolite mud

Surge pressure gradients of unweighted fresh water sepiolite mud system were predicted using semi-analytical solution based on rheological parameters obtained from conventional viscometer and HTHP rheometer measurements. The results were listed in Appendix-I in Tables I.1 thru I.4 and also pictured in Appendix-J in Figures J.1 thru J.4 for Bingham Plastic, Power Law, and Herschel Bulkley rheology models. Surge pressure tended to increase with increasing pipe velocity at all temperatures for all three rheological models. For example, the value of predicted surge pressure gradient increased from 1.5276 kPa/m while pipe was moving with 0.3048 m/sec to 4.4449 kPa/m when pipe was moved with 1.8288 m/sec at 27°C (around 83% increasing) in the case of Herschel Bulkley rheological fluid measured by conventional viscometer (Figure J.3). The rate of surge pressure increased with increasing pipe velocity and decreased with increasing temperature. So that this rate decreased to around 66% at 177°C. As another remark, it was observed that the value of surge pressure gradient based on conventional viscometer decreased continuously with increasing temperature up to gelation point, and then increased up to the final test temperature (232°C). For instance, the value of predicted surge pressure gradient based on Herschel Bulkley rheological parameters obtained from viscometer decreased from

4.4449 kPa/m at 27°C to 2.3037 kPa/m at 149°C, and then again increased to 3.1315 kPa/m at 232°C while pipe was moving with 1.8288 m/sec, (Figure J.3). The similar trends on surge pressure variation based on Herschel Bulkley rheological parameters obtained by HTHP rheometer were observed too. However, the minimum surge pressure gradient was recorded at 193°C which was the gelation point of fresh water sepiolite mud defined previously based on HTHP rheometer rheology data, (Figure J.4). In general and as a bottom line, it could be inferred that the variation of surge pressure was strongly depends on rheological properties of sepiolite mud such that the quite similar behavior was seen between surge pressure and rheological variations.

The difference between surge pressure gradients that was predicted based on Herschel Bulkley rheological parameters from conventional viscometer and HTHP rheometer measurements at different temperatures was also illustrated in Appendix-J in Figures J.5 thru J.10 for the unweighted fresh water sepiolite mud. These figures clearly exhibited the gap in estimated pressures surges based on viscometer and HTHP rheometer data. Figure 7.9 also presented the variation of surge pressure gradients predicted for Herschel Bulkley model based on conventional viscometer and HTHP rheometer measurements while pipe was moving with 0.3048 m/sec. The difference in the results between two measurement methods was so impressive.

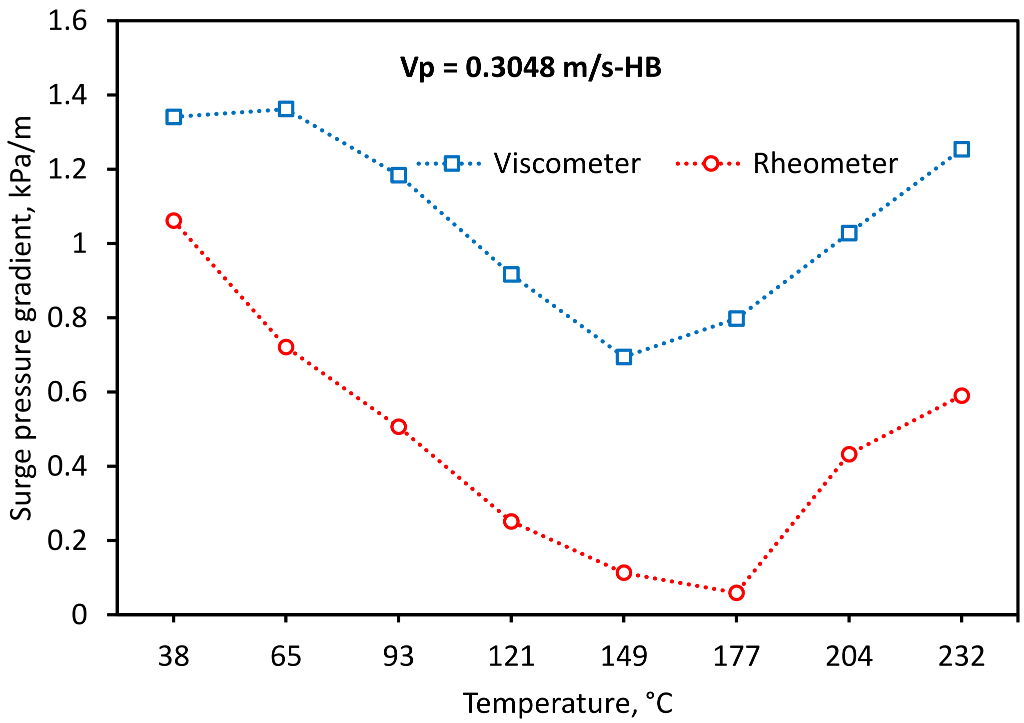

Figure 7.9: Variation of surge pressure gradients based on conventional viscometer and HTHP rheometer.

As seen from Figure 7.9, the difference between amounts of surge pressure based on the viscometer and rheometer measurements increased from 0.2791 kPa/m at 38°C to 0.7386 kPa/m at 177°C with 0.3048 m/sec of pipe velocity. Surge pressure gradient based on viscometer reading (0.694 kPa/m) was approximately six times higher than that of predicted using direct measurement data (0.113 kPa/m) at 149°C when the pipe was moved with 0.3048 m/sec, (Figure 7.9). However, based on the HTHP rheometer measurements, it is possible to run drillpipe with a speed of six-fold higher (1.8288 m/s) without putting drilling safety at risk, particularly at 149°C, (Figure 7.10). The difference was also more eminent at lower temperatures and diminished with increasing temperature, and it became almost the same at 149°C, (Figure 7.10).

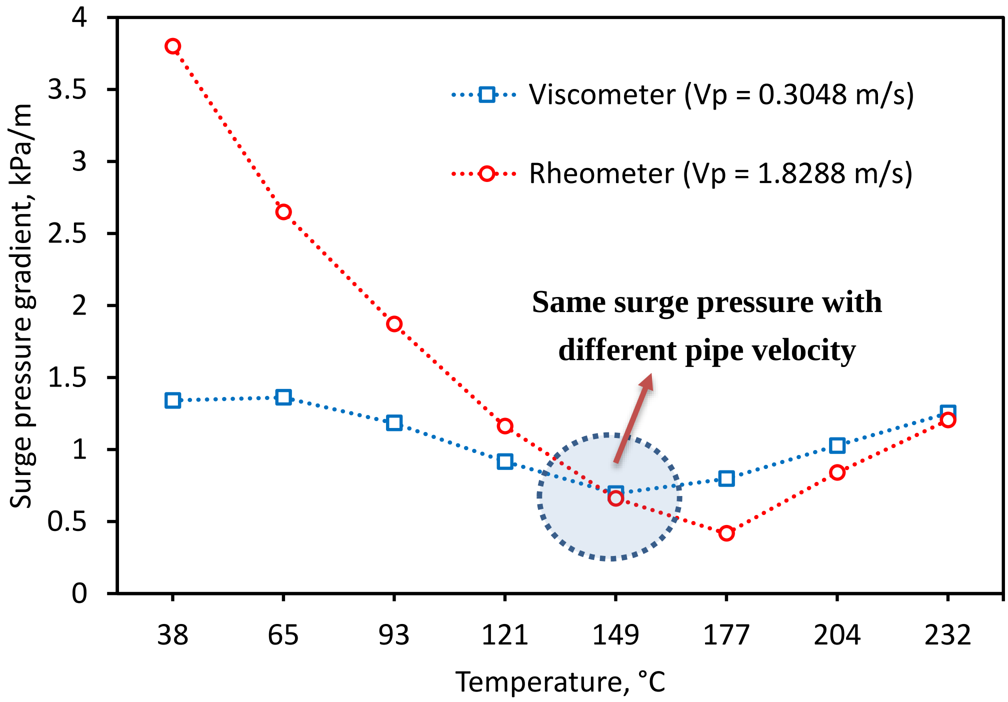

Figure 7.10: Same surge pressures with different pipe velocity based on conventional viscometer and HTHP rheometer.

Similar observations were seen through other pipe velocities depicted in Figures J.6 to J.10, (Appendix J). Surge pressure gradient variations with pipe velocities decreased with increasing temperature and made a minimum at the temperature where mud gelation was observed.

Results, presented herein, definitely proved that the surge pressures predicted based on conventional viscometer overestimates surge pressures. Using the result of conventional viscometer can lead to obtain fallacy outputs in terms of surge pressure as a critical part of wellbore hydraulic optimization, especially in the narrow annular geometry. Therefore, the speed of pipe movement can be modified considering the surge pressure based on HTHP rheometer which simulates the in-situ wellbore condition better than that of conventional viscometer.

7.8 Semi-Analytical Solution for Flow through a Concentric Annulus with Fixed Boundaries for a Herschel Bulkley Fluid

As mentioned in Chapter 5, Herschel Bulkley model usually gives the best fit in comparison to Power Law and Bingham Plastic models for the rheological measured data. Merlo et al., (1995) presented an analytical solution method including the most important equations of Herschel Bulkley model to calculate frictional pressure losses through pipe and annular flow in both laminar and turbulent flow regimes. These equations were listed in Appendix-K through Table K.1. However, this method is based on using the apparent Newtonian viscosity approach applied in determining Reynolds number for a non-Newtonian fluid. Besides, it consist of some coefficient (C_c and C_a) to calculate the corrected Reynolds number. These coefficients are the function of rheological parameters, geometry, and flow rate.

In this section, it was aimed to obtain relationships for flow through a concentric annulus with fixed boundaries (considering circulation only) for a Herschel Bulkley fluid using slot flow geometry approximation similar to the semi-analytical method applied to calculate surge and swab pressures. The steady state laminar flow equation was solved for a narrow slot geometry to approximate the flow in concentric annulus while circulating the fluid (Figure 7.11).

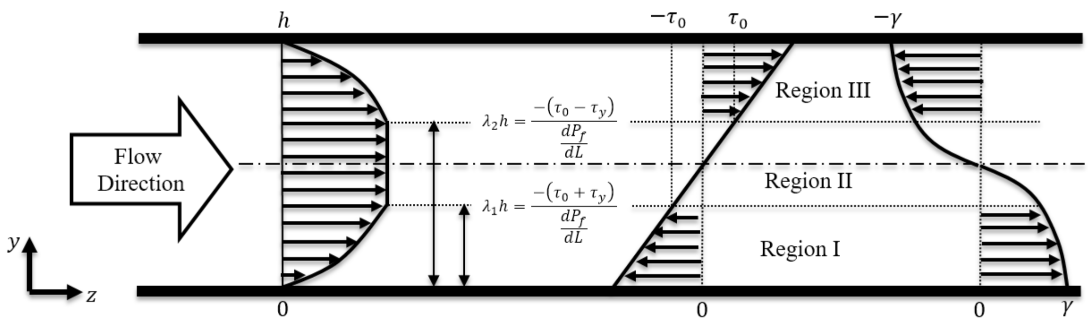

Figure 7.11: Slot geometry for a Herschel Bulkley fluid while circulating fluid.

Equation 7.59 for a concentric annulus with fixed boundaries can be rearranged by removing upper plate velocity (pipe velocity v_p) as follows:

$$\frac{1}{1+\frac{1}{n}}\left(\frac{1}{K}\frac{dP_f}{dL}\right)^{\frac{1}{n}}\left[(h-\lambda_2 h)^{1+\frac{1}{n}}-(\lambda_1 h)^{1+\frac{1}{n}}\right]=0 \tag{7.78}$$

Similarly Equation 7.70 takes the following form by eliminating pipe velocity;

$$\frac{dP_f}{dL}=\frac{K}{h^{n+1}}\frac{[\bar{v}]^n\left(2+\frac{1}{n}\right)^n}{\left[(\lambda_1)^{2+\frac{1}{n}}+(1-\lambda_2)^{2+\frac{1}{n}}+\frac{2n+1}{1+n}(\lambda_1)^{1+\frac{1}{n}}(\lambda_2-\lambda_1)\right]^n} \tag{7.79}$$

Equation 7.72 can also be applied exactly in this section;

$$\frac{dP_f}{dL}=\frac{2\tau_y}{(\lambda_2-\lambda_1)h} \tag{7.80}$$

To make Equation 7.78 zero, following part of that must be equal to zero:

$$\left[(h-\lambda_2 h)^{1+\frac{1}{n}}-(\lambda_1 h)^{1+\frac{1}{n}}\right]=0 \tag{7.81}$$

Equation 7.81 reduces to:

$$(1-\lambda_2)^{1+\frac{1}{n}}-(\lambda_1)^{1+\frac{1}{n}}=0 \tag{7.82}$$

By applying factoring rule to Equation 7.82, following series expansion would be appeared:

$$(1-\lambda_2)^{1+\frac{1}{n}}-(\lambda_1)^{1+\frac{1}{n}}$$
$$=[(1-\lambda_2)-\lambda_1]\left[(1-\lambda_2)^{\frac{1}{n}}+(1-\lambda_2)^{\frac{1}{n}-1}\lambda_1+(1-\lambda_2)^{\frac{1}{n}-2}{\lambda_1}^2+\cdots\right.$$
$$\left.+(1-\lambda_2){\lambda_1}^{1+\frac{1}{n}}+{\lambda_1}^{\frac{1}{n}}\right] \tag{7.83}$$

The second part of equation 7.83 is always positive because $0<\lambda_1<1$, $0<\lambda_2<1$ and also $0<n<1$. Therefore, the following part must be zero to make Equation 7.83 equal to zero:

$$(1-\lambda_2)-\lambda_1=0 \tag{7.84}$$

This relationship along with Equations 7.79 and 7.80 can be used to obtain a semi-analytical solution for flow through a concentric annulus with fixed boundaries for a Herschel Bulkley fluid. Replacing Equation 7.84 into Equations 7.79 and 7.80, the result is two equations with two unknown parameters.

$$\frac{dP_f}{dL} = \frac{2\tau_y}{(\lambda_2 - 1 + \lambda_2)h} = \frac{2\tau_y}{(2\lambda_2 - 1)h} \tag{7.85}$$

$$\frac{dP_f}{dL} = \frac{K}{h^{n+1}} \frac{[\bar{v}]^n \left(2 + \frac{1}{n}\right)^n}{\left[2(1-\lambda_2)^{2+\frac{1}{n}} + \frac{2n+1}{1+n}(1-\lambda_2)^{1+\frac{1}{n}}(2\lambda_2 - 1)\right]^n} \tag{7.86}$$

Equalizing Equations 7.85 and 7.86 leads to obtain a relation with only one unknown parameter as λ_2.

$$\frac{2\tau_y}{(2\lambda_2 - 1)h} = \frac{K}{h^{n+1}} \frac{[\bar{v}]^n \left(2 + \frac{1}{n}\right)^n}{\left[2(1-\lambda_2)^{2+\frac{1}{n}} + \frac{2n+1}{1+n}(1-\lambda_2)^{1+\frac{1}{n}}\left(2\lambda_2 - 1\right)\right]^n} \tag{7.87}$$

$$\lambda_2 = \frac{\tau_y}{K}\left(\frac{h\left[2(1-\lambda_2)^{2+\frac{1}{n}} + \frac{2n+1}{1+n}(1-\lambda_2)^{1+\frac{1}{n}}(2\lambda_2 - 1)\right]}{\bar{v}\left(2 + \frac{1}{n}\right)}\right)^n + \frac{1}{2} \tag{7.88}$$

To get the numerical solution, a Matlab iteration code based on grid search method given in Appendix-H was developed to solve a system of two equations to find λ_2 and frictional pressure drop ($\frac{dP_f}{dL}$).

7.9 Comparison with analytical method

The rheological properties obtained for the unweighted fresh water sepiolite mud base on classic viscometer measurements at different temperatures were used to make a comparison between already existed analytical method (Merlo et.al, 1995) and new developed semi-analytical method for a Herschel Bulkley fluid flowing through a concentric annulus. The results were illustrated in Appendix-L in Figures L1 thru L10. In addition, Figure 7.12 represents the variation of λ_2 and λ_1 with respect to average velocity, and Figure 7.13 pictured the comparison of frictional pressure drop obtained through two above mentioned methods at 38°C.

Model predictions were compared with those published by Merlo et. al (1995). Predictions of the new model were predominantly consistent with the analytical model and demonstrated excellent agreement. However, the difference between semi-analytical and analytical method was appeared at low velocities, (Figure 7.14). The gap between the results obtained based on these two methods was bridged gradually with increasing velocity. The superb consistency between the results was observed at high velocity, (Figure L.3).

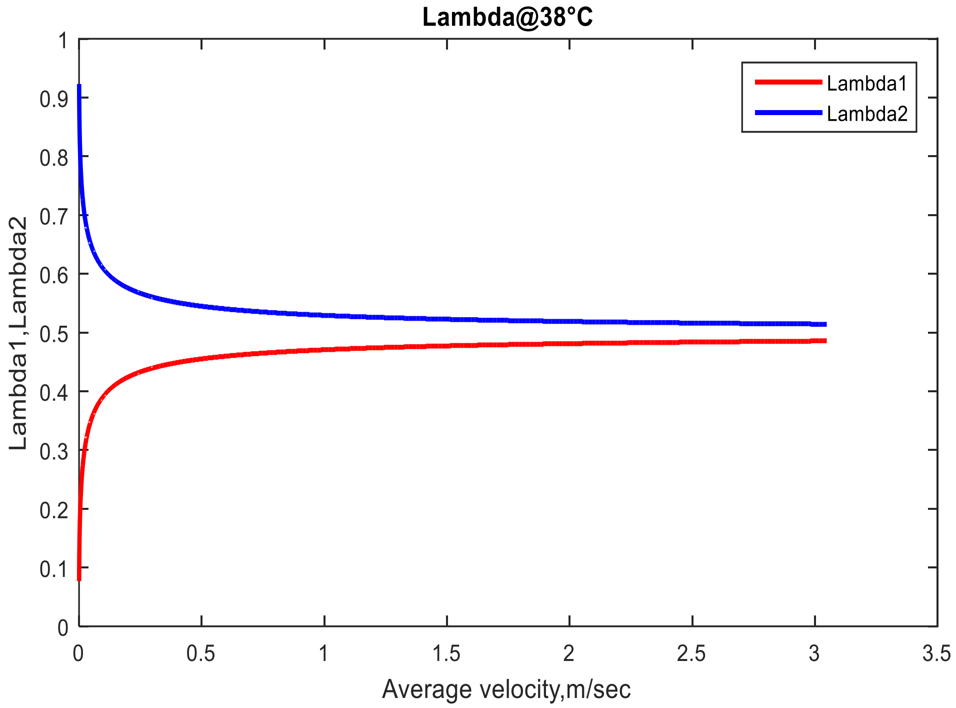

Figure 7.12: Variation of λ_2 and λ_1 with average velocity for fresh water sepiolite mud @38°C, (plug region wideness).

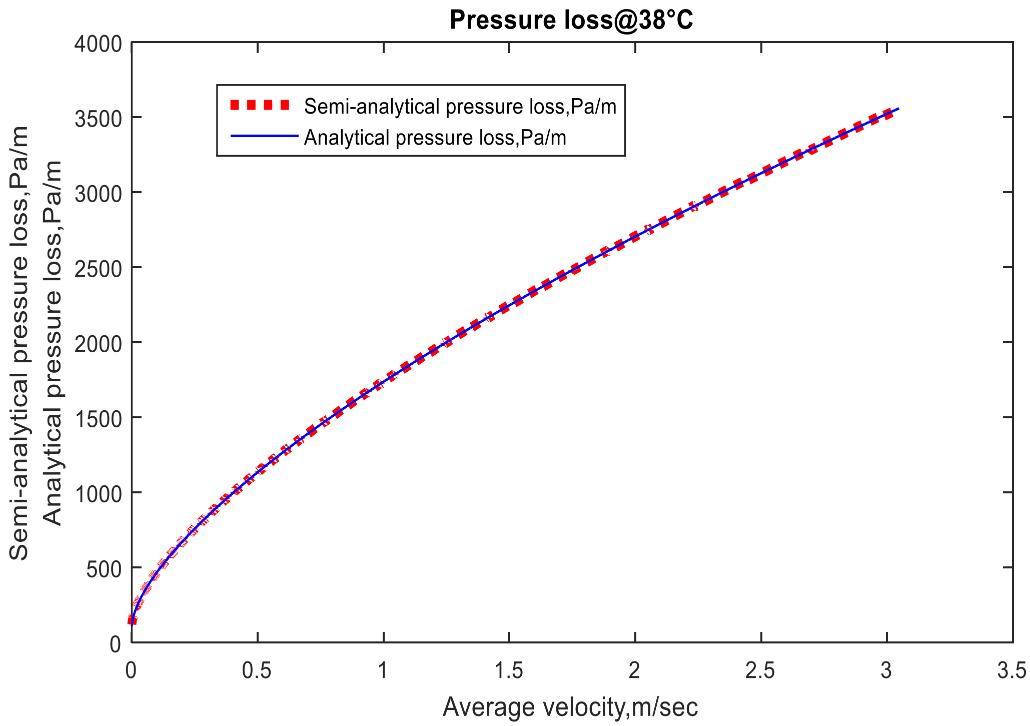

Figure 7.13: Comparison of frictional pressure drops obtained using semi-analytical and existing analytical method for fresh water sepiolite mud @38°C.

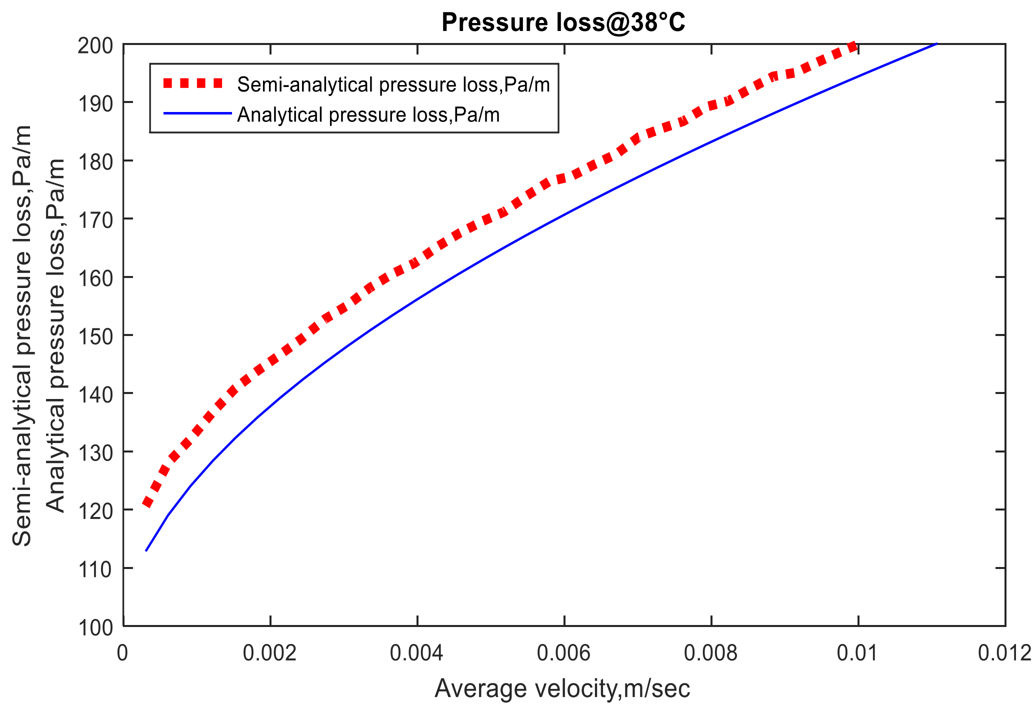

Figure 7.14: Difference between obtained frictional pressure drop using semi-analytical and existing analytical method for fresh water sepiolite mud @38°C.

The variations on pressure losses were directly proportional with rheological behavior and dominantly with shear stress and consistency index as expected (Figure 7.15). The frictional pressure losses decreased up to 149°C corresponding to the gelation point temperature where the fresh water sepiolite mud provided a lower consistency index (0.1243 Pa-s^n), and then increased with increasing temperature up to the final test temperature (232°C). The agreement between the pressure loss variations and rheological behavior of fluid could be the solid evidence verifying dependency of wellbore hydraulic deign to the fluid rheological properties.

Similar to the pressure drop, the difference between λ_2 and λ_1 known as plug region for Herschel Bulkley model, decreased with increasing temperature and related to the variation on the rheological parameters. The length of plug region decreased up to 93°C where the fresh water sepiolite mud provided a lower yield point (0.4643 Pa), and then increased up to 121°C with increasing yield point to 0.9125 Pa. Afterward, the value of pressure drop again decreased up to 177°C, and then increased to higher value at 232°C where the yield point of mud system raised to maximum value (2.0233 Pa). The plug region was the widest at 232°C because the mud system yielded the highest amount of viscosity and yield point at this temperature among all temperatures, (Figure 7.16).

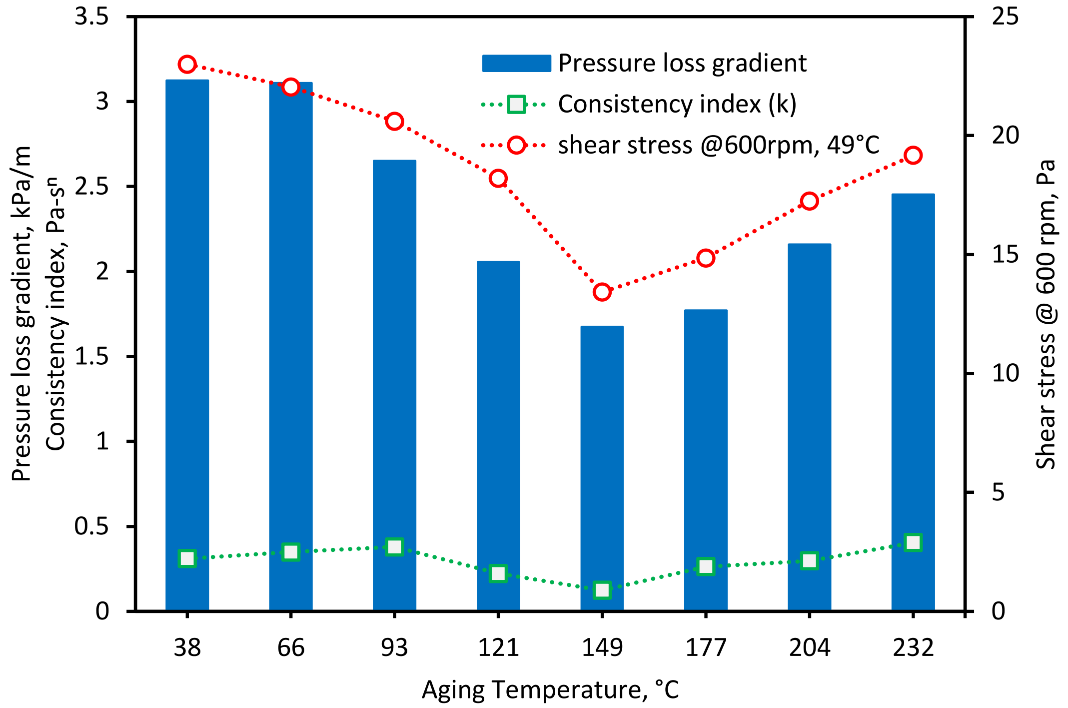

Figure 7.15: Agreement between pressure loss and rheological behavior of the fresh water sepiolite mud -viscometer results.

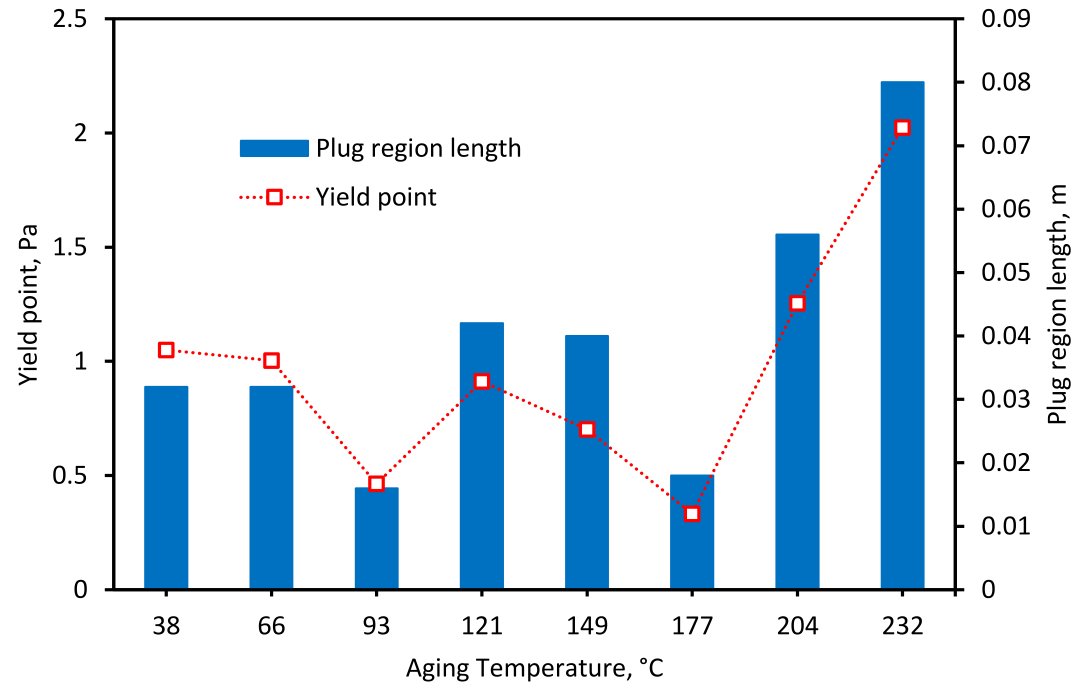

Figure 7.16: Agreement between the length of plug region and yield point of the fresh water sepiolite mud -viscometer results.

7.10 Chapter Conclusions

A new simplified and dimensional semi-analytical model were developed to calculate frictional pressure loss causing by drillstring movement for non-Newtonian fluids based on slot geometry solution method. The proposed semi-analytical method was applied on unweighted fresh water sepiolite mud rheological parameters to obtain surge and swab pressures at different temperatures. The results were compared with already developed Burkhardt method for Bingham Plastic fluid and Schuh model for Power Law fluid. The results revealed that:

- A satisfactory agreement was recorded between the semi-analytical method results on the one hand and Burkhardt and Schuh model on the other hand for Bingham Plastic and Power Law fluids, respectively. The maximum 5% error band was the strong indication confirming such agreement through examined models.
- The results of semi-analytical method for Herschel-Bulkley model were compared with experimental surge pressure results existing in literature. The results were very close indicating efficient performance of semi-analytical model in terms of employing for Herschel-Bulkley fluid.
- Surge pressure gradient calculated using semi-analytical method based on viscometer and rheometer measurements for sepiolite mud demonstrated noticeable differences between the results. The gap between the results got spread more with increasing temperature up to gelation temperature. Beyond this temperature, the gap began to get narrow.
- Surge pressure gradient for sepiolite mud varied through a trend similar to the rheological behavior of this mud with respect to temperature.
- It was observed that in the case of sepiolite muds, the surge pressures based on viscometer data overestimated the surge pressures based on in-situ data from rheometer. Therefore, the higher speed of pipe in wellbore is possible and results in saving power, time, and cost.
- The semi-analytical method could also be used to obtain frictional pressure losses in the case of circulating fluid through a concentric annulus with fixed boundaries for a Herschel Bulkley fluid by removing pipe velocity terms from the equations. The frictional pressure losses using this method were calculated

and in good agreement with touchy analytical method. The results employing various approaches indicated the validity and reliability of semi-analytical method presented in this study first time ever.

- The height of plug region associated and characterized with Herschel Bulkley model was investigated using semi-analytical method by the application of rheological properties of sepiolite mud. The height of plug region decreased with increasing temperature, in general.

8. EVALUATION OF STAND PIPE PRESSURES USING COMPUTATIONAL FLUID DYNAMICS

8.1 Introduction

Drilling engineers open holes in harsh environmental regions where advanced technology and good engineering methods are essential, particularly in deep water offshore wells where safe mud weight windows are reported to be almost zero. Such a low mud weight margin dictates calculating accurate equivalent circulation density (ECD) even for managed pressure drilling (MPD) operations. In addition, cost of power consumed in drilling operations is quite high and aimed to be minimized. As a result, calculations of precise frictional pressure losses (FPL) to realize better stand pipe pressures (SPP) and effective optimization of drilling hydraulics become extremely crucial. Consequently, more accurate FPL predictive methods are required in advance to develop efficient strategy for experimentally expensive and unpredictable oil and gas wells drilling. Commonly used rheological models like Bingham Plastic, Power Law, and Herschel-Bulkley to determine SPPs and optimum drilling hydraulics in a circulation system have no analytical solution for some vital parameters such as temperature, eccentricity and rotation of drillstring. Computational Fluid Dynamics (CFD) is a powerful tool to investigate the effects of aforementioned parameters on a hydraulic system in details.

This part of study is an attempt to calculate FPLs through a given drill collar and its corresponding annulus geometry (Table 8.1) while circulating unweighted fresh water sepiolite mud at a given circulation rate. The rheological constant parameters obtained from both conventional viscometer and HTHP rheometer were considered through three rheological models as Bingham Plastic, Power Law, and Herschel-Bulkley. Analytical methods and CFD analysis were used to calculate FPLs in above mentioned geometry. In addition, effects of temperature on FPL was also investigated using both methods at 8 common temperatures between rheometer and viscometer measurements as 38, 65, 93, 121, 149, 177, 204, 232°C. In short, this study completely evaluates

FPLs and details the successful application of CFD techniques to optimize hydraulic behavior.

8.2 Literature Review

Oil and gas production increases through drilling thousands of wells yearly over the entire world. It is obvious that the number of oil well and subsequently depth of the wells are supposed to increase in order to meet world's oil demand.

Assuming constant drilling fluid properties, the conventional calculations of wellbore pressure are both practical and accurate enough for routine wells. Downhole static pressures are easy to calculate from mud weight measured at the surface, while additional pressures caused by circulation can be calculated using established relationships between pump rate and drilling fluid rheological properties.

In relatively shallow wells, the difficulties stem from ignoring variations in the mud properties are small. In these situations, it is recommended to concentrate on formulating drilling fluid properties for maximum rates of penetration and optimal hole conditions. Drilled formations are stable and can commonly tolerate moderate overpressure without being fractured. This, in turn, allows mud engineers to consider a comfortable safety margin when using weighted mud.

However, mud properties might be changed with downhole pressure and temperature especially in high pressure and high temperature (HPHT), extended reach, and deep-water wells. It causes some fallacious on the accuracy of both surface measurements and downhole estimations of mud weight and viscosity. Moreover, these variations can be more critical due to availability of limited safety margins. The accurate prediction of these effects is so important in terms of successful drilling through HPHT, extended reach, and deep-water wells. Errors in calculating the drilling fluid pressure at the reservoir might appear due to neglecting uncertainties either in the temperature or in the fluid properties. Modelling downhole temperature profiles at all phases of the drilling operation is the essential factor to figure out the behavior of drilling fluids. The calculations become increasingly complicated when changes in viscosity with temperature are considered.

As a known fact, the foundation for modelling fluid motion are provided by governing equations namely the Navier-Stokes equations. There are some engineering approaches to solve numerically the equations governing fluid dynamics. Unfortunately, these approaches cannot represent the true reality condition of the well hydraulics due to some assumptions. In reality, the effects of the eccentricity, rotation of the string, temperature and multiphase fluid flow should be taken under consideration in a good optimization. One of the methods which include all these physical properties of the fluid hydraulics is Computational Fluid Dynamics (CFD). The CFD as a branch of fluid dynamics can provide a cost-effective means of simulating real flows by numerical solution of the governing equations.

Computational fluid dynamics (CFD) provides engineers, researchers and designers a validated simulation tool to help them better understand the performance, design and troubleshooting in applications ranging from reservoir injector design and drilling to production and transport. It can help to simulate flows involving single and multiple phases with or without heat and mass transfer. Therefore, in petroleum industry the application of the Computational Fluid Dynamics in the cutting transport, flow of mud, cement operations, and in bit optimization is growing day by day.

In drilling industry, it is always very crucial to exactly know the pressure drop in a hydraulic circulation system for many reasons. When drilling fluid is circulated, pressure drop takes place due to friction between the fluid and the surface in contact. The pressure that forces the drilling fluid to circulate through the hydraulic system is supplied by a mud pump. The mud pump pressure is partly used in overcoming the friction between the fluid and the open hole or casing or the surface equipment used. The remaining pump pressure is consumed as bit nozzle pressure loss where the high nozzle speed assist in cuttings removal from the bit and its surroundings. The total pressure drop that occurs due to fluid friction is termed as Stand Pipe Pressure and abbreviated as SPP. SPP is an important drilling parameter that must be known with sufficient accuracy for selecting proper jet bit nozzle size, determining optimum flow rate to ensure efficient hole cleaning, and selecting proper mud pump liner. Continuous monitoring of SPP also helps in identifying downhole problems. Thus, reliable indication of SPP provides an early warning of circulation problems, and this warns the driller to make corrections avoiding major problems.

Quick research in literature reveals that investigation on frictional pressure loss calculation was a major focus of researchers since 1950’s. To date, numerous investigators attempted to determine frictional pressure loss using non-Newtonian fluids flow mainly in horizontal, concentric, and eccentric annuli.

Fredrickson and Bird (1958) solved the problem of concentric, nonrotating annular flow using numerical method and obtained an expression of flow rate and frictional pressure loss in a laminar regime for Power Law and Bingham Plastic fluids. Heyda (1959) studied Newtonian fluid velocity distribution in an eccentric annuli and indicated the impressive effect of eccentricity on the velocity profile of a laminar flowing Newtonian fluid. Vaughn and Bergman (1965) developed a design model which uses circular capillary rheometer data on non-time-dependent fluids and supported experimental data for a laminar flow. Mitsuishi and Aoyagi (1973) experimentally determined the relation between the volumetric flow rate and pressure drop for high polymer aqueous solutions flowing in an eccentric annulus. They concluded that the pressure drop decreases as the eccentricity increases at a certain flow rate for flow in an eccentric annulus.

Iyoho and Azar (1981) determined the velocity profile for Power Law fluid flow through eccentric annuli using a slot-flow model. Langlinais et al. (1983) conducted an experimental study and compared obtained frictional pressure losses predicted by Bingham Plastic and Power Law models for the flow of drilling mud and mud/gas mixtures through a concentric annulus. Analytic, experimental, and also numerical approaches have been employed to explain flow in pipes and annulus by many researchers (Bourgouyn et al., 1986, Uner et al., (1989), Luo and Peden (1990), Haciislamoglu and Langlinais (1990), Fordham et.al 1991, Beverly and Tanner 1992, Filip and David 2003, Kelessidis et al., 2006). They developed analytical and numerical models in order to obtain velocity, volumetric flow rate, and frictional pressure loss for laminar flowing non-Newtonian fluids in an eccentric and concentric annuli. They also concluded that using numerical solutions for fluids having complex rheological properties in composite geometries are unavoidable.

The concept of effective diameter was proposed by Reed and Pilehvari (1993) in order to establish a relation between Newtonian and non-Newtonian flow through a concentric annulus. Moreover, the effects of eccentricity and pipe rotation on frictional pressure losses for Newtonian and non-Newtonian fluids were investigated by Escudier et al., (2002). Introduction of CFD technique into fluid flow model through oil and gas wells has been made for last decade. Bilgesu et al., (2002) used CFD simulation in an annular section to study the effect of cutting transport parameters in vertical and horizontal wells. It established CFD approach to visualize the velocity gradients and confirmed the obtained results with experimental results from literature. Singhal et al., (2005) compared friction pressure losses predicted by correlations with the data obtained from computational fluid dynamics (CFD) analysis. They concluded that the correlation proposed by Reed and Pilehvari (1993) results were confirmed by the CFD simulation results.

S.Won et al., (2008) carried out a study to investigate dynamic filtration process and related penetration into oil and gas bearing reservoir using CFD. This study mainly focused on the effect of formation porosity, permeability, time, and overbalanced pressure on contact between fluid and formations while drilling. Founargiotakis et al., (2008) used slot flow approximation to predict pressure drop through laminar, transitional, and turbulent flow of Herschel-Bulkley fluids in a concentric annuli. Gallego and Shah (2009) presented friction pressure correlations for turbulent flow of polymer solutions in straight and coiled tubing. The comparison of obtained results showed good agreement with experimental data.

8.3 Analytical Methods to Calculate Frictional Pressure Losses

Pressure drops are generated due to friction between the drilling fluid and the wall of the drill pipe and annulus during circulating of drilling fluid. It is known that the pump pressure (ΔP_p) is affected by frictional pressure losses in the surface equipment (ΔP_s), inside the drillstring (ΔP_{ds}), across the bit (ΔP_b), and in the annulus around the drillstring, (ΔP_a). It can be mathematically expressed as:

$$\Delta P_p = \Delta P_s + \Delta P_{ds} + \Delta P_b + \Delta P_a \qquad (8.1)$$

Miscalculation in (ΔP_p) consists primarily from inaccuracies in friction pressure losses in the drillstring and annulus. The drillstring pressure losses represent the largest component of error in the pump pressure. Several parameters are known to be important factors in variation of frictional pressure loss such as rheological behavior of the drilling fluid (Newtonian or non-Newtonian), flow regime of the drilling fluid (laminar, turbulent, or intermediate flow), drilling fluid properties (density and viscosity), flow rate of the drilling fluid (q), drillstring configuration and wellbore geometry. The best fit rheological model and rheological parameters obtained for all considered rheological models were determined according to procedure mentioned in Chapter 5. Calculation of Reynolds number depending on specific flow rate can help to determine the flow regime. Comparing calculated Reynolds number with critical Reynolds number lead to decide if the flow is laminar or turbulent. Then, the calculation of friction factor would be the next step. This factor is a function of the fluid rheological properties, pipe roughness, and the Reynolds number. The frictional pressure loss can be calculated using the appropriate equation from each rheological model after determination of the friction factor.

Analytical solution of frictional pressure gradient can be calculated using slot flow approximation for Bingham Plastic and Power Law fluids. Such calculation can be found in literature for pipe and annular flow (Bourgoyne et al., 1991). There are some studies related to frictional pressure loss calculation for a fluid with Herschel Bulkley rheological behavior which looks like combination of Bingham Plastic and Power Law models. However, these studies follow the study of Antonino Merlo, et al., (1995) to analytically calculate FPL for a HB fluid.

This chapter consists of determination of possible pressure losses while circulating unweighted fresh water sepiolite mud based on rheological parameters obtained from both viscometer and HTHP rheometer. All three rheological models were considered in the calculation of frictional pressure losses using analytical method corresponding to each rheological method.

8.3.1 Frictional pressure loss calculation for Bingham Plastic model

For Bingham Plastic model, pressure loss calculations are calculated with different formulas for different flow regimes. Accurate prediction of the onset of turbulent flow is even more difficult for non-Newtonian fluids than Newtonian fluids. When only the frictional pressure loss is desired, this problem can be avoided by calculating both frictional pressure loss with laminar and turbulent equations, and then selecting the result which is numerically higher.

8.3.1.1 Calculations in Pipe Flow:

Frictional pressure loss in pipe is calculated using formulas given below (Bourgoyne et al., 1991):

For laminar flow:

$$\frac{dp_f}{dL} = \frac{\mu_p v}{1500d^2} + \frac{\tau_y}{225d} \tag{8.2}$$

For turbulent flow:

$$\frac{dp_f}{dL} = \frac{\rho^{0.75} v^{1.75} \mu^{0.25}}{1800d^{1.25}} = \frac{\rho^{0.75} q^{1.75} \mu^{0.25}}{8624d^{4.75}} \tag{8.3}$$

where;

$\frac{dP_f}{dL}$: Frictional pressure loss per unit length, psi/ft
ρ : Density of drilling fluid, pound per gallon, lb_m/gal
v: Velocity of drilling fluid, ft/s
μ : Plastic viscosity of drilling fluid, cP
q: Flow rate of drilling fluid
d: Diameter of pipe, in
τ_y : Yield point, $lb_f/100\ ft^2$

8.3.1.2 Calculations in Annular Flow:

Frictional Pressure loss in annuli is calculated with the formula given below (Bourgoyne et al., 1991):

For laminar flow:

$$\frac{dp_f}{dL} = \frac{\mu_p v}{1000(d_2 - d_1)^2} + \frac{\tau_y}{200(d_2 - d_1)} \tag{8.4}$$

For turbulent flow:

$$\frac{dp_f}{dL} = \frac{\rho^{0.75} v^{1.75} \mu^{0.25}}{1396(d_2 - d_1)^{1.25}} = \frac{\rho^{0.75} q^{1.75} \mu^{0.25}}{8624d^{4.75}} \tag{8.5}$$

where,

$\frac{dP_f}{dL}$: Frictional pressure loss per unit length, psi/ft
ρ : Density of drilling fluid, pound per gallon, lbm/gal
V: Velocity of drilling fluid, ft/s
μ : Plastic viscosity of drilling fluid, cP
q: Flow rate of drilling fluid
d_1: Outer diameter of inner pipe, in
d_2: Inner diameter of outer pipe/annulus, in
τ_y : Yield point, $lb_f/100\ ft^2$

8.3.2 Frictional pressure loss calculation for power law model

Similar to Bingham Plastic model, different equations in Power Law model are used to calculate frictional pressure losses for laminar and turbulent flow regimes. To avoid uncertainties related to beginning of turbulent flow, the frictional pressure losses for both laminar and turbulent flow are calculated and the higher one is selected.

8.3.2.1 Calculations in Pipe Flow:

Frictional pressure loss in pipe is calculated using equations given below (Bourgoyne et al., 1991):

For laminar flow:

$$\frac{dp_f}{dL} = \frac{K\bar{V}^n\left(\frac{3+1/n}{0.0416}\right)}{144000\, d^{1+n}} \tag{8.6}$$

For turbulent flow:

$$\frac{dp_f}{dL} = \frac{f\rho V^2}{25.8\, d} \tag{8.7}$$

where,

$\frac{dP_f}{dL}$: Frictional pressure loss per unit length, psi/ft
ρ : Density of drilling fluid, pound per gallon, lbm/gal
V: Velocity of drilling fluid, ft/s
n: Flow behavior index
q: Flow rate of drilling fluid
d: Diameter of pipe, in
K : Consistency index, eq cp

8.3.2.2 Calculations in Annular Flow:

Frictional Pressure loss in annuli for Power Law fluid is calculated with the equations given below (Bourgoyne et al., 1991):

For laminar flow:

$$\frac{dp_f}{dL} = \frac{K\bar{V}^n\left(\frac{2+\frac{1}{n}}{0.0208}\right)^n}{144000\,(d_2-d_1)^{1+n}} \tag{8.8}$$

For turbulent flow:

$$\frac{dp_f}{dL} = \frac{f\rho V^2}{25.8\, d} \tag{8.9}$$

where,

$\frac{dP_f}{dL}$: Frictional pressure loss per unit length, psi/ft
ρ : Density of drilling fluid, pound per gallon, lbm/gal
V: Velocity of drilling fluid, ft/s
n: Flow behavior index
q: Flow rate of drilling fluid
d_1: Outer diameter of inner pipe, in
d_2: Inner diameter of outer pipe/annulus, in
K : Consistency index, eq cp

To find the value of friction factor, the graphical procedure is used according to Bourgoyne et al., 1991. The unit conversions are given in Appendix-R.

8.3.3 Frictional pressure loss calculation for Herschel Bulkley model

To calculate the frictional pressure loss in pipe flow the first step is to determine flow regime. Then, the appropriate equations will be used to calculate pressure loss. Reynolds number will used to determine flow regime. It is know that Reynolds number for pipe flow is, in general, defined as follows (Merlo et. al., 1995);

$$Re = \frac{2\rho Q}{\mu \pi R} \tag{8.10}$$

Equation 8.10 is known as generalized Reynolds number. In Herschel Bulkley model, it is required to determine equivalent Reynolds number which is defined as follows;

$$Re_{eq} = Cc * Re \tag{8.11}$$

Here C_c is correction factor and is defined as follows;

$$Cc = 1 - \frac{1}{2n+1} \left\{ \frac{\tau_0}{\tau_0 + k\left[\frac{(3n+1)Q}{n\pi R^3}\right]^n} \right\} \tag{8.12}$$

Reynolds number is a function of viscosity that can be expressed as:

$$\mu = \frac{\tau_0 + k\left[\left(\frac{3n+1}{nCc}\right)\left(\frac{Q}{\pi R^3}\right)\right]^n}{\left(\frac{3n+1}{nCc}\right)\left(\frac{Q}{\pi R^3}\right)} \tag{8.13}$$

Flow rate can be written as cross sectional area multiplied by velocity of fluid passing through that cross sectional area;

$$Q = (\pi R^2) V_p \tag{8.14}$$

After making substitutions for flow rate and viscosity, equivalent Reynolds number becomes as follow;

$$Re_{eq} = \left(2\frac{3n+1}{n}\right)\frac{\rho V_p^{(2-n)}R^n}{\tau_0\left(\frac{R}{V_p}\right)^n + k\left(\frac{3n+1}{nCc}\right)^n} \tag{8.16}$$

To decide whether flow is laminar or turbulent, equivalent Reynolds number should be compared with critical Reynolds number which is described as follows;

$$Re_{eqcr} = (Cc * Re)_{cr} = \left[\frac{4(3n+1)}{ny}\right]^{\left(\frac{1}{1-z}\right)} \tag{8.17}$$

where,

$$y = \frac{\log(n) + 3.93}{50} \tag{8.18}$$

$$z = \frac{1.75 - \log(n)}{7} \tag{8.19}$$

As a criteria the following should be taken into account;

If Re_{eq}<Re_{eqcr} the flow is considered as laminar, otherwise in the case of Re_{eq}>Re_{eqcr} then the flow is considered as turbulent.

8.3.3.1 Calculations in Pipe Flow:

Now let's consider pressure drop calculations for laminar flow. It is calculated using Fanning expression:

$$\Delta p = f\rho\frac{Q^2}{\pi^2 R^5}L \tag{8.20}$$

The friction factor in the equation above is determined by the following equation;

$$f = \frac{4}{Re_{eq}}\left(\frac{3n+1}{n}\right) \tag{8.21}$$

Now let's substitute friction factor equation and Reynolds number equation into Equation 8.20;

$$\Delta p = \frac{2Lk}{R}\left[\frac{\tau_0}{k} + \left[\left(\frac{3n+1}{nCc}\right)\left(\frac{Q}{\pi R^3}\right)\right]^n\right] \tag{8.22}$$

Now let's concentrate on the pressure drop equation for turbulent flow;

$$\Delta p = f\rho \frac{Q^2}{\pi^2 R^5} \tag{8.23}$$

The friction factor in the equation above is determined by the following equation;

$$f = y(Cc * Re)^{-z} \tag{8.24}$$

where y and z are the coefficients which are described in Equations (8.18) and (8.19).

8.3.3.2 Calculations in Annular Flow:

As made in pressure drop calculations for pipe, the flow regime should be determined before starting calculations. To determine flow regime, equivalent Reynolds number must be calculated and compared with critical Reynolds number. Equivalent Reynolds number can be calculated as follow;

$$Re_{eq} = Ca * Re \tag{8.25}$$

where;

$$Ca = 1 - \frac{1}{2n+1}\left\{\frac{\tau_0}{\tau_0 + k\left[\left(\frac{2(2n+1)}{n(R_2 - R_1)}\right)\left(\frac{Q}{\pi(R_2^2 - R_1^2)}\right)\right]^n}\right\} \tag{8.26}$$

$$Re = \frac{2\rho Q}{\mu\pi(R_1 + R_2)} \tag{8.27}$$

As it can be seen from Equation 8.27, viscosity and flow rate are required for Reynolds number calculation.

$$\mu = \frac{\tau_0 + k\left\{\left[\frac{2(2n+1)}{n(R_2 - R_1)}\right]\left[\frac{Q}{\pi Ca(R_2^2 - R_1^2)}\right]\right\}^n}{\left[\frac{2(2n+1)}{n(R_2 - R_1)}\right]\left[\frac{Q}{\pi Ca(R_2^2 - R_1^2)}\right]} \tag{8.28}$$

$$Q = \pi(R_2^2 - R_1^2)V_a \tag{8.29}$$

By substituting Equations 8.28 and 8.29 into 8.27, the following equation is obtained;

$$Re_{eq} = \left(4\frac{2n+1}{n}\right)\frac{\rho V_a^{(2-n)}(R_2 - R_1)^n}{\tau_0\left(\frac{R_2 - R_1}{VV_a}\right)^n + k\left(2\frac{2n+1}{nCa}\right)^n} \tag{8.30}$$

Now let’s define critical Reynolds number;

$$Re_{eqcr} = (Ca * Re)_{cr} = \left[\frac{8(2n+1)}{ny}\right]^{\left(\frac{1}{1-z}\right)} \tag{8.31}$$

where;

$$y = \frac{\log(n) + 3.93}{50} \tag{8.32}$$

$$z = \frac{1.75 - \log(n)}{7} \tag{8.33}$$

As mentioned above, to determine flow regime equivalent Reynolds must be compared with critical Reynolds number. If Re_{eq}<Re_{eqcr}, the flow is considered as laminar. If Re_{eq}>Re_{eqcr}, then the flow is considered as turbulent. Now let's consider frictional pressure loss equations. For laminar flow, frictional pressure loss can be calculated by using the following equation;

$$\Delta p = f\rho \frac{Q^2}{\pi^2 (R_2 - R_1)(R_2^2 - R_1^2)^2} L \tag{8.34}$$

where f is dimensionless friction factor and calculated as follows;

$$f = \frac{8}{Re_{eq}}\left(\frac{2n+1}{n}\right) \tag{8.35}$$

Now let's combine friction factor and Reynolds number with frictional pressure loss;

$$\Delta p = \frac{2Lk}{(R_2 - R_1)}\left[\frac{\tau_0}{k} + \left[\left(\frac{2(2n+1)}{nCa(R_2 - R_1)}\right)\left(\frac{Q}{\pi(R_2^2 - R_1^2)}\right)\right]^n\right] \tag{8.36}$$

If the flow regime is turbulent, the frictional pressure loss is calculated by using the formula as follows;

$$\Delta p = f\rho \frac{Q^2}{\pi^2 (R_2 - R_1)(R_2^1 - R_1^2)^2} L \tag{8.37}$$

where f is dimensionless friction factor and calculated as follows;

$$f = y(Ca * Re)^{-z} \tag{8.38}$$

y and z can be estimated by using the Equations 8.32 and 8.33.

8.4 Defined Geometry to Determine Frictional Pressure Loss

The rheological properties of unweighted fresh water sepiolite mud were selected to analytically determine frictional pressure loss at different temperatures. To investigate variation of frictional pressure losses, the selected geometry information was defined in Table 8.1. The objective was to focus the part of drill collar where the fluid was circulated with relatively high velocity. The frictional pressure losses would be extremely high in such geometry due to having high mud velocity. Therefore, the impact of temperature on variation of frictional pressure losses could clearly be demonstrated. In addition, it was tried to select a geometry commonly used in medium drilling depth. Moreover, the mud flow rate value was selected such that it could apply to form both laminar and turbulent flow regimes.

Table 8.1: Flow and geometry information to determine frictional pressure losses.

	Field unit	SI unit
Pipe inner diameter (ID)	2.75 in	0.06985 m
Pipe outer diameter (OD)	6.25 in	0.15875 m
Wellbore diameter (D_w)	7.875 in	0.2 m
Flow rate (Q)	0.9652 ft^3/s	1640 L/min
Fluid density	8.7 lb/gal	1043 kg/m^3

8.5 Circulation Pressure Losses-Analytical Solution Results

The variation of frictional pressure losses with temperature were analytically calculated for above-mentioned geometry and mud flow rate. The results were tabulated in Tables M.1 thru M.4 given in Appendix-M. The results involved in frictional pressure losses calculated based on rheological parameters obtained in Chapter 5 for Power Law, Bingham Plastic and Herschel Bulkley models using conventional viscosity and HTHP rheometer. The frictional pressure losses were calculated for 8 selected common temperatures (38, 65, 93, 121, 149, 177, 204, 232°C) in conventional viscometer and HTHP rheometer. The rheological constant parameters determined in Chapter 5 for unweighted sepiolite mud at these temperatures were used to calculate frictional pressure losses. The results consisted of frictional pressure losses both inside drill pipe (Tables M.1 and M.2) and its corresponding annulus (Tables M.3 and M.4) individually. The total frictional pressure losses through pipe and annulus can be easily calculated using the results given in these tables. The results were also pictured in Figures N.1 thru N.9 in Appendix-N to visually detail the pressure losses inside drill collar, annulus and both of them as total pressure drop. Through this problem, the only variable parameter affecting the frictional pressure losses was the temperature because the geometry and flow rate data were constant. Moreover, owing to this fact that the average mud velocity inside the pipe and in the annulus was different at constant flow rate. The effect of viscosity and mud flow rate on frictional pressure loss can also be evaluated. In other words, the effect of gelation on viscosity cannot be seen through a geometry where the fluid velocity is a dominant factor. In contrary, such effect might be observed in a geometry with low velocity. It was previously observed that (Chapter 5) the viscosity of sepiolite mud decreased with increasing temperature, and then tended to increase after the gelation temperature (where the gelation was started). Therefore, depending on the viscosity variation, the frictional pressure loss decreased up to the gelation point, and then beyond this point, it increased under the effect of increasing viscosity. The values of frictional pressure losses for unweighted fresh water sepiolite mud based on rheological parameters obtained for Bingham Plastic model using conventional viscometer at 8 aforementioned temperatures were listed in Table 8.2. In addition, the variation of calculated frictional pressure losses with temperature for Bingham Plastic model was depicted in Figure 8.1. Analytically calculated frictional pressure losses based on viscometer rheological parameters decreased from 14611 Pa/m at 38°C to 12504 Pa/m at 149°C (gelation point based on viscometer measurements) and, then increased to 13258 Pa/m at 232°C under the effect of increasing viscosity. In other words, the apparent viscosity of mud sample increased after gelation point and caused to increase the frictional pressure losses at constant flow rate.

Table 8.2: Frictional pressure losses-Bingham Plastic model-viscometer data.

	Viscometer results							
	Bingham Plastic							
	Rheological		**Drill Pipe**		**Annulus**		**Total**
Temperature (°C)	Plastic viscosity (Pa-s)	Yield point (pa)	ΔP (pa/m)	ΔP (psi/ft)	ΔP (pa/m)	ΔP (psi/ft)	ΔP (pa/m)
38	0.0335	3.99	10770	0.48	3841	0.17	14611
65	0.0328	4.14	10714	0.47	3820	0.17	14534
93	0.0278	3.56	10281	0.45	3666	0.16	13947
121	0.0215	2.93	9634	0.43	3435	0.15	13069
149	0.0180	2.00	9217	0.41	3287	0.15	12504
177	0.0184	2.44	9275	0.41	3307	0.15	12583
204	0.0213	3.66	9620	0.43	3430	0.15	13050
232	0.0227	4.97	9773	0.43	3485	0.15	13258

It could be concluded that the variation on average mud velocity was not able to suppress the effect of viscosity; therefore, pressure drops were observed in both drill pipe and annulus due to effect of gelation. In addition, as the flow area through drill pipe was quite low than the flow area in annulus, and the average mud velocity inside the pipe was higher than that of the in annulus. Therefore, the major portion of frictional pressure loss occurred during mud circulation in the drill pipe such that it was approximately %75. The pressure drop value at 232°C was close to the pressure drop value calculated at 38°C; therefore, it was inferred that the rheological parameters for this mud sample at 232°C were relatively close to the rheological parameters at 38°C.

Table 8.3 listed the values of frictional pressure losses for unweighted fresh water sepiolite mud based on rheological parameters obtained for Bingham Plastic model using HTHP rheometer at 8 aforementioned temperatures. In addition, the variation of calculated frictional pressure losses with temperature for Bingham Plastic model considering rheological constants from rheometer were depicted in Figure 8.1. The values of frictional pressure losses calculated considering the rheological parameters using HTHP rheometer were lower than those calculated based on viscometer data except for 38°C.

Table 8.3: Frictional pressure losses-Bingham Plastic model-rheometer data.

	Rheometer results						
	Bingham Plastic						
	Rheological		**Drill Pipe**		**Annulus**		**Total**
Temperature (°C)	Plastic viscosity (Pa-s)	Yield point (pa)	ΔP (pa/m)	ΔP (psi/ft)	ΔP (pa/m)	ΔP (psi/ft)	ΔP (pa/m)
38	0.0309	2.75	10551	0.47	3762	0.17	14313
65	0.0217	1.75	9663	0.43	3446	0.15	13109
93	0.0154	1.21	8864	0.39	3161	0.14	12024
121	0.0098	0.44	7929	0.35	2828	0.13	10757
149	0.0059	-0.01	6976	0.31	2488	0.11	9464
177	0.0039	-0.17	6310	0.28	2250	0.10	8560
204	0.0040	3.20	6340	0.28	2261	0.10	8601
232	0.0060	3.97	7000	0.31	2496	0.11	9497

As stemmed from the results in Chapter 5, the HTHP rheometer and viscometer measurements were in a good agreement and yielded approximately the same rheological results at lower temperatures. Spontaneously, a great consistency was observed between the hydraulic optimization results based on rheological parameters from both devices such that frictional pressure losses were the same at low temperatures. This observation was validated for the sepiolite mud in calculation of frictional pressure loss at 38°C. However, the values of pressure drop calculated using rheological parameters from these two devices yielded a difference after 38°C with increasing temperature. Moreover, it was exhibited that the generated gap between the results of two devices continuously increased with increasing temperature up to gelation point for the rheometer. As seen from the results depicted in Figure 8.1, the difference between the amounts of pressure drop calculated based on rheometer and viscometer data increased from 1425 Pa/m at 65°C to 4023 Pa/m at 177°C.

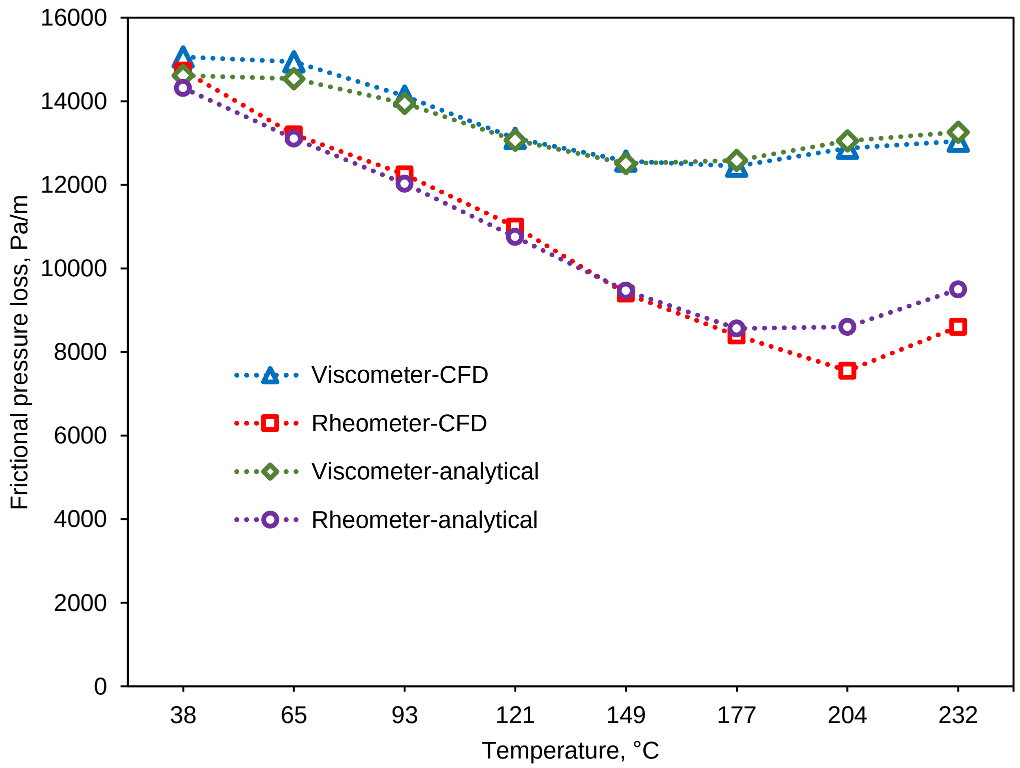

Figure 8.1: Variation of frictional pressure losses with temperature-Bingham Plastic model.

The gelation point temperature based on HTHP rheometer results was recorded at 190°C on contrary to the gelation point at 149°C considering the viscometer rheological data. The analytically calculated frictional pressure losses based on HTHP rheometer rheological parameters decreased from 14330 Pa/m at 38°C to 8560 Pa/m at 177°C, and then increased to 9497 Pa/m at 232°C under the effect of increasing viscosity. The frictional pressure losses obtained based on HTHP rheometer rheological results were lower than those calculated based on conventional viscometer at all temperatures. Similar to the results based on viscometer data, the frictional pressure losses calculated from the rheological parameters of rheometer inside drill pipe were about 75% higher than those of the annulus. Viscosity increasing after gelation point was also observed in HTHP rheometer rheological results. However, such increment was lower than that observed in the viscometer rheological results. Therefore, calculated pressure drops at 232°C in both drill pipe and annulus were lower than those obtained from the conventional viscometer at same temperature.

In previous chapters, it was concluded that the rheological behavior based on HTHP rheometer simulated the in-situ wellbore conditions better. Therefore, the frictional pressure losses calculated from rheometer parameters were accepted to be more accurate and close to the real in-situ conditions. In other words, it could be expected that the frictional pressure drops due to mud circulation would be low in hot wells depending on temperature values up to the gelation point.

Obtaining the same values for frictional pressure losses from both rheometer and viscometer rheological parameters at low temperature (38°C) confirmed the accuracy of measurements through this experimental study. In addition, the difference between frictional pressure losses calculated based on rheometer and viscometer for Bingham Plastic model were very important in term of hydraulic optimizations particularly in moderate to high temperatures. Therefore, it was concluded that l wellbore design hydraulics based on conventional viscometer data caused some sort of erroneous in the results for Bingham Plastic mode. On the other hand, it was observed that the hydraulic optimization based on viscometer data provided quite conservative results.

The results of analytical solution on frictional pressure losses calculated based on rheological parameters obtained in Chapter 5 for Power Law and Herschel Bulkley models using conventional viscosity and HTHP rheometer were listed in Tables M.1 thru M.4 and given in Appendix-M. The same geometry and flow rate were considered to calculate frictional pressure losses for the 8 selected common temperatures of 38, 65, 93, 121, 149, 177, 204, and 232°C in both conventional viscometer and HTHP rheometer. The frictional pressure losses were calculated both inside drill pipe (Tables M.1 and M.2) and its corresponding annulus (Tables M.3 and M.4) for the Power Law and Herschel Bulkley rheological parameters. The results were also pictured through

Figures N.1 thru N.6 and given in Appendix-N. These figures graphically illustrated the pressure drops inside drill collar, annulus and both of them as total pressure drop.

Unlike Bingham Plastic model, the frictional pressure losses calculated from Power Law and Herschel Bulkley rheological parameters using viscometer and HTHP rheometer data were relatively close to each other up to 177°C. The perfect agreement between the results based on viscometer and HTHP rheometer was more noticeable in the case of Herschel Bulkley model than those of Power Law model up to 177°C. This behavior was expected be continued up to the gelation temperature (193°C) based on HTHP rheological results. After this temperature, a big differences was observed between the pressure drop results based on viscometer and HTHP rheometer results in Power Law and Herschel Bulkley model.

More investigation on rheological behavior of sepiolite mud at different temperatures would be reasonable decision to get more insight in the variation of frictional pressure loss with temperature. The variation of analytically calculated frictional pressure losses with temperature for both Power Law and Herschel Bulkley models considering rheological constants from rheometer and viscometer were shown in Figures 8.2 and 8.3. As known, non-Newtonian fluid viscosities vary at different shear rates. Drilling fluids are normally shear thinning fluids, which means the viscosity of drilling fluid decreases with increasing shear rate. Shear thinning fluid exhibits relatively low viscosity in the drillstring where the shear rate is high and causes less frictional pressure loss if the velocity effect is neglected. Another type of non-Newtonian fluids is shear thickening fluid in which the viscosity of fluid increases as the shear rate increases. Shear thickening fluids are not favorable as drilling muds because they create excessive pressure drops in the circulation system. Considering this fact, it was logical to evaluate pressure drop changes through Power Law and Herschel Bulkley models with respect to variation in viscosity and flow behavior index. The rheological results obtained in Chapter 5 indicated that the unweighted fresh water sepiolite mud exhibited shear thinning behavior at all testing temperatures based on conventional viscometer measurements. However, the rheological parameters from HTHP rheometer imposed different rheological behaviors with increasing temperature. Therefore, it was expected that the frictional pressure losses based on rheometer parameters could be different from those obtained based on viscometer parameters.

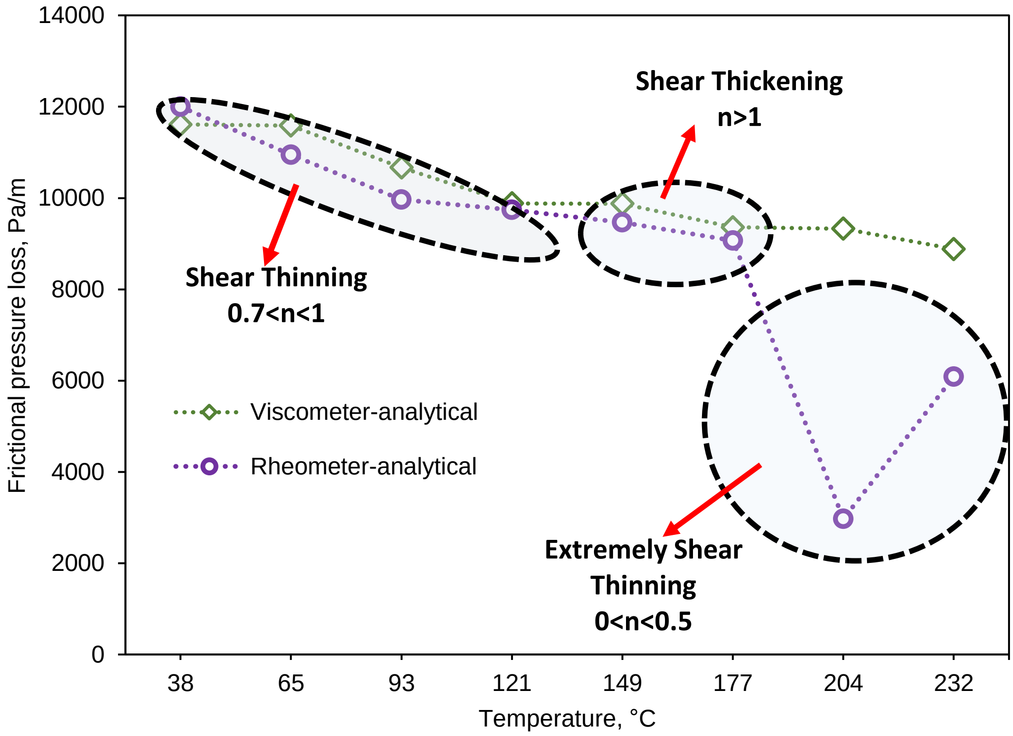

Figure 8.2: Variation of analytically calculated frictional pressure losses with temperature for Power Law sepiolite fluid.

As seen from Figure 8.2, frictional pressure losses decreased up to 121°C in Power Law model as fluid system exhibited shear thinning behavior. The flow behavior indexes for fluid at 149°C and 177°C were determined around 1 (1.007 and 1.094), and fluid system exhibited relatively shear thickening behavior. The value of frictional pressure losses at 149°C and 177°C were not significantly affected with variation on fluid system rheological behavior. However, extreme decrement in the value of flow behavior index (n=0.192) at 204°C resulted in high shear thinning behavior for the fluid system causing excessive decrease in frictional pressure losses. On the other hand, Herschel Bulkley model exhibited similar shear thinning behavior with the results of Power Law model up to 121°C (Figure 8.3). In addition, the fluid system presented shear thickening behavior by providing the flow behavior indexes higher than 1 (1.035 and 1.094) between the temperatures of 149°C and 177°C in the case of Herschel Bulkley fluid. However, the effect of such variation in rheological behavior on frictional pressure losses was not significant similar to Power Law model. Unlike Power Law model, extreme shear thickening behavior was dominant at 204°C for Herschel Bulkley fluid system since the flow behavior index increased excessively to 1.506 at this temperature. Therefore, the extreme increases in frictional pressure loss were unavoidable.

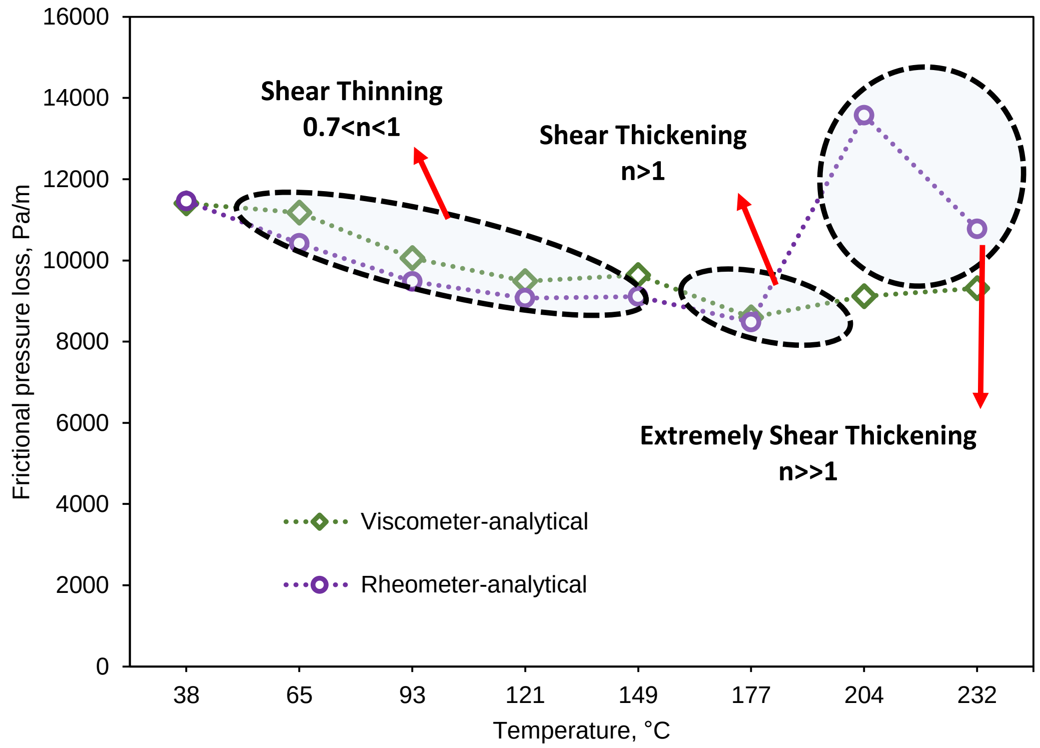

Figure 8.3: Variation of analytically calculated frictional pressure losses with temperature for Herschel Bulkley sepiolite fluid.

8.6 Prediction of Frictional Pressure Loss using CFD

In this study, CFD analysis using ANSYS Workbench 14.5 (2014) is used to simulate non-Newtonian fluids flowing through a vertical pipe and annulus. Navier-Stokes equations obtained from the conservation of momentum are solved numerically using ANSYS FLUENT. The flow is assumed to be a steady-state, incompressible, fully developed flow and $k-\varepsilon$ model was used as turbulent flow. The $k-\varepsilon$ model introduces two new variables into the system of equations. These are the turbulent kinetic energy k and turbulent dissipation ε. These two equations have to be solved along with the time-averaged continuity, momentum and energy equations. The continuity equation is then:

$$\frac{\partial \rho}{\partial t} + \nabla.(\rho U) = 0 \tag{8.39}$$

and the momentum equations become:

$$\frac{\partial \rho U}{\partial t} + \nabla.(\rho U \otimes U) - \nabla.\left(\mu_{eff} \nabla U\right) = -\nabla P' + \nabla.\left(\mu_{eff} \nabla U\right)^T + B \tag{8.40}$$

where B is the sum of body forces, U is the vector of velocity, μ_{eff} is the effective viscosity accounting for turbulence, and p' is the modified pressure.

The $k - \varepsilon$ model is based on the eddy viscosity concept, so that:

$$\mu_{eff} = \mu + \mu_t \tag{8.41}$$

According to the $k - \varepsilon$ model, turbulent viscosity is defined as

$$\mu_t = C_\mu \rho \frac{k^2}{\varepsilon} \tag{8.42}$$

In Equation 8.42, k is turbulent kinetic energy, ε is its dissipation rate, and C_μ is a constant; based on the best match with experiments, its value has been specified to be 0.09. The values of k and ε come directly from the differential transport equations for the turbulence kinetic energy and turbulence rate:

$$\frac{\partial(\rho k)}{\partial t} + \nabla.(\rho U k) = \nabla.\left[\left(\mu + \frac{\mu_t}{\sigma_k}\right)\nabla k\right] + P_k - \rho\varepsilon \tag{8.43}$$

$$\frac{\partial(\rho \varepsilon)}{\partial t} + \nabla.(\rho U \varepsilon) = \nabla.\left[\left(\mu + \frac{\mu_t}{\sigma_\varepsilon}\right)\nabla k\right] + \frac{\varepsilon}{k}(C_{\varepsilon 1} P_k - C_{\varepsilon 2}\rho\varepsilon) \tag{8.43}$$

where $C_{\varepsilon 1}$ is 1.44, $C_{\varepsilon 2}$ is 1.92, k is 1.0, and ε is 1.3; U is the vector of velocity (ANSYS FLUENT-Solver Theory Guide, 2014). P_k is the turbulence production due to viscous and buoyancy forces, which is modeled using:

$$P_k = \mu_t \nabla U.(\nabla U + \nabla U^T) - \frac{2}{3}\nabla.U(3\mu_t \nabla.U + \rho k) + P_{kb} \tag{8.44}$$

where P_{kb} is the buoyancy production term. For incompressible flow, $\nabla.U$ is small and the second term on the right side of Equation 8.42 does not contribute significantly to the production (ANSYS FLUENT-Solver Theory Guide, 2014). Three rheological fluid models describing before is used to characterize non-Newtonian fluids behavior. The concentric annulus and its corresponding drill pipe used in the CFD simulation were shown in Figure 8.4. Since the flow was asymmetric, considering half of pipe and annulus geometry through modelling was the reasonable decision to save in time and avoid excessive numerical calculation.

The mesh generation is one of the most important parts of CFD simulations in order to accurately simulate pipe and annular flow. Thus, a different mesh size was tried in this study and this process continued until simulation results were not dependent on mesh size. Afterward, the pipe and annulus geometries were divided approximately into 171520 and 139104 hexahedral meshes, respectively. The flow was assumed to be steady, incompressible, and isothermal. Figure 8.4 also shows a CFD model hexahedral mesh sample for concentric annulus and pipe.

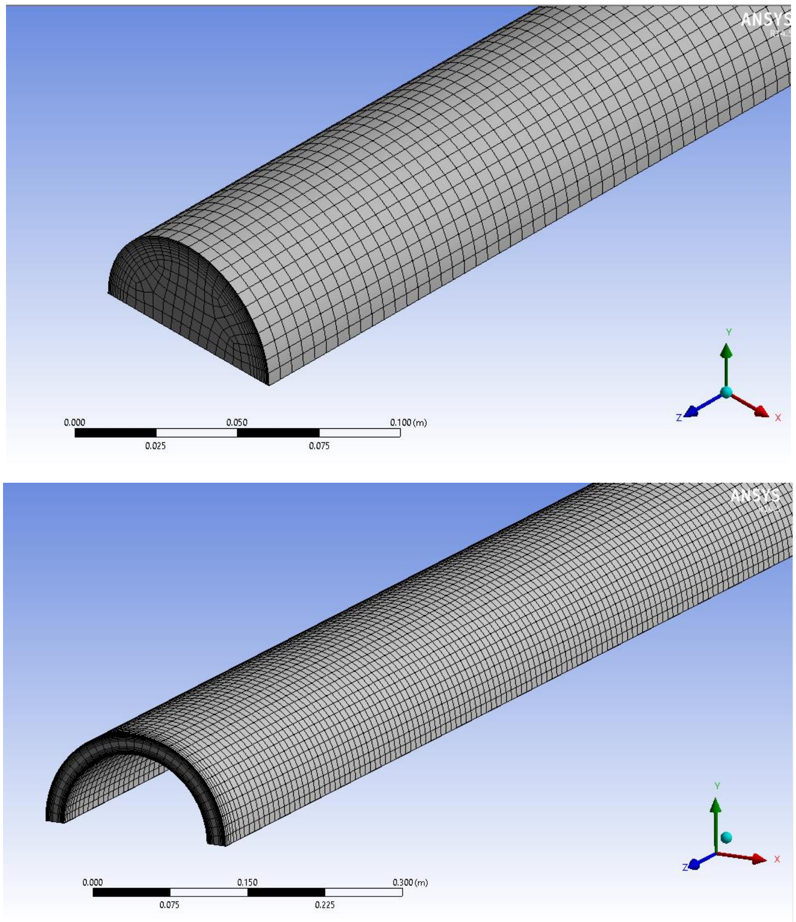

Figure 8.4: Hexahedral mesh type on a) Pipe b) Annulus.

The pipe length (L), is selected for simulation greater than the maximum entrance length (Le), in order to eliminate the end effects and to obtain fully developed flow. Then, the inlet fluid velocity and the outlet pressure were defined in a Fluent-Solver component of the package. The governing equation of turbulent flow was solved using finite volume method. No-slip boundary condition was chosen for all numerical solutions. The flow was assumed to be steady, incompressible, isothermal and k-ε model was used for turbulent flow. After completing numerical solution some criteria must be controlled to confirm the accuracy of the results. Some of these are y plus, centerline velocity, coefficient of skin friction, velocity profile, and pressure distribution. Turbulent flows are significantly affected by the presence of walls. The *k-epsilon* turbulence model is primarily valid away from walls and special treatment is required to make it valid near walls. The near-wall model is sensitive to the grid resolution which is assessed in the wall unit *y+* (defined in the FLUENT user manual). It is recommended to select the near-wall resolution such that $y+ > 30$ or < 5 for the wall-adjacent cell when using the *Enhanced Wall Treatment* option. In this section the y plus value tried to be less than 5 through all numerical analysis by applying fine mesh to the near walls. The visual results related to the CFD modelling on pipe and annular flow were given in Appendix-N through Figure N.10 to N.22. These figures depicted the pressure distribution profile, pressure drop per one meter, velocity profile, centerline velocity, y plus value through pipe and annulus while circulating unweighted fresh water sepiolite mud based on Herschel Bulkley rheological model at 38°C.

8.7 Circulation Pressure Losses-CFD Solution Results

The same geometry and flow rate were considered through CFD analysis under same selected 8 temperatures. The variation of frictional pressure losses with temperature were numerically calculated and the results were tabulated in Tables M.1 thru M.4 given in Appendix-M. Similar to analytical method, the results involved in frictional pressure losses calculated based on rheological parameters obtained in Chapter 5 for Power Law, Bingham Plastic and Herschel Bulkley models using conventional viscosity and HTHP rheometer. The results were also pictured through Figures N.1 thru N.9 in Appendix-N to detail pressure losses visually inside drill collar, annulus and through both of them as total pressure drop. Achieved results for CFD analysis indicated the great agreements and consistency between the results of frictional pressure losses obtained using CFD and analytical methods.

8.8 Chapter Conclusions

Frictional pressure loss of unweighted fresh water sepiolite mud at different temperatures were calculated and estimated using existing analytical method and CFD based on rheological parameters obtained from the viscometer and rheometer data. The results indicated that:

- Sepiolite mud using Bingham Plastic rheological model provided substantial difference between the frictional pressure losses calculated based on rheometer and viscometer. It meant that the wellbore hydraulic design using Bingham Plastic rheological parameters obtained from viscometer could lead to calculate excessive FPLs than those obtained from HTHP rheometer data.

- On contrary to Bingham Plastic model, relatively close and lower FPLs were calculated using viscometer and HTHP rheometer data in Power Law and Herschel Bulkley rheological model up to 177°C. It was expected that such behavior would be sustained up to the gelation point or temperature.
- After the gelation temperature, big differences were observed between the pressure drop results based on viscometer and HTHP rheometer data in both Power Law and Herschel Bulkley models.
- Through Power Law model, extremely low amount of flow behavior index resulted in high shear thinning behavior after the gelation point, thereby causing excessive decrease in frictional pressure losses. However, in Herschel Bulkley fluid system shear thickening behavior was ascendant after gelation point, and the extreme increase in frictional pressure loss was inevitable.
- Application of CFD analysis in prediction of FPLs directed that the convenient coincidence were witnessed between the results of frictional pressure losses obtained using CFD and analytical methods.

9. EFFECT OF TEMPERATURE ON HOLE CLEANING ABILITY OF UNWEIGHTED SEPIOLITE MUD

9.1 Introduction

The importance of efficient cutting transport during drilling operation is an undeniable fact. Poor transportation of cutting might causes some difficulties through well drilling. Stuck pipe could be a worse problem as a result of drill cutting accumulation. Effect of some parameters such as rheological properties and density of drilling fluid, size and density of drill-cutting, well inclination, drill pipe rotation, and mud circulation rate on cutting transport is among the top issues discussed in drilling industry.

This part of study is an attempt to investigate the hole cleaning ability of unweighted fresh water sepiolite mud using Computational Fluid Dynamics (CFD) analysis. The rheological model constants obtained through conventional viscometer and HTHP rheometer were used to evaluate effect of temperature on cutting transport while using unweighted fresh water sepiolite mud. Navier-Stokes equations, the continuity equation and the non-Newtonian Power Law rheological model were applied to establish the mathematical model of the cutting transport process in the annulus of the well. In addition analytical method based on Moore correlation (Bourgoyne et. al., 1991) was used to calculate cutting transport ratio and compared with CFD. Obtained results were compared to have better evaluation of CFD application.

9.2 Literature Review

Prediction of cutting transport or hole cleaning efficiency at a given circulation rate is an important issue that should to be determined particularly during well design phase. There is a direct relation between hole cleaning and energy consumption while drilling. Therefore, different drilling conditions should be simulated so that optimum drilling parameters are determined to achieve safe drilling and minimum drilling cost particularly in environments with narrow mud weight window. Yet simple, analytical model solutions do not consider or handle some realistic drilling conditions. Moreover, there is no analytical solution in some cases such as flow in eccentric annulus, rotation of drillstring, temperature effect, transient flow conditions, etc. In general, if validated, CFD can safely be used in modelling the aforementioned situations. Cutting transport is an important phenomenon while drilling operation. Numerous experimental works on this topic have been conducted to model and calculate required parameters in order to provide effective hole cleaning. However, all experimental works were limited with physical constraints. It is difficult and expensive to operate an experimental work in different well sizes using different particle sphericities and sizes. Some of leading studies were selected to review as literature. Hussain and Jamal (1983) investigated how particle size, flow rate, apparent viscosity, yield point and plastic viscosity affect carrying capacity of drilling mud. In addition, they analyzed semi empirical transport model of Zeidler (1972) and conclude that there is significant effect of fluid annular velocity on carrying capacity of the drilling fluid. Carrying capacity of mud increases with increasing ratio of yield point to plastic viscosity. They reported that parameters such as apparent viscosity, yield point and initial gel strength have major effect on fluid carrying capacity, at medium (18 in./sec) and low (12 in./sec) fluid annular velocities. Their effect were insignificant at high (23.9 in/sec) fluid annular velocities. Bilgesu et al., (2002) investigated the effect of fluid velocity, cutting size, rate of penetration, drill pipe rotation and well inclination on cutting transport using Computational Fluid Dynamics. They claimed that, contrary to smaller particles, hole cleaning was more efficient while using larger particles. They also indicated that for horizontal well effect of flow rate is more important for smaller particles than larger ones on hole cleaning. Drill pipe rotation has slightly effect on cutting transport especially for larger particles. Their studies presented that inclination has major effect on hole cleaning and increasing deviated angle has negative effect on hole cleaning. Tomren et. al. (1986) studied cutting transport ratio through inclined wells, at laboratory by changing the angles of inclination, pipe-hole eccentricity, fluid flow regimes, and pipe rotation. They observed that at high angles greater than 40° degree accumulation of bed was observed and increasing inclination of pipe, dramatically decreases the carrying capacity of fluid. They also presented that high viscous fluids give better result in cutting transport that those with low viscosity. At intermediate angles between 40° and 50° degrees, accumulated beds started to slide down against the fluid flow. For vertical wells there was not significant effect of eccentricity on cutting behavior. Since in inclined wells the minimum buildup of cuttings have observed at the concentric annulus and maximum buildup have observed at positive-eccentric annulus. Ford et al., (1990) analyzed Minimum Transport Velocity (MTV) for cuttings to movement in suspension and for rolling/sliding forward. This study reported that MTV is dependent on both rheology of fluid and fluid pattern. Increasing viscosity of fluid resulted in decreasing in MTV. The study resulted that pipe rotation has insignificant effect on cutting suspension or rolling/sliding mechanisms while circulating water as fluid. Horeland et al., (1993) investigated behavior of limestone cutting at water base and low toxicity invert emulsion mineral oil base muds in inclined wells. They concluded that in inclined wells, increasing yield point and plastic viscosity of both mud types decreased cutting transport rate. In addition they represented that at high angle inclined wells decreasing both yield point and plastic viscosity and increasing flow rate will improve hole cleaning. Okrajni et al. (1986) studied effect of rheological properties of water and bentonite polymer muds on cutting transport in inclined wells with angle between 0° to 90° degree through turbulent and laminar flow. They stated that the effect of mud yield value is insignificant on the cutting concentration in both vertical and horizontal wells. In turbulent flow, rheology of mud has insignificant effect on cutting transport performance. In laminar flow, increasing of yield point results in low cutting concentration for inclined wells between 0° and 45° degrees. Contrary to turbulent flow, cutting concentration is less in laminar flow at low inclined wells degrees between 0° to 45°. They described that there is not significant difference at cutting concentrations between laminar and turbulent flows in inclined wells degrees between 45° to 55°. Contrary to laminar flow, cutting concentration is less in turbulent flow at high inclined wells degrees between 55° to 90°. Sifferman et al., (1992) studied effect of annular mud velocity, mud density, mud rheology, mud type (oil or water base), cutting size, rate of penetration, drillpipe rotary speed, drillpipe eccentricity, drillpipe diameter and hole angle on hole cleaning. Zeidler et al., (1972) studied settling velocity of the drilled cuttings in the Newtonian fluid and develop correlations for it. They also studied cutting transport of the water and the drilling mud. Duan et al., (2007) experimentally investigated Critical Re-Suspension velocity (CRV), minimum velocity, to erode formed bed, and Critical Deposition Velocity (CDV), minimum velocity, to prevent bed formation. Some authors suggested additional runs for non-uniform cutting sizes and also for wellbore with inclination angles between vertical and horizontal. For this purpose H. Al-

Kayiem et al., (2010) conducted a study and examined the effect of non-uniform cuttings size and the inclination angle at different mud feeding rate using CFD simulation and analyses. Employing the real field data (a drilling site in Sudan) is the important aspect of this study. Impressive CFD achievement resulted in a significant effect of the cuttings size on hole cleaning so that fine particles are the easiest to clean out.

9.3 Particle Slip Velocity

Settling velocity of the particle due to its weight, defined as the slip velocity of the particle. It is function of the particle size, particle geometry, particle density, fluid rheological properties, carrying capacity of the mud and the fluid velocity in the annulus.

9.3.1 Particle slip velocity for Newtonian fluids

Bourgoyne et al. stated that, a particle which falls through the fluid is affected by the gravity force; buoyant force and viscous drag force caused by the fluid and the sum of acting forces are equal to the zero (Figure 9.1a). Considering this fact, relation between slip velocity and viscous drag force has been derived by the Stokes (1845) for the creeping flow (Figure 9.1b). Derived equations known as Stokes' law are given in Equations 9.1 and 9.2.

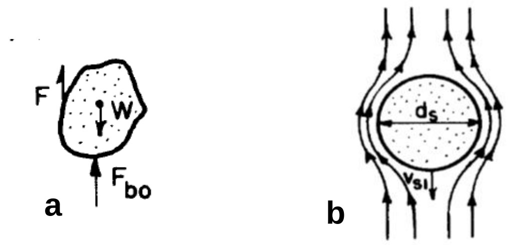

Figure 9.1: a) Forces acting to the particle b) creeping flow and slip velocity (Bourgoyne et al., 1991)

$$V_{sl} = \frac{d_s^2}{18\,\mu}\,(\rho_s - \rho_f)g \qquad (9.1)$$

$$V_{sl} = \frac{138\,d_s^2}{\mu}\,(\rho_s - \rho_f) \qquad (9.2)$$

where:

μ : Viscosity
V_{sl}: slip velocity
d_s : Diameter of spherical particle
ρ_f : Density of fluid
ρ_s : Density of particle

Stokes law is applicable for, Newtonian, laminar flows or flows with Reynolds number smaller than 0.1. For flows bigger than 0.1 empirically derived friction factor is used to obtain slip velocity as follows:

$$f = {}^{4}/_{3} \times {}^{gd_s}/_{v_{sl}^2} \times {}^{(\rho_s - \rho_f)}/_{\rho_f} \tag{9.3}$$

$$f = {}^{3.57d_s}/_{v_{sl}^2} \times {}^{(\rho_s - \rho_f)}/_{\rho_f} \tag{9.4}$$

$$V_{sl} = 1.89\sqrt{{}^{d_s}/_{f} \times {}^{(\rho_s - \rho_f)}/_{\rho_f}} \tag{9.5}$$

where:

f : Friction factor
d_s : Diameter of spherical particle
ρ_f : Density of fluid
V_{sl}: slip velocity

Since the friction factor was determined empirically, Figure 9.2 gives the friction factor as a function of Reynolds number and Sphericity Ψ. Sphericity is defined as the ratios of surface area of sphere particle to the surface area of the particle contains same volume (Bourgoyne et al., 1991).

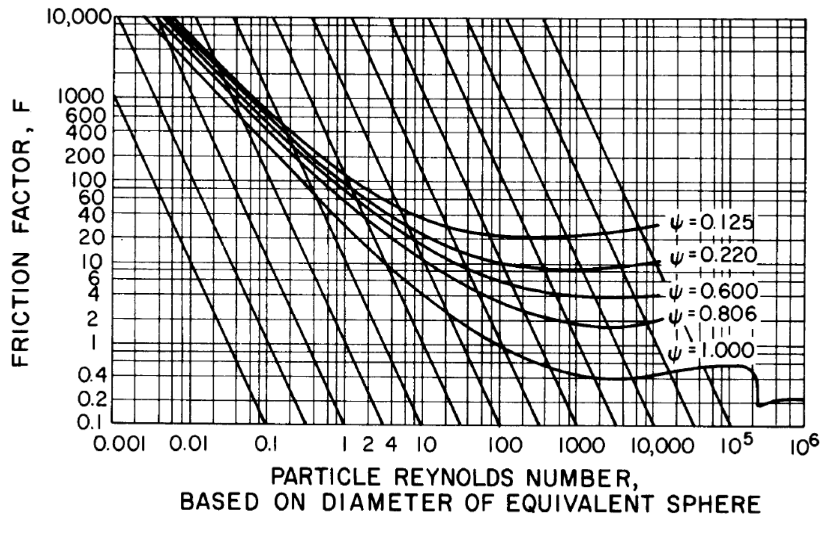

Figure 9.2: Friction factor as a function of Reynolds number and Sphericity (Bourgoyne et al., 1991).

9.3.2 Particle slip velocity for non-Newtonian fluids

Particles will not settle down unless buoyancy and gravity forces overcome the gel strength of the fluid (Bourgoyne et.al 1991). For the spherical particles with the surface area πd_s^2, minimum required force to overcome the buoyancy and gravity forces is equal to the surface area times gel strength (τ_g) given in Equation (9.6). This equation can be expressed in field units through Equation (9.7). On the other hand, by solving equation (9.7) for d_s, equation (9.8) will be obtained which is the minimum diameter of the spherical particle settled down in a fluid with a gel strength of τ_g. Unfortunately analytical solution for creeping flow has not been developed for non-Newtonian fluids (Bourgoyne et al, 1991).

$$\tau_g = {d_s(\rho_s - \rho_f)}/{6} \tag{9.6}$$

$$\tau_g = 10.4 d_s(\rho_s - \rho_f) \tag{9.7}$$

$$d_s = {\tau_g}/{10.4(\rho_s - \rho_f)} \tag{9.8}$$

where:

τ_g: Gel strength
ρ_f: Density of fluid
ρ_s : Density of particle

9.3.3 Moore correlation (an empirical solution)

Various equations have been derived to estimate the slip velocities of spherical particles in laminar and turbulent flows. The range of applicability of these equations depends on the particles Reynolds number which is a function of the particle diameter and settling velocity as well as the fluid density and viscosity. Moore P.L. (1974) has proposed an approaches to calculate the slip velocity for static fluids subjected to average flowing condition during drilling operation through a vertical well. According to this model an apparent Newtonian viscosity is computed based on equation proposed by Dodge and Metzner, 1959 (Equation 9.9). Computing an apparent Newtonian viscosity with equation (9.9) and using it instead of viscosity in equation (9.10) lead to find particles Reynolds number. Obtained Reynolds number can be used with the friction factor correlation given in Figure 9.3 which is based on the field data for limestone and shale cuttings. Finally, slip velocity may be calculated by entering the obtained friction factor value to the equation (9.5). Depending on the Reynolds number, slip velocity may be calculated by simplifying equation (9.5) based on obtained friction factor. Simplified versions of equation (9.5) were given as follows.

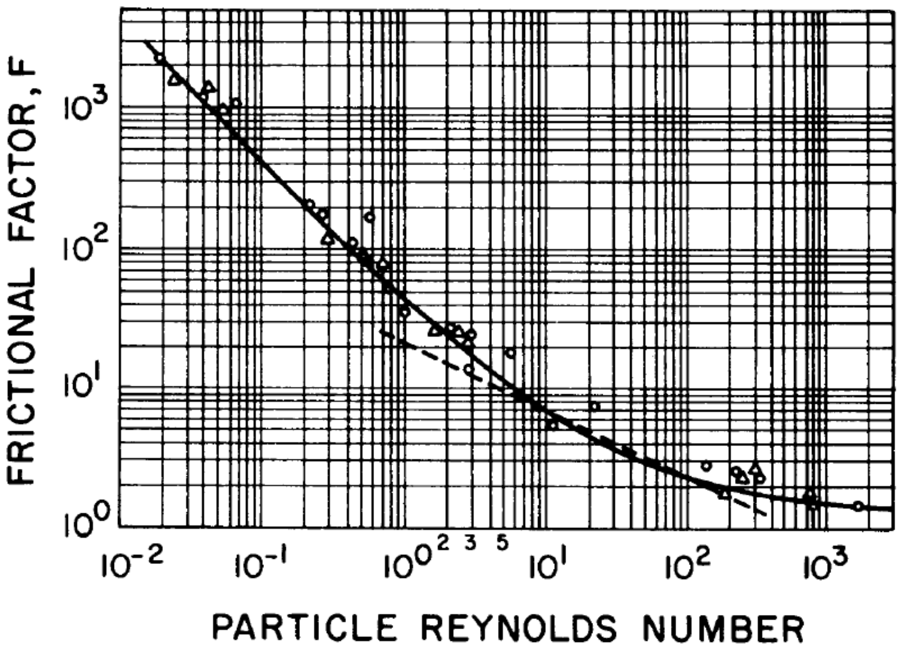

Figure 9.3: Friction factor F as a function of particle Reynolds number (Bourgoyne et al., 1991).

$$\mu_a = {}^{K}/_{144}\left({}^{d_2 - d_1}/_{\bar{v}_a}\right)^{(1-n)}\left({}^{2+\frac{1}{n}}/_{0.0208}\right)^{n} \tag{9.9}$$

$$N_{Re} = \frac{928\rho_f V_{sl} d_s}{\mu} \tag{9.10}$$

For Laminar flow, $N_{Re} < 3.0$, then

$$V_{sl} = 82.87\left(\frac{{d_s}^2}{\mu_a}\right)(\rho_s - \rho_f) \tag{9.11}$$

For Transitional flow,3 < N_{Re} < 300, then

$$v_{sl} = {}^{2.9 d_s (\rho_s - \rho_f)^{0.667}}/_{\rho_f^{0.333}\mu_a^{0.333}} \tag{9.12}$$

For Turbulent flow, N_{Re}> 300, then

$$V_{sl} = 1.54\sqrt{d_s(\,(\rho_s - \rho_f)\,/\,\rho_f)} \tag{9.13}$$

where:

f : Friction factor
d_2: Outer diameter of annulus
d_1: Inner diameter of annulus
ρ_f: Density of fluid
ρ_s : Density of particle
μ : Viscosity
V_{sl}: slip velocity
d_s : Diameter of spherical particle
N_{Re} : Reynolds number
μ_a : Apparent viscosity
K: Consistency index
n: Flow-behavior index

9.4 Cutting Transport Ratio

Cutting transport ratio F_T is defined as the ratio of transport velocity V_T to the mean annular velocity V_a where transport velocity is equal to the mean annular velocity minus slip velocity. On the other hand transport velocity may be defined as the velocity of cutting particle against the surface. Equations of F_T and V_T are given below.

$$V_T = V_a - V_{sl} \tag{9.13}$$

$$F_T = {}^{v_T}/_{v_a} = {}^{(v_a - v_{sl})}/_{v_a} = 1 - {}^{v_{sl}}/_{v_a} \tag{9.14}$$

where:

F_T: Cutting transport ratio
V_a: Mean annular velocity
V_T: Transport velocity
V_{sl}: Slip velocity

Cutting transport ratio is used to determine carrying capacity of drilling fluid. If slip velocity increases transport ratio decreases and cutting concentration increases in the annulus.

9.5 Modelling Cutting Transport Using CFD

Since investigated domain consists of fluid and particles, one of the mixture models built in Fluent must be used. In multiphase flow, a phase can be defined as an identifiable class of material that has a particular inertial response and interaction with the flow and the potential field in which it is immersed. FLUENT offers two types of two-phase flow approach, based on the Eulerian-Eulerian and the Eulerian-Lagrangian approaches.

9.5.1 Euler-Lagrange approach

Discrete Phase Model (DPM): In an Eulerian-Lagrangian formulation also called Lagrangian, the particles are treated as discrete entities. The fluid phase is treated as a continuum by solving the time-averaged Navier-Stokes equations, while the dispersed phase is solved by tracking a large number of particles, bubbles, or droplets through the calculated flow field. The dispersed phase can exchange momentum, mass, and energy with the fluid phase. A fundamental assumption made in this model is that the dispersed second phase occupies a low volume fraction. The particle or droplet trajectories are computed individually at specified intervals during the fluid phase calculation. This makes the model appropriate for any application where the volume fraction of the second phase is not negligible

9.5.2 Euler-Euler approach

In the Euler-Euler approach, the different phases are treated mathematically as interpenetrating continua. Since the volume of a phase cannot be occupied by the other phases, the concept of phasic volume fraction is introduced. These volume fractions are assumed to be continuous functions of space and time and their sum is equal to one. Conservation equations for each phase are derived to obtain a set of equations, which have similar structure for all phases. These equations are closed by providing constitutive relations that are obtained from empirical information, and in the case of granular flows, by application of kinetic theory. Three different Euler-Euler multiphase models are available: the volume of fluid (VOF) model, the mixture model, and the Eulerian model.

VOF model: This is a surface-tracking technique applied to a fixed Eulerian mesh. It is designed for two or more immiscible fluids where the position of the interface between the fluids is of interest. In the VOF model, a single set of momentum equations is shared by the fluids, and the volume fraction of each of the fluids in each computational cell is tracked throughout the domain.

Mixture Model: The mixture model is designed for two or more phases (fluid or particulate). As in the Eulerian model, the phases are treated as interpenetrating continua. The mixture model solves for the mixture momentum equation and prescribes relative velocities to describe the dispersed phases. The mixture model can also be used without relative velocities for the dispersed phases to model homogeneous multiphase flow.

Eulerian Model: The Eulerian model is the most complex of the multiphase models in Fluent. It solves a set of momentum and continuity equations for each phase. Coupling is achieved through the pressure and interphase exchange coefficients. The manner in which this coupling is handled depends upon the type of phases involved; granular (fluid-solid) flows are handled differently than non-granular (fluid-fluid) flows. For granular flows, the properties are obtained from application of kinetic theory. Momentum exchange between the phases is also dependent upon the type of mixture being modeled. With the Eulerian multiphase model, the number of secondary phases is limited only by memory requirements and convergence behavior. Any number of secondary phases can be modeled, provided that sufficient memory is available. For complex multiphase flows, however, one may find that the solution is limited by convergence behavior.

9.5.3 Turbulent dispersion of particles

In FLUENT, droplet dispersion due to turbulence can be treated either through the stochastic model or with the cloud model. The particle cloud model tracks the statistical evolution of a cloud of particles about a mean trajectory. However, the cloud model is not available for parallel processing, therefore this model cannot be used in this study. Hence the stochastic approach has been chosen for this investigation. In the stochastic tracking approach, the turbulent dispersion of particles is predicted using the instantaneous fluid velocity for the droplet trajectory equation integration. If we recorded the velocity at a particular point in the real (turbulent) fluid flow, the instantaneous velocity (U) is defined by:

$$u = \bar{u} + u(t) \tag{9.15}$$

where $\bar{u}$ is the time average of velocity and $u(t)$ presents the fluctuating velocity. By computing the trajectory in this manner for a sufficient number of representative particles, the random effects of turbulence on the particle dispersion may be accounted for. Generally a number of tries equal to 5 was specified so that the trajectories can be computed five times in order to get a good statistical representation of the spread of droplet due to turbulence. Each trajectory calculation includes a new stochastic representation of the turbulent contributions to the trajectory equation. Increasing the number of tries would lead to an increase in the number of droplet which would improve the statistical accuracy of the spray computation, but it would require a significant increase in the computational time, which is one of the main drawbacks highlighted using a Lagrangian method in the Literature review. Hence the maximum number of parcels and tries had to be limited. The total number of injection streams tracked for the surface injection will be equal to the number of diameters in each multiplied by the number of tries and the total number of injections.

To see the sensitivity of the solution to the number of tries, a simulation was carried out with 10 tries but this resulted in more than double computational time while the numerical predictions remained largely unchanged, therefore it was decided that setting to 4 the number of tries was sufficient. Typically a number of tries comprised between 3 and 5 is acceptable.

9.5.4 Particle force balance

The force balance is written in the Lagrangian reference frame. The force balance is represented by the particle inertia and the forces acting on the particle. As a result, FLUENT predicts the trajectory of a discrete phase particle in the following manner:

$$\frac{\mathrm{d}u_p}{\mathrm{dt}} = F_D\left(\vec{u} - \vec{u}_p\right) + {}^{\vec{g}(\rho_s - \rho)}\!\big/_{\rho_s} + \vec{F} \tag{9.16}$$

where F is an additional acceleration (force/unit particle mass) term, $F_D\left(\vec{u} - \vec{u}_p\right)$ represent the drag force per unit particle mass and

$$F_D = {}^{18\mu C_D Re}\!\big/_{\rho_s d_s^2 24} \tag{9.17}$$

where μ is the molecular fluid viscosity, ρ is the gas density, d_s is the particle diameter, ρ_s the particle density, u the gas velocity and $\vec{u}_p$ the particle viscosity. Re is the relative Reynolds number defined as follow:

$$\mathrm{Re} = {}^{\rho d_s\left|\vec{u}_p - \vec{u}\right|}\!\big/_{\mu} \tag{9.18}$$

The drag coefficient is described as:

$$C_D = \begin{cases} 0.424 & Re > 1000 \\ \frac{24}{Re}\left(1 + \frac{1}{6} Re^{2/3}\right) & Re \leq 1000 \end{cases} \tag{9.19}$$

In order to solve the discrete phase model, the following steps have to be followed:

1. solve the continuous phase prior to introduction of the discrete phase
2. set up the discrete phase properties
3. introduce the discrete phase by calculating the particle trajectories for each discrete phase injection
4. recalculate the continuous phase flow, using the interphase exchange of momentum, heat, and mass determined during the previous particle calculation
5. recalculate the discrete phase trajectories in the modified continuous phase flow field

While the particle travels throughout the domain, FLUENT keeps track of the heat, mass and momentum lost by the particles. The interaction between the continuous and the dispersed phase is taken into account by coupling both phases. FLUENT computes the particle/droplet trajectories and updates the interphase exchange of momentum, heat, and mass in each control volume. Convergence is reached when changes in solution variables from one iteration to the next is negligible and residuals are quite helpful in monitoring convergence. Generally, a decrease in residuals by at least three orders of magnitude indicates convergence. A relative error of 10^{-5} is used as the criterion for convergence for the continuity, velocity and turbulence terms and residuals of 10^{-6} are required for the energy equation. Rather than only relying on residuals, it is possible to get a complementary indication of convergence by checking the mass and energy balance; however, the energy balance being available only for cases with combustion from the particles to the gas phase.

This part of study covers the investigation of cutting transport ability of unweighted fresh water sepiolite mud through different annular velocities at elevated temperatures. The rheological constant parameters obtained using conventional viscometer and HTHP rheometer for Power Law model were used to apply Moore correlation as well as CFD analysis for this type of sepiolite mud sample. Table 9.1 presented the parameters used in calculation of cutting transport ratio in this part of study.

Table 9.1: Parameters for calculation of slip velocity.

Particle diameter	0.10	inch
Density of fluid	8.70	lbm/gal
Density of particle	21.44	lbm/gal
Hole diameter	7.88	inch
Pipe diameter	4.50	inch
Sphericity ψ	1	dimensionless

9.6 Results and Discussions

Hole cleaning ability of unweighted fresh water sepiolite mud was investigated using with both CFD and Moore analytical methods. Four common temperatures (38°C, 121°C, 149°C, and 232°C) were selected to evaluate the cutting transport ability of mud sample. The results were numerically listed in Tables P.1-P.15 located in Appendix-P. The comparative results were also presented graphically in Appendix-Q through Figures Q.1-Q.9 to compare the hole cleaning ability of mud sample based on rheological parameters obtained using conventional viscometer and HTHP rheometer.

Figure 9.4 shows the relation between cutting transport ratio and average annular velocity for fresh water sepiolite at 38°C. A detail comparison can be observed from the results depicted in this figure based on rheological constants measured by conventional viscometer and HTHP rheometer. No big differences were observed between cutting transport ratio calculated based on classic viscometer and HTHP rheometer at 38°C, as expected. The difference increased with increasing temperature so that it was observed an obvious difference in cutting transport ratio obtained based on rheological constants using viscometer and rheometer at 121°C and 149°C, (Figures Q.6 and Q.8).

For example at a constant annular velocity of 0.3 m/sec the value of transport ratio calculated based on viscometer measurements (87.79%) was 33% higher than that based on rheometer results (58.55%) at 121°C (Figure Q.6). This rate was increased to 63.4% with temperature increasing to 149°C. Generated gap in cutting transport ratio based on the rheometer and viscometer results decreased at 232°C due to increasing the viscosity of sepiolite mud sample as discussed in Chapter 6. It can be concluded that this gap will be increased up to 380°C (based on HTHP rheometer results) where the decreasing trend in sepiolite mud viscosity is changed to increase (gelation point). After that, it begins to be closed up with increasing temperature under effect of viscosity increasing. This observation can be confirmed through Figures Q.1 and Q.4 for cutting transport ratio obtained based on both rheometer and viscometer rheological constants. The transport ratio decreased from 87.80% at 38°C to 22.71% at 149°C and then increased to 85% at 232°C as a result of Moore correlation method applied on rheometer rheological parameters to obtain transport ratio (Figure Q.2).

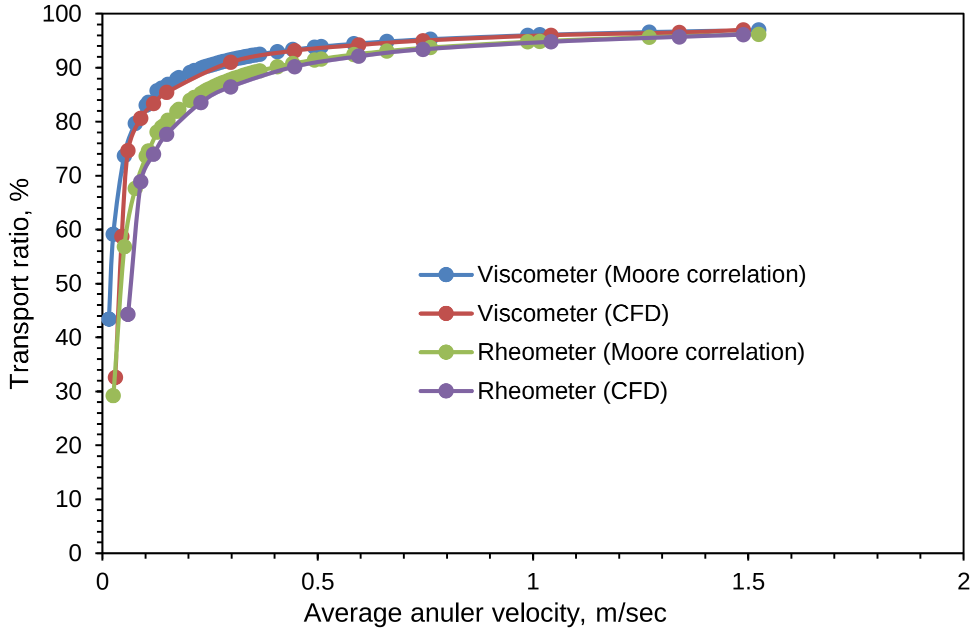

Figure 9.4: Hole cleaning ability of fresh water sepiolite mud @38°C-viscometer vs. HTHP rheometer.

The great agreements were observed between CFD and Moore analytical method at all temperatures. The slip velocity at 149°C was calculated using analytical methods for Newtonian fluid instead of Moore correlation to obtain better consistency with CFD cutting transport results. As observed in Chapter 6, it seemed the rheological behavior of sepiolite mud was changed to be Newtonian more than non-Newtonian through moderate temperatures (between 110- 193°C) due to extreme low amount of yield point. In addition, increasing the value of flow behavior index (n) to 1 at 149°C for Power Law model confirmed this observation. Further investigation on this concept will be highly appreciable. With increasing amount of flow behavior index near to 1 the cutting transport ratio calculated by Moore correlation began to keep aloof with CFD cutting transport results. Figure Q.6 and Q.7 illustrated the results of cutting transport ratio calculated using Moore correlation and CFD for unweighted fresh water sepiolite mud at 121°C and 149°C. The consistency between CFD and Moore correlation results based on HTHP rheometer rheological parameters tended to be declined with increasing temperature up to 149°C. On the other hand, Figure Q.8 depicted the results of cutting transport ratio calculated using Newtonian analytical method and CFD for unweighted fresh water sepiolite mud at 149°C. The proper conformity was observed in cutting transport ratio obtained based on CFD and Newtonian analytical method applied on both HTHP rheometer and conventional viscometer rheological measurements. Newtonian analytical calculations of slip velocity for sepiolite mud at 149°C based on rheometer rheological parameters were given as follow step by step:

For sepiolite mud at 149°C (rheometer results):

1) $v_{sl} = \frac{138\, d_s^2}{\mu}\,(\rho_s - \rho_f) = 138 \times 0.1^2 / 5.61 \times (21.44 - 8.70) = 3.13 \frac{ft}{sec}$

2) $f = 3.57 \times d_s / v_{sl}^2 \times (\rho_s - \rho_f) / \rho_f = 3.57 \times 0.1 / 3.13^2 \times (21.44 - 8.70) / 8.70 = 50 \times 10^{-3}$

$$N_{Re} = 928\, \rho_f\, v_{sl}\, d_s / \mu = 928 \times 8.70 \times 3.13 \times 0.1 / 5.61 = 451.16$$

3) Third step shown in the Figure 9.5: F=0.9 and $N_{Re} = 120$

4) $v_{sl} = 1.89\sqrt{(d_s/f)(\,(\rho_s - \rho_f)\,/\,\rho_f)} =$

$$1.89\sqrt{(0.1/0.7)(\,(21.44 - 8.70)\,/\,8.70)} = 0.76\, ft/sec$$

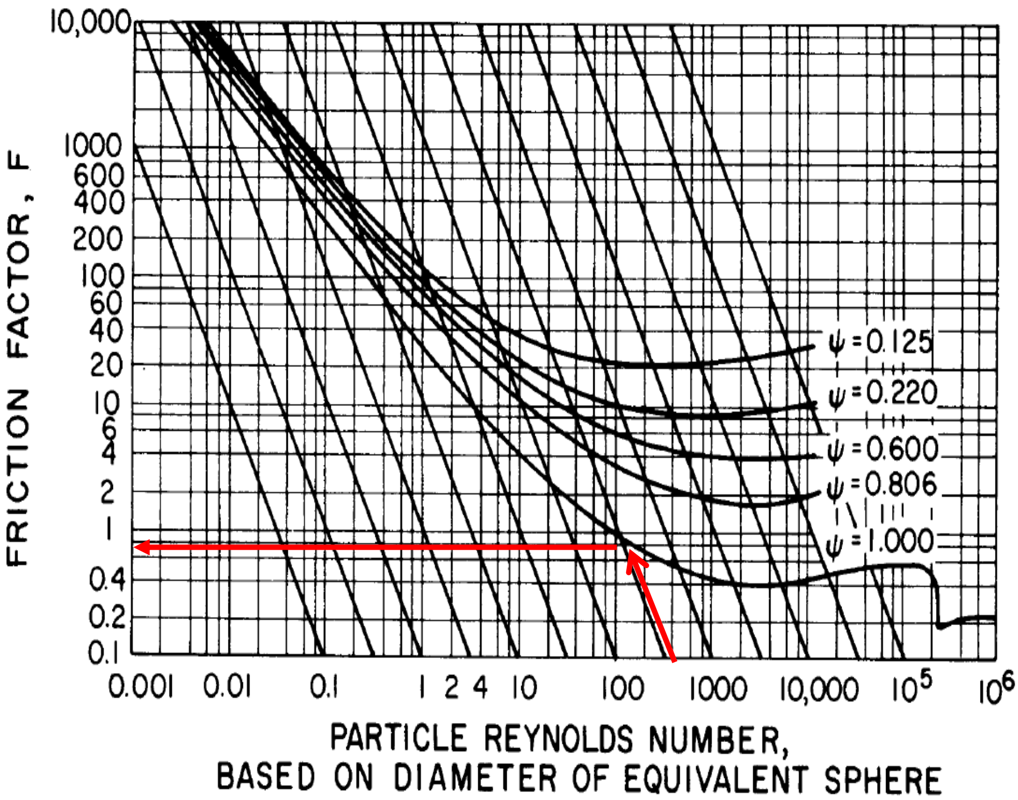

Figure 9.5: Determination of friction factor and Reynold number for sepiolite mud at 149°C (rheometer results).

It can be inferred that CFD method is a powerful tool in predicting cutting transport to provide an impressive idea prior to any operation and can be used to determine cutting transport related problems in advance along with taking necessary remedial actions. In addition, existence of good agreement between analytical and CFD results was a strong indicator for validating CFD results.

9.7 Chapter Conclusions

Thermal effects on hole cleaning ability of unweighted fresh water sepiolite mud based on rheological parameters obtained using both viscometer and rheometer were studies with a well-known analytical method and CFD. The results revealed that:

- The hole cleaning ability (cutting transport ratio) of sepiolite mud decreased with increasing temperature, however the decreasing trend keep up to the temperature at which fluid sample started to be gelling. Beyond this temperature decreasing trend in cutting transport switched to increase.
- Cutting transport ability of sepiolite mud changes with temperature parallel to the rheological behavior variation of mud sample.
- The difference observed in cutting transport ratios obtained based on viscometer and rheometer data increased with increasing temperature. The results inferred that the maximum difference will happened at the temperature corresponding to the gelation point.
- The great agreement between the results of empirical method and CFD indicated the successful application of CFD in drilling hydraulic optimization that can provide valuable insight to help engineers for understanding and simulating the physics in a circulation system prior to drill oil and gas wells.

10. CONCLUSIONS AND RECOMMENDATIONS

An exhaustive experimental and theoretical study was performed on developing and investigating thermal properties of sepiolite base drilling fluids. Seven types of sepiolite mud systems were formulated and experimentally evaluated in details by considering the hostile drilling conditions. Thermal effects on sepiolite mud properties contaminated with active-clay were examined through laboratorial work. In addition, the impact of elevated temperatures on differential pressure pipe sticking tendency and lubricity of developed sepiolite base mud systems were also investigated. However, the special emphasis was given for modelling thermal rheological properties of sepiolite mud systems. Conventional aging method using classic viscometer and direct measurement (in-situ) method using HTHP rheometer were followed to accomplish elaborative evaluation on thermal rheological variation of sepiolite fluid systems. Comparing the results of these two methods revealed the possible measurements fallacies that might happen and lead to mask real rheological behavior for a given fluid system.

Through theoretical part of this study, a new semi-analytical method was developed and examined/verified using the rheological properties of sepiolite mud systems to predict surge and/or swab pressures. The model can also be used to determine stand pipe pressures (SPP) by arranging the equations with zero pipe velocity. Hydraulic optimizations consist of prediction and calculation of frictional pressure losses and evaluation of hole cleaning ability of fluid system. The results obtained using analytical, semi-analytical and numerical approaches were compared and visually illustrated for terminative interpretations. The following results were turned out at the end of this study.

- The rheological and filtration properties of active-clay contaminated sepiolite base mud were investigated based on conventional aging method at elevated temperatures up to 204°C. The sepiolite base muds had exhibited particularly good rheological properties at temperatures above 177°C (350°F). The mud samples were not noticeably affected by the water salinity. In extreme temperatures, the sepiolite concentration of muds should be decreased to overcome problems related to degradation, particularly when formulating barite-weighted mud systems. Flocculation was observed when the sepiolite content exceeds 42.75 kg/m^3 (15 lb/bbl) for the barite-weighted muds at temperatures above 177°C (350°F) coupled with high amount of active solid contamination. Although sepiolite muds are known to yield high filtration rates as provided in Chapter 3, the formulation of sepiolite muds in special mixing order exhibited low filtration rates at harsh conditions. However, relatively high filtration rates due to the mud flocculation were observed when temperature was above 204°C (400°F) along with high salt content (343 kg/m^3) and active solid contamination (228 kg/m^3).

- Differential pressure pipe sticking tendency at high temperatures was studied for the sepiolite muds as well as two other commonly used mud systems. Compare to bentonite/polymer and lignosulfonate fluids that were rheologically stable up to 121°C, the sepiolite mud sample kept its stability up to 204°C. Extremely high amount of sticking coefficients were recorded for bentonite/polymer and lignosulfonate fluids at 121°C due to flocculation. However, the rate of increase in sticking coefficient values of sepiolite mud decreased substantially and became stable after 60 min of set time. The results also indicated that the sepiolite muds used in this study yielded acceptable amount of sticking coefficient even for the barite-weighted samples especially at high temperatures. Sticking times substantially decreased for the weighted mud systems indicating high tendency of differential pressure sticking phenomenon. In addition, the sticking times of sepiolite muds decreased with increasing temperature. High solid content increased the tendency of sticking phenomenon; therefore, a low solid mud system, a good solid control equipment operation, and/or usage of lubricating agents is a must to minimize sticking related borehole stability problems, especially for weighted mud system. Generally, excessive sticking coefficients must be expected once the flocculation was occurred. Special lubricants usage in sepiolite mud systems should be further investigated to characterize the efficiency of them.

- Thermal rheological properties of seven types of sepiolite base muds were investigated based on conventional aging method using classic viscometer and direct measurements using HTHP rheometer. In addition to unweighted and weighted fresh water sepiolite mud, semi and fully saturated sepiolite mud systems, sepiolite mud system with two different salt concentrations, and fresh water sepiolite suspension without additives were also subjected to thermal rheology testing using both methods. Comparing results from the two methods clearly indicated how important the knowledge of in-situ rheological properties of fluid system could be. The difference in viscosity from the both equipment increased with increasing temperature up to the gelation point where the decreasing trend in viscosity was halted. Beyond this point the viscosity increased with further temperature increment. As an important observation, in HTHP rheometer gelation point was occurred at the temperature higher than that of classic viscometer. It was also proven that the reason of gelation in sepiolite mud lied behind the degradation of polymers used in the mud systems rather than the sepiolite clay degradation. Rheological characterization from the both method with respect to temperature revealed that sepiolite muds were highly tolerable and efficient in saline environments. Comparing with the other two mud systems (bentonite/polymer and lignosulfonate muds) that are not applicable beyond 120°C, sepiolite mud provided effective rheological properties as well as filtration rate especially at temperature up to 204°C. Therefore, the usage of clay sepiolite instead of clay bentonite as the main component of drilling fluid could be reasonable decision at hot wells.

- The best rheological model representing the rheological behavior of each sepiolite mud systems was determined after viscometer and HTHP rheometer measurements. The Matlab curve fitting toolbox was used to analyze least-square regression to obtain residual mean squares (SSE), R-square, adjusted R-square and Root mean squared error (RMSE). The best fit rheological model was selected based on the minimum SSE, and minimum RMSE. The Herschel Bulkley model was the best fit rheological behavior model of all seven types of sepiolite muds based on classic viscometer data. However, while using HTHP rheometer rheological data, in addition to Herschel Bulkley, Power Law model exhibited the higher goodness of fit values especially in moderate temperatures. The effect of temperature on the rheological model constants of all seven types of sepiolite muds were determined and used in hydraulic optimization. Model constants were substantially varied with the temperature.

- A new semi-analytical derivation was introduced to estimate surge and swab pressures caused by tripping operation for Herschel Bulkley rheological model. The performance of semi-analytical model was examined using rheological properties of sepiolite mud based on aging method (Viscometer) and direct measurement (HTHP rheometer). The validity of calculated surge pressure was proved by comparing the results of semi-analytical method with the existing empirical models (Burkhardt and Schuh models) as well as experimental data. The effect of temperature on surge pressure was also identified through the semi-analytical model. The results disclosed the significant difference on surge pressure gradients obtained from viscometer and HTHP rheometer data. The existing gap expanded with increasing temperature such that surge pressures based on viscometer readings was approximately six fold higher than HTHP rheometer results at temperatures between 120-180°C. It can be inferred that determination of safe tripping speed from viscometer data can lead to waste of time, cost, and energy especially in hot wells.
- A comprehensive hydraulic optimization considering the fresh water sepiolite rheological parameters obtained using viscometer and HTHP rheometer were carried out in terms of determining circulation pressure loss, surge pressure, and hole cleaning. During the circulation, the difference in calculated frictional pressure drop results from both methods was so notable in the case of Bingham Plastic model. The rate of diversity increased with increasing temperature as expected. However, the difference in frictional pressure losses calculated based on Power Law and Herschel Bulkley models using viscometer and HTHP rheometer data was not significant up to 177°C. The rate of results consistency between two methods in Herschel Bulkley model was more than those were for Power Law model up to the gelation temperature. After this temperature, the big differences on the pressure drops were observed between the Power Law and Herschel Bulkley models.
- CFD and Moore empirical methods were applied to analyze hole cleaning ability of unweighted fresh water sepiolite mud based on Power Law model. Similar to FPL, the difference in cutting transport ratio obtained from

viscometer and rheometer measurements substantially increased up to gelation temperature. Beyond this point, the gap between the results begin to close up due to increasing in viscosity of sepiolite mud and became approximately the same at 232°C. Therefore, it can be concluded that the variation of cutting transport ability of sepiolite mud systems exhibited similar trend with rheological behavior of a fluid system.

- Successful performance of CFD through prediction of frictional pressure loss and cutting transport ratio dictated the imperative role of CFD method in analyzing and handling drilling problems in advance.
- The properties of sepiolite muds were comprehensively characterized through this study; however, Further investigations are recommended in following areas:

1. Effect of different salts on thermal properties of sepiolite mud system.
2. Effect of different lubricants on differential pipe sticking tendency of sepiolite muds.
3. Investigating critical shear rate for Herschel Bulkley model to determine the rheological constants
4. Proposing turbulent flow solution of surge pressures through Herschel Bulkley model.
5. Effect of eccentricity and pipe rotation on surge pressures through Herschel Bulkley model using CFD.
6. Modelling surge pressure with CFD using moving boundary and dynamic mesh.
7. Transient temperature modelling in wellbore hydraulic optimization.
8. Application of different numerical methods to solve non-linear equations obtained through semi-analytical method.

REFERENCES

Aadnoy, B.S., Larsen, K., Berg, P.C. (1999). Analysis of Stuck Pipe in Deviated Boreholes, SPE 56628, SPE Annual Technical Conference and Exhibition, Texas, Oct. 3-6. http://dx.doi.org/10.2118/56628-MS

Aadnoy, B. S. (2003). Introduction to special issue on borehole stability. J. Petrol. Sci. Eng., vol. 38, no. 3-4, pp. 79–82. DOI: 10.1016/S0920-4105(03)00022-6.

Aadnoy, B. S., Belayneh, M. (2004). Elasto-plastic fracturing model for wellbore stability using non-penetrating fluids. J. Petrol. Sci. Eng., vol. 45, no. 3-4, pp. 179–192. DOI: 10.1016/j.petrol.2004.07.006.

Adams, N. (1977). A Field Case Study of Differential Pressure Pipe Sticking. SPE 6716, SPE Annual Technical Conference and Exhibition, Denver, Oct. 12. http://dx.doi.org/10.2118/6716-MS

AEM, (2014). Anadolu Endustri Mineralleri (AEM), having the license rights of sepiolite clay deposits in Sivrihisar, Eskisehir, Turkey, (Address: Istinye Cad. ABC Yolu Lara Sok. Seba Home No: 4/1, Istinye, Sariyer, Istanbul, Turkey, Phone/Fax: +90 216 3234097).

Al-Ajmi, A. M., Zimmerman, R. W. (2006). Stability analysis of vertical boreholes using the Mogi-Coulomb failure criterion. Int. J. Rock. Mech. Min., vol. 43, no. 8, pp. 1200–1211. DOI: 10.1016/j.ijrmms.2006.04.001.

Al-Bazali, T., Zhang, J., Chenevert, M. E., Sharma, M. M. (2008). Factors controlling the compressive strength and acoustic properties of shales when interacting with water-based fluids. Int. J. Rock. Mech. Min., vol. 45, no. 5, pp. 729–738. DOI: 10.1016/j.ijrmms.2007.08.012.

Al-Kayiem, H., H., Zaki, M., N., Asyraf, Z., M., Elfeel, E., M., & Iskandar, S., B. (2010). Simulation of the cuttings cleaning during the drilling operation. *American Journal of Applied Sciences,7*(6):800-806.

Ali, P., Robert, S. and Vishal, L. (2001). Generalized Hydraulic Calculation Method Using Rational Polynomial Model. Paper SPE 71403 presented at the 2001 SPE Annual Technical Conference and Exhibition held in New Orleans, Louisiana, 30 September–3 October.

Altun, G., Serpen, U. (2005). Investigating Improved Rheological and Fluid Loss Performance of Sepiolite Muds under Elevated Temperatures. World Geothermal Congress, Antalya, Turkey, April 24-29.

Altun, G. and Serpen, U. (2005). Investigating Improved Rheological and Fluid Loss Performance of Sepiolite Muds under Elevated Temperatures, *Proceedings*, World Geothermal Congress, Antalya, Turkey, April 24-29.

Altun, G., Osgouei, A. E., Serpen, U. (2010). Controlling Rheological and Fluid Loss Properties of Sepiolite Based Muds under Elevated Temperatures. World Geothermal Congress, Bali, Indonesia, April 25-29.

Altun, G., Osgouei, A. E., Ozyurtkan, M. H. (2015). Sepiolite Based Muds as an Alternate Drilling Fluid for Hot Environments. Proceedings World Geothermal Congress, 19-24 April Australia, New Zealand

Altun, G., Osgouei, A. E. (2014). Investigation and remediation of active-clay contaminated sepiolite drilling muds, Appl. Clay. Sci., 102, pp. 238–245. http://dx.doi.org/10.1016/j.clay.2014.10.002.

Altun, Gursat., Osgouei, Ali Ettehadi., Ozyurtkan, M. Hakan. (2014). An Alternate Mud Proposal to Minimise Borehole Instability, IPTC 17871, International Petroleum Technology Conference, Kuala Lumpur, Malaysia, December. http://dx.doi.org/10.2523/17871-MS.

API RP 13B-1. (2004). Recommended practice for field testing water-based drilling fluids. API Recommended Practice 13B-1, 3rd Edition, July.

API RP 13D. (2006). Rheology and hydraulics of Oil-well drilling fluids. API Recommended Practice 13D, 5th Edition.

API RP 59. (2006). Recommended Practice for Well Control Operations. API Recommended Practice 59, Second Edition, May

API SPEC 13-A. (2010). Specification for drilling-fluid materials, 17th Edition, May.

Annis, M. R., Monaghan, P.H. (1962). Differential Pressure sticking – Laboratory Studies of Friction between Steel and Mud Filter Cake, SPE 151, J. Petr. Tech., 14 [5] 537, May. http://dx.doi.org/10.2118/151-PA.

ANSYS, Inc. (2011). ANSYS FLUENT Theory Guide. Release 14.0, ANSYS Inc. Southpointe 275 Technology Drive Canonsburg, PA 15317.

ASME Shale Shaker Committee. (2005). Drilling Fluids Processing Handbook, Gulf Professional Publishing, Burlington, USA.

Aswad,Z.A. and Saleh,M.M. (1990). Two-phase Flow Design Procedure For optimum Carrying Capacity in oil Well Drilling Operation. Int. conf. on Basic Principles and Industrial Application of Multiphase Flow, London, England, 24-25 April.

Balci, S. (1999). Thermal decomposition of sepiolite and variations in pore structure with and without acid pre-treatment", Journal of Chemical Technology & Biotechnology, Volume 66 Issue 1, pages72–78, Published Online: 26 March.

Bailey, L., Denis, J. H., Maitland, G. C. (1991). Drilling fluids and wellbore stability current performance and future challenges. Chemicals in the Oil Industry, by P.H.Ogden, Ed., Roy. Soc. of Chemistry, London, UK.

Bailey,W.J. and Peden, J.M. (2000). A Generalized and Consistent Pressure Drop and Flow Regime Transition Model for Drilling Hydraulics. Paper SPE 62167 presented at the SPE/IADC Middle East Drilling Technology Conference held in Bahrain, March.

Barrett, J .P. (1974). The coefficient of determination - some limitations. The American Statistician; 28, 19-20.

Bell, J. S. 2003. Practical methods for estimating in situ stresses for borehole stabilityapplications in sedimentary basins. J. Petrol. Sci. Eng., vol. 38, no. 3-4, pp. 111– 119. DOI: 10.1016/S0920-4105(03)00025-1.

Best, B. (1986). Casing Wear Caused by Tooljoint Hardfacing, *Article*, SPEDE, pp. 62-70, February, 1986

Beverly, C. R., and Tanner, R. I. (1992). Numerical analysis of three-dimensional Bingham plastic flow. J. Non-Newtonian Fluid Mechanics, Vol. 42, pp. 85-115.

Bourgoyne Jr. A.T. et al. (1991). Applied Drilling Engineering, SPE Textbook Series, Vol. 2, Richardson, TX, USA.

Biegler, M.W., Kuhn, G.R. (1994). Advances in Prediction of Stuck Pipe Using Multivariate Statistical Analysis. SPE 27529, SPE/IADC Drilling Conference, 15-18 February, Dallas, Texas. http://dx.doi.org/10.2118/27529-MS.

Bilgesu, H.I., Ali, M.W., Aminian, K., Amiri, S. (2002. Computational Fluid Dynamics (CFD) as a Tool to Study Cutting Transport in Wellbores. Society of Petroleum Engineers, USA.

Bing, Z., Kaiji, Z. and Qiji, Y. (1995). Equations Help Calculate Surge and Swab Pressures in Inclined Well, Oil & Gas Journal, Vol. 93, pp 74-77, 18 September.

Bowes, C., Procter, R. (1997). Drillers Stuck Pipe Handbook, Guidelines & Drillers Handbook Credits. Ballater, Scotland, Schlumberger.

Bol G.M. (1985). Effect of Mud Composition on Wear and Friction of Casing and Tool Joints, *Proceedings*, SPE Paper No: 13457, IADC/SPE Drilling Conference held in New Orleans, March 6-8.

Bradley, W. B. (1979). Mathematical concept-stress cloud can predict borehole failure. Oil. Gas. J., vol. 77, no. 8, pp. 92–101.

Bradley, W.B., Jarman, D., Plott, R.S., Wood, R.D., Schofield, T.R., Auflick, R.A., Cocking, D. (1991). A Task Force Approach to Reducing Stuck Pipe Costs, SPE 21999 IADC/SPE Drilling Conference, Amsterdam, 11–14 March. http://dx.doi.org/10.2118/21999-MS.

Bradley, W.B. and Fontenet, J.E. (1975) The Prediction and Control of Casing Wear, *Article*, JPT, pp. 43-233, February.

Burkhardt, J. A. (1961). Wellbore Pressure Surges Produced by Pipe Movement, Journal of Petroleum Technology, June, pp 595-605.

Cannon, G. E. (1934). Changes in Hydrostatic Pressure due to Withdrawing Drillpipe from the Hole, API Drilling and Production Practices, pp 42-47.

Cardwell, W. T. (1953). Pressure Changes in Drilling Wells Caused by Pipe Movement, API Drilling and Production Practices, pp 97-112.

Carney, L.L., Güven, N. (1980). Investigation of Changes in the Structure of Clays During Hydrothermal Study of Drilling Fluids. JPT J. Pet. Technol., pp. 385-390, October.

Carney, L.L., Güven, N., McGrew, G.T. 1982. Investigation of High-Temperature Fluid Loss Control Agents in Geothermal Drilling Fluids. SPE 10736, California Regional Meeting, San Francisco, CA, USA, March 24-26.

Carney, L.L., Meyer, R.L. (1976). A New Approach to High Temperature Drilling Fluids. SPE 6025, 51st SPE Annual Fall Meeting of Society of Petroleum Engineers, New Orleans, LA, USA, October 3-6.

Chen, X., Tan, C.P., Haberfield, C.M. (1998). A Comprehensive Practical Approach for Wellbore Instability Management, SPE 48898, SPE International Conference and Exhibition in China, Beijing, 2-6 November. http://dx.doi.org/10.2118/48898-MS.

Clark, E. H. (1955). Bottom-Hole Pressure Surges while Running Pipes, Petroleum Engineer International, pp 68-96.

Clark, E. H. (1956). A Graphic View of Pressure Surges and Lost Circulation, API Drilling & Production Practices, pp 424-438.

Crespo, F. (2011). Experimental Study and Modeling on Surge and Swab Pressures for Yield-Power-Law drilling fluids, Master's Dissertation Thesis, Mewbourne School of Petroleum & Geological Engineering, University of Oklahoma.

Crespo, F., Ahmed, R., Enfis M., Saasen A. and Amani M. (2012). Surge-and-Swab Pressure Predictions for Yield-Power-Law Drilling Fluids, SPE Drilling & Completions, December.

Crocker D .C. (1972). Some interpretations of the multiple correlation coefficient. The American Statistician, 26, 31-3

Cook, J.M., Goldsmith, G., Geehan, T.M., Audibert, A.M., Bieber, M.T., Lecourtier, J. (1993). Mud/shale interaction: model wellbore studies using X-ray tomography. SPE 25729. SPE/IADC Drilling Conference, Amsterdam, Netherlands, February 23–25.

Duan, M., Miska, S., Yu, M., Takach, N., Ahmed, R. (2007). Critical Conditions for Effective Sand-Sized Solids Transport in Horizontal and High-Angle Wells. Society of Petroleum Engineers, USA.

Draper, N .R., and Smith H. (1981). Applied regression analysis. 2nd edition. New York: Wiley.

Draper, N.R. (1984). The Box-Wetz Criterion versus R^2. J. R. Stat. Soc., Part 147, 100.

Escudier, M.P., Oliveira, P.J. Pinho, F.T. (2002). Fully Developed Laminar Flow of Purely Viscous Non-Newtonian Liquids Through Annuli, Including The Effects of Eccentricity and Inner- Cylinder Rotation'', Int. J. Heat and Fluid Flow. 23, 52-73.

Filip, P. and J. David. (2003). Axial Couette-Poiseuille Flow of Power-Law Viscoplastic Fluids in Concentric Annuli," J. Petr. Sci. Eng. 40, 111-119.

Ford, J.T., Peden, J.M., Oyeneyin, M.B., Gao, E., Zarrough, R. (1990). *Experimental Investigation of Drilled Cuttings Transport in Inclined Boreholes*, Society of Petroleum Engineers, USA.

Fontenot, J. E. and Clark, R. K. (1974). An Improved Method for Calculating Swab and Surge Pressures and Circulating Pressures in a Drilling Well. Society of Petroleum Engineers Journal, pp 451-462 (October).

Ford, J.T., Peden, J.M., Oyeneyin, M.B., Gao, E., Zarrough, R. (1990). Experimental Investigation of Drilled Cuttings Transport in Inclined Boreholes", Society of Petroleum Engineers, USA.

Fordham, E. J., S. H. Bittleston and M. A. Tehrani. (1991). Viscoplastic Flow in Centered Annuli, Pipes and Slots," IEC Res. 29, 517-524.

Founargiotakis, K., Kelessidis, V.C., Maglione, R. (2008). Laminar, transitional and turbulent flow of Herschel-Bulkley fluids in concentric annulus. The Canadian Journal of chemical Engineering. 86, 676-683.

Foxenberg, W.E. and Ke, M. (1998) Eliminate Formation Damage Caused By High Density Completion Fluid-Crude Oil Emulsion, Proceedings, SPE Paper No: 39444, SPE Formation Damage Control Conference, Lafayette, Louisiana, February 18-19.

Fredrickson, A. G., and Bird, R. B. (1958). Flow of non-Newtonian fluids in annuli. Ind. Eng. Chem. 50:347–352.

Gallego, F., and Shah, S. (2009). Friction pressure correlations for turbulent flow of drag reducing polymer solutions in straight and coiled tubing. J. Petrol. Sci. & Eng. 65:147–161.

Goins, W. C., Weichhert, J. P., Burba, J. L., Dawson, D. D. and Teplitz, A. J. (1951). Down-the-Hole Pressure Surges and their Effect on Loss of Circulation, API Drilling and Production Practices, pp 125-132.

Guo W. and Hong H. F. (2010). Utility Calculation Method of New Four-Parameter Rheological Model for Drilling Hydraulics. Paper SPE 130421 presented at CPS/SPE International Oil & Gas Conference and Exhibition held in Beijing, China, 8–10 June.

Güven, N., Panfill, D.J., Carney, L.L. (1988). Comparative Rheology of Water Based Drilling Fluids With Various Clays. SPE 17571, International Meeting on Petroleum Engineering, Tianjin, China, November 1-4.

Haden, E. L., Welch, G. R. (1961). Techniques for Preventing Differential Pressure Sticking of Drill Pipe, API Drilling and Production Practice, 39.

Haciislamoglu, M., and Langlinais, J. (1990). Non-Newtonian fluid flow in eccentric annuli. J. Energ. Res. Tech. 112:163–169.

Hareland, G., Azar, J.J., Rampersad, P.R. (1993). Comparison of Cuttings Transport in Directional Drilling Using Low-Toxicity Invert Emulsion Mineral-Oil-Based and Water-Based Muds. Society of Petroleum Engineers, USA.

Healy, M .J .R. (1984). The use of R^2 as a measure of goodness of fit. J R Statist Soc A, 147, Part 4 : 608-9.

Helland, I .S. (1987). On the interpretation and use of R^2 in regression analysis. Biometrics, 43, 61-9.

Hemphil, T., W. Campos, and A. Pilehvari. (1993), Yield-power law model accurately predicts mud rheology, Oil Gas J. 91, 45- 50

Heyda, J. F. (1959). A Green's function solution for the case of laminar flow between non-concentric circular cylinders. J. Franklin Inst. 267:25–34.

Hillscher, L.W. and Clements, W.R. (1982). High-Temperature Drilling Fluid for Geothermal and Deep Sensitive Formations, *Proceedings*, SPE Paper No: 10737, California Regional Meeting, San Francisco, CA, USA, March 24-26.

Horn, A. J. (1950). Well Blowouts in California Drilling Operations, Causes and Suggestions for Prevention, API Drilling and Production Practices, pp 112-128.

Hussaini, S.M. and Jamal, A.Z. (1983). Experimental Study of Drilled Cuttings Transport Using Common Drilling Muds. Society of Petroleum Engineers, USA.

Iyoho, A.W. and Azar, J.J. (1981). An Accurate Slot-Flow Model for Non-Newtonian Fluid Flow Through Eccentric Annuli,'' Society of Petroleum Engineers Journal, 21: 565-572.

Jardine, S.I., McCann, D.P., Barber, S.S. (1992). An Advanced System for the Early Detection of Sticking Pipe, SPE 23915, SPE Drilling Conference, New Orleans, 18–21 February. http://dx.doi.org/10.2118/23915-MS.

Jawad, R.H.and Akgun, F. (2002). Carrying Capacity Design for Directional Wells. SPE 77196, presented at the IADC/SPE Asia Pacific Drilling Technology held in Jakarta, Indonesia, 9–11 September.

Kavak, D. and Ozturk, N. (2004). Adsorption of Boron from Aqueous Solutions by Sepiolite: II. Column Studies", in Turkish, Second International Boron Symposium, 23-25 September, Eskisehir, Turkey.

KDS, (2001). Deepwater Drilling Fluid Design Example, Technical report, Kingdom Drilling Ltd., March 9.

Kelessidis, V. C., R. Maglione, C. Tsamantaki and Y. Aspirtakis. (2006). Optimal Determination of Rheological Parameters for Herschel-Bulkley Drilling Fluids and Impact on Pressure Drop, Velocity Profiles and Penetration Rates during Drilling," J. Petrol. Sci. Eng. 53, 203-224.

Ke, Y. C. and Stroeve, P. (2005). Polymer-Layered Silicate and Silica Nanocomposites. Amsterdam: Elsevier B. V.

Kvalseth, T .O. (1985). Cautionary note about R^2. The American Statistician, 39, 279-85.

Lal, M. (1983). Surge and Swab Modeling for Dynamic Pressures and Safe Trip Velocities, Paper SPE-11412, presented at the IADC/SPE Drilling Conference, New Orleans, Louisiana, 20-23 February.

Langlinais, J. P., Bourgoyne, A. T., and Holden, W. R. (1983). Frictional pressure losses for the flow of drilling mud and mud/gas mixtures. SPE Paper 11993. 58th Annular Technical Conference and Exhibition, San Francisco, CA, October 5–8.

Lomba, R., Chenevert, M.E., Sharma, M.M. (2000). The ion-selective membrane behavior of native shales. J. Petrol. Sci. Eng. 25, 9–23.

Luo, Y., and Peden, J. M. (1990). Flow of drilling fluids through eccentric annuli. SPE Production and Engineering Feb. 91–96.

Merlo, A., Maglione, R., and Piatti, C. (1995). An Innovative Model for Drilling Fluid Hydraulics. Paper SPE 29259 presented at SPE Oil and Gas Conference, Kuala Lumpur, 20-22 March.

Mitsuishi, N., and Aoyagi, Y. (1973). Non-Newtonian fluid flow in an eccentric annuli. J. Chem. Eng. Japan 6:402–408.

Mohiuddin, M.A., Awal, M.R., Abdulraheem, A., Khan, K. (2001). A New Diagnostic Approach to Identify the Causes of Borehole Instability Problems in an Offshore Arabian Field, SPE 68095, SPE Middle East Oil Show, Bahrain, 17-20 March. http://dx.doi.org/10.2118/68095-MS.

Mohiuddin, M.A., Khan, K., Abdulraheem, A., Al-Majed, A., Awal, M.R. (2006). Analysis of Wellbore Instability on Vertical, Directional, and Horizontal Wells Using Field Data, J. Petrol. Sci. Eng; pp: 83-92; vol: 55. doi:10.1016/j.petrol.2006.04.021.

Mahto, V. (2013). The Prevention of Differential Pipe Sticking Problems Caused by Water-based Drilling, Petrol Sci Technol, 31:21, 2237-2243, DOI: 10.1080/10916466.2011.5652

Mody, F.K., Hale, A.H. (1993). A borehole stability model to couple the mechanics and chemistry of drilling fluid shale interaction. SPE/IADC 25728. SPE/IADC Drilling Conference, Amsterdam, Netherlands. February 23–25.

Moore, P.L. (1974). Drilling practices manual, Petroleum Publishing Co, Tulsa

Motulsky, H. and Christopoulos, A. (2003). Fitting Models to Biological Data using Linear and Nonlinear Regression. A practical guide to curve fitting, GraphPad Software Inc., San Diego CA.

Murray, H.H. (2007). Applied clay mineralogy

Moussa, M.M. (1985): Dynamic Measurement of Drilling Fluid Rheology at Elevated Temperature and Pressure, Proceedings, SPE Paper No: 13691, *Middle East Oil Technical Conference and Exhibition*, Bahrain, March 11-14.

Nagelkerke, N .J .D. (1991). A note on a general definition of the coefficient of determination. Biometrika, 78, 691-2.

Okrajni, S.S. and Azar, J.J. (1986). The Effect of Mud Rheology on Annular Hole Cleaning in Directional Wells. Society of Petroleum Engineers, USA.

Ormsby, G. S. (1954). Calculation and Control of Mud Pressures in Drilling and Completion Operations, API Drilling and Production Practices, pp 44-55.

Osgouei, A. E. (2010). Controlling Rheological and Filtration Properties of Sepiolite Based Drilling Fluids under Elevated Temperatures and Pressures. Master Thesis, Istanbul Technical University, Istanbul, Turkey, June.

Osgouei, A. E., Altun G. (2015) .Kesinti Taşınımının Hesaplamalı Akışkanlar Dinamiği Yaklaşımıyla Kestirimi. Makine ve Mühendis, Vol 664, ISSN 1300-3402, 26 May

Osgouei, A. E., Altun G., Serpen, U. (2015). Sondaj Akışkanı Isıl Reolojik Özellikleri Üzerine Karşılaştırmalı Bir Çalışma: Klasik Viskometre ve Isıl Reometre. 12th HVAC and Sanitary Congress and Exhibition (TESKON 2015), Izmir, Turkey, 8-11 April

Osgouei, A. E., Ozyurtkan, M. H., Altun G. (2014). Dynamic Filtration Properties of Fresh Water Sepiolite-based Muds. Energ. Source. Part A. 36:19, 2079-2086, July.

Outmans, H.D. (1958). Mechanics of Differential Pressure Sticking of Drill Collars, Petrl. Trans., AIME, vol. 213, 265-274.

Ranney, G .B., and Thigpen C .C. (1981). The sample coefficient of determination in simple linear regression. The American Statistician, 35, 152 -3.

Redburn, M., Dearing, H. Growcock, F. (2013). Field Lubricity Measurements Corrilate With Improved Performance of Novel Water-Based Drilling Fluid, *Proceedings*, 11th Offshore Mediterranean Conference and Exhibition in Ravenna, Italy, March 20-22.

Reed, T.D., and Pilehvari, A.A. (1993). A New Model for Laminar, Transitional, and Turbulent Flow of Drilling Muds'', SPE paper 25456, presented at the Production Operations Symposium in Oklahoma City, OK, USA, 21-23 March.

Sabah, E. ve Çelik M.S. (1998). Sepiyolit, Afyon.

Samprit, C.R and Ali, S.H. (2006). *Regression Analysis by Example,* John Wiley & Sons, Inc., Hoboken, New Jersey.

Santoyo, E; Santoyo-Gutierrez, S; Garcia, A; Espinosa, G; Moya, SL. (2001). Rheological property measurement of drilling fluids used in geothermal wells, Applied Thermal Engineering 21, 283-302

Schlemmer, R., Friedheim, J.E., Growcock, F.B., Headley, J.A., Polnaszek, S.C., Bloys, J.B. (2002). Membrane Efficiency in Shale - An Empirical Evaluation of Drilling Fluid Chemistries and Implications for Fluid Design. SPE 74557. SPE/IADC Drilling Conference, Dallas, TX, USA. February 26–28.

Schmidt, V., Dodson, J., Dodson, T. (2004). Gulf of Mexico trouble time creates major drilling expenses: use of cost-effective technologies needed, Offshore, 64(1), pp. 46–48.

Schoenmakers, J.M. (1986). Prediction of Casing Wear Due to Drillstring Rotation: Field Validation of Laboratory Simulations, *Proceedings*, SPE Paper No: 14761, SPE/IADC Drilling Conference, Dallas, February 10-12.

Schuh, F. J. (1964). Computer Makes Surge-Pressure Calculations Useful, Oil & Gas Journal, Vol. 62, No. 31, pp 96-104.

Scott, A., and Wild C. (1991). Transformations and R^2. The American Statistician, 45, 127-9.

Serpen, U. (1999). Use of Sepiolite Clay and Other Minerals for Developing Geothermal Drilling Fluids. J. Appl. Mech. Eng, vol 4, special issue.

Serpen, U. (2000). Investigation on Geothermal Drilling Muds with High Temperature Stability. World Geothermal Congress, Kyushu-Tohoku, Japan, May 28-June 10.

Serpen, U., Haciislamoglu, M., Tuna, O. (1992). Use of Sepiolite Resources of Turkey in geothermal Muds. 9th International Petroleum Congress of Turkey, Ankara, Turkey, February 17-21.

Sifferman, T.R. and Becker, T.E. (1992). Hole Cleaning in Full-Scale İnclined Wellbores, Society of Petroleum Engineers, USA.

Siruvuri, C., Nagarakanti, S., Samuel, R. (2006). Stuck Pipe Prediction and Avoidance: A Convolutional Neural Network Approach. SPE 98378, IADC/SPE Drilling Conference, 21-23 February Miami, Florida, USA. http://dx.doi.org/10.2118/98378-MS.

Singhal N., Shah S.N., Jain S. (2005). Friction Pressure Correlations for Newtonian and Non-Newtonian Fluids in Concentric Annuli'', SPE paper 94280 presented at the SPE Conference, Oklahoma, USA , 17-19 April.

Stokes, G. G. (1845). On the theories of the internal friction of fluids in motion, and of the equilibrium and motion of elastic solids. Trans. Cambridge Phil. Soc. 8: 287- 341.

Stokes, G. G. (1851). On the effect of the internal friction of fluids on the motion of pendulums. Trans. Cambridge Phil. Soc. 9: 8-149.

Stuart, A., and Ord J .K. (1991). Kendall's advanced theory of statistics, 5th edition. Vol. 2: Classical inference and relationship. London: Edward Arnold.

Tomren, P.H., Iyoho, A.W., Azar, J.J. (1986). Experimental Study of Cuttings Transport in Directional Wells, Society of Petroleum Engineers, USA.

True, M.E. and Weiner, P.E. (1975). Optimum Means of Protecting Casing and Drillpipe Tool Joints Against Wear, *Article*, JPT, pp. 52-246, February.

Uner, D., Ozgen, C., and Tosun, I. (1989). Flow of a power law fluid in an eccentric annulus. SPE Drill. Eng. Sept.:269–272.

Url-1 < http://www.glossary.oilfield.slb.com/Terms/r/rheological.aspx>, date retrieved 15.12.2015.

Van Oort, E. (2003). On the physical and chemical stability of shales. J. Petrol. Sci. Eng. 38, 213–235.

Vaughn, R.D. and Bergman, P. (1966). Laminar Flow of Non-Newtonian Fluids in Concentric Annuli" Industrial & Engineering Chemistry Process Design and Development, Vol. 5, No. 1, January.

Wang, Y., Dusseault, M. B. (2003). A coupled conductive-convective thermo-poroelastic solution and implications for wellbore stability. J. Petrol. Sci. Eng., vol. 38, no. 3-4, pp. 187–198. DOI: 10.1016/S0920-4105(03)00032-9.

Weakley, R.R. (1990). Use of Stuck Pipe Statistics to Reduce the Occurrence of Stuck Pipe. SPE 20410, SPE Annual Technical Conference and Exhibition, 23-26 September, New Orleans, Louisiana. http://dx.doi.org/10.2118/20410-MS.

Weir, I.S. and Bailey, W.J. (1996). A Statistical Study of Rheological Models for Drilling Fluids, SPE 36359.

White, J.P. and Dawson, R. (1985). Casing Wear: Laboratory Measurements and Field Predictions, *Proceedings*, SPE Paper No: 14325, SPE Annual Technical Conference and Exhibition, Las Vegas, September 22-25, 1985.

Willett, J .B., and Singer J .D. (1988). Another cautionary note about R^2: its use in weighted least-squares regression analysis. The American Statistician, 42, 236-8.

William C. Lyons, Ph.D., P.E., Gary J. Plisga, B.S. (2005). Standard Handbook of Petroleum and Natural Gas Engineering. 2nd Edition, Gulf Professional Publishing. pp 4-378

Williamson, J.S. (1981) Casing Wear: The Effect of Contact Pressure, *Article*, JPT, pp. 88-2382, December.

Wisnie, A.P., Zheiwei, Z. (1994). Quantifying Stuck Pipe Risk in Gulf of Mexico Oil and Gas Drilling. SPE 28298, SPE Annual Technical Conference and Exhibition, 25-28 September, New Orleans, Louisiana, http://dx.doi.org/10.2118/20410-MS

Won, S., Bilgesu, H.I. and Ameri, S. (2008) "Investigation of Mud Filtrate Invasion Using Computational Fluid Dynamics" paper SPE 117769 presented at the SPE Eastern Regional/AAPG Eastern Section Joint Meeting, Pittburg, Pennsylvania, USA.

Zeynali, M. E. (2012). Mechanical and physico-chemical aspects of wellbore stability during drilling operations, J. Petrol. Sci. Eng., vol. 82-83, pp. 120–124. DOI: 10.1016/j.petrol.2012.01.006.

Zeidler, H.U. (1972). "An Experimental Analysis of the Transport of Drilled Particles", Rice University, Houston, Texas, USA.

Zilch, H.E., Otto, M.J. Pye, D.S. (1991). The Evolution of Geothermal Drilling Fluid in the Imperial Valley. SPE 21786, Western Regional Meeting, Long Beach, CA, USA, March 20-22.

Zoback, M. D., Barton, C. A., Brudy M., Castillo, D.A., Finkbeiner, T., Grollimund, B.R., Moos, D.B., Peska, P., Ward, C.D., Wiprut, D.J. (2003). Determination of stress orientation and magnitude in deep wells. Int. J. Rock. Mech. Min., vol. 40, no. 7-8, pp. 1049–1076. DOI: 10.1016/j.ijrmms.2003.07.001.

APPENDICES **Page**

Appendix A: Sepiolite clay particle size analysis report and determining dolomite content of sepiolite clay sample.

Sepiolite clay particle size analysis report:

MASTERSIZER 2000

MALVERN INSTRUMENTS

Result Analysis Report

Sample Name: 6 ince - Average	**SOP Name:**	**Measured:** 01 Nisan 2014 Salı 10:10:21
Sample Source & type:	**Measured by:** Hasan Gökçe	**Analysed:** 01 Nisan 2014 Salı 10:10:23
Sample bulk lot ref:	**Result Source:** Averaged	

Particle Name: Default	**Accessory Name:** Hydro 2000G (A)	**Analysis model:** General purpose	**Sensitivity:** Normal
Particle RI: 1.520	**Absorption:** 0.1	**Size range:** 0.020 to 2000.000 um	**Obscuration:** 4.39 %
Dispersant Name: Ethanol	**Dispersant RI:** 1.360	**Weighted Residual:** 8.028 %	**Result Emulation:** Off

Concentration: 0.0082 %Vol	**Span :** 1.575	**Uniformity:** 0.479	**Result units:** Volume
Specific Surface Area: 0.504 m²/g	**Surface Weighted Mean D[3,2]:** 11.905 um	**Vol. Weighted Mean D[4,3]:** 29.728 um	

d(0.1): 7.061 um   d(0.5): 29.013 um   d(0.9): 52.765 um

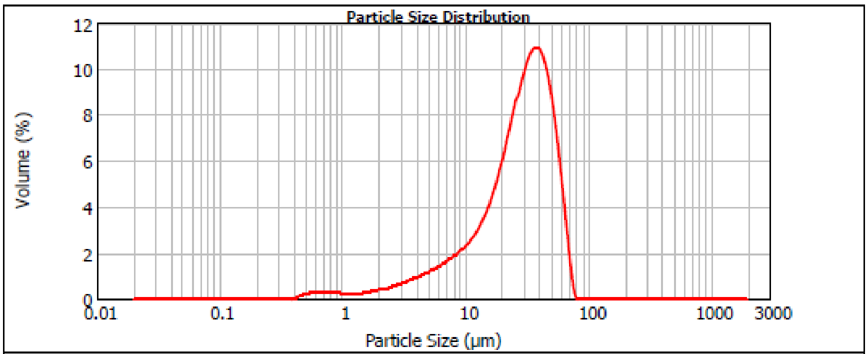

6 ince - Average, 01 Nisan 2014 Salı 10:10:21

Size (µm)	Volume In %	Size (µm)	Volume In %	Size (µm)	Volume In %
0.010	0.00	0.105	0.00	1.096	0.19
0.011	0.00	0.120	0.00	1.259	0.20
0.013	0.00	0.138	0.00	1.445	0.23
0.015	0.00	0.158	0.00	1.660	0.28
0.017	0.00	0.182	0.00	1.905	0.35
0.020	0.00	0.209	0.00	2.188	0.44
0.023	0.00	0.240	0.00	2.512	0.53
0.026	0.00	0.275	0.00	2.884	0.62
0.030	0.00	0.316	0.00	3.311	0.73
0.035	0.00	0.363	0.00	3.802	0.84
0.040	0.00	0.417	0.13	4.365	0.98
0.046	0.00	0.479	0.19	5.012	1.13
0.052	0.00	0.550	0.24	5.754	1.29
0.060	0.00	0.631	0.26	6.607	1.48
0.069	0.00	0.724	0.25	7.586	1.68
0.079	0.00	0.832	0.23	8.710	1.91
0.091	0.00	0.955	0.21	10.000	2.21
0.105		1.096		11.482	

Size (µm)	Volume In %	Size (µm)	Volume In %	Size (µm)	Volume In %
11.482	2.59	120.226	0.00	1258.925	0.00
13.183	3.13	138.038	0.00	1445.440	0.00
15.136	3.84	158.489	0.00	1659.587	0.00
17.378	4.79	181.970	0.00	1905.461	0.00
19.953	5.94	208.930	0.00	2187.762	0.00
22.909	7.22	239.883	0.00	2511.886	0.00
26.303	8.46	275.423	0.00	2884.032	0.00
30.200	9.44	316.228	0.00	3311.311	0.00
34.674	9.89	363.078	0.00	3801.894	0.00
39.811	9.54	416.869	0.00	4365.158	0.00
45.709	8.27	478.630	0.00	5011.872	0.00
52.481	6.13	549.541	0.00	5754.399	0.00
60.256	3.47	630.957	0.00	6606.934	0.00
69.183	0.69	724.436	0.00	7585.776	0.00
79.433	0.00	831.764	0.00	8709.636	0.00
91.201	0.00	954.993	0.00	10000.000	
104.713	0.00	1096.478	0.00		
120.226		1258.925			

Operator notes: *st 500*
Pump:1250
Ult 0

Malvern Instruments Ltd.
Malvern, UK
Tel := +[44] (0) 1684-892456 Fax +[44] (0) 1684-892789

Mastersizer 2000 Ver. 5.60
Serial Number : MAL100720

File name: Sultann
Record Number: 247
01.04.2014 13:54:03

Dolomite content of sepiolite clay:

Two different methods will be given below to determine the dolomite content of raw sepiolite clay sample used in this study. The first method is based on chemical compositions of sepiolite clay sample from XRF analysis. The second method is based on XRD pattern of sepiolite clay sample using Reference Intensity Ratio (RIR) approach.

Method 1: An ideal sepiolite has the formulation of Si12 Mg8 O30 (OH) 6 (OH) 4. 8H2O, or Si12 Mg9 O30 (OH) 6 (OH) 4. 6H2O. Generally, clay sepiolite does not contain calcium oxide (CaO). The results of XRF analysis (Table 1) of sepiolite sample showed that it contains 4.37% of calcium oxide (CaO). Therefore, it can be inferred that the most part of calcium oxide (CaO) originating from dolomite ((CaMg) $(CO_3)_2$) which is a carbonate mineral. On the other hand, it is also well known that an ideal dolomite consist of 30.41% of calcium oxide (CaO) in general. Even though this generalization can be negotiable due to existence of free Mg and Ca sourcing from other materials, it can be assumed as an extreme condition that all amount of calcium oxide (CaO) is sourcing from dolomite. Therefore, depending on this assumption, maximum dolomite content of this kind of sepiolite would be:

$$Dolomite\ Content = \frac{4.37 \times 100}{30.41} \cong 14\ \%$$

Generally it can be accepted as 10 % in the case of existing free Mg and Ca.

Method 2: Another way to determine the dolomite content of sepiolite sample is based on the ratio of silicon oxide to magnesium oxide which is around 2.22 for an ideal sepiolite. Here in this sepiolite sample if it is assumed that all Al2+ and Fe3+ are included within silica, the summation of these three gives the content of silicon oxide (52.31%+1.23%+2.69%) in sepiolite sample. Therefore,

$$\frac{\text{silicon oxide content \%}}{\text{magnesium oxide content \%}} = \frac{56.23}{23.22} = 2.46$$

However for ideal sepiolite magnesium oxide content for this particular case should be 56.23/2.22 = 25.33%. It is resulted that the amount of 2.11% (25.33-23.22) of magnesium oxide comes from the dolomite source. As ideal dolomite has 21.86% magnesium oxide, thus the dolomite content of this sepiolite sample would be:

$$Dolomite\ Content = \frac{2.11 \times 100}{21.86} \cong 10\ \%$$

Appendix B: Properties of sepiolite base mud subjected to active clay contamination.

Table B.1: Rheological and filtration properties of fresh water sepiolite muds.

Mud System		Property	Sample Code							
			S1	S2	S3	S4	S5	S6	S7	S8
Mud System	**BM1** **Unweighted (1042 kg/m^3) , pH = 8**	Aging temperature, °C	27	27	149	149	177	177	204	204
		Rheology measurement Temperature, ˚C	27	49	27	49	27	49	27	49
		Plastic Viscosity, Pa-s	0.025	0.021	0.021	0.015	0.014	0.011	0.014	0.011
		Yield Point, Pa	10.06	8.14	8.14	6.23	5.75	4.31	8.62	6.71
		Gel strength, dial reading[1] (10s./1min./10min.)	4/6/13	4/6/13	4/5/7	3/4/6	4/5/15	3/4/13	6/7/10	4/5/9
		Flow behavior index (n)	0.6285	0.6343	0.6343	0.6185	0.6211	0.6319	0.5323	0.5257
		Power law consistency index (K), $Pa\text{-}s^n$	0.474	0.371	0.371	0.302	0.276	0.198	0.625	0.480
		Minimum annular velocity (AV), m/s	0.493	0.630	0.630	0.772	0.848	1.179	0.376	0.488
		HTHP water loss, ml (7.5/30min)@149 °C		6.4/14.6		6.4/14.5		7.2/15.7		11.8/24.5
		Cake thickness, mm		2.0		2.0		2.5		3.0
	BM3 **Barite-Weighted (1330 kg/m^3), pH = 8**	Aging temperature, °C	27	27	149	149	177	177	204	204
		Rheology measurement Temperature, ˚C	27	49	27	49	27	49	27	49
		Plastic Viscosity, Pa-s	0.037	0.029	0.021	0.016	0.022	0.016	0.016	0.014
		Yield Point, Pa	15.81	10.54	6.71	5.27	8.14	6.71	15.32	11.50
		Gel strength, dial reading[1] (10s./1min./10min.)	7/13/23	6/11/19	3/3/5	3/3/5	4/5/14	4/5/13	4/7/18	3/5/16
		Flow behavior index (n)	0.6118	0.649	0.6776	0.6709	0.6449	0.6163	0.4147	0.4522
		Power law consistency index (K), $Pa\text{-}s^n$	0.786	0.454	0.261	0.210	0.356	0.328	0.184	0.115
		Minimum annular velocity (AV), m/s	0.234	0.403	0.701	0.874	0.513	0.556	0.102	0.158
		HTHP water loss, ml (7.5/30min)@ 149 °C		2.9/6.5		3.0/7.6		4.0/9.0		7.2/15.5
		Cake thickness, mm		3.0		3.5		3.5		4.0

[1] Multiply dial reading value by 0.478026 to obtain Pascal.

Table B.2: Properties of fresh water sepiolite muds subjected to active clay contamination.

Mud System		Property	Sample code					
			S1	S2	S3	S4	S5	S6
Mud System	BM2 Unweighted system, (pH = 8)	OCMA, kg/m^3	0	0	228	228	228	-
		Aging temperature, °C	27	177	149	177	177	-
		MBT, kg/m^3	14.28	14.28	34.28	34.28	34.28	-
		Mud density, kg/m^3	1042	1042	1066	1066	1066	-
		Temperature of rheology measurement, ˚C	27	27	49	27	49	-
		Plastic Viscosity, Pa-s	0.023	0.014	0.019	0.030	0.024	-
		Yield Point, Pa	7.18	4.79	11.02	16.29	13.89	-
		Gel strength, dial reading[1] (10s./1min./10min.)	3/3/5	2/3/5	8/10/13	8/10/16	8/11/20	-
		HTHP water loss, cc (7.5/30min)@ 149°C	5.5/13	6/14	2.2/5	-	3/6.5	-
		Cake thickness, mm	2.0	2.0	2.5	-	2.5	-
		Flow behavior index (n)	0.6824	0.6626	0.5381	0.5543	0.5386	-
		Power law consistency index (K), Pa-s^n	0.275	0.196	0.747	1.029	0.940	-
		Minimum annular velocity (AV), m/s	0.848	1.189	0.305	0.223	0.244	-
	BM4 Barite-Weighted system, (pH = 8)	Sepiolite, kg/m^3	57	57	28.5	28.5	28.5	28.5
		OCMA, kg/m^3	0	0	0	0	228	228
		Mud density, kg/m^3	1318	1318	1258	1258	1306	1306
		Aging temperature, °C	27	177	27	177	149	177
		MBT, kg/m^3	-	-	14.28	14.28	35.71	37.14
		Temperature of rheology measurement, ˚C	27	27	27	27	49	49
		Plastic Viscosity, Pa-s	0.032	0.024	0.027	0.016	0.024	0.024
		Yield Point, Pa	11.02	7.66	7.18	4.31	9.58	11.97
		Gel strength, dial reading[1] (10s./1min./10min.)	3/4/7	3/3/7	3/3/4	2/2/3	8/9/20	8/10/25
		HTHP water loss, cc (7.5/30min)@ 149°C	-	3.1/8	-	2.5/6.5	2.5/6	3.1/7.5
		Cake thickness, mm	-	3	-	3	6	6
		Flow behavior index (n)	0.6612	0.6777	0.7158	0.7133	0.6177	0.5748
		Power law consistency index (K), Pa-s^n	0.454	0.298	0.247	0.149	0.448	0.693
		Minimum annular velocity (AV), m/s	0.406	0.620	0.782	1.295	0.417	0.269

[1] Multiply dial reading value by 0.478026 to obtain Pascal.

Table B.3: Effect of reactive clay on barite-weighted sepiolite muds at high salinity.

		Property	Sample code			
			S1	S2	S3	S4
BM5	Weighted system (28.5 kg/m³ sepiolite) pH = 7.2	NaCl, kg/m³	0	343	343	343
		OCMA[1], kg/m³	0	0	228	228
		Aging temperature, °C	27	27	177	177
		MBT, kg/m³	-	-	31.43	31.43
		Mud density, kg/m³	1306	1486	1522	1522
		Temperature of rheology measurement, ˚C	27	27	27	49
		Plastic Viscosity, Pa-s	0.034	0.019	0.021	0.021
		Yield Point, Pa	12.93	4.79	6.23	9.58
		Gel strength, dial reading[2] (10s./1min./10min.)	3/4/5	2/2/5	3/4/9	5/7/15
		Flow behavior index (n)	0.6387	0.7266	0.6935	0.5963
		Power law consistency index (K), Pa-s^n	0.579	0.159	0.229	0.507
		Minimum annular velocity (AV), m/s	0.315	1.021	0.696	0.315
		HTHP water loss, cc (7.5/30min)@ 149 °C	-	-	4/8.5	4/8.5
		Cake thickness, mm	-	-	5	5
BM6	Weighted system (42.75 kg/m³ sepiolite) pH = 7.2	NaCl, kg/m³	343	343	343	343
		OCMA[1], kg/m³	143	143	228	228
		Aging temperature, °C	177	177	177	177
		MBT, kg/m³	32.85	32.85	34.28	34.28
		Mud density, kg/m³	1498	1498	1540	1540
		Temperature of rheology measurement, ˚C	27	49	27	49
		Plastic Viscosity, Pa-s	0.019	0.020	0.027	0.028
		Yield Point, Pa	6.71	10.54	11.97	14.37
		Gel strength, dial reading[2] (10s./1min./10min.)	3/5/12	10/12/23	5/7/17	13/18/32
		Flow behavior index (n)	0.6557	0.5616	0.6030	0.5680
		Power law consistency index (K), Pa-s^n	0.282	0.646	0.617	0.857
		Minimum annular velocity (AV), m/s	0.625	0.274	0.274	0.198
		HTHP water loss, cc (7.5/30min)@ 149 °C	6/13	6/13	4.6/9.5	4.6/9.5
		Cake thickness, mm	6	6	7	7

[1] Oil Company Materials Association (OCMA): Pertaining to a drilling-grade bentonite with API/ISO specifications
[2] Multiply dial reading value by 0.478026 to obtain Pascal.

Table B.3 (Continued): Effect of reactive clay on barite-weighted sepiolite muds at high salinity.

		Property	Sample code			
			S1	S2	S3	S4
BM7	**Weighted system (57 kg/m^3 sepiolite) pH = 7.2**	NaCl, kg/m^3	0	343	343	343
		OCMA[1], kg/m^3	0	0	143	143
		Aging temperature, °C	27	27	177	177
		MBT, kg/m^3	-	-	32.85	32.85
		Mud density, kg/m^3	1330	1498	1510	1510
		Temperature of rheology measurement, ˚C	27	27	27	49
		Plastic Viscosity, Pa-s	0.042	0.022	0.023	0.025
		Yield Point, Pa	20.12	10.06	12.93	15.81
		Gel strength, dial reading[2] (10s./1min./10min.)	11/15/25	6/8/15	6/8/18	20/25/38
		Flow behavior index (n)	0.5846	0.5958	0.5457	0.5168
		Power law consistency index (K), Pa-s^n	1.118	0.534	0.849	1.179
		Minimum annular velocity (AV), m/s	0.168	0.310	0.188	0.137
		HTHP water loss, cc (7.5/30min)@ 149 °C	-	-	8/16.5	8/16.5
		Cake thickness, mm	-	-	7	7

1 Oil Company Materials Association (OCMA): Pertaining to a drilling-grade bentonite with API/ISO specifications
2 Multiply dial reading value by 0.478026 to obtain Pascal.

Appendix C: Differential Pressure Sticking Tendency of Bentonite/Polymer, Lignosulfonate, and Sepiolite Muds.

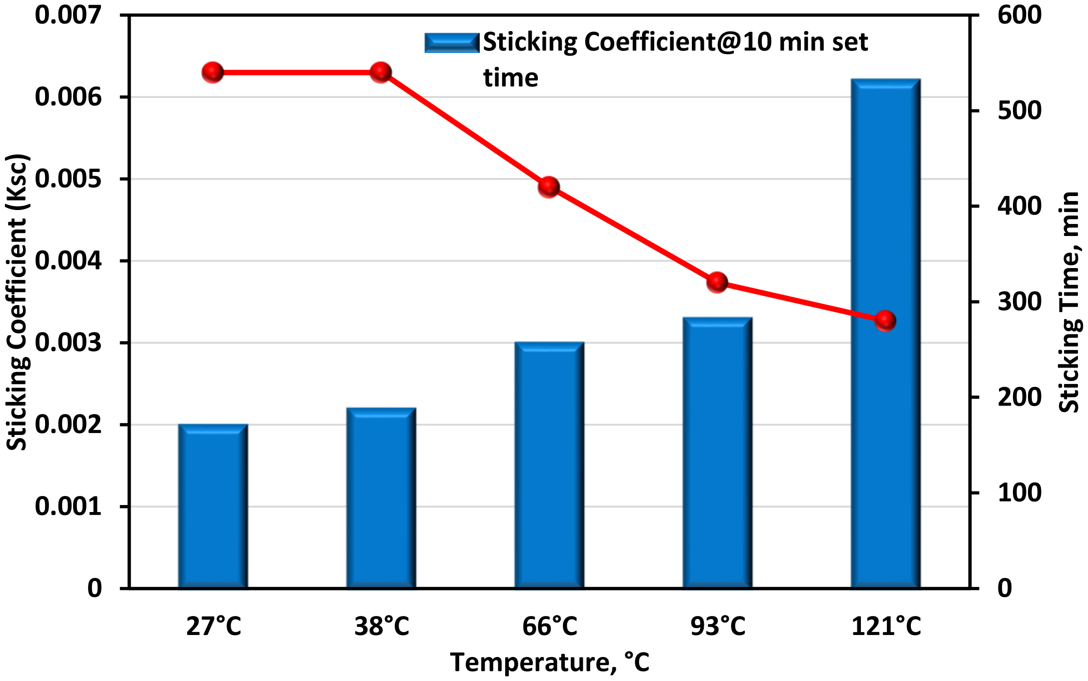

Figure C.1: Sticking coefficient for unweighted bentonite/polymer drilling fluid.

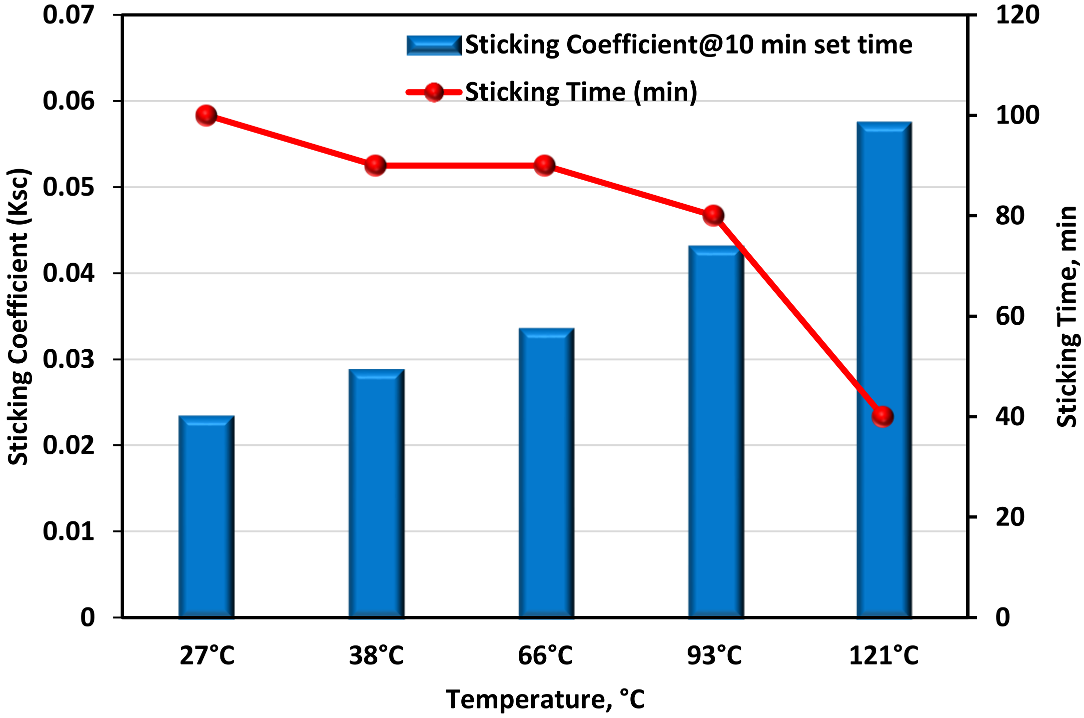

Figure C.2: Sticking coefficient for barite-weighted bentonite/polymer drilling fluid.

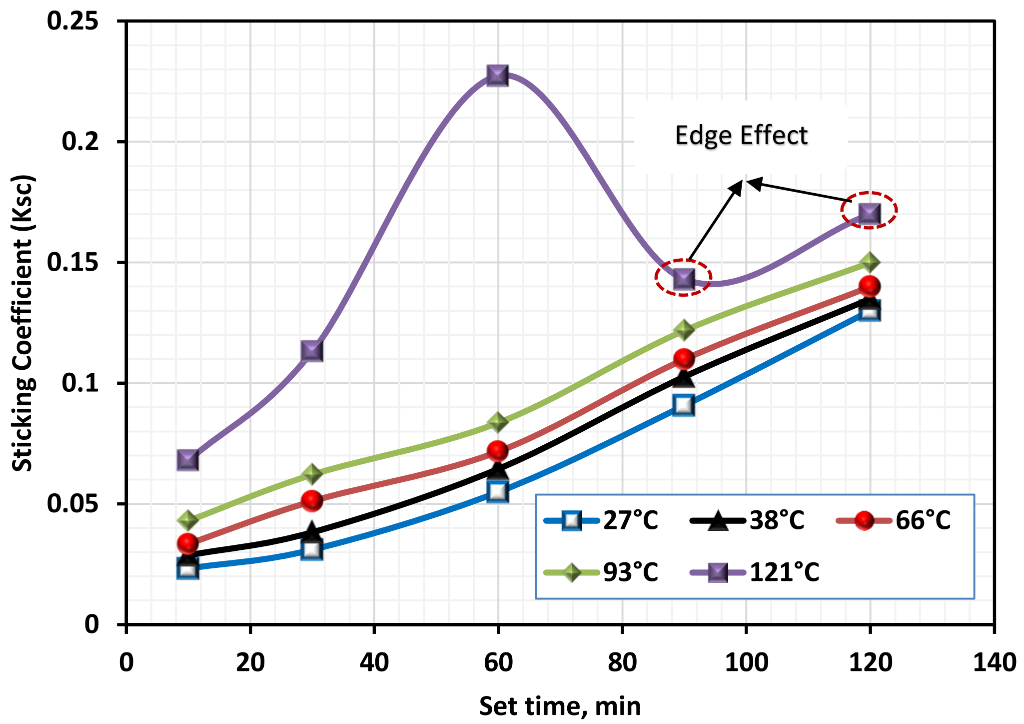

Figure C.3: Sticking coefficient vs. set time for weighted bentonite/polymer fluid.

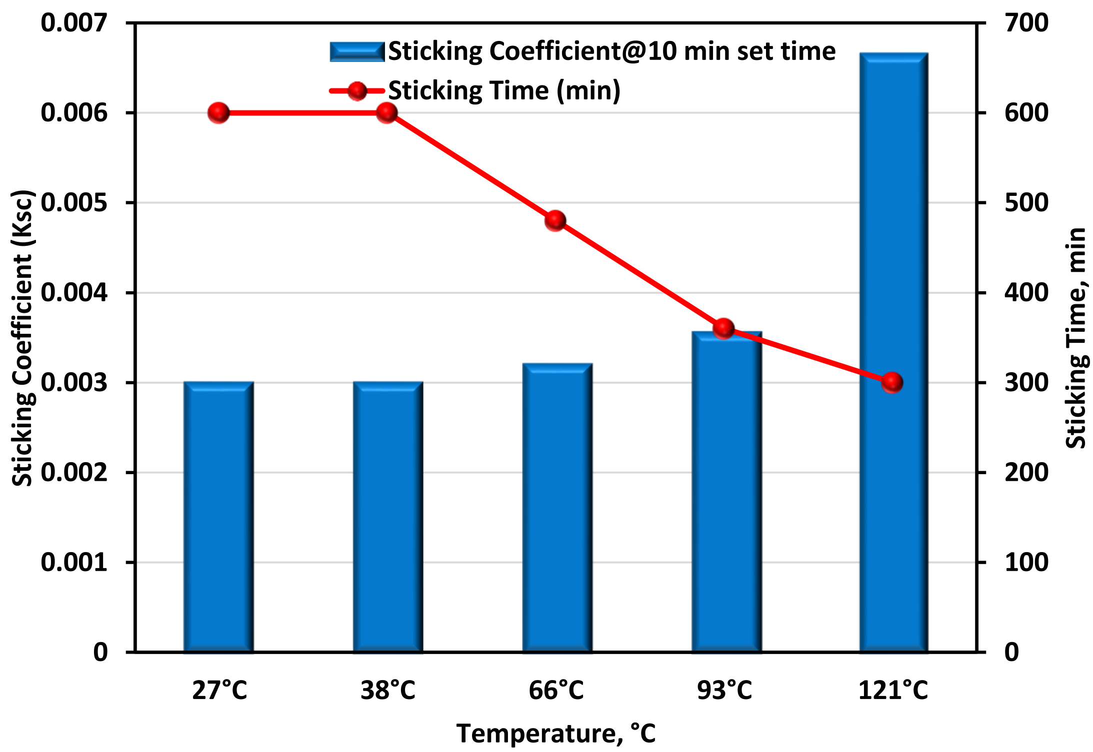

Figure C.4: Sticking coefficient for unweighted lignosulfonate fluid @10 minutes.

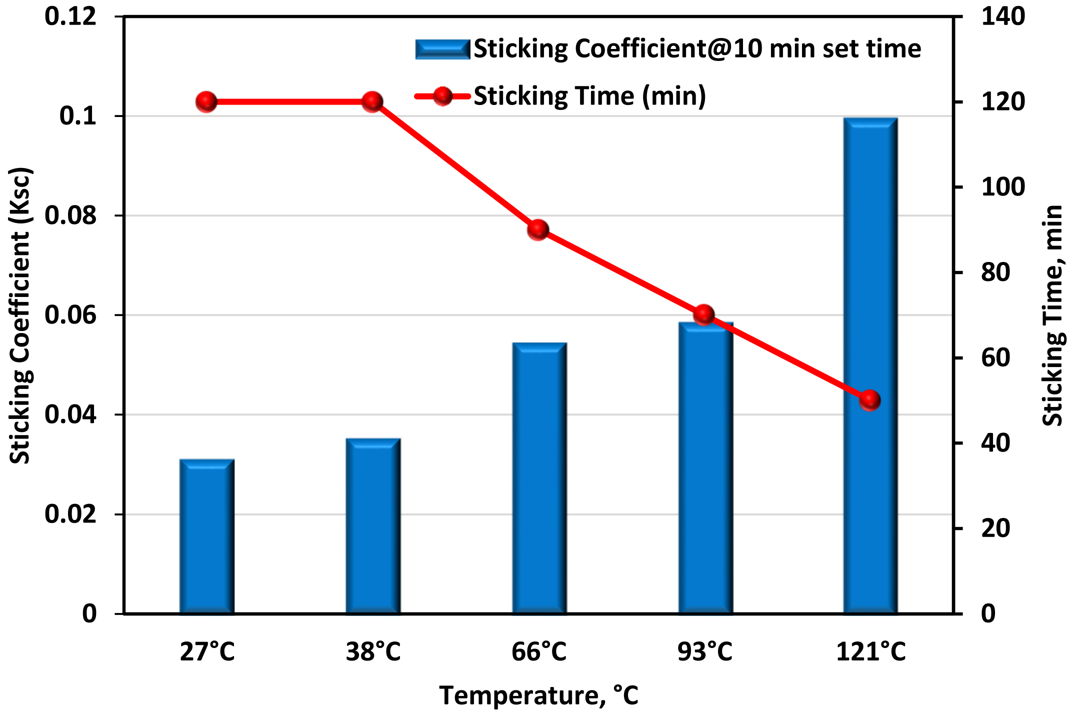

Figure C.5: Sticking coefficient for weighted lignosulfonate drilling fluid @10 minutes.

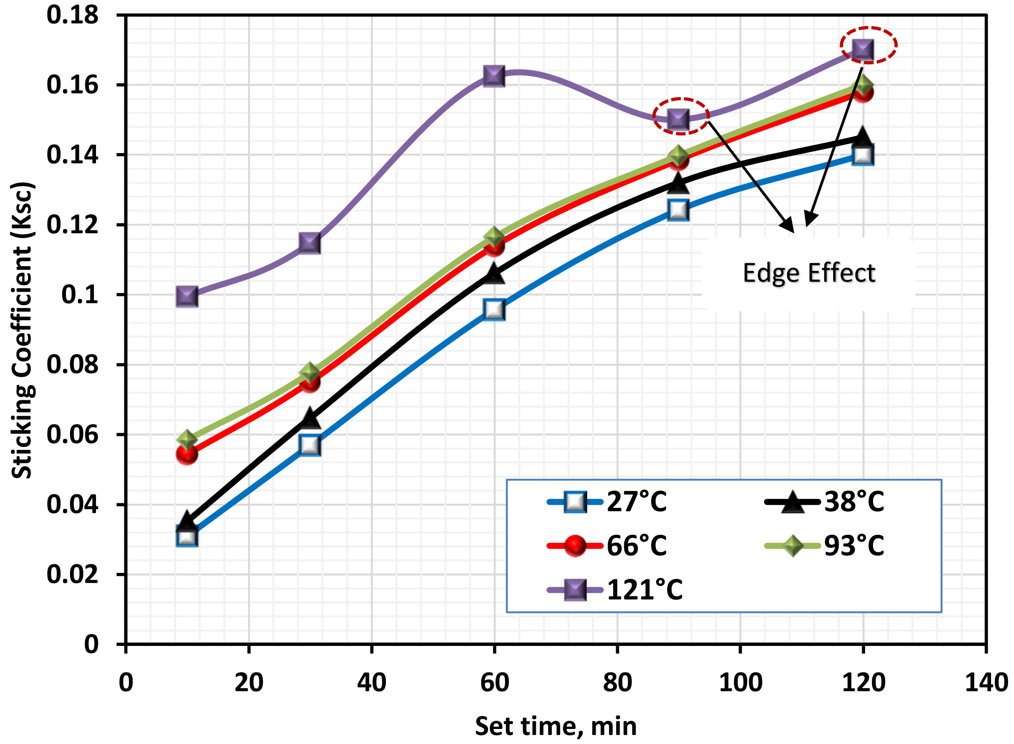

Figure C.6: Sticking coefficient vs. set time for weighted lignosulfonate drilling fluid.

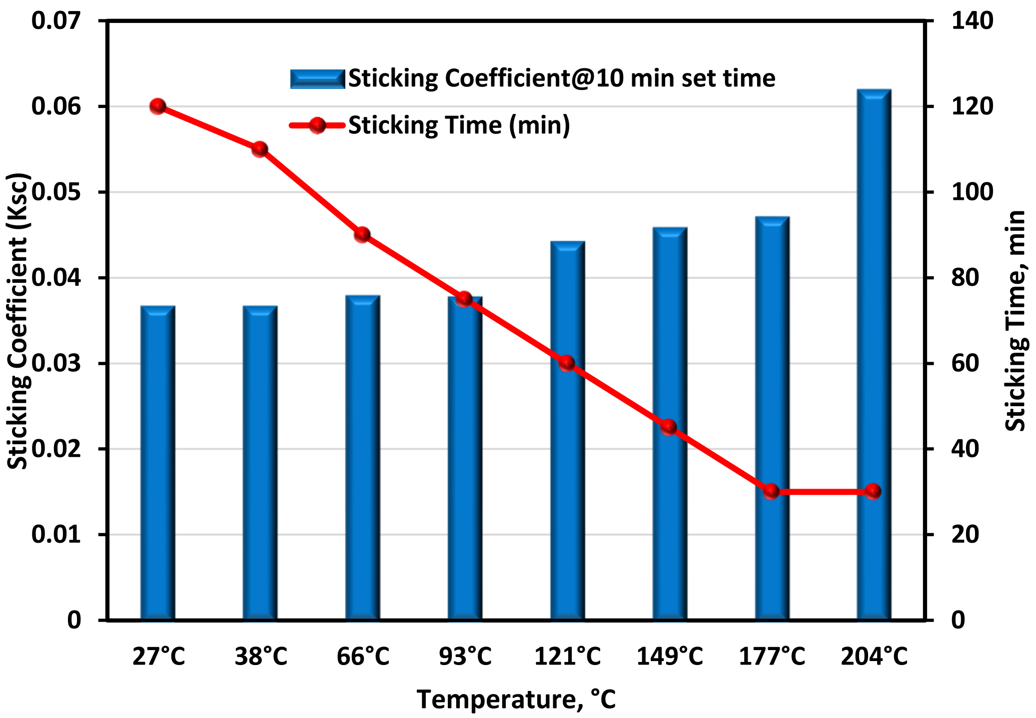

Figure C.7: Sticking coefficient for unweighted sepiolite drilling fluid.

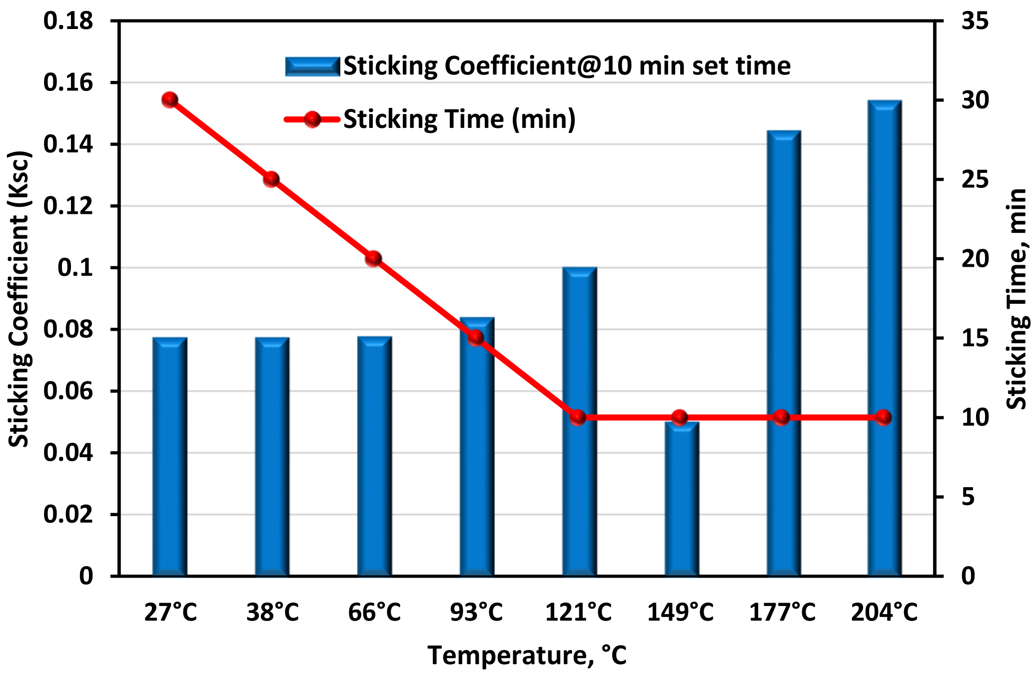

Figure C.8: Sticking coefficient for barite-weighted sepiolite drilling fluid.

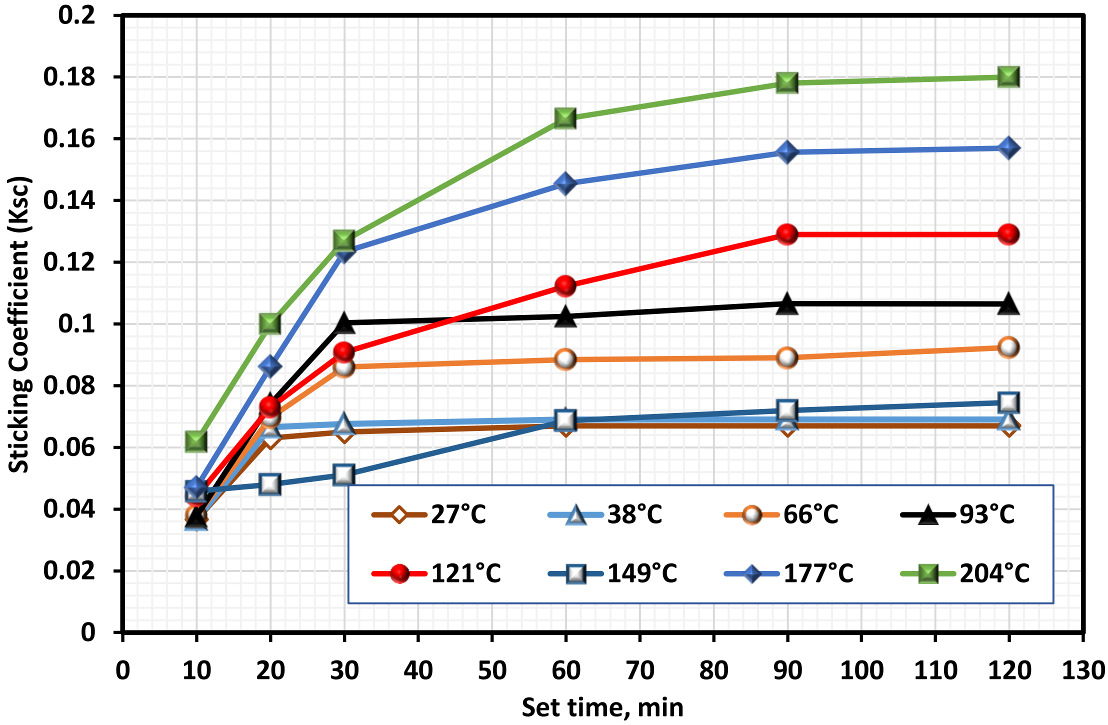

Figure C.9: Sticking coefficient vs. set time for unweighted sepiolite drilling fluid.

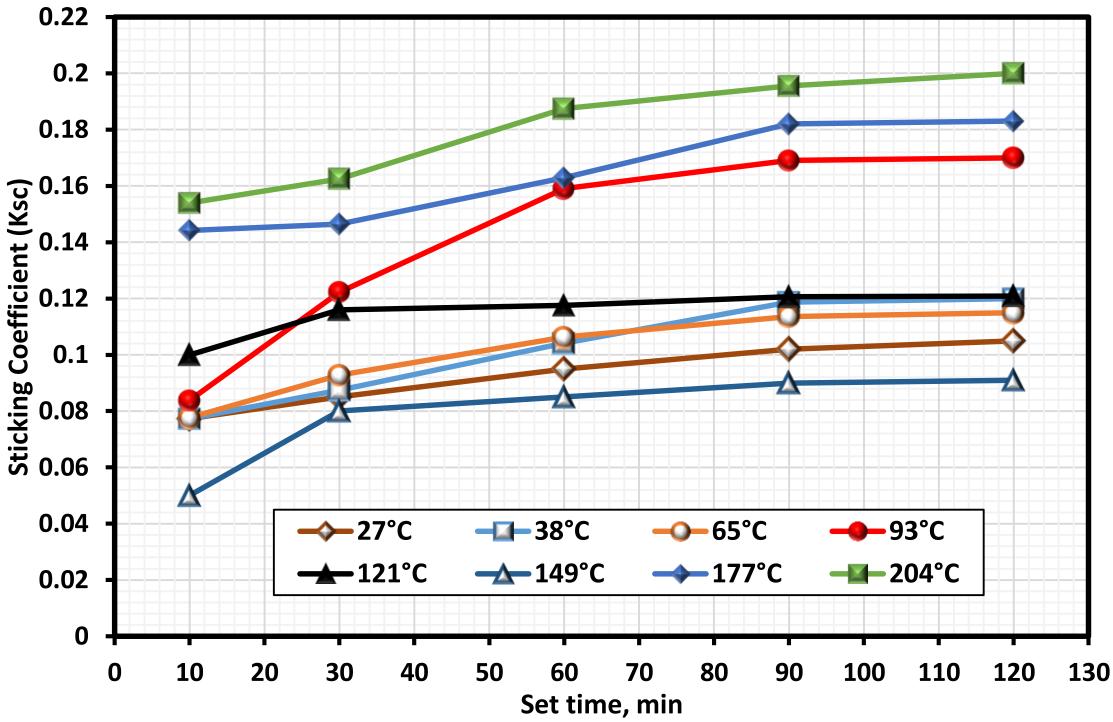

Figure C.10: Sticking coefficient vs. set time for weighted sepiolite drilling fluid.

APPENDIX D: Classic viscometer measurements at different aging temperatures.

Table D.1: Rheological measurements of sepiolite and fresh water suspension-viscometer results.

Aging Temperature, °C		27		38		65		93		121		149		177		204		232	
Measured Temperature, ˚C		27	49	27	49	27	49	27	49	27	49	27	49	27	49	27	49	27	49
*Dial Readings	600 rpm	37	33	34	27	26	21	25	21	23	18	20	18	13	13	18	19	53	52
	300 rpm	31	28	29	23	21	17	20	17	19	15	16	15	10	11	16	18	46	51
	200 rpm	28	25	25	21	19	16	18	15	17	14	15	14	8.5	10	14	16	46	51
	100 rpm	24	22	22	19	16	14	16	14	15	13	13	13	7.5	10	13	16	46	51
	6 rpm	16	17	15	15	10	11	11	11	12	13	12	13	7.5	10	13	16	46	49
	3 rpm	16	17	14	14	10	10.5	11	11	12	12	11	13	7.5	10	13	16	45	40
Plastic Viscosity (mPa-s)		6	5	5	4	5	4	5	4	4	3	4	3	3	2	2	1	7	1
Yeild Point (Pa)		11.98	11.02	11.50	9.10	7.66	6.23	7.19	6.23	7.19	5.75	5.75	5.75	3.35	4.31	6.71	8.14	18.68	23.95
*Gel Strenght (dial reading) 10 sec 1min 10min		19 25 36	19 21 26	15 20 26	14 15 19	12 16 24	10 11 22	12 16 25	12 14 19	15 24 27	15 19 24	14 20 35	21 26 36	15 23 43	25 33 53	28 38 48	40 50 70	93 113 147	58 70 98

*Multiplying dial reading to 0.479 to obtain in Pascal

Table D.2: Rheological measurements of unweighted fresh water sepiolite drilling fluid-viscometer results.

Aging Temperature, °C		27		38		65		93		121		149		177		204		232	
Measured Temperature, ˚C		27	49	27	49	27	49	27	49	27	27	49	27	49	27	49	27	49	27
*Dial Readings	600 rpm	74	51	71	48	70	46	59	43	46	38	38	28	39	31	47	36	52	40
	300 rpm	49	34	45	31	44	30	38	28	30	25	24	18	26	20	31	25	35	28
	200 rpm	38	27	35	24	35	23	30	22	23	20	18	14	20	16	25	20	29	23
	100 rpm	25	18	22	16	23	14	20	15	15	13	11	9	13	11	17	12	21	15
	6 rpm	6	5	5	4	5	3	4	4	4	4	3	3	3	3	5	4	7	5
	3 rpm	5	4	4	3	4	3	3	3	3	3	2	2	2	2	4	3	6	4
Plastic Viscosity (mPa-s)		25	17	26	17	26	16	21	15	16	13	14	10	13	11	16	11	17	12
Yeild Point (Pa)		11.42	8.09	9.04	6.66	8.57	6.66	8.09	6.19	6.66	5.71	4.76	3.81	6.19	4.28	7.14	6.66	8.57	7.62
*Gel strenght (dial reading) 10 sec/ 1min/ 10min		6/11/22	5/8/17	4/10/21	3/8/16	5/9/20	3/7/15	4/7/15	3/5/10	3/6/17	3/5/16	3/3/5	3/3/4	3/4/15	3/4/13	6/7/10	4/5/9	8/9/15	7/8/13

*Multiplying dial reading to 0.479 to obtain in Pascal

Table D.3: Rheological measurements of semi-saturated sepiolite drilling fluid-viscometer results.

Aging Temperature, °C		27		38		65		93		121		149		177		204		232	
Measured Temperature, ˚C		27	49	27	49	27	49	27	49	27	27	49	27	49	27	49	27	49	27
*Dial Readings	600 rpm	24	17	24	17	22	16	20	14	15	12	14	11	12	10	19	15	25	20
	300 rpm	13	10	13	10	13	9	11	8	8	7	8	6	7	6	11	10	15	12
	200 rpm	10	7	10	7	9	7	8	6	6	5	6	5	5	5	9	8	12	10
	100 rpm	6	5	6	5	6	4	5	4	4	3	3	3	3	3	6	6	9	7
	6 rpm	2	2	2	2	2	1	2	1	2	2	1	2	1	1	2	3	4	4
	3 rpm	1	1	1	1	1	1	1	1	1	2	1	2	1	1	2	3	4	4
Plastic Viscosity (mPa-s)		11	7	11	7	9	7	9	6	7	5	6	5	5	4	8	5	10	8
Yeild Point (Pa)		0.958	1.437	0.958	1.437	1.916	0.958	0.958	0.958	0.479	0.958	0.958	0.479	0.958	0.958	1.437	2.395	2.395	1.916
*Gel strenght (dial reading) 10 sec/ 1min/ 10min		1/2/2	1/2/2	1/2/2	1/2/2	1/2/2	1/2/2	2/2/2	2/2/2	2/2/2	2/2/2	2/2/2	2/2/2	2/2/2	2/2/2	2/2/2	2/2/2	3/4/5	4/5/6

*Multiplying dial reading to 0.479 to obtain in Pascal

Table D.4: Rheological measurements of fully-saturated sepiolite drilling fluid-viscometer results.

Aging Temperature, °C		27		38		65		93		121		149		177		204		232	
Measured Temperature, ˚C		27	49	27	49	27	49	27	49	27	27	49	27	49	27	49	27	49	27
*Dial Readings	600 rpm	22	18	22	18	20	15	18	15	15	12	14	12	11	9	18	14	23	18
	300 rpm	12	10	12	10	11	9	10	9	9	7	8	7	6	6	10	10	13	11
	200 rpm	9	8	9	8	8	7	7	7	7	5	5	5	5	4	8	8	10	9
	100 rpm	5	5	5	5	5	4	4	4	4	3	3	3	3	3	6	6	8	7
	6 rpm	2	2	2	2	2	2	2	2	2	2	2	2	1	1	2	3	4	4
	3 rpm	1	2	1	2	2	1			1	1	1	1	1	1	2	3	3	3
Plastic Viscosity (mPa-s)		10	8	10	8	9	6	8	6	6	5	6	5	5	3	8	4	10	7
Yeild Point (Pa)		0.958	0.958	0.958	0.958	0.958	1.437	0.958	1.437	1.437	0.958	0.958	0.958	0.479	1.437	0.958	2.874	1.437	1.916
*Gel strenght (dial reading) 10 sec/ 1min/ 10min		2/2/2	2/2/2	2/2/2	2/2/2	2/2/2	2/2/3	2/2/2	2/2/2	2/2/2	2/2/2	2/2/2	2/2/2	2/2/2	2/2/2	2/2/4	3/3/5	3/4/6	4/5/8

*Multiplying dial reading to 0.479 to obtain in Pascal

Table D.5: Rheological measurements of sepiolite drilling fluid with intrusion of 171 kg/m^3 NaCl-viscomete results.

Aging Temperature, °C		27		38		65		93		121		149		177		204		232	
Measured Temperature, ˚C		27	49	27	49	27	49	27	49	27	27	49	27	49	27	49	27	49	27
*Dial Readings	600 rpm	28	24	28	24	28	24	28	24	27	24	22	20	21	15	23	18	28	23
	300 rpm	17	16	17	16	18	16	18	16	17	16	13	12	12	9	15	12	20	17
	200 rpm	13	12	13	12	14	12	14	12	13	12	10	10	9	7	13	10	15	12
	100 rpm	9	8	9	8	9	8	9	8	8	8	7	7	6	5	9	7	11	9
	6 rpm	2	3	2	3	3	3	3	3	2	3	2	2	2	2	3	3	5	5
	3 rpm	2	2	2	2	2	2	2	2	2	2	2	2	2	2	3	3	4	4
Plastic Viscosity (mPa-s)		11	8	11	8	10	8	10	8	10	8	9	8	9	6	8	6	8	6
Yeild Point (Pa)		2.874	3.832	2.874	3.832	3.832	3.832	3.832	3.832	3.353	3.832	1.916	1.916	1.437	1.437	3.353	2.874	5.748	5.269
*Gel strenght (dial reading) 10 sec/ 1min/ 10min		2/3/6	3/4/9	2/3/6	3/4/9	2/3/7	3/4/9	2/3/7	3/4/9	2/3/4	2/3/5	2/2/3	2/2/4	2/2/2	2/2/2	2/4/8	2/4/11	4/6/12	4/6/15

*Multiplying dial reading to 0.479 to obtain in Pascal

Table D.6: Rheological measurements of sepiolite drilling fluid with intrusion of 342 kg/m^3 NaCl.

Aging Temperature, °C		27		38		65		93		121		149		177		204		232	
Measured Temperature, ˚C		27	49	27	49	27	49	27	49	27	27	49	27	49	27	49	27	49	27
*Dial Readings	600 rpm	32	21	32	21	32	21	32	21	31	20	28	18	29	24	48	46	55	52
	300 rpm	20	12	20	12	21	14	21	14	19	12	16	10	18	15	36	35	43	40
	200 rpm	11	10	11	10	11	10	11	10	12	9	11	8	14	12	32	29	35	31
	100 rpm	7	6	7	6	7	6	7	6	8	6	7	5	9	8	28	24	28	24
	6 rpm	2	2	2	2	2	2	2	2	2	2	2	2	2	2	18	15	22	18
	3 rpm	2	2	2	2	2	2	2	2	2	2	2	2	2	2	15	13	18	15
Plastic Viscosity (mPa-s)		12	9	12	9	11	7	11	7	12	8	12	8	11	9	12	11	12	12
Yeild Point (Pa)		3.832	1.437	3.832	1.437	4.79	3.353	4.79	3.353	3.353	1.916	1.916	0.958	3.353	2.874	11.496	11.496	14.849	13.412
*Gel strenght (dial reading) 10 sec/ 1min/ 10min		2/2/2	2/2/2	2/2/2	2/2/2	2/2/2	2/2/2	2/2/2	2/2/2	2/2/2	2/2/2	2/2/2	2/2/2	2/2/2	2/2/2	10/15/21	14/16/26	12/18/25	15/20/30

*Multiplying dial reading to 0.479 to obtain in Pascal

Table D.7: Rheological measurements weighted fresh water sepiolite drilling fluid-viscometer results.

Aging Temperature, °C		27		38		65		93		121		149		177		204		232	
Measured Temperature, ˚C		27	49	27	49	27	49	27	49	27	27	49	27	49	27	49	27	49	27
*Dial Readings	600 rpm	106	79	104	77	91	68	72	52	59	40	52	36	50	34	64	49	70	55
	300 rpm	69	51	68	50	59	45	45	33	36	25	31	22	29	20	44	34	50	39
	200 rpm	54	40	53	39	46	35	34	25	27	19	23	17	21	15	35	26	38	30
	100 rpm	35	26	35	26	30	23	21	16	17	12	14	11	12	10	23	17	26	20
	6 rpm	9	6	9	6	7	6	4	3	3	3	3	3	3	3	7	6	9	8
	3 rpm	6	5	6	5	5	4	3	2	2	2	3	2	3	2	6	5	8	7
Plastic Viscosity (mPa-s)		37	28	36	27	32	23	27	19	23	15	21	14	21	14	20	15	20	16
Yeild Point (Pa)		15.328	11.017	15.328	11.017	12.933	10.538	8.622	6.706	6.227	4.79	4.79	3.832	3.832	2.874	11.496	9.101	14.37	11.017
*Gel strenght (dial reading) 10 sec/ 1min/ 10min		8/14/25	6/10/19	8/13/22	5/9/17	6/11/21	6/8/13	5/6/15	3/4/10	3/4/5	3/3/4	3/3/4	2/2/3	3/5/10	3/4/6	6/9/15	5/7/13	8/10/20	6/7/15

*Multiplying dial reading to 0.479 to obtain in Pascal

Appendix E: HTHP Rheometer Rheological Measurments.

Table E.1: Rheological measurements of sepiolite and fresh water suspension-rheometer results.

Rheometer test @38°C				Rheometer test @43°C				Rheometer test @49°C			
Time (sec)	Shear rate (1/sec)	Shear stress (Pa)	Viscosity (mPa-s)	Time (sec)	Shear rate (1/sec)	Shear stress (Pa)	Viscosity (mPa-s)	Time (sec)	Shear rate (1/sec)	Shear stress (Pa)	Viscosity (mPa-s)
1740	1021.20	16.59	16.23	3413	1021.27	13.59	13.30	5376	1021.32	11.34	11.10
1800	510.72	13.34	26.11	3473	510.67	10.91	21.36	5436	510.78	9.00	17.60
1860	340.45	11.74	34.48	3533	340.48	9.66	28.37	5496	340.58	7.94	23.31
1920	170.17	10.12	59.43	3593	170.12	8.34	49.02	5556	170.13	6.90	40.51
1980	10.12	7.74	764.49	3653	10.02	6.49	649.02	5616	9.92	5.58	564.00
2040	4.80	7.45	1575.30	3713	4.90	6.32	1311.02	5676	5.16	5.46	1057.07

Rheometer test @54°C				Rheometer test @60°C				Rheometer test @66°C			
Time (sec)	Shear rate (1/sec)	Shear stress (Pa)	Viscosity (mPa-s)	Time (sec)	Shear rate (1/sec)	Shear stress (Pa)	Viscosity (mPa-s)	Time (sec)	Shear rate (1/sec)	Shear stress (Pa)	Viscosity (mPa-s)
6443	1021.16	10.27	10.05	7542	1021.33	9.22	9.03	8551	1021.37	8.31	8.14
6503	510.74	8.09	15.82	7602	510.96	7.20	14.08	8611	510.99	6.47	12.67
6563	340.49	7.14	20.97	7662	340.48	6.37	18.71	8671	340.49	5.72	16.79
6623	170.12	6.23	36.62	7722	170.20	5.57	32.71	8731	170.18	5.02	29.48
6683	9.96	5.19	521.87	7782	10.01	4.77	476.86	8791	10.02	4.38	438.47
6743	5.15	5.08	987.32	7842	4.80	4.63	983.07	8851	4.82	4.16	874.80

Rheometer test @71°C				Rheometer test @77°C				Rheometer test @82°C			
Time (sec)	Shear rate (1/sec)	Shear stress (Pa)	Viscosity (mPa-s)	Time (sec)	Shear rate (1/sec)	Shear stress (Pa)	Viscosity (mPa-s)	Time (sec)	Shear rate (1/sec)	Shear stress (Pa)	Viscosity (mPa-s)
9460	1021.43	7.58	7.42	10382	1021.37	6.89	6.74	11326	1021.35	6.37	6.24
9520	510.87	5.88	11.50	10442	510.80	5.36	10.48	11386	510.71	4.95	9.69
9580	340.44	5.17	15.19	10502	340.46	4.71	13.84	11446	340.54	4.37	12.81
9640	170.17	4.55	26.72	10562	170.17	4.15	24.39	11506	170.17	3.86	22.69
9700	9.91	4.09	413.40	10622	9.94	3.78	381.01	11566	9.94	3.55	358.34
9760	5.08	3.97	781.38	10682	5.16	3.53	683.07	11626	4.87	2.78	581.46

Table E.1 (Continued): Rheological measurements of sepiolite and fresh water suspension-rheometer results.

Rheometer test @88°C				Rheometer test @93°C				Rheometer test @99°C			
Time (sec)	Shear rate (1/sec)	Shear stress (Pa)	Viscosity (mPa-s)	Time (sec)	Shear rate (1/sec)	Shear stress (Pa)	Viscosity (mPa-s)	Time (sec)	Shear rate (1/sec)	Shear stress (Pa)	Viscosity (mPa-s)
11326	1021.35	5.91	6.24	12244	1021.45	5.59	5.79	13175	1021.37	5.26	5.47
11386	510.71	4.65	9.69	12304	510.79	4.37	9.09	13235	510.86	4.07	8.55
11446	340.54	4.11	12.81	12364	340.52	3.86	12.08	13295	340.46	3.55	11.33
11506	170.17	3.64	22.69	12424	170.16	3.41	21.38	13355	170.14	3.13	20.02
11566	9.94	3.38	358.34	12484	10.11	3.19	335.22	13415	10.00	2.93	319.71
11626	4.87	2.51	581.46	12544	4.85	2.54	523.89	13475	5.06	2.00	502.79

Rheometer test @104°C				Rheometer test @110°C				Rheometer test @116°C			
Time (sec)	Shear rate (1/sec)	Shear stress (Pa)	Viscosity (mPa-s)	Time (sec)	Shear rate (1/sec)	Shear stress (Pa)	Viscosity (mPa-s)	Time (sec)	Shear rate (1/sec)	Shear stress (Pa)	Viscosity (mPa-s)
15011	1021.48	5.01	4.91	15688	1021.48	4.85	4.75	16354	1021.45	4.70	4.60
15071	510.78	3.92	7.66	15748	510.82	3.78	7.39	16414	510.84	3.65	7.15
15131	340.51	3.49	10.23	15808	340.45	3.33	9.78	16474	340.48	3.28	9.64
15191	170.16	3.08	18.09	15868	170.16	2.97	17.43	16534	170.15	2.91	17.09
15251	10.05	2.87	286.07	15928	9.98	2.73	274.49	16594	9.99	2.66	267.30
15311	4.81	1.82	387.77	15988	4.80	1.66	354.46	16654	5.10	1.73	339.38

Rheometer test @121°C				Rheometer test @127°C				Rheometer test @132°C			
Time (sec)	Shear rate (1/sec)	Shear stress (Pa)	Viscosity (mPa-s)	Time (sec)	Shear rate (1/sec)	Shear stress (Pa)	Viscosity (mPa-s)	Time (sec)	Shear rate (1/sec)	Shear stress (Pa)	Viscosity (mPa-s)
17030	1021.50	4.58	4.48	17705	1021.45	4.43	4.34	18378	1021.51	4.33	4.24
17090	510.85	3.57	6.98	17765	510.87	3.46	6.77	18438	510.89	3.41	6.68
17150	340.51	3.19	9.35	17825	340.51	3.11	9.12	18498	340.50	3.09	9.08
17210	170.22	2.89	16.94	17885	170.20	2.77	16.29	18558	170.20	2.78	16.35
17270	9.91	2.54	256.56	17945	10.06	2.45	243.88	18618	9.94	2.29	231.30
17330	4.89	1.56	328.67	18005	5.14	1.56	303.29	18678	4.74	1.47	318.59

Table E.1 (Continued): Rheological measurements of sepiolite and fresh water suspension-rheometer results.

Rheometer test @138°C				Rheometer test @143°C				Rheometer test @149°C			
Time (sec)	Shear rate (1/sec)	Shear stress (Pa)	Viscosity (mPa-s)	Time (sec)	Shear rate (1/sec)	Shear stress (Pa)	Viscosity (mPa-s)	Time (sec)	Shear rate (1/sec)	Shear stress (Pa)	Viscosity (mPa-s)
18739	1021.12	4.30	4.21	19425	1021.53	4.23	4.14	20055	1021.65	4.20	4.11
18799	510.84	3.36	6.58	19485	510.95	3.39	6.64	20115	510.86	3.36	6.58
18859	340.48	3.05	8.97	19545	340.49	3.11	9.14	20175	340.45	3.09	9.07
18919	170.06	2.75	16.16	19605	170.19	2.82	16.55	20235	170.16	2.80	16.44
18979	9.97	2.29	230.37	19665	10.07	2.14	213.20	20295	9.96	2.04	205.99
19039	5.01	1.48	295.38	19725	4.95	1.44	295.10	20355	5.09	1.45	285.94

Rheometer test @154°C				Rheometer test @160°C				Rheometer test @166°C			
Time (sec)	Shear rate (1/sec)	Shear stress (Pa)	Viscosity (mPa-s)	Time (sec)	Shear rate (1/sec)	Shear stress (Pa)	Viscosity (mPa-s)	Time (sec)	Shear rate (1/sec)	Shear stress (Pa)	Viscosity (mPa-s)
20737	1021.30	4.19	4.10	21099	1021.42	4.21	4.12	21755	1021.51	4.27	4.18
20797	510.94	3.42	6.69	21159	510.88	3.43	6.71	21815	510.93	3.53	6.91
20857	340.52	3.15	9.24	21219	340.46	3.17	9.31	21875	340.59	3.29	9.66
20917	170.19	2.89	17.00	21279	170.14	2.91	17.12	21935	170.17	3.04	17.83
20977	10.04	1.90	189.86	21339	10.02	1.90	190.16	21995	10.14	1.80	177.57
21037	5.13	1.40	272.09	21399	4.82	1.33	281.09	22055	4.89	1.35	282.33

Rheometer test @171°C				Rheometer test @177°C				Rheometer test @182°C			
Time (sec)	Shear rate (1/sec)	Shear stress (Pa)	Viscosity (mPa-s)	Time (sec)	Shear rate (1/sec)	Shear stress (Pa)	Viscosity (mPa-s)	Time (sec)	Shear rate (1/sec)	Shear stress (Pa)	Viscosity (mPa-s)
22117	1021.72	4.31	4.22	22772	1021.62	4.43	4.34	23417	1021.59	4.50	4.40
22177	510.97	3.54	6.93	22832	510.93	3.73	7.30	23477	510.92	3.80	7.44
22237	340.59	3.30	9.69	22892	340.59	3.48	10.21	23537	340.58	3.52	10.33
22297	170.19	3.05	17.91	22952	170.20	3.22	18.90	23597	170.18	3.27	19.22
22357	10.11	1.79	177.12	23012	10.14	1.78	175.97	23657	10.08	1.74	173.33
22417	5.10	1.33	261.33	23072	4.80	1.37	290.32	23717	4.76	1.37	292.66

Table E.1 (Continued): Rheological measurements of sepiolite and fresh water suspension-rheometer results.

Rheometer test @188°C				Rheometer test @193°C				Rheometer test @199°C			
Time (sec)	Shear rate (1/sec)	Shear stress (Pa)	Viscosity (mPa-s)	Time (sec)	Shear rate (1/sec)	Shear stress (Pa)	Viscosity (mPa-s)	Time (sec)	Shear rate (1/sec)	Shear stress (Pa)	Viscosity (mPa-s)
24071	1021.39	4.55	4.46	24717	1021.49	4.64	4.54	25536	1021.55	4.66	4.56
24131	510.99	3.87	7.57	24777	510.95	3.98	7.78	25596	510.96	4.01	7.85
24191	340.59	3.60	10.55	24837	340.64	3.68	10.81	25656	340.51	3.69	10.83
24251	170.25	3.32	19.50	24897	170.23	3.37	19.78	25716	170.22	3.38	19.87
24311	10.13	1.75	173.33	24957	10.06	1.78	177.47	25776	9.97	1.74	175.28
24371	4.96	1.39	284.41	25017	5.12	1.47	287.24	25836	5.12	1.50	293.32

Rheometer test @204°C				Rheometer test @210°C				Rheometer test @216°C			
Time (sec)	Shear rate (1/sec)	Shear stress (Pa)	Viscosity (mPa-s)	Time (sec)	Shear rate (1/sec)	Shear stress (Pa)	Viscosity (mPa-s)	Time (sec)	Shear rate (1/sec)	Shear stress (Pa)	Viscosity (mPa-s)
26204	1021.63	4.66	4.56	26850	1021.60	4.66	4.56	27493	1021.52	4.68	4.58
26264	510.99	3.98	7.78	26910	510.97	4.00	7.82	27553	510.97	4.02	7.86
26324	340.51	3.65	10.71	26970	340.52	3.65	10.73	27613	340.65	3.64	10.68
26384	170.23	3.35	19.70	27030	170.27	3.36	19.75	27673	170.24	3.33	19.53
26444	10.10	1.75	173.22	27090	10.11	1.76	174.58	27733	10.20	1.75	171.97
26504	4.78	1.48	313.59	27150	4.88	1.55	322.04	27793	4.92	1.57	325.38

Rheometer test @221°C				Rheometer test @227°C				Rheometer test @232°C			
Time (sec)	Shear rate (1/sec)	Shear stress (Pa)	Viscosity (mPa-s)	Time (sec)	Shear rate (1/sec)	Shear stress (Pa)	Viscosity (mPa-s)	Time (sec)	Shear rate (1/sec)	Shear stress (Pa)	Viscosity (mPa-s)
28182	1021.73	4.57	4.47	28826	1021.68	4.49	4.39	29526	1021.54	4.38	4.29
28242	510.95	3.93	7.70	28886	510.93	3.84	7.51	29586	510.97	3.73	7.29
28302	340.59	3.56	10.46	28946	340.57	3.47	10.17	29646	340.68	3.35	9.84
28362	170.24	3.22	18.93	29006	170.27	3.14	18.44	29706	170.27	3.03	17.76
28422	10.12	1.70	167.64	29066	10.08	1.62	161.25	29766	10.12	1.57	155.06
28482	5.15	1.62	314.02	29126	4.87	1.57	327.02	29826	4.86	1.55	320.82

Table E.1 (Continued): Rheological measurements of sepiolite and fresh water suspension-rheometer results.

Rheometer test @238°C				Rheometer test @243°C				Rheometer test @249°C			
Time (sec)	Shear rate (1/sec)	Shear stress (Pa)	Viscosity (mPa-s)	Time (sec)	Shear rate (1/sec)	Shear stress (Pa)	Viscosity (mPa-s)	Time (sec)	Shear rate (1/sec)	Shear stress (Pa)	Viscosity (mPa-s)
30182	1021.40	4.30	4.21	30927	1021.58	4.22	4.13	31599	1021.46	4.14	4.05
30242	511.01	3.68	7.20	30987	510.99	3.60	7.04	31659	511.05	3.53	6.91
30302	340.62	3.28	9.63	31047	340.68	3.22	9.44	31719	340.52	3.13	9.18
30362	170.30	2.93	17.22	31107	170.27	2.88	16.88	31779	170.09	2.82	16.56
30422	10.14	1.48	146.28	31167	10.11	1.45	143.37	31839	10.14	1.39	136.67
30482	5.06	1.49	295.49	31227	4.95	1.47	299.76	31899	4.81	1.45	307.99

Rheometer test @254°C				Rheometer test @260°C			
Time (sec)	Shear rate (1/sec)	Shear stress (Pa)	Viscosity (mPa-s)	Time (sec)	Shear rate (1/sec)	Shear stress (Pa)	Viscosity (mPa-s)
32297	1021.59	4.13	4.04	34038	1021.76	3.66	3.58
32357	511.02	3.49	6.84	34098	511.16	3.16	6.18
32417	340.62	3.08	9.05	34158	340.58	2.80	8.21
32477	170.26	2.74	16.06	34218	170.30	2.44	14.29
32537	10.14	1.30	128.58	34278	9.97	1.03	103.26
32597	4.94	1.37	279.56	34338	5.12	0.97	189.49

Table E.2: Rheological measurements of unweighted fresh water sepiolite drilling fluid-rheometer results.

Rheometer test @38°C				Rheometer test @43°C				Rheometer test @49°C			
Time (sec)	Shear rate (1/sec)	Shear stress (Pa)	Viscosity (mPa-s)	Time (sec)	Shear rate (1/sec)	Shear stress (Pa)	Viscosity (mPa-s)	Time (sec)	Shear rate (1/sec)	Shear stress (Pa)	Viscosity (mPa-s)
1935	1020.88	33.00	32.32	3986	1020.80	31.38	30.72	6113	1020.60	29.35	28.74
1995	510.43	19.65	38.48	4046	510.65	18.68	36.56	6172	510.38	17.29	33.86
2055	340.35	14.74	43.29	4106	340.28	14.10	41.41	6233	340.31	13.05	38.32
2115	170.06	9.27	54.51	4166	170.05	8.90	52.30	6293	170.09	8.29	48.71
2175	9.81	1.82	184.77	4226	9.96	1.63	163.49	6353	9.98	1.49	149.58
2235	4.77	1.50	316.77	4286	4.83	1.23	255.34	6413	4.87	1.15	237.52

Rheometer test @54°C				Rheometer test @60°C				Rheometer test @66°C			
Time (sec)	Shear rate (1/sec)	Shear stress (Pa)	Viscosity (mPa-s)	Time (sec)	Shear rate (1/sec)	Shear stress (Pa)	Viscosity (mPa-s)	Time (sec)	Shear rate (1/sec)	Shear stress (Pa)	Viscosity (mPa-s)
7130	1020.98	26.77	26.21	8242	1020.71	24.92	24.40	9261	1020.62	23.10	22.63
7190	510.72	15.81	30.95	8302	510.52	14.36	28.11	9321	510.64	13.45	26.33
7250	340.31	12.01	35.28	8362	340.28	10.93	32.09	9381	340.31	10.19	29.93
7310	170.08	7.65	44.96	8422	170.10	6.98	41.00	9441	170.12	6.46	37.96
7370	9.97	1.35	134.91	8482	9.89	1.16	116.74	9501	10.03	1.13	112.78
7430	4.83	1.03	213.11	8542	4.71	0.85	180.73	9561	4.90	0.83	169.12

Rheometer test @71°C				Rheometer test @77°C				Rheometer test @82°C			
Time (sec)	Shear rate (1/sec)	Shear stress (Pa)	Viscosity (mPa-s)	Time (sec)	Shear rate (1/sec)	Shear stress (Pa)	Viscosity (mPa-s)	Time (sec)	Shear rate (1/sec)	Shear stress (Pa)	Viscosity (mPa-s)
10199	1020.82	21.64	21.19	11133	1020.98	20.25	19.83	12088	1020.88	18.93	18.53
10259	510.48	12.53	24.54	11133	1020.98	20.25	19.83	12148	510.50	10.94	21.43
10319	340.26	9.45	27.77	11193	510.49	11.75	23.01	12208	340.33	8.23	24.17
10379	170.08	6.00	35.28	11253	340.31	8.84	25.96	12268	170.12	5.22	30.69
10439	9.99	1.00	99.66	11313	170.11	5.58	32.81	12328	9.81	0.82	83.66
10499	4.74	0.70	148.26	11373	9.85	0.95	96.61	12388	5.04	0.60	118.63

Table E.2 (Continued): Rheological measurements of unweighted fresh water sepiolite drilling fluid-rheometer results.

Rheometer test @88°C				Rheometer test @93°C				Rheometer test @99°C			
Time (sec)	Shear rate (1/sec)	Shear stress (Pa)	Viscosity (mPa-s)	Time (sec)	Shear rate (1/sec)	Shear stress (Pa)	Viscosity (mPa-s)	Time (sec)	Shear rate (1/sec)	Shear stress (Pa)	Viscosity (mPa-s)
13040	1020.95	17.61	17.24	13981	1020.85	16.36	16.02	15104	1020.96	15.28	14.96
13100	510.58	10.09	19.76	14041	510.50	9.39	18.38	15164	510.65	8.71	17.05
13160	340.30	7.60	22.33	14101	340.40	7.20	21.13	15224	340.39	6.63	19.46
13220	170.10	4.76	28.00	14161	170.09	4.65	27.31	15284	170.06	4.28	25.14
13280	10.04	0.69	68.12	14221	9.91	0.75	75.89	15344	9.91	0.77	77.51
13340	5.14	0.45	87.87	14281	4.73	0.53	112.79	15404	4.82	0.51	106.55

Rheometer test @104°C				Rheometer test @110°C				Rheometer test @116°C			
Time (sec)	Shear rate (1/sec)	Shear stress (Pa)	Viscosity (mPa-s)	Time (sec)	Shear rate (1/sec)	Shear stress (Pa)	Viscosity (mPa-s)	Time (sec)	Shear rate (1/sec)	Shear stress (Pa)	Viscosity (mPa-s)
15829	1021.00	13.75	13.46	16499	1021.00	12.57	12.31	17156	1021.11	11.42	11.18
15889	510.47	7.65	14.98	16559	510.53	6.93	13.58	17216	510.52	6.23	12.19
15949	340.28	5.65	16.59	16619	340.32	5.09	14.94	17276	340.33	4.49	13.19
16009	170.13	3.41	20.06	16679	170.09	3.03	17.81	17336	170.10	2.62	15.37
16069	9.86	0.32	32.93	16739	9.93	0.27	27.28	17396	9.98	0.15	15.40
16129	4.82	0.10	19.66	16799	5.10	0.11	20.70	17456	4.83	-0.02	-5.06

Rheometer test @121°C				Rheometer test @127°C				Rheometer test @132°C			
Time (sec)	Shear rate (1/sec)	Shear stress (Pa)	Viscosity (mPa-s)	Time (sec)	Shear rate (1/sec)	Shear stress (Pa)	Viscosity (mPa-s)	Time (sec)	Shear rate (1/sec)	Shear stress (Pa)	Viscosity (mPa-s)
17825	1020.89	10.35	10.13	18513	1020.98	9.23	9.04	19168	1020.95	8.15	7.98
17885	510.49	5.53	10.84	18573	510.47	4.85	9.50	19228	510.65	4.17	8.15
17945	340.34	4.03	11.85	18633	340.31	3.49	10.26	19288	340.37	2.90	8.51
18005	170.01	2.38	13.97	18693	170.08	1.98	11.62	19348	170.14	1.57	9.21
18065	9.95	0.13	13.54	18753	9.88	0.04	4.21	19408	9.93	-0.07	-7.04
18125	5.06	-0.01	-2.23	18813	4.90	-0.09	-19.11	19468	4.72	-0.19	-41.60

Table E.2 (Continued): Rheological measurements of unweighted fresh water sepiolite drilling fluid-rheometer results.

Rheometer test @138°C				Rheometer test @143°C				Rheometer test @149°C			
Time (sec)	Shear rate (1/sec)	Shear stress (Pa)	Viscosity (mPa-s)	Time (sec)	Shear rate (1/sec)	Shear stress (Pa)	Viscosity (mPa-s)	Time (sec)	Shear rate (1/sec)	Shear stress (Pa)	Viscosity (mPa-s)
19783	1020.78	7.44	7.29	20457	1020.90	6.58	6.44	21088	1020.96	6.02	5.90
19843	510.48	3.78	7.40	20517	510.53	3.25	6.36	21148	510.74	2.99	5.84
19903	340.32	2.66	7.81	20577	340.22	2.21	6.50	21208	340.38	1.98	5.82
19963	170.02	1.45	8.53	20637	170.07	1.16	6.81	21268	170.14	1.01	5.95
20023	9.85	-0.06	-6.63	20697	9.85	-0.12	-12.59	21328	9.98	-0.17	-16.78
20083	4.78	-0.13	-28.77	20757	4.80	-0.19	-41.51	21388	4.83	-0.25	-51.57

Rheometer test @154°C				Rheometer test @160°C				Rheometer test @166°C			
Time (sec)	Shear rate (1/sec)	Shear stress (Pa)	Viscosity (mPa-s)	Time (sec)	Shear rate (1/sec)	Shear stress (Pa)	Viscosity (mPa-s)	Time (sec)	Shear rate (1/sec)	Shear stress (Pa)	Viscosity (mPa-s)
21761	1021.03	5.32	5.21	22123	1020.63	5.08	4.97	22752	1021.05	4.53	4.43
21821	510.56	2.56	5.02	22183	510.47	2.49	4.87	22812	510.60	2.11	4.14
21881	340.34	1.68	4.95	22243	340.42	1.68	4.93	22872	340.34	1.35	3.96
21941	170.11	0.76	4.49	22303	170.04	0.75	4.40	22932	170.17	0.63	3.71
22001	10.00	-0.20	-19.84	22363	10.12	-0.23	-22.26	22992	9.88	-0.22	-22.42
22061	5.12	-0.25	-47.90	22423	4.75	-0.30	-65.07	23052	4.79	-0.30	-63.91

Rheometer test @171°C				Rheometer test @177°C				Rheometer test @182°C			
Time (sec)	Shear rate (1/sec)	Shear stress (Pa)	Viscosity (mPa-s)	Time (sec)	Shear rate (1/sec)	Shear stress (Pa)	Viscosity (mPa-s)	Time (sec)	Shear rate (1/sec)	Shear stress (Pa)	Viscosity (mPa-s)
23370	1021.17	4.21	4.12	23988	1021.01	3.87	3.79	24609.	1021.05	3.62	3.55
23430	510.79	1.96	3.84	24048	510.52	1.84	3.59	24669.	510.53	1.74	3.40
23490	340.39	1.22	3.57	24108	340.41	1.17	3.43	24729.	340.38	1.10	3.24
23550	170.16	0.50	2.91	24168	170.12	0.52	3.03	24789.	170.15	0.51	2.97
23610	10.14	-0.30	-29.97	24228	9.86	-0.21	-20.93	24849.	9.88	-0.20	-19.98
23670	4.81	-0.35	-74.64	24288	5.12	-0.25	-49.92	24909.	4.84	-0.25	-51.42

Table E.2 (Continued): Rheological measurements of unweighted fresh water sepiolite drilling fluid-rheometer results.

Rheometer test @188°C				Rheometer test @193°C				Rheometer test @199°C			
Time (sec)	Shear rate (1/sec)	Shear stress (Pa)	Viscosity (mPa-s)	Time (sec)	Shear rate (1/sec)	Shear stress (Pa)	Viscosity (mPa-s)	Time (sec)	Shear rate (1/sec)	Shear stress (Pa)	Viscosity (mPa-s)
25222	1021.24	3.50	3.43	25848	1021.12	3.80	3.72	26508	1021.12	4.98	4.88
25282	510.66	1.66	3.25	25908	510.76	2.05	4.00	26568	510.64	3.09	6.05
25342	340.42	1.10	3.23	25968	340.38	1.50	4.42	26628	340.41	2.69	7.90
25402	170.14	0.49	2.85	26028	170.09	0.89	5.23	26688	170.06	2.09	12.28
25462	9.97	-0.24	-24.20	26088	10.02	0.04	3.48	26748	9.89	1.24	123.42
25522	4.83	-0.30	-62.80	26148	4.79	0.05	8.72	26808	5.09	1.70	335.24

Rheometer test @204°C				Rheometer test @210°C				Rheometer test @216°C			
Time (sec)	Shear rate (1/sec)	Shear stress (Pa)	Viscosity (mPa-s)	Time (sec)	Shear rate (1/sec)	Shear stress (Pa)	Viscosity (mPa-s)	Time (sec)	Shear rate (1/sec)	Shear stress (Pa)	Viscosity (mPa-s)
27179	1020.98	7.53	7.38	27855	1021.24	9.76	9.55	28516	1021.26	11.08	10.85
27239	510.63	4.95	9.69	27915	510.70	6.68	13.08	28576	510.62	7.77	15.21
27299	340.47	4.40	12.93	27975	340.44	5.97	17.54	28636	340.42	7.03	20.63
27359	170.08	3.75	22.02	28035	170.27	5.37	31.55	28696	170.19	6.28	36.86
27419	9.89	3.61	362.84	28095	10.02	6.57	654.13	28756	10.01	8.85	883.16
27479	5.07	4.55	897.47	28155	4.95	6.83	1405.38	28816	4.82	8.79	1861.49

Rheometer test @221°C				Rheometer test @227°C				Rheometer test @232°C			
Time (sec)	Shear rate (1/sec)	Shear stress (Pa)	Viscosity (mPa-s)	Time (sec)	Shear rate (1/sec)	Shear stress (Pa)	Viscosity (mPa-s)	Time (sec)	Shear rate (1/sec)	Shear stress (Pa)	Viscosity (mPa-s)
29174	1021.25	11.29	11.05	29815	1021.38	10.74	10.51	30484	1021.47	10.09	9.87
29234	510.64	8.30	16.24	29875	510.74	7.79	15.24	30544	510.70	7.03	13.75
29294	340.38	7.31	21.46	29935	340.46	6.85	20.11	30604	340.42	5.99	17.60
29354	170.12	6.67	39.19	29995	170.15	6.21	36.47	30664	170.11	5.00	29.40
29414	9.98	9.95	996.35	30055	10.17	9.68	949.94	30724	10.10	6.24	616.19
29474	4.82	7.79	1642.79	30115	5.08	7.99	1574.35	30784	4.88	7.25	1508.39

Table E.2 (Continued): Rheological measurements of unweighted fresh water sepiolite drilling fluid-rheometer results.

Rheometer test @238°C				Rheometer test @243°C				Rheometer test @249°C			
Time (sec)	Shear rate (1/sec)	Shear stress (Pa)	Viscosity (mPa-s)	Time (sec)	Shear rate (1/sec)	Shear stress (Pa)	Viscosity (mPa-s)	Time (sec)	Shear rate (1/sec)	Shear stress (Pa)	Viscosity (mPa-s)
31165	1021.42	10.82	10.59	31817	1021.43	13.44	13.16	32472	1021.32	15.51	15.18
31225	510.70	7.09	13.89	31877	510.76	9.39	18.39	32532	510.72	10.58	20.72
31285	340.40	6.27	18.41	31937	340.46	8.48	24.91	32592	340.42	9.09	26.68
31345	170.19	5.25	30.82	31997	170.18	7.66	44.96	32652	170.18	7.64	44.88
31405	10.07	3.97	392.77	32057	10.18	4.77	467.38	32712	10.07	3.04	302.24
31465	5.07	4.86	957.76	32117	4.95	3.55	724.53	32772	4.89	1.65	341.71

Rheometer test @254°C				Rheometer test @260°C			
Time (sec)	Shear rate (1/sec)	Shear stress (Pa)	Viscosity (mPa-s)	Time (sec)	Shear rate (1/sec)	Shear stress (Pa)	Viscosity (mPa-s)
33157	1021.29	10.82	10.59	33882	1021.30	8.03	7.86
33217	510.82	7.18	14.05	33942	510.69	5.51	10.79
33277	340.36	6.17	18.13	34002	340.41	4.97	14.61
33337	170.15	5.15	30.25	34062	170.21	4.21	24.75
33397	10.11	1.48	147.17	34122	10.06	1.09	107.91
33457	5.11	1.10	215.46	34182	4.90	0.97	198.56

Table E.3: Rheological measurements of semi-saturated sepiolite drilling fluid-rheometer results.

Rheometer test @38°C				Rheometer test @43°C				Rheometer test @49°C			
Time (sec)	Shear rate (1/sec)	Shear stress (Pa)	Viscosity (mPa-s)	Time (sec)	Shear rate (1/sec)	Shear stress (Pa)	Viscosity (mPa-s)	Time (sec)	Shear rate (1/sec)	Shear stress (Pa)	Viscosity (mPa-s)
1754	1021.11	13.25	12.97	3579	1021.16	12.70	12.43	5584	1021.18	11.76	11.51
1814	510.63	7.25	14.19	3639	510.60	6.94	13.59	5644	510.60	6.29	12.31
1874	340.59	5.22	15.31	3699	340.44	5.06	14.85	5704	340.52	4.68	13.74
1934	170.10	3.09	18.15	3759	170.12	3.00	17.60	5764	170.14	2.73	16.03
1994	10.11	0.75	74.25	3819	9.97	0.58	58.63	5824	10.11	0.46	45.21
2054	5.17	0.59	113.66	3879	5.18	0.43	83.42	5884	4.88	0.28	58.21

Rheometer test @54°C				Rheometer test @60°C				Rheometer test @66°C			
Time (sec)	Shear rate (1/sec)	Shear stress (Pa)	Viscosity (mPa-s)	Time (sec)	Shear rate (1/sec)	Shear stress (Pa)	Viscosity (mPa-s)	Time (sec)	Shear rate (1/sec)	Shear stress (Pa)	Viscosity (mPa-s)
6619	1021.17	10.73	10.50	7785	1021.15	9.93	9.72	8809	1021.15	9.29	9.10
6679	510.69	5.73	11.21	7845	510.58	5.24	10.26	8869	510.69	4.86	9.52
6739	340.35	4.02	11.82	7905	340.45	3.70	10.86	8929	340.38	3.50	10.27
6799	170.12	2.27	13.34	7965	170.12	2.03	11.93	8989	170.13	1.96	11.53
6859	10.10	0.26	25.95	8025	10.11	0.05	4.67	9049	10.13	0.25	24.36
6919	4.97	0.11	21.43	8085	4.93	-0.07	-14.30	9109	5.14	0.16	31.90

Rheometer test @71°C				Rheometer test @77°C				Rheometer test @82°C			
Time (sec)	Shear rate (1/sec)	Shear stress (Pa)	Viscosity (mPa-s)	Time (sec)	Shear rate (1/sec)	Shear stress (Pa)	Viscosity (mPa-s)	Time (sec)	Shear rate (1/sec)	Shear stress (Pa)	Viscosity (mPa-s)
9749	1021.07	8.65	8.47	10652	1021.13	8.15	7.98	11590	1021.23	7.64	7.48
9809	510.67	4.55	8.90	10712	510.65	4.20	8.23	11650	510.59	3.99	7.80
9869	340.39	3.21	9.41	10772	340.35	3.03	8.90	11710	340.34	2.85	8.38
9929	170.13	1.74	10.24	10832	170.07	1.64	9.64	11770	170.15	1.57	9.21
9989	10.02	0.07	7.10	10892	10.01	0.05	4.72	11830	10.11	0.07	7.05
10049	5.03	-0.01	-2.25	10952	5.06	-0.07	-13.80	11890	5.08	0.05	9.30

Table E.3 (Continued): Rheological measurements of semi-saturated sepiolite drilling fluid-rheometer results.

Rheometer test @88°C				Rheometer test @93°C				Rheometer test @99°C			
Time (sec)	Shear rate (1/sec)	Shear stress (Pa)	Viscosity (mPa-s)	Time (sec)	Shear rate (1/sec)	Shear stress (Pa)	Viscosity (mPa-s)	Time (sec)	Shear rate (1/sec)	Shear stress (Pa)	Viscosity (mPa-s)
12517	1021.32	7.22	7.07	13428	1021.28	6.82	6.68	14541	1021.27	6.42	6.28
12577	510.65	3.87	7.57	13488	510.62	3.56	6.97	14601	510.70	3.30	6.45
12637	340.43	2.63	7.71	13548	340.44	2.45	7.19	14661	340.46	2.33	6.84
12697	170.21	1.34	7.89	13608	170.11	1.27	7.44	14721	170.08	1.28	7.50
12757	10.08	-0.07	-7.47	13668	10.04	-0.16	-16.21	14781	10.08	-0.07	-6.93
12817	4.88	-0.13	-27.89	13728	4.91	-0.25	-50.49	14841	4.92	-0.11	-22.53

Rheometer test @104°C				Rheometer test @110°C				Rheometer test @116°C			
Time (sec)	Shear rate (1/sec)	Shear stress (Pa)	Viscosity (mPa-s)	Time (sec)	Shear rate (1/sec)	Shear stress (Pa)	Viscosity (mPa-s)	Time (sec)	Shear rate (1/sec)	Shear stress (Pa)	Viscosity (mPa-s)
15259	1021.31	5.97	5.85	15917	1021.35	5.63	5.51	16560	1021.44	5.30	5.19
15319	510.71	3.09	6.04	15977	510.78	2.89	5.66	16620	510.82	2.68	5.24
15379	340.43	2.13	6.25	16037	340.49	2.03	5.95	16680	340.51	1.87	5.49
15439	170.21	1.10	6.46	16097	170.20	1.08	6.35	16740	170.21	1.01	5.92
15499	10.13	-0.13	-13.20	16157	10.12	-0.09	-9.34	16800	10.07	-0.07	-6.93
15559	5.14	-0.19	-36.32	16217	4.85	-0.15	-31.10	16860	4.95	-0.13	-26.13

Rheometer test @121°C				Rheometer test @127°C				Rheometer test @132°C			
Time (sec)	Shear rate (1/sec)	Shear stress (Pa)	Viscosity (mPa-s)	Time (sec)	Shear rate (1/sec)	Shear stress (Pa)	Viscosity (mPa-s)	Time (sec)	Shear rate (1/sec)	Shear stress (Pa)	Viscosity (mPa-s)
17218	1021.38	4.95	4.84	17865	1021.38	4.65	4.55	18503	1021.39	4.37	4.28
17278	510.85	2.39	4.68	17925	510.80	2.28	4.46	18563	510.76	2.16	4.22
17338	340.38	1.68	4.95	17985	340.53	1.51	4.43	18623	340.38	1.50	4.42
17398	170.12	0.87	5.09	18045	170.16	0.73	4.29	18683	170.21	0.81	4.77
17458	10.04	-0.21	-20.53	18105	10.11	-0.30	-30.04	18743	10.13	-0.06	-5.47
17518	5.13	-0.30	-59.18	18165	4.97	-0.36	-73.31	18803	5.17	-0.07	-13.50

Table E.3 (Continued): Rheological measurements of semi-saturated sepiolite drilling fluid-rheometer results.

Rheometer test @138°C				Rheometer test @143°C				Rheometer test @149°C			
Time (sec)	Shear rate (1/sec)	Shear stress (Pa)	Viscosity (mPa-s)	Time (sec)	Shear rate (1/sec)	Shear stress (Pa)	Viscosity (mPa-s)	Time (sec)	Shear rate (1/sec)	Shear stress (Pa)	Viscosity (mPa-s)
19123	1021.43	4.21	4.12	19767	1021.29	4.01	3.93	20413	1021.36	3.81	3.73
19183	510.81	2.06	4.03	19827	510.82	1.95	3.82	20473	510.78	1.86	3.64
19243	340.51	1.38	4.04	19887	340.49	1.16	3.42	20533	340.49	1.26	3.69
19303	170.17	0.69	4.03	19947	170.19	0.46	2.71	20593	170.20	0.61	3.57
19363	10.18	-0.19	-18.35	20007	10.19	-0.42	-41.33	20653	10.15	-0.25	-25.18
19423	4.94	-0.21	-42.24	20067	4.93	-0.44	-90.40	20713	4.91	-0.30	-62.12

Rheometer test @154°C				Rheometer test @160°C				Rheometer test @166°C			
Time (sec)	Shear rate (1/sec)	Shear stress (Pa)	Viscosity (mPa-s)	Time (sec)	Shear rate (1/sec)	Shear stress (Pa)	Viscosity (mPa-s)	Time (sec)	Shear rate (1/sec)	Shear stress (Pa)	Viscosity (mPa-s)
21046	1021.40	3.71	3.63	21408	1021.27	3.69	3.61	22036	1021.50	3.53	3.45
21106	510.87	1.80	3.53	21468	510.79	1.81	3.54	22096	510.82	1.79	3.51
21166	340.45	1.22	3.57	21528	340.48	1.16	3.40	22156	340.51	1.22	3.57
21226	170.18	0.57	3.34	21588	170.17	0.52	3.05	22216	170.23	0.60	3.54
21286	10.10	-0.28	-27.71	21648	10.11	-0.30	-30.04	22276	10.17	-0.30	-29.88
21346	4.99	-0.32	-64.40	21708	5.02	-0.36	-72.63	22336	4.87	-0.35	-72.82

Rheometer test @171°C				Rheometer test @177°C				Rheometer test @182°C			
Time (sec)	Shear rate (1/sec)	Shear stress (Pa)	Viscosity (mPa-s)	Time (sec)	Shear rate (1/sec)	Shear stress (Pa)	Viscosity (mPa-s)	Time (sec)	Shear rate (1/sec)	Shear stress (Pa)	Viscosity (mPa-s)
22397	1021.50	3.63	3.56	23028	1021.48	3.60	3.52	23642	1021.48	3.80	3.72
22457	510.82	1.80	3.52	23088	510.85	1.87	3.66	23702	510.86	2.02	3.95
22517	340.50	1.23	3.62	23148	340.44	1.37	4.02	23762	340.49	1.52	4.47
22577	170.23	0.61	3.57	23208	170.26	0.75	4.40	23822	170.30	0.90	5.31
22637	10.14	-0.28	-28.09	23268	10.07	-0.20	-19.59	23882	10.13	-0.06	-6.55
22697	4.83	-0.30	-63.10	23328	5.18	-0.19	-36.01	23942	5.04	-0.05	-9.64

Table E.3 (Continued): Rheological measurements of semi-saturated sepiolite drilling fluid-rheometer results.

Rheometer test @188°C				Rheometer test @193°C				Rheometer test @199°C			
Time (sec)	Shear rate (1/sec)	Shear stress (Pa)	Viscosity (mPa-s)	Time (sec)	Shear rate (1/sec)	Shear stress (Pa)	Viscosity (mPa-s)	Time (sec)	Shear rate (1/sec)	Shear stress (Pa)	Viscosity (mPa-s)
24291	1021.48	3.96	3.88	24951	1021.47	4.15	4.06	25609	1021.24	4.29	4.20
24351	510.87	2.17	4.24	25011	510.80	2.30	4.50	25669	510.87	2.43	4.75
24411	340.47	1.67	4.90	25071	340.54	1.81	5.32	25729	340.52	1.90	5.59
24471	170.30	1.10	6.43	25131	170.27	1.22	7.14	25789	170.18	1.29	7.55
24531	10.21	0.11	10.23	25191	10.14	0.20	19.82	25849	10.18	0.28	27.29
24591	4.94	0.18	36.70	25251	4.95	0.33	66.04	25909	5.08	0.47	91.78

Rheometer test @204°C				Rheometer test @210°C				Rheometer test @216°C			
Time (sec)	Shear rate (1/sec)	Shear stress (Pa)	Viscosity (mPa-s)	Time (sec)	Shear rate (1/sec)	Shear stress (Pa)	Viscosity (mPa-s)	Time (sec)	Shear rate (1/sec)	Shear stress (Pa)	Viscosity (mPa-s)
26259	1021.55	4.46	4.36	26923	1021.47	4.62	4.52	27582	1021.60	4.66	4.56
26319	510.86	2.58	5.04	26983	510.86	2.68	5.24	27642	510.89	2.70	5.28
26379	340.52	2.08	6.10	27043	340.47	2.08	6.12	27702	340.47	2.13	6.26
26439	170.19	1.47	8.61	27103	170.16	1.42	8.32	27762	170.27	1.42	8.35
26499	10.13	0.48	47.10	27163	10.20	0.39	38.43	27822	10.13	0.41	40.42
26559	5.11	0.69	134.85	27223	4.86	0.58	118.24	27882	4.96	0.60	120.63

Rheometer test @221°C				Rheometer test @227°C				Rheometer test @232°C			
Time (sec)	Shear rate (1/sec)	Shear stress (Pa)	Viscosity (mPa-s)	Time (sec)	Shear rate (1/sec)	Shear stress (Pa)	Viscosity (mPa-s)	Time (sec)	Shear rate (1/sec)	Shear stress (Pa)	Viscosity (mPa-s)
28241	1021.39	4.68	4.58	28906	1021.56	4.57	4.47	29568	1021.19	4.47	4.38
28301	510.87	2.66	5.20	28966	510.94	2.54	4.97	29628	510.90	2.48	4.86
28361	340.57	2.07	6.07	29026	340.55	1.98	5.80	29688	340.49	1.93	5.68
28421	170.22	1.37	8.06	29086	170.26	1.29	7.60	29748	170.18	1.23	7.20
28481	10.07	0.32	32.03	29146	10.15	0.22	21.74	29808	10.08	0.14	14.19
28541	5.01	0.47	93.21	29206	4.93	0.32	65.27	29868	5.11	0.23	44.54

Table E.3 (Continued): Rheological measurements of semi-saturated sepiolite drilling fluid-rheometer results.

Rheometer test @238°C				Rheometer test @243°C				Rheometer test @249°C			
Time (sec)	Shear rate (1/sec)	Shear stress (Pa)	Viscosity (mPa-s)	Time (sec)	Shear rate (1/sec)	Shear stress (Pa)	Viscosity (mPa-s)	Time (sec)	Shear rate (1/sec)	Shear stress (Pa)	Viscosity (mPa-s)
30236	1021.57	4.43	4.34	30892	1021.70	4.51	4.41	31559	1021.39	4.70	4.60
30296	510.98	2.53	4.95	30952	510.94	2.62	5.13	31619	510.89	2.84	5.57
30356	340.49	1.96	5.75	31012	340.52	2.06	6.06	31679	340.55	2.23	6.55
30416	170.24	1.28	7.52	31072	170.29	1.35	7.92	31739	170.26	1.51	8.86
30476	10.16	0.17	16.54	31132	10.06	0.29	28.83	31799	10.00	0.51	50.91
30536	4.95	0.20	39.79	31192	4.93	0.29	57.96	31859	5.08	0.48	94.65

Rheometer test @254°C				Rheometer test @260°C			
Time (sec)	Shear rate (1/sec)	Shear stress (Pa)	Viscosity (mPa-s)	Time (sec)	Shear rate (1/sec)	Shear stress (Pa)	Viscosity (mPa-s)
32268	1021.41	4.94	4.83	33024	1021.56	5.39	5.27
32328	510.89	3.01	5.88	33084	510.87	3.29	6.44
32388	340.43	2.44	7.15	33144	340.57	2.68	7.86
32448	170.17	1.74	10.24	33204	170.18	2.07	12.19
32508	10.08	0.66	65.04	33264	10.11	0.87	85.56
32568	4.81	0.63	131.58	33324	5.03	0.82	163.32

Table E.4: Rheological measurements of fully-saturated sepiolite drilling fluid-rheometer results.

Rheometer test @38°C				Rheometer test @43°C				Rheometer test @49°C			
Time (sec)	Shear rate (1/sec)	Shear stress (Pa)	Viscosity (mPa-s)	Time (sec)	Shear rate (1/sec)	Shear stress (Pa)	Viscosity (mPa-s)	Time (sec)	Shear rate (1/sec)	Shear stress (Pa)	Viscosity (mPa-s)
1697	1021.21	13.12	12.85	3563	1021.06	12.47	12.21	5560	1021.26	11.48	11.23
1757	510.60	7.03	13.76	3623	510.58	6.50	12.73	5620	510.85	5.84	11.43
1817	340.45	5.07	14.89	3683	340.32	4.58	13.45	5680	340.39	3.97	11.65
1877	170.14	2.97	17.46	3743	170.10	2.56	15.06	5740	170.07	2.04	11.96
1937	10.12	0.96	95.43	3803	10.05	0.40	40.23	5800	10.05	-0.06	-5.53
1997	4.93	0.89	181.53	3863	5.15	0.29	55.54	5860	4.87	-0.13	-26.51

Rheometer test @54°C				Rheometer test @60°C				Rheometer test @66°C			
Time (sec)	Shear rate (1/sec)	Shear stress (Pa)	Viscosity (mPa-s)	Time (sec)	Shear rate (1/sec)	Shear stress (Pa)	Viscosity (mPa-s)	Time (sec)	Shear rate (1/sec)	Shear stress (Pa)	Viscosity (mPa-s)
6606	1021.13	10.40	10.18	7665	1021.10	9.58	9.38	8714	1021.12	8.87	8.69
6666	510.76	5.27	10.31	7725	510.81	4.81	9.41	8774	510.53	4.41	8.63
6726	340.35	3.61	10.62	7785	340.38	3.26	9.58	8834	340.46	3.02	8.87
6786	170.10	1.86	10.93	7845	170.15	1.71	10.07	8894	170.04	1.57	9.22
6846	10.01	-0.01	-1.13	7905	10.03	-0.10	-10.30	8954	9.93	-0.13	-12.95
6906	4.88	-0.09	-19.68	7965	4.95	-0.24	-49.10	9014	4.81	-0.23	-48.96

Rheometer test @71°C				Rheometer test @77°C				Rheometer test @82°C			
Time (sec)	Shear rate (1/sec)	Shear stress (Pa)	Viscosity (mPa-s)	Time (sec)	Shear rate (1/sec)	Shear stress (Pa)	Viscosity (mPa-s)	Time (sec)	Shear rate (1/sec)	Shear stress (Pa)	Viscosity (mPa-s)
9641	1021.15	8.34	8.16	10575	1021.09	7.85	7.69	11513	1021.20	7.42	7.26
9701	510.80	4.08	7.99	10635	510.62	3.89	7.62	11573	510.78	3.59	7.03
9761	340.34	2.77	8.13	10695	340.37	2.64	7.75	11633	340.41	2.50	7.35
9821	170.19	1.45	8.49	10755	170.15	1.39	8.18	11693	170.14	1.28	7.49
9881	10.01	-0.13	-12.85	10815	9.96	-0.07	-7.03	11753	10.02	-0.17	-16.64
9941	5.03	-0.19	-37.14	10875	4.90	-0.13	-26.67	11813	4.98	-0.29	-60.09

Table E.4 (Continued): Rheological measurements of fully-saturated sepiolite drilling fluid-rheometer results.

Rheometer test @88°C				Rheometer test @93°C				Rheometer test @99°C			
Time (sec)	Shear rate (1/sec)	Shear stress (Pa)	Viscosity (mPa-s)	Time (sec)	Shear rate (1/sec)	Shear stress (Pa)	Viscosity (mPa-s)	Time (sec)	Shear rate (1/sec)	Shear stress (Pa)	Viscosity (mPa-s)
12453	1021.22	6.99	6.84	13374	1021.25	6.63	6.49	14473	1021.24	6.24	6.10
12513	510.62	3.43	6.71	13434	510.62	3.22	6.30	14533	510.67	3.03	5.92
12573	340.41	2.35	6.89	13494	340.49	2.15	6.32	14593	340.43	2.00	5.88
12633	170.15	1.23	7.21	13554	170.15	1.08	6.32	14653	170.13	0.94	5.55
12693	9.90	-0.07	-7.08	13614	9.96	-0.28	-28.05	14713	10.09	-0.25	-25.29
12753	5.13	-0.18	-35.44	13674	4.94	-0.30	-62.68	14773	4.91	-0.36	-74.48

Rheometer test @154°C				Rheometer test @160°C				Rheometer test @166°C			
Time (sec)	Shear rate (1/sec)	Shear stress (Pa)	Viscosity (mPa-s)	Time (sec)	Shear rate (1/sec)	Shear stress (Pa)	Viscosity (mPa-s)	Time (sec)	Shear rate (1/sec)	Shear stress (Pa)	Viscosity (mPa-s)
15184	1021.29	5.81	5.69	15840	1021.37	5.49	5.37	16485.	1021.34	5.21	5.10
15244	510.73	2.78	5.43	15900	510.67	2.63	5.14	16545.	510.75	2.39	4.67
15304	340.43	1.80	5.29	15960	340.47	1.69	4.96	16605.	340.45	1.51	4.43
15364	170.12	0.87	5.09	16020	170.15	0.82	4.83	16665.	170.22	0.64	3.74
15424	10.21	-0.28	-27.86	16080	10.11	-0.25	-24.26	16725.	10.10	-0.35	-34.38
15484	5.04	-0.32	-64.16	16140	4.95	-0.30	-61.96	16785.	5.01	-0.42	-84.06

Rheometer test @121°C				Rheometer test @127°C				Rheometer test @132°C			
Time (sec)	Shear rate (1/sec)	Shear stress (Pa)	Viscosity (mPa-s)	Time (sec)	Shear rate (1/sec)	Shear stress (Pa)	Viscosity (mPa-s)	Time (sec)	Shear rate (1/sec)	Shear stress (Pa)	Viscosity (mPa-s)
17135	1021.35	4.93	4.82	17801	1021.40	4.68	4.58	18433	1021.40	4.41	4.31
17195	510.73	2.31	4.53	17861	510.81	2.12	4.16	18493	511.03	2.09	4.09
17255	340.37	1.51	4.43	17921	340.51	1.42	4.17	18553	340.41	1.33	3.92
17315	170.23	0.69	4.05	17981	170.20	0.69	4.06	18613	170.18	0.58	3.43
17375	10.11	-0.30	-30.06	18041	10.07	-0.24	-23.83	18673	10.11	-0.25	-24.22
17435	4.94	-0.40	-80.62	18101	4.91	-0.31	-63.25	18733	5.08	-0.30	-59.76

Table E.4 (Continued): Rheological measurements of fully-saturated sepiolite drilling fluid-rheometer results.

Rheometer test @138°C				Rheometer test @143°C				Rheometer test @149°C			
Time (sec)	Shear rate (1/sec)	Shear stress (Pa)	Viscosity (mPa-s)	Time (sec)	Shear rate (1/sec)	Shear stress (Pa)	Viscosity (mPa-s)	Time (sec)	Shear rate (1/sec)	Shear stress (Pa)	Viscosity (mPa-s)
19060	1021.15	4.26	4.17	19711	1021.38	4.03	3.95	20338	1021.44	3.90	3.81
19120	510.78	1.99	3.90	19771	510.79	1.92	3.75	20398	510.76	1.83	3.58
19180	340.49	1.28	3.76	19831	340.52	1.27	3.73	20458	340.47	1.16	3.42
19240	170.19	0.52	3.05	19891	170.17	0.52	3.08	20518	170.16	0.47	2.74
19300	10.14	-0.31	-30.45	19951	10.09	-0.25	-24.32	20578	10.10	-0.30	-30.09
19360	4.94	-0.36	-73.65	20011	4.99	-0.30	-61.25	20638	4.92	-0.32	-66.42

Rheometer test @154°C				Rheometer test @160°C				Rheometer test @166°C			
Time (sec)	Shear rate (1/sec)	Shear stress (Pa)	Viscosity (mPa-s)	Time (sec)	Shear rate (1/sec)	Shear stress (Pa)	Viscosity (mPa-s)	Time (sec)	Shear rate (1/sec)	Shear stress (Pa)	Viscosity (mPa-s)
21000	1021.37	3.70	3.62	21361	1021.37	3.61	3.54	21986	1021.09	3.40	3.32
21060	510.76	1.67	3.26	21421	510.79	1.67	3.27	22046	510.77	1.56	3.05
21120	340.54	1.05	3.07	21481	340.50	1.04	3.06	22106	340.56	0.92	2.71
21180	170.14	0.40	2.34	21541	170.20	0.41	2.40	22166	170.16	0.33	1.97
21240	10.07	-0.30	-30.16	21601	10.11	-0.30	-30.05	22226	10.17	-0.38	-37.09
21300	4.97	-0.36	-73.35	21661	4.81	-0.35	-72.87	22286	4.98	-0.43	-87.46

Rheometer test @171°C				Rheometer test @177°C				Rheometer test @182°C			
Time (sec)	Shear rate (1/sec)	Shear stress (Pa)	Viscosity (mPa-s)	Time (sec)	Shear rate (1/sec)	Shear stress (Pa)	Viscosity (mPa-s)	Time (sec)	Shear rate (1/sec)	Shear stress (Pa)	Viscosity (mPa-s)
22591	1021.45	3.32	3.25	23218	1021.48	3.23	3.17	23579	1021.47	3.21	3.14
22651	510.78	1.50	2.94	23278	510.83	1.49	2.92	23639	510.76	1.50	2.94
22711	340.56	0.93	2.73	23338	340.45	0.92	2.71	23699	340.49	0.93	2.74
22771	170.12	0.32	1.85	23398	170.22	0.37	2.17	23759	170.18	0.34	1.99
22831	10.11	-0.42	-41.15	23458	10.05	-0.30	-30.22	23819	10.16	-0.32	-31.33
22891	4.89	-0.46	-95.62	23518	4.92	-0.31	-64.44	23879	5.17	-0.38	-73.01

Table E.4 (Continued): Rheological measurements of fully-saturated sepiolite drilling fluid-rheometer results.

Rheometer test @188°C				Rheometer test @193°C				Rheometer test @199°C			
Time (sec)	Shear rate (1/sec)	Shear stress (Pa)	Viscosity (mPa-s)	Time (sec)	Shear rate (1/sec)	Shear stress (Pa)	Viscosity (mPa-s)	Time (sec)	Shear rate (1/sec)	Shear stress (Pa)	Viscosity (mPa-s)
24194	1021.52	3.05	2.99	24803	1021.28	3.12	3.05	25424	1021.52	3.19	3.12
24254	510.84	1.41	2.76	24863	510.89	1.46	2.85	25484	510.91	1.49	2.91
24314	340.48	0.92	2.71	24923	340.52	0.97	2.84	25544	340.58	1.00	2.93
24374	170.16	0.34	1.99	24983	170.18	0.42	2.48	25604	170.22	0.46	2.68
24434	10.12	-0.36	-35.28	25043	10.13	-0.25	-24.23	25664	10.08	-0.30	-30.16
24494	5.07	-0.42	-82.96	25103	4.97	-0.30	-61.57	25724	4.97	-0.36	-72.29

Rheometer test @204°C				Rheometer test @210°C				Rheometer test @216°C			
Time (sec)	Shear rate (1/sec)	Shear stress (Pa)	Viscosity (mPa-s)	Time (sec)	Shear rate (1/sec)	Shear stress (Pa)	Viscosity (mPa-s)	Time (sec)	Shear rate (1/sec)	Shear stress (Pa)	Viscosity (mPa-s)
26053	1021.49	3.26	3.19	26688	1021.25	3.33	3.26	27306	1021.56	3.32	3.25
26113	510.91	1.60	3.13	26748	510.93	1.61	3.14	27366	510.87	1.66	3.24
26173	340.56	1.11	3.27	26808	340.60	1.09	3.20	27426	340.46	1.16	3.42
26233	170.17	0.54	3.17	26868	170.26	0.51	3.00	27486	170.19	0.57	3.34
26293	10.09	-0.27	-26.76	26928	10.20	-0.32	-31.26	27486	170.19	0.57	3.34
26353	4.98	-0.28	-56.64	26988	5.15	-0.31	-59.91	27546	10.11	-0.30	-29.59

Rheometer test @221°C				Rheometer test @227°C				Rheometer test @232°C			
Time (sec)	Shear rate (1/sec)	Shear stress (Pa)	Viscosity (mPa-s)	Time (sec)	Shear rate (1/sec)	Shear stress (Pa)	Viscosity (mPa-s)	Time (sec)	Shear rate (1/sec)	Shear stress (Pa)	Viscosity (mPa-s)
27917	1021.23	3.40	3.32	28546	1021.31	3.45	3.38	29179	1021.59	3.49	3.42
27977	510.83	1.68	3.30	28606	510.89	1.82	3.56	29239	510.99	1.79	3.51
28037	340.59	1.15	3.39	28666	340.50	1.35	3.97	29299	340.48	1.29	3.79
28097	170.22	0.54	3.20	28726	170.23	0.79	4.66	29359	170.30	0.70	4.11
28157	10.10	-0.32	-32.03	28786	10.13	-0.06	-6.45	29419	10.18	-0.17	-16.98
28217	4.93	-0.32	-66.47	28846	5.08	-0.07	-14.66	29479	4.97	-0.20	-40.21

Table E.4 (Continued): Rheological measurements of fully-saturated sepiolite drilling fluid-rheometer results.

Rheometer test @238°C				Rheometer test @243°C				Rheometer test @249°C			
Time (sec)	Shear rate (1/sec)	Shear stress (Pa)	Viscosity (mPa-s)	Time (sec)	Shear rate (1/sec)	Shear stress (Pa)	Viscosity (mPa-s)	Time (sec)	Shear rate (1/sec)	Shear stress (Pa)	Viscosity (mPa-s)
29812	1021.56	3.60	3.53	30444	1021.53	3.79	3.70	31103	1021.56	4.16	4.07
29872	510.99	2.00	3.91	30504	510.96	2.13	4.16	31163	511.00	2.39	4.67
29932	340.54	1.49	4.37	30564	340.58	1.66	4.86	31223	340.54	1.82	5.33
29992	170.29	0.90	5.31	30624	170.26	1.10	6.43	31283	170.27	1.23	7.23
30052	10.04	0.08	8.08	30684	10.12	0.21	20.53	31343	10.00	0.32	32.44
30112	4.96	0.05	10.49	30744	5.12	0.19	37.74	31403	4.97	0.32	65.61

Rheometer test @254°C				Rheometer test @260°C			
Time (sec)	Shear rate (1/sec)	Shear stress (Pa)	Viscosity (mPa-s)	Time (sec)	Shear rate (1/sec)	Shear stress (Pa)	Viscosity (mPa-s)
31798	1021.57	4.54	4.44	32870	1021.46	5.39	5.28
31858	510.90	2.80	5.48	32930	510.85	3.24	6.35
31918	340.61	2.25	6.59	32990	340.49	2.66	7.82
31978	170.29	1.67	9.78	33050	170.20	2.06	12.13
32038	10.12	0.78	76.77	33110	10.10	0.82	81.39
32098	4.91	0.76	156.43	33170	4.85	0.81	167.21

Table E.5: Rheological measurements of sepiolite drilling fluid with entrusion of 342 kg/m^3 NaCl-rheometer results.

Rheometer test @38°C				Rheometer test @43°C				Rheometer test @49°C			
Time (sec)	Shear rate (1/sec)	Shear stress (Pa)	Viscosity (mPa-s)	Time (sec)	Shear rate (1/sec)	Shear stress (Pa)	Viscosity (mPa-s)	Time (sec)	Shear rate (1/sec)	Shear stress (Pa)	Viscosity (mPa-s)
1746	1020.76	18.08	17.71	3741	1021.18	17.84	17.46	5861	1021.19	16.63	16.28
1806	510.52	10.69	20.93	3801	510.71	10.74	21.03	5921	510.56	9.97	19.52
1866	340.30	8.22	24.15	3861	340.34	8.29	24.34	5981	340.34	7.65	22.45
1926	170.12	5.48	32.18	3921	170.15	5.55	32.60	6041	170.19	5.08	29.82
1986	9.97	1.65	165.11	3981	10.01	1.62	162.06	6101	9.95	1.27	127.67
2046	5.09	1.52	298.35	4041	4.87	1.37	282.38	6161	4.97	1.06	213.42

Rheometer test @54°C				Rheometer test @60°C				Rheometer test @66°C			
Time (sec)	Shear rate (1/sec)	Shear stress (Pa)	Viscosity (mPa-s)	Time (sec)	Shear rate (1/sec)	Shear stress (Pa)	Viscosity (mPa-s)	Time (sec)	Shear rate (1/sec)	Shear stress (Pa)	Viscosity (mPa-s)
6940	1021.06	15.47	15.14	8081	1021.15	14.70	14.39	9108	1021.15	13.90	13.61
7000	510.76	9.24	18.09	8141	510.57	8.81	17.24	9168	510.60	8.40	16.44
7060	340.36	7.14	20.98	8201	340.42	6.86	20.14	9228	340.36	6.59	19.35
7120	170.08	4.77	28.06	8261	170.14	4.56	26.76	9288	170.08	4.45	26.17
7180	10.11	1.35	133.20	8321	10.11	1.23	121.21	9348	10.09	1.26	124.35
7240	4.88	1.18	242.40	8381	4.85	1.04	215.59	9408	4.99	1.07	215.73

Rheometer test @71°C				Rheometer test @77°C				Rheometer test @82°C			
Time (sec)	Shear rate (1/sec)	Shear stress (Pa)	Viscosity (mPa-s)	Time (sec)	Shear rate (1/sec)	Shear stress (Pa)	Viscosity (mPa-s)	Time (sec)	Shear rate (1/sec)	Shear stress (Pa)	Viscosity (mPa-s)
10047	1021.21	13.22	12.94	10985	1021.11	12.59	12.32	11951	1021.27	12.02	11.76
10107	510.60	7.93	15.53	11045	510.63	7.60	14.88	12011	510.57	7.24	14.17
10167	340.39	6.22	18.27	11105	340.34	5.89	17.29	12071	340.38	5.71	16.77
10227	170.10	4.11	24.13	11165	170.12	3.95	23.21	12131	170.08	3.85	22.62
10287	10.15	1.10	107.64	11225	10.11	1.02	100.48	12191	10.14	1.09	107.34
10347	4.92	0.95	193.20	5728	3.53	42.74	88.79	12251	4.95	0.94	190.84

Table E.5 (Continued): Rheological measurements of sepiolite drilling fluid with entrusion of 342 kg/m^3 NaCl-rheometer results.

Rheometer test @88°C				Rheometer test @93°C				Rheometer test @99°C			
Time (sec)	Shear rate (1/sec)	Shear stress (Pa)	Viscosity (mPa-s)	Time (sec)	Shear rate (1/sec)	Shear stress (Pa)	Viscosity (mPa-s)	Time (sec)	Shear rate (1/sec)	Shear stress (Pa)	Viscosity (mPa-s)
12893	1021.21	11.50	11.26	13834	1021.25	11.07	10.83	14946	1021.38	10.72	10.49
12953	510.65	6.96	13.63	13894	510.62	6.73	13.17	15006	510.67	6.59	12.90
13013	340.43	5.52	16.19	13954	340.37	5.41	15.90	15066	340.53	5.26	15.43
13073	170.14	3.71	21.78	14014	170.24	3.72	21.85	15126	170.17	3.65	21.46
13133	10.25	0.98	95.78	14074	10.15	1.10	108.64	15186	10.10	1.29	127.12
13193	4.99	0.89	177.50	14134	5.02	0.99	197.71	15246	5.01	1.29	257.83

Rheometer test @104°C				Rheometer test @110°C				Rheometer test @116°C			
Time (sec)	Shear rate (1/sec)	Shear stress (Pa)	Viscosity (mPa-s)	Time (sec)	Shear rate (1/sec)	Shear stress (Pa)	Viscosity (mPa-s)	Time (sec)	Shear rate (1/sec)	Shear stress (Pa)	Viscosity (mPa-s)
15674	1021.36	10.20	9.98	16316	1021.32	9.98	9.77	16989	1021.32	9.71	9.50
15734	510.70	6.21	12.16	16376	510.70	6.12	11.99	17049	510.76	6.08	11.90
15794	340.41	4.95	14.55	16436	340.42	4.89	14.36	17109	340.50	4.92	14.45
15854	170.18	3.50	20.54	16496	170.19	3.38	19.86	17169	170.11	3.45	20.27
15914	10.16	1.12	109.94	16556	10.14	1.01	99.53	17229	10.12	1.15	113.72
15974	4.94	1.03	207.72	16616	5.01	0.96	191.11	17289	4.97	1.13	227.07

Rheometer test @121°C				Rheometer test @127°C				Rheometer test @132°C			
Time (sec)	Shear rate (1/sec)	Shear stress (Pa)	Viscosity (mPa-s)	Time (sec)	Shear rate (1/sec)	Shear stress (Pa)	Viscosity (mPa-s)	Time (sec)	Shear rate (1/sec)	Shear stress (Pa)	Viscosity (mPa-s)
17658	1021.27	9.64	9.43	18370	1021.19	9.58	9.38	19048	1021.12	9.60	9.40
17718	510.70	6.04	11.83	18430	510.72	6.02	11.79	19108	510.75	6.11	11.95
17778	340.45	4.91	14.41	18490	340.46	4.91	14.40	19168	340.48	5.07	14.89
17838	170.11	3.52	20.67	18550	170.21	3.58	21.03	19228	170.19	3.80	22.32
17898	10.07	1.29	127.77	18610	10.20	1.31	128.59	19288	10.19	1.55	151.55
17958	5.10	1.28	250.83	18670	5.11	1.33	259.73	19348	4.93	1.67	338.31

Table E.5 (Continued): Rheological measurements of sepiolite drilling fluid with entrusion of 342 kg/m^3 NaCl-rheometer results.

Rheometer test @138°C				Rheometer test @143°C				Rheometer test @149°C			
Time (sec)	Shear rate (1/sec)	Shear stress (Pa)	Viscosity (mPa-s)	Time (sec)	Shear rate (1/sec)	Shear stress (Pa)	Viscosity (mPa-s)	Time (sec)	Shear rate (1/sec)	Shear stress (Pa)	Viscosity (mPa-s)
19409	1021.46	9.84	9.63	20112	1021.45	9.71	9.50	20758	1021.19	9.98	9.77
19469	510.81	6.18	12.10	20172	510.78	6.45	12.63	20818	510.83	6.57	12.86
19529	340.46	5.08	14.91	20232	340.55	5.51	16.17	20878	340.47	5.69	16.71
19589	170.21	3.79	22.26	20292	170.22	4.38	25.75	20938	170.16	4.55	26.70
19649	10.14	1.56	153.28	20352	10.12	2.25	221.41	20998	10.16	2.37	232.23
19709	4.98	1.70	341.33	20412	4.98	2.66	533.12	21058	4.96	2.81	564.36

Rheometer test @154°C				Rheometer test @160°C				Rheometer test @166°C			
Time (sec)	Shear rate (1/sec)	Shear stress (Pa)	Viscosity (mPa-s)	Time (sec)	Shear rate (1/sec)	Shear stress (Pa)	Viscosity (mPa-s)	Time (sec)	Shear rate (1/sec)	Shear stress (Pa)	Viscosity (mPa-s)
21459	1021.37	10.14	9.92	21821	1021.20	10.26	10.04	22476	1021.23	10.49	10.26
21519	510.80	6.97	13.64	21881	510.83	6.92	13.54	22536	510.78	7.56	14.80
21579	340.42	6.18	18.14	21941	340.38	6.07	17.81	22596	340.51	6.86	20.13
21639	170.16	5.14	30.19	22001	170.18	5.08	29.85	22656	170.17	5.98	35.12
21699	10.11	3.32	327.50	22061	10.04	3.38	335.74	22716	10.14	4.83	475.84
21759	4.93	3.92	795.36	22121	4.94	4.02	814.25	22776	5.10	5.47	1072.22

Rheometer test @171°C				Rheometer test @177°C				Rheometer test @182°C			
Time (sec)	Shear rate (1/sec)	Shear stress (Pa)	Viscosity (mPa-s)	Time (sec)	Shear rate (1/sec)	Shear stress (Pa)	Viscosity (mPa-s)	Time (sec)	Shear rate (1/sec)	Shear stress (Pa)	Viscosity (mPa-s)
22837	1021.32	10.40	10.18	23496	1021.43	10.88	10.64	24121	1021.43	10.97	10.73
22897	510.81	7.27	14.22	23556	510.86	8.19	16.02	24181	510.80	8.26	16.17
22957	340.60	6.58	19.32	23616	340.49	7.57	22.22	24241	340.50	7.73	22.69
23017	170.18	5.77	33.88	23676	170.23	6.83	40.11	24301	170.16	7.05	41.39
23077	10.08	4.66	461.26	23736	10.08	6.22	615.81	24361	10.05	6.47	642.99
23137	4.95	5.43	1096.18	23796	4.92	6.77	1380.98	24421	5.02	7.02	1405.63

Table E.5 (Continued): Rheological measurements of sepiolite drilling fluid with entrusion of 342 kg/m^3 NaCl-rheometer results.

Rheometer test @188°C				Rheometer test @193°C				Rheometer test @199°C			
Time (sec)	Shear rate (1/sec)	Shear stress (Pa)	Viscosity (mPa-s)	Time (sec)	Shear rate (1/sec)	Shear stress (Pa)	Viscosity (mPa-s)	Time (sec)	Shear rate (1/sec)	Shear stress (Pa)	Viscosity (mPa-s)
24764	1021.40	11.34	11.10	25388	1021.48	11.75	11.50	26037	1021.52	12.63	12.36
24824	510.91	8.77	17.16	25448	510.85	9.19	17.97	26097	510.82	10.11	19.79
24884	340.48	8.26	24.26	25508	340.51	8.68	25.49	26157	340.50	9.73	28.55
24944	170.12	7.63	44.83	25568	170.17	8.06	47.37	26217	170.22	9.18	53.91
25004	10.15	7.30	719.16	25628	10.14	7.67	756.49	26277	10.04	8.73	868.38
25064	5.14	7.65	1487.11	25688	5.13	8.00	1557.93	26337	5.07	8.78	1729.82

Rheometer test @204°C				Rheometer test @210°C				Rheometer test @216°C			
Time (sec)	Shear rate (1/sec)	Shear stress (Pa)	Viscosity (mPa-s)	Time (sec)	Shear rate (1/sec)	Shear stress (Pa)	Viscosity (mPa-s)	Time (sec)	Shear rate (1/sec)	Shear stress (Pa)	Viscosity (mPa-s)
26662	1021.42	13.21	12.93	27324	1021.19	14.31	14.01	27985	1021.51	14.77	14.45
26722	510.89	10.43	20.40	27384	510.94	11.60	22.69	28045	510.87	11.55	22.61
26782	340.54	9.93	29.14	27444	340.53	11.10	32.59	28105	340.46	10.92	32.05
26842	170.20	9.32	54.75	27504	170.16	10.46	61.46	28165	170.15	10.14	59.54
26902	10.11	8.66	855.35	27564	10.12	9.28	916.15	28225	10.10	8.55	845.70
26962	5.00	8.80	1764.33	27624	5.11	9.21	1801.49	28285	4.87	8.37	1728.47

Rheometer test @221°C				Rheometer test @227°C				Rheometer test @232°C			
Time (sec)	Shear rate (1/sec)	Shear stress (Pa)	Viscosity (mPa-s)	Time (sec)	Shear rate (1/sec)	Shear stress (Pa)	Viscosity (mPa-s)	Time (sec)	Shear rate (1/sec)	Shear stress (Pa)	Viscosity (mPa-s)
28637	1021.51	14.78	14.46	29296	1021.44	13.51	13.22	29949	1021.58	11.68	11.43
28697	510.78	11.21	21.94	29356	510.86	10.12	19.80	30009	510.92	8.56	16.75
28757	340.56	10.35	30.37	29416	340.49	9.11	26.74	30069	340.60	7.59	22.27
28817	170.23	9.47	55.60	29476	170.21	8.02	47.07	30129	170.22	6.54	38.43
28877	10.16	7.31	718.69	29536	10.19	5.71	558.97	30189	10.11	4.18	412.20
28937	4.91	7.28	1489.53	29596	5.06	5.90	1166.76	30249	4.96	4.14	838.93

Table E.5 (Continued): Rheological measurements of sepiolite drilling fluid with entrusion of 342 kg/m^3 NaCl-rheometer results.

Rheometer test @238°C				Rheometer test @243°C				Rheometer test @249°C			
Time (sec)	Shear rate (1/sec)	Shear stress (Pa)	Viscosity (mPa-s)	Time (sec)	Shear rate (1/sec)	Shear stress (Pa)	Viscosity (mPa-s)	Time (sec)	Shear rate (1/sec)	Shear stress (Pa)	Viscosity (mPa-s)
30600	1021.56	10.20	9.98	31269	1021.64	9.18	8.98	31940	1021.18	8.63	8.45
30660	510.94	7.28	14.24	31329	510.88	6.41	12.55	32000	510.87	5.99	11.73
30720	340.60	6.40	18.78	31389	340.53	5.50	16.13	32060	340.54	5.12	15.03
30780	170.24	5.33	31.27	31449	170.29	4.52	26.51	32120	170.20	4.27	25.09
30840	10.26	3.15	306.75	31509	10.12	2.46	242.77	32180	10.12	2.32	228.97
30900	5.07	3.08	607.41	31569	4.97	2.21	447.08	32240	4.94	2.04	415.25

Rheometer test @254°C				Rheometer test @260°C			
Time (sec)	Shear rate (1/sec)	Shear stress (Pa)	Viscosity (mPa-s)	Time (sec)	Shear rate (1/sec)	Shear stress (Pa)	Viscosity (mPa-s)
32648	1021.47	8.47	8.29	33328	1021.59	8.64	8.46
32708	510.94	5.81	11.37	33388	510.95	5.92	11.59
32768	340.56	5.11	15.00	33448	340.67	5.27	15.47
32828	170.24	4.43	26.00	33508	170.31	4.75	27.88
32888	10.15	2.53	249.47	33568	10.11	2.86	282.40
32948	5.15	2.37	459.72	33628	5.14	2.72	528.45

Table E.6: Rheological measurements of sepiolite drilling fluid with entrusion of 171 kg/m^3 NaCl-rheometer results.

Rheometer test @38°C				Rheometer test @43°C				Rheometer test @49°C			
Time (sec)	Shear rate (1/sec)	Shear stress (Pa)	Viscosity (mPa-s)	Time (sec)	Shear rate (1/sec)	Shear stress (Pa)	Viscosity (mPa-s)	Time (sec)	Shear rate (1/sec)	Shear stress (Pa)	Viscosity (mPa-s)
1704	1021.17	16.15	15.81	3541	1021.49	16.10	15.75	5538	1021.28	15.20	14.88
1764	510.70	9.18	17.97	3598	510.63	9.06	17.73	5598	510.67	8.54	16.72
1824	340.53	6.84	20.07	3658	340.39	6.76	19.85	5658	340.41	6.45	18.93
1884	170.16	4.26	25.04	3718	170.14	4.12	24.21	5718	170.15	4.04	23.73
1944	10.12	1.04	102.90	3778	10.16	0.85	83.76	5778	10.05	0.99	98.80
2004	5.15	0.86	166.25	3838	4.91	0.68	138.28	5838	4.87	0.83	170.46

Rheometer test @54°C				Rheometer test @60°C				Rheometer test @66°C			
Time (sec)	Shear rate (1/sec)	Shear stress (Pa)	Viscosity (mPa-s)	Time (sec)	Shear rate (1/sec)	Shear stress (Pa)	Viscosity (mPa-s)	Time (sec)	Shear rate (1/sec)	Shear stress (Pa)	Viscosity (mPa-s)
6592	1021.02	14.10	13.81	7670	1021.16	13.37	13.08	8726	1021.36	12.66	12.39
6652	510.60	7.88	15.43	7730	510.67	7.46	14.61	8786	510.70	7.06	13.82
6712	340.39	5.90	17.31	7790	340.40	5.46	16.04	8846	340.37	5.28	15.51
6772	170.13	3.61	21.24	7850	170.11	3.39	19.89	8906	170.21	3.32	19.48
6832	10.00	0.69	69.16	7910	10.01	0.72	71.87	8966	10.08	0.62	61.24
6892	5.07	0.46	90.12	7970	5.06	0.57	113.33	9026	4.92	0.42	84.91

Rheometer test @71°C				Rheometer test @77°C				Rheometer test @82°C			
Time (sec)	Shear rate (1/sec)	Shear stress (Pa)	Viscosity (mPa-s)	Time (sec)	Shear rate (1/sec)	Shear stress (Pa)	Viscosity (mPa-s)	Time (sec)	Shear rate (1/sec)	Shear stress (Pa)	Viscosity (mPa-s)
9676	1021.33	12.03	11.77	10579	1021.34	11.50	11.25	11515	1021.33	11.11	10.87
9736	510.71	6.67	13.05	10639	510.69	6.42	12.57	11575	510.73	6.28	12.29
9796	340.43	4.99	14.66	10699	340.42	4.95	14.52	11635	340.50	4.77	14.00
9856	170.16	3.11	18.29	10759	170.21	3.17	18.59	11695	170.19	3.22	18.88
9916	10.19	0.55	54.37	10819	10.08	0.68	67.51	11755	10.12	0.91	90.29
9976	5.00	0.39	77.97	10879	5.13	0.53	104.25	11815	4.92	0.83	169.57

Table E.6 (Continued): Rheological measurements of sepiolite drilling fluid with entrusion of 171 kg/m^3 NaCl-rheometer results.

Rheometer test @88°C				Rheometer test @93°C				Rheometer test @99°C			
Time (sec)	Shear rate (1/sec)	Shear stress (Pa)	Viscosity (mPa-s)	Time (sec)	Shear rate (1/sec)	Shear stress (Pa)	Viscosity (mPa-s)	Time (sec)	Shear rate (1/sec)	Shear stress (Pa)	Viscosity (mPa-s)
12435	1021.30	10.68	10.45	13358	1021.28	10.38	10.16	14468	1021.12	10.18	9.97
12495	510.72	6.01	11.76	13418	510.75	5.87	11.49	14528	510.82	5.84	11.43
12555	340.55	4.52	13.27	13478	340.46	4.52	13.26	14588	340.39	4.57	13.42
12615	170.16	2.87	16.88	13538	170.11	2.95	17.32	14648	170.17	3.08	18.11
12675	10.12	0.47	45.98	13598	10.14	0.61	60.35	14708	10.10	0.85	84.27
12735	4.98	0.36	72.00	13658	4.85	0.51	104.36	14768	5.02	0.75	150.70

Rheometer test @104°C				Rheometer test @110°C				Rheometer test @116°C			
Time (sec)	Shear rate (1/sec)	Shear stress (Pa)	Viscosity (mPa-s)	Time (sec)	Shear rate (1/sec)	Shear stress (Pa)	Viscosity (mPa-s)	Time (sec)	Shear rate (1/sec)	Shear stress (Pa)	Viscosity (mPa-s)
15195	1021.35	9.76	9.55	15879	1021.35	9.62	9.42	16560	1021.38	9.31	9.11
15255	510.71	5.62	11.00	15939	510.77	5.59	10.94	16620	510.83	5.45	10.67
15315	340.42	4.41	12.96	15999	340.56	4.38	12.84	16680	340.39	4.21	12.36
15375	170.18	2.94	17.25	16059	170.16	2.92	17.14	16740	170.15	2.78	16.31
15435	10.08	0.74	73.21	16119	10.08	0.83	81.90	16800	10.13	0.63	61.81
15495	4.83	0.65	135.12	16179	4.87	0.76	155.98	16860	4.94	0.46	93.12

Rheometer test @121°C				Rheometer test @127°C				Rheometer test @132°C			
Time (sec)	Shear rate (1/sec)	Shear stress (Pa)	Viscosity (mPa-s)	Time (sec)	Shear rate (1/sec)	Shear stress (Pa)	Viscosity (mPa-s)	Time (sec)	Shear rate (1/sec)	Shear stress (Pa)	Viscosity (mPa-s)
17234	1021.33	9.20	9.01	17933	1021.44	9.07	8.87	18596	1021.18	8.94	8.75
17294	510.86	5.40	10.56	17993	510.77	5.29	10.35	18656	510.85	5.23	10.23
17354	340.42	4.23	12.42	18053	340.48	4.17	12.23	18716	340.43	4.18	12.26
17414	170.20	2.86	16.79	18113	170.18	2.86	16.82	18776	170.14	2.89	17.00
17474	10.08	0.71	70.35	18173	10.08	0.72	71.20	18836	10.16	0.77	75.43
17534	4.99	0.69	138.69	18233	5.11	0.69	134.22	18896	4.92	0.73	147.54

Table E.6 (Continued): Rheological measurements of sepiolite drilling fluid with entrusion of 171 kg/m^3 NaCl-rheometer results.

Rheometer test @138°C				Rheometer test @143°C				Rheometer test @149°C			
Time (sec)	Shear rate (1/sec)	Shear stress (Pa)	Viscosity (mPa-s)	Time (sec)	Shear rate (1/sec)	Shear stress (Pa)	Viscosity (mPa-s)	Time (sec)	Shear rate (1/sec)	Shear stress (Pa)	Viscosity (mPa-s)
18958	1021.47	9.14	8.95	19642	1021.27	8.81	8.63	20004	1021.40	9.09	8.89
19018	510.76	5.38	10.54	19702	510.75	5.36	10.49	20064	510.78	5.44	10.65
19077	340.50	4.23	12.43	19762	340.46	4.39	12.90	20124	340.51	4.37	12.83
19138	170.09	2.96	17.40	19822	170.19	3.19	18.74	20184	170.20	3.10	18.22
19198	10.11	0.88	86.97	19882	10.02	1.06	104.98	20244	10.11	0.99	97.92
19257	4.87	0.90	183.66	19942	5.07	1.19	234.11	20304	4.92	1.13	230.18

Rheometer test @154°C				Rheometer test @160°C				Rheometer test @166°C			
Time (sec)	Shear rate (1/sec)	Shear stress (Pa)	Viscosity (mPa-s)	Time (sec)	Shear rate (1/sec)	Shear stress (Pa)	Viscosity (mPa-s)	Time (sec)	Shear rate (1/sec)	Shear stress (Pa)	Viscosity (mPa-s)
20687	1021.45	8.72	8.53	21048	1021.53	9.06	8.87	21710	1021.53	8.65	8.46
20747	510.89	5.36	10.50	21108	510.81	5.45	10.67	21770	510.90	5.47	10.71
20807	340.50	4.48	13.16	21168	340.49	4.44	13.04	21830	340.52	4.68	13.74
20867	170.20	3.39	19.91	21228	170.20	3.30	19.37	21890	170.21	3.71	21.80
20927	10.09	1.36	134.70	21288	10.16	1.19	116.85	21950	10.11	1.89	186.00
20987	4.95	1.70	341.97	21348	4.94	1.50	301.82	22010	5.05	2.44	481.93

Rheometer test @171°C				Rheometer test @177°C				Rheometer test @182°C			
Time (sec)	Shear rate (1/sec)	Shear stress (Pa)	Viscosity (mPa-s)	Time (sec)	Shear rate (1/sec)	Shear stress (Pa)	Viscosity (mPa-s)	Time (sec)	Shear rate (1/sec)	Shear stress (Pa)	Viscosity (mPa-s)
22072	1021.30	8.89	8.70	22734	1021.51	8.61	8.43	23381	1021.58	8.67	8.48
22132	510.76	5.49	10.74	22794	510.87	5.60	10.95	23441	510.83	5.66	11.08
22192	340.50	4.56	13.39	22854	340.50	4.88	14.33	23501	340.47	4.98	14.62
22252	170.24	3.60	21.17	22914	170.30	3.99	23.42	23561	170.17	4.14	24.32
22312	10.04	1.83	181.88	22974	10.12	2.53	248.94	23621	10.12	2.91	285.84
22372	4.87	2.34	480.03	23034	4.92	3.29	668.31	23681	5.15	3.79	735.31

Table E.6 (Continued): Rheological measurements of sepiolite drilling fluid with entrusion of 171 kg/m^3 NaCl-rheometer results.

Rheometer test @188°C				Rheometer test @193°C				Rheometer test @199°C			
Time (sec)	Shear rate (1/sec)	Shear stress (Pa)	Viscosity (mPa-s)	Time (sec)	Shear rate (1/sec)	Shear stress (Pa)	Viscosity (mPa-s)	Time (sec)	Shear rate (1/sec)	Shear stress (Pa)	Viscosity (mPa-s)
24042	1021.50	8.77	8.58	24710	1021.40	9.05	8.86	25364	1021.51	9.39	9.19
24102	510.84	6.00	11.75	24770	510.82	6.35	12.42	25424	510.87	6.84	13.38
24162	340.47	5.45	15.99	24830	340.53	5.81	17.06	25484	340.53	6.34	18.61
24222	170.22	4.70	27.58	24890	170.20	5.16	30.33	25544	170.23	5.77	33.90
24282	10.13	3.74	366.97	24950	10.08	4.58	452.63	25604	10.10	5.28	520.97
24342	4.83	4.85	1007.13	25010	4.99	5.98	1206.08	25664	4.89	6.46	1336.49

Rheometer test @204°C				Rheometer test @210°C				Rheometer test @216°C			
Time (sec)	Shear rate (1/sec)	Shear stress (Pa)	Viscosity (mPa-s)	Time (sec)	Shear rate (1/sec)	Shear stress (Pa)	Viscosity (mPa-s)	Time (sec)	Shear rate (1/sec)	Shear stress (Pa)	Viscosity (mPa-s)
26024	1021.52	9.83	9.62	26680	1021.47	10.10	9.88	27339	1021.55	9.99	9.78
26084	510.86	7.34	14.37	26740	510.87	7.57	14.81	27399	510.78	7.50	14.68
26144	340.50	7.02	20.60	26800	340.54	7.19	21.10	27459	340.54	7.05	20.68
26204	170.16	6.50	38.15	26860	170.21	6.57	38.60	27519	170.24	6.46	37.94
26264	10.05	6.11	606.25	26920	10.18	5.83	571.22	27579	10.14	5.34	524.84
26324	5.12	6.82	1333.71	26980	4.95	6.46	1316.60	27639	4.96	5.98	1219.20

Rheometer test @221°C				Rheometer test @227°C				Rheometer test @232°C			
Time (sec)	Shear rate (1/sec)	Shear stress (Pa)	Viscosity (mPa-s)	Time (sec)	Shear rate (1/sec)	Shear stress (Pa)	Viscosity (mPa-s)	Time (sec)	Shear rate (1/sec)	Shear stress (Pa)	Viscosity (mPa-s)
28008	1021.61	9.89	9.68	28654	1021.59	9.72	9.51	29310	1021.56	9.03	8.84
28068	510.82	7.45	14.57	28714	510.98	7.04	13.77	29370	510.90	6.39	12.51
28128	340.49	6.90	20.27	28774	340.52	6.37	18.71	29430	340.54	5.73	16.82
28188	170.18	6.23	36.60	28834	170.22	5.59	32.85	29490	170.23	4.84	28.41
28248	10.12	4.85	478.80	28894	10.10	4.03	398.60	29550	10.07	3.12	309.64
28308	4.86	5.13	1068.46	28954	4.86	3.87	803.67	29610	5.09	3.00	587.90

Table E.6 (Continued): Rheological measurements of sepiolite drilling fluid with entrusion of 171 kg/m^3 NaCl-rheometer results.

Rheometer test @238°C				Rheometer test @243°C				Rheometer test @249°C			
Time (sec)	Shear rate (1/sec)	Shear stress (Pa)	Viscosity (mPa-s)	Time (sec)	Shear rate (1/sec)	Shear stress (Pa)	Viscosity (mPa-s)	Time (sec)	Shear rate (1/sec)	Shear stress (Pa)	Viscosity (mPa-s)
29963	1021.45	8.40	8.22	30623	1021.53	7.83	7.66	31287	1021.46	7.38	7.22
30023	510.90	5.93	11.60	30683	510.84	5.24	10.25	31347	510.80	4.90	9.58
30083	340.54	5.08	14.92	30743	340.55	4.35	12.77	31407	340.50	4.07	11.94
30143	170.15	4.00	23.53	30803	170.26	3.29	19.30	31467	170.25	3.15	18.50
30203	10.12	2.27	224.49	30863	10.17	1.68	164.91	31527	10.10	1.73	170.88
30263	4.94	1.88	384.96	30923	4.83	1.32	277.40	31587	4.89	1.36	281.11

Rheometer test @254°C				Rheometer test @260°C			
Time (sec)	Shear rate (1/sec)	Shear stress (Pa)	Viscosity (mPa-s)	Time (sec)	Shear rate (1/sec)	Shear stress (Pa)	Viscosity (mPa-s)
31990	1021.55	7.29	7.14	33759	1021.46	8.16	7.98
32050	510.86	4.78	9.36	33819	510.94	6.99	13.67
32110	340.54	4.11	12.07	33879	340.62	6.16	18.07
32170	170.31	3.42	20.07	33939	170.22	5.60	32.90
32230	10.10	1.91	188.76	33999	10.11	1.85	182.87
32290	4.88	1.30	269.30	34059	4.92	1.12	230.93

Table E.7: Rheological measurements of weighted fresh water sepiolite drilling fluid-rheometer results.

Rheometer test @38°C				Rheometer test @43°C				Rheometer test @49°C			
Time (sec)	Shear rate (1/sec)	Shear stress (Pa)	Viscosity (mPa-s)	Time (sec)	Shear rate (1/sec)	Shear stress (Pa)	Viscosity (mPa-s)	Time (sec)	Shear rate (1/sec)	Shear stress (Pa)	Viscosity (mPa-s)
1829	1020.99	48.55	47.53	3760	1020.97	43.15	42.25	5853	1021.03	38.85	38.04
1889	510.67	30.39	59.49	3820	510.53	27.34	53.54	5913	510.61	24.59	48.14
1949	340.33	23.83	69.98	3880	340.31	21.29	62.54	5973	340.36	19.06	55.97
2009	170.14	15.66	92.02	3940	170.03	14.15	83.17	6033	170.13	12.46	73.21
2069	9.98	3.57	356.31	4000	10.03	3.21	318.99	6093	9.98	2.51	250.53
2129	4.87	2.87	595.98	4060	5.12	2.64	516.68	6153	5.10	2.05	401.16

Rheometer test @54°C				Rheometer test @60°C				Rheometer test @66°C			
Time (sec)	Shear rate (1/sec)	Shear stress (Pa)	Viscosity (mPa-s)	Time (sec)	Shear rate (1/sec)	Shear stress (Pa)	Viscosity (mPa-s)	Time (sec)	Shear rate (1/sec)	Shear stress (Pa)	Viscosity (mPa-s)
6934	1021.08	35.80	35.04	8075	1021.01	32.92	32.23	9096	1021.13	30.58	29.93
6994	510.47	22.37	43.81	8135	510.69	20.58	40.28	9156	510.57	18.91	37.03
7054	340.45	17.21	50.52	8195	340.43	15.85	46.55	9216	340.38	14.51	42.62
7114	170.08	11.32	66.50	8255	170.12	10.37	60.93	9276	170.02	9.44	55.52
7174	10.06	2.26	224.51	8315	9.92	2.04	204.64	9336	9.96	1.98	198.05
7234	4.90	1.69	345.65	8375	4.98	1.54	309.53	9396	4.79	1.51	316.47

Rheometer test @71°C				Rheometer test @77°C				Rheometer test @82°C			
Time (sec)	Shear rate (1/sec)	Shear stress (Pa)	Viscosity (mPa-s)	Time (sec)	Shear rate (1/sec)	Shear stress (Pa)	Viscosity (mPa-s)	Time (sec)	Shear rate (1/sec)	Shear stress (Pa)	Viscosity (mPa-s)
10058	1020.94	28.17	27.58	10986	1021.06	25.95	25.41	11943	1021.01	24.06	23.55
10118	510.55	17.33	33.94	11046	510.54	15.93	31.18	12003	510.55	14.69	28.76
10178	340.36	13.25	38.93	11106	340.41	12.00	35.24	12063	340.42	11.00	32.31
10238	170.08	8.59	50.46	11166	170.11	7.78	45.73	12123	170.07	7.02	41.24
10298	9.97	1.75	175.00	11226	9.95	1.56	156.63	12183	10.04	1.25	123.93
10358	4.92	1.33	270.84	11286	5.10	1.20	235.88	12243	4.89	0.89	182.11

Table E.7 (Continued): Rheological measurements of weighted fresh water sepiolite drilling fluid-rheometer results.

Rheometer test @88°C				Rheometer test @93°C				Rheometer test @99°C			
Time (sec)	Shear rate (1/sec)	Shear stress (Pa)	Viscosity (mPa-s)	Time (sec)	Shear rate (1/sec)	Shear stress (Pa)	Viscosity (mPa-s)	Time (sec)	Shear rate (1/sec)	Shear stress (Pa)	Viscosity (mPa-s)
12885	1021.15	22.18	21.72	13790	1021.09	20.42	19.99	14922	1021.42	18.62	18.23
12945	510.60	13.33	26.09	13850	510.62	12.12	23.73	14979	510.60	10.81	21.16
13005	340.36	9.98	29.32	13910	340.35	9.04	26.55	15039	340.42	8.10	23.79
13065	170.16	6.30	37.01	13970	170.09	5.82	34.19	15099	170.14	5.18	30.43
13125	9.99	1.13	112.83	14030	10.02	1.02	101.86	15159	10.08	0.94	93.53
13185	4.84	0.78	161.81	14090	5.11	0.73	142.89	15219	4.92	0.68	137.56

Rheometer test @104°C				Rheometer test @110°C				Rheometer test @116°C			
Time (sec)	Shear rate (1/sec)	Shear stress (Pa)	Viscosity (mPa-s)	Time (sec)	Shear rate (1/sec)	Shear stress (Pa)	Viscosity (mPa-s)	Time (sec)	Shear rate (1/sec)	Shear stress (Pa)	Viscosity (mPa-s)
15639	1021.26	16.83	16.47	16318	1021.29	15.28	14.95	16957	1021.34	13.88	13.59
15699	510.67	9.60	18.80	16378	510.70	8.48	16.60	17017	510.67	7.59	14.86
15759	340.44	6.98	20.49	16438	340.41	6.08	17.86	17077	340.44	5.54	16.28
15819	170.10	4.24	24.94	16498	170.24	3.65	21.45	17137	170.19	3.36	19.71
15879	10.10	0.67	65.87	16558	10.16	0.59	58.33	17197	10.11	0.63	62.54
15939	4.94	0.46	92.65	16618	5.11	0.44	86.48	17257	4.87	0.45	92.89

Rheometer test @121°C				Rheometer test @127°C				Rheometer test @132°C			
Time (sec)	Shear rate (1/sec)	Shear stress (Pa)	Viscosity (mPa-s)	Time (sec)	Shear rate (1/sec)	Shear stress (Pa)	Viscosity (mPa-s)	Time (sec)	Shear rate (1/sec)	Shear stress (Pa)	Viscosity (mPa-s)
17623	1021.28	12.57	12.30	18322	1021.07	11.19	10.95	18999	1021.36	9.81	9.60
17683	510.68	6.75	13.21	18382	510.78	5.84	11.43	19059	510.68	4.94	9.67
17743	340.41	4.78	14.05	18442	340.41	4.04	11.86	19119	340.54	3.31	9.72
17803	170.16	2.77	16.28	18502	170.16	2.33	13.68	19179	170.14	1.80	10.59
17863	10.12	0.33	33.04	18562	10.09	0.28	27.87	19239	10.06	0.04	3.73
17923	4.89	0.16	32.53	18622	5.15	0.16	31.85	19299	4.96	-0.13	-25.99

Table E.7 (Continued): Rheological measurements of weighted fresh water sepiolite drilling fluid-rheometer results.

Rheometer test @138°C				Rheometer test @143°C				Rheometer test @149°C			
Time (sec)	Shear rate (1/sec)	Shear stress (Pa)	Viscosity (mPa-s)	Time (sec)	Shear rate (1/sec)	Shear stress (Pa)	Viscosity (mPa-s)	Time (sec)	Shear rate (1/sec)	Shear stress (Pa)	Viscosity (mPa-s)
19360	1021.39	9.20	9.00	20052	1021.28	7.90	7.74	20724	1021.36	7.20	7.04
19420	510.70	4.77	9.34	20112	510.74	3.93	7.68	20784	510.70	3.54	6.92
19480	340.49	3.25	9.54	20172	340.48	2.74	8.04	20844	340.44	2.34	6.86
19540	170.18	1.74	10.24	20232	170.17	1.57	9.21	20904	170.16	1.25	7.32
19600	10.15	0.06	6.08	20292	10.05	0.22	22.16	20964	10.18	0.08	7.49
19660	4.90	-0.07	-14.33	20352	4.91	0.13	25.51	21024	5.01	-0.01	-2.27

Rheometer test @154°C				Rheometer test @160°C				Rheometer test @166°C			
Time (sec)	Shear rate (1/sec)	Shear stress (Pa)	Viscosity (mPa-s)	Time (sec)	Shear rate (1/sec)	Shear stress (Pa)	Viscosity (mPa-s)	Time (sec)	Shear rate (1/sec)	Shear stress (Pa)	Viscosity (mPa-s)
21407	1021.31	6.41	6.27	21769	1021.39	6.18	6.05	22411	1021.34	5.37	5.26
21467	510.77	3.06	6.00	21829	510.69	3.08	6.03	22471	510.74	2.56	5.01
21527	340.50	2.00	5.88	21889	340.45	2.00	5.88	22531	340.44	1.66	4.88
21587	170.16	1.10	6.43	21949	170.24	1.08	6.34	22591	170.24	0.87	5.08
21647	10.00	0.16	15.89	22009	10.06	0.11	11.04	22651	10.07	0.04	3.74
21707	4.93	0.11	21.57	22069	5.01	0.07	14.22	22711	5.00	-0.07	-14.05

Rheometer test @171°C				Rheometer test @177°C				Rheometer test @182°C			
Time (sec)	Shear rate (1/sec)	Shear stress (Pa)	Viscosity (mPa-s)	Time (sec)	Shear rate (1/sec)	Shear stress (Pa)	Viscosity (mPa-s)	Time (sec)	Shear rate (1/sec)	Shear stress (Pa)	Viscosity (mPa-s)
22773	1021.26	5.16	5.05	23425	1021.40	4.60	4.50	24064	1021.37	4.56	4.46
22833	510.74	2.45	4.79	23485	510.75	2.11	4.13	24124	510.79	2.19	4.28
22893	340.41	1.54	4.52	23545	340.48	1.26	3.70	24184	340.54	1.46	4.29
22953	170.15	0.71	4.17	23605	170.28	0.52	3.05	24244	170.22	0.75	4.40
23013	10.12	-0.12	-12.21	23665	10.06	-0.22	-21.98	24304	10.21	-0.03	-2.99
23073	5.14	-0.13	-24.94	23725	4.92	-0.30	-61.96	24364	4.95	-0.08	-16.00

Table E.7 (Continued): Rheological measurements of weighted fresh water sepiolite drilling fluid-rheometer results.

Rheometer test @188°C				Rheometer test @193°C				Rheometer test @199°C			
Time (sec)	Shear rate (1/sec)	Shear stress (Pa)	Viscosity (mPa-s)	Time (sec)	Shear rate (1/sec)	Shear stress (Pa)	Viscosity (mPa-s)	Time (sec)	Shear rate (1/sec)	Shear stress (Pa)	Viscosity (mPa-s)
24697	1021.40	4.73	4.62	25343	1021.41	5.95	5.83	26011	1021.42	8.65	8.47
24757	510.85	2.43	4.75	25403	510.78	3.53	6.90	26071	510.86	5.90	11.55
24817	340.42	1.79	5.25	25463	340.59	3.01	8.82	26131	340.46	5.46	16.02
24877	170.21	1.13	6.63	25523	170.18	2.31	13.56	26191	170.18	4.95	29.07
24937	10.15	0.24	23.33	25583	10.15	1.45	141.97	26251	10.12	5.05	497.69
24997	5.09	0.28	54.45	25643	4.94	1.92	388.71	26311	5.12	6.25	1224.03

Rheometer test @204°C				Rheometer test @210°C				Rheometer test @216°C			
Time (sec)	Shear rate (1/sec)	Shear stress (Pa)	Viscosity (mPa-s)	Time (sec)	Shear rate (1/sec)	Shear stress (Pa)	Viscosity (mPa-s)	Time (sec)	Shear rate (1/sec)	Shear stress (Pa)	Viscosity (mPa-s)
26669	1021.48	11.54	11.29	27326	1021.43	13.40	13.11	27974	1021.29	13.48	13.20
26729	510.83	8.30	16.24	27386	510.85	10.29	20.13	28034	510.85	10.51	20.57
26789	340.52	7.72	22.66	27446	340.56	9.76	28.63	28094	340.50	9.49	27.87
26849	170.26	7.34	43.08	27506	170.23	9.33	54.77	28154	170.28	9.26	54.38
26909	10.17	9.31	913.50	27566	10.07	13.06	1296.36	28214	10.13	13.53	1334.02
26969	5.18	9.14	1766.97	27626	5.17	11.94	2310.28	28274	4.96	10.05	2060.33

Rheometer test @221°C				Rheometer test @227°C				Rheometer test @232°C			
Time (sec)	Shear rate (1/sec)	Shear stress (Pa)	Viscosity (mPa-s)	Time (sec)	Shear rate (1/sec)	Shear stress (Pa)	Viscosity (mPa-s)	Time (sec)	Shear rate (1/sec)	Shear stress (Pa)	Viscosity (mPa-s)
28637	1021.46	13.42	13.13	29302	1021.23	12.90	12.63	29954	1021.54	12.25	11.99
28697	510.87	10.24	20.03	29362	510.81	9.68	18.94	30014	510.78	8.49	16.62
28757	340.51	9.29	27.28	29422	340.44	8.79	25.80	30074	340.50	7.40	21.71
28817	170.16	9.18	53.93	29482	170.19	8.44	49.57	30134	170.26	6.42	37.67
28877	10.10	13.54	1338.85	29542	10.11	12.65	1249.25	30194	10.05	7.67	761.76
28937	4.89	9.92	2047.62	29602	4.91	9.61	1983.51	30254	5.09	8.26	1620.64

Table E.7 (Continued): Rheological measurements of weighted fresh water sepiolite drilling fluid-rheometer results.

Rheometer test @238°C				Rheometer test @243°C				Rheometer test @249°C			
Time (sec)	Shear rate (1/sec)	Shear stress (Pa)	Viscosity (mPa-s)	Time (sec)	Shear rate (1/sec)	Shear stress (Pa)	Viscosity (mPa-s)	Time (sec)	Shear rate (1/sec)	Shear stress (Pa)	Viscosity (mPa-s)
30629	1021.52	12.73	12.46	31286	1021.50	16.42	16.07	31953	1021.51	22.27	21.79
30689	510.84	8.35	16.33	31346	510.82	13.28	26.00	32013	510.83	16.28	31.85
30749	340.52	7.36	21.61	31406	340.51	12.62	37.04	32073	340.60	14.26	41.85
30809	170.16	6.12	35.98	31466	170.23	11.38	66.82	32133	170.23	12.28	72.08
30869	10.13	5.16	507.47	31526	10.02	6.83	679.81	32193	10.13	5.01	494.99
30929	4.87	5.73	1179.11	31586	5.12	5.34	1045.22	32253	4.91	3.03	624.28

Rheometer test @254°C				Rheometer test @260°C			
Time (sec)	Shear rate (1/sec)	Shear stress (Pa)	Viscosity (mPa-s)	Time (sec)	Shear rate (1/sec)	Shear stress (Pa)	Viscosity (mPa-s)
32656	1021.44	17.62	17.24	33359	1021.26	14.60	14.29
32716	510.79	12.48	24.43	33419	510.92	10.37	20.30
32776	340.51	10.81	31.74	33479	340.56	9.07	26.63
32836	170.23	8.88	52.13	33539	170.22	7.30	42.86
32896	10.04	3.48	346.82	33599	10.08	3.12	309.26
32956	4.91	2.78	569.49	33659	5.10	3.21	629.09

Appendix F: Rheological constant of model parameters.

Table F.1: Rheological parameter for sepiolite clay with fresh water suspension – viscometer results.

		sepiolite clay with fresh water suspesion - Viscometer								
		Temperature, °C								
Model	**Parameter**	**27**	**38**	**66**	**93**	**121**	**149**	**177**	**204**	**232**
Bingham Plastic	μp (mPa-s)	10.5524	9.8578	7.9993	6.9599	5.5708	4.3005	2.8515	2.6762	3.4972
	τy (Pa)	9.3261	8.4591	5.9444	6.2126	6.4378	5.9348	3.6212	6.4905	22.8196
	SSE	39.0900	34.3000	20.1600	10.1200	4.3460	0.9640	0.9671	1.2660	10.4500
	R^2	0.9023	0.9018	0.9114	0.9394	0.9678	0.9842	0.9646	0.9483	0.7913
	Adjusted R^2	0.8778	0.8773	0.8893	0.9243	0.9598	0.9802	0.9558	0.9353	0.7391
	RMSE	3.1260	2.9280	2.2450	1.5910	0.9146	0.4909	0.4617	0.5626	1.6170
Power Law	n	0.1704	0.1746	0.1964	0.1636	0.1258	0.1015	0.0944	0.0534	0.0173
	K (mPa-s^n)	5513.290	4933.700	3219.359	3796.554	4489.667	4514.096	2902.261	5738.420	22144.170
	SSE	13.0700	11.5500	7.1410	10.1200	11.8000	11.9500	11.5000	9.9160	32.9200
	R^2	0.9673	0.9669	0.9686	0.9395	0.8865	0.8038	0.5791	0.5949	0.3429
	Adjusted R^2	0.9592	0.9587	0.9608	0.9244	0.8582	0.7547	0.4739	0.4936	0.1786
	RMSE	1.8070	1.6990	1.3360	1.5900	1.7170	1.7290	1.6960	1.5740	2.8690
Herschel Bulkley	n	0.4433	0.4442	0.4642	0.5469	0.6642	0.8501	1.3410	1.1310	4.3920
	K (mPa-s^n)	562.8250	522.1100	364.1837	171.4820	58.9649	12.2385	0.2687	1.0811	0.0000
	τo (Pa)	6.8210	6.1264	4.2008	5.1349	5.9061	5.7911	3.7645	6.5527	23.3656
	SSE	0.4411	1.0540	0.2184	0.3557	0.0806	0.6436	0.4083	1.1740	0.8279
	R^2	0.9989	0.9970	0.9990	0.9979	0.9992	0.9894	0.9851	0.9520	0.9835
	Adjusted R^2	0.9982	0.9950	0.9984	0.9965	0.9987	0.9824	0.9751	0.9201	0.9725
	RMSE	0.3835	0.5928	0.2698	0.3443	0.1639	0.4632	0.3689	0.6259	0.5253
Best fit model		Herschel Bulkley	Herschel Bulkley	Herschel Bulkley	Herschel Bulkley	Herschel Bulkley	Herschel Bulkley	Herschel Bulkley	Herschel Bulkley	Herschel Bulkley

Table F.2: Rheological parameter for unweighted fresh water sepiolite mud – viscometer results.

		Unweighted fresh water sepiolite mud- Viscometer								
		Temperature, °C								
Model	**Parameter**	**27**	**38**	**66**	**93**	**121**	**149**	**177**	**204**	**232**
Bingham Plastic	μp (mPa-s)	34.5599	33.5204	32.8211	27.8299	21.4592	17.9817	18.4367	21.3347	22.7238
	τy (Pa)	4.9050	3.9858	4.1410	3.5556	2.9344	1.9989	2.4381	3.6562	4.9672
	SSE	150.4000	102.4000	111.4000	100.0000	47.1700	22.2200	46.6700	60.0900	82.9700
	R^2	0.9626	0.9726	0.9691	0.9617	0.9694	0.9792	0.9594	0.9609	0.9528
	Adjusted R^2	0.9532	0.9658	0.9613	0.9521	0.9617	0.9741	0.9492	0.9511	0.9410
	RMSE	6.1320	5.0610	5.2780	5.0010	3.4340	2.3570	3.4160	3.8760	4.5540
Power Law	n	0.5881	0.6360	0.6183	0.6053	0.6047	0.6627	0.5976	0.5454	0.4799
	K (mPa-s^n)	638.5070	439.5304	518.1822	451.7449	353.2146	195.8152	316.5711	539.8330	929.7390
	SSE	5.8390	5.3130	5.3430	1.1670	3.7220	2.9840	0.7106	5.6380	12.1600
	R^2	0.9985	0.9986	0.9985	0.9996	0.9976	0.9972	0.9994	0.9963	0.9931
	Adjusted R^2	0.9982	0.9982	0.9981	0.9994	0.9970	0.9965	0.9992	0.9954	0.9913
	RMSE	1.2080	1.1530	1.1560	0.5402	0.9646	0.8637	0.4215	1.1870	1.7430
Herschel Bulkley	n	0.6356	0.6830	0.6633	0.6287	0.6668	0.7271	0.6225	0.6256	0.5917
	K (mPa-s^n)	448.4398	310.0567	349.3347	379.4638	222.7829	124.3005	263.0189	297.5548	404.4197
	τo (Pa)	1.1745	1.0500	1.0035	0.4643	0.9125	0.7022	0.3320	1.2540	2.0233
	SSE	0.4470	0.3040	1.0550	0.3172	0.2055	0.5234	0.2824	0.1424	0.8730
	R^2	0.9999	0.9999	0.9997	0.9999	0.9999	0.9995	0.9998	0.9999	0.9995
	Adjusted R^2	0.9998	0.9999	0.9995	0.9998	0.9998	0.9992	0.9996	0.9998	0.9992
	RMSE	0.3860	0.3183	0.5929	0.3252	0.2617	0.4177	0.3068	0.2179	0.5394
Best fit model		Herschel Bulkley	Herschel Bulkley	Herschel Bulkley	Herschel Bulkley	Herschel Bulkley	Herschel Bulkley	Herschel Bulkley	Herschel Bulkley	Herschel Bulkley

Table F.3: Rheological parameter for semi-saturated sepiolite drilling fluid – viscometer results.

		Semi-saturated sepiolite mud - Viscometer								
		Temperature, °C								
Model	**Parameter**	**27**	**38**	**66**	**93**	**121**	**149**	**177**	**204**	**232**
Bingham Plastic	μp (mPa-s)	11.2517	11.2517	10.3225	9.2782	6.7300	6.6102	5.5660	8.4639	10.4326
	τy (Pa)	0.9005	0.9005	0.9642	0.8114	0.7516	0.5370	0.5552	1.2622	2.2858
	SSE	1.8310	1.8310	2.7230	0.7995	0.6501	0.6733	0.3082	2.4580	2.6610
	R^2	0.9956	0.9956	0.9922	0.9971	0.9956	0.9953	0.9969	0.9895	0.9925
	Adjusted R^2	0.9944	0.9944	0.9902	0.9964	0.9945	0.9941	0.9962	0.9869	0.9906
	RMSE	0.6766	0.6766	0.8251	0.4471	0.4031	0.4103	0.2776	0.7840	0.8157
Power Law	n	0.7831	0.7831	0.7384	0.7861	0.7626	0.7883	0.7512	0.6298	0.5227
	K (mPa-s^n)	53.0732	53.0732	66.5810	43.3208	37.8171	30.1866	33.2713	119.6063	321.2174
	SSE	3.3420	3.3420	2.8240	3.4560	4.1990	1.3600	1.2090	4.5230	17.6800
	R^2	0.9919	0.9919	0.9919	0.9877	0.9715	0.9904	0.9880	0.9807	0.9503
	Adjusted R^2	0.9899	0.9899	0.9899	0.9846	0.9644	0.9881	0.9850	0.9759	0.9379
	RMSE	0.9141	0.9141	0.8404	0.9295	1.0250	0.5830	0.5498	1.0630	2.1020
Herschel Bulkley	n	0.8912	0.8912	0.8427	0.9278	0.9866	0.8987	0.8933	0.8110	0.8472
	K (mPa-s^n)	24.0123	24.0123	30.9338	15.3472	7.3910	13.3928	11.7068	31.6763	30.2920
	τo (Pa)	0.6375	0.6375	0.5973	0.6725	0.7338	0.3942	0.4280	0.8876	1.9275
	SSE	0.7409	0.7409	0.6866	0.4803	0.6447	0.3250	0.0388	0.4677	0.7680
	R^2	0.9982	0.9982	0.9980	0.9983	0.9956	0.9977	0.9996	0.9980	0.9978
	Adjusted R^2	0.9970	0.9970	0.9967	0.9971	0.9270	0.9962	0.9994	0.9970	0.9964
	RMSE	0.4970	0.4970	0.4784	0.4001	0.4636	0.3291	0.1138	0.3948	0.5060
Best fit model		Herschel Bulkley	Herschel Bulkley	Herschel Bulkley	Herschel Bulkley	Herschel Bulkley	Herschel Bulkley	Herschel Bulkley	Herschel Bulkley	Herschel Bulkley

Table F.4: Rheological parameter for fully-saturated sepiolite drilling fluid – viscometer results.

		Fully-saturated sepiolite mud - Viscometer								
		Temperature, °C								
Model	**Parameter**	**27**	**38**	**66**	**93**	**121**	**149**	**177**	**204**	**232**
Bingham Plastic	μp (mPa-s)	10.3464	10.3464	9.0675	8.3681	6.8545	6.3947	4.9960	7.8987	9.6471
	τy (Pa)	0.7947	0.7947	0.9781	0.7056	0.8842	0.6160	0.5858	1.2080	1.8863
	SSE	0.9800	0.9800	0.0198	0.6002	1.7210	1.1500	0.5095	1.9430	2.2290
	R^2	0.9972	0.9972	0.9999	0.9974	0.9888	0.9914	0.9937	0.9905	0.9927
	Adjusted R^2	0.9965	0.9965	0.9999	0.9967	0.9860	0.9893	0.9922	0.9881	0.9908
	RMSE	0.4950	0.4950	0.0703	0.3874	0.6559	0.5362	0.3569	0.6970	0.7466
Power Law	n	0.8072	0.8072	0.7746	0.8168	0.6730	0.8333	0.7111	0.6379	0.5814
	K (mPa-s^n)	41.4335	41.4335	46.8510	31.7433	71.1794	22.0771	39.7618	106.1943	196.9169
	SSE	3.3190	3.3190	6.1670	3.6780	2.5800	4.5160	1.4870	6.2350	18.7700
	R^2	0.9905	0.9905	0.9769	0.9838	0.9821	0.9662	0.9817	0.9695	0.9382
	Adjusted R^2	0.9881	0.9881	0.9711	0.9798	0.9776	0.9578	0.9772	0.9618	0.9228
	RMSE	0.9109	0.9109	1.2420	0.6588	0.8304	1.0630	0.6098	1.2490	2.1660
Herschel Bulkley	n	0.9273	0.9273	0.9852	0.9762	0.8296	1.0560	0.8800	0.8658	0.9436
	K (mPa-s^n)	17.1578	17.1578	10.0494	9.8770	22.5274	4.3321	11.5295	20.1324	14.2838
	τo (Pa)	0.6390	0.6390	0.9518	0.6658	0.6160	0.6821	0.4554	0.9743	1.7752
	SSE	0.5713	0.5713	0.0074	0.5723	0.6272	1.0630	0.2447	1.1460	2.0350
	R^2	0.9984	0.9984	1.0000	0.9975	0.9959	0.9921	0.9970	0.9944	0.9933
	Adjusted R^2	0.9973	0.9973	1.0000	0.9958	0.9932	0.9868	0.9950	0.9906	0.9888
	RMSE	0.4364	0.4364	0.0496	0.4368	0.4573	0.5951	0.2856	0.6180	0.8236
Best fit model		Herschel Bulkley	Herschel Bulkley	Herschel Bulkley	Herschel Bulkley	Herschel Bulkley	Herschel Bulkley	Herschel Bulkley	Herschel Bulkley	Herschel Bulkley

Table F.5: Rheological parameter for sepiolite drilling fluid with intrusion of 171 kg/m^3 NaCl – viscometer results.

		Sepiolite mud with 171 kg/m³ NaCl - Viscometer								
		Temperature, °C								
Model	**Parameter**	**27**	**38**	**66**	**93**	**121**	**149**	**177**	**204**	**232**
Bingham Plastic	μp (mPa-s)	13.0049	13.0049	12.8899	12.8899	12.6552	9.9872	9.5273	9.9824	11.9558
	τy (Pa)	1.5855	1.5855	1.8806	1.8806	1.5342	1.3426	1.1601	2.1972	2.9664
	SSE	10.6500	10.6500	14.0700	14.0700	10.7200	3.7830	1.0730	14.1000	17.8900
	R^2	0.9809	0.9809	0.9745	0.9745	0.9798	0.9884	0.9964	0.9581	0.9628
	Adjusted R^2	0.9762	0.9762	0.9682	0.9682	0.9747	0.9855	0.9955	0.9477	0.9535
	RMSE	1.6320	1.6320	1.8750	1.8750	1.6370	0.9725	0.5179	1.8780	2.1150
Power Law	n	0.6480	0.6480	0.5998	0.5998	0.6484	0.6485	0.7042	0.4828	0.4550
	K (mPa-s^n)	157.9742	157.9742	221.3459	221.3459	153.2800	122.6719	79.7535	401.2583	593.0020
	SSE	2.9030	2.9030	3.1420	3.1420	2.1980	4.1890	5.1790	4.0240	10.4100
	R^2	0.9948	0.9948	0.9943	0.9943	0.9959	0.9872	0.9825	0.9881	0.9784
	Adjusted R^2	0.9935	0.9935	0.9929	0.9929	0.9948	0.9840	0.9781	0.9851	0.9730
	RMSE	0.8520	0.8520	0.8863	0.8863	0.7413	1.0230	1.1380	1.0030	1.6140
Herschel Bulkley	n	0.7336	0.7336	0.6950	0.6950	0.7272	0.7940	0.8825	0.6208	0.6494
	K (mPa-s^n)	83.9687	83.9687	109.4515	109.4515	85.5973	42.1328	21.6173	143.9874	140.6344
	τo (Pa)	0.6931	0.6931	0.8129	0.8129	0.6352	0.8512	0.9178	1.0514	1.7488
	SSE	0.5661	0.5661	0.2632	0.2632	0.2080	0.4346	0.1435	0.7332	1.3080
	R^2	0.9990	0.9990	0.9995	0.9995	0.9996	0.9987	0.9995	0.9978	0.9973
	Adjusted R^2	0.9983	0.9983	0.9992	0.9992	0.9993	0.9978	0.9992	0.9964	0.9955
	RMSE	0.4344	0.4344	0.2962	0.2962	0.2633	0.3806	0.2187	0.4944	0.6604
Best fit model		Herschel Bulkley	Herschel Bulkley	Herschel Bulkley	Herschel Bulkley	Herschel Bulkley	Herschel Bulkley	Herschel Bulkley	Herschel Bulkley	Herschel Bulkley

Table F.6: Rheological parameter for sepiolite drilling fluid with intrusion of 342 kg/m^3 NaCl – viscometer results.

		Sepiolite mud with 342 kg/m³ NaCl - Viscometer								
		Temperature, °C								
Model	**Parameter**	**27**	**38**	**66**	**93**	**121**	**149**	**177**	**204**	**232**
Bingham Plastic	μp (mPa-s)	15.4573	15.4573	15.5723	15.5723	14.7532	13.1294	13.5844	15.5531	18.0056
	τy (Pa)	0.9992	0.9992	1.0452	1.0452	1.2406	1.1165	1.6420	9.7429	10.9452
	SSE	10.4000	10.4000	17.2100	17.2100	6.2990	1.3250	13.6200	53.4900	39.2900
	R^2	0.9868	0.9868	0.9786	0.9786	0.9912	0.9976	0.9777	0.9361	0.9640
	Adjusted R^2	0.9834	0.9834	0.9732	0.9732	0.9889	0.9970	0.9722	0.9202	0.9549
	RMSE	1.6120	1.6120	2.0740	2.0740	1.2550	0.5754	1.8450	3.6570	3.1340
Power Law	n	0.8317	0.8317	0.8137	0.8137	0.7636	0.7848	0.6427	0.2213	0.2206
	K (mPa-s^n)	51.8278	51.8278	58.9649	58.9649	79.6577	61.6473	0.3566	4876.2200	5546.8200
	SSE	13.2900	13.2900	18.3200	18.3200	6.6020	5.2930	1.8540	38.8300	109.8000
	R^2	0.9831	0.9831	0.9772	0.9772	0.9907	0.9906	0.9970	0.9536	0.8993
	Adjusted R^2	0.9788	0.9788	0.9715	0.9715	0.9884	0.9882	0.9962	0.9420	0.8741
	RMSE	1.8230	1.8230	2.1400	2.1400	1.2850	1.1500	0.6808	3.1160	5.2390
Herschel Bulkley	n	0.9234	0.9234	0.8946	0.8946	0.8580	0.9109	0.7114	0.5416	0.6989
	K (mPa-s^n)	26.3450	26.3450	32.4666	32.4666	39.7283	24.4338	102.6976	397.5700	148.7774
	τo (Pa)	0.7530	0.7530	0.6931	0.6931	0.7736	0.8699	0.6007	7.2856	9.4746
	SSE	9.3060	9.3060	15.0100	15.0100	2.8240	0.3105	0.1384	6.1580	12.3400
	R^2	0.9881	0.9881	0.9813	0.9813	0.9960	0.9994	0.9998	0.9926	0.9887
	Adjusted R^2	0.9802	0.9802	0.9689	0.9689	0.9934	0.9991	0.9996	0.9877	0.9811
	RMSE	1.7610	1.7610	2.2370	2.2370	0.9703	0.3217	0.2148	1.4330	2.0280
Best fit model		Herschel Bulkley	Herschel Bulkley	Herschel Bulkley	Herschel Bulkley	Hersche l Bulkley	Herschel Bulkley	Herschel Bulkley	Herschel Bulkley	Herschel Bulkley

Table F.7: Rheological parameter for weighted sepiolite drilling mud – viscometer results.

		Weighted fresh water sepiolite mud - Viscometer								
		Temperature, °C								
Model	**Parameter**	**27**	**38**	**66**	**93**	**121**	**149**	**177**	**204**	**232**
Bingham Plastic	μp (mPa-s)	49.6723	48.6185	42.8370	34.6030	28.4478	24.7404	23.8159	29.1328	31.3362
	τy (Pa)	6.7156	6.7347	5.5756	3.3741	2.5037	2.2436	1.8786	5.2498	6.3659
	SSE	288.2000	286.2000	213.4000	93.6800	54.3800	22.2800	9.5510	130.5000	154.3000
	R^2	0.9652	0.9640	0.9654	0.9764	0.9797	0.9889	0.9948	0.9547	0.9538
	Adjusted R^2	0.9565	0.9550	0.9567	0.9705	0.9746	0.9861	0.9935	0.9434	0.9422
	RMSE	8.4880	8.4580	7.3050	4.8390	3.6870	2.3600	1.5450	5.7120	6.2100
Power Law	n	0.6005	0.5940	0.6075	0.6759	0.6975	0.7220	0.7726	0.5307	0.5035
	K (mPa-s^n)	839.2080	861.2420	686.8860	339.6110	239.1168	177.3737	120.3248	820.5270	1081.103
	SSE	11.3500	10.7400	5.6030	2.1260	1.0540	5.9150	8.6380	11.1500	27.9900
	R^2	0.9986	0.9987	0.9991	0.9995	0.9996	0.9971	0.9953	0.9961	0.9916
	Adjusted R^2	0.9983	0.9983	0.9989	0.9993	0.9995	0.9963	0.9942	0.9952	0.9895
	RMSE	1.6850	1.6380	1.1840	0.7291	0.5134	1.2160	1.4700	1.6690	2.6450
Herschel Bulkley	n	0.6464	0.6402	0.6462	0.7038	0.7216	0.7908	0.8582	0.6067	0.6107
	K (mPa-s^n)	596.8340	610.7250	515.4040	276.0477	199.9825	106.7212	64.0423	0.9722	487.1430
	τo (Pa)	1.5955	1.5888	1.1577	0.6232	0.4301	1.0006	1.1271	1.6918	2.5981
	SSE	1.0460	0.7532	0.1143	0.2076	0.1017	0.1994	0.5830	1.6650	6.7020
	R^2	0.9999	0.9999	1.0000	0.9999	1.0000	0.9999	0.9997	0.9994	0.9980
	Adjusted R^2	0.9998	0.9998	1.0000	0.9999	0.9999	0.9998	0.9995	0.9990	0.9967
	RMSE	0.5906	0.5011	0.1952	0.2631	0.1841	0.2578	0.4408	0.7450	1.4950
Best fit model		Herschel Bulkley	Herschel Bulkley	Herschel Bulkley	Herschel Bulkley	Herschel Bulkley	Herschel Bulkley	Herschel Bulkley	Herschel Bulkley	Herschel Bulkley

Table F.8: Rheological parameter for sepiolite clay with fresh water suspension – rheometer results.

		Sepiolite clay with fresh water suspension - Rheometer								
		Temperature, °C								
Model	**Parameter**	**38**	**43**	**49**	**54**	**60**	**66**	**71**	**77**	**82**
Bingham Plastic	μp (mPa-s)	8.9046	7.1084	5.7672	5.0918	4.4858	4.0078	3.5360	3.2198	3.1667
	τy (Pa)	8.1095	6.7826	5.7241	5.2546	4.7541	4.3033	3.9944	3.6327	3.2280
	SSE	9.3950	5.0670	1.7690	0.7748	0.3027	0.2400	0.0659	0.1579	1.4540
	R^2	0.9647	0.9700	0.9839	0.9909	0.9954	0.9954	0.9984	0.9953	0.9572
	Adjusted R^2	0.9559	0.9625	0.9798	0.9886	0.9942	0.9943	0.9980	0.9942	0.9465
	RMSE	1.5330	1.1260	0.6650	0.4401	0.2751	0.2449	0.1283	0.1987	0.6030
Power Law	n	0.1552	0.1479	0.1402	0.1331	0.1269	0.1248	0.1165	0.1177	0.1340
	K (mPa-s^n)	5154.040	4421.170	3842.538	3623.635	3366.412	3071.348	2937.707	2654.618	2225.4340
	SSE	25.5900	18.0700	15.3100	14.0100	12.5700	10.5300	9.9760	7.9330	6.2180
	R^2	0.9039	0.8929	0.8603	0.8345	0.8080	0.7987	0.7542	0.7649	0.8168
	Adjusted R^2	0.8798	0.8661	0.8254	0.7931	0.7601	0.7484	0.6927	0.7061	0.7710
	RMSE	2.5290	2.1250	1.9560	1.8720	1.7730	1.6220	1.5790	1.4080	1.2470
Herschel Bulkley	n	0.6473	0.6716	0.7538	0.8125	0.8698	0.8932	0.9897	0.9693	0.8224
	K (mPa-s^n)	106.1943	71.2752	32.3086	18.8487	11.1224	8.4352	3.7989	3.9867	10.9356
	τo (Pa)	7.1994	6.1312	5.3696	5.0295	4.6262	4.2123	3.9872	3.6131	3.0987
	SSE	0.1324	0.0512	0.0435	0.0351	0.0386	0.1017	0.0649	0.1509	1.2160
	R^2	0.9995	0.9997	0.9996	0.9996	0.9994	0.9981	0.9984	0.9955	0.9642
	Adjusted R^2	0.9992	0.9995	0.9993	0.9993	0.9990	0.9968	0.9973	0.9925	0.9403
	RMSE	0.2100	0.1306	0.1204	0.1081	0.1134	0.1841	0.1471	0.2243	0.6366
Best fit model		Herschel Bulkley	Herschel Bulkley	Herschel Bulkley	Herschel Bulkley	Herschel Bulkley	Herschel Bulkley	Herschel Bulkley	Herschel Bulkley	Herschel Bulkley

Table F.8 (Continued): Rheological parameter for sepiolite clay with fresh water suspension – rheometer results.

		Sepiolite clay with fresh water suspension - Rheometer								
		Temperature, °C								
Model	**Parameter**	**88**	**93**	**99**	**104**	**110**	**116**	**121**	**127**	**132**
Bingham Plastic	μp (mPa-s)	2.9300	2.7006	2.7547	2.6225	2.5981	2.4520	2.4611	2.3653	2.3706
	τy (Pa)	3.0292	2.8989	2.5459	2.4630	2.3279	2.3160	2.2087	2.1526	2.0841
	SSE	1.9120	0.9664	2.1080	2.8390	2.9980	2.3200	2.8090	2.3510	2.5870
	R^2	0.9357	0.9607	0.9211	0.8870	0.8795	0.8936	0.8748	0.8852	0.8756
	Adjusted R^2	0.9196	0.9509	0.9013	0.8588	0.8494	0.8670	0.8435	0.8565	0.8445
	RMSE	0.6913	0.4915	0.7259	0.8424	0.8658	0.7616	0.8380	0.7667	0.8042
Power Law	n	0.1346	0.1275	0.1484	0.1502	0.1571	0.1504	0.1593	0.1581	0.1653
	K (mPa-s^n)	2074.549	2039.582	1670.273	1594.591	1472.446	1494.480	1380.478	1347.906	1269.829
	SSE	5.1550	4.8360	4.7910	4.1030	3.9720	3.4110	3.0720	2.7270	1.9350
	R^2	0.8266	0.8033	0.8206	0.8367	0.8404	0.8435	0.8631	0.8668	0.9070
	Adjusted R^2	0.7833	0.7542	0.7758	0.7959	0.8004	0.8044	0.8289	0.8336	0.8837
	RMSE	1.1350	1.1000	1.0940	1.0130	0.9965	0.9234	0.8764	0.8257	0.6955
Herschel Bulkley	n	0.7656	0.8522	0.7645	0.6634	0.6435	0.6609	0.5813	0.5942	0.4880
	K (mPa-s^n)	15.0885	7.5730	14.2886	27.8155	31.7529	26.4839	46.9803	41.2180	89.4772
	τo (Pa)	2.8606	2.8103	2.3869	2.2159	2.0616	2.0817	1.8825	1.8533	1.6286
	SSE	1.5460	0.8477	1.7850	2.2170	2.3110	1.7680	1.9380	1.5870	1.2770
	R^2	0.9480	0.9655	0.9332	0.9118	0.9071	0.9189	0.9136	0.9225	0.9386
	Adjusted R^2	0.9133	0.9425	0.8886	0.8530	0.8452	0.8648	0.8561	0.8709	0.8977
	RMSE	0.7178	0.5316	0.7714	0.8596	0.8777	0.7678	0.8037	0.7272	0.6524
Best fit model		Herschel Bulkley	Herschel Bulkley	Herschel Bulkley	Herschel Bulkley	Herschel Bulkley	Herschel Bulkley	Herschel Bulkley	Herschel Bulkley	Herschel Bulkley

Table F.8 (Continued): Rheological parameter for sepiolite clay with fresh water suspension – rheometer results.

		Sepiolite clay with fresh water suspension - Rheometer								
		Temperature, °C								
Model	**Parameter**	**138**	**143**	**149**	**154**	**160**	**166**	**171**	**177**	**182**
Bingham Plastic	μp (mPa-s)	2.3351	2.3481	2.3557	2.4266	2.4745	2.5617	2.6086	2.7083	2.7849
	τy (Pa)	2.0717	2.0501	2.0166	1.9922	1.9759	2.0017	1.9926	2.0731	2.0793
	SSE	2.4170	2.9000	2.6970	3.6730	4.1790	5.1960	5.3470	6.8200	7.3480
	R^2	0.8796	0.8604	0.8696	0.8383	0.8260	0.8037	0.8049	0.7771	0.7738
	Adjusted R^2	0.8496	0.8255	0.8370	0.7979	0.7825	0.7546	0.7561	0.7214	0.7173
	RMSE	0.7773	0.8514	0.8212	0.9589	1.0220	1.1400	1.1560	1.3060	1.3550
Power Law	n	0.1640	0.1717	0.1751	0.1863	0.1904	0.1976	0.2017	0.2036	0.2078
	K (mPa-s^n)	1266.955	1209.954	1174.987	1107.448	1084.935	1064.338	1043.262	1075.834	1062.901
	SSE	2.0470	1.1630	0.9244	0.4889	0.5264	0.2657	0.3132	0.2327	0.2284
	R^2	0.8981	0.9440	0.9553	0.9785	0.9781	0.9900	0.9886	0.9924	0.9930
	Adjusted R^2	0.8726	0.9300	0.9441	0.9731	0.9726	0.9875	0.9857	0.9905	0.9912
	RMSE	0.7153	0.5393	0.4807	0.3496	0.3628	0.2577	0.2798	0.2412	0.2389
Herschel Bulkley	n	0.5152	0.3824	0.3841	0.2785	0.2506	0.1976	0.2017	0.2036	0.2078
	K (mPa-s^n)	72.2332	197.9228	196.1984	478.904	621.263	1064.338	1043.262	1075.834	1062.901
	τo (Pa)	1.6669	1.3484	1.314855	0.8052	0.5829	0.0000	0.0000	0.0000	0.0000
	SSE	1.3020	0.8712	0.6238	0.4230	0.4972	0.2657	0.3132	0.2327	0.2284
	R^2	0.9352	0.9581	0.9698	0.9814	0.9793	0.9900	0.9886	0.9924	0.9930
	Adjusted R^2	0.8919	0.9301	0.9497	0.9690	0.9655	0.9875	0.9857	0.9905	0.9912
	RMSE	0.6588	0.5389	0.4560	0.3755	0.4071	0.2577	0.2798	0.2412	0.2389
Best fit model		Herschel Bulkley	Herschel Bulkley	Herschel Bulkley	Herschel Bulkley	Herschel Bulkley	Power Law	Power Law	Power Law	Power Law

Table F.8 (Continued): Rheological parameter for sepiolite clay with fresh water suspension – rheometer results.

		Sepiolite clay with fresh water suspension - Rheometer								
		Temperature, °C								
Model	**Parameter**	**188**	**193**	**199**	**204**	**210**	**216**	**221**	**227**	**232**
Bingham Plastic	μp (mPa-s)	2.8295	2.8726	2.8917	2.9018	2.8668	2.8960	2.8055	2.7758	2.7231
	τy (Pa)	2.1105	2.1680	2.1723	2.1502	2.1814	2.1723	2.1387	2.0693	2.0003
	SSE	7.8020	7.8810	7.9820	7.5930	7.2860	6.8670	6.1700	5.8640	5.2170
	R^2	0.7687	0.7724	0.7725	0.7824	0.7852	0.7983	0.8052	0.8099	0.8216
	Adjusted R^2	0.7109	0.7154	0.7156	0.7280	0.7315	0.7479	0.7565	0.7623	0.7770
	RMSE	1.3970	1.4040	1.4130	1.3780	1.3500	1.3100	1.2420	1.2110	1.1420
Power Law	n	0.2094	0.2079	0.2087	0.2089	0.2048	0.2063	0.2039	0.2059	0.2072
	K (mPa-s^n)	1069.607	1103.137	1102.179	1094.994	1126.129	1116.549	1106.969	1067.212	1029.371
	SSE	0.2270	0.1565	0.1465	0.1324	0.1184	0.0909	0.0967	0.1350	0.1584
	R^2	0.9933	0.9955	0.9958	0.9962	0.9965	0.9973	0.9969	0.9956	0.9946
	Adjusted R^2	0.9916	0.9943	0.9948	0.9953	0.9956	0.9967	0.9962	0.9945	0.9932
	RMSE	0.2382	0.1978	0.1914	0.1819	0.1720	0.1508	0.1555	0.1837	0.1990
Herschel Bulkley	n	0.2094	0.2079	0.2087	0.2089	0.2048	0.2063	0.2194	0.2347	0.2600
	K (mPa-s^n)	1069.607	1103.137	1102.179	1094.994	1126.129	1116.549	955.605	817.653	638.507
	τo (Pa)	0.0000	0.0000	0.0000	0.0000	0.0000	0.0000	0.1900	0.3171	0.5082
	SSE	0.2270	0.1565	0.1465	0.1324	0.1184	0.0909	0.0935	0.1243	0.1235
	R^2	0.9933	0.9955	0.9958	0.9962	0.9965	0.9973	0.9970	0.9960	0.9958
	Adjusted R^2	0.9916	0.9943	0.9948	0.9953	0.9956	0.9967	0.9951	0.9933	0.9930
	RMSE	0.2382	0.1978	0.1914	0.1819	0.1720	0.1508	0.1766	0.2035	0.2029
Best fit model		Power Law	Power Law	Power Law	Power Law	Power Law	Power Law	Herschel Bulkley	Herschel Bulkley	Herschel Bulkley

Table F.8 (Continued): Rheological parameter for sepiolite clay with fresh water suspension – rheometer results.

		Sepiolite clay with fresh water suspension - Rheometer				
		Temperature, °C				
Model	**Parameter**	**238**	**243**	**249**	**254**	**260**
Bingham Plastic	μp (mPa-s)	2.4175	2.3778	2.3591	2.4348	2.5804
	τy (Pa)	2.1430	2.0961	2.0314	1.9491	1.4571
	SSE	3.9420	3.7760	3.7560	3.7760	5.6430
	R^2	0.7966	0.7983	0.7965	0.8058	0.7928
	Adjusted R^2	0.7288	0.7310	0.7287	0.7410	0.7409
	RMSE	1.1460	1.1220	1.1190	1.1220	1.1880
Power Law	n	0.2273	0.2281	0.2325	0.2456	0.2577
	K (mPa-s^n)	889.5030	867.9480	826.2750	752.5090	624.6160
	SSE	0.0458	0.0434	0.0664	0.0499	0.1060
	R^2	0.9976	0.9977	0.9964	0.9974	0.9961
	Adjusted R^2	0.9969	0.9969	0.9952	0.9966	0.9951
	RMSE	0.1235	0.1202	0.1488	0.1289	0.1628
Herschel Bulkley	n	0.2273	0.2281	0.2325	0.2456	0.2577
	K (mPa-s^n)	889.5030	867.9480	826.2750	752.5090	624.6160
	τo (Pa)	0.0000	0.0000	0.0000	0.0000	0.0000
	SSE	0.0458	0.0434	0.0664	0.0499	0.1060
	R^2	0.9976	0.9977	0.9964	0.9974	0.9961
	Adjusted R^2	0.9969	0.9969	0.9952	0.9966	0.9951
	RMSE	0.1235	0.1202	0.1488	0.1289	0.1628
Best fit model		Power Law	Power Law	Power Law	Power Law	Power Law

Table F.9: Rheological parameter for unweighted fresh water sepiolite mud – rheometer results.

		Unweighted fresh water sepiolite mud - Rheometer								
		Temperature, °C								
Model	**Parameter**	**38**	**43**	**49**	**54**	**60**	**66**	**71**	**77**	**82**
Bingham Plastic	μp (mPa-s)	30.8668	29.4585	27.5425	25.1236	23.4327	21.7179	20.3910	18.2020	17.8715
	τy (Pa)	2.7523	2.5535	2.330814	2.1584	1.8336	1.7503	1.5649	1.9500	1.3316
	SSE	44.4800	45.6100	36.54	33.2600	24.5300	21.4300	18.4200	11.1900	13.9400
	R^2	0.9858	0.6840	0.9853	0.9840	0.9846	0.9862	0.9865	0.9916	0.9867
	Adjusted R^2	0.9822	0.9800	0.9817	0.9800	0.9830	0.9827	0.9831	0.9895	0.9834
	RMSE	3.3350	3.3770	3.022	2.8830	2.4760	2.3150	2.1460	1.6730	1.8670
Power Law	n	0.7125	0.7110	0.7186	0.7124	0.7335	0.7282	0.7360	0.7432	0.7405
	K ($mPa\text{-}s^n$)	235.2848	225.9922	200.4615	190.8336	153.2800	147.5320	130.9586	117.1634	111.0801
	SSE	5.4420	3.2670	3.463	2.6620	2.9500	2.2020	1.7500	1.1970	1.2120
	R^2	0.9983	0.9989	0.9986	0.9987	0.9984	0.9986	0.9987	0.9991	0.9988
	Adjusted R^2	0.9978	0.9986	0.9983	0.9984	0.9980	0.9982	0.9984	0.9989	0.9986
	RMSE	1.1660	0.9037	0.9305	0.8158	0.8588	0.7419	0.6615	0.5471	0.5505
Herschel Bulkley	n	0.7644	0.7512	0.7614	0.7517	0.7723	0.7684	0.7718	0.7829	0.7731
	K ($mPa\text{-}s^n$)	160.2255	167.8895	146.1429	142.7420	115.0558	109.6431	100.5421	86.8427	87.2738
	τo (Pa)	0.9642	0.7185	0.705088	0.5968	0.5355	0.5164	0.4298	0.5116	0.3430
	SSE	0.2716	0.4531	0.7122	0.7213	1.3220	0.7070	0.6997	0.4668	0.5431
	R^2	0.9999	0.9998	0.9997	0.9997	0.9993	0.9995	0.9995	0.9970	0.9995
	Adjusted R^2	0.9999	0.9997	0.9995	0.9994	0.9988	0.9992	0.9991	0.9994	0.9991
	RMSE	0.3009	0.3886	0.4872	0.4903	0.6637	0.4855	0.4830	0.3945	0.4255
Best fit model		Herschel Bulkley	Herschel Bulkley	Herschel Bulkley	Herschel Bulkley	Herschel Bulkley	Herschel Bulkley	Herschel Bulkley	Herschel Bulkley	Herschel Bulkley

Table F.9 (Continued): Rheological parameter for unweighted fresh water sepiolite mud – rheometer results.

		Unweighted fresh water sepiolite mud - Rheometer								
		Temperature, °C								
Model	**Parameter**	**88**	**93**	**99**	**104**	**110**	**116**	**121**	**127**	**132**
Bingham Plastic	μp (mPa-s)	16.7123	15.3759	14.3269	13.2731	12.1522	10.8781	9.8482	8.8902	7.7311
	τy (Pa)	1.1376	1.2095	1.1189	0.5968	0.5001	0.5178	0.4448	0.2709	0.2478
	SSE	11.8600	11.2500	8.3410	5.7440	3.9780	1.8550	1.3730	0.8336	0.0062
	R^2	0.9871	0.9855	0.9876	0.9900	0.9917	0.9941	0.9947	0.9960	0.9999
	Adjusted R^2	0.9838	0.9819	0.9845	0.9875	0.9897	0.9921	0.9929	0.9947	0.9999
	RMSE	1.7220	1.6770	1.4440	1.1980	0.9973	0.7863	0.6766	0.5271	0.0556
Power Law	n	0.7530	0.7306	0.7389	0.8056	0.8208	0.8464	0.8560	0.8893	0.9419
	K (mPa-s^n)	94.8420	102.5539	90.3873	51.5404	42.4442	32.3086	27.3653	19.4043	11.9079
	SSE	0.8262	1.4650	1.5130	0.3373	0.2338	0.1356	0.2404	0.1660	0.0406
	R^2	0.9991	0.9981	0.9978	0.9994	0.9995	0.9996	0.9991	0.9992	0.9996
	Adjusted R^2	0.9989	0.9976	0.9972	0.9993	0.9994	0.9994	0.9988	0.9989	0.9994
	RMSE	0.4545	0.6053	0.6151	0.2904	0.2418	0.2126	0.2831	0.2353	0.1425
Herschel Bulkley	n	0.7762	0.7674	0.7843	0.8056	0.8208	0.8464	0.8560	0.8893	1.0180
	K (mPa-s^n)	79.8972	78.1728	64.6650	51.5404	42.4442	32.3086	27.3653	19.4043	6.8018
	τo (Pa)	0.2258	0.3338	0.3770	0.0000	0.0000	0.0000	0.0000	0.0000	0.3102
	SSE	0.5337	0.8395	0.6982	0.3373	0.2338	0.1356	0.2404	0.1660	0.0044
	R^2	0.9994	0.9989	0.9990	0.9994	0.9995	0.9996	0.9991	0.9992	1.0000
	Adjusted R^2	0.9990	0.9982	0.9989	0.9993	0.9994	0.9994	0.9981	0.9989	0.9999
	RMSE	0.4218	0.5290	0.4824	0.2904	0.2418	0.2126	0.3467	0.2353	0.0665
Best fit model		Herschel Bulkley	Herschel Bulkley	Herschel Bulkley	Power Law	Power Law	Power Law	Power Law	Power Law	Herschel Bulkley

Table F.9 (Continued): Rheological parameter for unweighted fresh water sepiolite mud – rheometer results.

		Unweighted fresh water sepiolite mud - Rheometer								
		Temperature, °C								
Model	**Parameter**	**138**	**143**	**149**	**154**	**160**	**166**	**171**	**177**	**182**
Bingham Plastic	μp (mPa-s)	7.0365	6.3851	5.9013	5.3504	5.0630	4.6027	4.3728	3.9484	3.6758
	τy (Pa)	0.2414	0.0412	-0.0128	-0.1492	-0.0845	-0.1948	-0.2619	-0.1688	-0.1335
	SSE	0.0165	0.0174	0.0042	0.0028	0.0112	0.0202	0.0017	0.0015	0.0017
	R^2	0.9998	0.9998	0.9999	0.9999	0.9998	0.9995	0.9999	0.9999	0.9999
	Adjusted R^2	0.9997	0.9996	0.9999	0.9999	0.9996	0.9992	0.9999	0.9999	0.9999
	RMSE	0.0909	0.0932	0.0458	0.0374	0.0749	0.1004	0.0292	0.0278	0.0292
Power Law	n	0.9394	0.9925	1.0070	1.0590	1.0310	1.1000	1.1340	1.0940	1.0790
	K (mPa-s^n)	11.0553	6.7683	5.6091	3.4656	4.0236	2.2149	1.6276	1.9797	2.0554
	SSE	0.0608	0.0230	0.0029	0.0074	0.0164	0.0001	0.0215	0.0061	0.0037
	R^2	0.9993	0.9997	1.0000	0.9999	0.9996	1.0000	0.9994	0.9998	0.9998
	Adjusted R^2	0.9990	0.9995	0.9999	0.9998	0.9994	1.0000	0.9990	0.9997	0.9998
	RMSE	0.1744	0.1072	0.0383	0.0608	0.0985	0.0058	0.1037	0.0553	0.0429
Herschel Bulkley	n	1.0390	1.0630	1.0350	1.0590	1.0310	1.1010	1.1340	1.0940	1.0790
	K (mPa-s^n)	5.2882	4.0131	4.5783	3.4656	4.0236	2.2015	1.6276	1.9797	2.0554
	τo (Pa)	0.3647	0.2188	0.0797	0.0000	0.0000	0.0017	0.0000	0.0000	0.0000
	SSE	0.0094	0.0019	0.0002	0.0074	0.0164	0.0001	0.0215	0.0061	0.0037
	R^2	0.9990	1.0000	1.0000	0.9999	0.9996	1.0000	0.9994	0.9998	0.9998
	Adjusted R^2	0.9997	0.9999	1.0000	0.9998	0.9994	1.0000	0.9990	0.9997	0.9998
	RMSE	0.0970	0.0441	0.01363	0.0608	0.0985	0.0058	0.1037	0.0553	0.0429
Best fit model		Herschel Bulkley	Herschel Bulkley	Herschel Bulkley	Power Law	Power Law	Power Law	Power Law	Power Law	Power Law

Table F.9 (Continued): Rheological parameter for unweighted fresh water sepiolite mud – rheometer results.

		Unweighted fresh water sepiolite mud - Rheometer								
		Temperature, °C								
Model	Parameter	**188**	**193**	**199**	**204**	**210**	**216**	**221**	**227**	**232**
Bingham Plastic	μp (mPa-s)	3.5403	3.6203	3.5772	4.0260	5.2690	5.7336	5.5468	5.4367	5.9827
	τy (Pa)	-0.1205	0.1703	1.3503	3.1973	4.2554	5.1109	5.5612	5.1205	3.9723
	SSE	0.0045	0.2371	0.2671	1.4400	0.6144	0.5288	0.2633	0.2504	0.0020
	R^2	0.9998	0.9932	0.9922	0.9675	0.9876	0.9910	0.9952	0.9952	1.0000
	Adjusted R^2	0.9997	0.9902	0.9895	0.6566	0.9815	0.9865	0.9928	0.9928	1.0000
	RMSE	0.0475	0.2811	0.2984	0.6929	0.5542	0.5142	0.3628	0.3539	0.0314
Power Law	n	1.0740	0.8459	0.4282	0.1920	0.3739	0.3506	0.3242	0.3383	0.4238
	K (mPa-s^n)	2.0506	10.782	238.877	1672.668	706.046	943.630	1159.659	1000.631	524.026
	SSE	0.0052	0.0402	2.8430	17.0000	3.6770	3.9850	3.2420	3.0400	1.5110
	R^2	0.9998	0.9988	0.9166	0.6158	0.9260	0.9321	0.9407	0.9421	0.9761
	Adjusted R^2	0.9996	0.9985	0.8888	0.4878	0.8891	0.8981	0.9111	0.9131	0.9642
	RMSE	0.0511	0.1157	0.9735	2.3800	1.3560	1.4120	1.2730	1.2330	0.8693
Herschel Bulkley	n	1.0740	0.8459	0.8806	1.5060	1.5380	1.4420	1.2870	1.2980	1.0170
	K (mPa-s^n)	2.0506	10.7823	8.3394	0.1169	0.1099	0.2360	0.6926	0.6275	5.2690
	τo (Pa)	0.0000	0.0000	1.2200	3.5724	5.0870	5.9109	6.1264	5.6905	4.0202
	SSE	0.0052	0.0402	0.1710	0.0691	0.0041	0.0234	0.0404	0.0223	0.0009
	R^2	0.9998	0.9988	0.9950	0.9984	0.9999	0.9996	0.9993	0.9996	1.0000
	Adjusted R^2	0.9996	0.9985	0.9900	0.9969	0.9998	0.9988	0.9978	0.9987	1.0000
	RMSE	0.0511	0.1157	0.2924	0.1858	0.0640	0.1530	0.2010	0.1492	0.0306
Best fit model		Power Law	Power Law	Herschel Bulkley	Herschel Bulkley	Herschel Bulkley	Herschel Bulkley	Herschel Bulkley	Herschel Bulkley	Herschel Bulkley

Table F.9 (Continued): Rheological parameter for unweighted fresh water sepiolite mud – rheometer results.

		Unweighted fresh water sepiolite mud - Rheometer				
		Temperature, °C				
Model	**Parameter**	**238**	**243**	**249**	**254**	**260**
Bingham Plastic	μp (mPa-s)	6.6437	8.8328	12.6312	9.1154	6.6485
	τy (Pa)	3.9527	4.8523	3.5868	2.1919	1.8499
	SSE	0.4439	17.9300	47.0100	22.9200	18.4400
	R^2	0.9962	0.9338	0.9166	0.9215	0.8860
	Adjusted R^2	0.9949	0.9172	0.8958	0.9019	0.8575
	RMSE	0.3847	2.1170	3.4280	2.3940	2.1470
Power Law	n	0.2809	0.2436	0.3998	0.4423	0.4013
	K (mPa-s^n)	1371.3770	2256.0900	934.0500	489.0590	485.7060
	SSE	21.2200	16.7400	7.6840	2.8940	1.7460
	R^2	0.8187	0.9382	0.9864	0.9901	0.9892
	Adjusted R^2	0.7583	0.9227	0.9830	0.9876	0.9865
	RMSE	2.6590	2.0460	1.3860	0.8505	0.6608
Herschel Bulkley	n	1.0280	0.5769	0.4822	0.4947	0.4013
	K (mPa-s^n)	5.4414	174.4039	499.1180	329.0251	485.7060
	τo (Pa)	4.0030	3.6533	1.0754	0.4582	0.0000
	SSE	0.4278	6.1580	6.0030	2.5160	1.7460
	R^2	0.9963	0.9773	0.9894	0.9914	0.9892
	Adjusted R^2	0.9927	0.9621	0.9823	0.9856	0.9865
	RMSE	0.4625	1.4330	1.4150	0.9159	0.6608
Best fit model		Herschel Bulkley	Herschel Bulkley	Herschel Bulkley	Herschel Bulkley	Power Law

Table F.10: Rheological parameter for semi-saturated sepiolite drilling fluid – rheometer results.

		Semi-saturated sepiolite mud - Rheometer								
		Temperature, °C								
Model	**Parameter**	**38**	**43**	**49**	**54**	**60**	**66**	**71**	**77**	**82**
Bingham Plastic	μp (mPa-s)	12.3917	11.9894	11.1751	10.3751	9.6040	8.9286	8.3586	7.8796	7.4485
	τy (Pa)	0.7736	0.6740	0.5346	0.2937	0.2457	0.2759	0.2121	0.1816	0.1408
	SSE	1.0160	1.6410	1.6100	0.8915	0.7330	0.4857	0.4265	0.4058	0.4737
	R^2	0.9980	0.9965	0.9960	0.9974	0.9970	0.9981	0.9977	0.9975	0.9974
	Adjusted R^2	0.9975	0.9956	0.9950	0.9968	0.9960	0.9977	0.9969	0.9967	0.9967
	RMSE	0.5040	0.6405	0.6345	0.4721	0.4943	0.3485	0.3770	0.3678	0.3441
Power Law	n	0.8243	0.8229	0.8379	0.8846	0.9023	0.8895	0.9081	0.9146	0.9044
	K (mPa-s^n)	43.4884	42.1376	35.1394	23.2938	0.0399	19.4714	15.9842	14.3796	14.4754
	SSE	1.9270	0.9657	0.6550	0.0830	0.0858	0.1824	0.0412	0.1057	0.0651
	R^2	0.9961	0.9979	0.9984	0.9998	0.9996	0.9993	0.9998	0.9994	0.9996
	Adjusted R^2	0.9952	0.9974	0.9980	0.9997	0.9995	0.9991	0.9997	0.9991	0.9995
	RMSE	0.6941	0.4914	0.4047	0.1441	0.1691	0.2135	0.1172	0.1877	0.1276
Herschel Bulkley	n	0.9069	0.8802	0.8794	0.8972	0.9023	0.9162	0.9081	0.9146	0.9044
	K (mPa-s^n)	23.7057	27.6431	25.8995	21.2389	0.0399	16.0034	15.9842	14.3796	14.4754
	τo (Pa)	0.5298	0.3622	0.2426	0.0666	0.0000	0.1194	0.0000	0.0000	0.0000
	SSE	0.0411	0.1008	0.2633	0.0522	0.0858	0.0826	0.0412	0.1057	0.0651
	R^2	0.9999	0.9980	0.9994	0.9999	0.9996	0.9997	0.9998	0.9994	0.9996
	Adjusted R^2	0.9999	0.9996	0.9989	0.9998	0.9995	0.9995	0.9997	0.9991	0.9995
	RMSE	0.1171	0.1833	0.2963	0.1919	0.1691	0.1659	0.1172	0.1877	0.1276
Best fit model		Herschel Bulkley	Herschel Bulkley	Herschel Bulkley	Herschel Bulkley	Power Law	Herschel Bulkley	Power Law	Power Law	Power Law

Table F.10 (Continued): Rheological parameter for semi-saturated sepiolite drilling fluid – rheometer results.

		Semi-saturated sepiolite mud - Rheometer								
		Temperature, °C								
Model	**Parameter**	**88**	**93**	**99**	**104**	**110**	**116**	**121**	**127**	**132**
Bingham Plastic	μp (mPa-s)	6.8593	6.4952	6.0306	5.7049	5.3265	5.0439	4.7900	4.6051	4.1879
	τy (Pa)	0.2609	0.2071	0.2501	0.1598	0.1861	0.1389	0.0253	-0.0604	0.0724
	SSE	0.0916	0.0214	0.0074	0.0089	0.0044	0.0075	0.0384	0.0010	0.0179
	R^2	0.9989	0.9997	0.9999	0.9998	0.9999	0.9998	0.9991	1.0000	0.9994
	Adjusted R^2	0.9984	0.9996	0.9998	0.9998	0.9999	0.9998	0.9986	1.0000	0.9991
	RMSE	0.2141	0.1034	0.0610	0.0666	0.0470	0.0610	0.1385	0.0220	0.0945
Power Law	n	0.9212	0.9362	0.9256	0.9445	0.9352	0.9514	0.9976	1.0280	0.9741
	K (mPa-s^n)	12.2289	10.3943	10.4853	8.5885	8.6172	7.2425	4.9050	3.7491	5.1014
	SSE	0.0196	0.0009	0.0388	0.0017	0.0139	0.0241	0.0413	0.0004	0.0289
	R^2	0.9998	1.0000	0.9994	1.0000	0.9997	0.9995	0.9990	1.0000	0.9991
	Adjusted R^2	0.9996	1.0000	0.9991	1.0000	0.9996	0.9992	0.9985	1.0000	0.9986
	RMSE	0.0991	0.0209	0.1393	0.0289	0.0833	0.1098	0.1437	0.0141	0.1203
Herschel Bulkley	n	0.9212	0.9362	1.0170	0.9520	0.9915	1.0390	1.0990	1.0280	1.0920
	K (mPa-s^n)	12.2289	10.3943	5.3169	8.1191	5.6714	3.7985	2.3303	3.7491	2.1325
	τo (Pa)	0.0000	0.0000	0.2978	0.0244	0.1647	0.2266	0.2255	0.0000	0.2373
	SSE	0.0196	0.0009	0.0064	0.0015	0.0042	0.0038	0.0179	0.0004	0.0040
	R^2	0.9998	1.0000	0.9999	1.0000	0.9999	0.9999	0.9996	1.0000	0.9999
	Adjusted R^2	0.9996	1.0000	0.9997	0.9999	0.9997	0.9997	0.9987	1.0000	0.9996
	RMSE	0.0991	0.0209	0.0801	0.0384	0.0650	0.0620	0.1337	0.0141	0.0634
Best fit model		Power Law	Power Law	Herschel Bulkley	Power Law	Herschel Bulkley	Herschel Bulkley	Herschel Bulkley	Power Law	Herschel Bulkley

Table F.10 (Continued): Rheological parameter for semi-saturated sepiolite drilling fluid – rheometer results.

		Semi-saturated sepiolite mud - Rheometer								
		Temperature, °C								
Model	**Parameter**	**138**	**143**	**149**	**154**	**160**	**166**	**171**	**177**	**182**
Bingham Plastic	μp (mPa-s)	4.1510	4.1783	3.7587	3.6849	3.7204	3.4229	3.5475	3.3291	3.3904
	τy (Pa)	-0.0356	-0.2359	-0.0363	-0.0570	-0.1066	0.0364	0.0056	0.1965	0.3307
	SSE	0.0041	0.0174	0.0033	0.0042	0.4948	0.0025	0.0034	0.0105	0.0166
	R^2	0.9999	0.9994	0.9999	0.9998	1.0000	0.9999	0.9998	0.9995	0.9992
	Adjusted R^2	0.9998	0.9992	0.9998	0.9997	0.9999	0.9998	0.9998	0.9992	0.9988
	RMSE	0.4502	0.0932	0.0409	0.0460	0.0227	0.0354	0.0414	0.0724	0.0910
Power Law	n	1.0210	1.1150	1.0220	1.0330	1.0570	0.9764	0.9982	0.8954	0.8398
	K (mPa-s^n)	3.5623	1.7819	3.2064	2.8936	2.4434	4.0677	3.5978	7.2473	11.2134
	SSE	0.0017	0.0707	0.0023	0.0041	0.0098	0.0009	0.0035	0.0222	0.0635
	R^2	0.9999	0.9977	0.9999	0.9998	0.9996	1.0000	0.9998	0.9989	0.9969
	Adjusted R^2	0.9999	0.9966	0.9999	0.9997	0.9994	0.9999	0.9998	0.9983	0.9953
	RMSE	0.0289	0.1880	0.0338	0.0450	0.0700	0.0215	0.0420	0.1056	0.1782
Herschel Bulkley	n	1.0460	1.1150	1.0290	1.0330	1.0570	0.9764	1.0160	0.9955	1.0400
	K (mPa-s^n)	2.9550	1.7819	3.0369	2.8936	2.4434	4.0677	3.1571	3.4407	2.5339
	τo (Pa)	0.0504	0.0000	0.0135	0.0000	0.0000	0.0000	0.0316	0.1894	0.3913
	SSE	0.0005	0.0707	0.0022	0.0041	0.0098	0.0009	0.0031	0.0105	0.0149
	R^2	1.0000	0.9977	0.9999	0.9998	0.9996	1.0000	0.9999	0.9995	0.9993
	Adjusted R^2	0.9999	0.9966	0.9997	0.9997	0.9994	0.9999	0.9996	0.9984	0.9978
	RMSE	0.0230	0.1880	0.0469	0.0450	0.0700	0.0215	0.0559	0.1023	0.1220
Best fit model		Herschel Bulkley	Power Law	Power Law	Power Law	Power Law	Power Law	Herschel Bulkley	Herschel Bulkley	Herschel Bulkley

Table F.10 (Continued): Rheological parameter for semi-saturated sepiolite drilling fluid – rheometer results.

		Semi-saturated sepiolite mud - Rheometer								
		Temperature, °C								
Model	**Parameter**	**188**	**193**	**199**	**204**	**210**	**216**	**221**	**227**	**232**
Bingham Plastic	μp (mPa-s)	3.6519	3.7357	3.8109	3.7774	4.0384	4.0600	4.1539	4.1352	4.1122
	τy (Pa)	0.3001	0.4021	0.4729	0.6610	0.5810	0.5983	0.5154	0.4232	0.3639
	SSE	0.4555	0.4860	0.4492	0.4153	0.4315	0.4346	0.4493	0.4978	0.5741
	R^2	0.9872	0.9870	0.9884	0.9891	0.9901	0.9901	0.9902	0.9891	0.9873
	Adjusted R^2	0.9830	0.9827	0.9846	0.9855	0.9868	0.9868	0.9870	0.9855	0.9831
	RMSE	0.3897	0.4025	0.3869	0.3721	0.3793	0.3806	0.3870	0.4073	0.4375
Power Law	n	0.7740	0.7362	0.7139	0.6473	0.6883	0.6836	0.7171	0.7471	0.7616
	K (mPa-s^n)	18.3457	24.8936	30.0333	49.0017	38.5978	40.1737	32.0499	25.4684	22.6232
	SSE	0.1341	0.2088	0.2410	0.5840	0.3418	0.3663	0.2642	0.1898	0.1225
	R^2	0.9962	0.9944	0.9938	0.9847	0.9921	0.9917	0.9943	0.9958	0.9973
	Adjusted R^2	0.9950	0.9925	0.9917	0.9796	0.9895	0.9889	0.9923	0.9945	0.9964
	RMSE	0.2114	0.2638	0.2834	0.4412	0.3375	0.3494	0.2967	0.2515	0.2021
Herschel Bulkley	n	0.7940	0.7961	0.8005	0.8133	0.8063	0.8064	0.8104	0.8054	0.7852
	K (mPa-s^n)	15.8118	15.9411	15.7447	14.2407	16.0082	16.0896	15.9938	16.5063	18.9636
	τo (Pa)	0.0465	0.1461	0.2188	0.4286	0.3211	0.3371	0.2550	0.1556	0.0635
	SSE	0.1281	0.1517	0.1149	0.1322	0.0746	0.0721	0.0888	0.1232	0.1114
	R^2	0.9964	0.9959	0.9970	0.9965	0.9983	0.9984	0.9981	0.9973	0.9975
	Adjusted R^2	0.9928	0.9919	0.9941	0.9931	0.9966	0.9967	0.9961	0.9946	0.9951
	RMSE	0.2530	0.2754	0.2397	0.2571	0.1931	0.1898	0.2107	0.2482	0.2361
Best fit model		Herschel Bulkley	Herschel Bulkley	Herschel Bulkley	Herschel Bulkley	Herschel Bulkley	Herschel Bulkley	Herschel Bulkley	Herschel Bulkley	Herschel Bulkley

Table F.10 (Continued): Rheological parameter for semi-saturated sepiolite drilling fluid – rheometer results.

		Semi-saturated sepiolite mud - Rheometer				
		Temperature, °C				
Model	**Parameter**	**238**	**243**	**249**	**254**	**260**
Bingham Plastic	μp (mPa-s)	4.0394	4.1223	4.1232	4.1922	4.4078
	τy (Pa)	0.4158	0.4386	0.6308	0.7975	1.0083
	SSE	0.6819	0.8056	0.6865	0.8289	0.9725
	R^2	0.9844	0.9856	0.9877	0.9857	0.9848
	Adjusted R^2	0.9792	0.9820	0.9846	0.9821	0.9810
	RMSE	0.4768	0.4488	0.4143	0.4552	0.4931
Power Law	n	0.7318	0.6858	0.6143	0.5515	0.4937
	K ($mPa\text{-}s^n$)	27.5569	38.2769	64.8087	103.7514	165.7340
	SSE	0.1053	0.2932	0.8628	1.5060	2.5950
	R^2	0.9976	0.9948	0.9845	0.9739	0.9594
	Adjusted R^2	0.9968	0.9934	0.6807	0.9674	0.9493
	RMSE	0.1874	0.2707	0.4644	0.6137	0.8055
Herschel Bulkley	n	0.7570	0.7693	0.7809	0.7718	0.7797
	K ($mPa\text{-}s^n$)	22.8244	20.6928	19.0738	20.6593	20.5539
	τo (Pa)	0.0698	0.2052	0.4121	0.5643	0.7731
	SSE	0.0927	0.0686	0.0230	0.0910	0.2377
	R^2	0.9979	0.9988	0.9996	0.9984	0.9960
	Adjusted R^2	0.9958	0.9980	0.9993	0.9974	0.9938
	RMSE	0.2153	0.1513	0.0875	0.1741	0.2815
Best fit model		Herschel Bulkley	Herschel Bulkley	Herschel Bulkley	Herschel Bulkley	Herschel Bulkley

Table F.11: Rheological parameter for fully-saturated sepiolite drilling fluid – rheometer results.

		Fully-saturated sepiolite mud - Rheometer								
		Temperature, °C								
Model	**Parameter**	**38**	**43**	**49**	**54**	**60**	**66**	**71**	**77**	**82**
Bingham Plastic	μp (mPa-s)	12.0229	11.9319	11.0745	10.0159	9.2591	8.5885	8.1238	7.6113	7.2090
	τy (Pa)	0.8838	0.3758	0.1752	0.1722	0.1146	0.0829	0.0108	0.0578	0.0099
	SSE	0.0756	0.3723	0.0049	0.0079	0.0091	0.0201	0.0429	0.0215	0.0681
	R^2	0.9998	0.9992	1.0000	1.0000	0.9999	0.9998	0.9996	0.9998	0.9993
	Adjusted R^2	0.9998	0.9990	1.0000	0.9999	0.9999	0.9998	0.9994	0.9997	0.9989
	RMSE	0.1375	0.3051	0.0496	0.6287	0.0675	0.1003	0.1465	0.1037	0.1846
Power Law	n	0.8367	0.9034	0.9686	0.9670	0.9788	0.9849	1.0040	0.9902	1.0050
	K (mPa-s^n)	39.4217	23.7488	13.9676	12.7845	10.8589	9.6327	7.9227	8.2149	7.0174
	SSE	4.8510	0.4842	0.0035	0.0163	0.0261	0.0333	0.0423	0.0312	0.0674
	R^2	0.9896	0.9990	1.0000	0.9999	0.9998	0.9997	0.9996	0.9997	0.9993
	Adjusted R^2	0.9871	0.9987	1.0000	0.9999	0.9997	0.9996	0.9995	0.9995	0.9989
	RMSE	1.1010	0.3479	0.0417	0.0902	0.1143	0.1291	0.1454	0.1249	0.1835
Herschel Bulkley	n	0.9759	0.9447	0.9821	0.9954	1.0320	1.0440	1.0800	1.0610	1.0890
	K (mPa-s^n)	14.2167	17.5314	12.6312	10.3608	7.3335	6.2318	45.1026	4.8619	3.7558
	τo (Pa)	0.8268	0.2416	0.0804	0.1503	0.2483	0.2514	0.2927	0.2631	0.2862
	SSE	0.0174	0.0649	0.0011	0.0077	0.0008	0.0067	0.0030	0.0010	0.0297
	R^2	1.0000	0.9999	1.0000	1.0000	1.0000	0.9999	1.0000	1.0000	0.9997
	Adjusted R^2	0.9999	0.9998	1.0000	0.9999	1.0000	0.9998	0.9999	1.0000	0.9990
	RMSE	0.0761	0.1470	0.0327	0.0877	0.0285	0.0818	0.0550	0.3104	0.1722
Best fit model		Herschel Bulkley	Herschel Bulkley	Herschel Bulkley	Herschel Bulkley	Herschel Bulkley	Herschel Bulkley	Herschel Bulkley	Herschel Bulkley	Herschel Bulkley

Table F.11: (Continued): Rheological parameter for fully-saturated sepiolite drilling fluid – rheometer results.

		Fully-saturated sepiolite mud - Rheometer								
		Temperature, °C								
Model	**Parameter**	**88**	**93**	**99**	**104**	**110**	**116**	**121**	**127**	**132**
Bingham Plastic	μp (mPa-s)	6.7874	6.5384	6.2174	5.8342	5.5133	5.3935	4.9864	4.7177	4.5007
	τy (Pa)	0.0330	-0.0690	-0.1239	-0.1651	-0.1583	-0.3186	-0.1874	-0.1801	-0.1949
	SSE	0.0309	0.0168	0.0043	0.0161	0.0174	0.0195	0.0146	0.0776	0.0020
	R^2	0.9996	0.9998	0.9999	0.9997	0.9997	0.9996	0.9997	0.9980	0.9999
	Adjusted R^2	0.9994	0.9997	0.9999	0.9996	0.9995	0.9994	0.9995	0.9970	0.9999
	RMSE	0.1243	0.0915	0.0463	0.0897	0.0932	0.0986	0.0855	0.1970	0.0317
Power Law	n	0.9967	1.0260	1.0430	1.0650	1.0670	1.1390	1.0860	1.0990	1.0950
	K (mPa-s^n)	6.9838	5.3983	4.5404	3.6236	3.3899	1.9558	2.6513	2.2987	2.2369
	SSE	0.0356	0.0068	0.0029	0.0001	0.0011	0.0098	0.0021	0.0243	0.0084
	R^2	0.9996	0.9999	1.0000	1.0000	1.0000	0.9998	1.0000	0.9994	0.9998
	Adjusted R^2	0.9993	0.9999	0.9999	1.0000	1.0000	0.9997	0.9999	0.9991	0.9996
	RMSE	0.1335	0.0585	0.0381	0.0077	0.0236	0.0700	0.0322	0.1101	0.0648
Herschel Bulkley	n	1.0770	1.0620	1.0430	1.0710	1.0760	1.1390	1.0860	1.1880	1.0950
	K (mPa-s^n)	3.8627	4.1625	4.5404	3.4771	3.1643	1.9558	2.6513	1.1975	2.2369
	τo (Pa)	0.2595	0.1082	0.0000	0.0148	0.0232	0.0000	0.0000	0.1659	0.0000
	SSE	0.0053	0.0014	0.0029	0.0000	0.0008	0.0098	0.0021	0.0076	0.0084
	R^2	0.9999	1.0000	1.0000	1.0000	1.0000	0.9998	1.0000	0.9998	0.9998
	Adjusted R^2	0.9998	0.9999	0.9999	1.0000	1.0000	0.9997	0.9999	0.9994	0.9996
	RMSE	0.0729	0.0377	0.0381	0.0033	0.2905	0.0700	0.0322	0.0872	0.0648
Best fit model		Herschel Bulkley	Herschel Bulkley	Herschel Bulkley	Herschel Bulkley	Herschel Bulkley	Power Law	Power Law	Herschel Bulkley	Bingham Plastic

Table F.11: (Continued): Rheological parameter for fully-saturated sepiolite drilling fluid – rheometer results.

		Fully-saturated sepiolite mud - Rheometer								
		Temperature, °C								
Model	**Parameter**	**138**	**143**	**149**	**154**	**160**	**166**	**171**	**177**	**182**
Bingham Plastic	μp (mPa-s)	4.3876	4.1041	4.0260	3.8813	3.7712	3.6064	3.5274	3.3736	3.3635
	τy (Pa)	-0.2281	-0.1591	-0.2167	-0.2804	-0.2424	-0.2885	-0.2836	-0.2187	-0.2207
	SSE	0.0030	0.0069	0.0007	0.0083	0.0013	0.0015	0.0015	0.0021	0.0014
	R^2	0.9999	0.9998	1.0000	0.9997	1.0000	0.9999	0.9999	0.9999	0.9999
	Adjusted R^2	0.9999	0.9997	1.0000	0.9995	0.9999	0.9999	0.9999	0.9998	0.9999
	RMSE	0.0388	0.0587	0.0191	0.0642	0.0251	0.0275	0.0269	0.0323	0.0262
Power Law	n	1.1140	1.0800	1.1170	1.1700	1.1450	1.1840	1.1850	1.1480	1.1410
	K (mPa-s^n)	1.8470	2.2657	1.7028	1.1137	1.2967	0.9321	0.9072	0.0024	1.1855
	SSE	0.0203	0.0212	0.0220	0.0179	0.0197	0.0387	0.0392	0.0125	0.0357
	R^2	0.9994	0.9993	0.9992	0.9993	0.9992	0.9983	0.9982	0.9994	0.9982
	Adjusted R^2	0.9991	0.9989	0.9988	0.9990	0.9988	0.9975	0.9973	0.9991	0.9973
	RMSE	0.1008	0.1029	0.1050	0.0945	0.0993	0.1391	0.1400	0.0791	0.1337
Herschel Bulkley	n	1.1140	1.0800	1.1170	1.1700	1.1450	1.1840	1.1850	1.1480	1.1410
	K (mPa-s^n)	1.8470	2.2657	1.7028	1.1137	1.2967	0.9321	0.9072	0.0024	1.1855
	τo (Pa)	0.0000	0.0000	0.0000	0.0000	0.0000	0.0000	0.0000	0.0000	0.0000
	SSE	0.0203	0.0212	0.0220	0.0179	0.0197	0.0387	0.0392	0.0125	0.0357
	R^2	0.9994	0.9993	0.9992	0.9993	0.9992	0.9983	0.9982	0.9994	0.9982
	Adjusted R^2	0.9991	0.9989	0.9988	0.9990	0.9988	0.9975	0.9973	0.9991	0.9973
	RMSE	0.1008	0.1029	0.1050	0.0945	0.0993	0.1391	0.1400	0.0791	0.1337
Best fit model		Bingham Plastic	Bingham Plastic	Bingham Plastic	Bingham Plastic	Bingham Plastic	Bingham Plastic	Bingham Plastic	Bingham Plastic	Bingham Plastic

Table F.11: (Continued): Rheological parameter for fully-saturated sepiolite drilling fluid – rheometer results.

		Fully-saturated sepiolite mud - Rheometer								
		Temperature, °C								
Model	**Parameter**	**188**	**193**	**199**	**204**	**210**	**216**	**221**	**227**	**232**
Bingham Plastic	μp (mPa-s)	3.1710	3.1638	3.2141	3.1815	3.3094	3.2160	3.3343	1.6779	3.2673
	τy (Pa)	-0.1871	-0.1249	-0.1083	0.0036	-0.05566	0.0348	-0.0083	0.2645	0.1497
	SSE	0.0071	0.0076	0.0115	0.0068	0.0053	0.0079	0.0044	0.0090	0.0069
	R^2	0.9996	0.9996	0.9994	0.9996	0.9997	0.9996	0.9998	0.9995	0.9996
	Adjusted R^2	0.9994	0.9994	0.9991	0.9994	0.9996	0.9994	0.9997	0.9992	0.9995
	RMSE	0.0595	0.0616	0.0757	0.0582	0.0517	0.0628	0.0470	0.0671	0.0587
Power Law	n	1.1280	1.0890	1.0790	0.9991	1.0370	0.9786	1.0030	0.8578	0.9181
	K (mPa-s^n)	1.2329	1.6454	1.8073	3.2069	2.5234	3.7669	3.2562	9.0004	6.0067
	SSE	0.0259	0.0052	0.0041	0.0068	0.0041	0.0080	0.0046	0.0397	0.0172
	R^2	0.9985	0.9997	0.9998	0.9996	0.9998	0.9996	0.9998	0.9977	0.9991
	Adjusted R^2	0.9978	0.9996	0.9997	0.9994	0.9997	0.9993	0.9996	0.9965	0.9986
	RMSE	0.1137	0.0509	0.0454	0.0584	0.0455	0.0633	0.0482	0.1409	0.0927
Herschel Bulkley	n	1.1280	1.0890	1.0880	1.0160	1.0370	0.9921	1.0030	1.0330	1.0150
	K (mPa-s^n)	1.2329	1.6454	1.6890	2.8366	2.5234	3.4071	3.2562	2.4439	2.9329
	τo (Pa)	0.0000	0.0000	0.0130	0.0266	0.0000	0.0229	0.0000	0.3112	0.1720
	SSE	0.0259	0.0052	0.0040	0.0065	0.0041	0.0078	0.0046	0.0080	0.0067
	R^2	0.9985	0.9997	0.9998	0.9996	0.9998	0.9993	0.9998	0.9995	0.9996
	Adjusted R^2	0.9978	0.9996	0.9993	0.9989	0.9997	0.9989	0.9996	0.9986	0.9989
	RMSE	0.1137	0.0509	0.0635	0.0808	0.0455	0.0884	0.0482	0.0895	0.0817
Best fit model		Bingham Plastic	Power Law	Power Law	Power Law	Power Law	Power Law	Power Law	Herschel Bulkley	Herschel Bulkley

Tabl Table F.11: (Continued): Rheological parameter for fully-saturated sepiolite drilling fluid – rheometer results.

		Fully-saturated sepiolite mud - Rheometer				
		Temperature, °C				
Model	**Parameter**	**238**	**243**	**249**	**254**	**260**
Bingham Plastic	μp (mPa-s)	3.4646	3.4938	3.7448	3.6811	4.4279
	τy (Pa)	0.1664	0.3123	0.4220	0.8689	0.9815
	SSE	0.3839	0.4671	0.3757	0.3778	1.0010
	R^2	0.9902	0.9883	0.9918	0.9915	0.9845
	Adjusted R^2	0.9878	0.9854	0.9898	0.9893	0.9806
	RMSE	0.3098	0.3417	0.3065	0.3073	0.5003
Power Law	n	0.8019	0.7255	0.6978	0.4925	0.5048
	K (mPa-s^n)	13.8431	24.4290	32.3660	140.4428	153.7590
	SSE	0.0300	0.1953	0.4807	2.2480	2.6380
	R^2	0.9992	0.9951	0.9895	0.9492	0.9591
	Adjusted R^2	0.9990	0.9939	0.9869	0.9366	0.9489
	RMSE	0.0867	0.2215	0.3467	0.7496	0.8120
Herschel Bulkley	n	0.8066	0.7980	0.8274	0.8230	0.7862
	K (mPa-s^n)	13.3737	14.3657	12.4875	12.6648	19.7204
	τo (Pa)	0.0090	0.1447	0.2738	0.7185	0.7544
	SSE	0.0295	0.0782	0.0538	0.0495	0.3101
	R^2	0.9992	0.9980	0.9988	0.9989	0.9952
	Adjusted R^2	0.9987	0.9967	0.9980	0.9981	0.9920
	RMSE	0.0992	0.1614	0.1339	0.1284	0.3215
Best fit model		Power Law	Herschel Bulkley	Herschel Bulkley	Herschel Bulkley	Herschel Bulkley

Table F.12: Rheological parameter for sepiolite drilling fluid with intrusion of 171 kg/m^3 NaCl – rheometer results.

		Sepiolite mud with 171 kg/m^3 NaCl intrusion - Rheometer								
		Temperature, °C								
Model	**Parameter**	**38**	**43**	**49**	**54**	**60**	**66**	**71**	**77**	**82**
Bingham Plastic	μp (mPa-s)	15.7208	16.0417	15.1747	12.4971	13.2970	12.4827	11.9606	11.4002	10.7727
	τy (Pa)	2.0530	2.0683	1.7388	1.7484	1.6377	1.6650	1.4863	1.4164	1.4475
	SSE	8.5740	11.9000	11.6900	8.5350	8.9810	8.7170	7.6230	7.1440	6.4370
	R^2	0.9900	0.9859	0.9846	0.9866	0.9846	0.9830	0.9838	0.9833	0.9832
	Adjusted R^2	0.9875	0.9824	0.9807	0.9833	0.9807	0.9788	0.9798	0.9791	0.9789
	RMSE	1.4640	1.7250	1.7100	1.4610	1.4980	1.4760	1.3810	1.3360	1.2690
Power Law	n	0.6646	0.6481	0.6676	0.6558	0.6540	0.6337	0.6504	0.6490	0.6327
	K (mPa-s^n)	177.3258	196.2942	160.5608	161.4230	155.4834	168.8475	143.4126	137.9520	146.8614
	SSE	9.4160	7.0540	3.7690	5.2300	3.8360	3.9840	3.0060	2.5630	3.1170
	R^2	0.9890	0.9917	0.9950	0.9918	0.9934	0.9922	0.9936	0.9940	0.9918
	Adjusted R^2	0.9863	0.9896	0.9938	0.9897	0.9918	0.9903	0.9920	0.9925	0.9898
	RMSE	1.5340	1.3280	0.9707	1.1430	0.9792	0.9980	0.8669	0.8005	0.8827
Herschel Bulkley	n	0.8020	0.7663	0.7561	0.7723	0.7567	0.7459	0.7513	0.7471	0.7475
	K (mPa-s^n)	64.6171	82.1964	83.5855	68.4491	72.9038	73.8618	68.1617	66.9163	63.0364
	τo (Pa)	1.2952	1.1462	0.8157	0.9733	0.8320	0.8636	0.7396	0.6869	0.7616
	SSE	0.3923	0.3319	0.3275	0.3206	0.3140	0.3533	0.2606	0.2237	0.2928
	R^2	0.9995	0.9996	0.9996	0.9995	0.9995	0.9993	0.9994	0.9995	0.9992
	Adjusted R^2	0.9992	0.9993	0.9993	0.9992	0.9991	0.9989	0.9991	0.9991	0.9987
	RMSE	0.3616	0.3326	0.3304	0.3269	0.3235	0.3432	0.2947	0.2731	0.3124
Best fit model		Herschel Bulkley	Herschel Bulkley	Herschel Bulkley	Herschel Bulkley	Herschel Bulkley	Herschel Bulkley	Herschel Bulkley	Herschel Bulkley	Herschel Bulkley

Table F.12 (Continued): Rheological parameter for sepiolite drilling fluid with intrusion of 171 kg/m^3 NaCl – rheometer results.

		Sepiolite mud with 171 kg/m^3 NaCl intrusion - Rheometer								
		Temperature, °C								
Model	**Parameter**	**88**	**93**	**99**	**104**	**110**	**116**	**121**	**127**	**132**
Bingham Plastic	μp (mPa-s)	10.3464	9.7908	9.2447	8.9142	8.7992	8.3825	8.1670	7.7981	7.5730
	τy (Pa)	1.3771	1.4801	1.6296	1.4447	1.3733	1.5314	1.6444	1.8796	2.1172
	SSE	6.6990	6.2620	4.1670	4.6600	5.0470	5.0560	4.3250	3.4240	3.4380
	R^2	0.9810	0.9802	0.9852	0.9855	0.9803	0.9783	0.9804	0.9791	0.9778
	Adjusted R^2	0.9763	0.9753	0.9815	0.9778	0.9753	0.9728	0.9755	0.9722	0.9704
	RMSE	1.2940	1.2510	1.0210	1.0760	1.1230	1.1240	1.0400	1.0680	1.0710
Power Law	n	0.6301	0.6006	0.5721	0.5878	0.5933	0.5504	0.5263	0.5505	0.5093
	K (mPa-s^n)	143.3647	168.1290	196.8690	168.6559	159.5070	207.5507	241.4639	205.7784	272.1678
	SSE	2.3860	3.2270	5.5750	3.7220	2.7950	3.5800	4.8650	2.6400	3.3720
	R^2	0.9932	0.9898	0.9802	0.9858	0.9891	0.9846	0.9779	0.9850	0.9782
	Adjusted R^2	0.9916	0.9873	0.9752	0.9822	0.9863	0.9808	0.9724	0.9800	0.9710
	RMSE	0.7723	0.8982	1.1810	0.9646	0.8360	0.9460	1.1030	0.9055	1.0600
Herschel Bulkley	n	0.7329	0.7293	0.7628	0.7435	0.7287	0.7162	0.7304	0.7172	0.7126
	K (mPa-s^n)	67.1079	65.1440	48.5706	53.6480	58.8212	61.2641	53.9354	58.7733	58.9649
	τo (Pa)	0.6663	0.7951	1.0864	0.8656	0.7559	0.9058	1.0763	1.0619	1.3058
	SSE	0.2743	0.3661	0.2065	0.3373	0.2359	0.2056	0.2488	0.3223	0.4297
	R^2	0.9992	0.9988	0.9993	0.9987	0.9991	0.9991	0.9989	0.9980	0.9972
	Adjusted R^2	0.9987	0.9981	0.9988	0.9979	0.9985	0.9985	0.9981	0.9961	0.9944
	RMSE	0.3024	0.3493	0.2624	0.3353	0.2804	0.2618	0.2880	0.4014	0.4635
Best fit model		Herschel Bulkley	Herschel Bulkley	Herschel Bulkley	Herschel Bulkley	Herschel Bulkley	Herschel Bulkley	Herschel Bulkley	Herschel Bulkley	Herschel Bulkley

Table F.12 (Continued): Rheological parameter for sepiolite drilling fluid with intrusion of 171 kg/m^3 NaCl – rheometer results.

		Sepiolite mud with 171 kg/m^3 NaCl intrusion - Rheometer								
		Temperature, °C								
Model	**Parameter**	**138**	**143**	**149**	**154**	**160**	**166**	**171**	**177**	**182**
Bingham Plastic	μp (mPa-s)	7.8221	6.9886	7.1179	6.4234	6.5288	5.4606	5.5516	4.6200	4.4552
	τy (Pa)	2.0793	2.7921	2.9085	3.7142	3.6605	4.9002	4.6549	6.0402	6.2653
	SSE	2.9610	3.0880	3.1680	1.8090	1.1320	0.2731	0.3888	0.3433	0.5636
	R^2	0.9820	0.9766	0.9769	0.9837	0.9900	0.9965	0.9952	0.9940	0.9894
	Adjusted R^2	0.9760	0.9688	0.9692	0.9782	0.9867	0.9954	0.9937	0.9919	0.9858
	RMSE	0.9934	1.0150	1.0280	0.7765	0.6144	0.3017	0.3600	0.3383	0.4335
Power Law	n	0.5271	0.4038	0.3970	0.2963	0.3026	0.1897	0.1998	0.1249	0.1150
	K (mPa-s^n)	246.685	559.951	600.666	1194.147	1147.684	2501.338	2291.057	4015.457	4332.076
	SSE	3.8280	5.8930	6.7600	10.3400	12.8400	15.5500	17.7600	17.5900	17.6300
	R^2	0.9767	0.9554	0.9507	0.9066	0.8871	0.8032	0.7830	0.6900	0.6674
	Adjusted R^2	0.9690	0.9405	0.9342	0.8755	0.8495	0.7376	0.7107	0.5867	0.5566
	RMSE	1.1300	1.4020	1.5010	1.8570	2.0690	2.2770	2.4330	2.4210	2.4240
Herschel Bulkley	n	0.7408	0.7100	0.7192	0.7706	0.8411	0.9514	1.0290	1.1770	1.2410
	K (mPa-s^n)	49.6723	55.4682	52.8337	32.9025	20.1851	7.7023	4.5127	1.3331	0.8181
	τo (Pa)	1.3508	2.0343	2.1708	3.2040	3.3295	4.8283	4.6980	6.2318	6.5048
	SSE	0.4167	0.4907	0.6954	0.5316	0.5446	0.2381	0.3768	0.0690	0.1244
	R^2	0.9975	0.9963	0.9949	0.9952	0.9952	0.9970	0.9954	0.9988	0.9977
	Adjusted R^2	0.9949	0.9926	0.9898	0.9904	0.9904	0.9940	0.9908	0.9976	0.9953
	RMSE	0.4565	0.4953	0.5897	0.5156	0.5218	0.3451	0.4341	0.1858	0.2494
Best fit model		Herschel Bulkley	Herschel Bulkley	Herschel Bulkley	Herschel Bulkley	Herschel Bulkley	Herschel Bulkley	Herschel Bulkley	Herschel Bulkley	Herschel Bulkley

Table F.12 (Continued): Rheological parameter for sepiolite drilling fluid with intrusion of 171 kg/m^3 NaCl – rheometer results.

		Sepiolite mud with 171 kg/m^3 NaCl intrusion - Rheometer								
		Temperature, °C								
Model	**Parameter**	**188**	**193**	**199**	**204**	**210**	**216**	**221**	**227**	**232**
Bingham Plastic	μp (mPa-s)	4.0725	4.0835	3.8612	4.4691	4.8619	6.0546	7.1994	7.2856	7.2952
	τy (Pa)	6.9886	7.3958	8.4879	8.4735	9.3261	8.6412	7.5969	6.2989	4.6118
	SSE	0.9476	0.8220	0.9008	0.7408	0.7995	1.7840	3.4380	3.6710	6.2580
	R^2	0.9788	0.9817	0.9777	0.9862	0.9897	0.9852	0.9799	0.9745	0.9650
	Adjusted R^2	0.9718	0.9756	0.9702	0.9815	0.9871	0.9815	0.9749	0.9660	0.9562
	RMSE	0.5620	0.5235	0.5480	0.4969	0.4471	0.6678	0.9271	1.1060	1.2510
Power Law	n	0.0915	0.0877	0.0727	0.0862	0.0737	0.0984	0.1320	0.2075	0.2141
	K (mPa-s^n)	5278.580	5647.410	6811.380	6471.29	7702.320	6634.150	5245.050	2941.060	2390.689
	SSE	17.7700	17.3200	15.8100	18.6100	17.3500	22.3000	25.2300	14.7000	13.9100
	R^2	0.6032	0.6141	0.6077	0.6523	0.7758	0.8150	0.8528	0.8979	0.9222
	Adjusted R^2	0.4709	0.4854	0.4770	0.5365	0.7197	0.7688	0.8160	0.8639	0.9027
	RMSE	2.4340	2.4030	2.2960	2.4900	2.0830	2.3610	2.5110	2.2140	1.8650
Herschel Bulkley	n	1.3960	1.3610	1.3870	1.2630	0.9212	0.8412	0.7712	0.7010	0.6529
	K (mPa-s^n)	0.2536	0.3252	0.2560	0.7060	8.4160	18.3218	35.6424	61.5994	84.5914
	τo (Pa)	7.3095	7.6927	8.7897	8.7322	9.2447	8.4208	7.1946	5.4750	3.8861
	SSE	0.0544	0.0652	0.1764	0.2461	0.7031	1.1310	1.3640	0.6710	0.6175
	R^2	0.9988	0.9985	0.9956	0.9954	0.9909	0.9906	0.9920	0.9953	0.9965
	Adjusted R^2	0.9976	0.9971	0.9912	0.9908	0.9849	0.9844	0.9867	0.9907	0.9942
	RMSE	0.1648	0.1805	0.2970	0.3508	0.4841	0.6139	0.6743	0.5792	0.4537
Best fit model		Herschel Bulkley	Herschel Bulkley	Herschel Bulkley	Herschel Bulkley	Herschel Bulkley	Herschel Bulkley	Herschel Bulkley	Herschel Bulkley	Herschel Bulkley

Table F.12 (Continued): Rheological parameter for sepiolite drilling fluid with intrusion of 171 kg/m^3 NaCl – rheometer results.

		Sepiolite mud with 171 kg/m^3 NaCl intrusion - Rheometer				
		Temperature, °C				
Model	**Parameter**	**238**	**243**	**249**	**254**	**260**
Bingham Plastic	μp (mPa-s)	6.8784	6.6485	6.2557	5.7863	5.5899
	τy (Pa)	3.5446	2.7648	2.5842	2.8026	3.1106
	SSE	5.6010	5.6210	5.0350	3.9750	3.6790
	R^2	0.9648	0.9623	0.9618	0.9646	0.9649
	Adjusted R^2	0.9560	0.9528	0.9522	0.9558	0.9561
	RMSE	1.1830	1.1850	1.1220	0.9968	0.9591
Power Law	n	0.2566	0.3065	0.3074	0.2688	0.2373
	K (mPa-s^n)	1567.767	1010.690	942.672	1186.483	1486.337
	SSE	10.0900	7.0130	6.3220	7.6770	9.3030
	R^2	0.9365	0.9529	0.9520	0.9317	0.9113
	Adjusted R^2	0.9207	0.9411	0.9400	0.9146	0.8891
	RMSE	1.5880	1.3240	1.2570	1.3850	1.5250
Herschel Bulkley	n	0.6483	0.6360	0.6376	0.6686	0.6974
	K (mPa-s^n)	81.4779	85.9326	79.8493	59.2044	46.5780
	τo (Pa)	2.8443	2.0530	1.9208	2.2657	2.6570
	SSE	0.4142	0.4010	0.5210	0.9220	1.4270
	R^2	0.9974	0.9973	0.9960	0.9918	0.9864
	Adjusted R^2	0.9957	0.9955	0.9934	0.9863	0.9773
	RMSE	0.3716	0.3656	0.4167	0.5544	0.6896
Best fit model		Herschel Bulkley	Herschel Bulkley	Herschel Bulkley	Herschel Bulkley	Herschel Bulkley

Table F.13: Rheological parameter for sepiolite drilling fluid with intrusion of 342 kg/m^3 NaCl – rheometer results.

		Sepiolite mud with 342 kg/m^3 NaCl intrusion - Rheometer								
		Temperature, °C								
Model	**Parameter**	**38**	**43**	**49**	**54**	**60**	**66**	**71**	**77**	**82**
Bingham Plastic	μp (mPa-s)	14.9448	15.0646	14.0203	13.2779	12.4971	11.8888	11.3188	10.6434	10.0063
	τy (Pa)	1.2617	1.0936	1.2004	0.8881	0.8761	0.8143	0.7420	0.8909	1.0883
	SSE	4.5230	4.8970	3.8390	4.2650	2.5560	3.6420	3.1090	3.2710	2.0460
	R^2	0.9938	0.9934	0.9940	0.9926	0.9950	0.9921	0.9926	0.9912	0.9937
	Adjusted R^2	0.9922	0.9917	0.9925	0.9907	0.9937	0.9901	0.9907	0.9890	0.9922
	RMSE	1.0630	1.1060	0.9796	1.0330	0.7994	0.9543	0.8816	0.9043	0.7153
Power Law	n	0.7535	0.7726	0.7538	0.7792	0.7866	0.7748	0.7826	0.7452	0.7140
	K (mPa-s^n)	86.2679	75.4904	80.9031	63.2280	56.9052	58.3901	52.5942	64.8566	77.3106
	SSE	3.3480	1.9730	3.4740	1.1360	1.6250	1.0670	0.9175	1.6520	3.7570
	R^2	0.9954	0.9973	0.9946	0.9980	0.9968	0.9977	0.9978	0.9955	0.9885
	Adjusted R^2	0.9943	0.9967	0.9932	0.9975	0.9960	0.9971	0.9973	0.9944	0.9856
	RMSE	0.9149	0.7023	0.9319	0.5329	0.6374	0.5164	0.4789	0.6426	0.9691
Herschel Bulkley	n	0.8410	0.8368	0.8468	0.8295	0.8577	0.8266	0.8320	0.8207	0.8515
	K (mPa-s^n)	45.3230	47.0618	40.8108	43.6465	33.7072	39.8911	36.5477	37.2231	28.1939
	τo (Pa)	0.7238	0.5350	0.7185	0.3698	0.4819	0.3413	0.3079	0.4492	0.7563
	SSE	0.1692	0.2038	0.3089	0.2948	0.1561	0.3542	0.3337	0.4643	0.3874
	R^2	0.9998	0.9997	0.9995	0.9995	0.9997	0.9992	0.9992	0.9987	0.9988
	Adjusted R^2	0.9996	0.9995	0.9992	0.9991	0.9995	0.9987	0.9987	0.9979	0.9980
	RMSE	0.2375	0.2606	0.3209	0.3135	0.2281	0.3436	0.3335	0.3934	0.3593
Best fit model		Herschel Bulkley	Herschel Bulkley	Herschel Bulkley	Herschel Bulkley	Herschel Bulkley	Herschel Bulkley	Herschel Bulkley	Herschel Bulkley	Herschel Bulkley

Table F.13 (Continued): Rheological parameter for sepiolite drilling fluid with intrusion of 342 kg/m^3 NaCl – rheometer results.

		Sepiolite mud with 342 kg/m^3 NaCl intrusion - Rheometer								
		Temperature, °C								
Model	**Parameter**	**88**	**93**	**99**	**104**	**110**	**116**	**121**	**127**	**132**
Bingham Plastic	μp (mPa-s)	10.0446	9.5992	9.1537	8.8519	8.6364	8.5789	8.3107	8.1574	7.9801
	τy (Pa)	0.7056	0.8478	1.0734	0.9853	1.0533	0.8641	0.9987	1.0006	1.0528
	SSE	3.2760	3.1630	2.8270	3.0920	2.5730	3.6160	3.1550	3.1350	3.2260
	R^2	0.9901	0.9895	0.9897	0.9880	0.9895	0.9851	0.9861	0.9857	0.9846
	Adjusted R^2	0.9876	0.9869	0.9871	0.9850	0.9868	0.9813	0.9826	0.9821	0.9807
	RMSE	0.9055	0.8892	0.8407	0.8792	0.8020	0.9508	0.8881	0.8853	0.8981
Power Law	n	0.7625	0.7300	0.6818	0.6855	0.6722	0.6923	0.6645	0.6600	0.6426
	K (mPa-s^n)	53.6959	65.0482	88.4713	82.8670	89.4293	75.8257	90.3394	91.5848	101.5959
	SSE	0.6573	1.3410	2.8050	1.9600	2.5470	0.9090	1.8120	1.9530	2.2410
	R^2	0.9980	0.9956	0.9898	0.9924	0.9896	0.9962	0.9920	0.9911	0.9893
	Adjusted R^2	0.9975	0.9944	0.9872	0.9905	0.9870	0.9953	0.9900	0.9888	0.9866
	RMSE	0.4054	0.5791	0.8373	0.6999	0.7980	0.4767	0.6730	0.6987	0.7486
Herschel Bulkley	n	0.8060	0.8042	0.8077	0.7905	0.8018	0.7623	0.7735	0.7734	0.7673
	K (mPa-s^n)	38.9475	37.6877	35.0724	38.2721	34.4736	45.2272	40.4803	39.7666	40.6048
	τo (Pa)	0.2473	0.4056	0.6605	0.5422	0.6495	0.3593	0.5394	0.5489	0.5964
	SSE	0.2943	0.3943	0.4181	0.3613	0.2599	0.2228	0.2974	0.4045	0.4609
	R^2	0.9991	0.9987	0.9985	0.9986	0.9989	0.9991	0.9987	0.9981	0.9978
	Adjusted R^2	0.9985	0.9987	0.9975	0.9977	0.9982	0.9985	0.9978	0.9969	0.9963
	RMSE	0.3123	0.3625	0.3733	0.3470	0.2943	0.2725	0.3149	0.3672	0.3919
Best fit model		Herschel Bulkley	Herschel Bulkley	Herschel Bulkley	Herschel Bulkley	Herschel Bulkley	Herschel Bulkley	Herschel Bulkley	Herschel Bulkley	Herschel Bulkley

Table F.13 (Continued): Rheological parameter for sepiolite drilling fluid with intrusion of 342 kg/m^3 NaCl – rheometer results.

		Sepiolite mud with 342 kg/m^3 NaCl intrusion - Rheometer								
		Temperature, °C								
Model	**Parameter**	**138**	**143**	**149**	**154**	**160**	**166**	**171**	**177**	**182**
Bingham Plastic	μp (mPa-s)	7.8556	7.2952	7.6640	6.9072	7.4245	6.3563	6.6964	5.7815	5.5277
	τy (Pa)	1.2957	1.5673	1.4523	1.8279	1.6415	2.2705	2.1248	2.7490	3.0009
	SSE	2.0060	2.8360	2.3800	2.4170	2.3140	1.7610	1.2180	0.7892	0.4281
	R^2	0.9878	0.9802	0.9849	0.9812	0.9844	0.9838	0.9898	0.9911	0.9947
	Adjusted R^2	0.9838	0.9736	0.9799	0.9749	0.9791	0.9784	0.9864	0.9882	0.9930
	RMSE	0.8176	0.9723	0.8907	0.8975	0.8783	0.7662	0.6371	0.5129	0.3778
Power Law	n	0.6549	0.5817	0.6184	0.5286	0.5809	0.4409	0.4834	0.3516	0.3099
	K (mPa-s^n)	95.8479	152.4657	122.3845	215.4063	156.9204	384.3975	295.2077	690.7180	911.5370
	SSE	1.6500	2.0250	1.9120	3.3820	2.9610	5.7870	6.6620	9.1030	11.6600
	R^2	0.9900	0.9859	0.9879	0.9737	0.9800	0.9467	0.9443	0.8978	0.8565
	Adjusted R^2	0.9867	0.9812	0.9838	0.9649	0.9733	0.9289	0.9258	0.8637	0.8087
	RMSE	0.7416	0.8216	0.7983	1.0260	0.9936	1.3890	1.4900	1.7420	1.9710
Herschel Bulkley	n	0.7874	0.7337	0.7638	0.7495	0.7710	0.7804	0.8391	0.8626	0.9481
	K (mPa-s^n)	35.6568	48.7622	41.2467	41.1988	37.9081	30.3542	20.9898	15.3232	7.9849
	τo (Pa)	0.7290	0.8636	0.8200	1.2133	1.0533	1.7934	1.7804	2.5013	2.9190
	SSE	0.3540	0.4974	0.3970	0.6159	0.6101	0.6371	0.5839	0.4533	0.3878
	R^2	0.9979	0.9965	0.9975	0.9952	0.9959	0.9941	0.9951	0.9949	0.9952
	Adjusted R^2	0.9957	0.9931	0.9950	0.9904	0.9918	0.9883	0.9902	0.9898	0.9905
	RMSE	0.4207	0.4987	0.4455	0.5549	0.5523	0.5644	0.5403	0.4761	0.4404
Best fit model		Herschel Bulkley	Herschel Bulkley	Herschel Bulkley	Herschel Bulkley	Herschel Bulkley	Herschel Bulkley	Herschel Bulkley	Herschel Bulkley	Herschel Bulkley

Table F.13 (Continued): Rheological parameter for sepiolite drilling fluid with intrusion of 342 kg/m^3 NaCl – rheometer results.

		Sepiolite mud with 342 kg/m^3 NaCl intrusion - Rheometer								
		Temperature, °C								
Model	**Parameter**	**188**	**193**	**199**	**204**	**210**	**216**	**221**	**227**	**232**
Bingham Plastic	μp (mPa-s)	4.8619	4.4207	4.0820	3.6893	4.1328	4.4044	4.7205	5.5708	5.7815
	τy (Pa)	3.7328	4.3757	5.0487	5.8438	5.7528	5.4606	5.1253	4.1932	3.3683
	SSE	0.3237	0.5996	0.7140	1.1230	0.5180	0.6239	1.0270	2.0980	3.0800
	R^2	0.9948	0.9885	0.9840	0.9697	0.9887	0.9880	0.9829	0.9796	0.9724
	Adjusted R^2	0.9931	0.9847	0.9787	0.9596	0.9849	0.9840	0.9772	0.9745	0.9655
	RMSE	0.3285	0.4471	0.4879	0.6117	0.4155	0.4560	0.5850	0.7242	0.8775
Power Law	n	0.2183	0.1624	0.1288	0.0985	0.1196	0.1399	0.1637	0.1792	0.2284
	K (mPa-s^n)	1700.450	5.289	3328.092	4315.311	3885.169	3381.740	2874.00	2478.346	1662.130
	SSE	13.0900	16.1200	15.4800	14.8500	13.3800	11.0900	9.2680	12.4500	9.5710
	R^2	0.7917	0.6914	0.6540	0.5996	0.7068	0.7863	0.8454	0.8789	0.9141
	Adjusted R^2	0.7223	0.5885	0.5387	0.4661	0.6091	0.7151	0.7938	0.8486	0.8927
	RMSE	2.0890	2.2180	2.2720	2.2250	2.1120	1.9220	1.7580	1.7640	1.5470
Herschel Bulkley	n	1.0290	1.2530	1.3220	1.4800	1.1480	0.9408	0.8000	0.7507	0.6950
	K (mPa-s^n)	3.9700	0.7477	0.4251	0.1277	1.4533	6.6964	19.5815	31.8679	49.0975
	τo (Pa)	3.7697	4.6224	5.3217	6.1791	5.9013	5.3840	4.8092	3.8459	2.8917
	SSE	0.3149	0.1325	0.1074	0.1866	0.3712	0.5921	0.5339	0.5777	0.4765
	R^2	0.9950	0.9975	0.9976	0.9950	0.9919	0.9886	0.9911	0.9944	0.9957
	Adjusted R^2	0.9900	0.9949	0.9952	0.9899	0.9837	0.9772	0.9822	0.9906	0.9929
	RMSE	0.3968	0.2574	0.2317	0.3054	0.4308	0.5441	0.5167	0.4388	0.3986
Best fit model		Herschel Bulkley	Herschel Bulkley	Herschel Bulkley	Herschel Bulkley	Herschel Bulkley	Herschel Bulkley	Herschel Bulkley	Herschel Bulkley	Herschel Bulkley

Table F.13 (Continued): Rheological parameter for sepiolite drilling fluid with intrusion of 342 kg/m^3 NaCl – rheometer results.

		Sepiolite mud with 342 kg/m^3 NaCl intrusion - Rheometer				
		Temperature, °C				
Model	**Parameter**	**238**	**243**	**249**	**254**	**260**
Bingham Plastic	μp (mPa-s)	6.1839	6.1887	5.6953	5.4798	5.6953
	τy (Pa)	2.4740	1.8274	1.8101	1.9227	1.8097
	SSE	5.1420	3.6340	2.5230	3.9410	2.5210
	R^2	0.9602	0.9716	0.9766	0.9611	0.9766
	Adjusted R^2	0.9502	0.9645	0.9707	0.9514	0.9707
	RMSE	1.1340	0.9532	0.7942	0.9926	0.7939
Power Law	n	0.3165	0.4024	0.3810	0.3488	0.3811
	K (mPa-s^n)	869.3850	451.8886	487.6220	596.8340	487.1430
	SSE	5.3890	4.6010	5.3110	5.2690	5.3050
	R^2	0.9582	0.9640	0.9507	0.9480	0.9507
	Adjusted R^2	0.9478	0.9550	0.9384	0.9350	0.9384
	RMSE	1.1610	1.0730	1.1520	1.1480	1.1520
Herschel Bulkley	n	0.6254	0.6804	0.7139	0.6690	0.7140
	K (mPa-s^n)	86.2679	58.2943	42.2861	55.8993	42.2526
	τo (Pa)	1.7814	1.2828	1.3814	1.4174	1.3814
	SSE	0.2439	0.2142	0.2932	1.2390	0.2948
	R^2	0.9981	0.9983	0.9973	0.9878	0.9973
	Adjusted R^2	0.9968	0.9972	0.9955	0.9797	0.9954
	RMSE	0.2852	0.2672	0.3126	0.6426	0.3135
Best fit model		Herschel Bulkley	Herschel Bulkley	Herschel Bulkley	Herschel Bulkley	Herschel Bulkley

Table F.14: Rheological parameter for weighted sepiolite drilling mud – rheometer results.

		Weighted fresh water sepiolite mud - Rheometer								
		Temperature, °C								
Model	**Parameter**	**38**	**43**	**49**	**54**	**60**	**66**	**71**	**77**	**82**
Bingham Plastic	μp (mPa-s)	44.5566	39.5750	36.0064	33.2570	30.6225	28.3616	26.2061	24.1895	22.6519
	τy (Pa)	5.5372	5.0630	4.2401	3.7055	3.3827	3.0991	2.7533	2.4434	2.0520
	SSE	178.5000	151.6000	128.5000	99.4300	84.8600	62.5200	50.7200	39.5400	34.2700
	R^2	0.9730	0.9710	0.9703	0.9730	0.9728	0.9766	0.9777	0.9796	0.9798
	Adjusted R^2	0.6992	0.9637	0.9629	0.9662	0.9660	0.9707	0.9721	0.9744	0.9747
	RMSE	6.6800	6.1570	5.6680	4.9860	4.6060	3.9530	3.5610	3.1440	2.9270
Power Law	n	0.6271	0.6184	0.6324	0.6463	0.6473	0.6566	0.5801	0.6764	0.6933
	K (mPa-s^n)	623.1790	587.2540	482.8320	403.6533	368.6863	320.7384	318.7745	237.6319	196.3900
	SSE	3.7200	9.5440	3.8380	3.5280	2.6580	3.8430	2.9550	2.5320	1.0300
	R^2	0.9979	0.9982	0.9991	0.9990	0.9991	0.9986	0.9987	0.9987	0.9994
	Adjusted R^2	0.9974	0.9977	0.9989	0.9988	0.9989	0.9986	0.9984	0.9984	0.9992
	RMSE	1.8520	1.5450	0.9795	0.9392	0.8151	0.9802	0.8595	0.7956	0.5076
Herschel Bulkley	n	0.6837	0.6726	0.6695	0.6834	0.6824	0.7034	0.7098	0.7210	0.7227
	K (mPa-s^n)	409.7845	394.0733	366.4350	306.5600	284.1428	226.6628	200.1741	170.7635	157.9263
	τo (Pa)	1.6722	1.4418	0.9005	0.8138	0.7099	0.8569	0.7415	0.6802	0.4179
	SSE	1.1020	0.5236	0.2446	0.4629	0.3244	0.2825	0.2503	0.2047	0.1265
	R^2	0.9998	0.9999	0.9999	0.9999	0.9999	0.9999	0.9999	0.9999	0.9999
	Adjusted R^2	0.9997	0.9998	0.9999	0.9998	0.9998	0.9998	0.9998	0.9998	0.9999
	RMSE	0.6060	0.4178	0.2856	0.3928	0.3288	0.3069	0.2889	0.2612	0.2053
Best fit model		Herschel Bulkley	Herschel Bulkley	Herschel Bulkley	Herschel Bulkley	Herschel Bulkley	Herschel Bulkley	Herschel Bulkley	Herschel Bulkley	Herschel Bulkley

Table F.14 (Continued): Rheological parameter for weighted sepiolite drilling mud – rheometer results.

		Weighted fresh water sepiolite mud - Rheometer								
		Temperature, °C								
Model	**Parameter**	**88**	**93**	**99**	**104**	**110**	**116**	**121**	**127**	**132**
Bingham Plastic	μp (mPa-s)	20.8988	19.2127	17.4739	16.0130	14.5233	13.0959	12.1139	10.7775	9.5800
	τy (Pa)	1.7867	1.6056	1.3963	0.9719	0.7726	0.7516	0.4076	0.2773	0.0480
	SSE	24.9000	19.1100	12.6500	7.1240	3.3190	2.3170	1.5570	0.4680	0.1190
	R^2	0.9827	0.9843	0.9874	0.9915	0.9952	0.9958	0.9967	0.9988	0.9995
	Adjusted R^2	0.9784	0.9803	0.9842	0.9894	0.9940	0.9948	0.9959	0.9984	0.9993
	RMSE	2.4950	2.1860	1.7780	1.3350	0.9109	0.7611	0.6239	0.3421	0.1992
Power Law	n	0.7092	0.7171	0.7338	0.7834	0.8181	0.8166	0.8680	0.9093	0.9764
	K (mPa-s^n)	162.0457	141.0176	114.2894	73.5744	52.4984	48.0437	30.6033	20.4581	11.2900
	SSE	1.0710	1.3140	1.6490	0.5963	0.7698	1.1900	0.1995	0.2352	0.0785
	R^2	0.9993	0.9989	0.9984	0.9993	0.9989	0.9979	0.9996	0.9994	0.9997
	Adjusted R^2	0.9991	0.9986	0.9979	0.9991	0.9986	0.9973	0.9995	0.9992	0.9996
	RMSE	0.5175	0.5732	0.6422	0.3861	0.4387	0.5454	0.2233	0.2425	0.1617
Herschel Bulkley	n	0.7418	0.7531	0.7784	0.8145	0.8588	0.8721	0.8852	0.9342	0.9764
	K (mPa-s^n)	127.3182	108.1103	82.2443	58.4859	38.8852	31.9397	26.9581	17.0428	11.2900
	τo (Pa)	0.4174	0.4164	0.4564	0.2805	0.3174	0.3859	0.1080	0.1316	0.0000
	SSE	0.1324	0.3722	0.4673	0.1132	0.1169	0.2157	0.1199	0.1115	0.0785
	R^2	0.9999	0.9997	0.9995	0.9999	0.9998	0.9996	0.9997	0.9997	0.9997
	Adjusted R^2	0.9998	0.9995	0.9992	0.9998	0.9997	0.9994	0.9996	0.9995	0.9996
	RMSE	0.2101	0.3522	0.3947	0.1943	0.1974	0.2681	0.1999	0.1928	0.1617
Best fit model		Herschel Bulkley	Herschel Bulkley	Herschel Bulkley	Herschel Bulkley	Herschel Bulkley	Herschel Bulkley	Herschel Bulkley	Herschel Bulkley	Power Law

Tab Table F.14 (Continued): Rheological parameter for weighted sepiolite drilling mud – rheometer results.

		Weighted fresh water sepiolite mud - Rheometer								
		Temperature, °C								
Model	**Parameter**	**138**	**143**	**149**	**154**	**160**	**166**	**171**	**177**	**182**
Bingham Plastic	μp (mPa-s)	8.9477	7.5682	7.0221	6.1935	5.9971	5.2786	5.2594	4.8235	4.4992
	τy (Pa)	0.1310	0.1512	-0.0040	0.0036	0.0304	-0.0671	-0.2202	-0.3417	-0.0587
	SSE	0.2141	0.1277	0.0366	0.1710	0.0318	0.0682	0.0117	0.0156	0.0229
	R^2	0.9990	0.9993	0.9997	0.9983	0.9997	0.9991	0.9998	0.9996	0.9994
	Adjusted R^2	0.9987	0.9991	0.9996	0.9978	0.9997	0.9988	0.9996	0.9994	0.9990
	RMSE	0.2671	0.1781	0.1105	0.2388	0.0892	0.1507	0.0765	0.0884	0.1070
Power Law	n	0.9420	0.9525	1.0100	1.0370	1.0020	1.0550	1.0950	1.1670	1.0360
	K (mPa-s^n)	13.4503	10.6913	6.5527	4.8427	5.9492	3.5896	2.7974	1.4193	3.4766
	SSE	0.0250	0.2733	0.0308	0.1129	0.0440	0.0181	0.0058	0.0262	0.0114
	R^2	0.9999	0.9985	0.9998	0.9989	0.9996	0.9998	0.9999	0.9994	0.9997
	Adjusted R^2	0.9998	0.9982	0.9997	0.9985	0.9995	0.9997	0.9998	0.9990	0.9995
	RMSE	0.0913	0.2614	0.1014	0.1940	0.1048	0.0776	0.0540	0.1145	0.0756
Herschel Bulkley	n	0.9420	0.9927	1.0210	1.0910	1.0240	1.0630	1.0950	1.1670	1.1090
	K (mPa-s^n)	13.4503	7.9658	6.0402	3.2625	5.0870	3.3889	2.7974	1.4193	2.0257
	τo (Pa)	0.0000	0.1404	0.0359	0.1446	0.0571	0.0181	0.0000	0.0000	0.1475
	SSE	0.0250	0.1257	0.0258	0.0269	0.0185	0.0167	0.0058	0.0262	0.0005
	R^2	0.9999	0.9993	0.9998	0.9997	0.9998	0.9998	0.9999	0.9994	1.0000
	Adjusted R^2	0.9998	0.9989	0.9996	0.9995	0.9997	0.9995	0.9998	0.9990	1.0000
	RMSE	0.0913	0.2047	0.1135	0.1159	0.0785	0.0915	0.0540	0.1145	0.0229
Best fit model		Power Law	Herschel Bulkley	Herschel Bulkley	Herschel Bulkley	Herschel Bulkley	Herschel Bulkley	Power Law	Power Law	Herschel Bulkley

Table F.14 (Continued): Rheological parameter for weighted sepiolite drilling mud – rheometer results.

		Weighted fresh water sepiolite mud - Rheometer								
		Temperature, °C								
Model	**Parameter**	**188**	**193**	**199**	**204**	**210**	**216**	**221**	**227**	**232**
Bingham Plastic	μp (mPa-s)	4.3512	4.3637	4.4494	5.1301	4.9433	5.2163	5.2834	5.4750	6.9311
	τy (Pa)	0.2743	1.4562	3.9680	6.1025	8.1670	8.0233	7.8317	7.1563	5.1014
	SSE	0.1125	0.1990	0.8160	1.6010	1.3380	1.1640	1.9060	1.2160	0.2151
	R^2	0.9978	0.9961	0.9772	0.9667	0.9699	0.9764	0.9628	0.9776	0.9975
	Adjusted R^2	0.9970	0.9947	0.9658	0.9501	0.9549	0.9646	0.9442	0.9664	0.9962
	RMSE	0.1936	0.2576	0.6387	0.8948	0.8180	0.7630	0.9763	0.7796	0.3280
Power Law	n	0.8628	0.4813	0.3491	0.2830	0.2197	0.2337	0.2388	0.2648	0.3979
	K (mPa-s^n)	11.8313	197.7791	739.0970	1553.397	2810.293	2578.936	2461.581	1983.060	756.820
	SSE	0.2813	4.9990	3.5090	6.3810	6.1240	5.9020	7.5900	6.2200	3.6460
	R^2	0.9944	0.9010	0.9021	0.8674	0.8625	0.8802	0.8520	0.8853	0.9572
	Adjusted R^2	0.9925	0.8680	0.8531	0.8011	0.7937	0.8204	0.7780	0.8279	0.9358
	RMSE	0.3062	1.2910	1.3250	1.7860	1.7500	1.7180	1.9480	1.7630	1.3500
Herschel Bulkley	n	0.9640	1.0030	1.7660	1.9960	1.9320	1.6570	1.9280	1.7220	1.2250
	K (mPa-s^n)	5.6139	4.2578	0.0186	0.0042	0.0064	0.0470	0.0071	0.0311	1.3479
	τo (Pa)	0.2302	1.4605	4.8235	7.2233	9.2160	8.9477	8.9477	8.1765	5.6857
	SSE	0.1004	0.1989	0.0462	0.0012	0.0111	0.2537	0.2560	0.0761	0.0000
	R^2	0.9980	0.9961	0.9987	1.0000	0.9998	0.9949	0.9950	0.9986	1.0000
	Adjusted R^2	0.9960	0.9921	0.9961	0.9999	0.9993	0.9846	0.9850	0.9958	1.0000
	RMSE	0.2240	0.3154	0.2150	0.0340	0.1055	0.5037	0.5060	0.2758	0.0043
Best fit model		Herschel Bulkley	Herschel Bulkley	Herschel Bulkley	Herschel Bulkley	Herschel Bulkley	Herschel Bulkley	Herschel Bulkley	Herschel Bulkley	Herschel Bulkley

Table F.14 (Continued): Rheological parameter for weighted sepiolite drilling mud – rheometer results.

Model	Parameter	238	243	249	254	260
		Weighted fresh water sepiolite mud - Rheometer				
		Temperature, °C				
Bingham Plastic	μp (mPa-s)	7.5155	9.8099	17.4739	13.9724	10.4230
	τy (Pa)	4.8571	7.6113	6.1935	4.5495	4.6132
	SSE	0.9325	66.3200	135.2000	56.6900	21.1200
	R^2	0.9938	0.8246	0.8797	0.9178	0.9315
	Adjusted R^2	0.9917	0.7808	0.8497	0.8972	0.9086
	RMSE	0.5575	4.0720	5.8150	3.7650	2.6530
Power Law	n	0.2536	0.1974	0.3459	0.3678	0.3707
	K (mPa-s^n)	1913.605	4059.046	1972.043	1325.872	1080.624
	SSE	36.8200	4.1250	9.5070	6.2790	4.1860
	R^2	0.7548	0.9891	0.9915	0.9909	0.9864
	Adjusted R^2	0.6731	0.9864	0.9894	0.9886	0.9819
	RMSE	3.5030	1.0160	1.5420	1.2530	1.1810
Herschel Bulkley	n	1.1780	0.2395	0.3730	0.4761	0.5134
	K (mPa-s^n)	2.1426	2740.8380	1591.238	579.590	353.9331
	τo (Pa)	5.1732	1.6636	0.7070	1.6870	2.0362
	SSE	0.1915	3.8830	9.1550	2.6220	1.1280
	R^2	0.9987	0.9897	0.9919	0.9962	0.9963
	Adjusted R^2	0.9974	0.9829	0.9864	0.9937	0.9927
	RMSE	0.3095	1.1380	1.7470	0.9348	0.7511
Best fit model		Herschel Bulkley	Herschel Bulkley	Herschel Bulkley	Herschel Bulkley	Herschel Bulkley

Appendix-G. Best fit and variation of rheological model prameters.

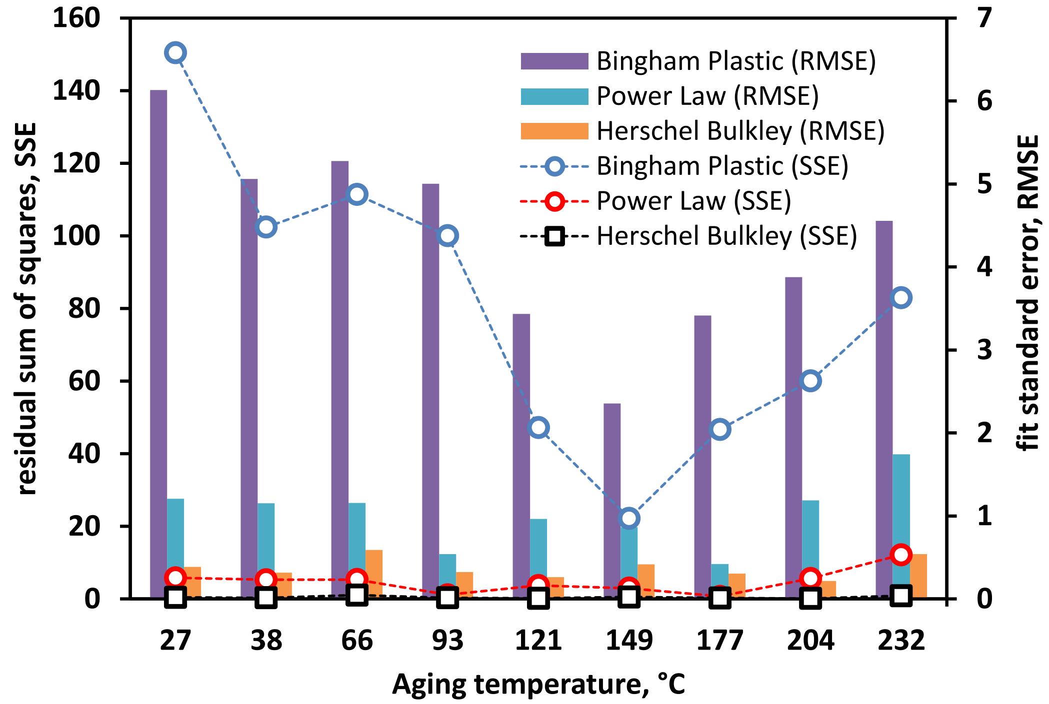

Figure G.1: SSE and RMSE for unweighted fresh water sepiolite mud-Viscometer.

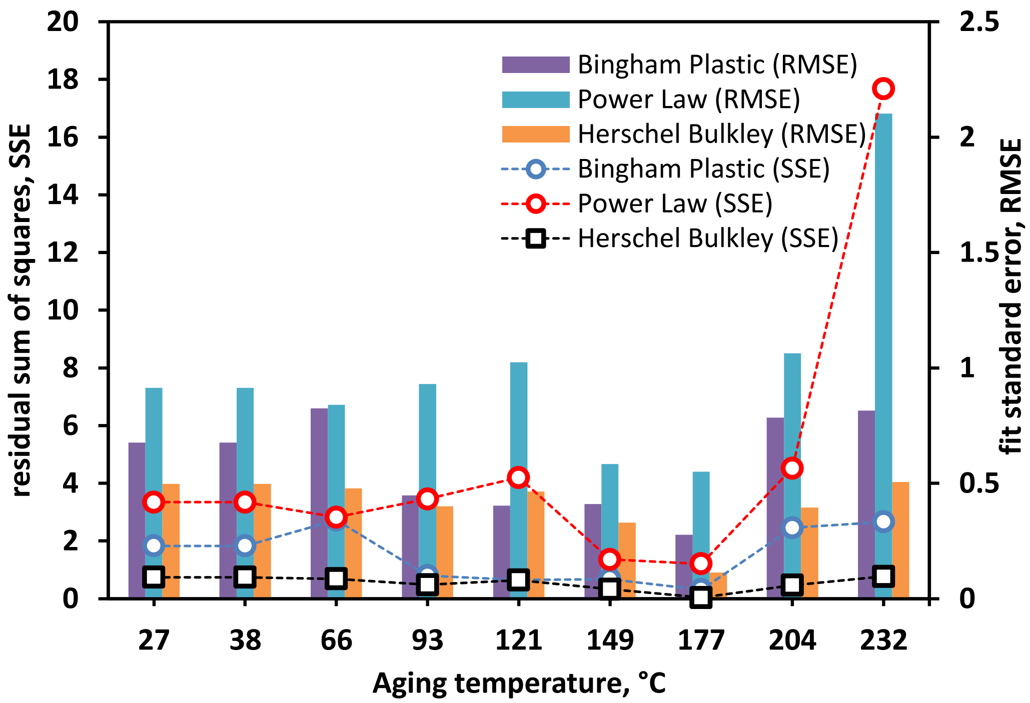

Figure G.2: SSE and RMSE for unweighted semi saturated sepiolite mud-Viscometer.

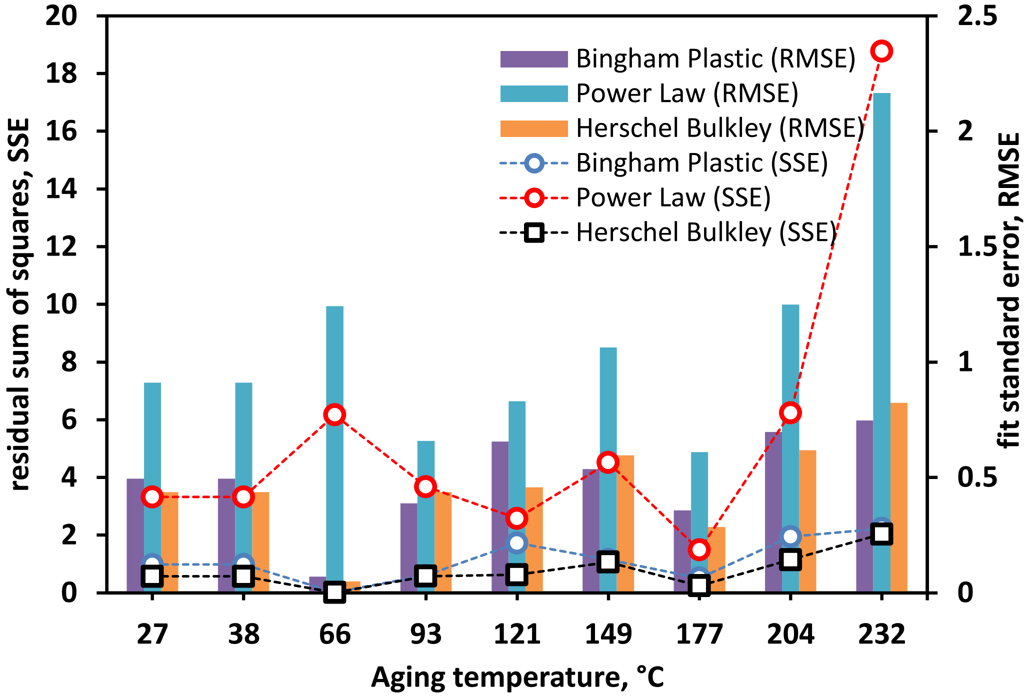

Figure G.3: SSE and RMSE for unweighted fully saturated sepiolite mud-Viscometer.

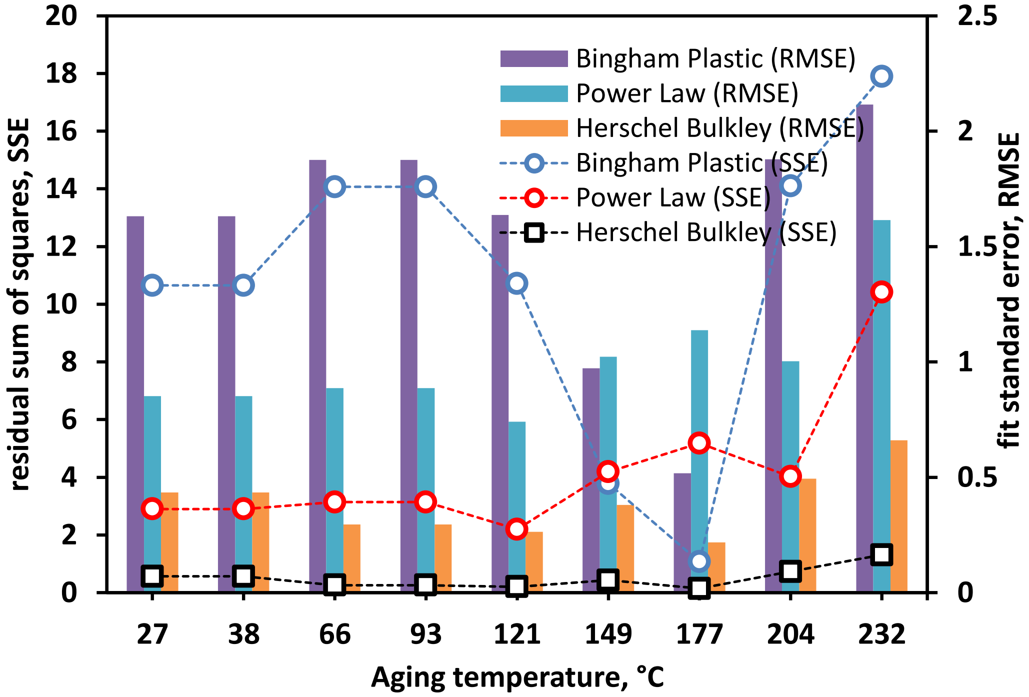

Figure G.4: SSE and RMSE for sepiolite mud with 171 kg/m^3 of NaCl -Viscometer

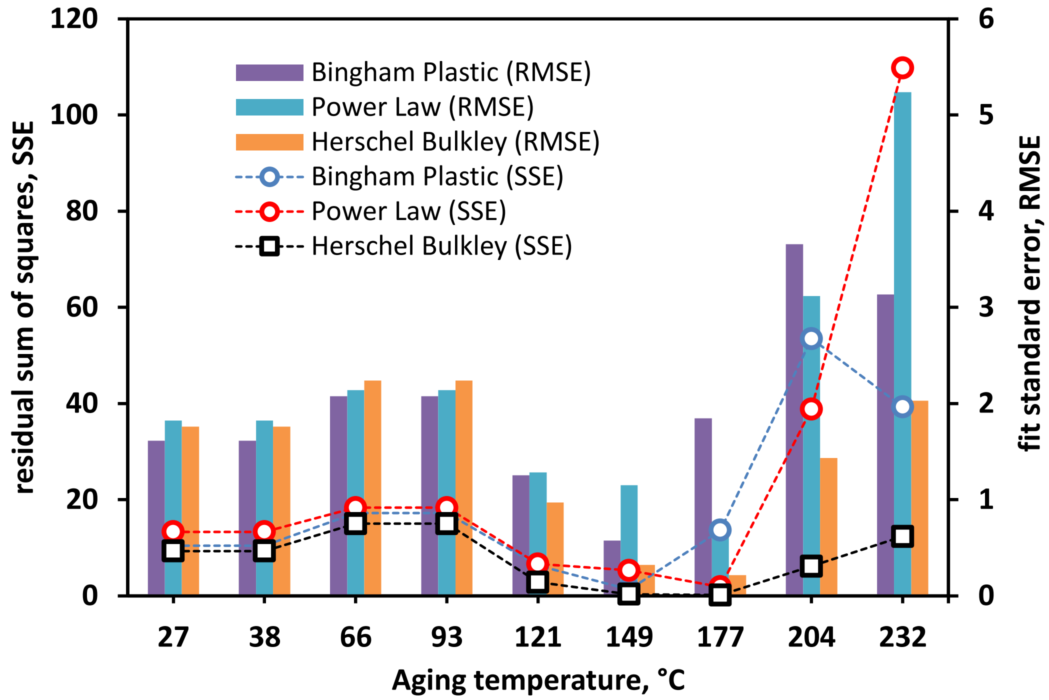

Figure G.5: SSE and RMSE for sepiolite mud with 342 kg/m^3 of NaCl -Viscometer

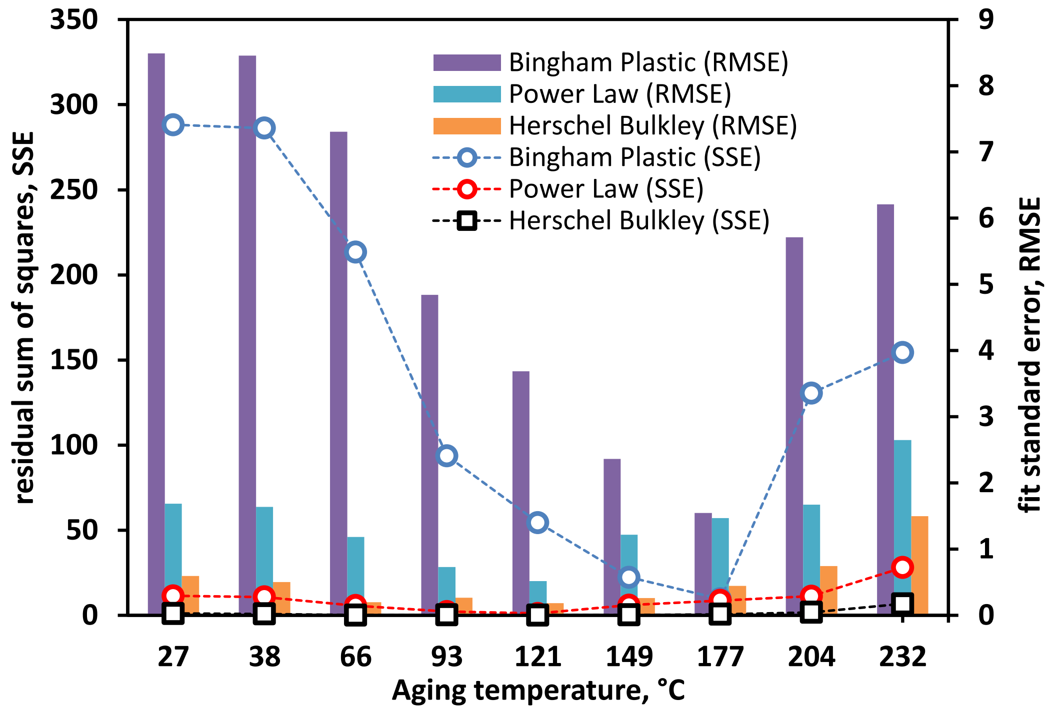

Figure G.6: SSE and RMSE for weighted fresh water sepiolite mud-Viscometer.

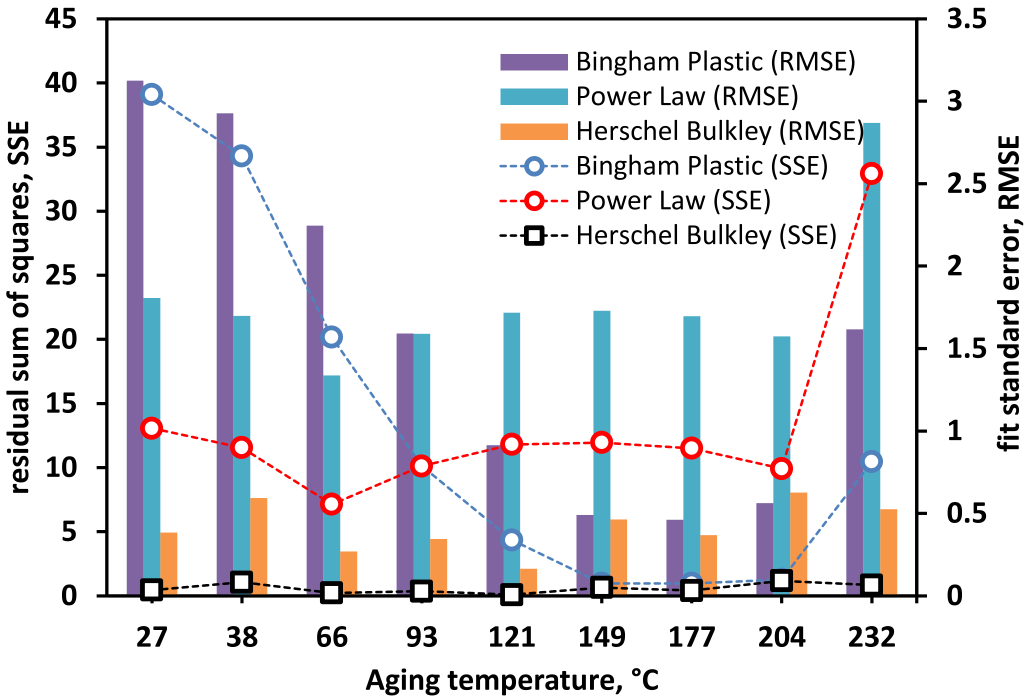

Figure G.7: SSE and RMSE for sepiolite and fresh water suspension-Viscometer

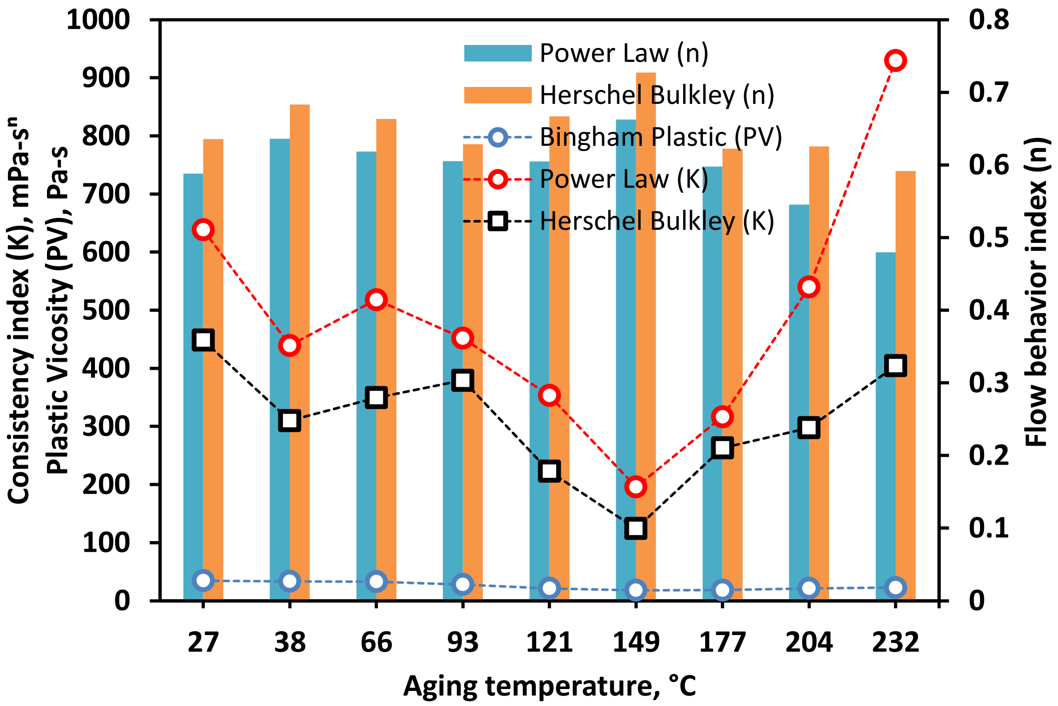

Figure G.8: Rheological parameters of unweighted fresh water sepiolite mud-Viscometer.

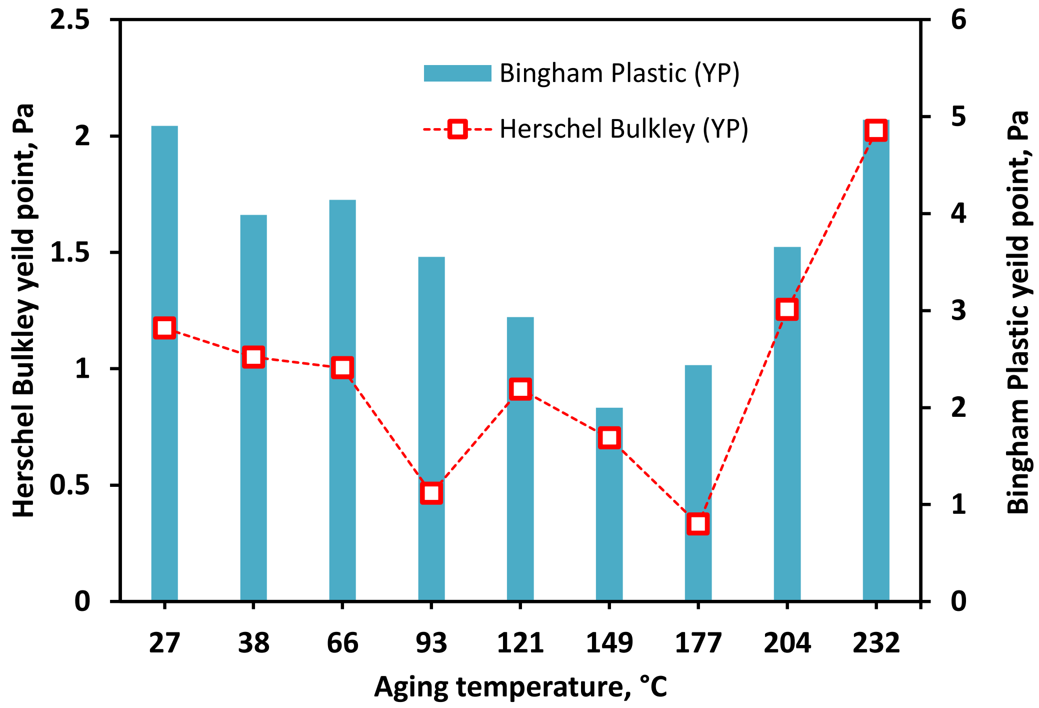

Figure G.9: Yield point for unweighted fresh water sepiolite mud-Viscometer

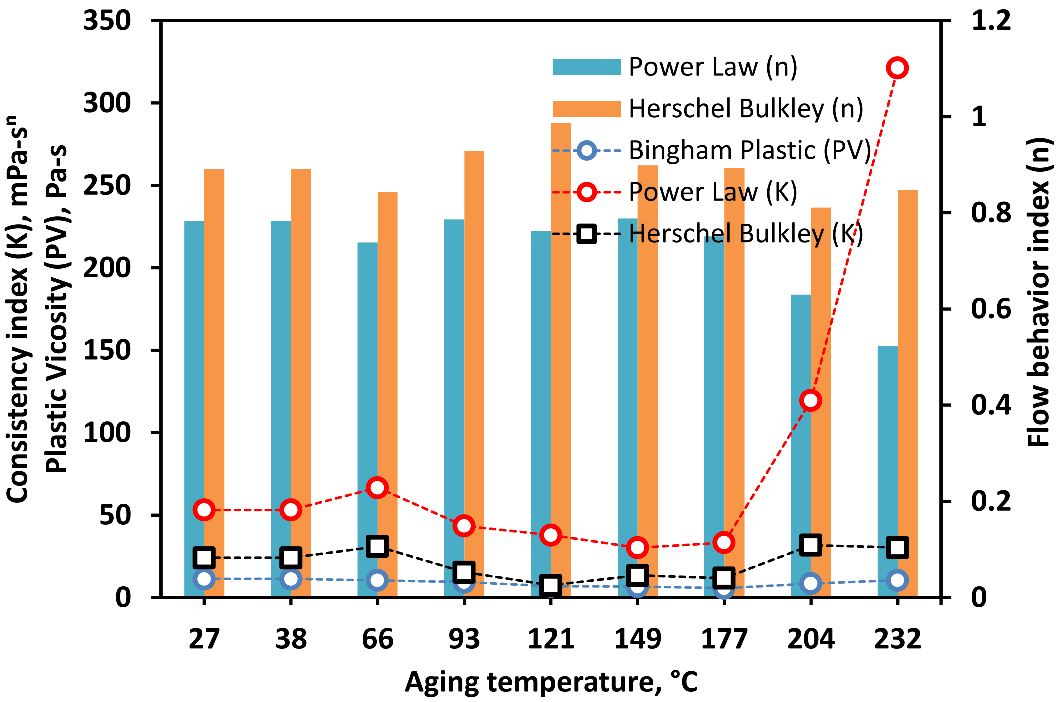

Figure G.10: Rheological parameters of semi saturated sepiolite mud-Viscometer

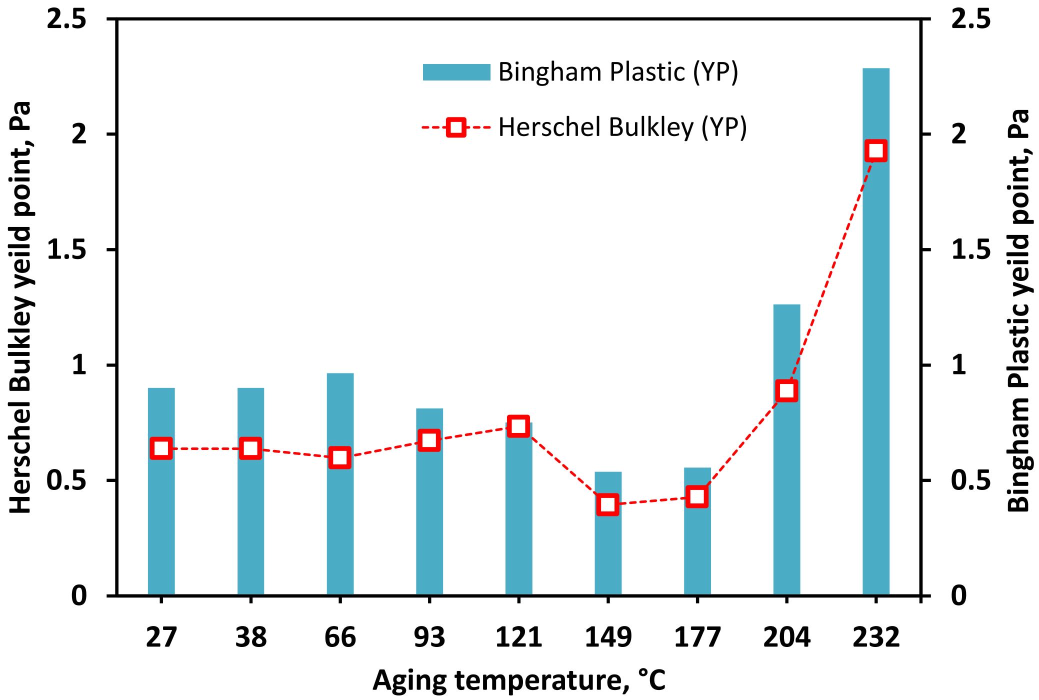

Figure G.11: Yield point for semi saturated sepiolite mud-Viscometer

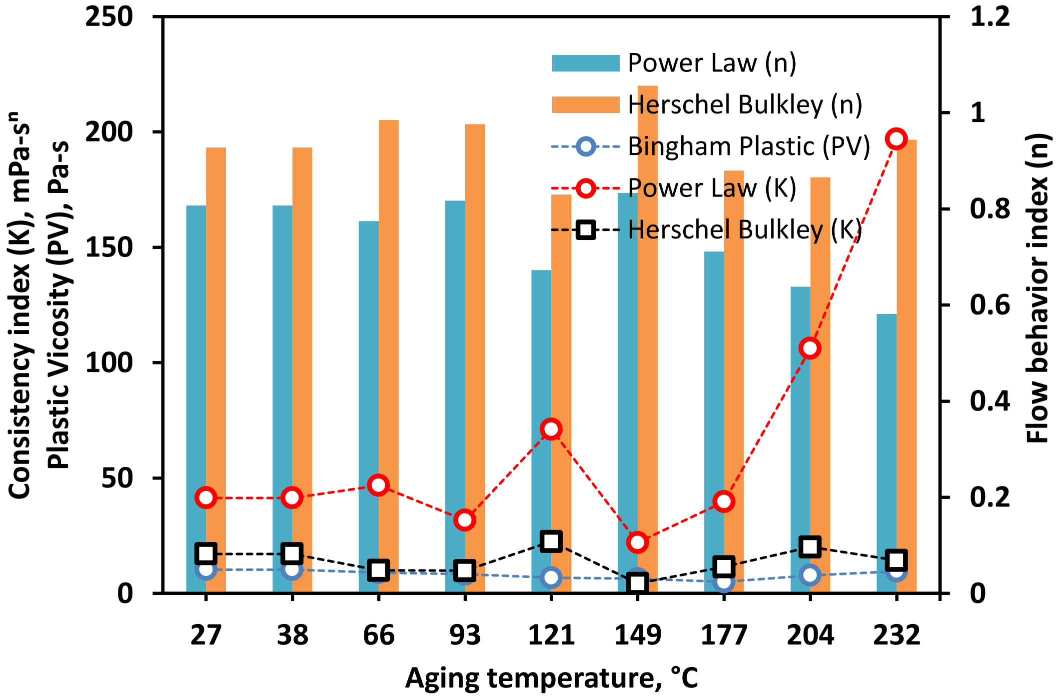

Figure G.12: Rheological parameters of fully saturated sepiolite mud-Viscometer

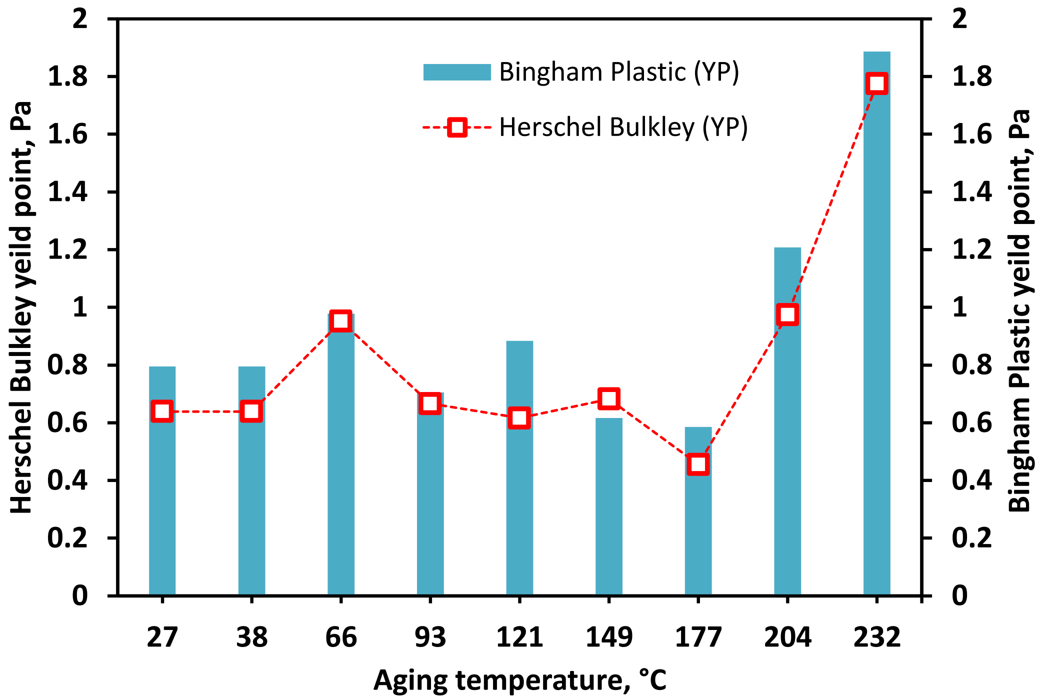

Figure G.13: Yield point for fully saturated sepiolite mud-Viscometer

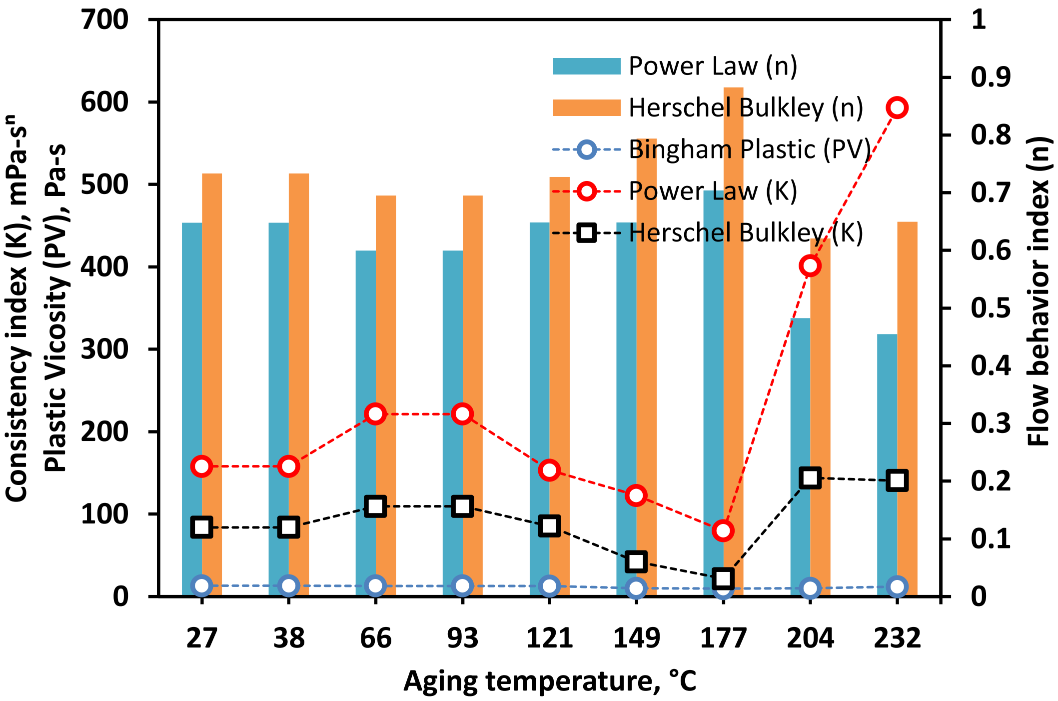

Figure G.14: Rheological parameters of sepiolite mud with 171 kg/m^3 of NaCl -Viscometer

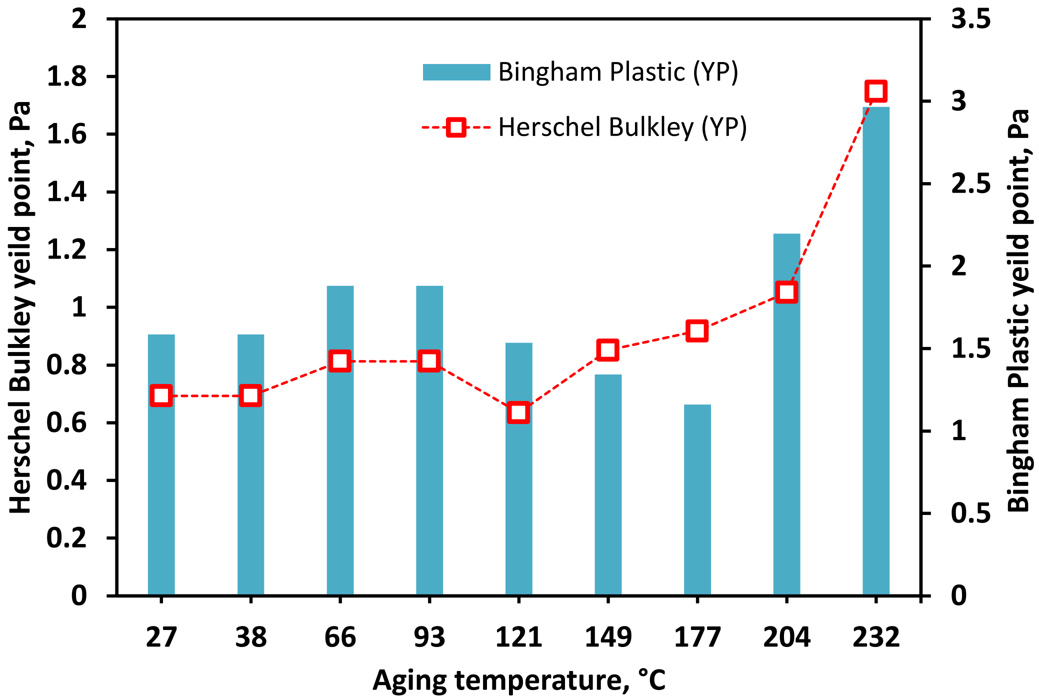

Figure G.15: Yield point for sepiolite mud with 171 kg/m^3 of NaCl -Viscometer

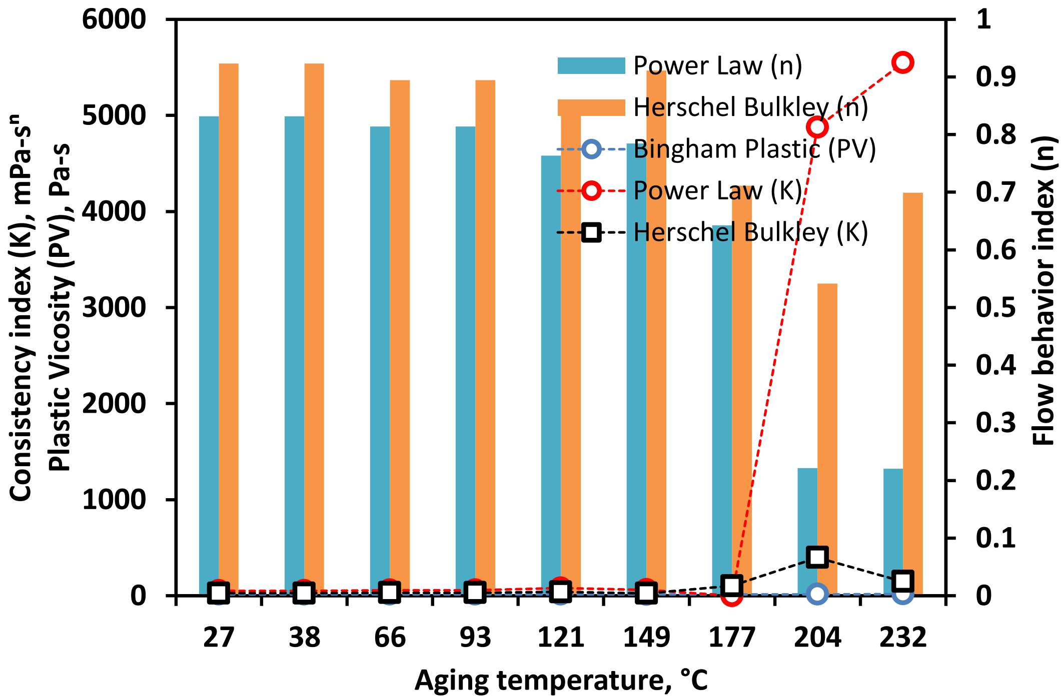

Figure G.16: Rheological parameters of sepiolite mud with 342 kg/m^3 of NaCl –Viscometer

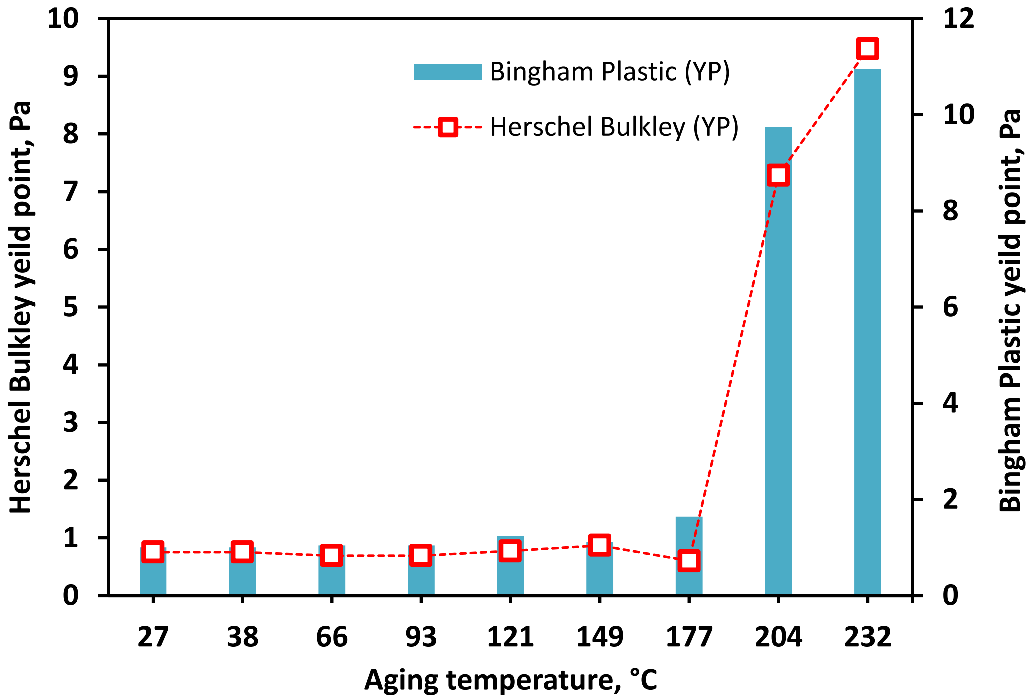

Figure G.17: Yield point for sepiolite mud with 342 kg/m^3 of NaCl -Viscometer

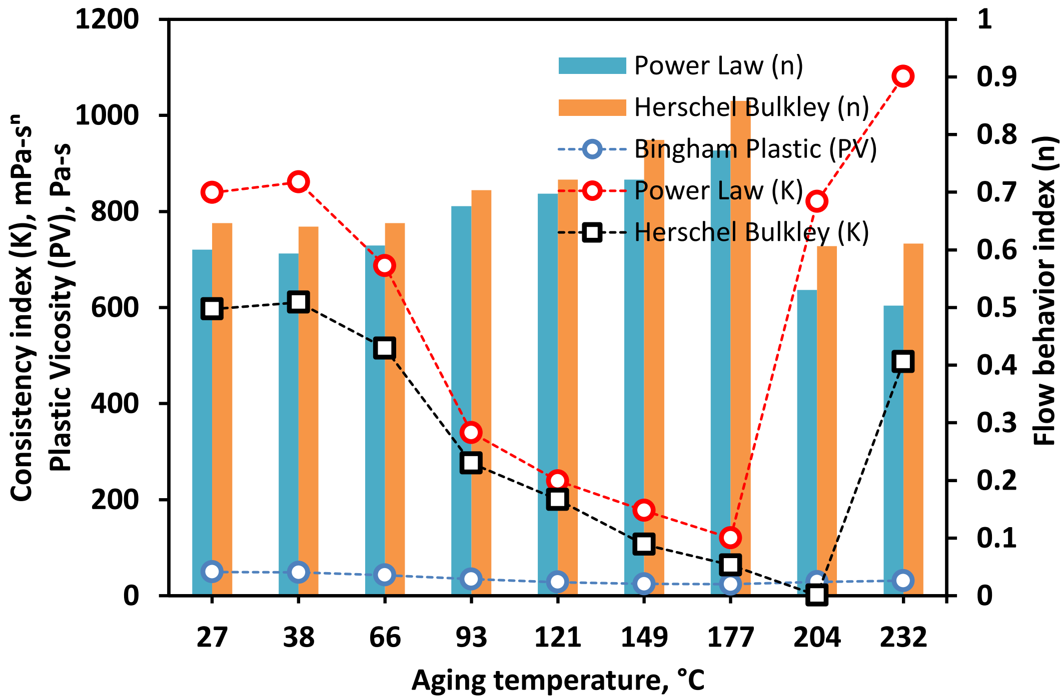

Figure G.18: Rheological parameters of weighted sepiolite mud-Viscometer

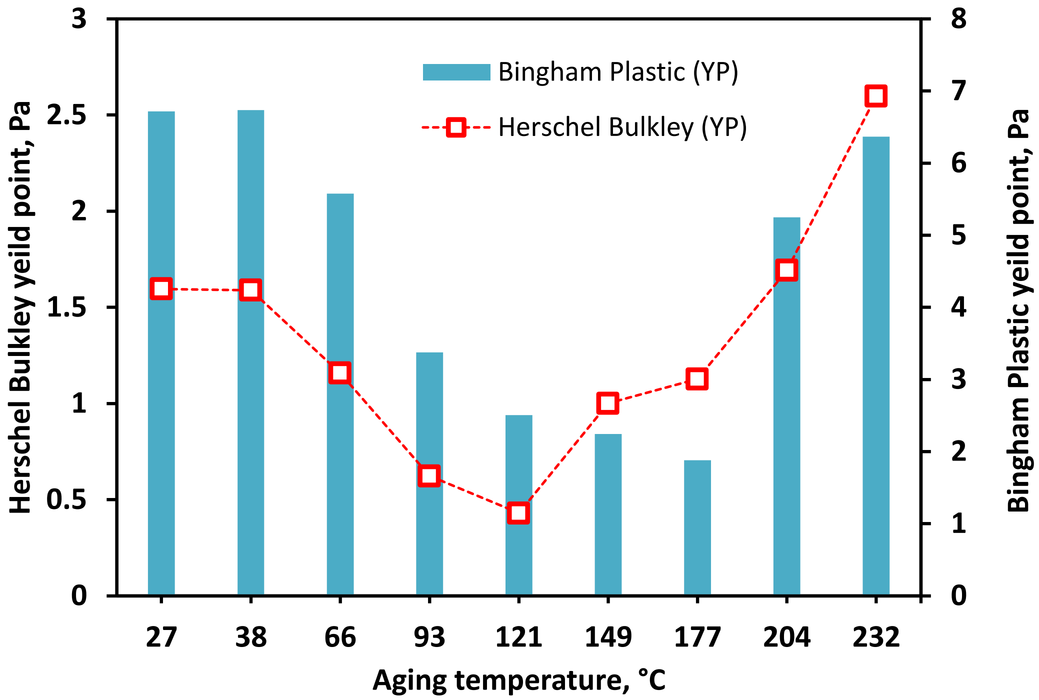

Figure G.19: Yield point for weighted sepiolite mud-Viscometer

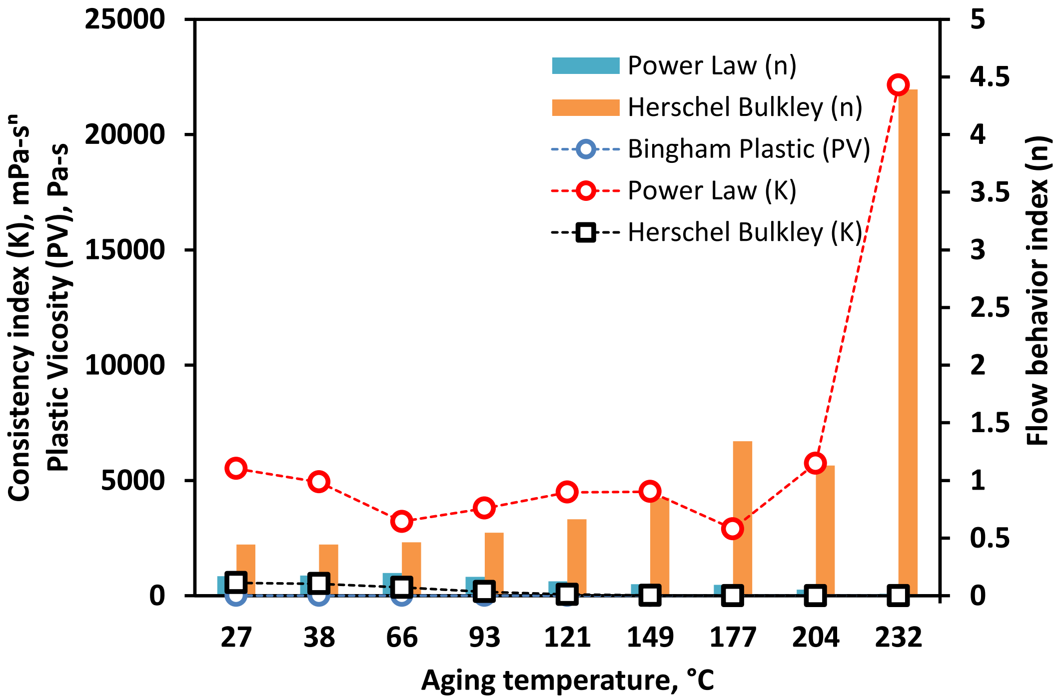

Figure G.20: Rheological parameters of sepiolite and fresh water suspension-Viscometer

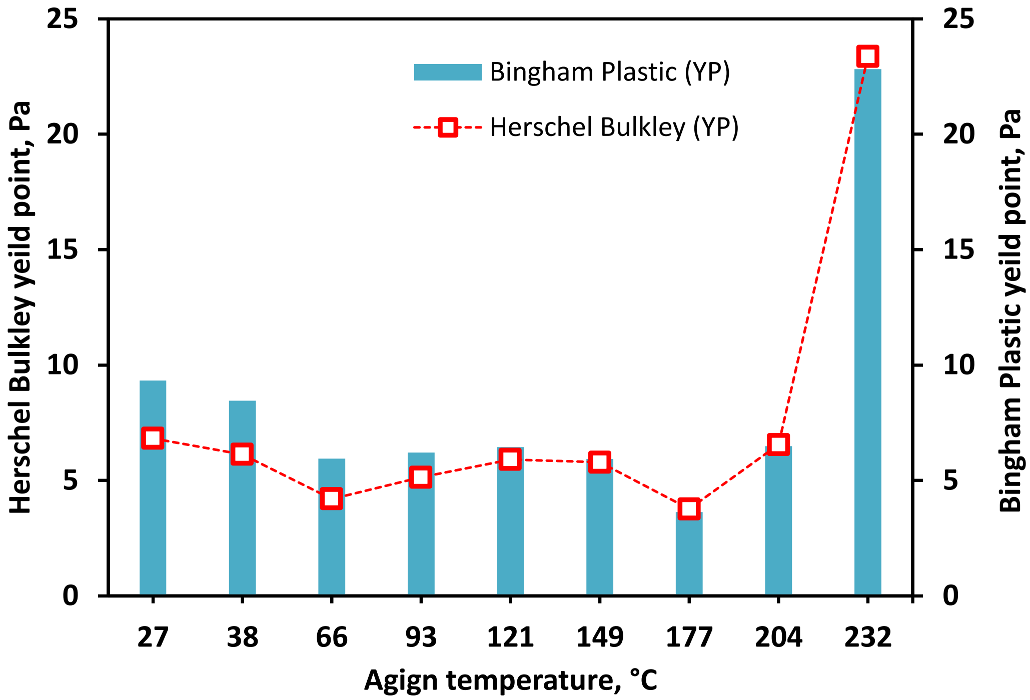

Figure G.21: Yield point for sepiolite and fresh water suspension-Viscometer

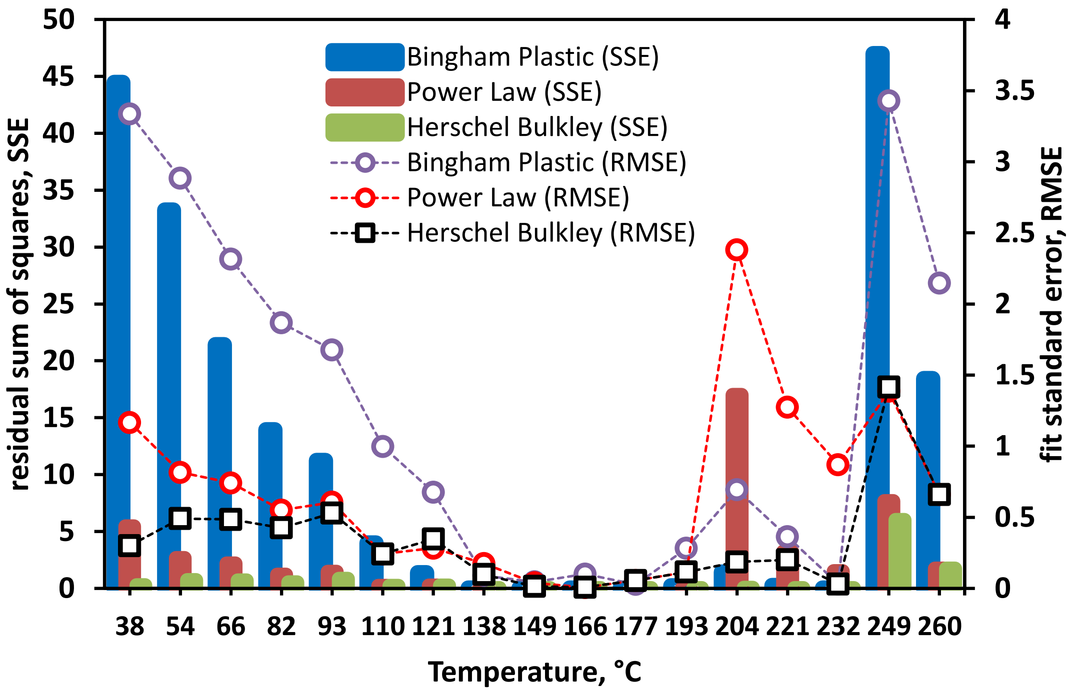

Figure G.22: SSE and RMSE for unweighted fresh water sepiolite mud-HTHP rheometer.

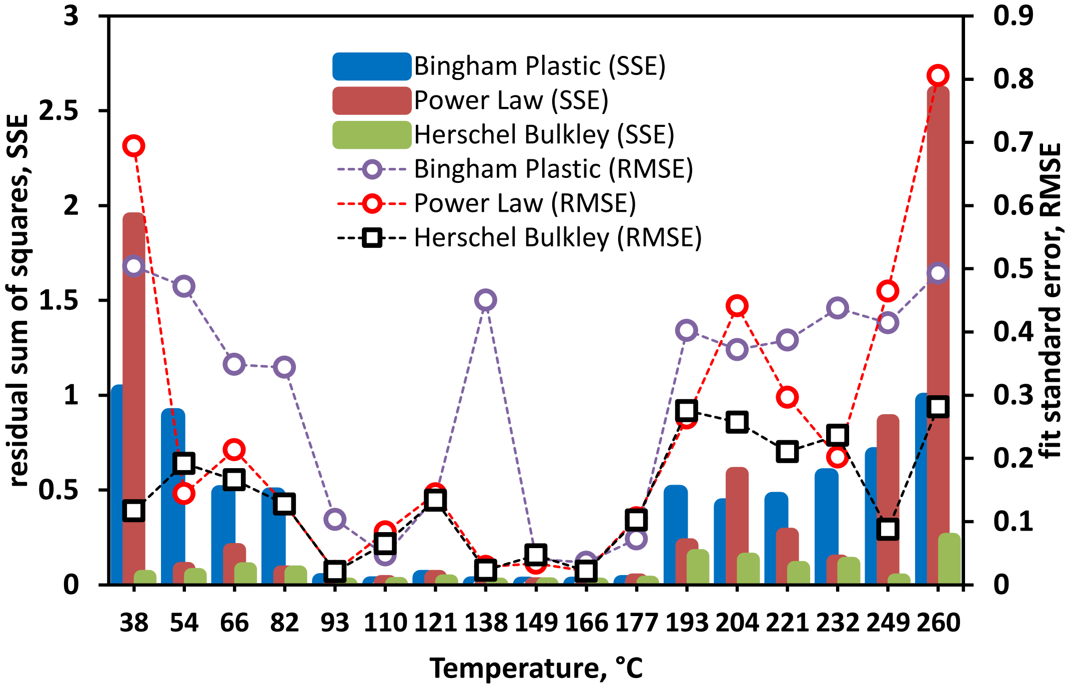

Figure G.23: SSE and RMSE for unweighted semi saturated sepiolite mud-HTHP rheometer.

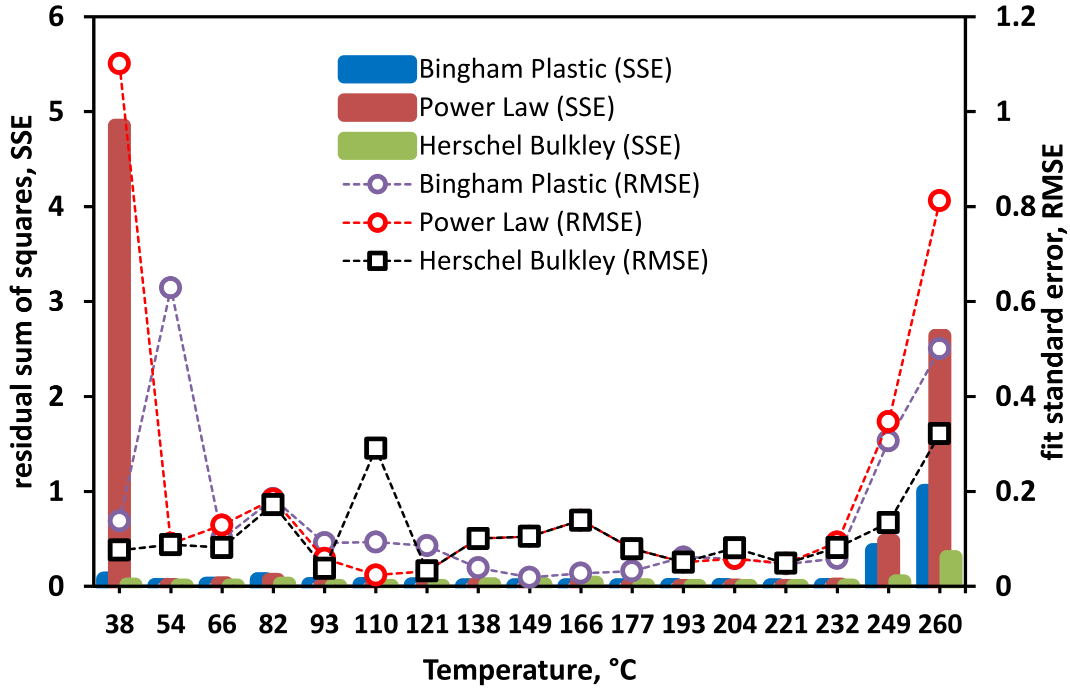

Figure G.24: SSE and RMSE for unweighted fully saturated sepiolite mud-HTHP rheometer.

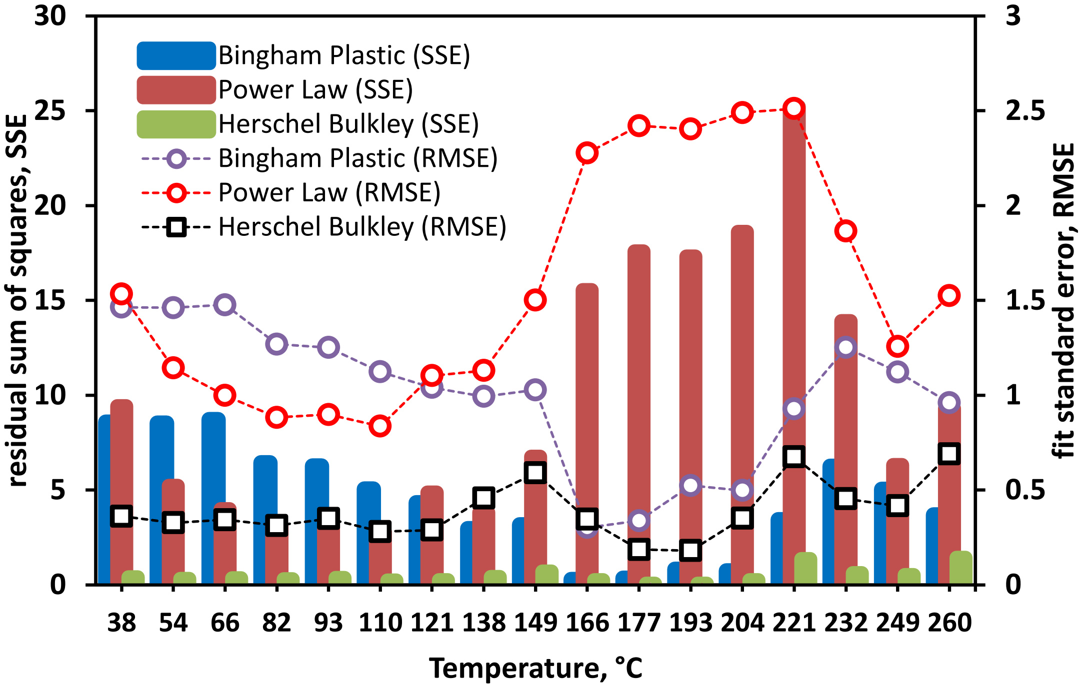

Figure G.25: SSE and RMSE for sepiolite mud with 171 kg/m^3 of NaCl - HTHP rheometer

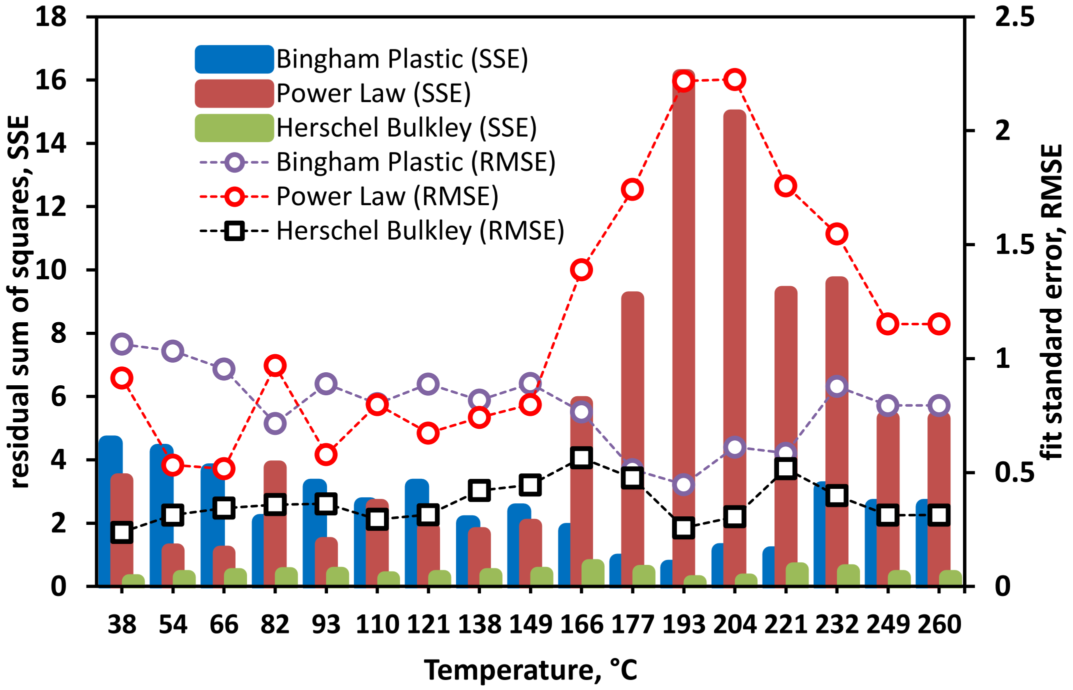

Figure G.26: SSE and RMSE for sepiolite mud with 342 kg/m^3 of NaCl - HTHP rheometer.

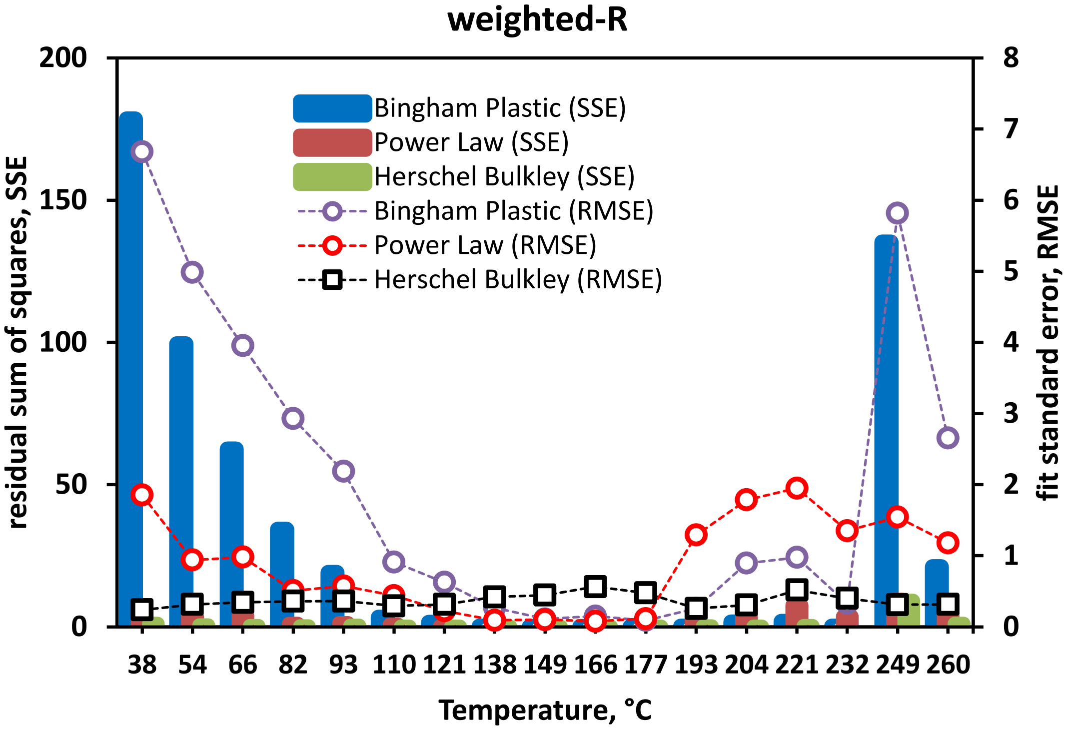

Figure G.27: SSE and RMSE for weighted fresh water sepiolite mud- HTHP rheometer.

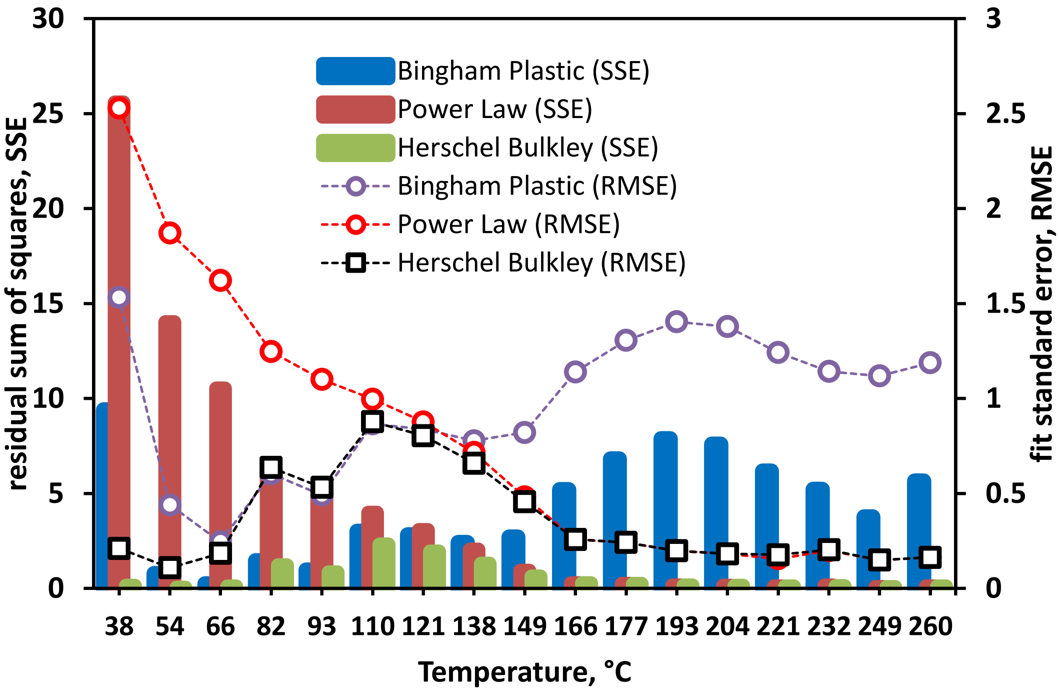

Figure G.28: SSE and RMSE for sepiolite and fresh water suspension- HTHP rheometer.

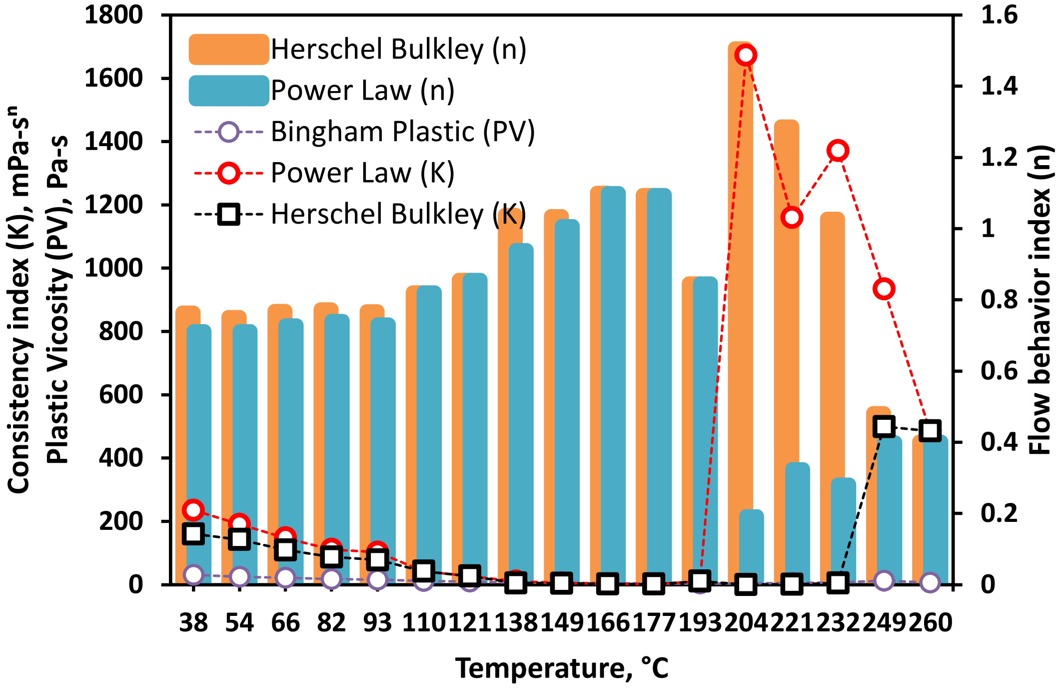

Figure G.29: Rheological parameters of unweighted fresh water sepiolite mud-HTHP rheometer.

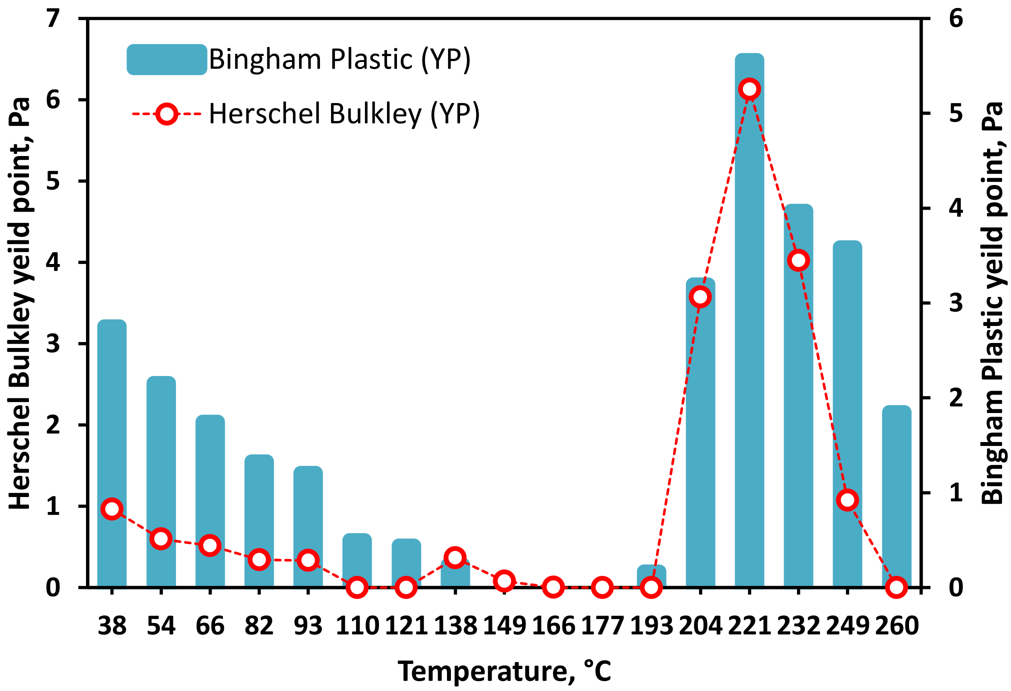

Figure G.30: Yield point for unweighted fresh water sepiolite mud-HTHP rheometer

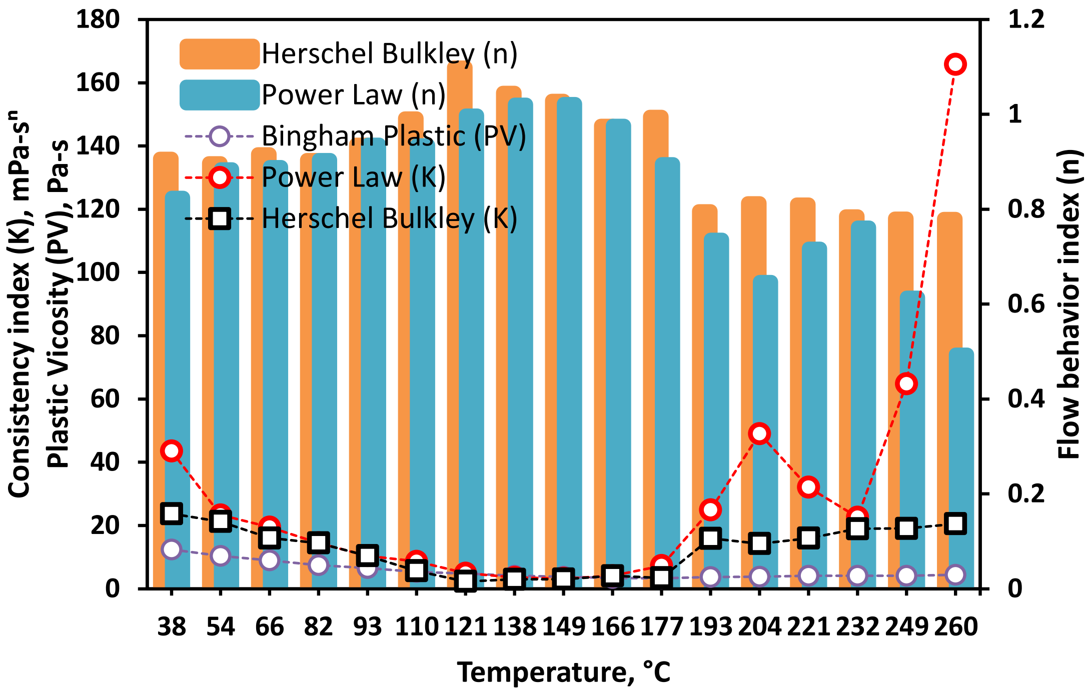

Figure G.31: Rheological parameters of semi saturated sepiolite mud- HTHP rheometer

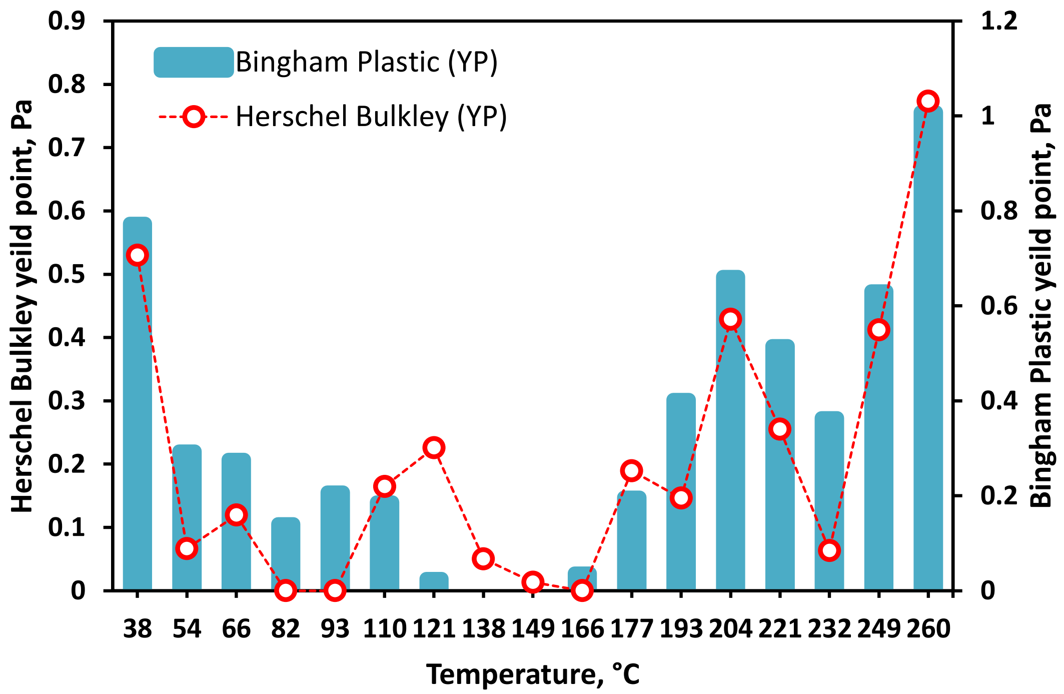

Figure G.32: Yield point for semi saturated sepiolite mud- HTHP rheometer

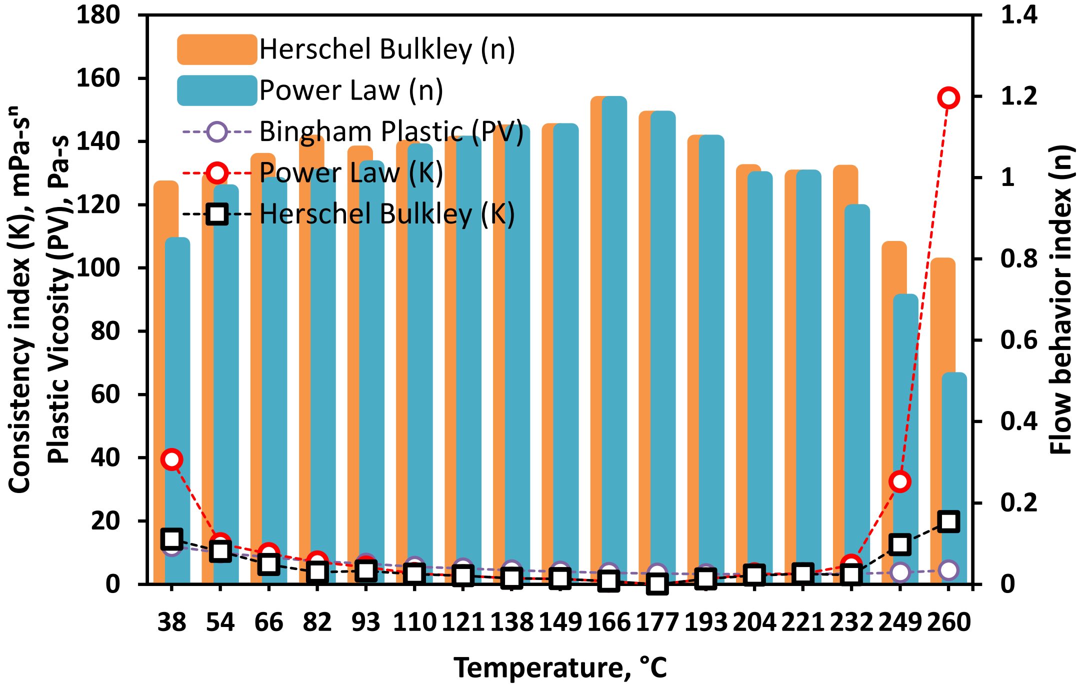

Figure G.33: Rheological parameters of fully saturated sepiolite mud- HTHP rheometer

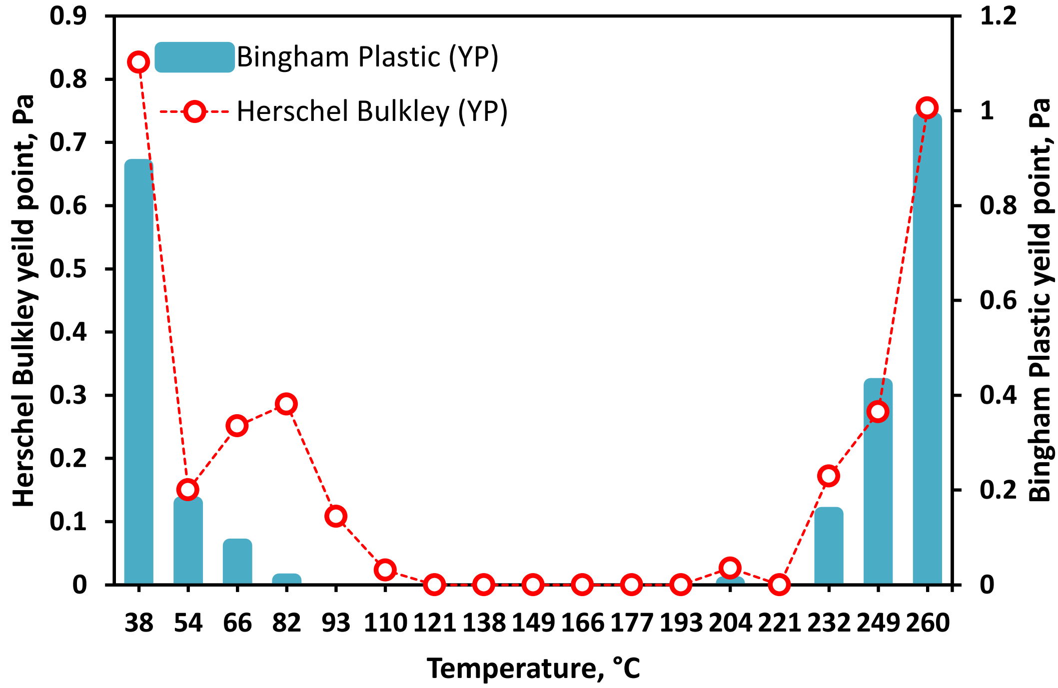

Figure G.34: Yield point for fully saturated sepiolite mud- HTHP rheometer

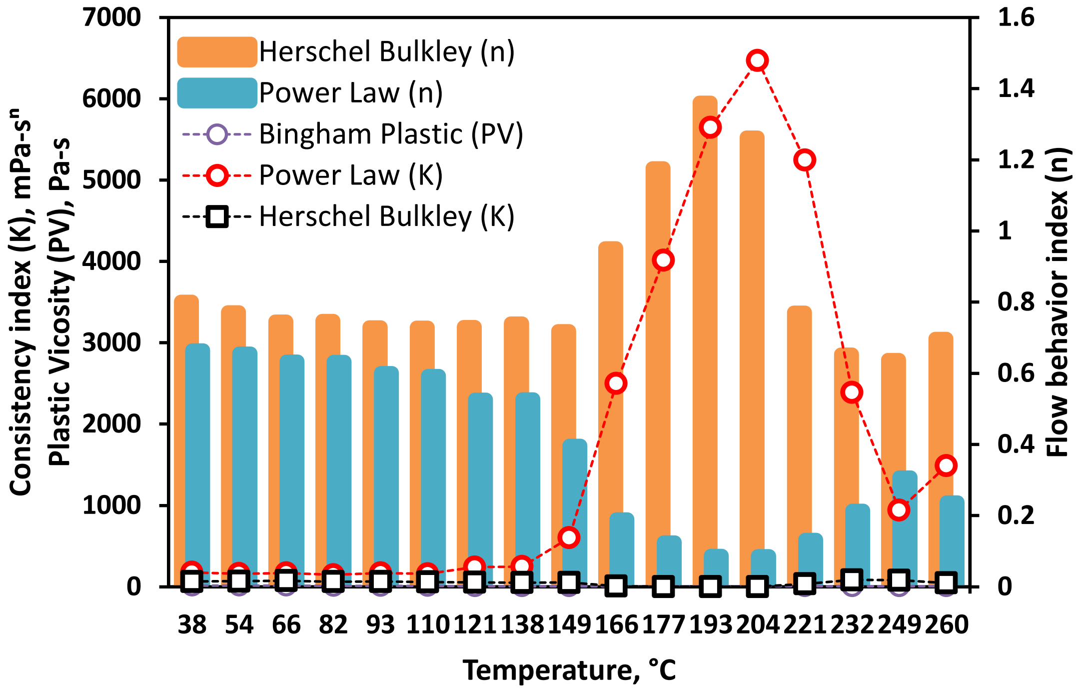

Figure G.35: Rheological parameters of sepiolite mud with 171 kg/m^3 of NaCl - HTHP rheometer.

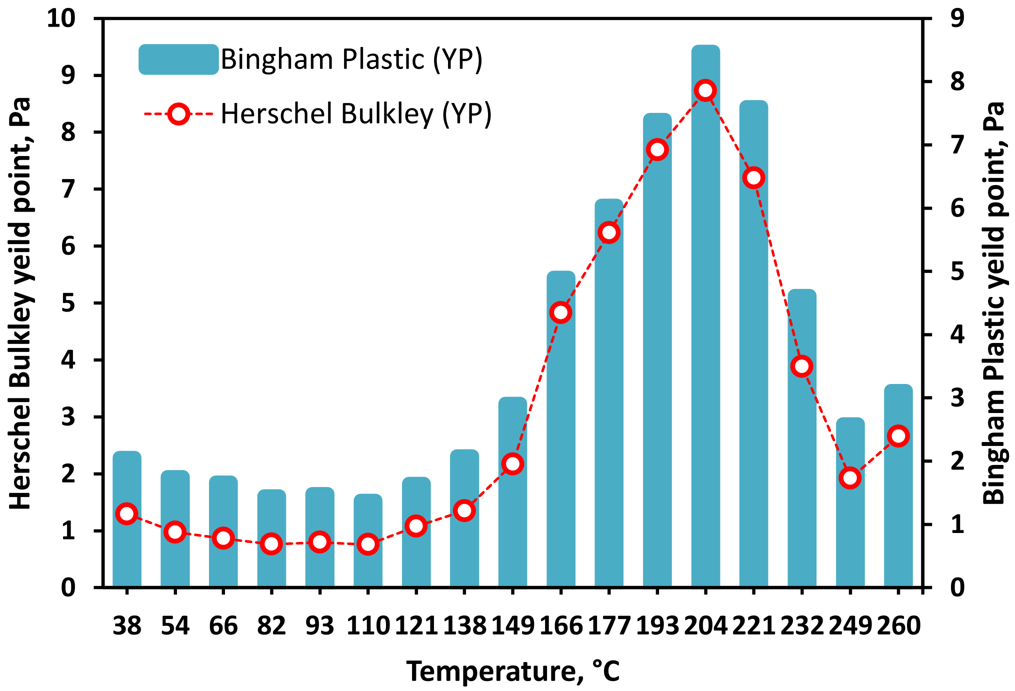

Figure G.36: Yield point for sepiolite mud with 171 kg/m^3 of NaCl - HTHP rheometer

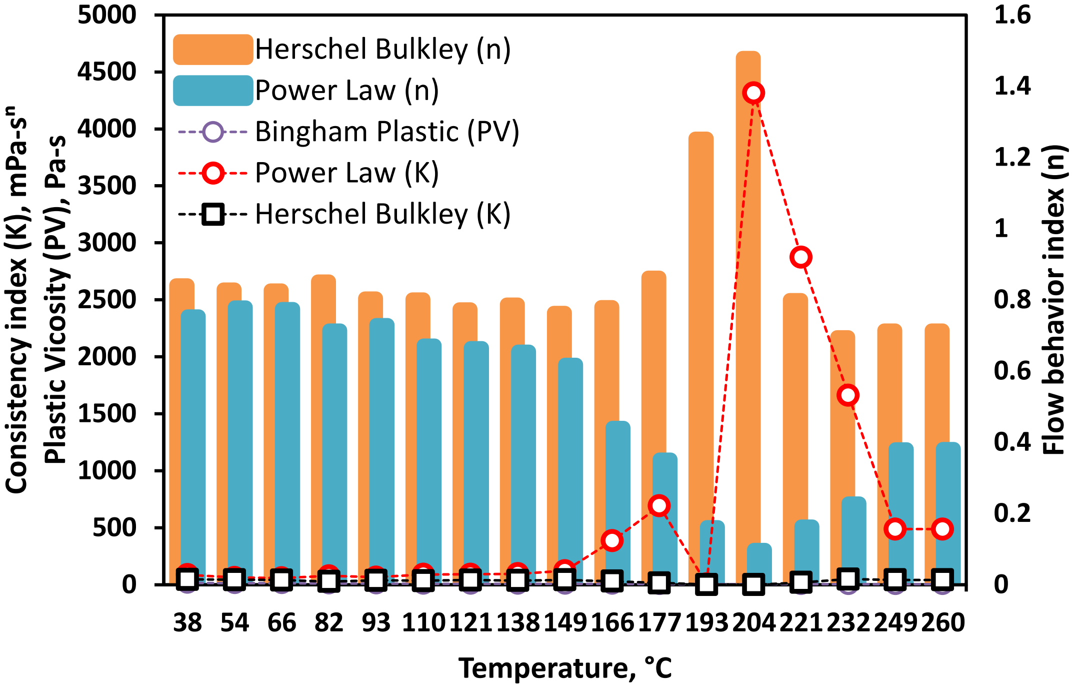

Figure G.37: Rheological parameters of sepiolite mud with 342 kg/m^3 of NaCl – HTHP rheometer.

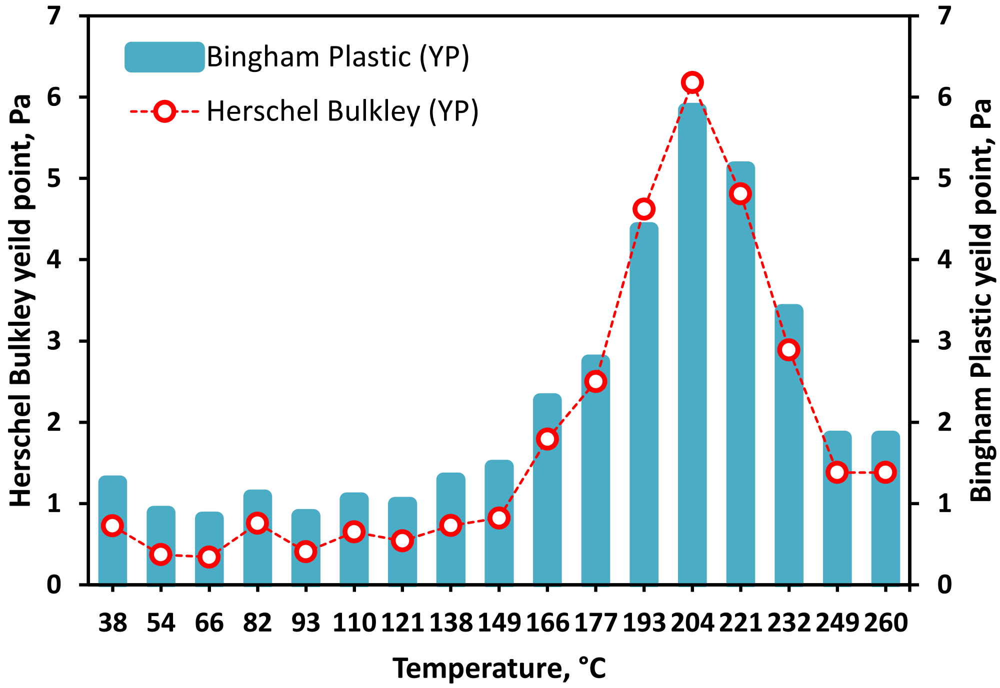

Figure G.38: Yield point for sepiolite mud with 342 kg/m^3 of NaCl - HTHP rheometer

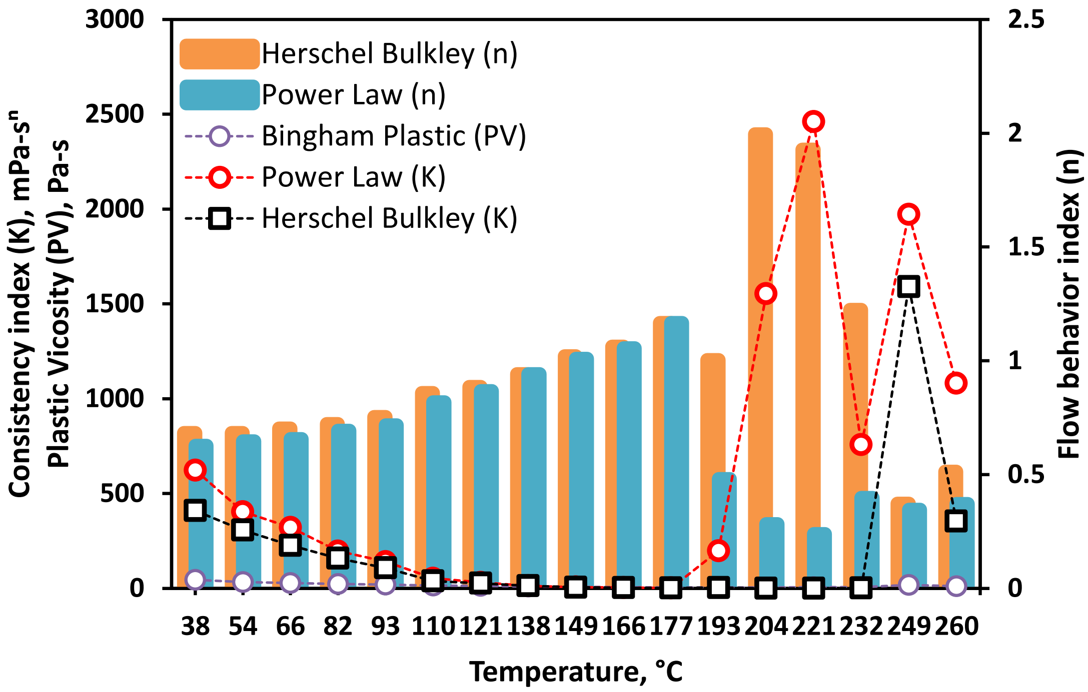

Figure G.39: Rheological parameters of weighted sepiolite mud- HTHP rheometer.

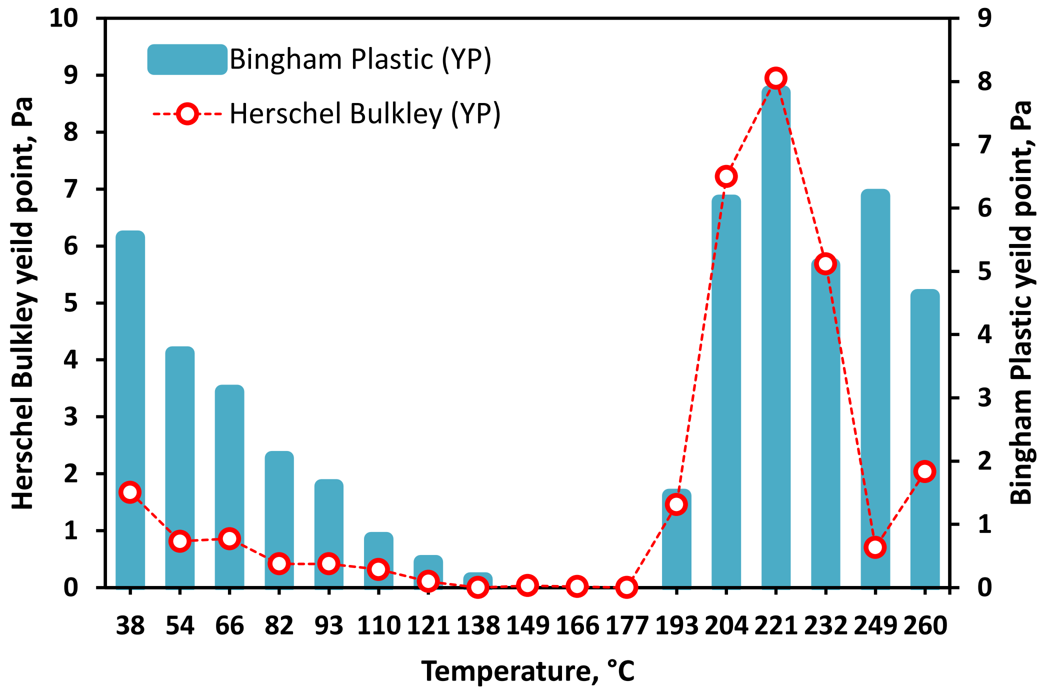

Figure G.40: Yield point for weighted sepiolite mud- HTHP rheometer

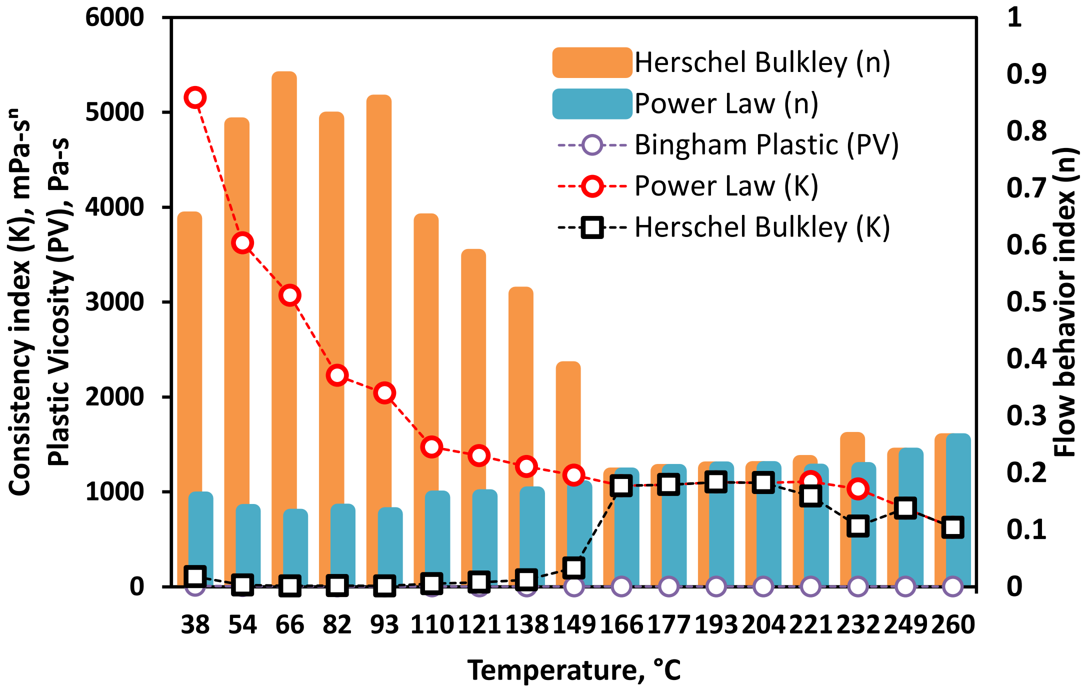

Figure G.41: Rheological parameters of sepiolite and fresh water suspension- HTHP rheometer.

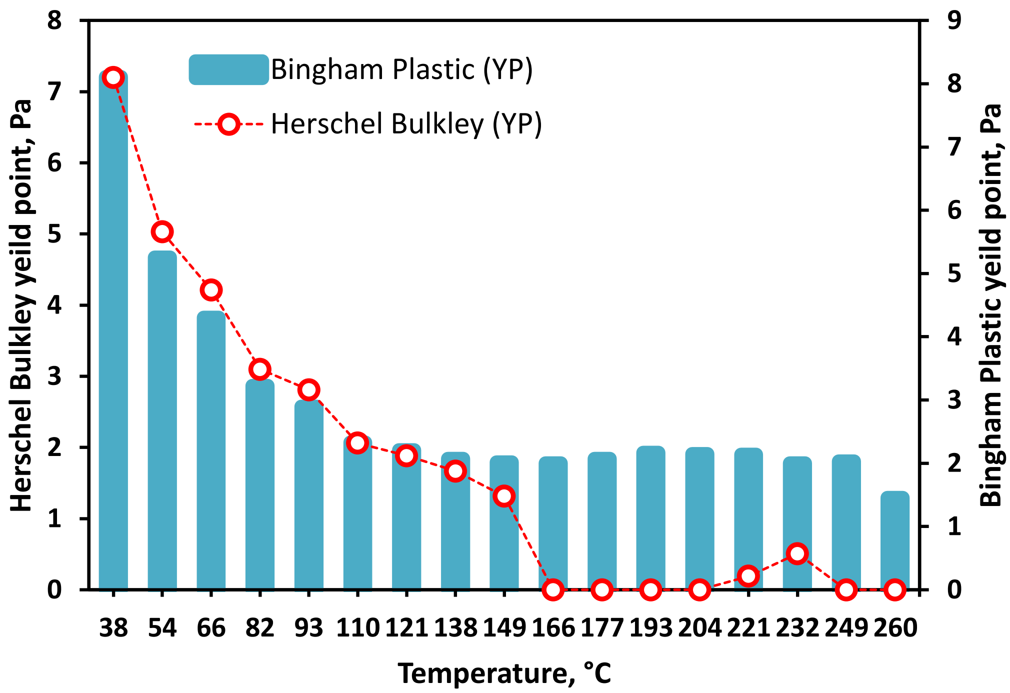

Figure G.42: Yield point for sepiolite and fresh water suspension- HTHP rheometer.

Appendix H: This appendix involves the Matlab codes to estimate frictional pressure losses due to pipe movement through tripping (Surge and Swab) period for Power Law, Bingham Plastic, and Herschel Bulkley fluids. Moreover, it contains a Matlab code to estimate frictional pressure losses through a concentric annulus with fixed boundaries for a Herschel Bulkley Fluid.

Matlab code H.1: Semi-Analytical Solution for Surge and Swab Pressure for a Herschel Bulkley and Bingham Plastic Fluid.

```
clear all
clc
close all
--------------------------------------------------------------------
-
% Semi-Analytical Solution for Surge and Swab Pressure for a
% Herschel Bulkley and Bingham Plastic Fluid
% n: flow behavior index, CON: consistency index, TY: Yield point
% Dout: outer diameter (hole diameter), Din: drill pipe diameter
% ro: density of fluid, h: annulus clearance, VpF: pipe velocity
ft/s
% Vp: pipe velocity m/s, VbarF: average velocity ft/s
% Vbar: average velocity m/s
% Dp: frictional pressure loss obtained from semi analytical method
% Qcf: flow rate ft³/m³. Qgal: flow rate gal/min
% to use code for Bingham plastic simply do n = 1 and CON = Plastic
% viscosity
--------------------------------------------------------------------
---
n = input('Enter value of n:');
Dout = input('Enter value of Dout in inch:');
Din = input('Enter value of Din in inch:');
CON = input('Enter value of CON in eq cp:');
TY = input('Enter value of TY in lb/100ft2:');
VpF = input('Enter value of VP in ft/s:');
h = 0.5*0.0254*(Dout-Din);
TY =TY*0.4788;
CON=CON*0.001;
tolerance = 0.1;
epsilon=0.0001;
Vp=VpF*0.3048;
Qcf=(pi/4)*VpF*(Din^2)/144;
Qgal=Qcf*448.831169;
VbarF=Qgal/(2.488*((Dout^2)-(Din^2)));
Vbar=abs(VbarF)*0.3048;
lambda1=0:0.001:1;
lambda2=0:0.001:1;
real_lambda1=zeros(size(length(Vp)));
real_lambda2=zeros(size(length(Vp)));
% real_lambda1=zeros(length(Vp),length(Vbar));
% real_lambda2=zeros(length(Vp),length(Vbar));
Dp=zeros(size(length(Vp)));
for k=1:length(Vp)
    for i=1:length(Vbar)
        for j=1:length(lambda1)
            for m=1:length(lambda2)
```

```
                    A=((1-lambda2(m))^(1+(1/n)));
                    F=(((lambda1(j)^(2+(1/n)))+((1-
lambda2(m))^(2+(1/n)))+((((((2*n)+1)/(1+n))*(lambda1(j)^(1+(1/n))))*
(lambda2(m)-lambda1(j)))))/(2+(1/n)));
                    G=(((2*TY)/(CON*(lambda2(m)-lambda1(j))))^(1/n));
                    B=((h*G*F)-Vbar(i))/Vp(k);
                    C=(Vbar(i)+(Vp(k)*(1-lambda2(m))));
                    D=lambda1(j)^(1+(1/n));
                    Q=Vp(k)*(1+(1/n));
                    E=((Q/h)*((CON/TY)^(1/n))*(((lambda2(m)-
lambda1(j))/2)^(1/n)));
                    err1=D-(A-((F*Q)/C));
                    err2=D-A+E;
                    err3=lambda2(m)-1+B;
                    if (((abs(err1) < tolerance) && (abs(err1) <
old_err1)) && ((abs(err2) < tolerance) && (abs(err2) < old_err2)) &&
((abs(err3) < tolerance) && (abs(err3) < old_err3)))
                         real_lambda1(k,i)=lambda1(j);
                         real_lambda2(k,i)=lambda2(m);
                    Dp(k,i) = (CON/(h^(n+1)))*(C^n)*((1/F)^n);
                    end
                    old_err1=abs(err1);
                    old_err2=abs(err2);
                    old_err3=abs(err3);
               end

          end
     end
end
```

Matlab code H.2: Semi-Analytical Solution for Surge and Swab Pressure for a Power Law Fluid.

```
clear all
clc
close all
-----------------------------------------------------------------------
% Semi-Analytical Solution for Surge and Swab Pressure for a
% Power Law Fluid
% n: flow behavior index, CON: consistency index, TY: Yield point
% Dout: outer diameter (hole diameter), Din: drill pipe diameter
% ro: density of fluid, h: annulus clearance, VpF: pipe velocity
ft/s
% Vp: pipe velocity m/s, VbarF: average velocity ft/s
% Vbar: average velocity m/s
% Dp: frictional pressure loss obtained from semi analytical method
% Qcf: flow rate ft³/m³. Qgal: flow rate gal/min
-----------------------------------------------------------------------
-
n = input('Enter value of n:');
Dout = input('Enter value of Dout in inch:');
Din = input('Enter value of Din in inch:');
CON = input('Enter value of CON in eq cp:');
VpF = input('Enter value of VP in ft/s:');
tolerance = 0.05;
CON=CON*0.001;
h = 0.5*0.0254*(Dout-Din);
Vp=VpF*0.3048;
Qcf=(pi/4)*VpF*(Din^2)/144;
Qgal=Qcf*448.831169;
VbarF=Qgal/(2.488*((Dout^2)-(Din^2)));
Vbar=VbarF*0.3048;

landa=0:0.0001:1;
landa1=zeros(size(length(Vbar)));
Dp=zeros(size(length(Vbar)));
est_landa=zeros(size(landa));
real_landa=zeros(size(length(Vp)));
err=zeros(length(landa),length(Vbar));
new_err=0;
for k=1:length(Vp)
    for i=1:length(Vbar)
        for j=1:length(landa)
            A=(1-landa(j))^(1+(1/n));

            B=Vp(k)*(1+(1/n))*((landa(j)^(2+(1/n)))+((1-
landa(j))^(2+(1/n))));
            C=(Vbar(i)+Vp(k)*(1-landa(j)))*(2+(1/n));
            est_landa(j)=((A-(B/C))^(n/(n+1)));
            err(j,i)=est_landa(j)-landa(j);
            if ((abs(err(j,i)) < tolerance) && (abs(err(j,i)) <
old_err))
                real_landa(k,i)=landa(j);

            end
                        old_err=abs(err(j,i));

        end
    end
```

```
end
            landa1(j)=real_landa(i);
                F=((landa1(j)^(2+(1/n)))+((1-landa1(j))^(2+(1/n))));
                C=(Vbar(i)+Vp(k)*(1-landa1(j)))*(2+(1/n));
            Dp(k,i) = (CON/(h^(n+1)))*((C/F)^n)

figure;plot(VpF,real_landa)
```

Matlab code H.3: Semi-Analytical Solution for Flow through a Concentric Annulus with Fixed Boundaries for a Herschel Bulkley Fluid

```
clear all
clc
close all
--------------------------------------------------------------------
% Semi-Analytical Solution for Flow through a Concentric Annulus
with
% Fixed Boundaries for a Herschel Bulkley Fluid
% n: flow behavior index, CON: consistency index, TY: Yield point
% Dout: Geometry outer diameter (hole diameter), Din: drill pipe
diameter
% ro: density of fluid, h: annulus clearance, y and z: Coefficients
% R:subtraction of squares of geometry radius, Vbar: average
velocity
% Dp: frictional pressure loss obtained from semi analytical method
% DpA: existing analytical frictional pressure loss method,
% Re: Reynold number, Reeq: equivalent Reynold number, Q: flow rate
% mu:viscosity, fic:friction factor, Ca: correlation coefficient
--------------------------------------------------------------------
--
n = input('Enter value of n:');
Dout = input('Enter value of Dout in inch:');
Din = input('Enter value of Din in inch:');
CON = input('Enter value of CON in Pa-s:');
TY = input('Enter value of TY in Pa:');
ro = input('Enter value of ro in kg/m³:');
h = 0.5*0.0254*(Dout-Din);
O = 0.5*0.0254*(Dout+Din);
R = ((0.5*0.0254*Dout)^2)-((0.5*0.0254*Din)^2);
y = (log(n)+3.93)/50;
z = (1.75-log(n))/7;
tolerance = 0.05;
dx=0.001;
dx=dx*0.3048;
Vbar=0.001*0.3048:dx:10*0.3048;
lambda=0:0.001:1;
est_lambda=zeros(size(lambda));
real_lambda=zeros(size(length(Vbar)));
err=zeros(length(lambda),length(Vbar));
new_err=0;
lambda2=zeros(size(length(Vbar)));
lambda1=zeros(size(length(Vbar)));
Dp2=zeros(size(length(Vbar)));
Dp1=(size(length(Vbar)));
DpA=zeros(size(length(Vbar)));
Q=zeros(size(length(Vbar)));
Ca=zeros(size(length(Vbar)));
Re=zeros(size(length(Vbar)));
mu=zeros(size(length(Vbar)));
Reeq=zeros(size(length(Vbar)));
fic=zeros(size(length(Vbar)));
    for i=1:length(Vbar)
        for j=1:length(lambda)
A=(h*(2*(1-lambda(j))^(2+(1/n))+((((2*n)+1)/(1+n))*((1-
lambda(j))^(1+(1/n)))*((2*lambda(j))-1))));
            B=(Vbar(i)*(2+(1/n)));
            C=TY/CON;
            est_lambda(j)=(C*((A/B))^n)+0.5;
            err(j,i)=est_lambda(j)-lambda(j);
```

```
        if ((abs(err(j,i)) < tolerance) && (abs(err(j,i)) <
old_err))
                real_lambda(i)=lambda(j);

lambda2(i)=real_lambda(i);
lambda1(i)=1-lambda2(i);
Dp1(i)=(2*TY)/((lambda2(i)-lambda1(i))*h);
D=(((lambda1(i))^(2+(1/n)))+((1-
lambda2(i))^(2+(1/n)))+((((2*n)+1)/(1+n))*(lambda1(i)^(1+(1/n)))*(la
mbda2(i)-lambda1(i))));
E=CON/(h^(1+n));
Dp2(i)=E*((B/D)^n);

            end
            old_err=abs(err(j,i));
        end

    end

figure,plot(Vbar,lambda1,'-r',Vbar,lambda2,':b')
legend('Lambda1', 'Lambda2');
title('Lambda');
xlabel('Average velocity,m/sec');
ylabel('Lambda1,Lambda2');

F = 1/(1+n);
    G = (2*((2*n)+1)/(n*h));

for i=1:length(Vbar)

Q(i) = pi*R*Vbar(i);
Ca(i) = 1-(F*(TY/(TY+(CON*((G*(Q(i)/(pi*R)))^n)))));
mu(i) =
(TY+(CON*((G*(Q(i)/(pi*Ca(i)*R)))^n)))/(G*(Q(i)/(pi*Ca(i)*R)));
Re(i) = (2*ro*Q(i))/(mu(i)*pi*O);
Reeq(i) = Ca(i)*Re(i);
fic(i) = (8/Reeq(i))*(((2*n)+1)/n);
DpA(i) = ((fic(i)*ro)*(Q(i)^2))/((pi^2)*h*(R^2));
end
figure,plot(Vbar,Dp2,':r',Vbar,DpA,'-b')
legend('Semi-analytical pressure loss,Pa/m','Analytical pressure
loss,Pa/m');
title('Pressure loss');
xlabel('Average velocity,m/sec');
ylabel('Semi-analytical pressure loss,Pa/m');
```

Appendix I: Surge pressure gradient for unweighted fresh water sepiolite mud – semi analytical method.

Table I.1: Surge pressure gradient for unweighted fresh water sepiolite mud: Burkhardt model vs. Semi analytical model.

Pipe velocity (m/s)	Temperature °C	Plastic viscosity (mPa-s)	Yield Point (Pa)	Effective velocity (m/s)	Plasticity (S)	Conductance (Y)	Reynold number	Friction factor	Surge pressure gradient (kPa/m)	
									Burkhardt method	Semi analytical method
0.3048	27	34.56	4.905	0.659	8.880	0.478	820	0.061	1.347	1.316
	38	33.52	3.986	0.659	7.440	0.521	845	0.054	1.198	1.174
	65	32.82	4.141	0.659	7.894	0.506	863	0.055	1.207	1.180
	93	27.83	3.556	0.659	7.994	0.503	1018	0.047	1.030	1.006
	121	21.46	2.934	0.659	8.555	0.487	1320	0.037	0.821	0.802
	149	17.98	1.999	0.659	6.955	0.537	1576	0.028	0.623	0.610
	177	18.44	2.438	0.659	8.274	0.495	1537	0.032	0.694	0.678
	204	21.33	3.656	0.659	10.722	0.432	1328	0.042	0.920	0.892
	232	22.72	4.967	0.659	13.677	0.375	1247	0.051	1.128	1.087
0.6096	27	34.56	4.905	1.319	4.440	0.644	1640	0.023	1.998	1.974
	38	33.52	3.986	1.319	3.720	0.683	1691	0.021	1.827	1.808
	65	32.82	4.141	1.319	3.947	0.670	1727	0.021	1.823	1.808
	93	27.83	3.556	1.319	3.997	0.668	2036	0.018	1.552	1.542
	121	21.46	2.934	1.319	4.278	0.653	2641	0.014	1.225	1.210
	149	17.98	1.999	1.319	3.477	0.698	3152	0.011	0.960	0.952
	177	18.44	2.438	1.319	4.137	0.660	3074	0.012	1.040	1.030
	204	21.33	3.656	1.319	5.361	0.600	2656	0.015	1.324	1.302
	232	22.72	4.967	1.319	6.838	0.541	2494	0.018	1.563	1.534

Table I.1 (Continued): Surge pressure gradient for unweighted fresh water sepiolite mud: Burkhardt model vs. Semi analytical model.

Pipe velocity (m/s)	Temperature °C	Plastic viscosity (mPa-s)	Yield Point (Pa)	Effective velocity (m/s)	Plasticity (S)	Conductance (Y)	Reynold number	Friction factor	Surge pressure gradient (kPa/m)	
									Burkhardt method	Semi analytical method
0.9144	27	34.56	4.905	1.978	2.960	0.730	2460	0.013	2.644	2.632
	38	33.52	3.986	1.978	2.480	0.764	2536	0.012	2.452	2.442
	65	32.82	4.141	1.978	2.631	0.753	2590	0.012	2.436	2.432
	93	27.83	3.556	1.978	2.665	0.750	3054	0.010	2.072	2.062
	121	21.46	2.934	1.978	2.852	0.738	3961	0.008	1.625	1.615
	149	17.98	1.999	1.978	2.318	0.776	4727	0.007	1.295	1.290
	177	18.44	2.438	1.978	2.758	0.744	4611	0.007	1.384	1.377
	204	21.33	3.656	1.978	3.574	0.692	3984	0.009	1.723	1.705
	232	22.72	4.967	1.978	4.559	0.638	3741	0.010	1.990	1.967
1.2192	27	34.56	4.905	2.638	2.220	0.783	3279	0.009	3.288	3.282
	38	33.52	3.986	2.638	1.860	0.811	3381	0.009	3.077	3.074
	65	32.82	4.141	2.638	1.973	0.802	3453	0.009	3.047	3.043
	93	27.83	3.556	2.638	1.998	0.800	4073	0.007	2.590	2.580
	121	21.46	2.934	2.638	2.139	0.789	5282	0.006	2.025	2.019
	149	17.98	1.999	2.638	1.739	0.822	6303	0.005	1.630	1.629
	177	18.44	2.438	2.638	2.068	0.795	6147	0.005	1.728	1.722
	204	21.33	3.656	2.638	2.681	0.749	5312	0.006	2.121	2.108
	232	22.72	4.967	2.638	3.419	0.701	4988	0.007	2.414	2.397

Table I.1 (Continued): Surge pressure gradient for unweighted fresh water sepiolite mud: Burkhardt model vs. Semi analytical model.

Pipe velocity (m/s)	Temperature °C	Plastic viscosity (mPa-s)	Yield Point (Pa)	Effective velocity (m/s)	Plasticity (S)	Conductance (Y)	Reynold number	Friction factor	Surge pressure gradient (kPa/m)	
									Burkhardt method	Semi analytical method
1.524	27	34.56	4.905	3.297	1.776	0.818	4099	0.007	3.932	3.927
	38	33.52	3.986	3.297	1.488	0.843	4226	0.007	3.701	3.702
	65	32.82	4.141	3.297	1.579	0.835	4317	0.007	3.661	3.651
	93	27.83	3.556	3.297	1.599	0.834	5091	0.006	3.109	3.106
	121	21.46	2.934	3.297	1.711	0.824	6602	0.004	2.425	2.421
	149	17.98	1.999	3.297	1.391	0.852	7879	0.004	1.965	1.962
	177	18.44	2.438	3.297	1.655	0.829	7684	0.004	2.071	2.065
	204	21.33	3.656	3.297	2.144	0.789	6641	0.005	2.518	2.509
	232	22.72	4.967	3.297	2.735	0.746	6235	0.005	2.838	2.817
1.8288	27	34.56	4.905	3.957	1.480	0.844	4919	0.006	4.575	4.564
	38	33.52	3.986	3.957	1.240	0.866	5072	0.005	4.325	4.329
	65	32.82	4.141	3.957	1.316	0.859	5180	0.005	4.270	4.268
	93	27.83	3.556	3.957	1.332	0.857	6109	0.005	3.627	3.631
	121	21.46	2.934	3.957	1.426	0.849	7922	0.004	2.825	2.820
	149	17.98	1.999	3.957	1.159	0.873	9455	0.003	2.300	2.299
	177	18.44	2.438	3.957	1.379	0.853	9221	0.003	2.415	2.414
	204	21.33	3.656	3.95653	1.787	0.817	7969	0.004	2.916	2.909
	232	22.72	4.967	3.95653	2.279	0.778	7482	0.004	3.261	3.249

Table I.2: Surge pressure gradient for unweighted fresh water sepiolite mud: Schuh model vs. Semi analytical model.

Pipe velocity (m/s)	Temperature °C	Flow behavior index (n)	Consistency index (Pa-s^n)	Effective velocity (m/s)	Reynold number	Friction factor	Surge pressure gradient (kPa/m)	
							Schuh method	Semi analytical method
0.3048	27	0.588	0.639	0.659	342	0.070	1.540	1.540
	38	0.636	0.440	0.659	392	0.061	1.347	1.348
	65	0.618	0.518	0.659	363	0.066	1.454	1.454
	93	0.605	0.452	0.659	444	0.054	1.188	1.188
	121	0.605	0.353	0.659	570	0.042	0.926	0.926
	149	0.663	0.196	0.659	769	0.031	0.686	0.686
	177	0.598	0.317	0.659	659	0.036	0.801	0.801
	204	0.545	0.540	0.659	502	0.048	1.051	1.051
	232	0.480	0.930	0.659	405	0.059	1.302	1.300
0.6096	27	0.588	0.639	1.319	911	0.026	2.315	2.315
	38	0.636	0.440	1.319	1008	0.024	2.093	2.094
	65	0.618	0.518	1.319	945	0.025	2.232	2.232
	93	0.605	0.452	1.319	1168	0.021	1.807	1.807
	121	0.605	0.353	1.319	1499	0.016	1.408	1.408
	149	0.663	0.196	1.319	1944	0.012	1.085	1.086
	177	0.598	0.317	1.319	1741	0.014	1.212	1.212
	204	0.545	0.540	1.319	1375	0.017	1.534	1.534
	232	0.480	0.930	1.319	1162	0.021	1.815	1.814

Table I.2 (Continued): Surge pressure gradient for unweighted fresh water sepiolite mud: Schuh model vs. Semi analytical model.

Pipe velocity (m/s)	Temperature °C	Flow behavior index (n)	Consistency index (Pa-s^n)	Effective velocity (m/s)	Reynold number	Friction factor	Surge pressure gradient (kPa/m)	
							Schuh method	Semi analytical method
0.9144	27	0.588	0.639	1.978	1615	0.015	2.939	2.939
	38	0.636	0.440	1.978	1752	0.014	2.709	2.710
	65	0.618	0.518	1.978	1656	0.014	2.867	2.868
	93	0.605	0.452	1.978	2056	0.012	2.309	2.310
	121	0.605	0.353	1.978	2639	0.009	1.799	1.799
	149	0.663	0.196	1.978	3343	0.007	1.420	1.421
	177	0.598	0.317	1.978	3074	0.008	1.544	1.544
	204	0.545	0.540	1.978	2480	0.010	1.914	1.913
	232	0.480	0.930	1.978	2153	0.011	2.205	2.203
1.2192	27	0.588	0.639	2.638	2425	0.010	3.480	3.481
	38	0.636	0.440	2.638	2594	0.009	3.253	3.255
	65	0.618	0.518	2.638	2464	0.010	3.425	3.427
	93	0.605	0.452	2.638	3070	0.008	2.748	2.749
	121	0.605	0.353	2.638	3942	0.006	2.141	2.141
	149	0.663	0.196	2.638	4912	0.005	1.718	1.719
	177	0.598	0.317	2.638	4602	0.005	1.834	1.834
	204	0.545	0.540	2.638	3769	0.006	2.239	2.238
	232	0.480	0.930	2.638	3333	0.007	2.532	2.529

Table I.2 (Continued): Surge pressure gradient for unweighted fresh water sepiolite mud: Schuh model vs. Semi analytical model.

Pipe velocity (m/s)	Temperature °C	Flow behavior index (n)	Consistency index (Pa-s^n)	Effective velocity (m/s)	Reynold number	Friction factor	Surge pressure gradient (kPa/m)	
							Schuh method	Semi analytical method
1.524	27	0.588	0.639	3.297	3323	0.007	3.968	3.969
	38	0.636	0.440	3.297	3517	0.007	3.749	3.751
	65	0.618	0.518	3.297	3353	0.007	3.932	3.934
	93	0.605	0.452	3.297	4191	0.006	3.146	3.147
	121	0.605	0.353	3.297	5382	0.004	2.450	2.451
	149	0.663	0.196	3.297	6620	0.004	1.992	1.993
	177	0.598	0.317	3.297	6293	0.004	2.095	2.096
	204	0.545	0.540	3.297	5215	0.005	2.529	2.528
	232	0.480	0.930	3.297	4680	0.005	2.818	2.815
1.8288	27	0.588	0.639	3.957	4298	0.006	4.418	4.418
	38	0.636	0.440	3.957	4510	0.005	4.210	4.212
	65	0.618	0.518	3.957	4314	0.006	4.402	4.403
	93	0.605	0.452	3.957	5405	0.004	3.513	3.514
	121	0.605	0.353	3.957	6941	0.003	2.736	2.736
	149	0.663	0.196	3.957	8448	0.003	2.248	2.249
	177	0.598	0.317	3.957	8127	0.003	2.336	2.337
	204	0.545	0.539833	3.956528	6798	0.004	2.793	2.792
	232	0.480	0.929739	3.956528	6174	0.004	3.075	3.072

Table I.3: Surge pressure gradient for unweighted fresh water sepiolite mud: Semi analytical model using Herschel Bulkley parameters-viscometer.

Pipe velocity (m/s)	Temperature °C	Flow behavior index (n)	Consistency index (mPa-s^n)	Yield Point (Pa)	Surge pressure gradient (kPa/m)
0.3048	27	0.6356	448.4398	1.1745	1.5276
	38	0.6830	310.0567	1.05	1.3403
	65	0.6633	349.3347	1.0035	1.3616
	93	0.6287	379.4638	0.4643	1.1835
	121	0.6668	222.7829	0.9125	0.9159
	149	0.7271	124.3005	0.7022	0.6940
	177	0.6225	263.0189	0.3320	0.7976
	204	0.6256	297.5548	1.2540	1.0274
	232	0.5917	404.4197	2.0233	1.2531
0.6096	27	0.6356	448.4398	1.1745	2.2861
	38	0.6830	310.0567	1.05	2.0992
	65	0.6633	349.3347	1.0035	2.0769
	93	0.6287	379.4638	0.4643	1.7964
	121	0.6668	222.7829	0.9125	1.3861
	149	0.7271	124.3005	0.7022	1.0890
	177	0.6225	263.0189	0.3320	1.2052
	204	0.6256	297.5548	1.2540	1.4985
	232	0.5917	404.4197	2.0233	1.7587
0.9144	27	0.6356	448.4398	1.1745	2.9154
	38	0.6830	310.0567	1.05	2.6848
	65	0.6633	349.3347	1.0035	2.6784
	93	0.6287	379.4638	0.4643	2.3013
	121	0.6668	222.7829	0.9125	1.7812
	149	0.7271	124.3005	0.7022	1.4316
	177	0.6225	263.0189	0.3320	1.5382
	204	0.6256	297.5548	1.2540	1.8878
	232	0.5917	404.4197	2.0233	2.1640
1.2192	27	0.6356	448.4398	1.1745	3.4702
	38	0.6830	310.0567	1.05	3.2393
	65	0.6633	349.3347	1.0035	3.2124
	93	0.6287	379.4638	0.4643	2.7421
	121	0.6668	222.7829	0.9125	2.1292
	149	0.7271	124.3005	0.7022	1.7409
	177	0.6225	263.0189	0.3320	1.8318
	204	0.6256	297.5548	1.2540	2.2268
	232	0.5917	404.4197	2.0233	2.5193

Table I.3 (Continued): Surge pressure gradient for unweighted fresh water sepiolite mud: Semi analytical model using Herschel Bulkley parameters-viscometer.

Pipe velocity (m/s)	Temperature °C	Flow behavior index (n)	Consistency index (mPa-s^n)	Yield Point (Pa)	Surge pressure gradient (kPa/m)
1.524	27	0.6356	448.4398	1.1745	3.9762
	38	0.6830	310.0567	1.05	3.7495
	65	0.6633	349.3347	1.0035	3.7035
	93	0.6287	379.4638	0.4643	3.1463
	121	0.6668	222.7829	0.9125	2.4532
	149	0.7271	124.3005	0.7022	2.0295
	177	0.6225	263.0189	0.3320	2.0963
	204	0.6256	297.5548	1.2540	2.5380
	232	0.5917	404.4197	2.0233	2.8363
1.8288	27	0.6356	448.4398	1.1745	4.4449
	38	0.6830	310.0567	1.05	4.2292
	65	0.6633	349.3347	1.0035	4.1624
	93	0.6287	379.4638	0.4643	3.5227
	121	0.6668	222.7829	0.9125	2.7534
	149	0.7271	124.3005	0.7022	2.3037
	177	0.6225	263.0189	0.3320	2.3445
	204	0.6256	297.5548	1.2540	2.8199
	232	0.5917	404.4197	2.0233	3.1315

Table I.4: Surge pressure gradient for unweighted fresh water sepiolite mud: Semi analytical model using Herschel Bulkley parameters-HTHP rheometer.

Pipe velocity (m/s)	Temperature °C	Flow behavior index (n)	Consistency index (mPa-s^n)	Yield Point (Pa)	Surge pressure gradient (kPa/m)
0.3048	38	0.7644	160.2255	0.96423	1.0612
	54	0.7517	142.7420	0.59683	0.861
	66	0.7684	109.6431	0.51636	0.721
	82	0.7731	87.2738	0.34296	0.576
	93	0.7674	78.1728	0.33377	0.506
	110	0.8208	42.4442	0.0000	0.327
	121	0.8560	27.3653	0.0000	0.251
	138	1.0390	5.2882	0.36471	0.17
	149	1.0350	4.5783	0.07671	0.113
	166	1.1010	2.2015	0.0016	0.068
	177	1.0940	1.9797	0.0000	0.059
	193	0.8459	10.7823	0.0000	0.094
	204	1.5060	0.1169	3.57238	0.432
	221	1.2870	0.6926	6.12641	0.754
	232	1.0170	5.2690	4.02025	0.59
	249	0.4822	499.1180	1.07536	0.84
	260	0.4013	485.7060	0.0000	0.455
0.6096	38	0.7644	160.2255	0.96423	1.7143
	54	0.7517	142.7420	0.59683	1.3929
	66	0.7684	109.6431	0.51636	1.1784
	82	0.7731	87.2738	0.34296	0.953
	93	0.7674	78.1728	0.33377	0.83
	110	0.8208	42.4442	0.0000	0.576
	121	0.8560	27.3653	0.0000	0.454
	138	1.0390	5.2882	0.36471	0.297
	149	1.0350	4.5783	0.07671	0.219
	166	1.1010	2.2015	0.0016	0.145
	177	1.0940	1.9797	0.0000	0.125
	193	0.8459	10.7823	0.0000	0.168
	204	1.5060	0.1169	3.57238	0.521
	221	1.2870	0.6926	6.12641	0.879
	232	1.0170	5.2690	4.02025	0.725
	249	0.4822	499.1180	1.07536	1.12
	260	0.4013	485.7060	0.0000	0.601

Table I.4 (Continued): Surge pressure gradient for unweighted fresh water sepiolite mud: Semi analytical model using Herschel Bulkley parameters-HTHP rheometer.

Pipe velocity (m/s)	Temperature °C	Flow behavior index (n)	Consistency index (mPa-s^n)	Yield Point (Pa)	Surge pressure gradient (kPa/m)
0.9144	38	0.7644	160.2255	0.96423	2.2881
	54	0.7517	142.7420	0.59683	1.8613
	66	0.7684	109.6431	0.51636	1.5827
	82	0.7731	87.2738	0.34296	1.2849
	93	0.7674	78.1728	0.33377	1.1183
	110	0.8208	42.4442	0.0000	0.805
	121	0.8560	27.3653	0.0000	0.642
	138	1.0390	5.2882	0.36471	0.426
	149	1.0350	4.5783	0.07671	0.328
	166	1.1010	2.2015	0.0016	0.227
	177	1.0940	1.9797	0.0000	0.195
	193	0.8459	10.7823	0.0000	0.238
	204	1.5060	0.1169	3.57238	0.604
	221	1.2870	0.6926	6.12641	0.995
	232	1.0170	5.2690	4.02025	0.852
	249	0.4822	499.1180	1.07536	1.3362
	260	0.4013	485.7060	0.0000	0.708
1.2192	38	0.7644	160.2255	0.96423	2.8208
	54	0.7517	142.7420	0.59683	2.2904
	66	0.7684	109.6431	0.51636	1.9568
	82	0.7731	87.2738	0.34296	1.5956
	93	0.7674	78.1728	0.33377	1.3823
	110	0.8208	42.4442	0.0000	1.019
	121	0.8560	27.3653	0.0000	0.821
	138	1.0390	5.2882	0.36471	0.556
	149	1.0350	4.5783	0.07671	0.438
	166	1.1010	2.2015	0.0016	0.311
	177	1.0940	1.9797	0.0000	0.268
	193	0.8459	10.7823	0.0000	0.303
	204	1.5060	0.1169	3.57238	0.696
	221	1.2870	0.6926	6.12641	1.1186
	232	1.0170	5.2690	4.02025	0.972
	249	0.4822	499.1180	1.07536	1.484
	260	0.4013	485.7060	0.0000	0.794

Table I.4 (Continued): Surge pressure gradient for unweighted fresh water sepiolite mud: Semi analytical model using Herschel Bulkley parameters-HTHP rheometer.

Pipe velocity (m/s)	Temperature °C	Flow behavior index (n)	Consistency index (mPa-s^n)	Yield Point (Pa)	Surge pressure gradient (kPa/m)
1.8288	38	0.7644	160.2255	0.96423	3.8005
	54	0.7517	142.7420	0.59683	3.0795
	66	0.7684	109.6431	0.51636	2.6488
	82	0.7731	87.2738	0.34296	2.164
	93	0.7674	78.1728	0.33377	1.8703
	110	0.8208	42.4442	0.0000	1.4214
	121	0.8560	27.3653	0.0000	1.1622
	138	1.0390	5.2882	0.36471	0.822
	149	1.0350	4.5783	0.07671	0.661
	166	1.1010	2.2015	0.0016	0.486
	177	1.0940	1.9797	0.0000	0.417
	193	0.8459	10.7823	0.0000	0.427
	204	1.5060	0.1169	3.57238	0.426
	221	1.2870	0.6926	6.12641	1.3656
	232	1.0170	5.2690	4.02025	1.2034
	249	0.4822	499.1180	1.07536	1.7763
	260	0.4013	485.7060	0.0000	0.935

Appendix J: Surge pressure gradients predicted using semi-analytical model for unweighted fresh water sepiolite mud system.

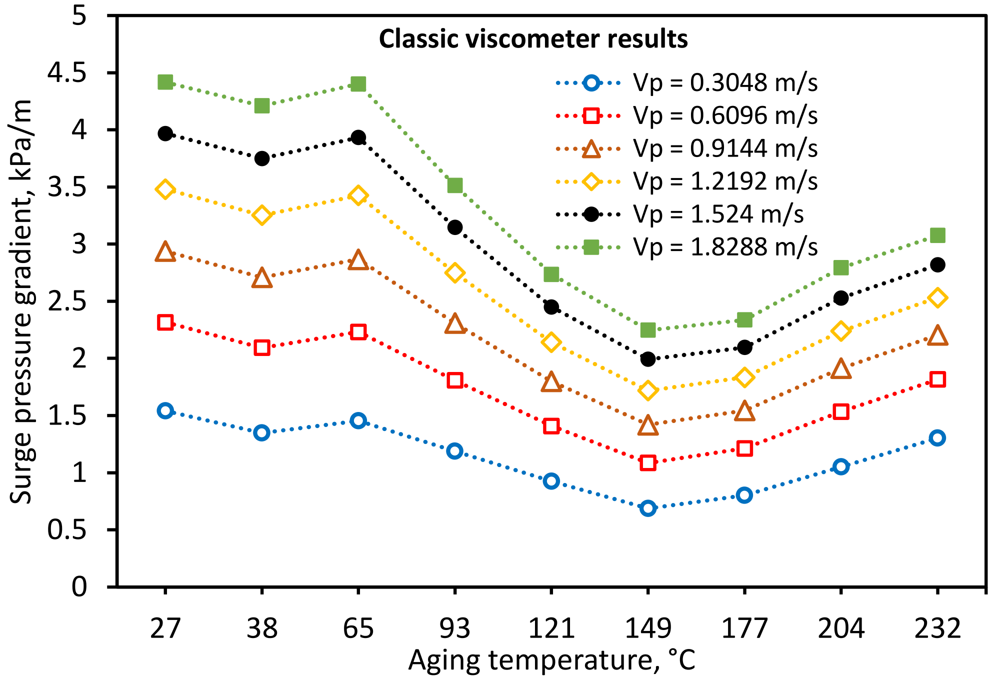

Figure J.1: Surge pressure gradients predicted based on Power Law viscometer parameters using semi-analytical model for unweighted fresh water sepiolite mud.

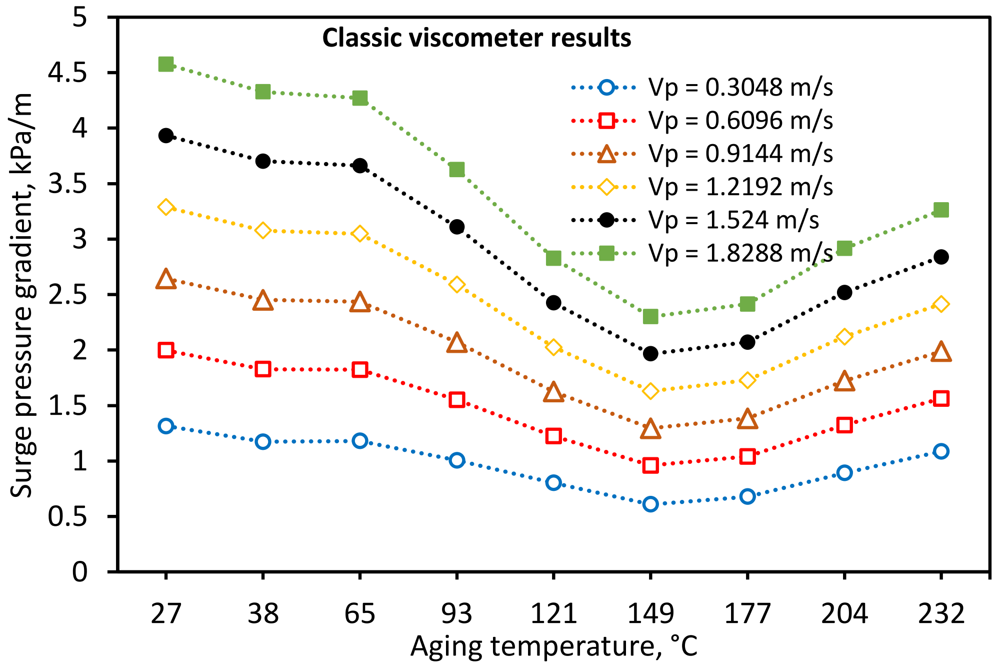

Figure J.2: Surge pressure gradients predicted based on Bingham Plastic viscometer parameters using semi-analytical model for unweighted fresh water sepiolite mud.

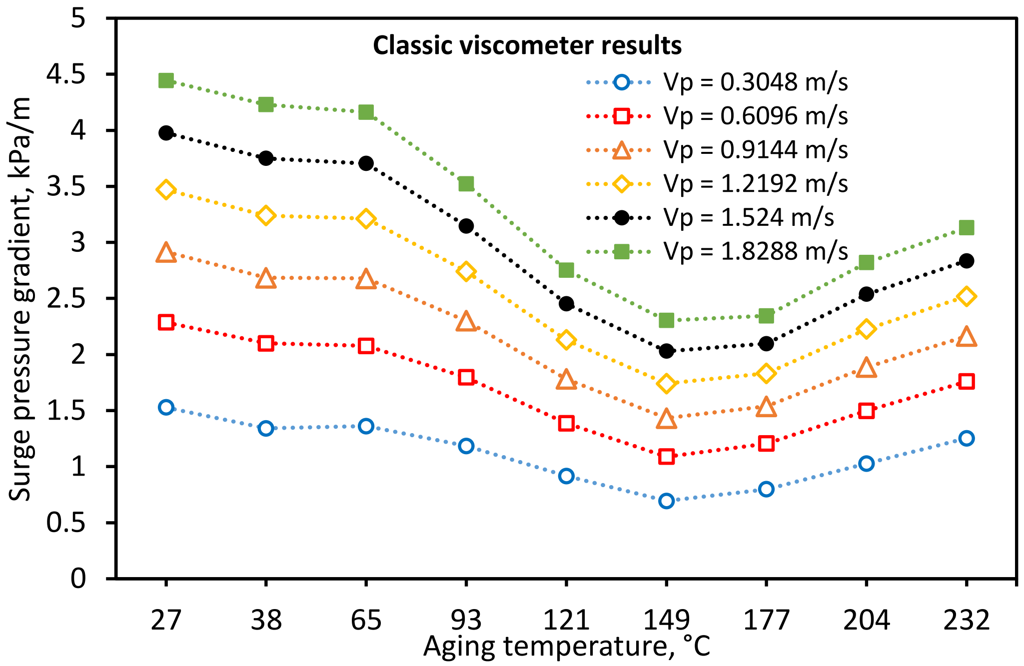

Figure J.3: Surge pressure gradients predicted based on Herschel Bulkley viscometer parameters using semi-analytical model for unweighted fresh water sepiolite mud.

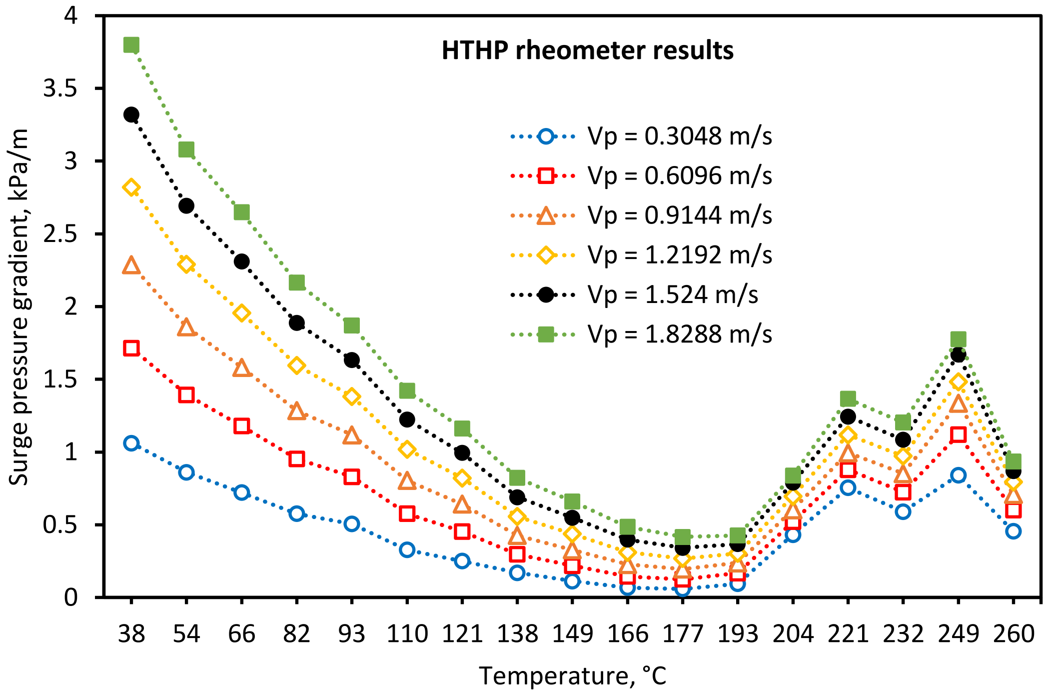

Figure J.4: Surge pressure gradients predicted based on Herschel Bulkley rheometer parameters using semi-analytical model for unweighted fresh water sepiolite mud.

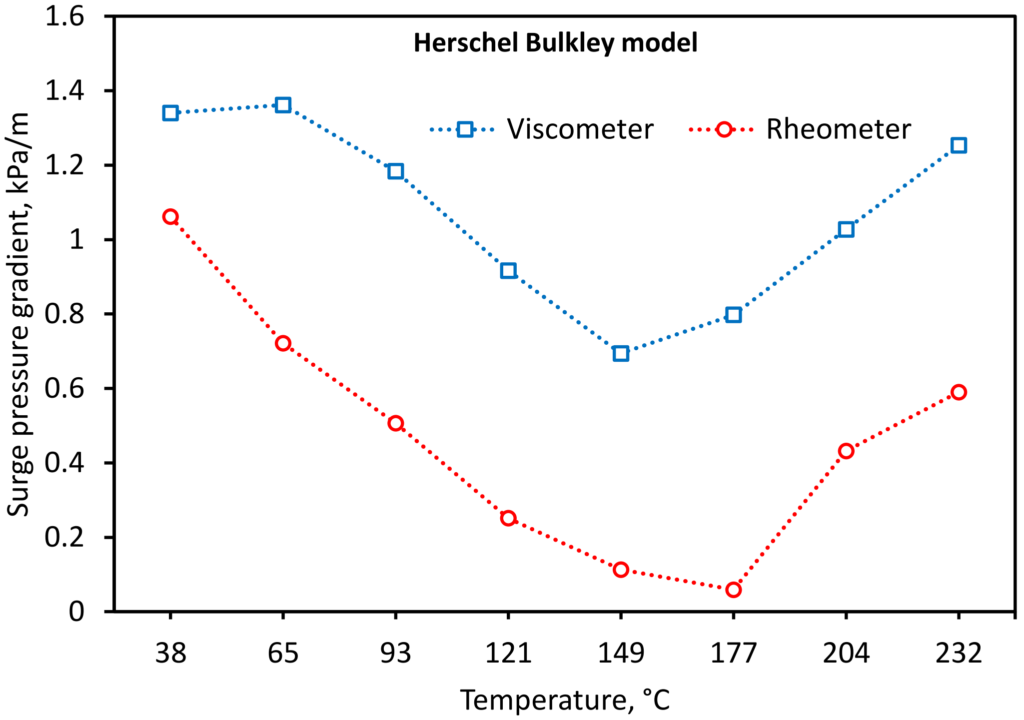

Figure J.5: Variation of surge pressure gradients predicted based on conventional viscometer and HTHP rheometer @Vp = 0.3048 m/sec.

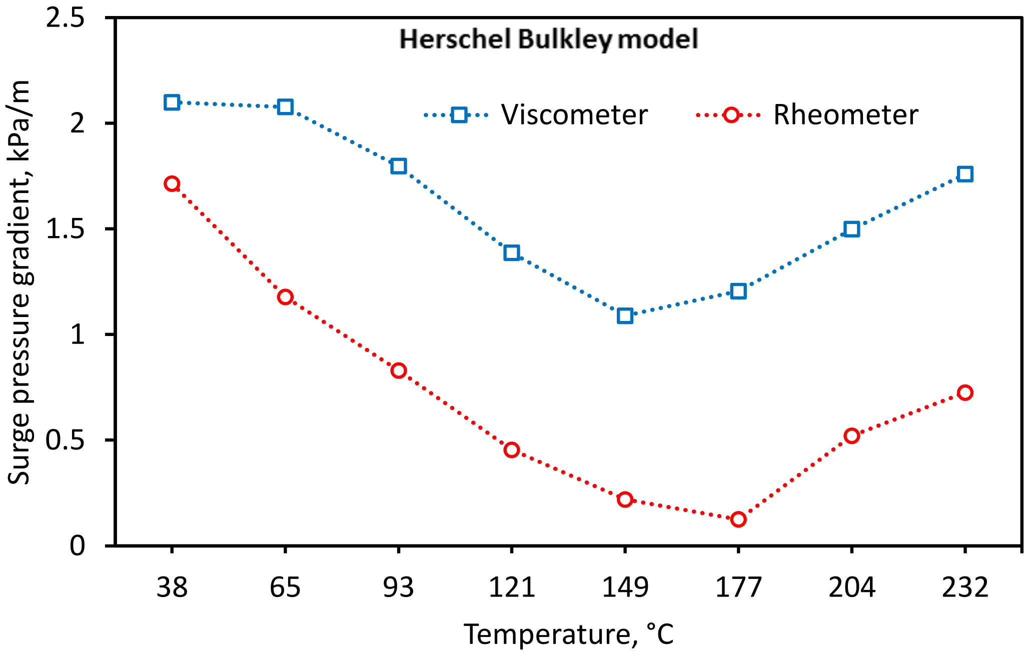

Figure J.6: Variation of surge pressure gradients predicted based on conventional viscometer and HTHP rheometer @Vp = 0.6096 m/sec.

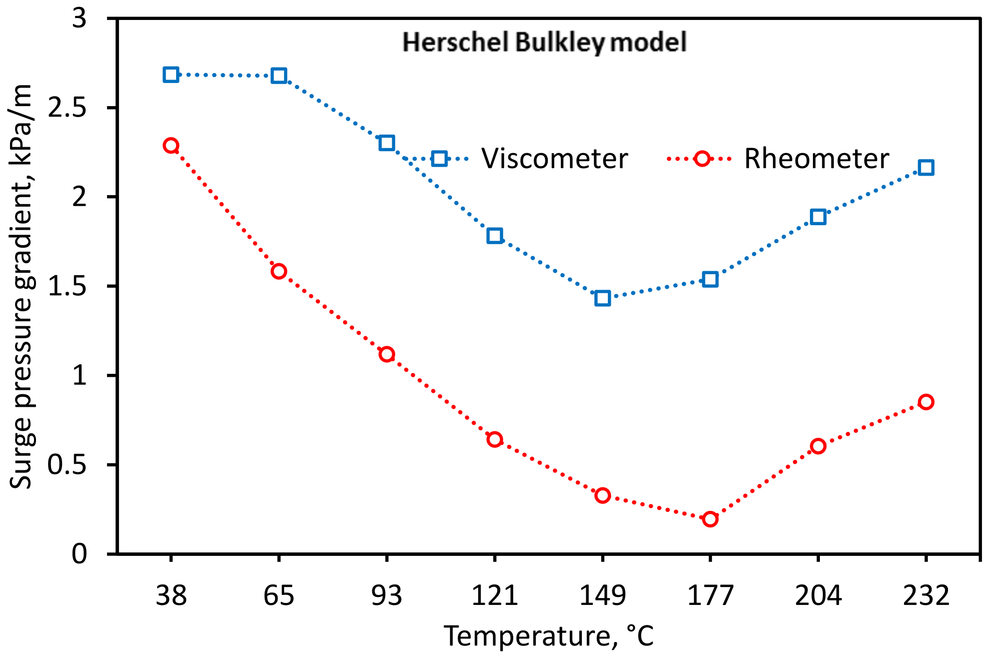

Figure J.7: Variation of surge pressure gradients predicted based on conventional viscometer and HTHP rheometer @Vp = 0.9144 m/sec.

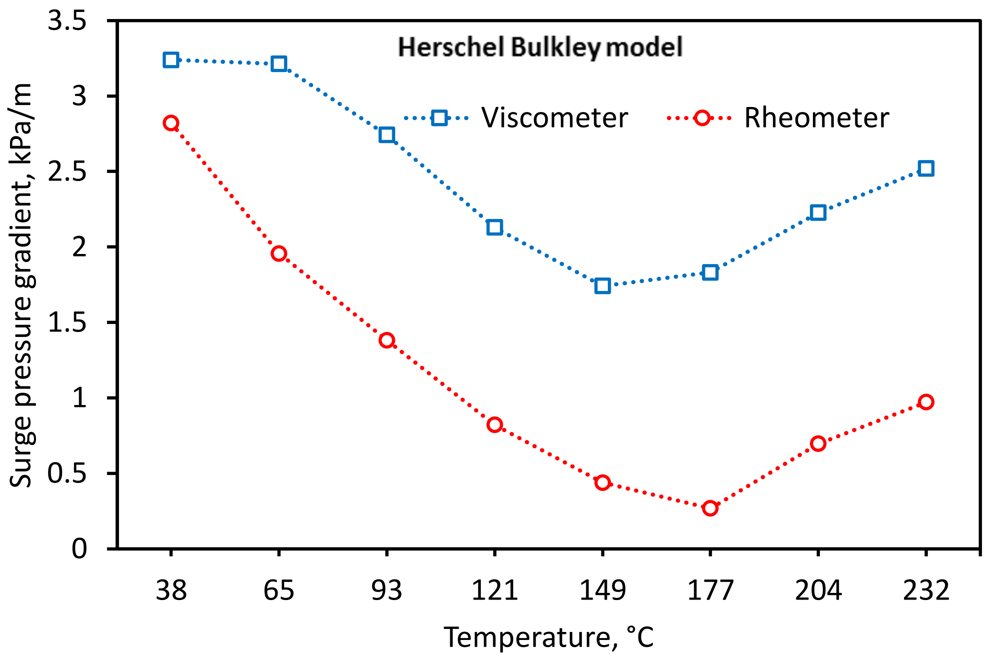

Figure J.8: Variation of surge pressure gradients predicted based on conventional viscometer and HTHP rheometer @Vp = 1.2192 m/sec.

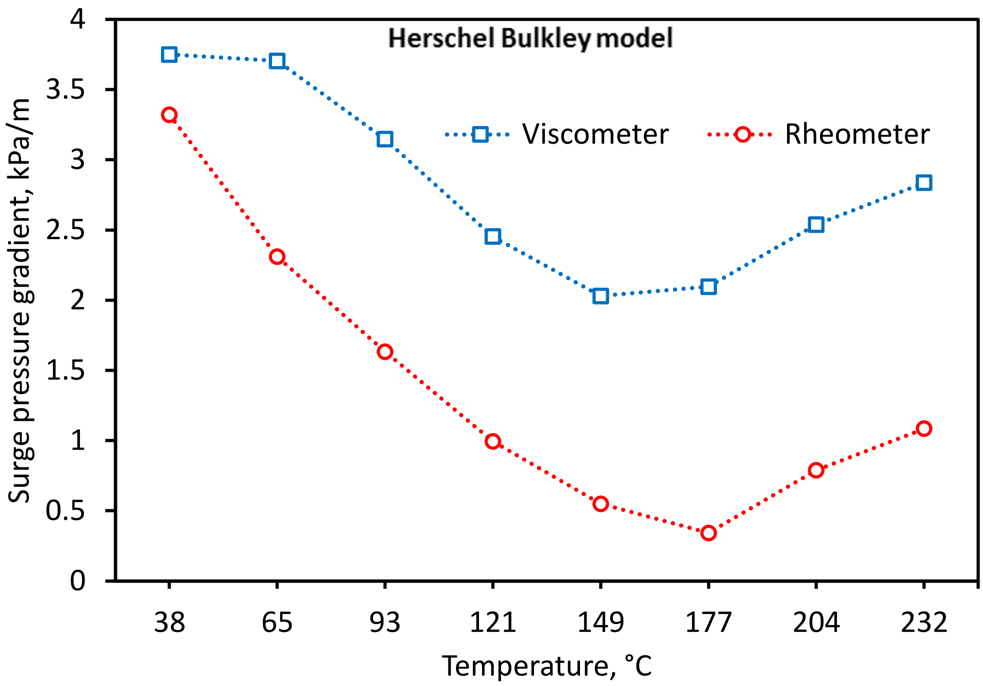

Figure J: Variation of surge pressure gradients predicted based on conventional viscometer and HTHP rheometer @Vp = 1.524 m/sec.

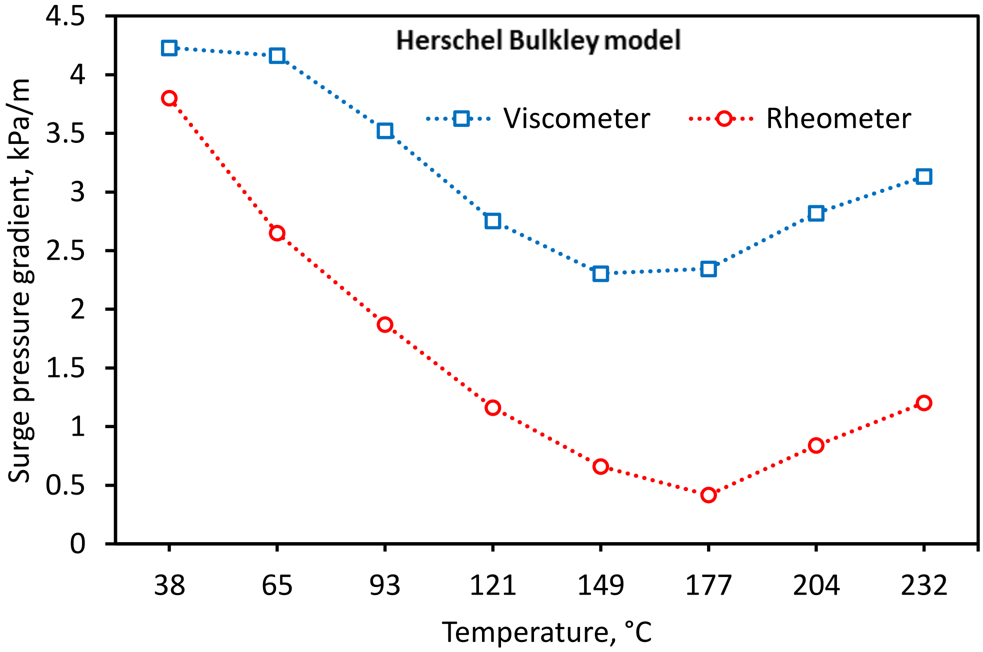

Figure J.10: Variation of surge pressure gradients predicted based on conventional viscometer and HTHP rheometer @Vp = 1.8288 m/sec.

Appendix K: Rheology and hydraulics equations for Herschel-Bulkley model.

Table K.1: Rheology and hydraulics equations for Herschel-Bulkley model, (Merlo et.al, 1995).

Hydraulic Equation: HERSCHEL BULKLEY MODEL	
Pipe Flow	**Annulus Flow**
$v_a = \frac{0.408\, q}{D_p^2}$	$v_a = \frac{0.408\, q}{D_2^2 - D_1^2}$
$Re_{eq} = \left(2\frac{3n+1}{n}\right)\frac{\rho V_p^{(2-n)} R^n}{\tau_0\left(\frac{R}{V_p}\right)^n + k\left(\frac{3n+1}{nCc}\right)^n}$	$Re_{eq} = \left(4\frac{2n+1}{n}\right)\frac{\rho V_a^{(2-n)} (R_2 - R_1)^n}{\tau_0\left(\frac{R_2 - R_1}{VV_a}\right)^n + k\left(2\frac{2n+1}{nCa}\right)^n}$
$Re_{eqcr} = (Cc * Re)_{cr} = \left[\frac{4(3n+1)}{ny}\right]^{\left(\frac{1}{1-z}\right)}$	$Re_{eqcr} = (Cc * Re)_{cr} = \left[\frac{4(3n+1)}{ny}\right]^{\left(\frac{1}{1-z}\right)}$
$y = \frac{\log(n) + 3.93}{50}$	$z = \frac{1.75 - \log(n)}{7}$
$R_{e_{eq}} < R_{e_{eqcr}} \rightarrow$ *Laminar Flow*	
$\Delta p = \frac{2Lk}{R}\left[\frac{\tau_0}{k} + \left[\left(\frac{3n+1}{nCc}\right)\left(\frac{Q}{\pi R^3}\right)\right]^n\right]$	$\Delta p = \frac{2Lk}{(R_2 - R_1)}\left[\frac{\tau_0}{k} + \left[\left(\frac{2(2n+1)}{nCa(R_2 - R_1)}\right)\left(\frac{Q}{\pi(R_2^2 - R_1^2)}\right)\right]^n\right]$
$R_{e_{eq}} > R_{e_{eqcr}} \rightarrow$ *Turbulent Flow*	
$f = y(Cc * Re)^{-z}$	$f = y(Ca * Re)^{-z}$
$Cc = 1 - \frac{1}{2n+1}\left\{\frac{\tau_0}{\tau_0 + k\left[\frac{(3n+1)Q}{n\pi R^3}\right]^n}\right\}$	$Ca = 1 - \frac{1}{2n+1}\left\{\frac{\tau_0}{\tau_0 + k\left[\left(\frac{2(2n+1)}{n(R_2 - R_1)}\right)\left(\frac{Q}{\pi(R_2^2 - R_1^2)}\right)\right]^n}\right\}$
$\Delta p = f\rho\frac{Q^2}{\pi^2 R^5}L$	$\Delta p = f\rho\frac{Q^2}{\pi^2(R_2 - R_1)(R_2^2 - R_1^2)^2}L$

Appendix L: Semi-analytical solution for flow through a concentric annulus with fixed boundaries for a Herschel Bulkley fluid-unweighted fresh water sepiolite mud.

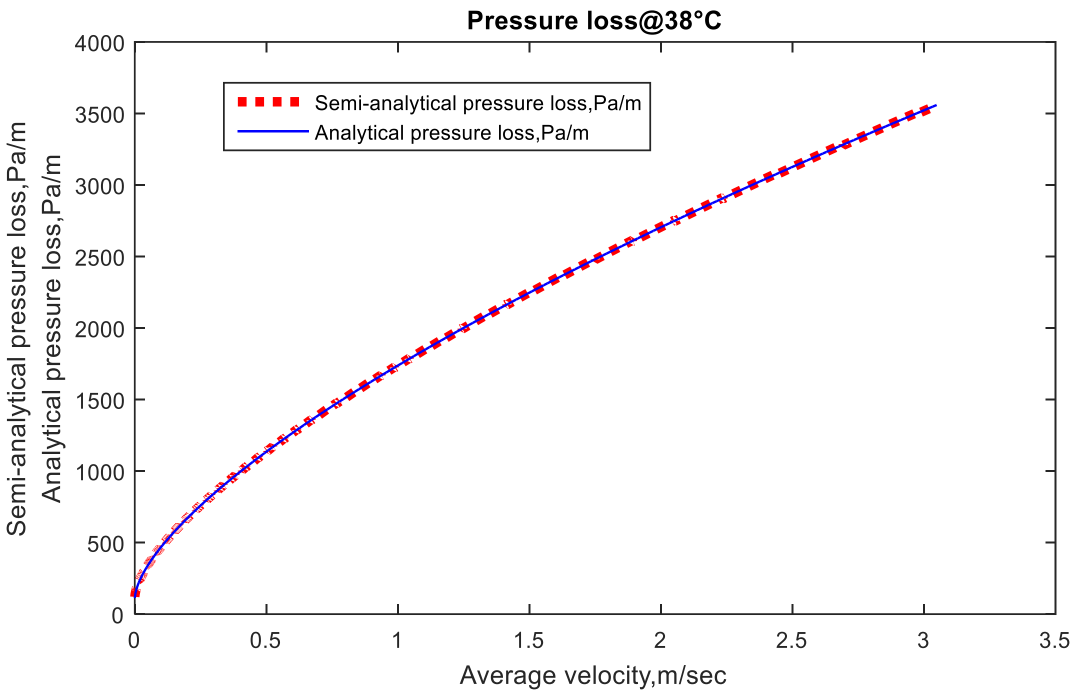

Figure L.1: Comparison of frictional pressure drop obtained using semi-analytical and existing analytical method for fresh water sepiolite mud @38°C.

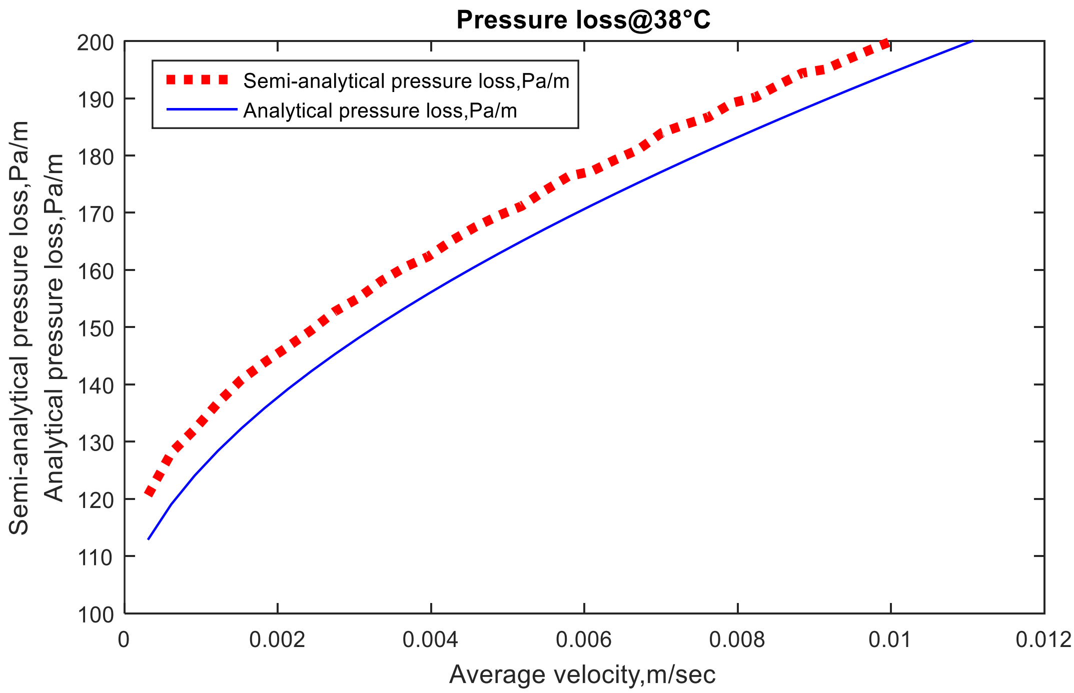

Figure L.2: Difference between obtained frictional pressure drop using semi-analytical and existing analytical method for fresh water sepiolite mud @38°C.

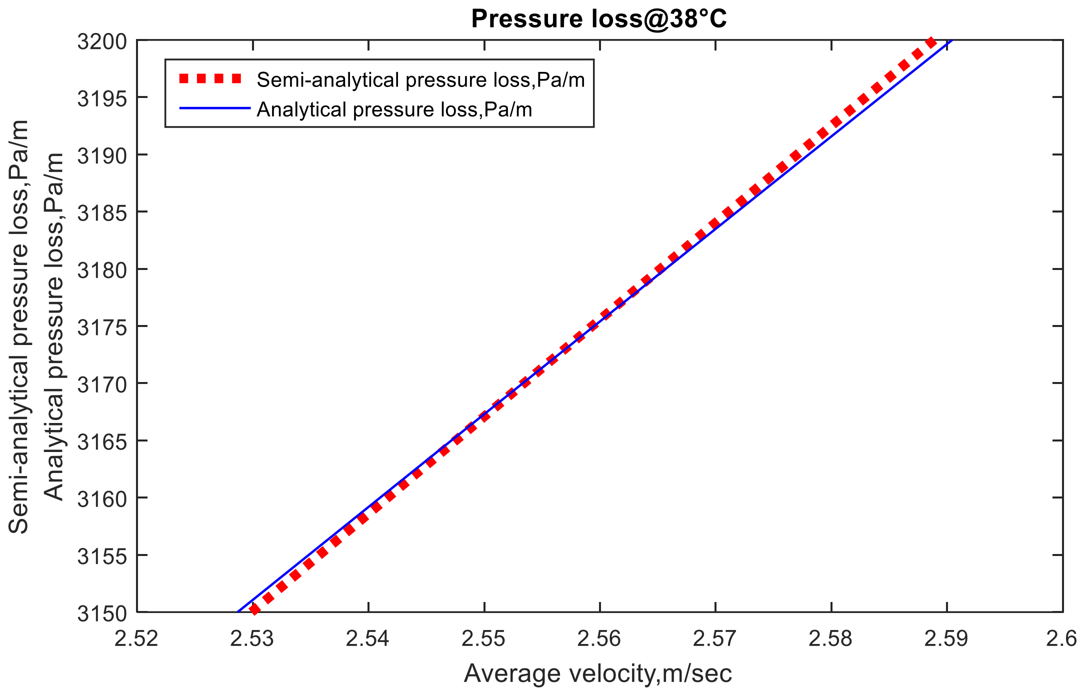

Figure L.3: Agreement between obtained frictional pressure drop using semi-analytical and existing analytical method for fresh water sepiolite mud @38°C.

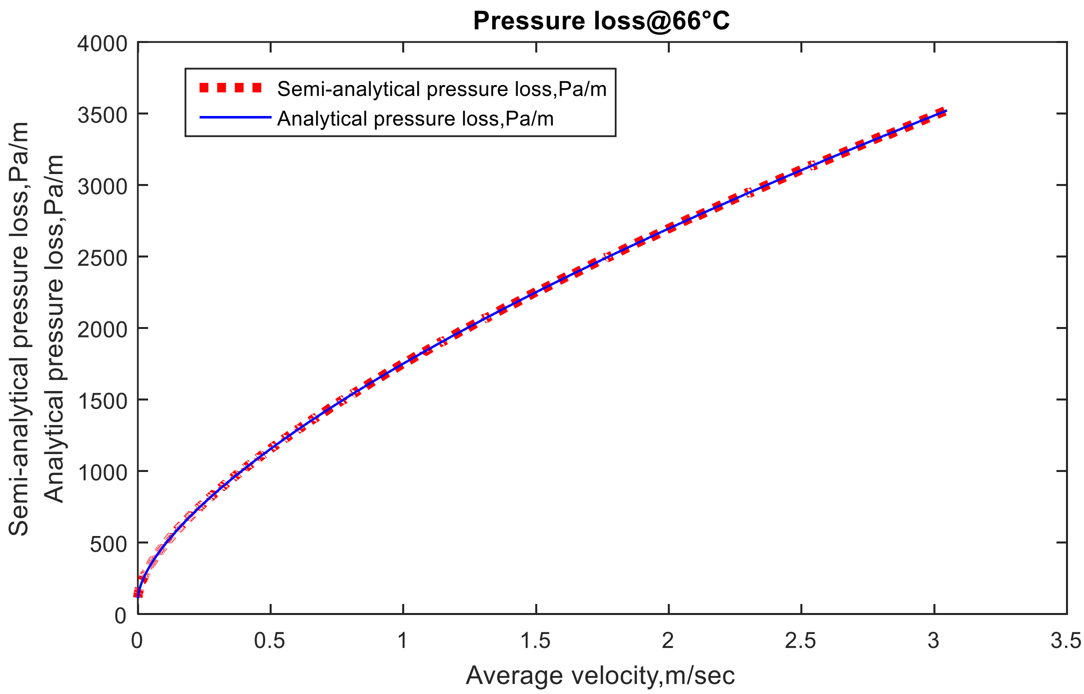

Figure L.4: Comparison of frictional pressure drop obtained using semi-analytical and existing analytical method for fresh water sepiolite mud @66°C.

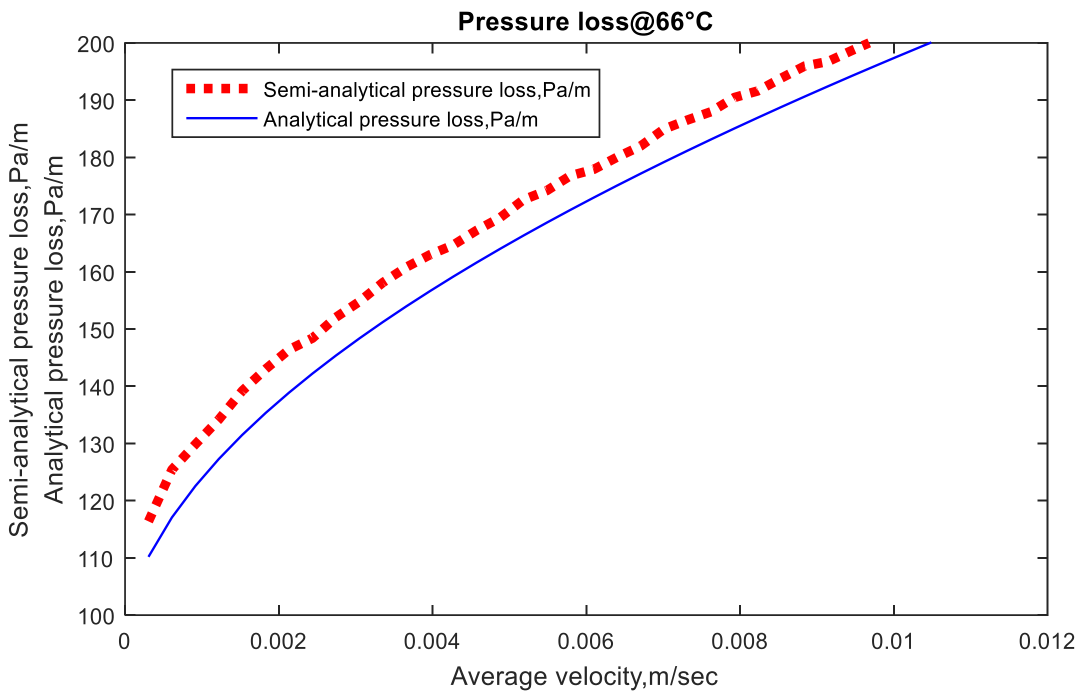

Figure L.5: Difference between obtained frictional pressure drop using semi-analytical and existing analytical method for fresh water sepiolite mud @66°C.

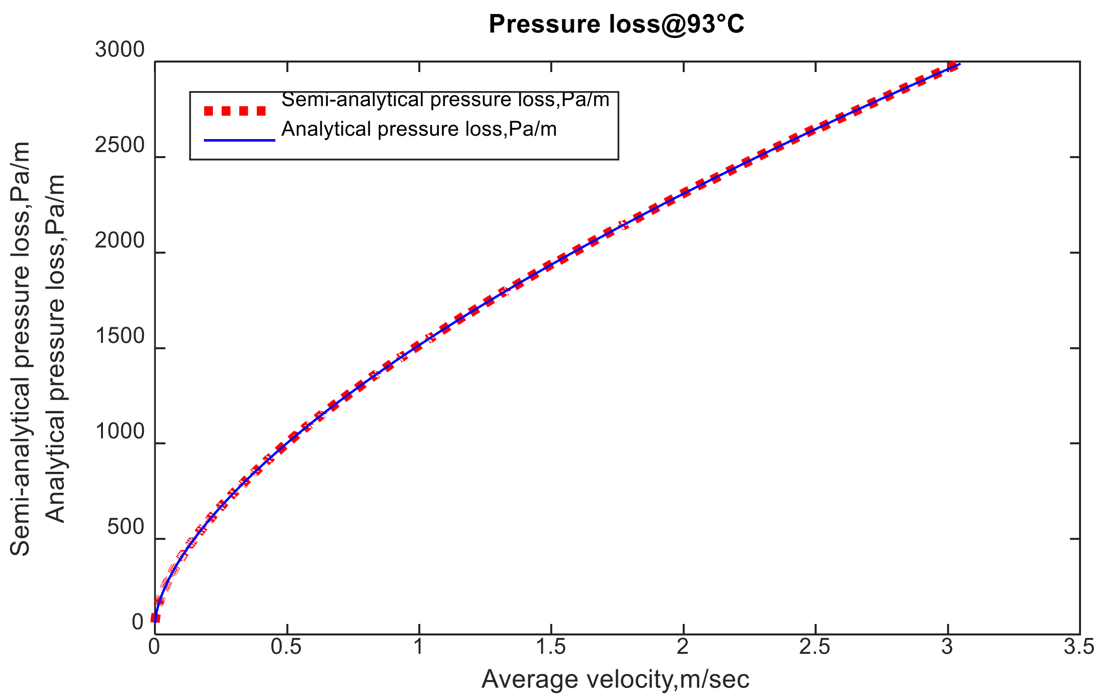

Figure L.6: Comparison of frictional pressure drop obtained using semi-analytical and existing analytical method for fresh water sepiolite mud @93°C.

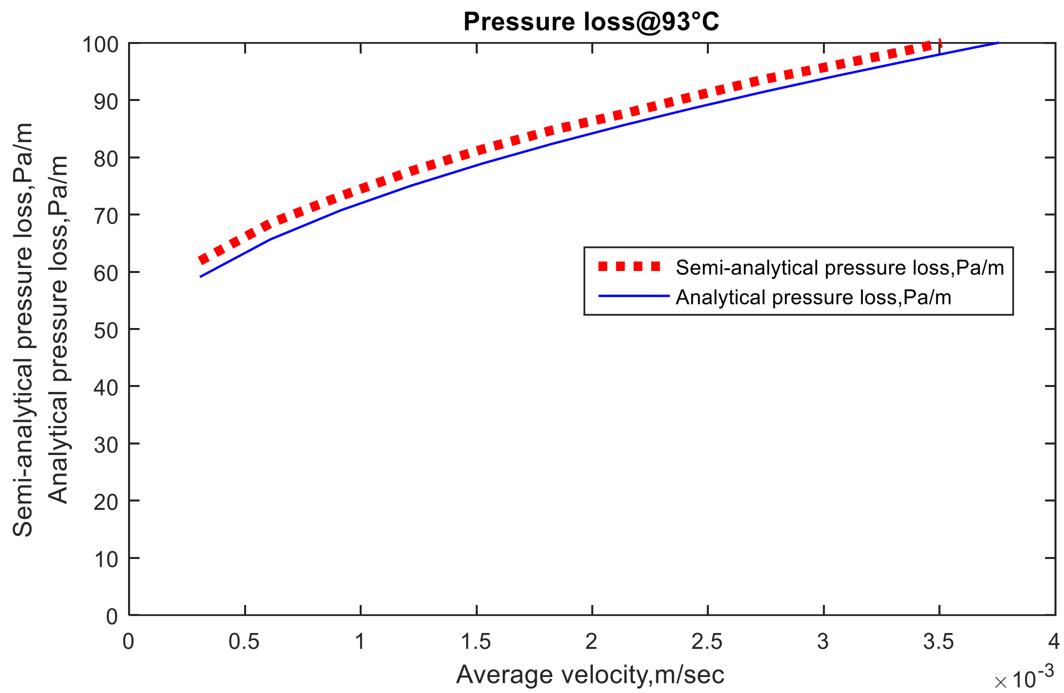

Figure L.7: Difference between obtained frictional pressure drop using semi-analytical and existing analytical method for fresh water sepiolite mud @93°C.

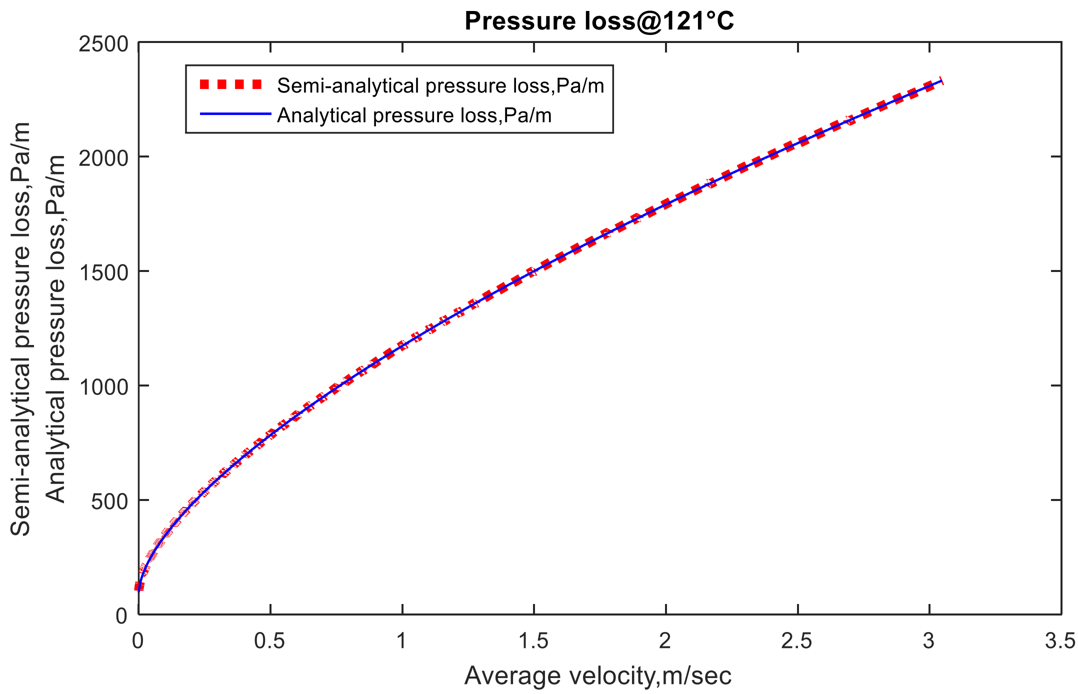

Figure L.8: Comparison of frictional pressure drop obtained using semi-analytical and existing analytical method for fresh water sepiolite mud @121°C.

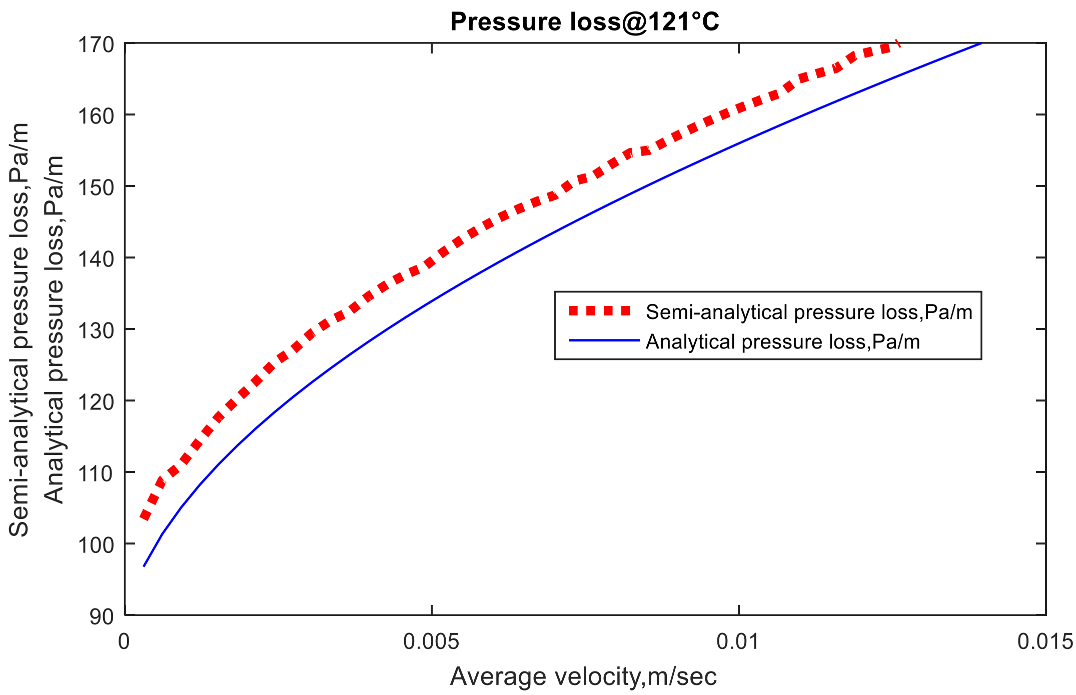

Figure L.9: Difference between obtained frictional pressure drop using semi-analytical and existing analytical method for fresh water sepiolite mud @121°C.

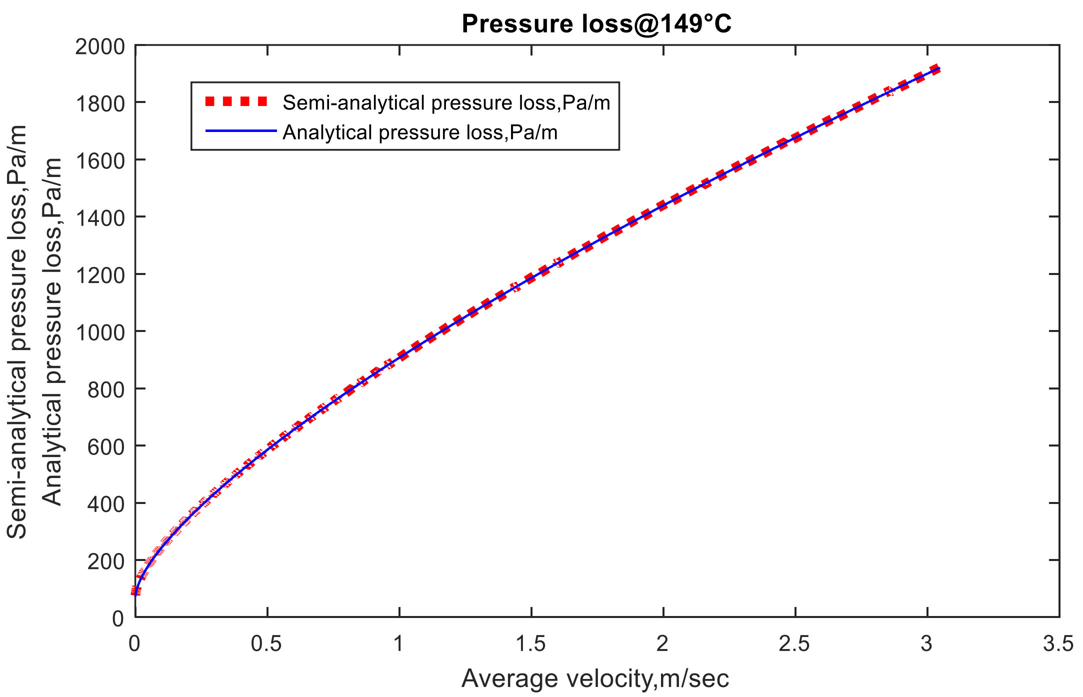

Figure L.10: Comparison of frictional pressure drop obtained using semi-analytical and existing analytical method for fresh water sepiolite mud @149°C.

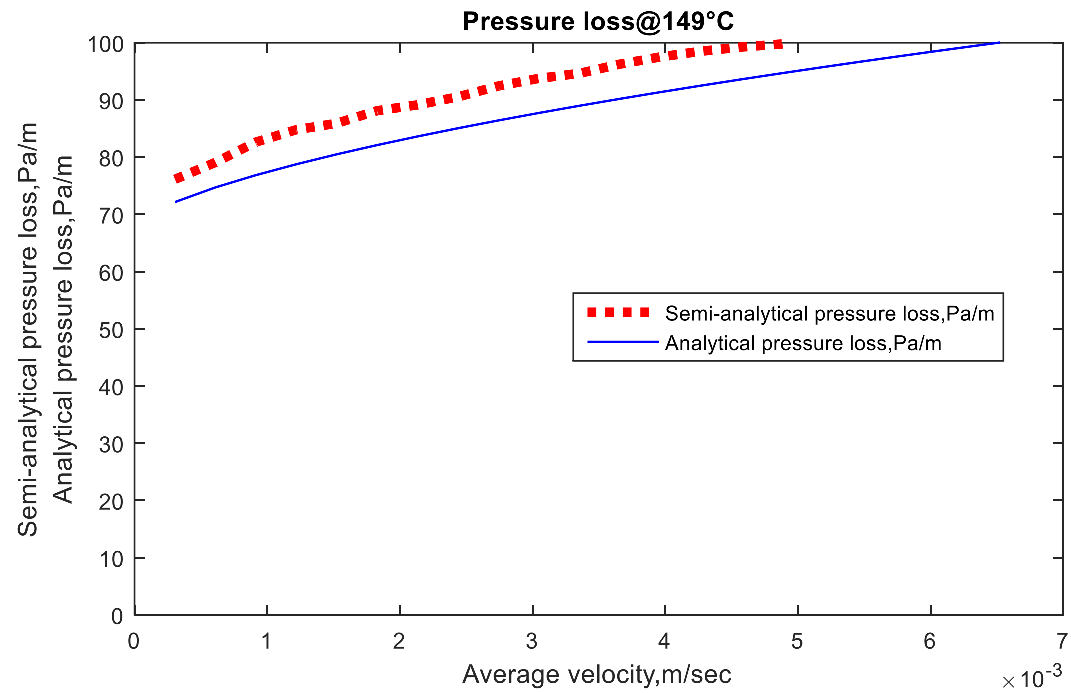

Figure L.11: Difference between obtained frictional pressure drop using semi-analytical and existing analytical method for fresh water sepiolite mud @149°C.

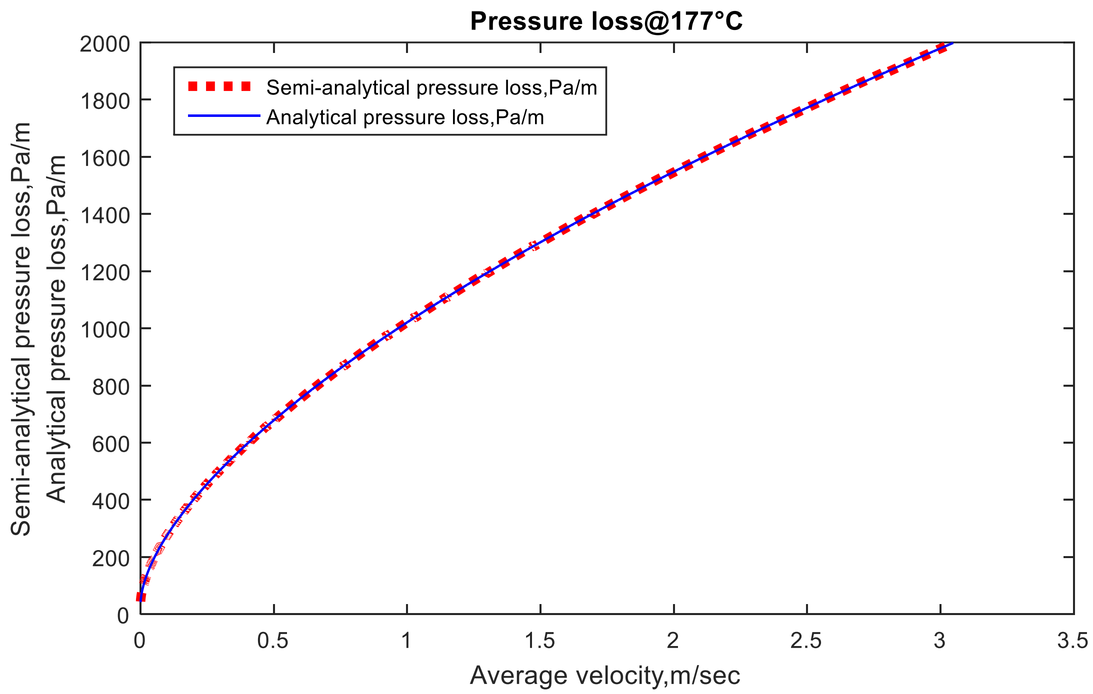

Figure L.12: Comparison of frictional pressure drop obtained using semi-analytical and existing analytical method for fresh water sepiolite mud @177°C.

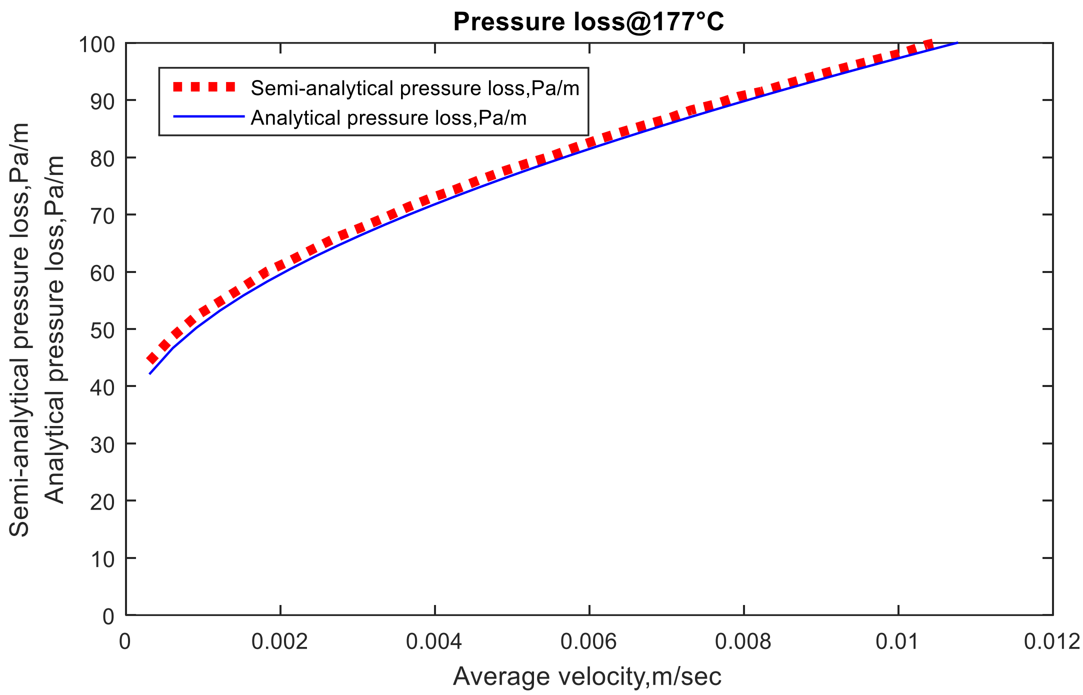

Figure L.13: Difference between obtained frictional pressure drop using semi-analytical and existing analytical method for fresh water sepiolite mud @177°C.

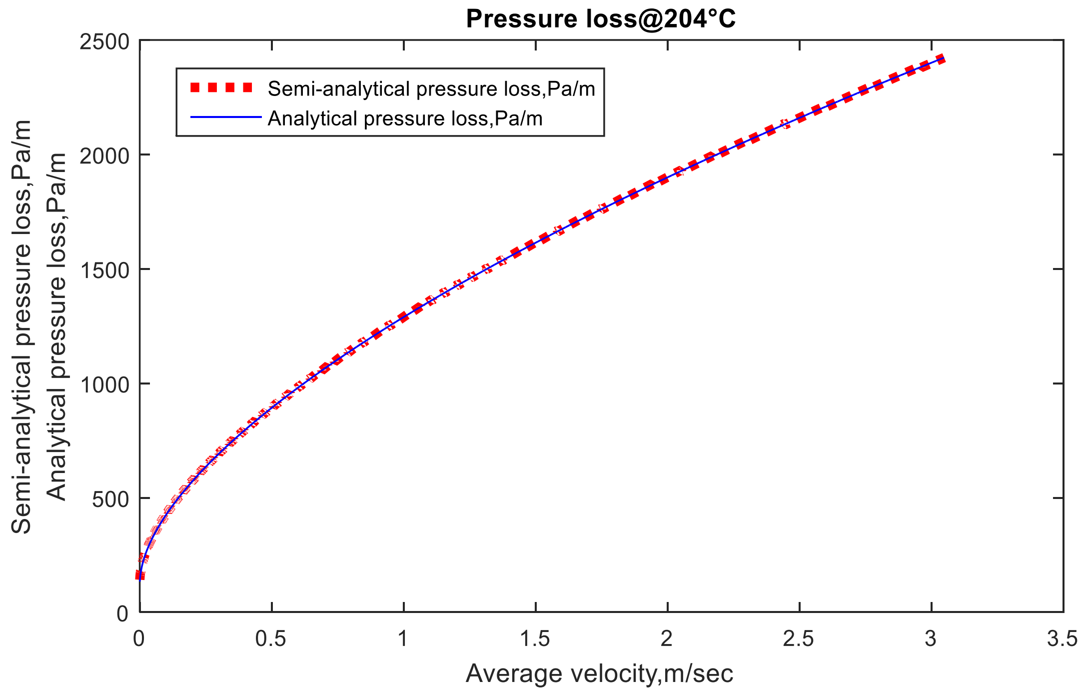

Figure L.14: Comparison of frictional pressure drop obtained using semi-analytical and existing analytical method for fresh water sepiolite mud @204°C.

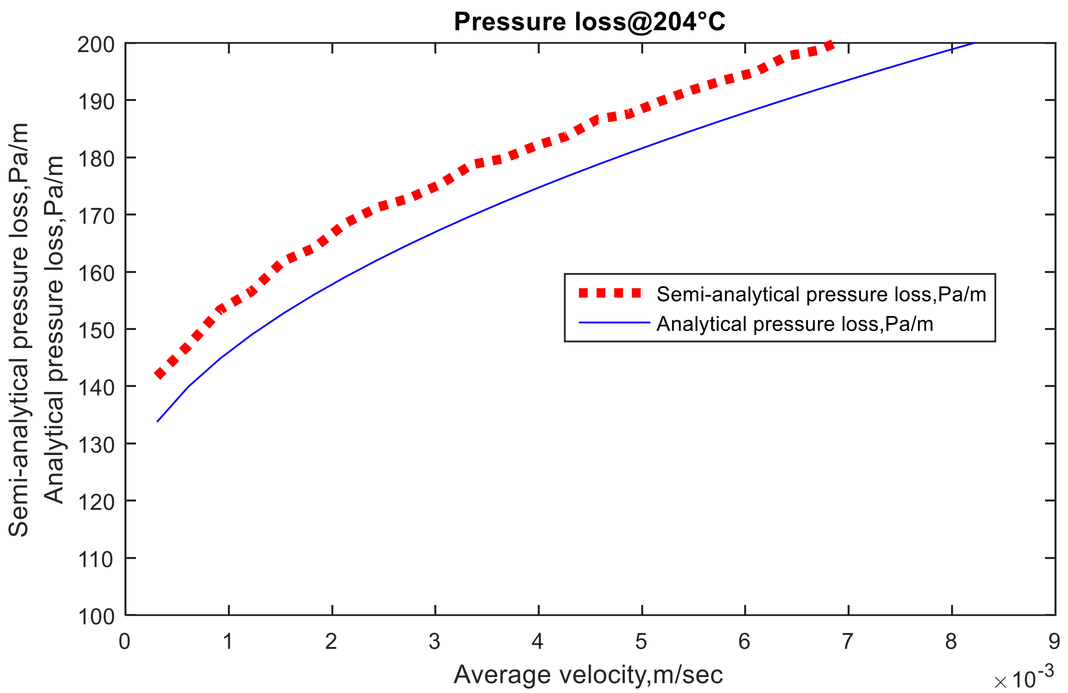

Figure L.15: Difference between obtained frictional pressure drop using semi-analytical and existing analytical method for fresh water sepiolite mud @204°C.

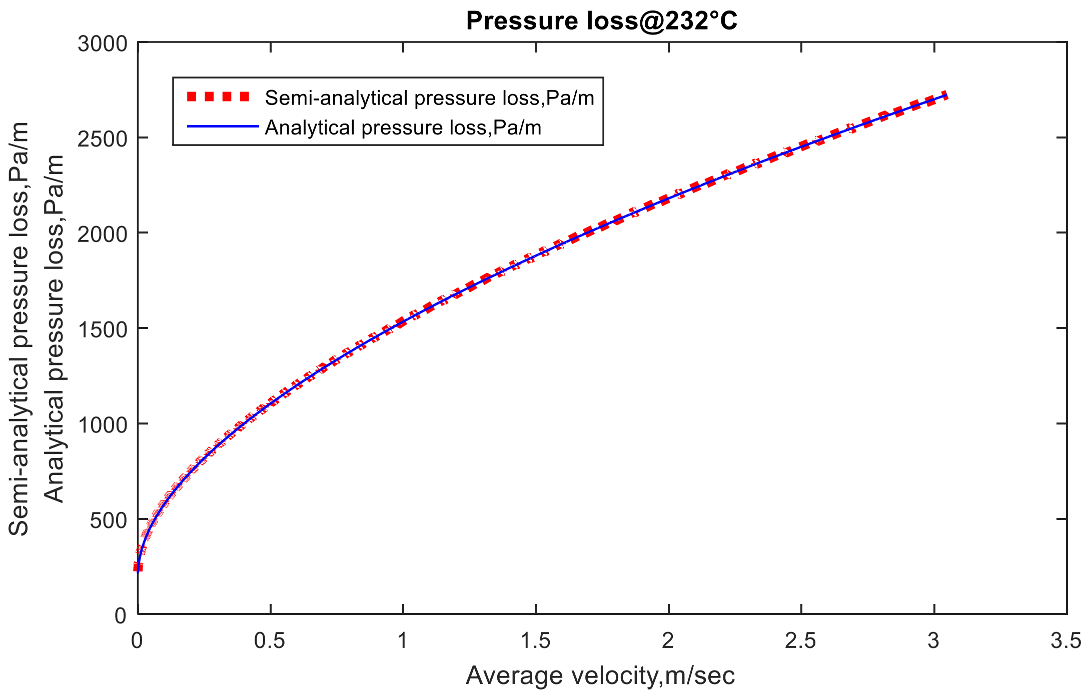

Figure L.16: Comparison of frictional pressure drop obtained using semi-analytical and existing analytical method for fresh water sepiolite mud @232°C.

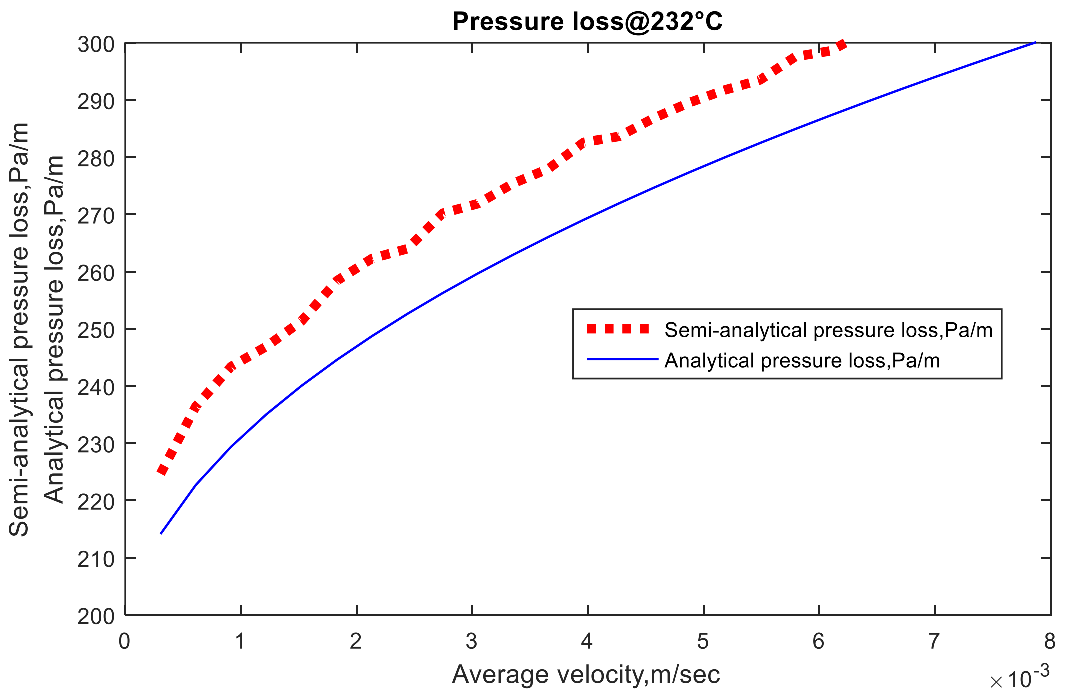

Figure L.17: Difference between obtained frictional pressure drop using semi-analytical and existing analytical method for fresh water sepiolite mud @232°C.

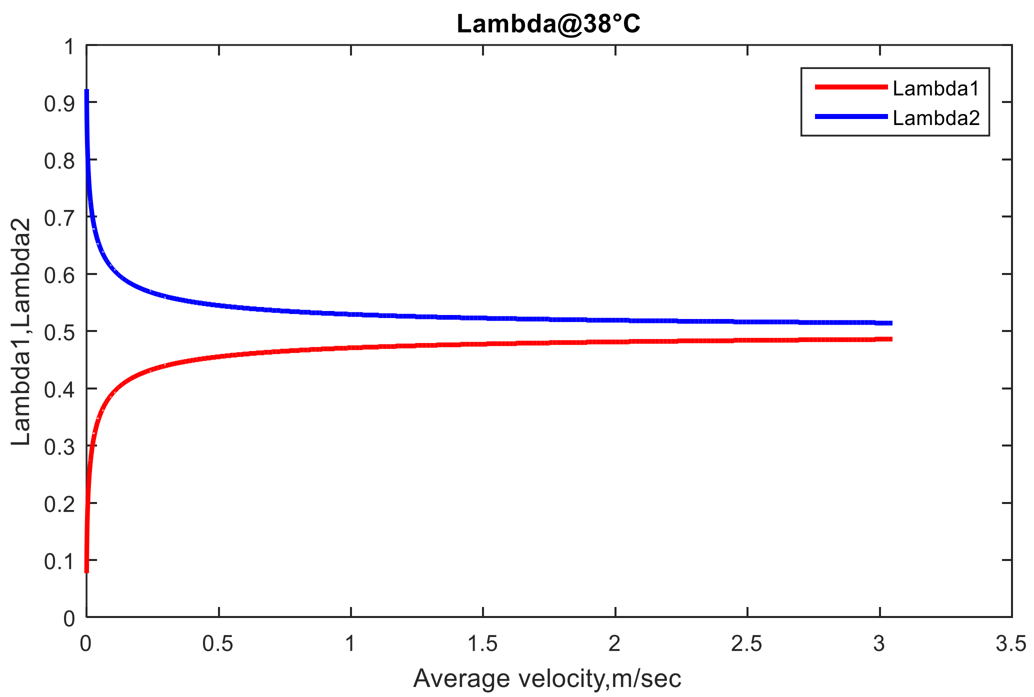

Figure L.18: Variation of λ_2 and λ_1 with average velocity for fresh water sepiolite mud @38°C, (plug region wideness).

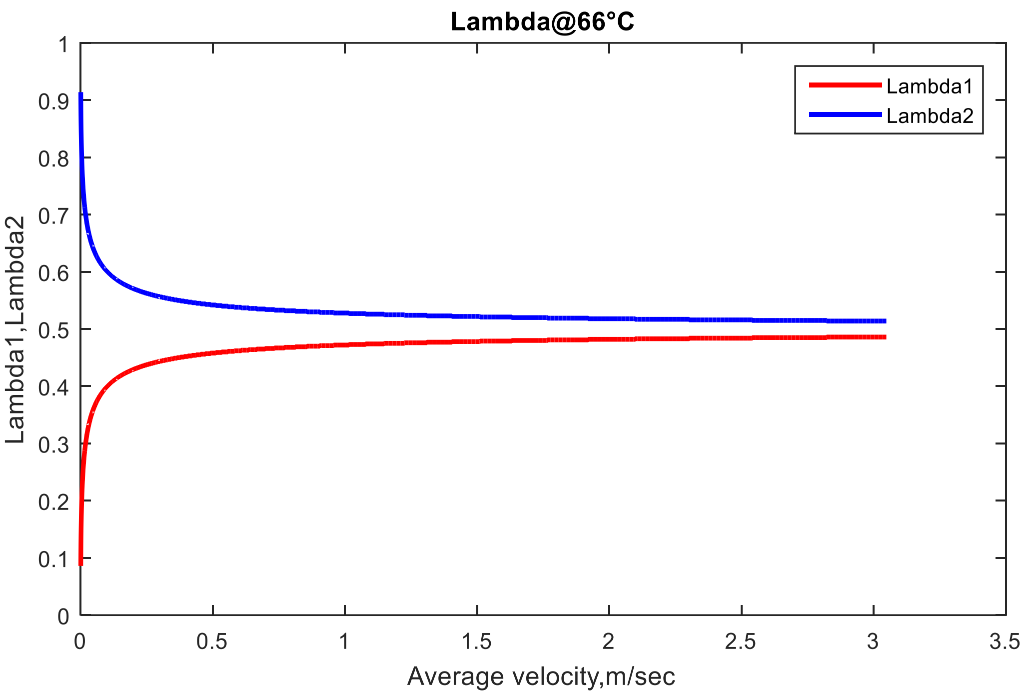

Figure L.19: Variation of λ_2 and λ_1 with average velocity for fresh water sepiolite mud @66°C, (plug region wideness).

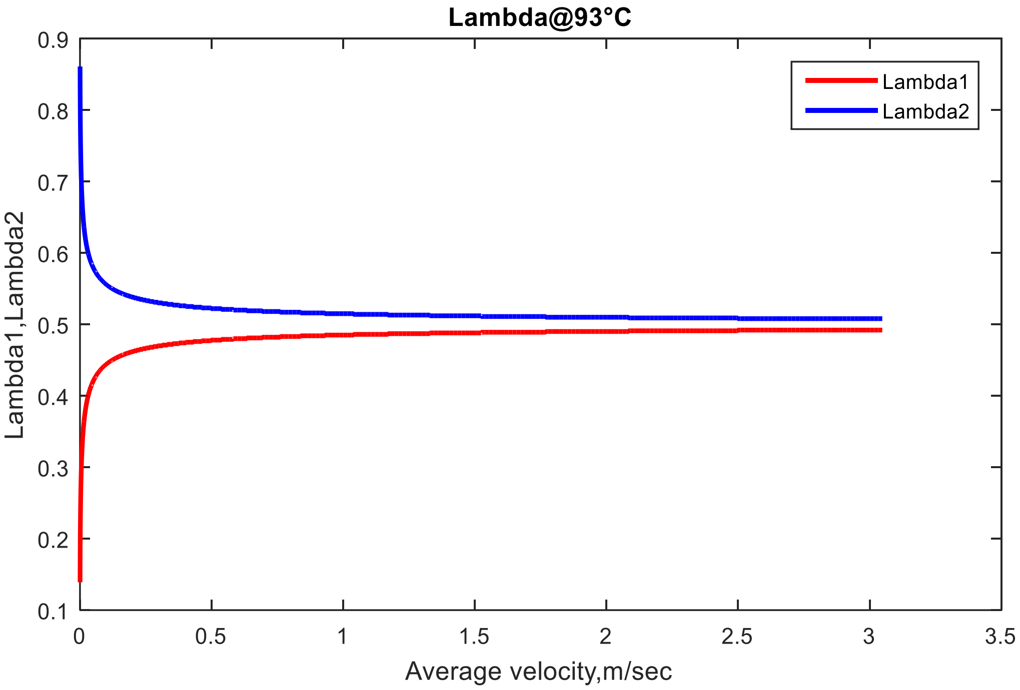

Figure L.20: Variation of λ_2 and λ_1 with average velocity for fresh water sepiolite mud @93°C, (plug region wideness).

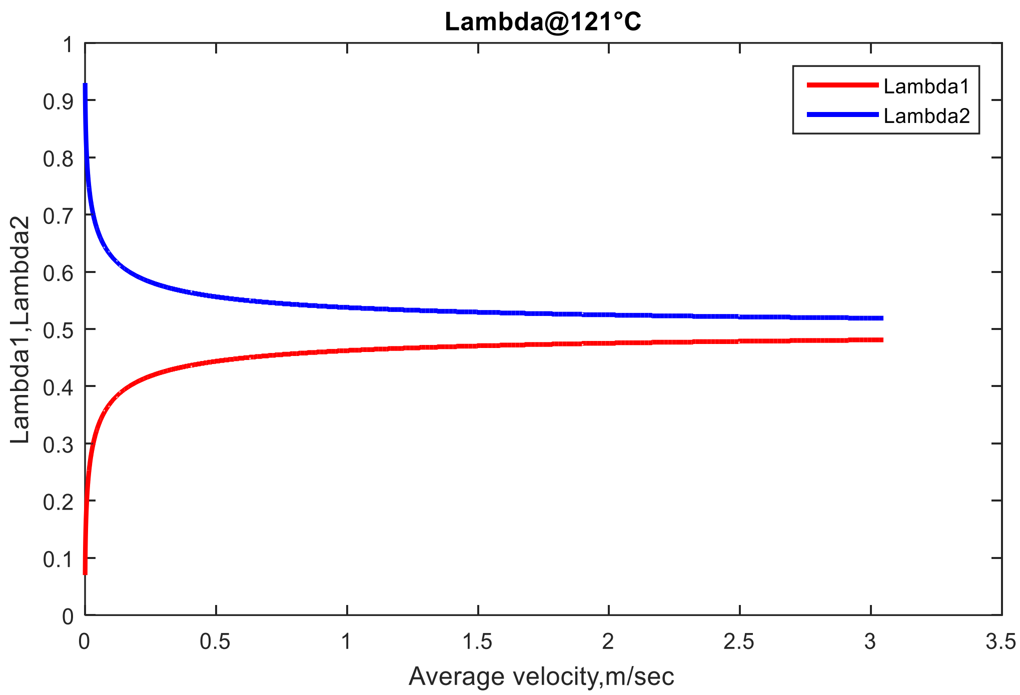

Figure L.21: Variation of λ_2 and λ_1 with average velocity for fresh water sepiolite mud @121°C, (plug region wideness).

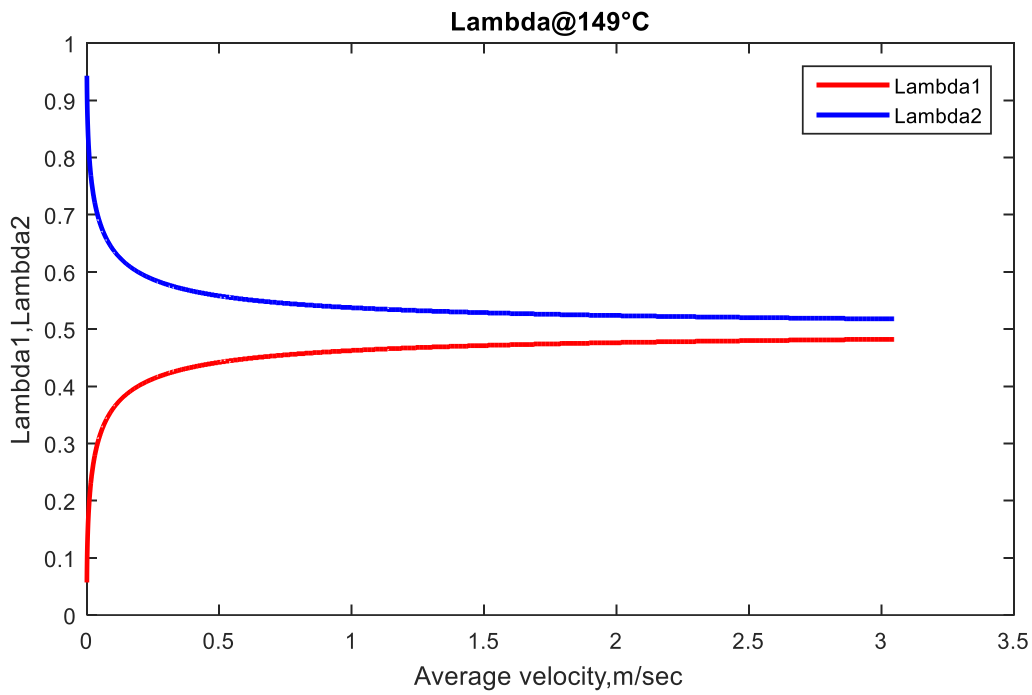

Figure L.22: Variation of λ_2 and λ_1 with average velocity for fresh water sepiolite mud @149°C, (plug region wideness).

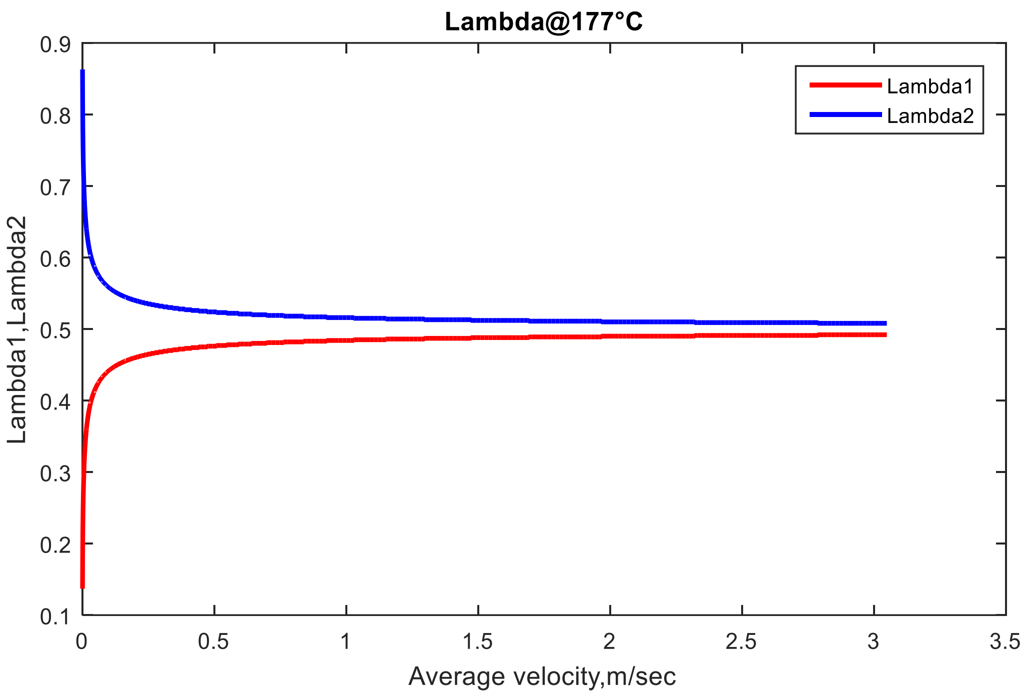

Figure L.23: Variation of λ_2 and λ_1 with average velocity for fresh water sepiolite mud @177°C, (plug region wideness).

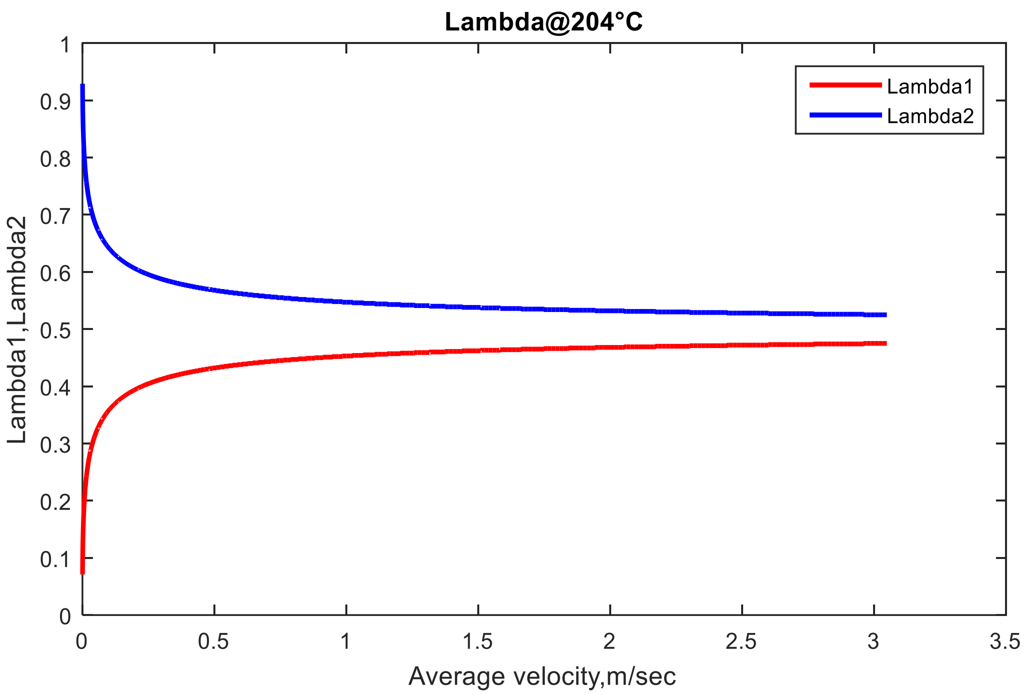

Figure L.24: Variation of λ_2 and λ_1 with average velocity for fresh water sepiolite mud @204°C, (plug region wideness).

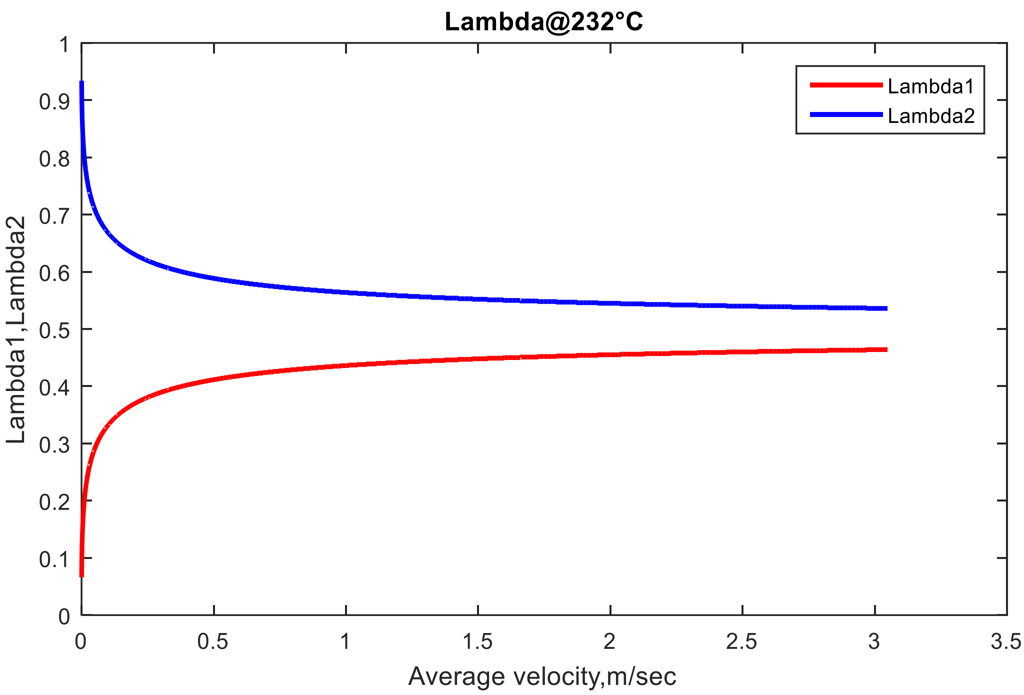

Figure L.25: Variation of λ_2 and λ_1 with average velocity for fresh water sepiolite mud @232°C, (plug region wideness).

Appendix M: Circulation pressure losses for unweighted fresh water sepiolite mud-Analytical solution and CFD results.

Table M.1: Pipe flow based on viscometer rheological parameters.

Pipe flow based on viscometer rheological parameters				**Temperature, °C**							
Model		**Properties**	**unit**	**38**	**65**	**93**	**121**	**149**	**177**	**204**	**232**
Power Law	**Analytical solution**	Flow behavior index (n)	-	0.636	0.618	0.605	0.605	0.663	0.598	0.545	0.480
		Consistency index (K)	$Pa\text{-}s^n$	0.4395	0.5182	0.4517	0.3532	0.1958	0.3166	0.5398	0.9297
		Fluid velocity inside pipe (v)	m/sec	7.13	7.13	7.13	7.13	7.13	7.13	7.13	7.13
		Reynold Number (Nre)	-	12456	11853	14795	18997	23507	22197	18286	16280
		Flow regime	-	Turbulent	Turbulent	Turbulent	Turbulent	Turbulent	Turbulent	Turbulent	Turbulent
		Friction factor(f)	-	0.0054	0.0054	0.0049	0.0046	0.0047	0.0044	0.0043	0.0041
		Pressure drop (ΔP/ΔL)	Pa/m	8176	8134	7517	7002	7064	6651	6567	6191
	CFD	Pressure drop (ΔP/ΔL)	Pa/m	7600	7530	6788	6206	6385	5816	5662	5234
Bingham Plastic	**Analytical solution**	Plastic viscosity (PV)	Pa-s	0.0335	0.0328	0.0278	0.0215	0.0180	0.0184	0.0213	0.0227
		Yield point (YP)	Pa	3.99	4.14	3.56	2.93	2.00	2.44	3.66	4.97
		Fluid velocity inside pipe (v)	m/sec	7.13	7.13	7.13	7.13	7.13	7.13	7.13	7.13
		Reynold Number (Nre)	-	15500	15831	18670	24213	28895	28182	24354	22865
		Flow regime	-	Turbulent	Turbulent	Turbulent	Turbulent	Turbulent	Turbulent	Turbulent	Turbulent
		Pressure drop (ΔP/ΔL)	Pa/m	10770	10714	10281	9634	9217	9275	9620	9773
	CFD	Pressure drop (ΔP/ΔL)	Pa/m	10890	10810	10340	9673	9340	9350	9560	9600
Herschel Bulkley	**Analytical solution**	Consistency index (K)	$Pa\text{-}s^n$	0.3104	0.3497	0.3799	0.2230	0.1244	0.2633	0.2979	0.4048
		Flow behavior index (n)	-	0.68	0.66	0.63	0.67	0.72	0.62	0.63	0.59
		Yield point (YP)	Pa	1.05	1.01	0.46	0.91	0.70	0.33	1.25	2.03
		Cc	-	0.99	0.99	0.99	0.98	0.98	0.99	0.98	0.96
		Y	-	0.0753	0.0750	0.0746	0.0751	0.0758	0.0745	0.0745	0.0740
		Z	-	0.2737	0.2755	0.2788	0.2751	0.2698	0.2794	0.2791	0.2826
		Reynold Number (Nre)	-	14152	14443	17148	21863	25798	25822	21631	19847
		Equivalent Reynold Number (Nre)	-	13965	14256	17024	21474	25390	25621	21102	19126
		Critical Reynold Number (Nre)	-	1862	1932	2069	1919	1723	2096	2082	2241
		Flow regime	-	Turbulent	Turbulent	Turbulent	Turbulent	Turbulent	Turbulent	Turbulent	Turbulent
		Friction factor(f)	-	0.0055	0.0054	0.0049	0.0048	0.0049	0.0044	0.0046	0.0046
		Pressure drop (ΔP/ΔL)	Pa/m	8401	8192	7497	7337	7473	6640	7036	6944
	CFD	Pressure drop (ΔP/ΔL)	Pa/m	8720	8275	7670	7270	7260	6470	6946	6966

Table M.2: Pipe flow based on rheometer rheological parameters.

Pipe flow based on Rheometer rheological parameters				Temperature, °C							
Model		Properties	unit	38	65	93	121	149	177	204	232
Power Law	Analytical solution	Flow behavior index (n)	-	0.7125	0.7282	0.7306	0.856	1.007	1.094	0.192	0.4238
		Consistency index (K)	$Pa\text{-}s^n$	0.2353	0.1475	0.1026	0.0274	0.0056	0.0020	1.6727	0.5240
		Fluid velocity inside pipe (v)	m/sec	7.13	7.13	7.13	7.13	7.13	7.13	7.13	7.13
		Reynold Number (Nre)	-	14162	20400	28894	48078	88407	142861	60991	41706
		Flow regime	-	Turbulent	Turbulent	Turbulent	Turbulent	Turbulent	Turbulent	Turbulent	Turbulent
		Friction factor(f)	-	0.0056	0.0052	0.0047	0.0047	0.0046	0.0045	0.0013	0.0028
		Pressure drop ($\Delta P/\Delta L$)	Pa/m	8530	7849	7190	7142	7048	6803	2036	4304
	CFD	Pressure drop ($\Delta P/\Delta L$)	Pa/m	8126	7394	6700	6768	6924	6856	1387	3269
Bingham Plastic	Analytical solution	Plastic viscosity (PV)	Pa-s	0.0309	0.0217	0.0154	0.0098	0.0059	0.0039	0.0040	0.0060
		Yield point (YP)	Pa	2.75	1.75	1.21	0.44	-0.01	-0.17	3.20	3.97
		Fluid velocity inside pipe (v)	m/sec	7.13	7.13	7.13	7.13	7.13	7.13	7.13	7.13
		Reynold Number (Nre)	-	16833	23924	33792	52759	88046	131593	129057	86847
		Flow regime	-	Turbulent	Turbulent	Turbulent	Turbulent	Turbulent	Turbulent	Turbulent	Turbulent
		Pressure drop ($\Delta P/\Delta L$)	Pa/m	10551	9663	8864	7929	6976	6310	6340	7000
	CFD	Pressure drop ($\Delta P/\Delta L$)	Pa/m	10761	9870	9148	8252	7043	6332	5850	6800
Herschel Bulkley	Analytical solution	Consistency index (K)	$Pa\text{-}s^n$	0.1602	0.1096	0.0782	0.0274	0.0046	0.0020	0.0001	0.0053
		Flow behavior index (n)	-	0.76	0.77	0.77	0.86	1.04	1.09	1.51	1.02
		Yield point (YP)	Pa	0.96	0.52	0.33	0.00	0.08	0.00	3.57	4.02
		Cc	-	0.99	0.99	0.99	1.00	0.99	1.00	0.85	0.85
		Y	-	0.0763	0.0763	0.0763	0.0772	0.0789	0.0794	0.0822	0.0787
		Z	-	0.2667	0.2663	0.2664	0.2596	0.2479	0.2444	0.2246	0.2490
		Reynold Number (Nre)	-	15553	22282	31505	50176	88281	140040	67695	51357
		Equivalent Reynold Number (Nre)	-	15352	22061	31220	50176	87800	140040	57754	43647
		Critical Reynold Number (Nre)	-	1622	1612	1614	1421	1155	1090	801	1176
		Flow regime	-	Turbulent	Turbulent	Turbulent	Turbulent	Turbulent	Turbulent	Turbulent	Turbulent
		Friction factor(f)	-	0.0058	0.0053	0.0048	0.0046	0.0047	0.0044	0.0070	0.0055
		Pressure drop ($\Delta P/\Delta L$)	Pa/m	8870	8094	7362	7069	7139	6664	10645	8376
	CFD	Pressure drop ($\Delta P/\Delta L$)	Pa/m	8973	8250	7400	7281	7030	7000	10635	7600

Table M.3: Annular flow based on viscometer rheological parameters.

Annular flow based on viscometer rheological parameters				Temperature, °C							
Model		Properties	unit	38	65	93	121	149	177	204	232
Power Law	Analytical solution	Flow behavior index (n)	-	0.636	0.618	0.605	0.605	0.663	0.598	0.545	0.480
		Consistency index (K)	Pa-s^n	0.4395	0.5182	0.4517	0.3532	0.1958	0.3166	0.5398	0.9297
		Annular velocity (v)	m/sec	2.35	2.35	2.35	2.35	2.35	2.35	2.35	2.35
		Reynold Number (Nre)	-	1806	1711	2130	2734	3429	3189	2597	2279
		Laminar pressure drop (ΔP/ΔL)	Pa/m	3018	3185	2559	1993	1589	1709	2099	2391
		Friction factor(f)	-	0.0101	0.0101	0.0092	0.0084	0.0082	0.0079	0.0081	0.0079
		Turbulent pressure drop (ΔP/ΔL)	Pa/m	3438	3454	3150	2879	2812	2710	2762	2694
	CFD	Turbulent pressure drop (ΔP/ΔL)	Pa/m	3936	4037	3451	2942	2710	2667	2895	3003
Bingham Plastic	Analytical solution	Plastic viscosity (PV)	Pa-s	0.0335	0.0328	0.0278	0.0215	0.0180	0.0184	0.0213	0.0227
		Yield point (YP)	Pa	3.99	4.14	3.56	2.93	2.00	2.44	3.66	4.97
		Annular velocity (v)	m/sec	2.35	2.35	2.35	2.35	2.35	2.35	2.35	2.35
		Reynold Number (Nre)	-	2462	2514	2965	3845	4589	4476	3868	3631
		Hedstrom Reynold number (NHe)	-	4202	4554	5438	7549	7323	8497	9516	11396
		Laminar pressure drop (ΔP/ΔL)	Pa/m	2793	2770	2355	1844	1478	1572	1940	2223
		Turbulent pressure drop (ΔP/ΔL)	Pa/m	3841	3820	3666	3435	3287	3307	3430	3485
	CFD	Turbulent pressure drop (ΔP/ΔL)	Pa/m	4167	4136	3783	3442	3230	3100	3313	3445
Herschel Bulkley	Analytical solution	Consistency index (K)	Pa-s^n	0.3104	0.3497	0.3799	0.2230	0.1244	0.2633	0.2979	0.4048
		Flow behavior index (n)	-	0.68	0.66	0.63	0.67	0.72	0.62	0.63	0.59
		Yield point (YP)	Pa	1.05	1.01	0.46	0.91	0.70	0.33	1.25	2.03
		Ca	-	0.9796	0.9802	0.9891	0.9727	0.9750	0.9883	0.9633	0.9465
		Y	-	0.0753	0.0750	0.0746	0.0751	0.0758	0.0745	0.0745	0.0740
		Z	-	0.2737	0.2755	0.2788	0.2751	0.2698	0.2794	0.2791	0.2826
		Reynold Number (Nre)	-	2630	2677	3173	4057	4813	4776	4003	3670
		Equivalent Reynold Number (Nre)	-	2576	2624	3139	3947	4693	4720	3857	3474
		Critical Reynold Number (Nre)	-	3410	3557	3848	3530	3120	3905	3876	4216
		Flow regime	-	laminar	laminar	laminar	turbulent	turbulent	turbulent	laminar	laminar
		Laminar Friction factor (f)		0.0108	0.0107	0.0092	0.0071	0.0058	0.0061	0.0075	0.0085
		Turbulent Friction factor (f)	-	0.0088	0.0086	0.0079	0.0077	0.0078	0.0070	0.0074	0.0074
		Laminar pressure drop (ΔP/ΔL)	Pa/m	3004	2986	2556	1981	1607	1707	2085	2373
		Turbulent pressure drop (ΔP/ΔL)	Pa/m	2451	2396	2207	2148	2165	1957	2077	2066
	CFD	Turbulent pressure drop (ΔP/ΔL)	Pa/m	2990	2850	2543	2142	2240	2000	2245	2355

Table M.4: Annular flow based on rheometer rheological parameters.

Annular flow based on Rheometer rheological parameters				Temperature, °C							
Model		**Properties**	**unit**	**38**	**65**	**93**	**121**	**149**	**177**	**204**	**232**
Power Law	**Analytical solution**	Flow behavior index (n)	-	0.7125	0.7282	0.7306	0.856	1.007	1.094	0.192	0.4238
		Consistency index (K)	$Pa\text{-}s^n$	0.2353	0.1475	0.1026	0.0274	0.0056	0.0020	1.6727	0.5240
		Annular velocity (v)	m/sec	2.35	2.35	2.35	2.35	2.35	2.35	2.35	2.35
		Reynold Number (Nre)	-	2091	3023	4284	7355	14063	23254	8132	5772
		Flow regime		turbulent	turbulent	turbulent	turbulent	turbulent	turbulent	turbulent	turbulent
		Laminar pressure drop (ΔP/ΔL)	Pa/m	2607	1803	1272	741	388	234	670	944
		Friction factor(f)	-	0.0102	0.0091	0.0081	0.0076	0.0071	0.0066	0.0027	0.0052
		Turbulent pressure drop (ΔP/ΔL)	Pa/m	3470	3098	2773	2599	2422	2262	934	1781
	CFD	Turbulent pressure drop (ΔP/ΔL)	Pa/m	3771	3076	2572	2319	2199	1974	877	1557
Bingham Plastic	**Analytical solution**	Plastic viscosity (PV)	Pa-s	0.0309	0.0217	0.0154	0.0098	0.0059	0.0039	0.0040	0.0060
		Yield point (YP)	Pa	2.75	1.75	1.21	0.44	-0.01	-0.17	3.20	3.97
		Annular velocity (v)	m/sec	2.35	2.35	2.35	2.35	2.35	2.35	2.35	2.35
		Reynold Number (Nre)	-	2673	3800	5367	8379	13983	20899	20496	13793
		Flow regime		turbulent	turbulent	turbulent	turbulent	turbulent	turbulent	turbulent	turbulent
		Hedstrom Reynold number (NHe)	-	3422	4396	6060	5434	0	0	233683	131474
		Laminar pressure drop (ΔP/ΔL)	Pa/m	2439	1689	1191	715	388	236	731	972
		Turbulent pressure drop (ΔP/ΔL)	Pa/m	3762	3446	3161	2828	2488	2250	2261	2496
	CFD	Turbulent pressure drop (ΔP/ΔL)	Pa/m	3965	3336	3100	2750	2354	2060	1700	1800
Herschel Bulkley	**Analytical solution**	Consistency index (K)	$Pa\text{-}s^n$	0.1602	0.1096	0.0782	0.0274	0.0046	0.0020	0.0001	0.0053
		Flow behavior index (n)	-	0.76	0.77	0.77	0.86	1.04	1.09	1.51	1.02
		Yield point (YP)	Pa	0.96	0.52	0.33	0.00	0.08	0.00	3.57	4.02
		Ca	-	0.98	0.98	0.99	1.00	0.99	1.00	0.74	0.75
		Y	-	0.0763	0.0763	0.0763	0.0772	0.0789	0.0794	0.0822	0.0787
		Z	-	0.2667	0.2663	0.2664	0.2596	0.2479	0.2444	0.2246	0.2490
		Reynold Number (Nre)	-	2914	4175	5907	9539	17237	27745	12931	9766
		Equivalent Reynold Number (Nre)	-	2853	4108	5821	9539	17066	27745	9511	7340
		Critical Reynold Number (Nre)	-	2912	2891	2896	2503	1972	1846	1298	2014
		Flow regime	-	laminar	turbulent	turbulent	turbulent	turbulent	turbulent	turbulent	turbulent
		Laminar Friction factor (f)		0.0093	0.0064	0.0045	0.0027	0.0014	0.0008	0.0022	0.0033
		Turbulent Friction factor (f)	-	0.0091	0.0083	0.0076	0.0072	0.0070	0.0065	0.0105	0.0086
		Laminar pressure drop (ΔP/ΔL)	Pa/m	2591	1796	1268	742	388	235	626	908
		Turbulent pressure drop (ΔP/ΔL)	Pa/m	2552	2324	2116	1998	1968	1819	2932	2398
	CFD	Turbulent pressure drop (ΔP/ΔL)	Pa/m	2594	2389	2097	1988	2172	1974	2865	2045

Appendix N: Circulation pressure losses for unweighted fresh water sepiolite based on viscometer and HTHP Rheometer measurements: Analytical method vs. CFD.

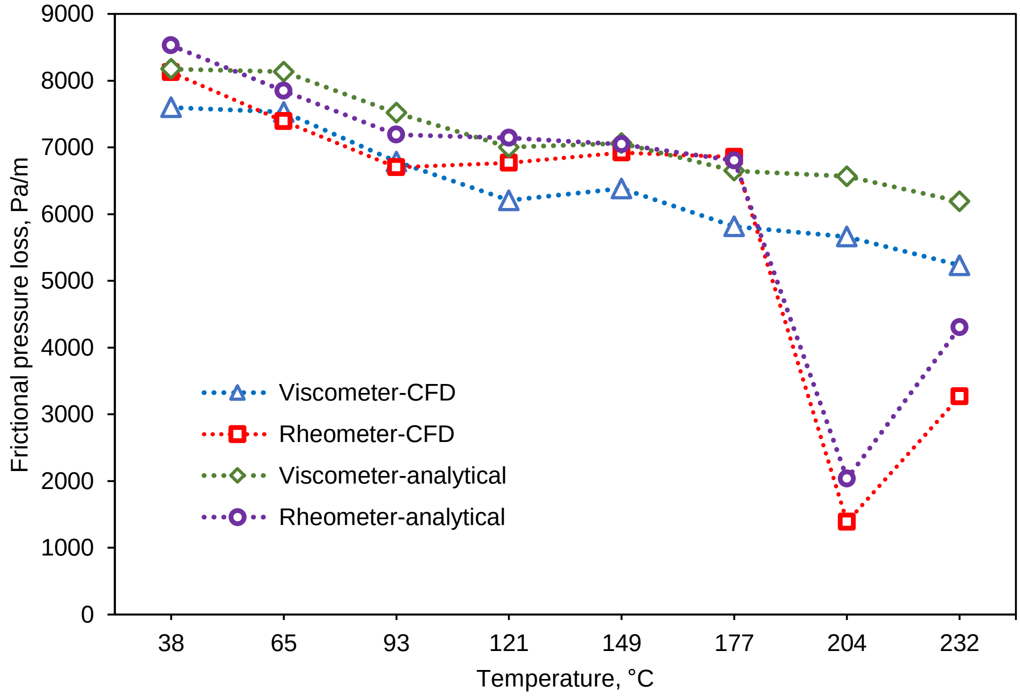

Figure N.1: Variation of frictional pressure losses with temperature-Power Law model- Drill pipe.

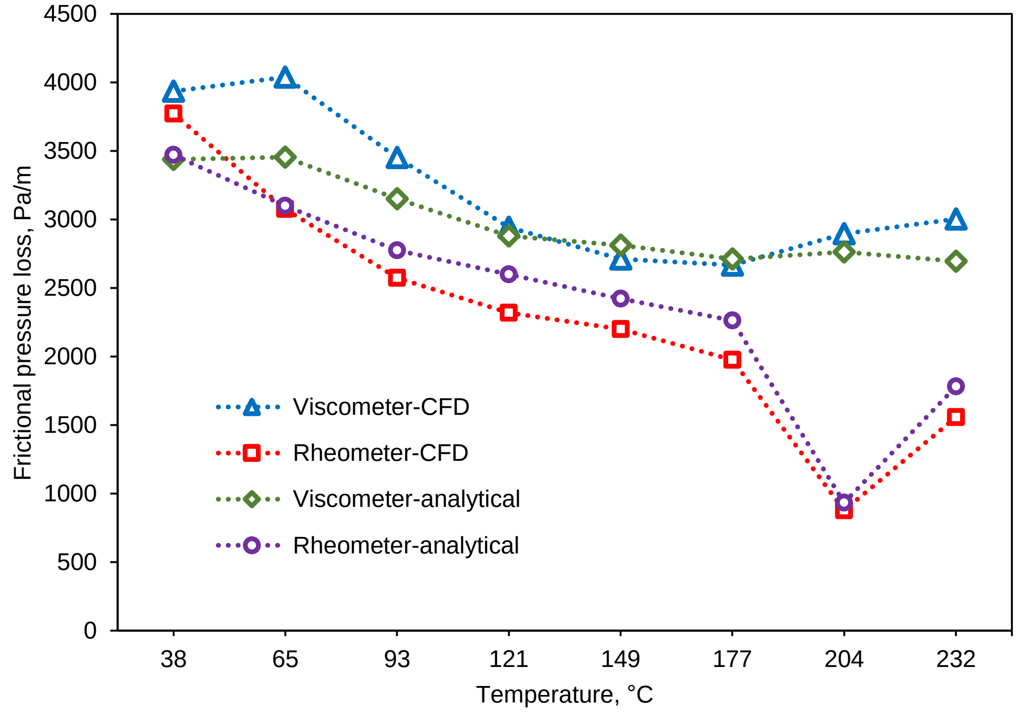

Figure N.2: Variation of frictional pressure losses with temperature-Power Law model- Annulus.

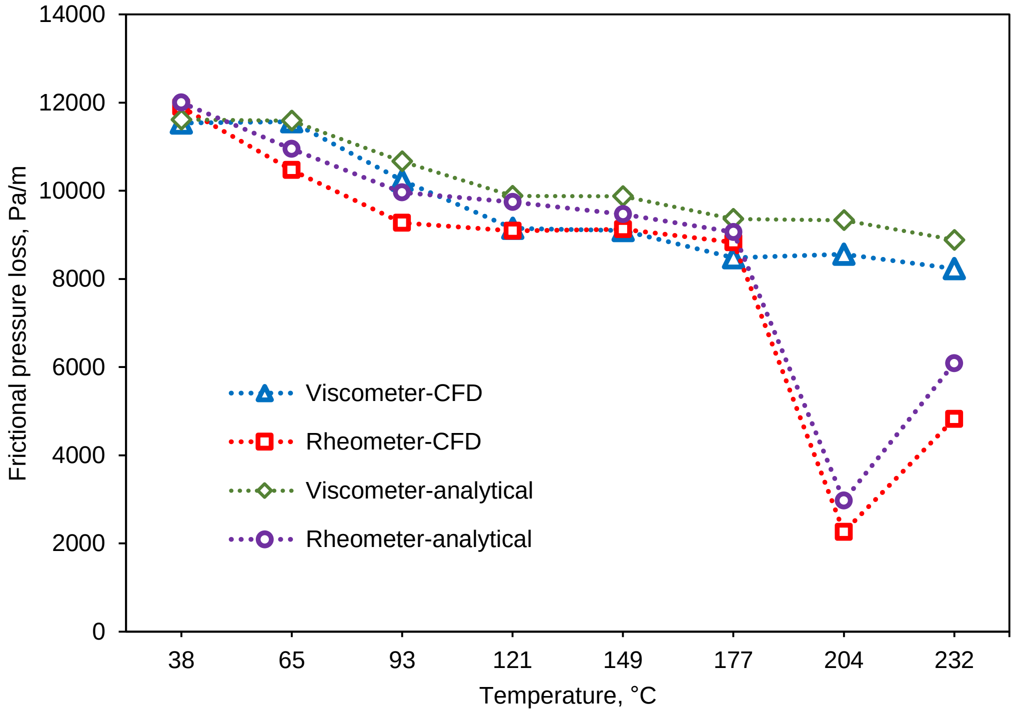

Figure N.3: Variation of frictional pressure losses with temperature-Power Law model- Total.

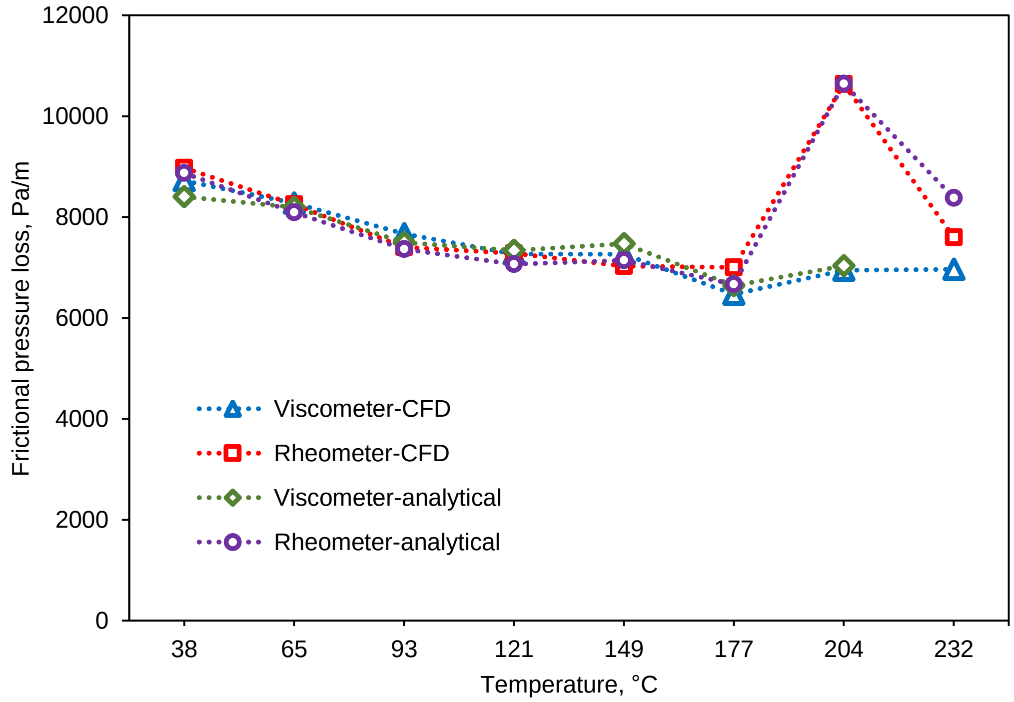

Figure N.4: Variation of frictional pressure losses with temperature-Herschel Bulkley model- Drill pipe.

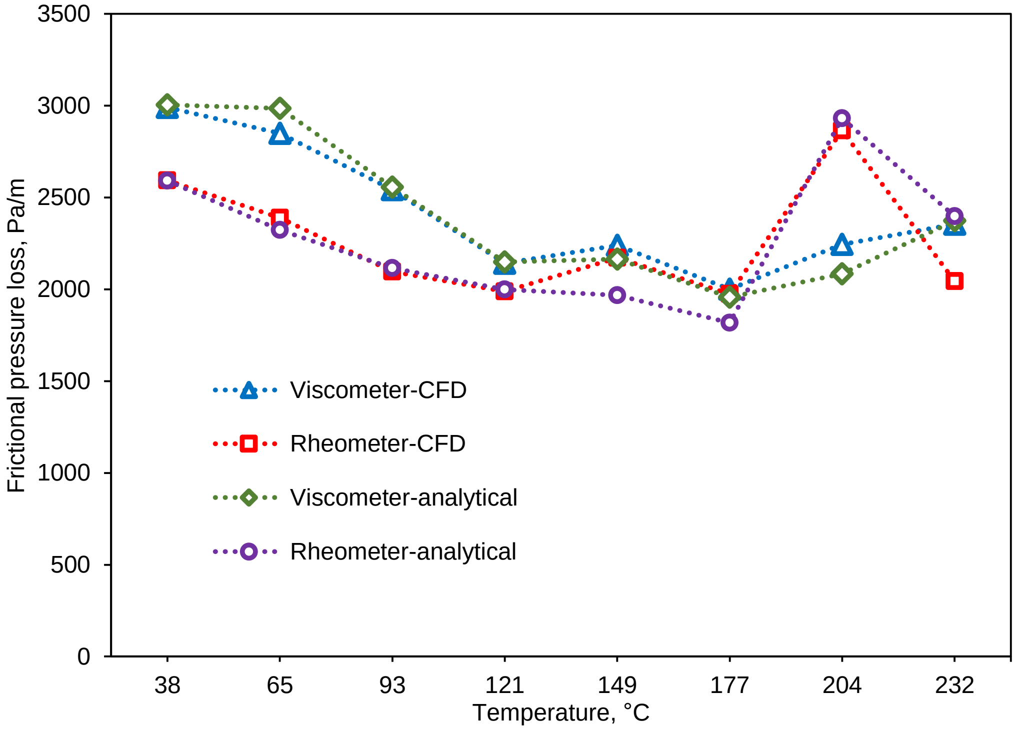

Figure N.5: Variation of frictional pressure losses with temperature-Herschel Bulkley model- Annulus.

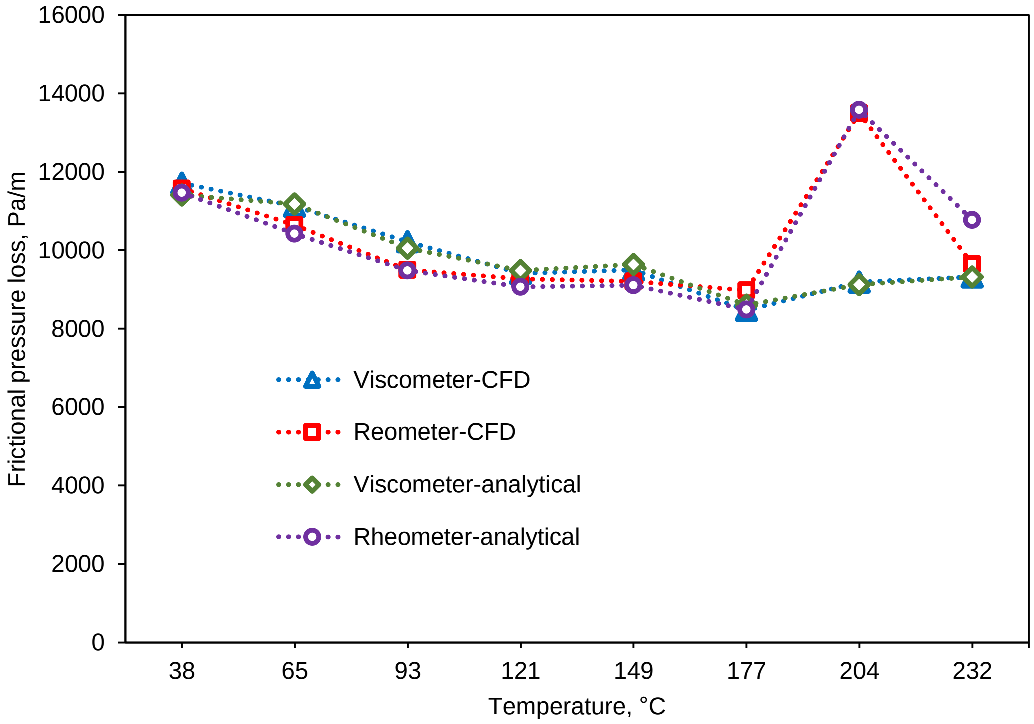

Figure N.6: Variation of frictional pressure losses with temperature-Herschel Bulkley model- Total.

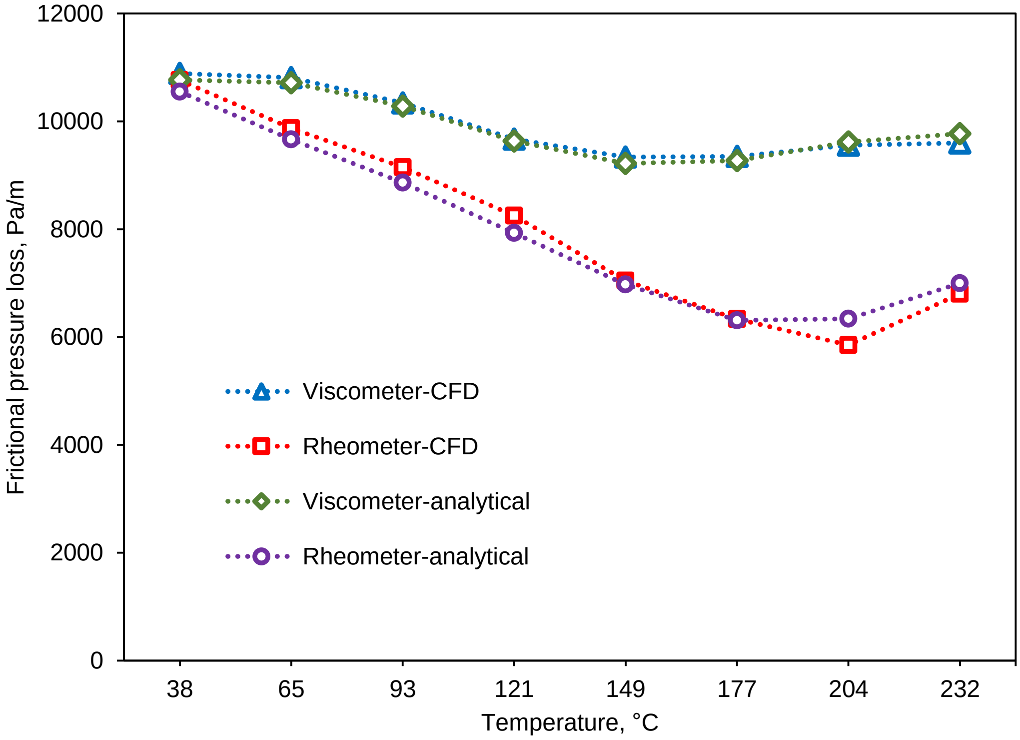

Figure N.7: Variation of frictional pressure losses with temperature-Bingham Plastic model- Drill pipe.

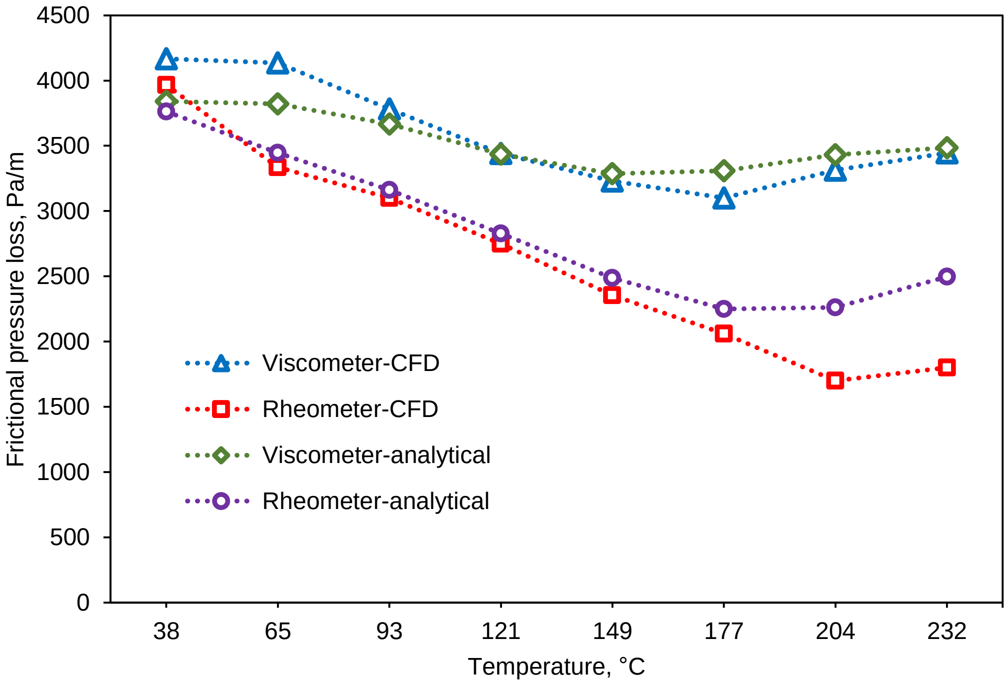

Figure N.8: Variation of frictional pressure losses with temperature-Bingham Plastic model- Annulus.

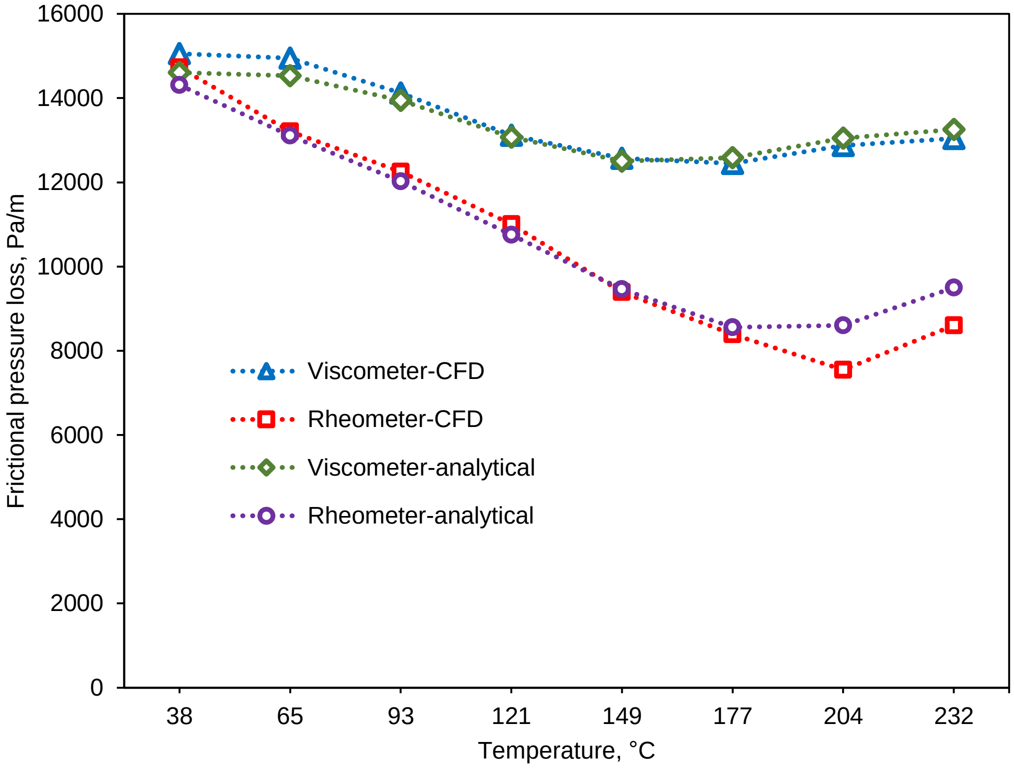

Figure N.9: Variation of frictional pressure losses with temperature-Bingham Plastic model- Total.

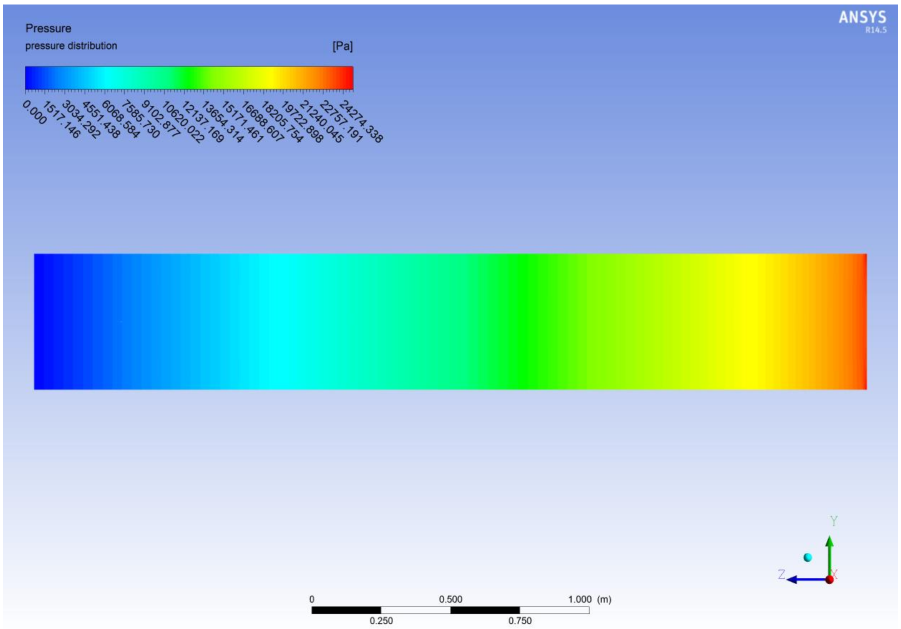

Figure N.10: Cross sectional pressure distribution inside drill pipe while circulating fresh water sepiolite mud.

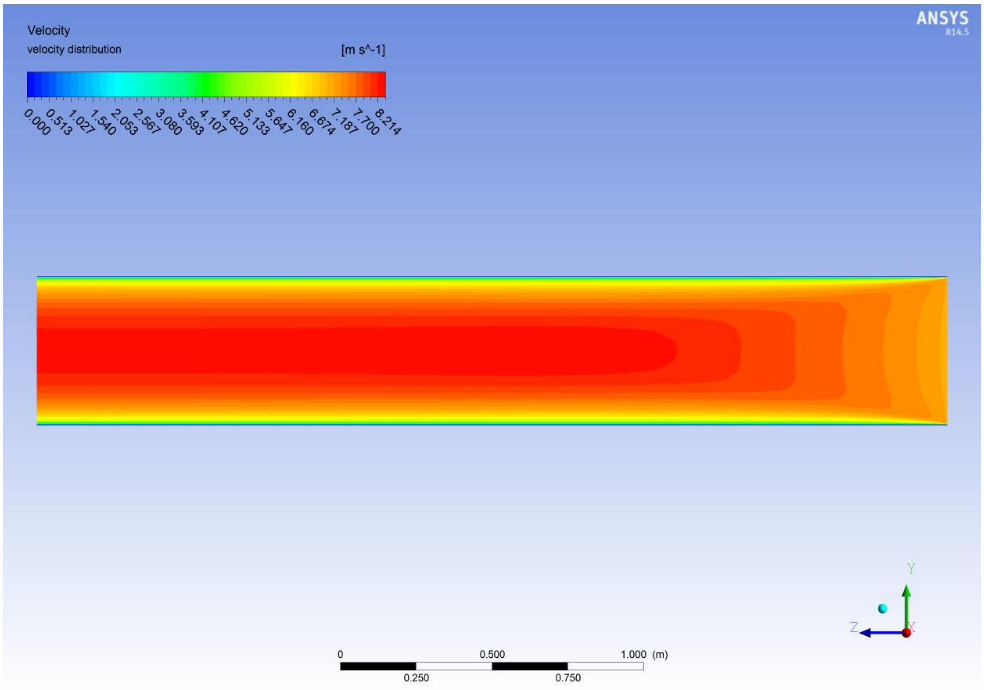

Figure N.11: Velocity distribution inside drill pipe while circulating fresh water sepiolite mud.

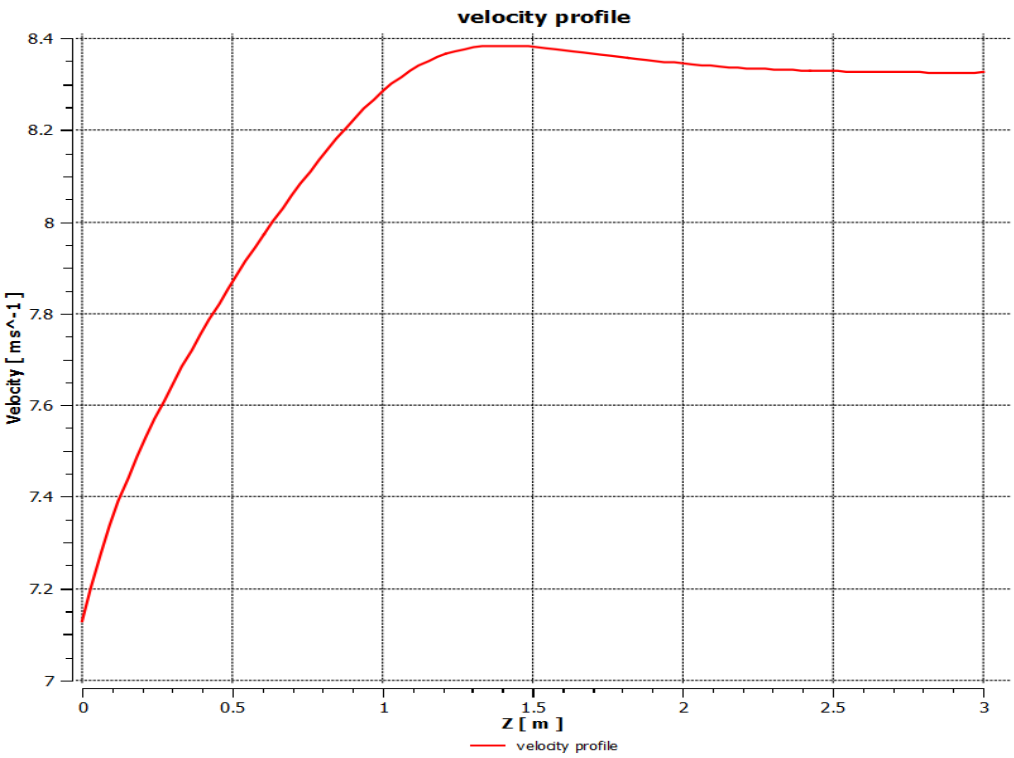

Figure N.12: Centerline velocity change inside drill pipe; fully developed flow after 2 meter.

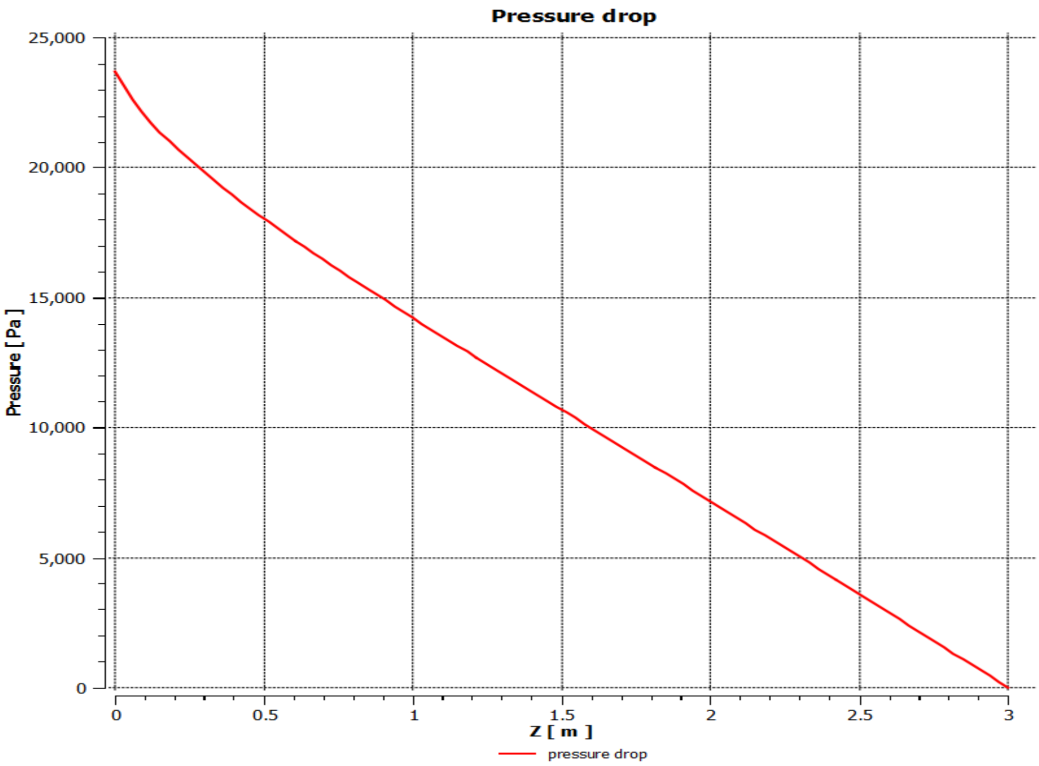

Figure N.13: Pressure drop inside drill pipe while circulating fresh water sepiolite mud.

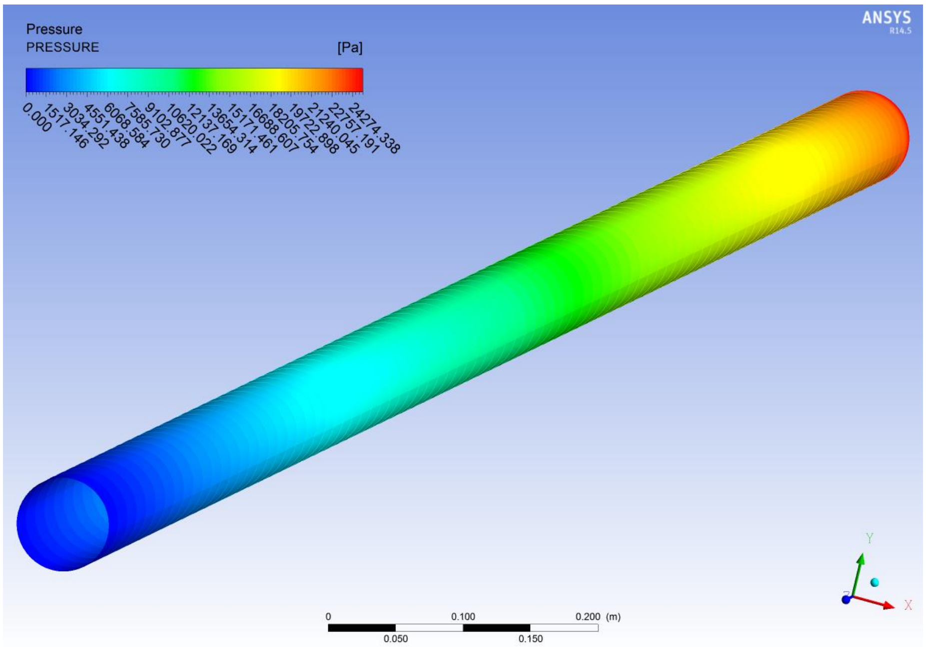

Figure N.14: Pressure distribution profile inside drill pipe while circulating fresh water sepiolite mud.

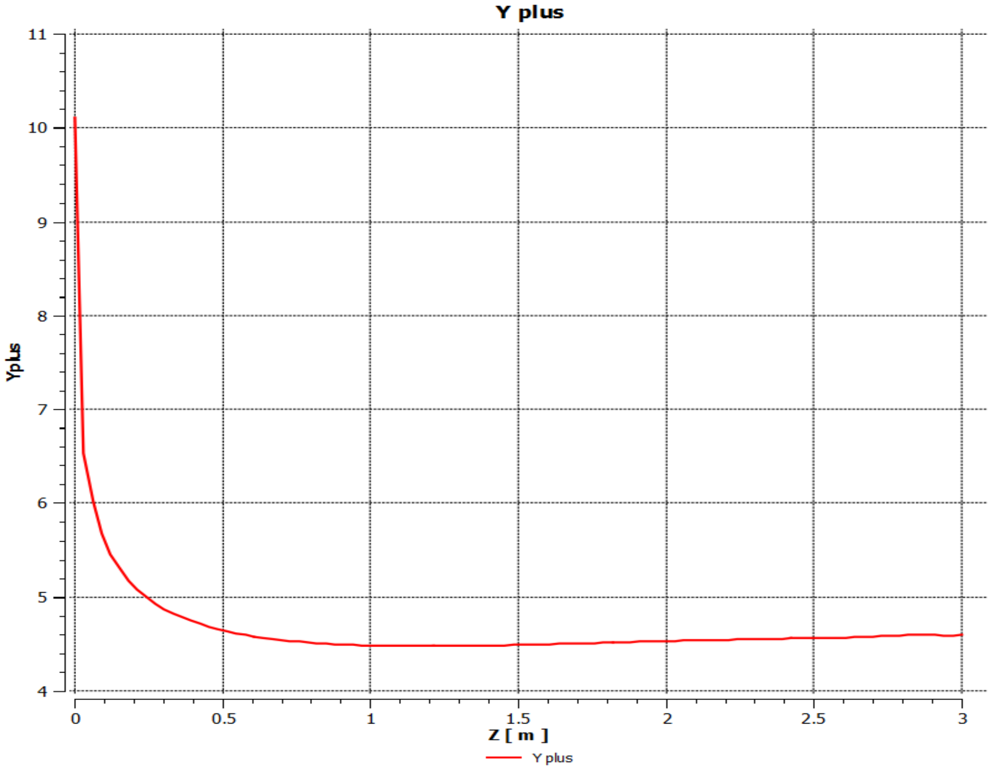

Figure N.15: Yplus variation through drill pipe.

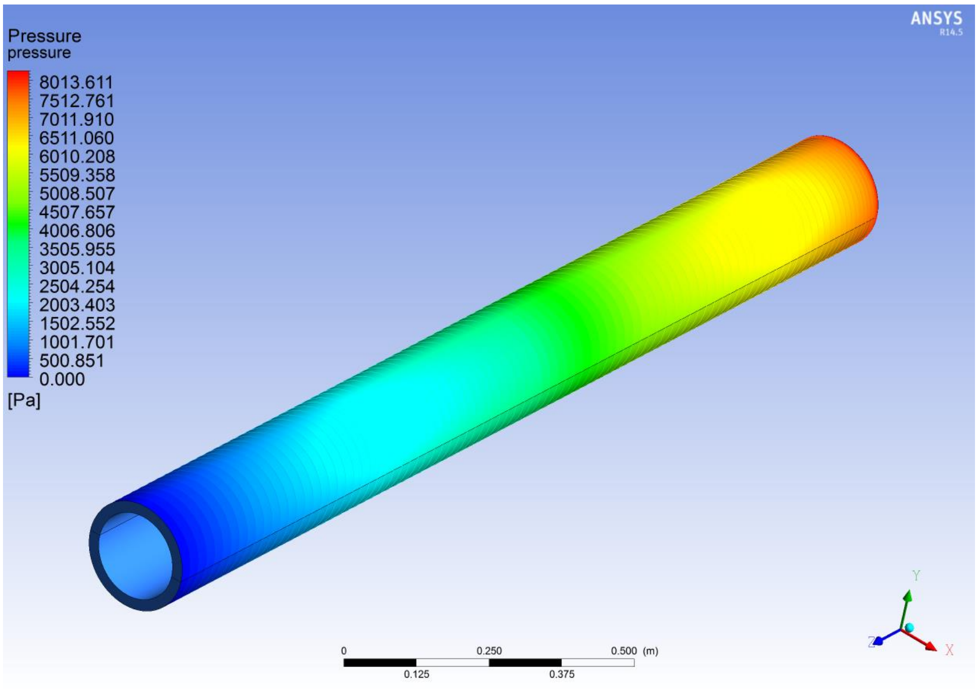

Figure N.16: Pressure distribution profile through annulus while circulating fresh water sepiolite mud.

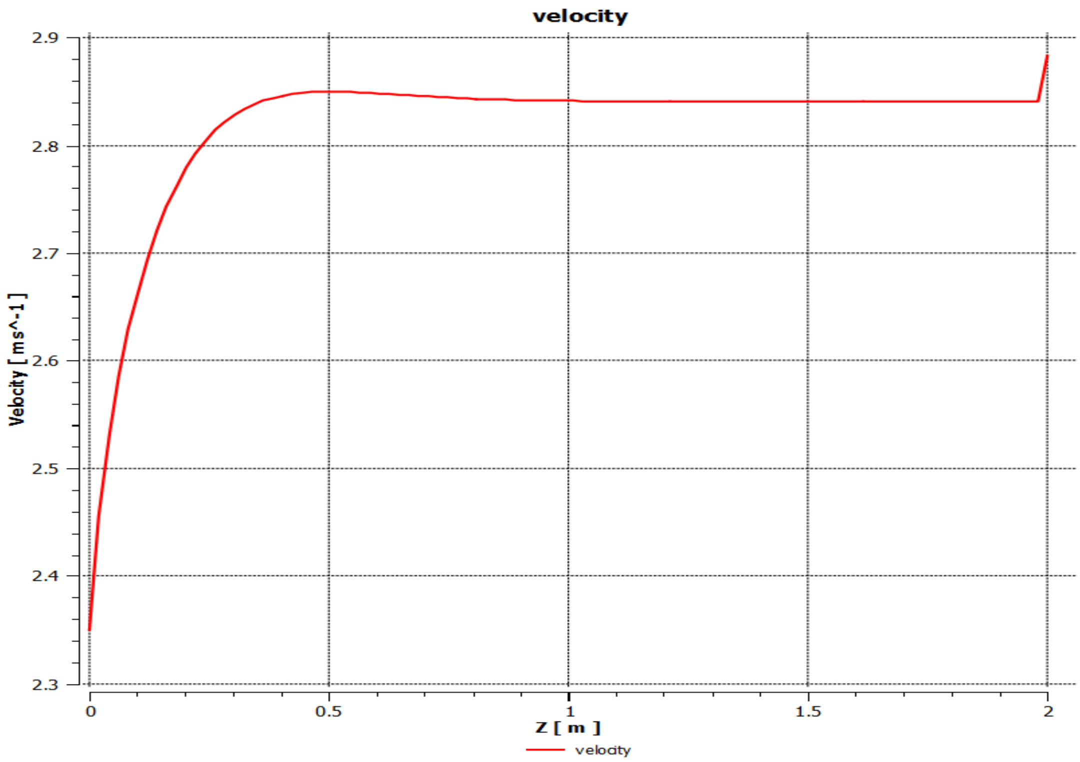

Figure N.17: Centerline velocity change through annulus; fully developed flow after 1 meter.

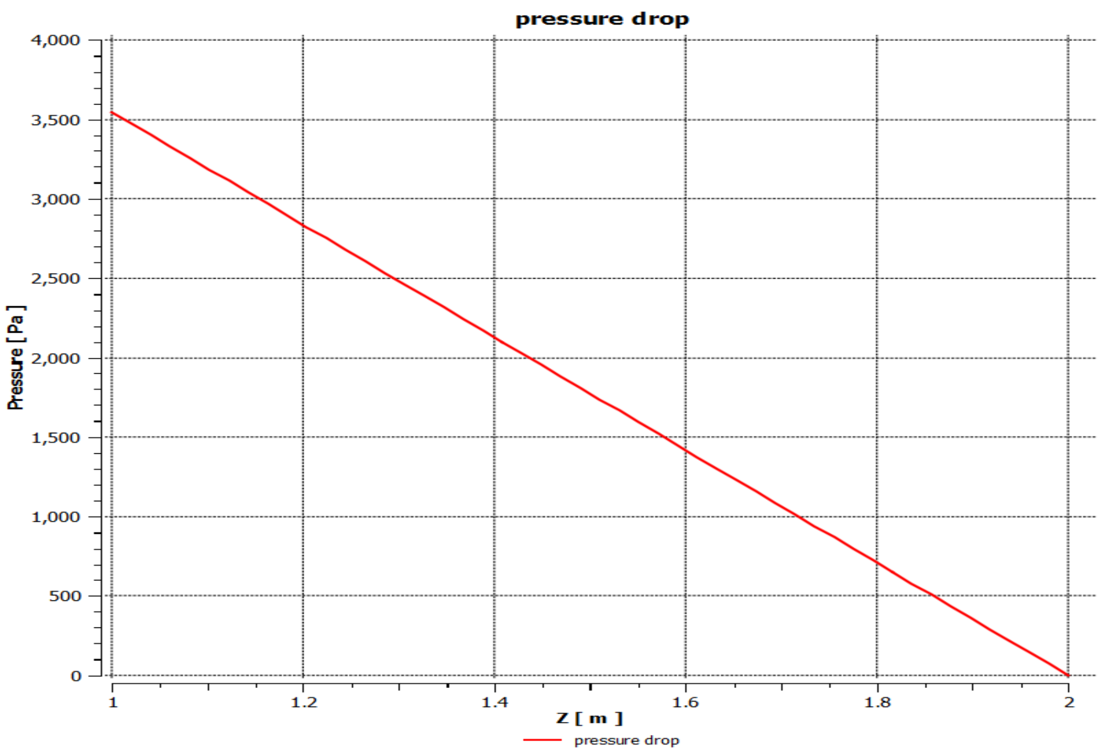

Figure N.18: Pressure drop through annulus while circulating fresh water sepiolite mud.

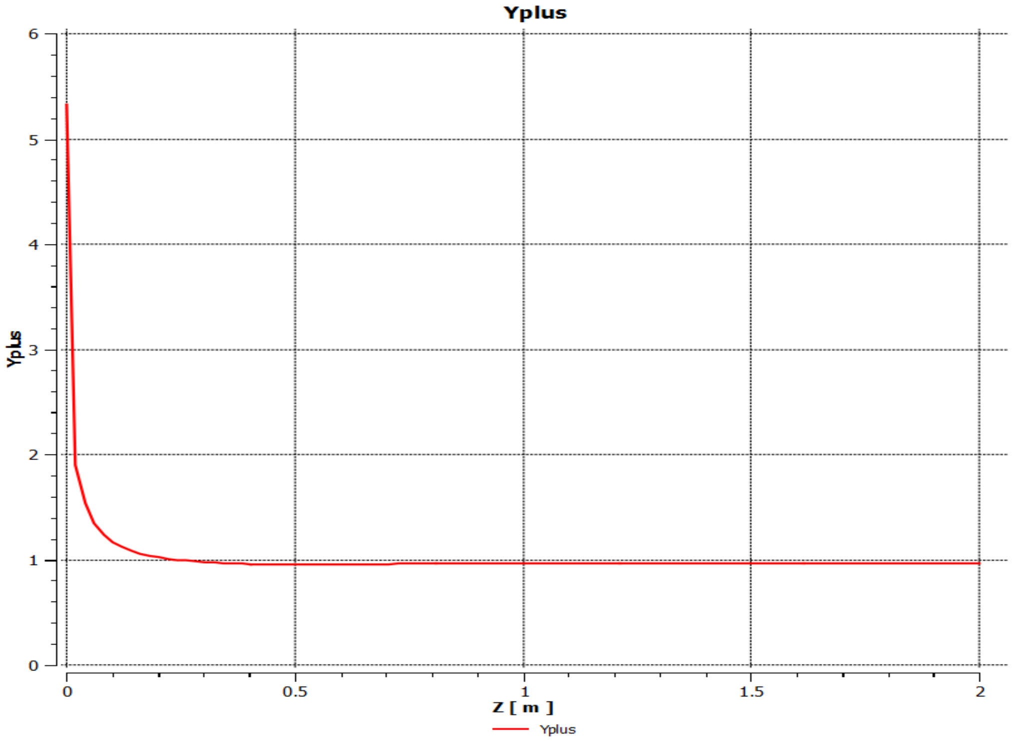

Figure N.19: Yplus variation through annulus.

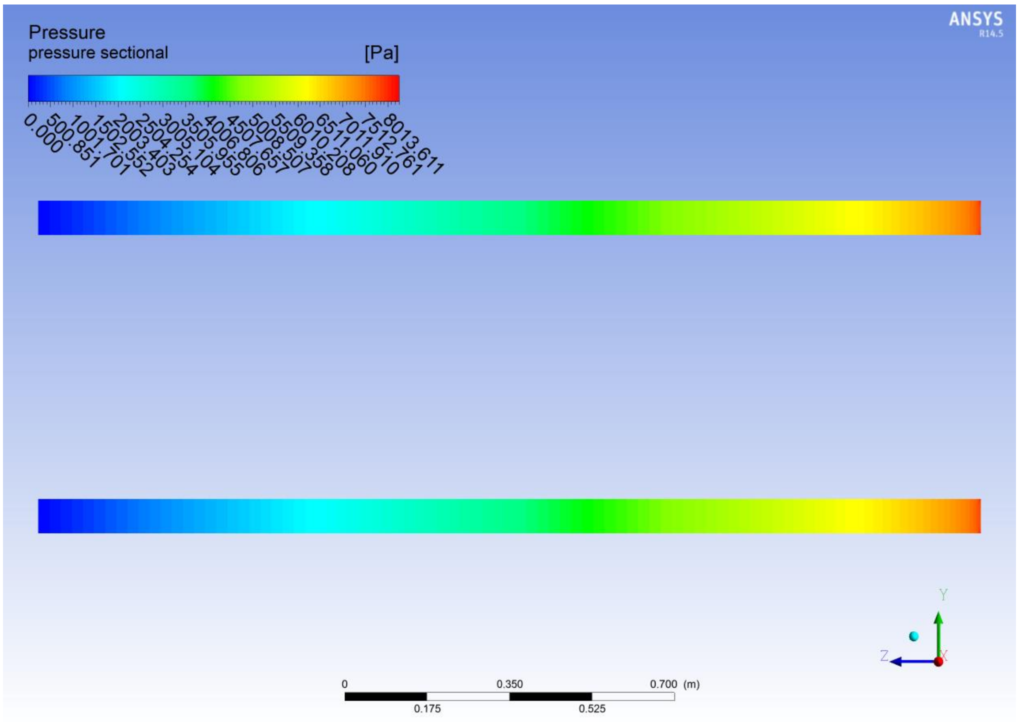

Figure N.20: Cross sectional pressure distribution through annulus while circulating fresh water sepiolite mud.

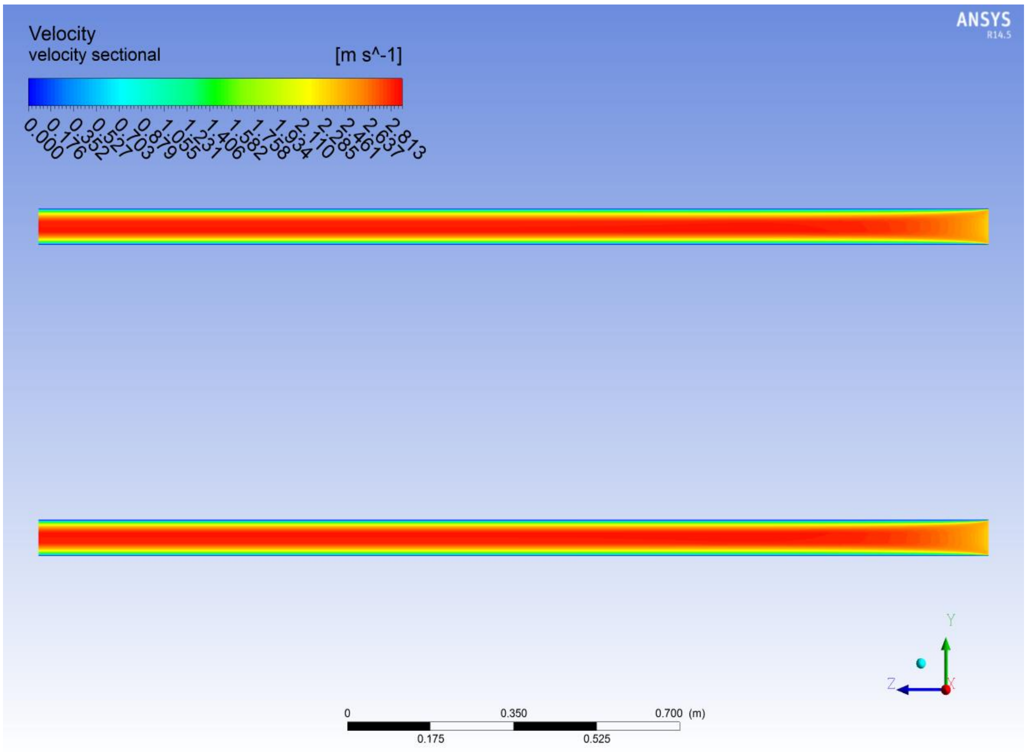

Figure N.21: Cross sectional velocity distribution through annulus while circulating fresh water sepiolite mud.

Appendix P: Numerical results of Hole cleaning ability of unweighted fresh water sepiolite mud system based on rheological properties obtained using viscometer and HTHP rheometer.

Table P.1: Cutting transport ratio of sepiolite mud based on viscometer rheological constants@38°C- Empirical method (Moore correlation).

Average annular velocity (m/s)	Slip velocities (m/s)	Va-Vsl (m/s)	Transport ratio	Transport ratio %
0.0152	0.0086	0.0066	0.4341	43.41
0.0254	0.0104	0.0150	0.5911	59.11
0.0508	0.0134	0.0374	0.7369	73.69
0.0762	0.0155	0.0607	0.7967	79.67
0.1016	0.0172	0.0844	0.8307	83.07
0.1067	0.0175	0.0892	0.8359	83.59
0.1270	0.0181	0.1089	0.8575	85.75
0.1372	0.0189	0.1182	0.8620	86.20
0.1422	0.0194	0.1228	0.8633	86.33
0.1524	0.0199	0.1325	0.8692	86.92
0.2134	0.0225	0.1908	0.8944	89.44
0.2286	0.0231	0.2055	0.8989	89.89
0.2337	0.0233	0.2104	0.9003	90.03
0.2388	0.0235	0.2153	0.9017	90.17
0.2438	0.0237	0.2202	0.9030	90.30
0.2489	0.0238	0.2251	0.9042	90.42
0.2540	0.0240	0.2300	0.9055	90.55
0.2591	0.0242	0.2349	0.9066	90.66
0.2642	0.0244	0.2398	0.9078	90.78
0.2692	0.0245	0.2447	0.9089	90.89
0.2743	0.0247	0.2496	0.9100	91.00
0.2794	0.0249	0.2545	0.9110	91.10
0.2845	0.0250	0.2595	0.9120	91.20
0.2896	0.0252	0.2644	0.9130	91.30
0.2946	0.0253	0.2693	0.9140	91.40
0.2997	0.0255	0.2742	0.9149	91.49
0.3048	0.0257	0.2791	0.9158	91.58
0.3099	0.0258	0.2841	0.9167	91.67
0.3150	0.0260	0.2890	0.9175	91.75
0.3200	0.0261	0.2939	0.9184	91.84
0.3251	0.0263	0.2988	0.9192	91.92
0.3302	0.0264	0.3038	0.9200	92.00
0.3353	0.0266	0.3087	0.9208	92.08
0.3404	0.0267	0.3136	0.9215	92.15
0.3454	0.0269	0.3186	0.9223	92.23
0.3505	0.0270	0.3235	0.9230	92.30
0.3556	0.0271	0.3285	0.9237	92.37
0.3658	0.0274	0.3383	0.9250	92.50
0.4064	0.0285	0.3779	0.9299	92.99
0.4420	0.0294	0.4126	0.9335	93.35
0.4928	0.0306	0.4622	0.9380	93.80
0.5080	0.0309	0.4771	0.9392	93.92
0.5842	0.0325	0.5517	0.9443	94.43
0.6604	0.0340	0.6264	0.9485	94.85
0.7620	0.0358	0.7262	0.9530	95.30
0.9875	0.0394	0.9481	0.9601	96.01
1.0160	0.0398	0.9762	0.9609	96.09
1.2700	0.0431	1.2269	0.9660	96.60
1.5240	0.0461	1.4779	0.9698	96.98

Table P.2: Cutting transport ratio of sepiolite mud based on viscometer rheological constants@121°C- Empirical method (Moore correlation).

Average annular velocity (m/s)	Slip velocities (m/s)	Va-Vsl (m/s)	Transport ratio	Transport ratio %
0.0152	0.0109	0.0043	0.2848	28.48
0.0254	0.0133	0.0121	0.4748	47.48
0.0508	0.0175	0.0333	0.6546	65.46
0.0762	0.0206	0.0556	0.7297	72.97
0.1016	0.0231	0.0785	0.7729	77.29
0.1067	0.0235	0.0832	0.7795	77.95
0.1270	0.0244	0.1026	0.8080	80.80
0.1372	0.0256	0.1116	0.8134	81.34
0.1422	0.0264	0.1159	0.8147	81.47
0.1524	0.0271	0.1253	0.8223	82.23
0.2134	0.0309	0.1824	0.8550	85.50
0.2286	0.0318	0.1968	0.8609	86.09
0.2337	0.0321	0.2016	0.8628	86.28
0.2388	0.0323	0.2064	0.8645	86.45
0.2438	0.0326	0.2112	0.8662	86.62
0.2489	0.0329	0.2160	0.8679	86.79
0.2540	0.0331	0.2209	0.8695	86.95
0.2591	0.0334	0.2257	0.8711	87.11
0.2642	0.0337	0.2305	0.8726	87.26
0.2692	0.0339	0.2353	0.8740	87.40
0.2743	0.0342	0.2402	0.8754	87.54
0.2794	0.0344	0.2450	0.8768	87.68
0.2845	0.0347	0.2498	0.8781	87.81
0.2896	0.0349	0.2547	0.8794	87.94
0.2946	0.0351	0.2595	0.8807	88.07
0.2997	0.0354	0.2643	0.8819	88.19
0.3048	0.0356	0.2692	0.8831	88.31
0.3099	0.0359	0.2740	0.8843	88.43
0.3150	0.0361	0.2789	0.8854	88.54
0.3200	0.0363	0.2837	0.8865	88.65
0.3251	0.0365	0.2886	0.8876	88.76
0.3302	0.0368	0.2934	0.8886	88.86
0.3353	0.0370	0.2983	0.8897	88.97
0.3404	0.0372	0.3031	0.8907	89.07
0.3454	0.0374	0.3080	0.8916	89.16
0.3505	0.0376	0.3129	0.8926	89.26
0.3556	0.0379	0.3177	0.8935	89.35
0.3658	0.0383	0.3275	0.8953	89.53
0.4064	0.0399	0.3665	0.9018	90.18
0.4420	0.0413	0.4007	0.9066	90.66
0.4928	0.0431	0.4497	0.9126	91.26
0.5080	0.0436	0.4644	0.9142	91.42
0.5842	0.0461	0.5381	0.9211	92.11
0.6604	0.0484	0.6120	0.9268	92.68
0.7620	0.0512	0.7108	0.9328	93.28
0.9875	0.0567	0.9308	0.9426	94.26
1.0160	0.0573	0.9587	0.9436	94.36
1.2700	0.0632	1.2068	0.9502	95.02
1.5240	0.0648	1.4592	0.9575	95.75

Table P.3: Cutting transport ratio of sepiolite mud based on viscometer rheological constants@149°C- Empirical method (Moore correlation).

Average annular velocity (m/s)	Slip velocities (m/s)	Va-Vsl (m/s)	Transport ratio	Transport ratio %
0.0254	0.0227	0.0027	0.1064	10.64
0.0508	0.0287	0.0221	0.4355	43.55
0.0762	0.0329	0.0433	0.5685	56.85
0.1016	0.0362	0.0654	0.6434	64.34
0.1067	0.0368	0.0698	0.6548	65.48
0.1270	0.0380	0.0890	0.7010	70.10
0.1372	0.0396	0.0976	0.7114	71.14
0.1422	0.0406	0.1017	0.7147	71.47
0.1524	0.0415	0.1109	0.7274	72.74
0.1727	0.0433	0.1294	0.7491	74.91
0.2286	0.0476	0.1810	0.7917	79.17
0.2337	0.0480	0.1857	0.7947	79.47
0.2388	0.0483	0.1904	0.7976	79.76
0.2438	0.0487	0.1952	0.8004	80.04
0.2489	0.0490	0.1999	0.8031	80.31
0.2540	0.0494	0.2046	0.8057	80.57
0.2591	0.0497	0.2094	0.8082	80.82
0.2642	0.0500	0.2142	0.8107	81.07
0.2692	0.0503	0.2189	0.8131	81.31
0.2743	0.0506	0.2237	0.8154	81.54
0.2794	0.0510	0.2284	0.8176	81.76
0.2845	0.0513	0.2332	0.8198	81.98
0.2896	0.0516	0.2380	0.8219	82.19
0.2946	0.0519	0.2428	0.8239	82.39
0.2997	0.0522	0.2475	0.8259	82.59
0.3048	0.0525	0.2523	0.8278	82.78
0.3099	0.0528	0.2571	0.8297	82.97
0.3150	0.0531	0.2619	0.8315	83.15
0.3200	0.0534	0.2667	0.8333	83.33
0.3251	0.0536	0.2715	0.8350	83.50
0.3302	0.0539	0.2763	0.8367	83.67
0.3353	0.0542	0.2811	0.8384	83.84
0.3404	0.0545	0.2859	0.8400	84.00
0.3454	0.0547	0.2907	0.8415	84.15
0.3505	0.0550	0.2955	0.8431	84.31
0.3556	0.0553	0.3003	0.8445	84.45
0.3658	0.0558	0.3100	0.8474	84.74
0.4064	0.0578	0.3486	0.8577	85.77
0.4420	0.0595	0.3825	0.8654	86.54
0.4928	0.0617	0.4310	0.8748	87.48
0.5080	0.0623	0.4457	0.8773	87.73
0.5842	0.0654	0.5188	0.8881	88.81
0.6604	0.0681	0.5923	0.8969	89.69
0.7620	0.0715	0.6905	0.9062	90.62
0.9875	0.0504	0.9371	0.9490	94.90
1.0160	0.0506	0.9654	0.9502	95.02
1.2700	0.0518	1.2182	0.9592	95.92
1.5240	0.0529	1.4711	0.9653	96.53

Table P.4: Cutting transport ratio of sepiolite mud based on viscometer rheological constants@232°C- Empirical method (Moore correlation).

Average annular velocity (m/s)	Slip velocities (m/s)	Va-Vsl (m/s)	Transport ratio	Transport ratio %
0.00508	0.0024981	0.002582	0.508257	50.8257
0.0254	0.0057695	0.019631	0.772855	77.28553
0.0508	0.0082737	0.042526	0.837131	83.71311
0.0762	0.0102161	0.065984	0.86593	86.59299
0.1016	0.011865	0.089735	0.883219	88.32185
0.10668	0.0121699	0.09451	0.885921	88.59211
0.127	0.0127596	0.11424	0.899531	89.95308
0.13716	0.0135997	0.12356	0.900848	90.08479
0.14224	0.0141341	0.128106	0.900632	90.06319
0.1524	0.0146505	0.137749	0.903868	90.38681
0.21336	0.0174523	0.195908	0.918202	91.82023
0.2286	0.01809	0.21051	0.920866	92.08663
0.23368	0.0182979	0.215382	0.921697	92.16966
0.23876	0.0185038	0.220256	0.922501	92.25006
0.24384	0.0187075	0.225133	0.92328	92.32797
0.24892	0.0189092	0.230011	0.924035	92.40351
0.254	0.0191089	0.234891	0.924768	92.4768
0.25908	0.0193068	0.239773	0.92548	92.54796
0.26416	0.0195027	0.244657	0.926171	92.61708
0.26924	0.0196969	0.249543	0.926843	92.68426
0.27432	0.0198893	0.254431	0.927496	92.74959
0.2794	0.02008	0.25932	0.928132	92.81316
0.28448	0.0202691	0.264211	0.92875	92.87503
0.28956	0.0204566	0.269103	0.929353	92.9353
0.29464	0.0206424	0.273998	0.92994	92.99402
0.29972	0.0208268	0.278893	0.930513	93.05126
0.3048	0.0210096	0.28379	0.931071	93.10708
0.30988	0.021191	0.288689	0.931615	93.16154
0.31496	0.021371	0.293589	0.932147	93.21469
0.32004	0.0215496	0.29849	0.932666	93.2666
0.32512	0.0217268	0.303393	0.933173	93.31729
0.3302	0.0219027	0.308297	0.933668	93.36683
0.33528	0.0220773	0.313203	0.934153	93.41525
0.34036	0.0222507	0.318109	0.934626	93.4626
0.34544	0.0224228	0.323017	0.935089	93.50892
0.35052	0.0225937	0.327926	0.935542	93.55423
0.3556	0.0227634	0.332837	0.935986	93.59859
0.36576	0.0230994	0.342661	0.936845	93.68455
0.4064	0.0244005	0.381999	0.939959	93.99594
0.44196	0.0254886	0.416471	0.942328	94.23283
0.49276	0.0269725	0.465787	0.945262	94.52623
0.508	0.0274032	0.480597	0.946057	94.60566
0.5842	0.0294694	0.554731	0.949556	94.9556
0.6604	0.0314097	0.62899	0.952438	95.24384
0.762	0.0338366	0.728163	0.955595	95.5595
0.9874504	0.0387195	0.948731	0.960788	96.07884
1.016	0.0392977	0.976702	0.961321	96.13211
1.27	0.0441337	1.225866	0.965249	96.5249
1.524	0.0485236	1.475476	0.96816	96.81604

Table P.5: Cutting transport ratio of sepiolite mud based on HTHP rheometer rheological constants@38°C- Empirical method (Moore correlation).

Average annular velocity (m/s)	Slip velocities (m/s)	Va-Vsl (m/s)	Transport ratio	Transport ratio %
0.0254	0.0180	0.0074	0.2921	29.21
0.0508	0.0219	0.0289	0.5680	56.80
0.0762	0.0247	0.0515	0.6764	67.64
0.1016	0.0268	0.0748	0.7363	73.63
0.1067	0.0272	0.0795	0.7454	74.54
0.1270	0.0279	0.0991	0.7804	78.04
0.1372	0.0289	0.1083	0.7894	78.94
0.1422	0.0295	0.1127	0.7926	79.26
0.1524	0.0301	0.1223	0.8025	80.25
0.2134	0.0332	0.1802	0.8446	84.46
0.2286	0.0338	0.1948	0.8521	85.21
0.2337	0.0340	0.1996	0.8544	85.44
0.2388	0.0342	0.2045	0.8566	85.66
0.2438	0.0345	0.2094	0.8587	85.87
0.2489	0.0347	0.2143	0.8608	86.08
0.2540	0.0349	0.2191	0.8628	86.28
0.2591	0.0351	0.2240	0.8647	86.47
0.2642	0.0353	0.2289	0.8665	86.65
0.2692	0.0354	0.2338	0.8683	86.83
0.2743	0.0356	0.2387	0.8701	87.01
0.2794	0.0358	0.2436	0.8718	87.18
0.2845	0.0360	0.2485	0.8734	87.34
0.2896	0.0362	0.2534	0.8750	87.50
0.2946	0.0364	0.2583	0.8765	87.65
0.2997	0.0366	0.2632	0.8780	87.80
0.3048	0.0367	0.2681	0.8795	87.95
0.3099	0.0369	0.2730	0.8809	88.09
0.3150	0.0371	0.2779	0.8823	88.23
0.3200	0.0373	0.2828	0.8836	88.36
0.3251	0.0374	0.2877	0.8849	88.49
0.3302	0.0376	0.2926	0.8862	88.62
0.3353	0.0378	0.2975	0.8874	88.74
0.3404	0.0379	0.3024	0.8886	88.86
0.3454	0.0381	0.3074	0.8898	88.98
0.3505	0.0382	0.3123	0.8909	89.09
0.3556	0.0384	0.3172	0.8920	89.20
0.3658	0.0387	0.3270	0.8942	89.42
0.4064	0.0399	0.3665	0.9018	90.18
0.4420	0.0409	0.4011	0.9075	90.75
0.4928	0.0422	0.4506	0.9144	91.44
0.5080	0.0425	0.4655	0.9162	91.62
0.5842	0.0443	0.5399	0.9242	92.42
0.6604	0.0459	0.6145	0.9305	93.05
0.7620	0.0478	0.7142	0.9373	93.73
0.9875	0.0515	0.9359	0.9478	94.78
1.0160	0.0519	0.9641	0.9489	94.89
1.2700	0.0554	1.2146	0.9564	95.64
1.5240	0.0584	1.4656	0.9617	96.17

Table P.6: Cutting transport ratio of sepiolite mud based on HTHP rheometer rheological constants@121°C- Empirical method (Moore correlation).

Average annular velocity (m/s)	Slip velocities (m/s)	Va-Vsl (m/s)	Transport ratio	Transport ratio %
0.1016	0.0874	0.0142	0.1419	14.19
0.1067	0.0878	0.0189	0.1808	18.08
0.1270	0.0883	0.0387	0.3089	30.89
0.1372	0.0886	0.0486	0.3563	35.63
0.1422	0.0889	0.0533	0.3771	37.71
0.1524	0.0894	0.0630	0.4167	41.67
0.2134	0.0906	0.1227	0.5766	57.66
0.2286	0.0907	0.1379	0.6035	60.35
0.2337	0.0908	0.1428	0.6117	61.17
0.2388	0.0909	0.1478	0.6196	61.96
0.2438	0.0910	0.1528	0.6271	62.71
0.2489	0.0911	0.1578	0.6344	63.44
0.2540	0.0912	0.1628	0.6413	64.13
0.2591	0.0913	0.1678	0.6480	64.80
0.2642	0.0914	0.1728	0.6545	65.45
0.2692	0.0914	0.1778	0.6607	66.07
0.2743	0.0915	0.1828	0.6667	66.67
0.2794	0.0916	0.1878	0.6724	67.24
0.2845	0.0917	0.1928	0.6780	67.80
0.2896	0.0918	0.1978	0.6834	68.34
0.2946	0.0918	0.2028	0.6886	68.86
0.2997	0.0919	0.2078	0.6936	69.36
0.3048	0.0920	0.2128	0.6985	69.85
0.3099	0.0920	0.2178	0.7032	70.32
0.3150	0.0921	0.2228	0.7078	70.78
0.3200	0.0922	0.2279	0.7122	71.22
0.3251	0.0923	0.2329	0.7165	71.65
0.3302	0.0923	0.2379	0.7206	72.06
0.3353	0.0924	0.2429	0.7246	72.46
0.3404	0.0925	0.2479	0.7286	72.86
0.3454	0.0925	0.2529	0.7324	73.24
0.3505	0.0926	0.2579	0.7360	73.60
0.3556	0.0927	0.2629	0.7396	73.96
0.3658	0.0932	0.2726	0.7465	74.65
0.4064	0.0936	0.3128	0.7707	77.07
0.4420	0.0940	0.3479	0.7883	78.83
0.4928	0.0942	0.3986	0.8091	80.91
0.5080	0.0948	0.4132	0.8146	81.46
0.5842	0.0954	0.4888	0.8377	83.77
0.6604	0.0960	0.5644	0.8556	85.56
0.7620	0.0972	0.6648	0.8740	87.40
0.9875	0.0974	0.8901	0.9015	90.15
1.0160	0.0984	0.9176	0.9042	90.42
1.2700	0.0993	1.1707	0.9225	92.25
1.5240	0.0000	1.5240	0.9349	93.49

Table P.7: Cutting transport ratio of sepiolite mud based on HTHP rheometer rheological constants@232°C- Empirical method (Moore correlation).

Average annular velocity (m/s)	Slip velocities (m/s)	Va-Vsl (m/s)	Transport ratio	Transport ratio %
0.0152	0.0081	0.0071	0.4682	46.82
0.0254	0.0109	0.0145	0.5717	57.17
0.0508	0.0162	0.0346	0.6807	68.07
0.0762	0.0205	0.0557	0.7311	73.11
0.1016	0.0242	0.0774	0.7620	76.20
0.1067	0.0249	0.0818	0.7669	76.69
0.1270	0.0262	0.1008	0.7936	79.36
0.1372	0.0281	0.1090	0.7949	79.49
0.1422	0.0294	0.1129	0.7936	79.36
0.1524	0.0305	0.1219	0.7996	79.96
0.2134	0.0371	0.1763	0.8262	82.62
0.2286	0.0386	0.1900	0.8312	83.12
0.2337	0.0391	0.1946	0.8328	83.28
0.2388	0.0396	0.1992	0.8343	83.43
0.2438	0.0400	0.2038	0.8358	83.58
0.2489	0.0405	0.2084	0.8372	83.72
0.2540	0.0410	0.2130	0.8386	83.86
0.2591	0.0415	0.2176	0.8399	83.99
0.2642	0.0419	0.2222	0.8412	84.12
0.2692	0.0424	0.2268	0.8425	84.25
0.2743	0.0429	0.2315	0.8438	84.38
0.2794	0.0433	0.2361	0.8450	84.50
0.2845	0.0438	0.2407	0.8462	84.62
0.2896	0.0442	0.2453	0.8473	84.73
0.2946	0.0447	0.2500	0.8484	84.84
0.2997	0.0451	0.2546	0.8495	84.95
0.3048	0.0455	0.2593	0.8506	85.06
0.3099	0.0460	0.2639	0.8516	85.16
0.3150	0.0464	0.2686	0.8527	85.27
0.3200	0.0468	0.2732	0.8536	85.36
0.3251	0.0473	0.2779	0.8546	85.46
0.3302	0.0477	0.2825	0.8556	85.56
0.3353	0.0481	0.2872	0.8565	85.65
0.3404	0.0485	0.2918	0.8574	85.74
0.3454	0.0489	0.2965	0.8583	85.83
0.3505	0.0494	0.3012	0.8592	85.92
0.3556	0.0498	0.3058	0.8600	86.00
0.3658	0.0506	0.3152	0.8617	86.17
0.4064	0.0538	0.3526	0.8677	86.77
0.4420	0.0564	0.3855	0.8724	87.24
0.4928	0.0624	0.4304	0.8734	87.34
0.5080	0.0627	0.4453	0.8765	87.65
0.5842	0.0644	0.5198	0.8897	88.97
0.6604	0.0660	0.5944	0.9001	90.01
0.7620	0.0678	0.6942	0.9110	91.10
0.9875	0.0713	0.9162	0.9278	92.78
1.0160	0.0717	0.9443	0.9295	92.95
1.2700	0.0748	1.1952	0.9411	94.11
1.5240	0.0775	1.4465	0.9492	94.92

Table P.8: Cutting transport ratio of sepiolite mud based on viscometer rheological constants@38°C- CFD.

Average annular velocity (m/s)	DPM velocity (m/s)	Transport ratio	Transport ratio %
0.0300	0.0098	0.3260	32.60
0.0450	0.0264	0.5870	58.70
0.0596	0.0444	0.7460	74.60
0.0893	0.0720	0.8060	80.60
0.1191	0.0993	0.8334	83.34
0.1489	0.1271	0.8540	85.40
0.2978	0.2710	0.9100	91.00
0.4466	0.4160	0.9314	93.14
0.5955	0.5608	0.9418	94.18
0.7444	0.7072	0.9500	95.00
1.0421	1.0005	0.9600	96.00
1.3399	1.2930	0.9650	96.50
1.4888	1.4441	0.9700	97.00

Table P.9: Cutting transport ratio of sepiolite mud based on viscometer rheological constants@121°C- CFD.

Average annular velocity (m/s)	DPM velocity (m/s)	Transport ratio	Transport ratio %
0.0298	0.0046	0.1560	15.60
0.0450	0.0181	0.4030	40.30
0.0596	0.0360	0.6050	60.50
0.0893	0.0670	0.7500	75.00
0.1191	0.0936	0.7857	78.57
0.1489	0.1207	0.8107	81.07
0.2978	0.2614	0.8779	87.79
0.4466	0.4059	0.9089	90.89
0.5955	0.5512	0.9256	92.56
0.7444	0.6985	0.9384	93.84
1.0421	0.9916	0.9515	95.15
1.3399	1.2863	0.9600	96.00
1.4888	1.4337	0.9630	96.30

Table P.10: Cutting transport ratio of sepiolite mud based on viscometer rheological constants@149°C- CFD.

Average annular velocity (m/s)	DPM velocity (m/s)	Transport ratio	Transport ratio %
0.0450	0.0027	0.0590	5.90
0.0596	0.0152	0.2547	25.47
0.0893	0.0512	0.5727	57.27
0.1191	0.0818	0.6865	68.65
0.1489	0.1067	0.7170	71.70
0.2978	0.2471	0.8300	83.00
0.4466	0.3916	0.8768	87.68
0.5955	0.5373	0.9022	90.22
0.7444	0.6836	0.9183	91.83
1.0421	0.9796	0.9400	94.00
1.3399	1.2744	0.9511	95.11
1.4888	1.4209	0.9544	95.44

Table P.11: Cutting transport ratio of sepiolite mud based on viscometer rheological constants@232°C- CFD.

Average annular velocity (m/s)	DPM velocity (m/s)	Transport ratio	Transport ratio %
0.0149	0.0034	0.2275	22.75
0.0298	0.0205	0.6900	69.00
0.0596	0.0511	0.8580	85.80
0.0893	0.0790	0.8846	88.46
0.1191	0.1068	0.8967	89.67
0.1489	0.1350	0.9067	90.67
0.2978	0.2772	0.9310	93.10
0.4466	0.4198	0.9400	94.00
0.5955	0.5633	0.9460	94.60
0.7444	0.7072	0.9500	95.00
1.0421	1.0005	0.9600	96.00
1.3399	1.2997	0.9700	97.00
1.4888	1.4441	0.9700	97.00

Table P.12: Cutting transport ratio of sepiolite mud based on HTHP rheometer rheological constants@38°C- CFD.

Average annular velocity (m/s)	DPM velocity (m/s)	Transport ratio	Transpor t ratio %
0.0596	0.0264	0.4429	44.29
0.0893	0.0615	0.6889	68.89
0.1191	0.0881	0.7395	73.95
0.1489	0.1156	0.7763	77.63
0.2286	0.1909	0.8353	83.53
0.2978	0.2574	0.8646	86.46
0.4466	0.4029	0.9020	90.20
0.5955	0.5485	0.9210	92.10
0.7444	0.6953	0.9340	93.40
1.0421	0.9880	0.9481	94.81
1.3399	1.2825	0.9572	95.72
1.4888	1.4311	0.9613	96.13

Table P.13: Cutting transport ratio of sepiolite mud based on HTHP rheometer rheological constants@121°C- CFD.

Average annular velocity (m/s)	DPM velocity (m/s)	Transport ratio	Transport ratio %
0.1489	0.0257	0.1726	17.26
0.2084	0.0888	0.4262	42.62
0.2978	0.1743	0.5855	58.55
0.4466	0.3216	0.7200	72.00
0.5955	0.4684	0.7866	78.66
0.7444	0.6156	0.8270	82.70
1.0421	0.9125	0.8756	87.56
1.3399	1.2039	0.8985	89.85
1.4888	1.3521	0.9082	90.82

Table P.14: Cutting transport ratio of sepiolite mud based on HTHP rheometer rheological constants@149°C- CFD.

Average annular velocity (m/s)	DPM velocity (m/s)	Transport ratio	Transport ratio %
0.2084	0.0055	0.0265	2.65
0.2680	0.0606	0.2260	22.60
0.2978	0.0896	0.3010	30.10
0.3573	0.1465	0.4100	41.00
0.4466	0.2327	0.5210	52.10
0.5955	0.3793	0.6370	63.70
0.7444	0.5263	0.7070	70.70
1.0421	0.8191	0.7860	78.60
1.3399	1.1121	0.8300	83.00
1.4888	1.2595	0.8460	84.60

Table P.15: Cutting transport ratio of sepiolite mud based on HTHP rheometer rheological constants@232°C- CFD.

Average annular velocity (m/s)	DPM velocity (m/s)	Transport ratio	Transport ratio %
0.0298	0.0046	0.1551	15.51
0.0450	0.0176	0.3903	39.03
0.0596	0.0433	0.7267	72.67
0.0893	0.0706	0.7900	79.00
0.1191	0.0957	0.8035	80.35
0.1489	0.1220	0.8196	81.96
0.2978	0.2590	0.8700	87.00
0.4466	0.4038	0.9042	90.42
0.5955	0.5490	0.9219	92.19
0.7444	0.6967	0.9360	93.60
1.0421	0.9924	0.9523	95.23
1.3399	1.2899	0.9627	96.27
1.4888	1.4384	0.9662	96.62

Appendix Q: Graphical results of hole cleaning ability of unweighted fresh water sepiolite mud system based on rheological properties obtained using viscometer and HTHP rheometer.

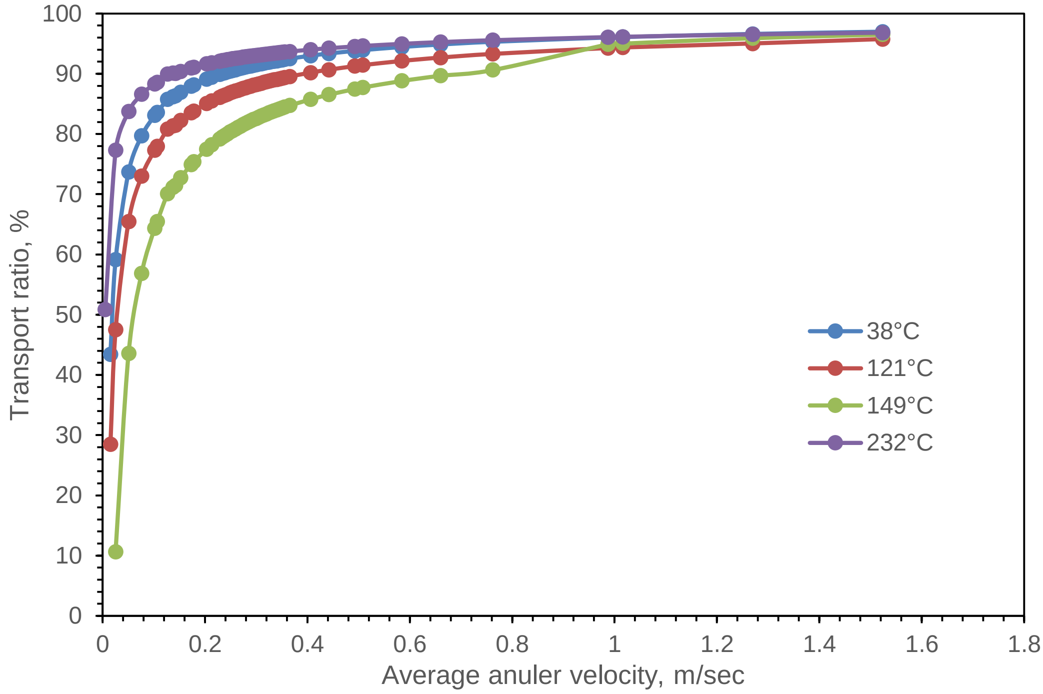

Figure Q.1: Hole cleaning ability of fresh water sepiolite mud based on viscometer rheological parameters- Empirical method (Moore correlation).

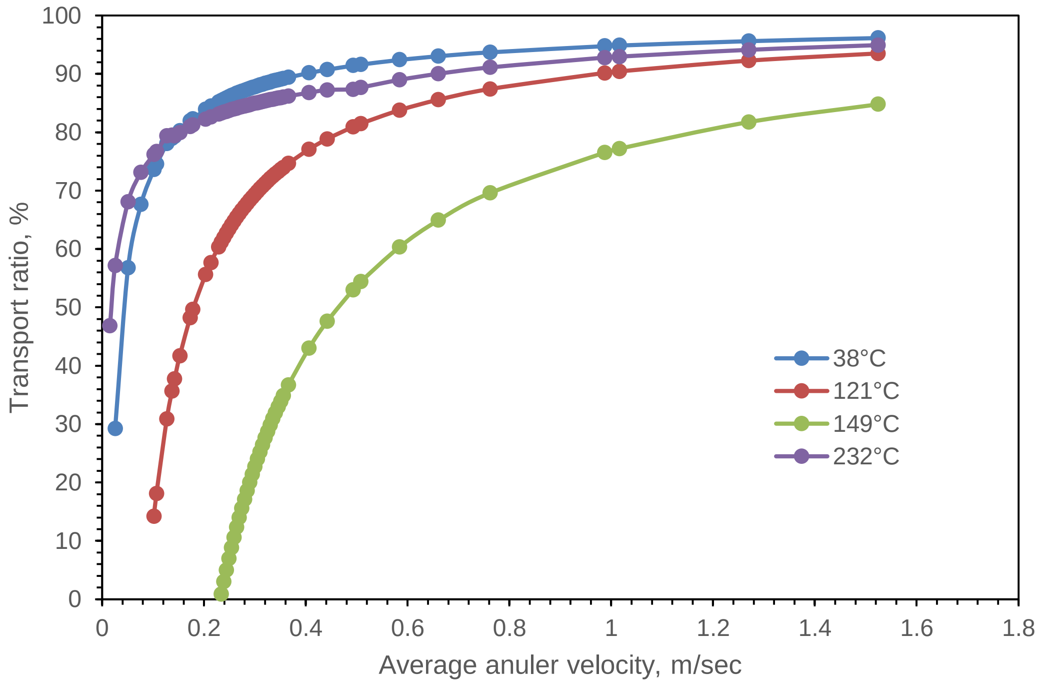

Figure Q.2: Hole cleaning ability of fresh water sepiolite mud based on HTHP rheometer rheological parameters- Empirical method (Moore correlation).

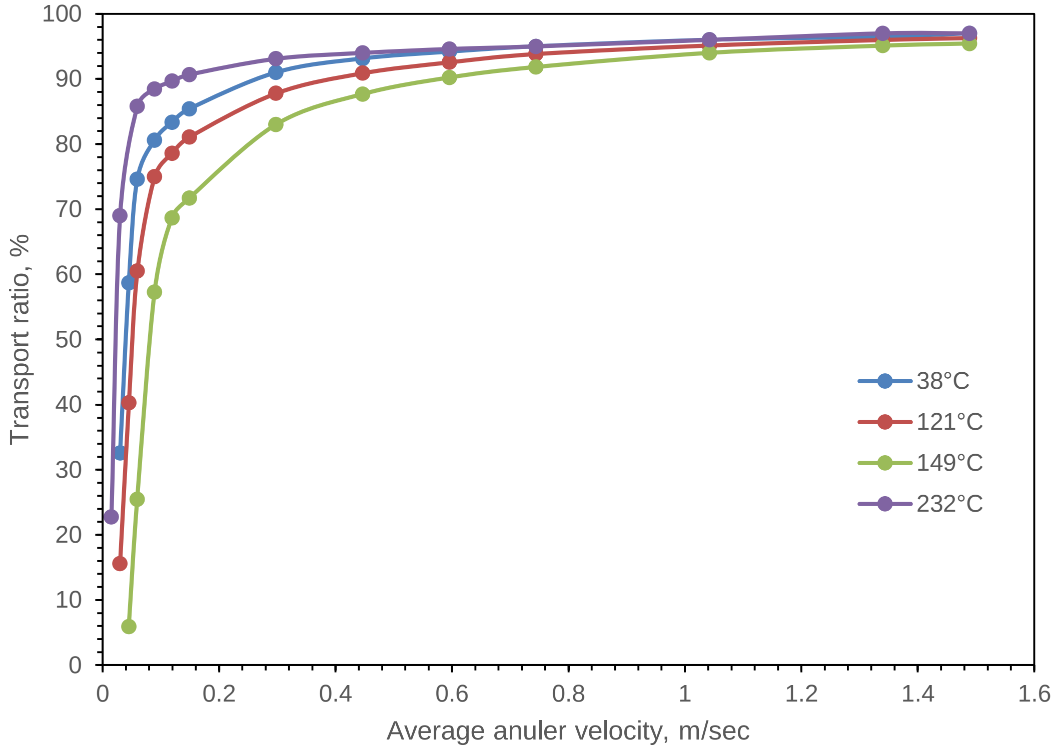

Figure Q.3: Hole cleaning ability of fresh water sepiolite mud based on viscometer rheological parameters- CFD.

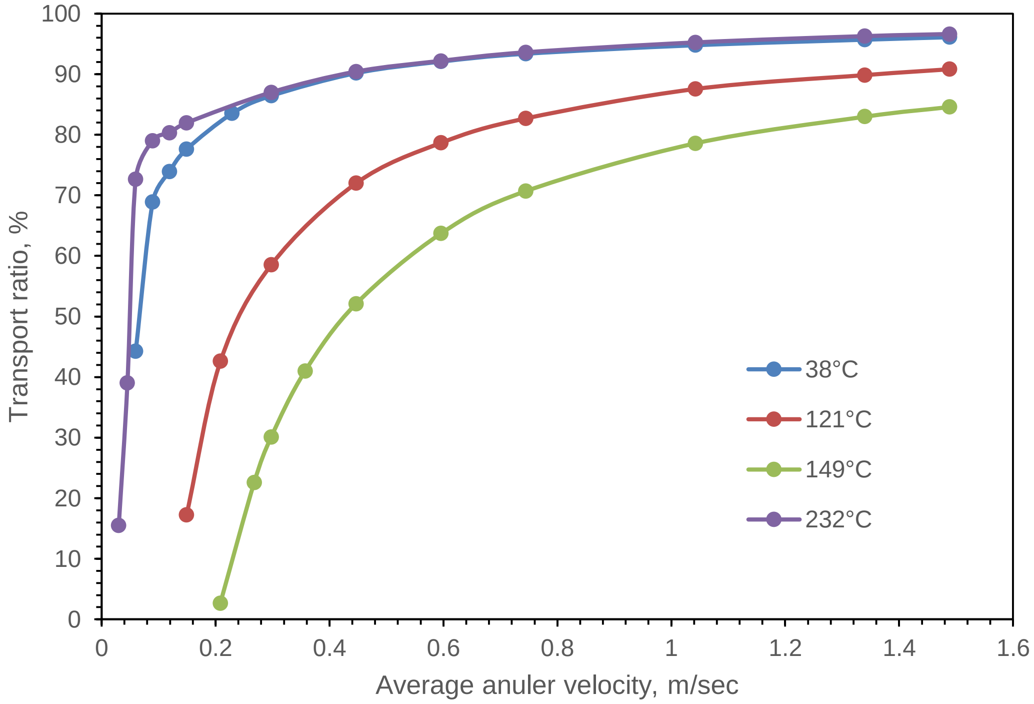

Figure Q.4: Hole cleaning ability of fresh water sepiolite mud based on HTHP rheometer rheological parameters- CFD.

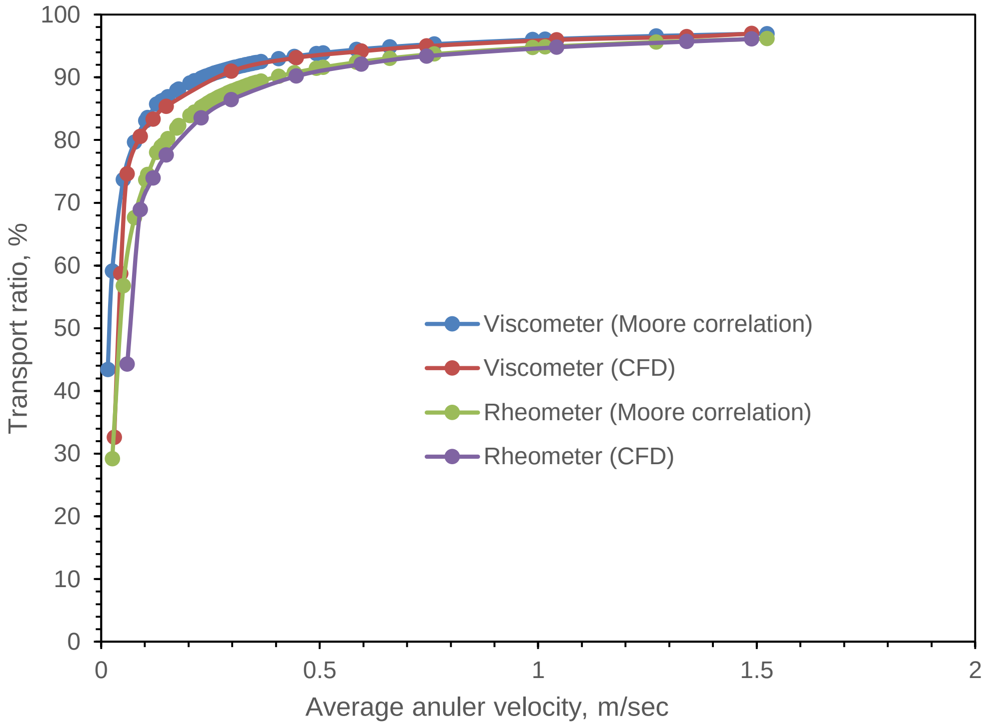

Figure Q.5: Hole cleaning ability of fresh water sepiolite mud @38°C-viscometer vs. HTHP Rheometer.

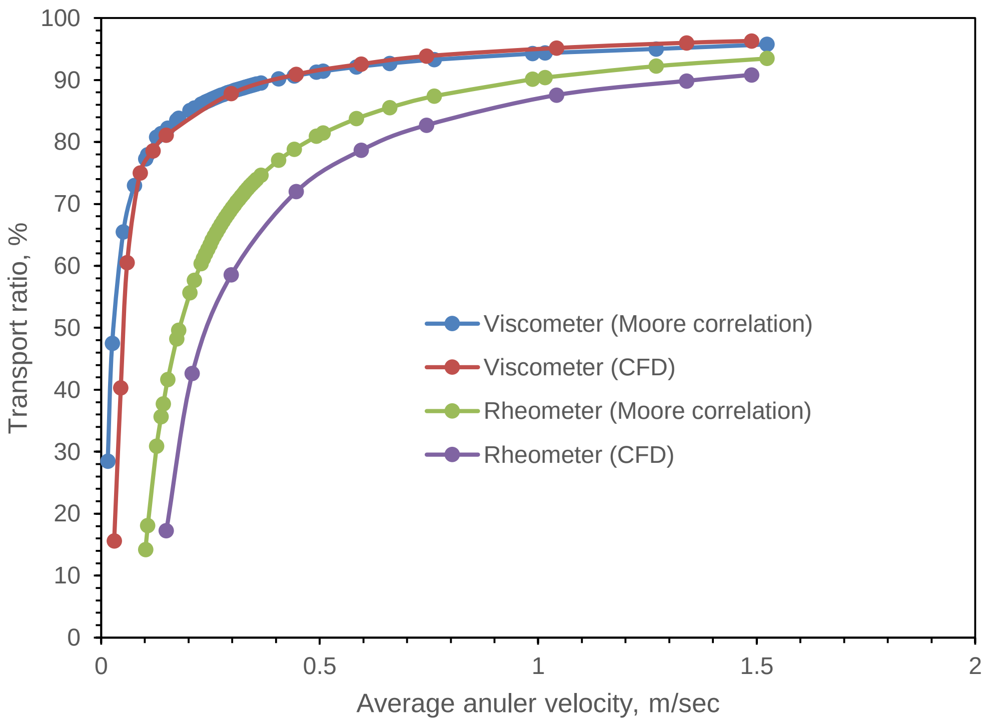

Figure Q.6: Hole cleaning ability of fresh water sepiolite mud @121°C-viscometer vs. HTHP Rheometer.

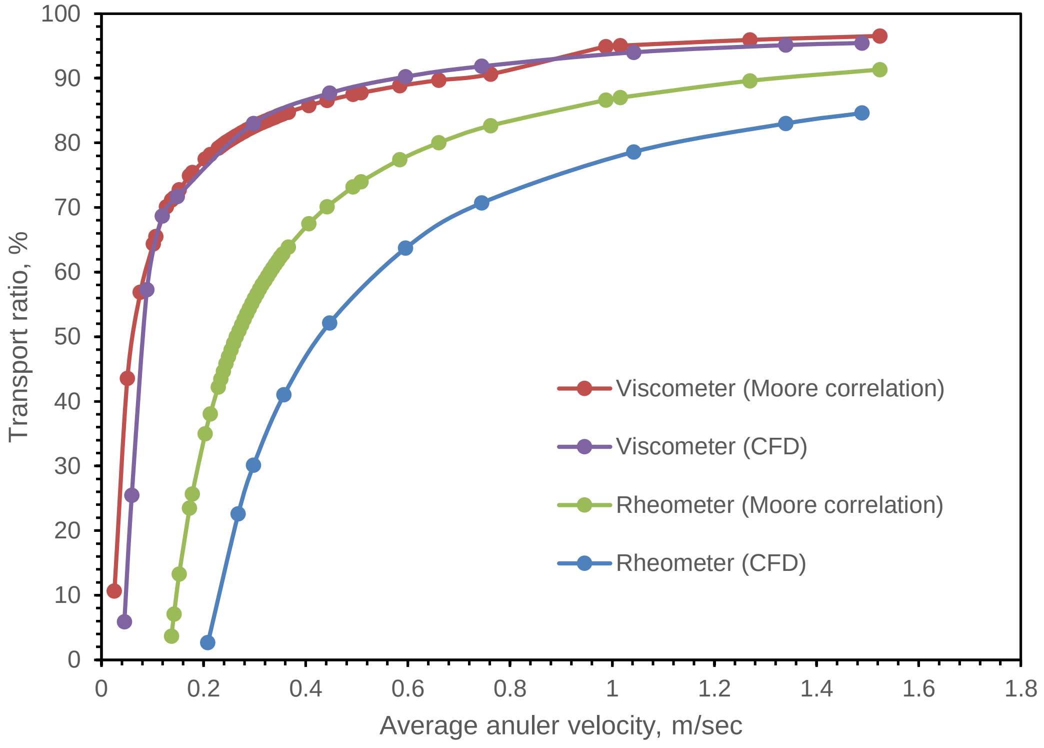

Figure Q.7: Hole cleaning ability of fresh water sepiolite mud @149°C-viscometer vs. HTHP rheometer, (non-Newtonian method).

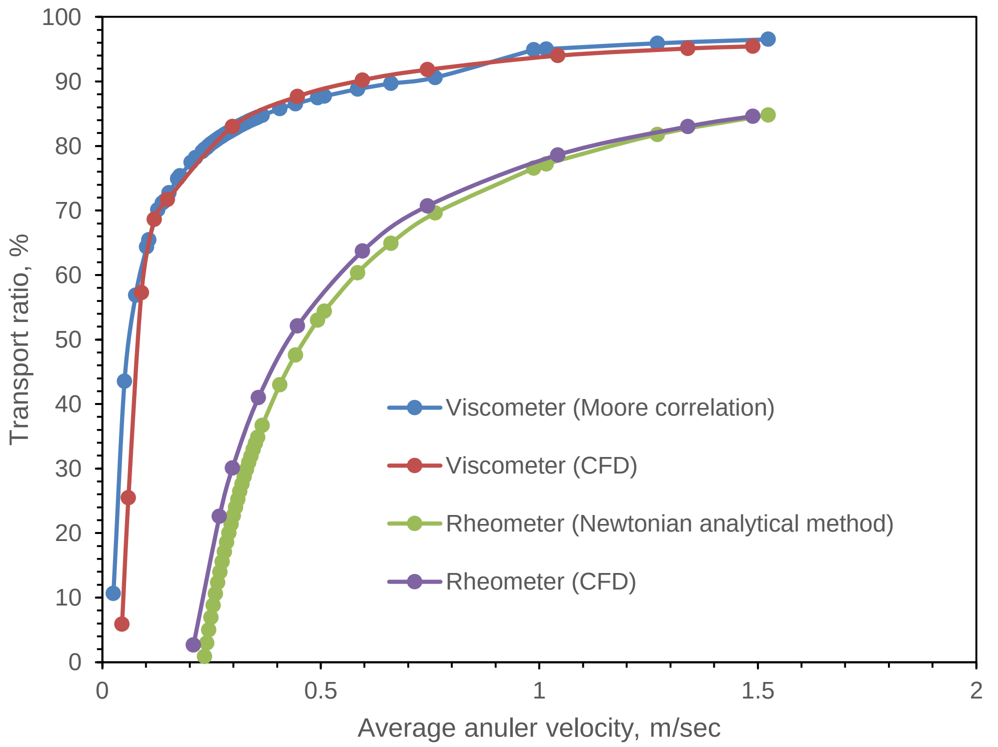

Figure Q.8: Hole cleaning ability of fresh water sepiolite mud @149°C-viscometer vs. HTHP rheometer, (Newtonian method).

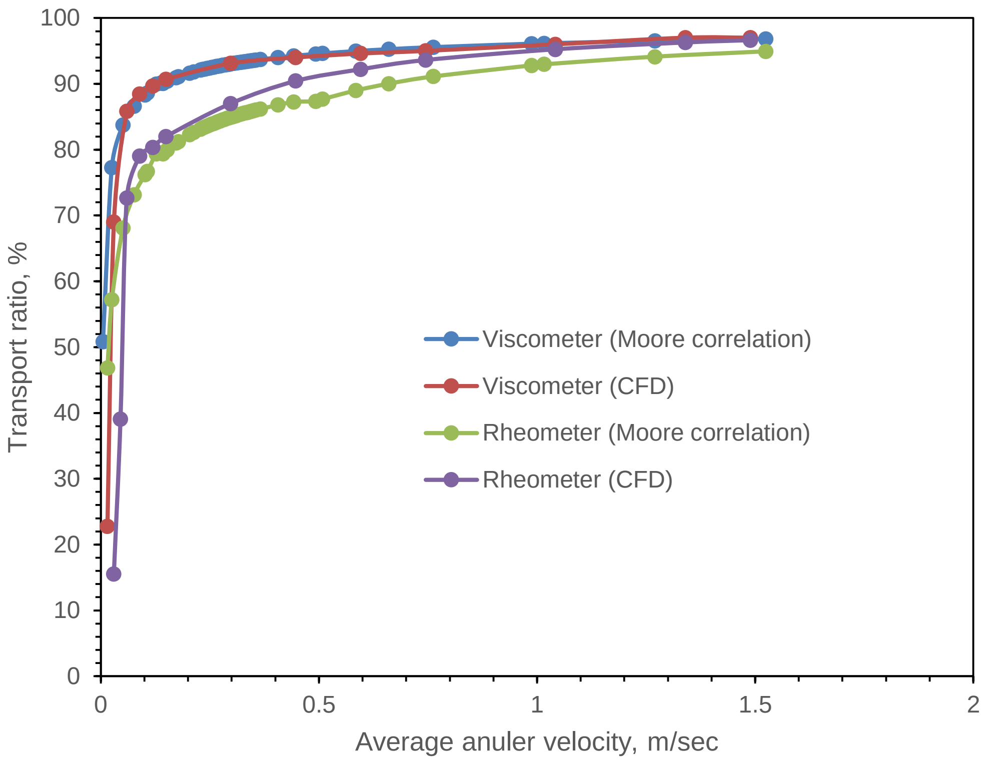

Figure Q.9: Hole cleaning ability of fresh water sepiolite mud @232°C-viscometer vs. HTHP rheometer.

Appendix R: Unit conversions.

Unit Conversion:

- Pa-s = eq cp × 10^{-3}
- Pa = lb/100 ft^2 × 0.479
- Pa = psi × 6894.7572
- Pa/m = psi/ft × 22620.5948
- m/s = ft/s ×3.2808
- lb_m/gal = kg/m^3× 119.83
- eq cp = Pa-s × 10^3
- lb/100 ft^2 = Pa × 2.0877
- psi = Pa × 145×10^{-3}
- psi/ft = Pa/m × 422×10^{-4}
- ft/s = m/s × 0.3048
- kg/m^3 = lb_m/gal ×0.00834

CURRICULUM VITAE

Name Surname: Ali ETTEHADI

Place and Date of Birth: 31/05/1979

E-Mail: ettehadi@itu.edu.tr

EDUCATION:

B.Sc.: Civil Engineering

Azarbaijan University of Tarbiat Moallem, Tabriz, Iran (2004)

M.Sc.: Petroleum and Natural Gas Engineering

Istanbul Technical University, Istanbul, Turkey (2010)

PUBLICATIONS, PRESENTATIONS AND PATENTS ON THE THESIS:

Journal Articals

- **Ali Ettehadi**, M. Hakan Ozyurtkan, and Gursat Altun, 2014. "*Dynamic Filtration Properties of Fresh Water Sepiolite-based Muds"*. Journal of Energy Resources, Part A Recovery, Utilization and Environmental Effects. Vol. 36, Issue 19, pp. 2079-2086, July. DOI**:**10.1080/15567036.2011.563267
- Gurşat Altun, **Ali Ettehadi**., 2014 "*Investigation and Remediation of Sepiolite Muds Contaminated with Reactive Clay*" Journal of Applied Clay Science,CLAY3193, DOI: 10.1016/j.clay.2014.10.002
- **Ali Ettehadi ,** Gürşat Altun, 2015 "*modelling cutting transport using computational fluid dynamics*" Mühendis ve Makina (Turkish Journal)

Conference Papers (International)

- **Ali Ettehadi** , Gursat Altun., 2015 "*Impressive Contribution of CFD in Modelling Wellbore Physics"* 20th International Petroleum and Natural Gas Congress and Exhibition of Turkey, 27-29 May, Ankara, Turkey
- Gursat Altun, **Ali Ettehadi** and Mustafa Hakan Ozyurtkan, 2015 " *Sepiolite Based Muds as an Alternate Drilling Fluid for Hot Environments* " Proceedings World Geothermal Congress, 19-24 April Australia, New Zealand
- Gursat Altun, **Ali Ettehadi** and Mustafa Hakan Ozyurtkan, 2014 " *An Alternate Mud Proposal to Minimize Borehole Instability* " IPTC2014, International Petroleum Technology Conference, 10-12 December, Kuala Lumpur, Malaysia
- Gürşat Altun, **Ali Ettehadi** ., Mustafa Hakan Ozyurtkan, 2014 "*Customization of Sepiolite Based Drilling Fluids at High Temperatures*" 48th US Rock Mechanics / Geomechanics Symposium, 1-4 June July, Minneapolis, MN, USA

- **Ali Ettehadi**, Gursat Altun., 2013 "*A Review of Application of Computational Fluid Dynamics in Prediction of Oil And Gas Wells Problems"* Conference paper accepted at 19th International Petroleum and Natural Gas Congress and Exhibition of Turkey, 15-17 May, Ankara, Turkey
- **Ali Ettehadi**, Mustafa Hakan Ozyurtkan, Gursat Altun., 2012 "*Dynamic Filtration Properties of Clay Based Drilling Muds at Elevated Tempratures"* Conference paper accepted (7-July-2012), Kuwait International Petroleum Conference and Exhibition, SPE-163325-MS, 10-12 December
- **Ali Ettehadi**., 2012 "*Sepiolite Muds for Hostile Drilling Environments"* accepted for presentation (6-August-2012) German Section of Society of Petroleum Engineering Student Technical Conference 2012, Wietze, Germany, 18/19 October.
- Gursat Altun, **Ali Ettehadi** and Umran Serpen., 2010 "*Controlling Rheological and Fluid Loss Properties of Sepiolite Based Muds under Elevated Temperatures*" Proceedings World Geothermal Congress 2010, Bali, Indonesia, 25-29 April.

Conference Papers (National)

- **Ali Ettehadi,** Bagtyyar Durdyyev, Gürşat Altun, 2015 "*Kesinti Taşınımının Hesaplamalı Akışkanlar Dinamiği Yaklaşımıyla Kestirimi*" 12th HVAC and Sanitary Congress and Exhibition (TESKON 2015), Izmir, Turkey ,8-11 April
- **Ali Ettehadi,** Gürşat Altun, Ümran Serpen, 2015 "*Sondaj Akışkanı Isıl Reolojik Özellikleri Üzerine Karşılaştırmalı Bir Çalışma: Klasik Viskometre ve Isıl Reometre*" 12th HVAC and Sanitary Congress and Exhibition (TESKON 2015), Izmir, Turkey ,8-11 April
- Gürşat Altun, **Ali Ettehadi**, Ümran Serpen, 2013 "S*u bazlı sepiolit çamurları özelliklerinin zorlu sondaj koşullarında deneysel olarak incelenmesi*" 11th HVAC and Sanitary Congress and Exhibition (TESKON 2013), Izmir, Turkey ,17-20 April
- Gürşat Altun, **Ali Ettehadi**, Ümran Serpen, Mehmet Çelik., 2011 "*Katkılı sepiolit temelli sondaj çamurlarının kil kirlenmesine karşı reolojik ve su kaybı özelliklerinin incelenmesi* " 10th HVAC and Sanitary Congress and Exhibition (TESKON 2011), Izmir, Turkey ,13-14 April.
- **Ali Ettehadi**, Eda Ay Dilsiz, Gürşat Altun, Ümran Serpen, Mehmet Çelik., 2009 "*Sivrihisar-Eskişehir Yöresi Sepiolit Killerinin Sondaj Çamuru Olarak Reoloji Ve Su Kaybı Özellikleri*" TMMOB Geothermal Congress 2009 , Ankara, Turkey, 23 - 25 December.

PARTICIPATED PROJECTS

- **TPAO – Istanbul Technical University** (Altun. G.), "Investigation of Sepiolite Based Drilling Fluids Properties at Elevated Temperatures and Pressures", Experimental and Theoretical Work, 2009, No: ITU Revolving Funds 861
- **Scientific Research Project (SRP-** Istanbul Technical University), "Investigation of Plugging Ability on Sepiolite Based Drilling Fluids at Different Type of Permeable Formations", Experimental and Theoretical Work, 2011-2012, No: ITU BAP 34455
- **The Scientific And Technological Research Council Of Turkey – ITU**, "Investigation rheological and cutting transport properties of sepiolite based muds using high temperature rheometer" Experimental and Theoretical Work, 2013, No: 113M601